

Rare Earth Magnetism

Structures and Excitations

JENS JENSEN

and

ALLAN R. MACKINTOSH

*H.C. Ørsted Institute
University of Copenhagen*

CLARENDON PRESS · OXFORD

1991

THE
INTERNATIONAL SERIES
OF
MONOGRAPHS ON PHYSICS

GENERAL EDITORS

J. BIRMAN S. F. EDWARDS
C. H. LLEWELLYN SMITH M. REES

PREFACE

The study of the magnetic properties of the rare earth metals may be said to have its origins in the 1930s, when the ferromagnetism of Gd was discovered, and the paramagnetism of the other heavy elements was investigated. The detailed exploration of these properties, and the concurrent development in our understanding of rare earth magnetism, occurred however as a result of two decisive advances in experimental technique during the 1950s. F.H. Spedding and his colleagues at Iowa State University began to produce large quantities of pure rare earth elements and to fashion them into single crystals, and during the same period, intense beams of thermal neutrons became available from research reactors. The neutron is a uniquely useful tool for studying the microscopic magnetic behaviour of materials, and neutron scattering has played the leading role in the progressive elucidation of the magnetic structures and excitations in the rare earths, and hence in understanding the magnetic interactions and their consequences.

This progress has of course been fully documented in the scientific literature and a number of compendia have served to consolidate the achievements of the many scientists involved. In particular, the review of the *Magnetic Properties of Rare Earth Metals*, edited by R.J. Elliott (Plenum Press 1972), which was written at a time when the field had recently become mature, set an exemplary standard of completeness, authoritativeness and, despite the large number of authors, coherence. More recently, a number of excellent surveys of different aspects of rare earth magnetism have appeared in the multi-volume series *Handbook on the Physics and Chemistry of Rare Earths*, edited by K.A. Gschneidner, Jr. and L. Eyring (North-Holland 1978 –), while Sam Legvold presented a largely experimental, but admirably balanced and complete review of the whole field in his chapter in Vol. 1 of *Ferromagnetic Materials*, edited by E.P. Wohlfarth (North-Holland 1980).

Our aim with this monograph has not been to produce a similarly comprehensive review, but rather to present a unified and coherent account of a limited but important area of rare earth magnetism, the magnetic structures and excitations, which both reflect the nature of the fundamental magnetic interactions, and determine many of the characteristic properties of the metals. We have tried to concentrate on the essential principles and their application to typical examples, generally restricting our discussion to the pure elements, and considering alloys and compounds only when they are necessary to illuminate particular

topics. We have been involved for some time in the effort which has been made in Denmark to study, both theoretically and experimentally, the magnetic structures and especially the excitations in the rare earths. This account of the subject represents the results of our experience, and we have written it in the hope that it will be useful not only to those who have a special interest in rare earth magnetism, but also to a wider audience who wish to learn something about the methods and achievements of modern research in magnetism. We have therefore attempted to make the theoretical treatment reasonably complete and self-contained, starting from first principles and developing the argument in some detail. On the other hand, no pretence is made to completeness in our survey of the experimental results. Rather, they are used for illustrative purposes, and the specific properties of the individual elements may therefore have to be found in one of the reviews to which we frequently refer. However, we have tried to include the most important developments from recent years, with the aim of incorporating in this book most of the available information about rare earth magnetism, or directions as to where it can be found.

With very few exceptions, the magnetic properties of the rare earth metals can be understood in terms of what we will call the standard model, according to which the magnetic $4f$ electrons in the metal have the same angular-momentum quantum numbers as in the free ion. They interact, however, with the surrounding electric field of the crystal, and with each other through an indirect exchange mediated by the conduction electrons. Since the emergence of the standard model in the late 1950s, a primary aim of the rare earth-research community has been to determine these interactions, by a combination of experiment and first-principles calculations, and thereby to explain qualitatively and, where possible, quantitatively all features of the magnetic behaviour. In this way the limitations of the model can be explored, and appropriate modifications and extensions formulated where necessary. In fact, the standard model is remarkably successful; only in the relatively rare instances where the number of $4f$ electrons per atom is non-integral does it fail seriously. We discuss one such example, the electronic structure of α -Ce, in some detail, but otherwise say rather little about the interesting phenomena associated with itinerant f electrons that are called, depending on the circumstances, intermediate valence, valence fluctuations, or heavy-fermion behaviour, and are manifested in both the lanthanides and the actinides.

We begin with a lengthy introductory chapter in which, after a brief historical survey, those elements of rare earth magnetism which constitute the standard model, and are necessary for the comprehension of the rest of the book, are concisely summarized. Our approach is

deliberately reductionist. The starting point is the electronic structure of the atoms, and we show how the magnetic moments and their interactions arise, and how they are expressed in the magnetic properties. In order that this survey should be reasonably comprehensive, there is some overlap with topics treated in more detail later in the book, but we have judged that this degree of repetition does no harm; rather the contrary. We then present the mean-field theory of magnetic structures, and in order to illustrate its power and generality, apply it in a number of typical but sometimes relatively complex situations, with emphasis on the disparate structures of Ho. To prepare for our discussion of the magnetic excitations, we give an account of linear response theory and its application to the magnetic scattering of neutrons, thus covering the principal theoretical and experimental techniques which are used in this field. The excitations are treated in three chapters, in each of which the theory, which is based on the use of the random-phase approximation, is presented in parallel with a selection of the experimental results which it purports to explain. The very extensive results which have been obtained on the ferromagnetic heavy rare earths, especially Tb, are treated in considerable detail, followed by a chapter on the spin waves in periodic structures, which are still under active investigation. The crystal-field excitations in the light rare earths, which have a somewhat different character from the previously discussed spin waves, are considered separately, and illustrated by the example of Pr, which has been by far the most comprehensively studied, and displays many interesting features. We conclude with a summarizing discussion, in which the emphasis is placed on those aspects of the subject which are not yet satisfactorily understood.

In the writing of this monograph, and during the many years of work which preceded it, we have benefitted inestimably from the advice and collaboration of our colleagues and friends in the rare earth-research community. To all of them, we express our sincere appreciation, while absolving them from responsibility for the faults which, despite their best efforts, remain. Two deserve special mention; Dr. Hans Skriver provided us with many unpublished results of his calculations of electronic structures, which we have used liberally in Chapter 1, and Professor Keith McEwen read the manuscript and made many constructive comments. We produced the book ourselves, in a form ready for printing, using \TeX , which we found admirably suited for the purpose, and enjoyed a harmonious and effective cooperation with Oxford University Press throughout this process. The illustrations were prepared by the drawing office of the H.C. Ørsted Institute, and we are grateful to them for the care which they took in translating our sketches into elegant and informative figures. At various stages during the writing of the book,

A.R.M. was director of NORDITA, visiting scientist at the Institute of Theoretical Physics and St. John's College, University of Oxford, and Miller Visiting Professor in the Physics Department of the University of California, Berkeley. The hospitality of all of these institutions is gratefully acknowledged. Finally, we thank our families for their support and forbearance with our mental abstraction during this lengthy enterprise.

Copenhagen
January 1991

J.J.
A.R.M.

A number of misprints has been removed in this digital version of the book compared to the printed one. Among these, the most disturbing one was the missing Kronecker delta, $\delta_{\alpha\beta}$, in the expressions (1.4.26) and (5.5.2*b*) for the magnetic dipole–dipole interaction. The factor $1/2S$ has been moved from (1.2.19) to (1.2.17). The right charge of the electron $-e$ has been introduced in (1.4.1) and (1.4.3). The signs in the argument of the last δ -function in equation (4.2.9*a*) have been changed. The lattice sum for the dipole–dipole interaction introduced by (5.5.6) is small but not zero in the case of an hcp lattice with an ideal c/a ratio. This circumstance has required some modifications in the text below (5.5.6). The big left-bracket in (5.6.4*a*) has been moved to its right position. The signs in front of $\frac{\hbar\omega}{2}$ have been changed in the Fermi function arguments in the last line on page 267. The expression for the denominator at the bottom of page 277 has been squared. The expression for $\chi_{xy}(\mathbf{q}, \omega)$ has been added to equation (6.1.18). The AB indices in some of the functions in (7.2.1*b*), (7.2.2*a*) and (7.2.3) now all read BA . A Δ was missing in the equations just before (7.2.8*a*). The fraction $\frac{1}{5}$ in front of A^2 in (7.3.25*b*) has been changed to its right value $\frac{1}{15}$, and the quadrupolar contribution makes a 1.5% correction to the susceptibility at T_N as told now in the sixth line on page 351. The intrinsic value of the quadrupole interaction is $P_{\parallel} = -0.128$ mK (not meV) in the fourth line on page 351. The phrase “magnetization density”, which appeared repeatedly in the text, has been replaced by “magnetization” or “moment density”. In addition to these corrections, a few number of trivial typographic errors has been removed. – I want to thank M. Rotter, H. M. Rønnow and M. S. S. Brooks for their contributions to this list of corrections.

October 2011

J.J.

August 2023 A review is added to the book as an appendix.

J.J.

November 2024 Aleksandra E. Szukiel has found a misplaced $1/N$ factor in (1.4.13). The right placing of this factor has improved/simplified the derivation of the indirect exchange interaction, (1.4.20).

J.J.

CONTENTS

1	ELEMENTS OF RARE EARTH MAGNETISM	1
1.1	A brief history	2
1.2	Rare earth atoms	8
1.3	The metallic state	16
1.4	Magnetic interactions	39
1.5	Rare earth magnetism	50
2	MAGNETIC STRUCTURES	68
2.1	Mean-field theory of magnetic ordering	68
2.1.1	The high-temperature susceptibility	71
2.1.2	The mean-field approximation	74
2.1.3	Transversely ordered phases	79
2.1.4	Longitudinally ordered phases	83
2.1.5	Competing interactions and structures	85
2.1.6	Multiply periodic structures	89
2.2	The magnetic anisotropy	94
2.2.1	Temperature dependence of the Stevens operators	94
2.2.2	Anisotropic contributions to the free energy	101
2.3	Magnetic structures of the elements	111
2.3.1	Bulk magnetic structures	112
2.3.2	The magnetization of Holmium	125
2.3.3	Films and superlattices	130
3	LINEAR RESPONSE THEORY	134
3.1	The generalized susceptibility	134
3.2	Response functions	137
3.3	Energy absorption and the Green function	142
3.4	Linear response of the Heisenberg ferromagnet	149
3.5	The random-phase approximation	154
3.5.1	The generalized susceptibility in the RPA	154
3.5.2	MF-RPA theory of the Heisenberg ferromagnet	160

4	MAGNETIC SCATTERING OF NEUTRONS	163
4.1	The differential cross-section in the dipole approximation	164
4.2	Elastic and inelastic neutron scattering	173
5	SPIN WAVES IN THE FERROMAGNETIC HEAVY RARE EARTHS	181
5.1	The ferromagnetic hcp-crystal	182
5.2	Spin waves in the anisotropic ferromagnet	186
5.3	The uniform mode and spin-wave theory	198
5.3.1	The magnetic susceptibility and the energy gap	198
5.3.2	The validity of the spin-wave theory	206
5.4	Magnetoelastic effects	211
5.4.1	Magnetoelastic effects on the energy gap	211
5.4.2	The magnon-phonon interaction	219
5.5	Two-ion anisotropy	231
5.5.1	The dipole-dipole interaction	232
5.5.2	General two-ion interactions	240
5.6	Binary rare earth alloys	247
5.7	Conduction-electron interactions	256
5.7.1	The indirect-exchange interaction	256
5.7.2	The mass-enhancement of the conduction electrons	270
5.7.3	Magnetic contributions to the electrical resistivity	275
6	SPIN WAVES IN PERIODIC STRUCTURES	285
6.1	Incommensurable periodic structures	286
6.1.1	The helix and the cone	287
6.1.2	The longitudinally polarized structure	300
6.2	Commensurable periodic structures	305
7	CRYSTAL-FIELD EXCITATIONS IN THE LIGHT RARE EARTHS	312
7.1	MF-RPA theory of simple model systems	313
7.2	Beyond the MF-RPA Theory	322

7.3	Perturbations of the crystal-field system	334
7.3.1	Magnetoelastic effects and two-ion anisotropy	334
7.3.2	Conduction-electron interactions	342
7.3.3	Coupling to the nuclear spins	349
7.4	Magnetic properties of Praseodymium	352
7.4.1	Induced magnetic ordering	352
7.4.2	The magnetic excitations	361
8	PERSPECTIVES FOR RARE EARTH RESEARCH	370
	REFERENCES	381
	INDEX	398
	APPENDIX (REVIEW)	404
A.1	Magnetic structures and excitations	405
A.2	Long-period magnetic structures	407
A.3	Magnetic excitations in the heavy rare earth metals	411
A.4	Films and superlattices of rare earth metals	414
A.5	Structures and excitations in the light rare earths	416
A.6	Conclusions	419
	References	420

ELEMENTS OF RARE EARTH MAGNETISM

The purpose of this introductory chapter is to describe in a synoptic way those features of rare earth magnetism which provide the foundation for the rest of the book. Since this material is presented in the form of a survey, it does not claim to be as systematic and complete as the later chapters. Consequently, it may be necessary for those who are unfamiliar with the rare earths and their magnetism to find further details in the original articles and reviews to which we shall refer, even though we have attempted to present a reasonably self-contained account. We shall also frequently refer forward to later sections for a more exhaustive treatment of some of the topics which are cursorily introduced here. We hope however that the information we have collected together will also provide a useful summary for those who have some familiarity with the subject.

We set the scene with a brief history of the field, outlining what we regard as the major advances. Even though we have striven to do justice to at least the majority of the important contributions, our viewpoint should not necessarily be considered as particularly objective. The magnetism of the rare earths has its origin in the angular momenta of the $4f$ electrons in the atoms and we therefore describe in Section 1.2 their electronic structure and magnetic characteristics, introducing such essential ideas as *density-functional theory*, *Russell-Saunders coupling* and *Hund's rules*, and outlining how to calculate the *magnetic moment* of an unfilled subshell. We condense these atoms into a metal in Section 1.3, which is concerned with the description of the *conduction-electron gas* and its influence on the *structural properties*. A physically transparent method for determining the electronic structure is outlined, and the way in which the *band structure* is built up from its constituent parts is described and illustrated, using the concepts of *canonical bands* and *potential parameters*. The nature of the $4f$ states in the metals, and the occurrence of $4f$ bands in Ce and its compounds, are briefly discussed. Our experimental knowledge of the electronic structure, and particularly of the *Fermi surface*, is summarized. The way in which the conduction electrons determine the *atomic volume* and *crystal structure* is explained, and the individual contributions of the different l -states described. In Section 1.4, the *magnetic interactions* are presented, both the *single-ion* terms resulting from the *crystal fields* and the *two-ion* coupling via

indirect exchange and other mechanisms. The *magnetoelastic effects*, due to the coupling between the lattice strains and the magnetic moments, are also discussed. The manner in which these interactions and the characteristics of the $4f$ electrons combine to determine the magnetic properties of the metals is described in the last section. The observed *magnetic structures* of the heavy rare earths are presented and their occurrence under different circumstances discussed. Some features of the structures and their temperature dependence are described in terms of an elementary *mean-field theory*. The magnetism of the light rare earths is then briefly treated and the importance of the crystal fields emphasized. The effect of a *magnetic field* on the magnetic structures is mentioned, and the factors which determine the *magnetic anisotropy* discussed. Finally, the way in which *magnetostriction* can change the crystal symmetry and influence the magnetic structure is illustrated.

1.1 A brief history

The quantum theory of magnetism was first placed on a sound footing in 1932 by J.H. Van Vleck in his classic monograph *The Theory of Electric and Magnetic Susceptibilities*. In it, he extended the calculations of the magnetic susceptibilities of isolated rare earth ions, which had been performed by Hund (1925), to encompass the anomalous cases of Eu and Sm, which have low-lying multiplets, giving rise to *Van Vleck paramagnetism*. He was thus able to obtain good agreement with experiment over the whole series from La to ‘Casseiopaium’ (now Lu). The study of the metallic elements began in earnest when Urbain, Weiss, and Trombe (1935) discovered the *ferromagnetism* of Gd. Klemm and Bommer (1937) determined the *paramagnetic Curie temperatures* of the heavy rare earths and Néel (1938) showed that, in the presence of strong spin-orbit coupling on the ion and an interionic exchange interaction between the spins, these should be proportional, as observed, to $(g - 1)^2 J(J + 1)$. This later became known as the *de Gennes factor*.

Very little work was done on the rare earths during the war, but immediately afterwards F.H. Spedding, at Iowa State University, resumed his programme of producing the pure elements, and by the early 1950s relatively large quantities had become available. One of the first fruits of this programme was the extension of physical measurements to the light rare earths, when Parkinson, Simon, and Spedding (1951) detected a number of anomalies of magnetic origin in the *heat capacity*. Just previously, Lawson and Tang (1949) had showed that the γ - α phase transition in Ce, which can be induced either by pressure or cooling, resulted in no change of the fcc symmetry, but a substantial reduction of the lattice parameter. Zachariasen and Pauling independently ascribed this shrinking to the transfer of the localized $4f$ electron to the conduc-

tion band, the so-called *promotional model*. Extensive measurements were carried out on polycrystalline samples of all the stable lanthanides through the 1950s, and summarized by Spedding, Legvold, Daane, and Jennings (1957) at the close of this early period of rare earth research. Of particular significance, in the light of later developments, was the observation of extra magnetic neutron-diffraction peaks in polycrystalline Er by Koehler and Wollan (1955).

The disparate theoretical components which were later brought together to form the *standard model* of rare earth magnetism were also formulated in the 1950s. Zener (1951) suggested that localized moments could be coupled together by an *indirect exchange* through the medium of the conduction electrons, and Ruderman and Kittel (1954) calculated this coupling quantitatively for nuclear moments embedded in a free-electron gas. Kasuya (1956) and Yosida (1957) extended the treatment of this *RKKY interaction* to localized electronic moments. Stevens (1952) invented his method of *operator equivalents*, which was of decisive importance for a satisfactory treatment of the crystal fields. Mason (1954) formulated a theory of *magnetoelastic effects*, while Zener (1954) showed how to calculate the temperature dependence of the magnetic anisotropy.

The classical period of rare earth magnetism was heralded by the publication of the *magnetization* measurements on monocrystalline Dy by Behrendt, Legvold, and Spedding (1957). The fabrication of single crystals of all the heavy rare earths followed successively, and their bulk magnetic properties were studied at Iowa State by Legvold and his students. They were also made available to Koehler and his colleagues at Oak Ridge for *neutron-diffraction* measurements, which revealed what he later described as ‘a panoply of exotic spin configurations’. By the time of the First Rare Earth Conference at Lake Arrowhead, California in October 1960, both the magnetic susceptibilities and structures had been extensively investigated. The papers of Legvold (1961) and Koehler, Wollan, Wilkinson, and Cable (1961) summarized the remarkable progress which had been made by that time.

Theoretical developments lagged little behind. Almost simultaneously with the observation of the *helical structure* in Dy, Enz (1960) showed that the magnetization curves implied such a structure, and pointed out the importance of magnetoelastic effects in inducing the transition to the ferromagnetic phase. Niira (1960) successfully interpreted the magnetization of Dy in the ferromagnetic phase by calculating the *spin-wave spectrum* of an anisotropic magnet, showing that a finite energy is required to create a long-wavelength excitation. This *energy gap* gives rise to an exponential decrease of the magnetization at low temperatures. Elliott (1961) considered the magnetic structures of the

heavy rare earths and their temperature dependences, utilizing a phenomenological *molecular-field model*. A similar approach was taken by Miwa and Yosida (1961), while Nagamiya, Nagata, and Kitano (1962) calculated the effect of a magnetic field on some of these structures, showing that a *fan* structure may exist between the helix and the ferromagnet. In these papers, the standard model first attained a coherent formulation.

The transport properties, particularly the *electrical resistivity*, were elucidated in the same period. De Gennes (1958) considered the *magnetic disorder scattering*, showing that it is proportional to the de Gennes factor in the paramagnetic phase, while Kasuya (1959) gave a very complete discussion of the same subject, including not only the paramagnetic phase but also scattering by spin waves and rare earth impurities. The first resistivity measurements on single crystals were made on Er by Green, Legvold, and Spedding (1961). The unusual temperature dependence of the resistance in the *c*-direction was explained by Mackintosh (1962) as a consequence of the incommensurable magnetic ordering, leading to *magnetic superzones*. Miwa (1963) and Elliott and Wedgwood (1963) made calculations of the magnitude of this effect, using the free electron model, which were in semi-quantitative agreement with the experimental results. Mackintosh (1963) pointed out that the spin-wave energy gap should also give rise to an exponential increase in the magnetic scattering at low temperature and deduced that the gap in Tb is about 20 K, a value later substantiated by direct measurements.

Until this time, the conduction electrons in the rare earths had been described by the *free-electron model*, but Dimmock and Freeman (1964) demonstrated that this simplification was unjustified when they calculated the *band structure* of Gd by the APW method. The conduction electrons were found to be largely *d*-like, as in the transition metals, and the Fermi surface far from spherical. At that time, single crystals of the purity required to allow conventional Fermi surface experiments were unavailable, so Gustafson and Mackintosh (1964) employed *positron annihilation*, initially in polycrystalline samples. Their most striking observation was that the number of *4f* electrons in Ce does not change greatly at the γ - α transition, in contradiction to the promotional model, and hence to the standard model. Later measurements on single crystals of the heavy rare earths showed that the conduction electrons are indeed far from free electron-like, and the experimental results could be well accounted for by relativistic APW calculations (Williams, Loucks, and Mackintosh 1966).

As the ground-state properties of the rare earth metals became progressively clarified, interest turned towards the *magnetic excitations*. Niira's pioneering theoretical work was followed by the calculation of

the spin-wave *dispersion relations* in a variety of heavy-rare-earth magnetic structures by Cooper, Elliott, Nettel, and Suhl (1962). The first observations of spin waves by *inelastic neutron scattering* were made at Risø by Bjerrum Møller and Houmann (1966), who obtained rather complete dispersion relations for Tb at 90 K. During the following years, Bjerrum Møller and his colleagues performed a series of experiments which revealed many novel phenomena, including the temperature- and field-dependence of the *magnon energies*, allowing the deduction of the exchange and its anisotropy, and crystal-field and magnetoelastic parameters. Magnons in the incommensurable helical phase, including *phason* excitations at long wavelengths, were also observed, as was the interaction of magnons with each other, with the conduction electrons, and with phonons, including coupling through a new mechanism involving the spin-orbit interaction of the conduction electrons, explained by Liu (1972a).

Callen and Callen (1963) further developed the theory of *magnetostriction*, putting it in the form used by Rhyne and Legvold (1965a) to interpret their pioneering measurements on single crystals. Callen and Callen (1965) also generalized the treatment of the temperature dependence of crystal-field and magnetoelastic parameters. Cooper (1968a,b) considered in detail the role of the magnetoelastic effects in the helical-ferromagnetic transition, and included them in calculations of the spin-wave energies. Turov and Shavrov (1965) had earlier proposed that, since the magneto-strain cannot follow the precession of the moments in a spin wave, the energy gap should not vanish when the hexagonal anisotropy is cancelled by an external magnetic field. This *frozen lattice* effect was observed by Nielsen, Bjerrum Møller, Lindgård, and Mackintosh (1970). In the late 1960s, the availability of separated isotopes allowed spin-wave measurements at Oak Ridge on a number of the heavy rare earths which, because of neutron absorption in the natural state, could otherwise only be studied with great difficulty. Of particular interest were experiments on the isotropic ferromagnet Gd, in which the *magnetic form factor* was studied by Moon and Koehler (1971) and the spin waves by Koehler, Child, Nicklow, Smith, Moon, and Cable (1970), and the clear evidence for a large *exchange anisotropy* in the *conical phase* of Er (Nicklow, Wakabayashi, Wilkinson, and Reed 1971a).

With the increasing understanding of the magnetic behaviour of the heavy rare earths, it was natural that attention began to turn to the lighter metals. Moon, Cable, and Koehler (1964) began what was destined to become a long-lasting study by a number of groups of the magnetic structure of Nd, and Cable, Moon, Koehler, and Wollan (1964) found indications of antiferromagnetic ordering in polycrystalline Pr. Bleaney (1963) had earlier shown that the crystal-field ground states

in Pr should be singlets, and in such *singlet ground-state systems* no magnetic ordering should occur unless the exchange exceeds a critical value. Johansson, Lebeck, Nielsen, Bjerrum Møller, and Mackintosh (1970) could indeed detect no signs of magnetic ordering at 4.2 K in monocrystalline Pr. Shortly afterwards, the crystal-field excitations, or *magnetic excitons*, were observed by Rainford and Houmann (1971) and, on the basis of these results, Rainford (1972) proposed a crystal-field level scheme which is very close to that accepted today.

The achievements of the classical period were summarized in the compendium on the *Magnetic Properties of Rare Earth Metals*, edited by R.J. Elliott, which was published in 1972 and, in a sense, also signalled the end of this period. In the modern era, the principles which had been established by the early 1970s have been applied to attaining a deeper and more complete understanding of the elements, even though the primary interest has increasingly turned towards rare earth compounds and alloys. For example, the magnetic interactions in the exchange-dominated system Tb were studied in exhaustive detail with inelastic neutron scattering by Jensen, Houmann, and Bjerrum Møller (1975). The crystal-field dominated system Pr was subjected to a similarly careful investigation by Houmann, Rainford, Jensen, and Mackintosh (1979) and, from his analysis of these results, Jensen (1976a) concluded that Pr could be induced to order antiferromagnetically either by the application of a modest *stress* or, through the *hyperfine interaction*, as first proposed by Murao (1971), by cooling to about 40 mK. The former effect was observed by McEwen, Stirling, and Vettier (1978) while magnetic ordering at very low temperatures had been inferred from heat-capacity measurements by Lindelof, Miller, and Pickett (1975). However, the controversy surrounding this phenomenon was only finally settled by the unambiguous observation of magnetic ordering by neutron diffraction (Bjerrum Møller, Jensen, Wulff, Mackintosh, McMasters, and Gschneidner 1982). The effects of the crystal field alone were studied by Touborg and Høg (1974), by dissolving small amounts of the magnetic rare earths in Sc, Y, and Lu and determining the crystal-field level scheme through susceptibility measurements, in conjunction with inelastic neutron scattering (Rathmann and Touborg 1977).

Efforts to increase the purity of rare earth samples were rewarded by the observation of the *de Haas-van Alphen (dHvA) effect* in Gd by Young, Jordan, and Jones (1973) and the subsequent detailed elucidation of its Fermi surface, which could be satisfactorily accounted for by band structures calculated with the inclusion of the exchange splitting between up- and down-spin levels. More recently, the careful study of the dHvA effect in paramagnetic Pr by Wulff, Lonzarich, Fort, and Skriver (1988) has confirmed the success of the band model in describ-

ing the conduction electrons, and given extensive information on their interaction with the $4f$ electrons.

The electronic structure of Ce has been of continued interest. Johansson (1974) elaborated the suggestion of Gustafson, McNutt, and Roellig (1969) that α -Ce is a *4f-band metal*, and Glötzel (1978) and others have further explored this model by band structure calculations. Single crystals of α -Ce suitable for dHvA experiments are extremely difficult to prepare, but Johansson, Crabtree, Edelstein, and McMasters (1981) have studied the related compound CeSn_3 , observing the $4f$ character of the electrons at the Fermi surface. *Photoemission experiments* by Wieliczka, Weaver, Lynch, and Olson (1982) and Mårtensson, Reihl, and Parks (1982) proved highly informative in exploring the electronic structure of Ce. This work reflects the intense interest in the 1980s in the problem of non-integral $4f$ occupancy, which gives rise to a variety of phenomena subsumed under the description *mixed-valent* behaviour, the most striking of which is the huge electronic heat capacity and associated effective masses measured in *heavy-fermion materials*. The discovery of *superconductivity* in CeCu_2Si_2 by Steglich, Aarts, Bredl, Lieke, Meschede, Franz, and Schäfer (1979) stimulated a major effort in studying lanthanide and actinide heavy-fermion systems, and underlined the significance of the earlier observation of superconductivity in Ce under pressure by Probst and Wittig (1975).

The properties of itinerant $4f$ electrons have predominantly been studied through rare earth compounds. Indeed the main thrust of the rare earth research programme has recently been towards understanding *compounds and alloys*, which are generally beyond the scope of this book, but which may nevertheless be largely understood in terms of the principles which we shall present. However, as will be discussed in later sections, there still remain a number of problems in the elements which await and occasionally obtain a solution. For example, the essential features of the classic puzzle of the magnetic structure of Nd have been clarified by McEwen, Forgan, Stanley, Bouillot, and Fort (1985). Gibbs, Moncton, D'Amico, Bohr, and Grier (1985) have re-examined the configurations of the moments in Ho and other heavy rare earths, using a combination of *synchrotron radiation*, which shows promise for very high-resolution structural studies, and neutron diffraction. They utilized the concept of *spin slips* to explain their results, and hence refocused attention on *commensurable magnetic structures*, which had originally been studied by Koehler, Cable, Wilkinson, and Wollan (1966). Initial studies of the excitations of such structures were performed by Larsen, Jensen, and Mackintosh (1987), who thereby explained the long-standing mystery of the stability of the cone structure in Ho at low temperatures. Other unexplained features of the neutron diffraction patterns from Ho

were accounted for by Jensen and Mackintosh (1990), who showed that intermediate structures, which they named *helifans*, could be stabilized by a magnetic field.

A new field of endeavour has been opened by the fabrication of *multilayers* of different species of rare earths and the study of their properties by Majkrzak, Cable, Kwo, Hong, McWhan, Yafet, Waszczak, and Vettier (1986), and by Salamon, Sinha, Rhyne, Cunningham, Erwin, Borchers, and Flynn (1986). The size of the teams working on a number of these modern projects in rare earth research reflects the technical complexity of the problems now being tackled, and no doubt also the collaborative spirit of the age.

1.2 Rare earth atoms

The starting point for the understanding of the magnetism of the rare earths is the description of the electronic states, particularly of the $4f$ electrons, in the atoms. The wavefunction $\Psi(\mathbf{r}_1\sigma_1, \mathbf{r}_2\sigma_2, \dots, \mathbf{r}_Z\sigma_Z)$ for the electrons, which is a function of the space and spin coordinates \mathbf{r} and σ of the Z electrons which constitute the electronic charge cloud (Z is the atomic number), is determined for the stationary state of energy E from the Schrödinger equation

$$\mathcal{H}\Psi = E\Psi, \quad (1.2.1)$$

where the non-relativistic Hamiltonian operator is

$$\mathcal{H} = -\frac{\hbar^2}{2m} \sum_i^Z \nabla_i^2 + \frac{1}{2} \sum_{ij}^Z \frac{e^2}{|\mathbf{r}_i - \mathbf{r}_j|} + \sum_i^Z v_{\text{ext}}(\mathbf{r}_i) \quad (1.2.2)$$

and, in the case of an atom, the ‘external’ potential $v_{\text{ext}}(\mathbf{r})$ is just the Coulomb potential $-Ze^2/r_i$ due to the nuclear attraction. As is well known, the difficulties in solving this problem reside in the second term, the Coulomb interaction between the electrons. For heavy atoms, exact solutions require a prohibitive amount of computation, while any possibility of an exact solution for the electronic states in a metal is clearly out of the question. It is therefore necessary to replace the Coulomb interaction by a self-consistent field, which is most satisfactorily determined by means of the density-functional theory of Hohenberg and Kohn (1964) and Kohn and Sham (1965).

The first step is to write the Hamiltonian (1.2.2) in the symbolic form

$$\mathcal{H} = T + U + V, \quad (1.2.3)$$

incorporating the kinetic energy, the Coulomb repulsion between the electrons, and the external potential, due to the nucleus in the atom or

the periodic lattice potential in the solid. Hohenberg and Kohn (1964) established two important results. Firstly, they showed that the external potential is a unique functional of the electron density $n(\mathbf{r})$, and hence that the ground-state wavefunction Φ and the energy functional

$$\langle \Phi | \mathcal{H} | \Phi \rangle = \langle \Phi | (T + U) | \Phi \rangle + \int v_{\text{ext}}(\mathbf{r})n(\mathbf{r})d\mathbf{r} \quad (1.2.4)$$

are unique functionals of $n(\mathbf{r})$. Secondly, they proved that the energy functional (1.2.4) attains its minimum value, the ground-state energy, for the correct ground-state density. Hence, if the universal functional $\langle \Phi | (T + U) | \Phi \rangle$ were known, it would be straightforward to use this variational principle to determine the ground-state energy for any specified external potential. However, the functional is not known, and the complexity of the many-electron problem is associated with its approximate determination.

Guided by the successes of the one-electron model, Kohn and Sham (1965) considered a system of non-interacting electrons with the same density as that of the real system, satisfying the single-particle Schrödinger equation

$$\left[-\frac{\hbar^2}{2m}\nabla^2 + v_{\text{eff}}(\mathbf{r}) \right] \psi_i(\mathbf{r}) = \varepsilon_i \psi_i(\mathbf{r}). \quad (1.2.5)$$

The ground state Φ_S of such a system is just the antisymmetrized product, or *Slater determinant*, formed from the Z lowest-lying one-electron orbitals, so that the electron density is the sum over these orbitals:

$$n(\mathbf{r}) = \sum_i^Z |\psi_i(\mathbf{r})|^2. \quad (1.2.6)$$

The effective potential $v_{\text{eff}}(\mathbf{r})$ must therefore be determined so that $n(\mathbf{r})$ is also the ground-state density of the real system. To accomplish this, the energy functional (1.2.4) may be written in the form

$$\begin{aligned} \langle \Phi | \mathcal{H} | \Phi \rangle &= \langle \Phi_S | T | \Phi_S \rangle \\ &+ \int \left[\frac{1}{2} \int \frac{e^2 n(\mathbf{r}')}{|\mathbf{r} - \mathbf{r}'|} d\mathbf{r}' + v_{\text{ext}}(\mathbf{r}) \right] n(\mathbf{r}) d\mathbf{r} + E_{\text{xc}}\{n(\mathbf{r})\}, \end{aligned} \quad (1.2.7)$$

where the first contribution is the kinetic energy of the non-interacting system, and the second is the Hartree energy of the charge cloud. The last term is the difference between the true kinetic energy and that of the non-interacting system, plus the difference between the true interaction energy of the system and the Hartree energy. This exchange-correlation

energy encompasses our ignorance of this problem, and is presumably relatively small. In the *local* approximation, which is adopted to convert the density-functional theory into a practical method, this energy is written

$$E_{\text{xc}}\{n(\mathbf{r})\} \approx \int \varepsilon_{\text{xc}}[n(\mathbf{r})]n(\mathbf{r})d\mathbf{r}, \quad (1.2.8)$$

and the effective potential is therefore

$$v_{\text{eff}}(\mathbf{r}) = \int \frac{e^2 n(\mathbf{r}')}{|\mathbf{r} - \mathbf{r}'|} d\mathbf{r}' + v_{\text{ext}}(\mathbf{r}) + v_{\text{xc}}[n(\mathbf{r})], \quad (1.2.9)$$

where

$$v_{\text{xc}}[n(\mathbf{r})] = d[n\varepsilon_{\text{xc}}(n)]/dn \equiv \mu_{\text{xc}}[n(\mathbf{r})] \quad (1.2.10)$$

is the local approximation to the exchange-correlation contribution to the chemical potential of the electron gas. Useful estimates of this quantity have been obtained from calculations for a homogeneous electron gas of density $n(\mathbf{r})$ by Hedin and Lundqvist (1971), von Barth and Hedin (1972), and Gunnarsson and Lundqvist (1976), and these are frequently used in calculations on both atoms and solids.

In order to determine the atomic structure, the Schrödinger equation (1.2.5) must be solved by the Hartree self-consistent procedure, in which, through a process of iteration, the potential (1.2.9) generates wavefunctions which, via (1.2.6), reproduce itself. Since this potential is spherically symmetric in atoms, the single-particle wavefunctions may be written as the product of a radial function, a spherical harmonic and a spin function

$$\psi_{nlm_l m_s}(\mathbf{r}\sigma) = i^l R_{nl}(r) Y_{lm_l}(\hat{\mathbf{r}}) \chi_{m_s}, \quad (1.2.11)$$

where $\hat{\mathbf{r}}$ is a unit vector in the direction of \mathbf{r} , the spin quantum number m_s can take the values $\pm\frac{1}{2}$, and the phase factor i^l is included for later convenience. The radial component satisfies the equation

$$-\frac{\hbar^2}{2m} \frac{d^2[rR_{nl}(r)]}{dr^2} + \left(v_{\text{eff}}(r) + \frac{l(l+1)\hbar^2}{2mr^2} - \varepsilon \right) [rR_{nl}(r)] = 0. \quad (1.2.12)$$

Some radial wavefunctions for rare earth atoms are shown in Fig. 1.1. The $4f$ electrons are well embedded within the atom, and shielded by the $5s$ and $5p$ states from the surroundings. The $5d$ and $6s$ electrons form the conduction bands in the metals. The incomplete screening of the increasing nuclear charge along the rare earth series causes the lanthanide contraction of the wavefunctions, which is reflected in the ionic and atomic radii in the solid state. In particular, as illustrated in Fig. 1.1, the $4f$ wavefunction contracts significantly between Ce, which has

one $4f$ electron, and Tm, which has one $4f$ hole in the atom, though two in the metallic state. The angular dependences of the $4f$ wavefunctions are depicted in Fig. 1.2. The charge clouds are highly anisotropic, with pronounced multipoles whose magnitudes and signs change dramatically with m_l . As we shall see, this anisotropy is clearly manifested in the magnetic properties of the metals.

Since they are among the heavier elements, relativistic effects are of substantial importance in the rare earths. These are most straightforwardly taken into account by solving the Dirac equation in the central

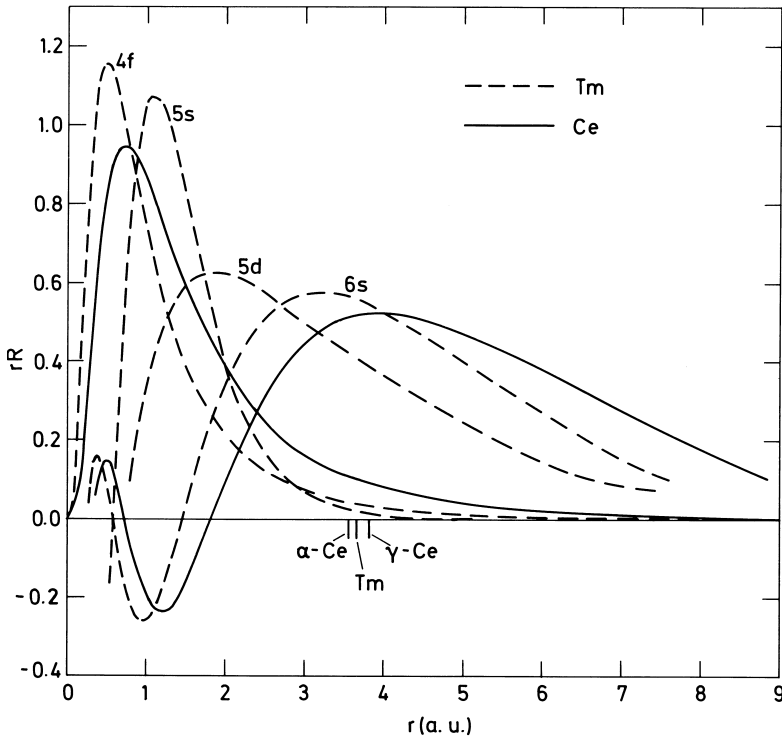


Fig. 1.1. The radial components of atomic wavefunctions for Ce, which has one $4f$ electron, and Tm, which has 13 $4f$ electrons, or one $4f$ hole. The Tm wavefunctions are contracted, relative to those of Ce, due to the incomplete shielding of the greater nuclear charge. As a consequence, the amplitude of the $4f$ wavefunction at the indicated Wigner-Seitz radius is much greater in Ce than in Tm, which has important consequences for the character of the $4f$ states in the metals.

field, rather than the Schrödinger equation, but it may be more instructive to consider them as perturbations which, to order $(p/mc)^2$, augment the one-electron potential with

$$-\frac{p^4}{8m^3c^2} - \frac{\hbar^2}{4m^2c^2} \frac{dv}{dr} \frac{\partial}{\partial r} + \frac{1}{2m^2c^2r} \frac{dv}{dr} \mathbf{s} \cdot \mathbf{l}. \quad (1.2.13)$$

The first term, which is due to the increase of mass with velocity, reduces the energy of all states by an amount which decreases with l , while the second ‘Darwin’ term increases the energy of s states only. These effects may both be incorporated into the central field, but the last term couples together the spin and orbital motion in a way that has far-reaching consequences for the magnetic properties.

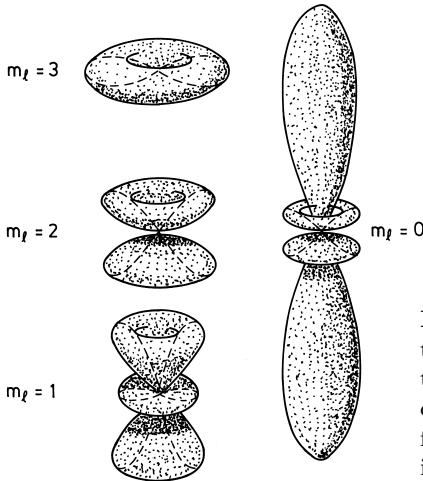


Fig. 1.2. The angular variation of the $4f$ wavefunctions. The interaction of the highly anisotropic charge clouds with the crystalline electric fields gives rise to the large single-ion anisotropies observed in the rare earth metals.

In the Russell–Saunders coupling scheme, which is an accurate procedure for the $4f$ electrons, the spins \mathbf{s}_i of the individual $4f$ electrons are coupled by the exchange interaction, diagonal in the total spin \mathbf{S} of the incompletely filled subshell, while the Coulomb interaction similarly combines the \mathbf{l}_i into the total orbital momentum \mathbf{L} . In terms of the one-electron functions, the wavefunction for the subshell may be written

$$\Psi(LSM_L M_S) = \sum_{m_l m_s} C(LSM_L M_S; m_l m_s) \psi(m_l m_s), \quad (1.2.14)$$

where the $C(LSM_L M_S; m_l m_s)$ are the *Clebsch–Gordan* or *Wigner* coefficients. It is convenient to write this expansion in a representation-

independent form, in terms of the state vectors

$$|LSM_L M_S\rangle = \sum_{m_l m_s} \langle m_l m_s | LSM_L M_S \rangle |m_l m_s\rangle. \quad (1.2.15)$$

The exchange and Coulomb interactions are sufficiently large that the magnetic properties at all accessible temperatures are determined by the S and L states of lowest energy. These are found from Hund's rules; S is maximized and, subject to this maximum S value, L is also maximized. This results in the values for the trivalent ions shown in Table 1.1.

Table 1.1. Properties of the tripositive rare earth ions.

$4f^n$	Ion ⁺⁺⁺	L	S	J	g	$(g-1)^2 J(J+1)$	$\Delta(K)$
0	La	0	0	0	—		
1	Ce	3	$\frac{1}{2}$	$\frac{5}{2}$	$\frac{6}{7}$	0.18	3150
2	Pr	5	1	4	$\frac{4}{5}$	0.80	3100
3	Nd	6	$\frac{3}{2}$	$\frac{9}{2}$	$\frac{8}{11}$	1.84	2750
4	Pm	6	2	4	$\frac{3}{5}$	3.20	2300
5	Sm	5	$\frac{5}{2}$	$\frac{5}{2}$	$\frac{2}{7}$	4.46	1450
6	Eu	3	3	0	—		500
7	Gd	0	$\frac{7}{2}$	$\frac{7}{2}$	2	15.75	
8	Tb	3	3	6	$\frac{3}{2}$	10.50	2900
9	Dy	5	$\frac{5}{2}$	$\frac{15}{2}$	$\frac{4}{3}$	7.08	4750
10	Ho	6	2	8	$\frac{5}{4}$	4.50	7500
11	Er	6	$\frac{3}{2}$	$\frac{15}{2}$	$\frac{6}{5}$	2.55	9350
12	Tm	5	1	6	$\frac{7}{6}$	1.17	11950 ^a
13	Yb	3	$\frac{1}{2}$	$\frac{7}{2}$	$\frac{8}{7}$	0.32	14800
14	Lu	0	0	0	—		

^a The lowest excited state in Tm is 3F_4 at 8490K.

It is a consequence of the *Wigner-Eckart theorem* that the spin-orbit term in (1.2.13) can be written

$$\mathcal{H}_{so} = \pm \zeta(LS) \mathbf{S} \cdot \mathbf{L}, \quad (1.2.16)$$

where

$$\zeta(LS) = \frac{\pi}{m^2 c^2 S} \int r R_{4f}^2(r) \frac{dv}{dr} dr, \quad (1.2.17)$$

and the + and – signs refer respectively to a less or more than half-filled subshell. The spin and orbital angular momenta are thus combined into the total angular momentum $\mathbf{J} = \mathbf{L} + \mathbf{S}$. These states may be written

$$|JM_JLS\rangle = \sum_{M_L M_S} \langle LSM_L M_S | JM_JLS\rangle |LSM_L M_S\rangle. \quad (1.2.18)$$

Because of the sign of (1.2.16), the value of J in the ground state is $L \mp S$, according as the subshell is less or more than half-full. Roughly speaking, \mathbf{L} is always parallel to \mathbf{J} , but \mathbf{S} is antiparallel in the first half of the series and parallel in the second half. The energy separation to the first excited multiplet may be determined from the matrix elements of (1.2.16), and is given by

$$\Delta = \zeta(LS) \begin{cases} (J+1) \\ J \end{cases} \quad (1.2.19)$$

again depending on whether the subshell is respectively less or more than half-filled. The values of J in the ground state and of Δ , obtained from spectroscopic measurements on rare earth salts (Dieke 1968), are given in Table 1.1.

The magnetization of an assembly of N rare earth atoms or ions is given by the derivative of the free energy with respect to magnetic field:

$$M = -\frac{1}{V} \frac{\partial F}{\partial H} \quad (1.2.20)$$

or, recalling that

$$F = -\frac{N}{\beta} \ln \sum_n e^{-\beta E_n(H)}, \quad (1.2.21)$$

where $E_n(H)$ are the atomic energy levels in the field, and $\beta = 1/k_B T$,

$$M = \frac{N}{V} \sum_n -\frac{\partial E_n}{\partial H} e^{-\beta E_n} / \sum_n e^{-\beta E_n}. \quad (1.2.22)$$

Neglecting the small diamagnetic susceptibility, the magnetic contribution to the Hamiltonian is given by the Zeeman term

$$\mathcal{H}_Z = -\mu_B (\mathbf{L} + g_0 \mathbf{S}) \cdot \mathbf{H}, \quad (1.2.23)$$

where μ_B is the Bohr magneton. Because of the negative charge on the electron, the angular momentum and the magnetic moment are *antiparallel*. This gives rise to certain difficulties, which are frequently ignored in the literature. We shall circumvent them by taking \mathbf{L} , \mathbf{S} , and \mathbf{J} as

signifying the *negative* of the corresponding angular-momentum vector. We shall furthermore from now on take the gyromagnetic ratio g_0 as 2. Second-order perturbation theory then gives the magnetic contribution to the energy:

$$\delta E_n(H) = -\mu_B \mathbf{H} \cdot \langle n | \mathbf{L} + 2\mathbf{S} | n \rangle + \sum_{m \neq n} \frac{|\langle n | \mu_B \mathbf{H} \cdot (\mathbf{L} + 2\mathbf{S}) | m \rangle|^2}{E_n - E_m}. \quad (1.2.24)$$

Problems of degeneracy are taken care of by using the $|JM_JLS\rangle$ basis, whose degeneracy is completely lifted by the field. In this basis, and within a particular JLS -multiplet, the Wigner–Eckart theorem implies that the matrix elements of $(\mathbf{L} + 2\mathbf{S})$ are proportional to those of \mathbf{J} , so that

$$\langle JLSM_J | \mathbf{L} + 2\mathbf{S} | JLSM'_J \rangle = g(JLS) \langle JLSM_J | \mathbf{J} | JLSM'_J \rangle, \quad (1.2.25)$$

and the proportionality constant, *the Landé factor*, is

$$g = \frac{3}{2} + \frac{S(S+1) - L(L+1)}{2J(J+1)}. \quad (1.2.26)$$

Within this multiplet, we may write eqn (1.2.25) in the shorthand form $\mathbf{L} + 2\mathbf{S} = g\mathbf{J}$, and consider the effective moment on the atom to be

$$\boldsymbol{\mu} = g\mu_B \mathbf{J}. \quad (1.2.27)$$

With the same proviso, we may similarly write

$$\mathbf{L} = (2 - g)\mathbf{J}, \quad (1.2.28)$$

and

$$\mathbf{S} = (g - 1)\mathbf{J}. \quad (1.2.29)$$

If J is non-zero, the first-order term in (1.2.24), combined with (1.2.22) gives a magnetization for the ground-state multiplet:

$$M(H, T) = \frac{N}{V} g\mu_B J B_J(\beta g\mu_B JH), \quad (1.2.30)$$

where the *Brillouin function* is

$$B_J(x) = \frac{2J+1}{2J} \coth \frac{2J+1}{2J} x - \frac{1}{2J} \coth \frac{1}{2J} x. \quad (1.2.31)$$

If $g\mu_B JH$ is small compared with $k_B T$, the susceptibility is constant and given by *Curie's law*:

$$\chi = \frac{M}{H} = \frac{g^2 \mu_B^2 J(J+1) N}{3k_B T} \frac{N}{V} \equiv \frac{C}{T}, \quad (1.2.32)$$

where C is the *Curie constant*. The second-order non-diagonal term in (1.2.24) gives a paramagnetic contribution to χ which is independent of temperature, provided that the thermal population of the excited states is negligible. This *Van Vleck paramagnetism* is very small in the heavy rare earths, but in the first half of the series it is given by

$$\chi_V = \frac{2\mu_B^2(L+1)S}{3(J+1)\Delta} \frac{N}{V}, \quad (1.2.33)$$

which may be significant, since

$$\frac{\chi_V}{\chi} = \frac{2(L+1)S}{g^2J(J+1)^2} \frac{k_B T}{\Delta} = \frac{\alpha k_B T}{\Delta}, \quad (1.2.34)$$

where, from Table 1.1, α takes the modest value of 0.19 for Pr, but is 12 for Sm. Since Δ is only 1450 K, the Van Vleck paramagnetism in Sm is significant even at rather low temperatures. In trivalent Eu, $J = 0$ in the ground state and the paramagnetic susceptibility is due entirely to the mixing of the excited states into the ground state by the field, and to the thermal excitation of these states. However, Eu metal is divalent and the $^8S_{7/2}$ ionic susceptibility follows Curie's law very closely. The Van Vleck paramagnetism arising from the mixing of states of different J will not play a significant role in our later discussion, but the analogous phenomenon of the mixing of states of different M_J , split by the crystalline electric field in the metal, will be of central importance.

1.3 The metallic state

When a large number of rare earth atoms are assembled to form a solid, the $4f$ electrons generally remain localized, in a sense which will be made more precise later, so that their magnetic properties closely resemble those in the free atoms. The external $5d$ and $6s$ electrons, on the other hand, become delocalized into *Bloch states*, extending throughout the metal and constituting the conduction-electron gas. The conduction electrons themselves make only a modest contribution to the magnetic moment, but by mediating the magnetic interactions they play a crucial role in determining the characteristic magnetic properties in the solid state. An understanding of the magnetism therefore requires a detailed description of the conduction electron gas, and this section is concerned with our theoretical and experimental knowledge of the Bloch states, and their influence on the structural properties of the metals. Some of these structural properties of the rare earth metals are collected in Table 1.2, from which it may be seen that the room-temperature structures are all close-packed, with a coordination number of 12, with the exception of Eu, which is bcc. The remaining elements all form hexagonal phases,

Table 1.2. Structural properties of the lanthanides.

Element	Structure (300 K)	Lattice const.		Atomic rad. S (a.u.)	Density (g/cm ³)	Melt. point (K)
		a (Å)	c (Å)			
La	dhcp	3.774	12.171	3.92	6.146	1191
Ce(β)	dhcp	3.681	11.857	3.83	6.689	1071
Ce(γ)	fcc	5.161		3.81	6.770	
Ce(α)	fcc	4.85 (77 K)		3.58	8.16	
Pr	dhcp	3.672	11.833	3.82	6.773	1204
Nd	dhcp	3.658	11.797	3.80	7.008	1294
Pm	dhcp	3.65	11.65	3.78	7.264	1315
Sm	rhomb	3.629	26.207	3.77	7.520	1347
Eu	bcc	4.583		4.26	5.244	1095
Gd	hcp	3.634	5.781	3.76	7.901	1586
Tb	hcp	3.606	5.697	3.72	8.230	1629
Dy	hcp	3.592	5.650	3.70	8.551	1687
Ho	hcp	3.578	5.618	3.69	8.795	1747
Er	hcp	3.559	5.585	3.67	9.066	1802
Tm	hcp	3.538	5.554	3.65	9.321	1818
Yb	fcc	5.485		4.05	6.966	1092
Lu	hcp	3.505	5.549	3.62	9.841	1936

although the hcp allotrope of Yb is only stable at low temperatures, and Ce has two separate fcc phases in addition to its dhcp form.

The heavy rare earths are all hcp, while the dhcp structure predominates among the lighter metals. These structures may be produced by stacking close-packed layers in the sequences ABAB and ABAC respectively, as shown in Fig. 1.3. The fcc structure corresponds to the stacking sequence ABCABC, while the Sm structure is ABABCBCAC. The latter has rhombohedral symmetry but it is frequently more convenient to consider it as hexagonal. The crystallographic a -axis is taken along the direction joining a pair of nearest neighbours in the hexagonal plane, the c -axis is normal to the plane, and the b -axis is orthogonal to the other two. The local, i.e. nearest-neighbour, symmetry in the fcc and hcp structure is, of course, cubic and hexagonal respectively. The dhcp structure, on the other hand, has two types of site and, for an ‘ideal’ $c/2a$ ratio of 1.633, their *local* symmetry alternates between cubic and hexagonal in the sequence chch, while the Sm structure corresponds to chhchh. As may be seen from Table 1.2, however, the $c/2a$ ratio is consistently smaller than the ideal value, so the ‘cubic’ sites have only approximate local cubic symmetry.

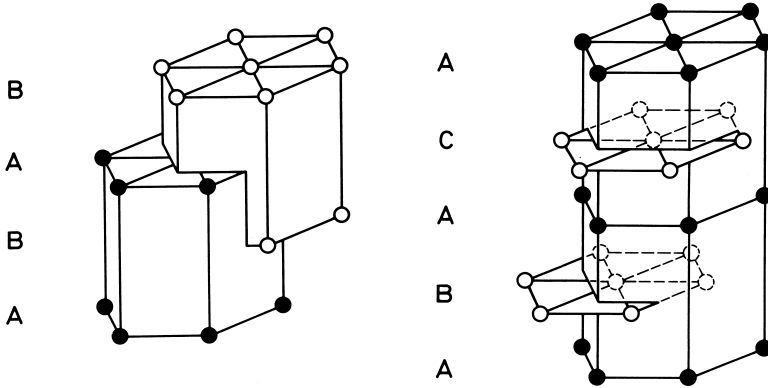


Fig. 1.3. The hcp and dhcp crystal structures. In the latter, the B and C sites have hexagonal symmetry, while the A sites have local cubic symmetry, for an ideal c/a ratio.

To determine the eigenstates for the conduction electron gas, we adopt the same procedure as that outlined for atoms in the previous section. The external potential $v_{\text{ext}}(\mathbf{r})$ in (1.2.2) is now the Coulomb attraction of the nuclei situated on the crystal lattice, shielded by the electrons of the ionic core, which are usually taken to have the same charge distribution as in the atoms. The potential consequently has the translational symmetry of the periodic lattice, and so therefore does the effective potential $v_{\text{eff}}(\mathbf{r})$, which arises when we make the single-particle approximation (1.2.5) and the local-density approximation (1.2.9). In the atom, the eigenfunctions are determined by the boundary condition that their amplitude must vanish for large values of r and, when (1.2.12) is integrated numerically, they are automatically continuous and differentiable. The translational symmetry of the solid is expressed in *Bloch's theorem*:

$$\psi(\mathbf{r}) = e^{i\mathbf{k}\cdot\mathbf{R}} \psi(\mathbf{r} - \mathbf{R}), \quad (1.3.1)$$

and this boundary condition gives rise to eigenfunctions $\psi_j(\mathbf{k}, \varepsilon, \mathbf{r})$ and eigenvalues $\varepsilon_j(\mathbf{k})$ which are functions of the wave-vector \mathbf{k} in reciprocal space. All the electron states may be characterized by values of \mathbf{k} lying within the *Brillouin zone*, illustrated for the hexagonal and fcc structures in Fig. 1.4, and by the band index j defined such that $\varepsilon_j(\mathbf{k}) \leq \varepsilon_{j+1}(\mathbf{k})$.

The determination of the eigenstates of the Schrödinger equation, subject to the Bloch condition (1.3.1) is the central problem of energy-band theory. It may be solved in a variety of ways, but by far the most

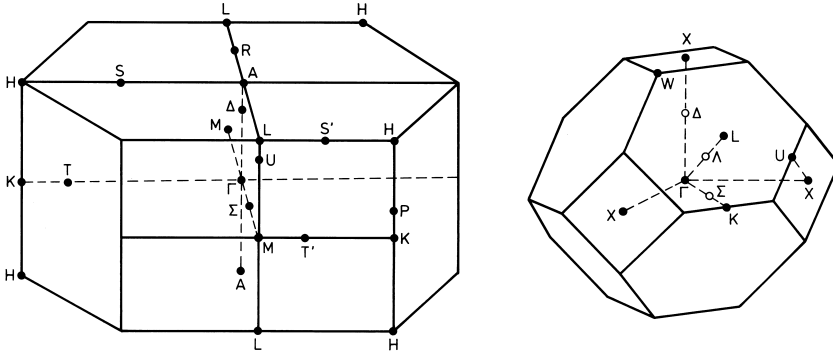


Fig. 1.4. The Brillouin zones for the hexagonal and fcc lattices.

effective procedure for the rare earths is to adopt one of the linear methods of Andersen (1975). In the following, we will use the *Atomic Sphere Approximation* (ASA) which will allow us to illustrate the construction and characteristics of the energy bands in a transparent way. This approximation, and the closely-related *Linear Muffin-Tin Orbitals Method* (LMTO), which allows computationally very efficient calculations of arbitrarily precise energy bands, for a given potential, have been concisely described by Mackintosh and Andersen (1980) and, in much more detail, by Skriver (1984).

In a close-packed solid, the electrons may to a very good approximation be assumed to move in a *muffin-tin potential*, which is spherically symmetric in a sphere surrounding each atomic site, and constant in the interstitial regions. We recall that the *atomic polyhedron*, or *Wigner-Seitz cell*, is bounded by the planes which perpendicularly bisect the vectors joining an atom at the origin with its neighbours, and has the same volume as the *atomic sphere*, whose radius S is chosen accordingly. If we surround each site in the crystal with an atomic sphere, the potential within each of these overlapping regions will, to a high degree of accuracy, be spherically symmetric. Neglecting the spin, we may therefore write the solutions of the Schrödinger equation for a single atomic sphere situated at the origin in the form

$$\psi_{lm}(\varepsilon, \mathbf{r}) = i^l R_l(\varepsilon, r) Y_{lm}(\hat{\mathbf{r}}), \quad (1.3.2)$$

where the radial function $R_l(\varepsilon, r)$ satisfies eqn (1.2.12) and is a function of the continuous energy variable ε . Examples of such radial functions are shown in Fig. 1.5.

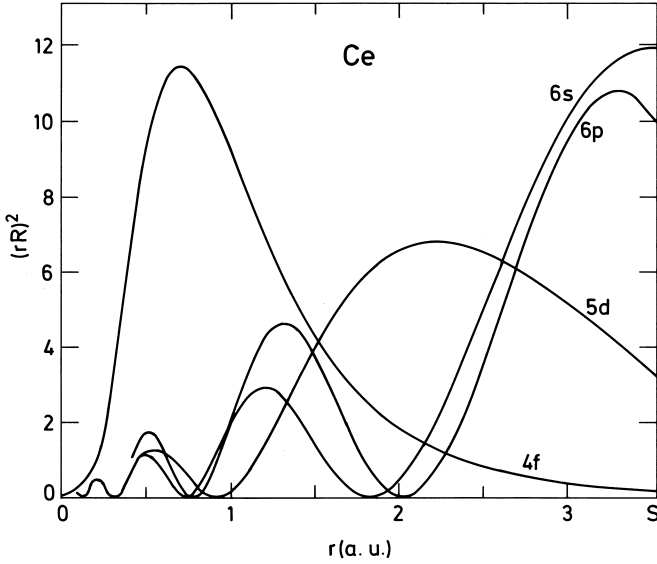


Fig. 1.5. Radial wavefunctions for α -Ce metal, calculated by Skriver from the self-consistent atomic-sphere potential, at the energies C_{nl} of the centres of the associated bands. Since these wavefunctions are normalized within the unit cell, the effective masses μ_{nl} are inversely proportional to the value of $R_l^2(C_{nl}, S)$ at the Wigner-Seitz radius, and this probability, and the consequent overlap between wavefunctions on neighbouring sites, therefore determines the corresponding band width.

Augmenting these partial waves by suitably-chosen regular solutions of Laplace's equation, we define the energy-dependent *muffin-tin orbitals*

$$\chi_{lm}(\varepsilon, \mathbf{r}) = i^l Y_{lm}(\hat{\mathbf{r}}) \begin{cases} R_l(\varepsilon, r) + p_l(\varepsilon)(r/S)^l; & r < S \\ (S/r)^{l+1} & ; \quad r > S, \end{cases} \quad (1.3.3)$$

which are continuous and differentiable if

$$p_l(\varepsilon) = \frac{D_l(\varepsilon) + l + 1}{D_l(\varepsilon) - l}, \quad (1.3.4)$$

where the *logarithmic derivative* is

$$D_l(\varepsilon) = S \frac{R_l'(\varepsilon, S)}{R_l(\varepsilon, S)}. \quad (1.3.5)$$

From muffin-tin orbitals located on the lattice sites of a solid, with one atom per unit cell, we now construct a wavefunction which is continuous and differentiable, and manifestly satisfies the Bloch condition (1.3.1):

$$\psi_j(\mathbf{k}, \varepsilon, \mathbf{r}) = \sum_{lm} a_{lm}^{jk} \sum_{\mathbf{R}} e^{i\mathbf{k}\cdot\mathbf{R}} \chi_{lm}(\varepsilon, \mathbf{r} - \mathbf{R}). \quad (1.3.6)$$

If we approximate the atomic polyhedra by spheres, and implicitly assume that they fill space, the condition that (1.3.6) is a solution of the Schrödinger equation is easily seen to be that the sum of the tails originating from terms of the form $(S/|\mathbf{r} - \mathbf{R}|)^{l+1}$, from the surrounding atoms, cancels the 'extra' contribution

$$\sum_{lm} a_{lm}^{jk} Y_{lm}(\hat{\mathbf{r}}) p_l(\varepsilon) (r/S)^l,$$

in the atomic sphere at the origin. To satisfy this condition, we expand the tails of the muffin-tin orbitals centred at \mathbf{R} about the origin, in the form

$$\begin{aligned} \sum_{\mathbf{R} \neq \mathbf{0}} e^{i\mathbf{k}\cdot\mathbf{R}} \left(\frac{S}{|\mathbf{r} - \mathbf{R}|} \right)^{l+1} i^l Y_{lm}(\widehat{\mathbf{r} - \mathbf{R}}) \\ = \sum_{l'm'} \frac{-1}{2(2l'+1)} \left(\frac{r}{S} \right)^{l'} i^{l'} Y_{l'm'}(\hat{\mathbf{r}}) \mathcal{S}_{l'm',lm}^{\mathbf{k}}, \end{aligned} \quad (1.3.7)$$

where the expansion coefficients, known as the *canonical structure constants*, are

$$\mathcal{S}_{l'm',lm}^{\mathbf{k}} = \sum_{\mathbf{R} \neq \mathbf{0}} e^{i\mathbf{k}\cdot\mathbf{R}} \mathcal{S}_{l'm',lm}(\mathbf{R}), \quad (1.3.8)$$

with

$$\mathcal{S}_{l'm',lm}(\mathbf{R}) = g_{l'm',lm} \sqrt{4\pi} (-i)^\lambda Y_{\lambda\mu}^*(\hat{\mathbf{R}}) (R/S)^{-\lambda-1},$$

where

$$g_{l'm',lm} \equiv (-1)^{m+1} 2 \sqrt{\frac{(2l'+1)(2l+1)}{2\lambda+1} \frac{(\lambda+\mu)!(\lambda-\mu)!}{(l'+m')!(l'-m')!(l+m)!(l-m)!}}$$

and

$$\lambda \equiv l + l' \quad ; \quad \mu \equiv m - m'.$$

From (1.3.3) and (1.3.7), the required *tail-cancellation* occurs if

$$\sum_{lm} [P_l(\varepsilon) \delta_{l'l} \delta_{m'm} - \mathcal{S}_{l'm',lm}^{\mathbf{k}}] a_{lm}^{jk} = 0, \quad (1.3.9)$$

where the *potential function* $P_l(\varepsilon)$ is defined by

$$P_l(\varepsilon) = 2(2l + 1)p_l(\varepsilon) = 2(2l + 1) \frac{D_l(\varepsilon) + l + 1}{D_l(\varepsilon) - l}. \quad (1.3.10)$$

The linear homogeneous equations (1.3.10) have solutions for the eigenvectors a_{lm}^{jk} only for those values of \mathbf{k} and ε for which

$$\det[P_l(\varepsilon)\delta_{l'l}\delta_{m'm} - \mathcal{S}_{l'm',lm}^{\mathbf{k}}] = 0. \quad (1.3.11)$$

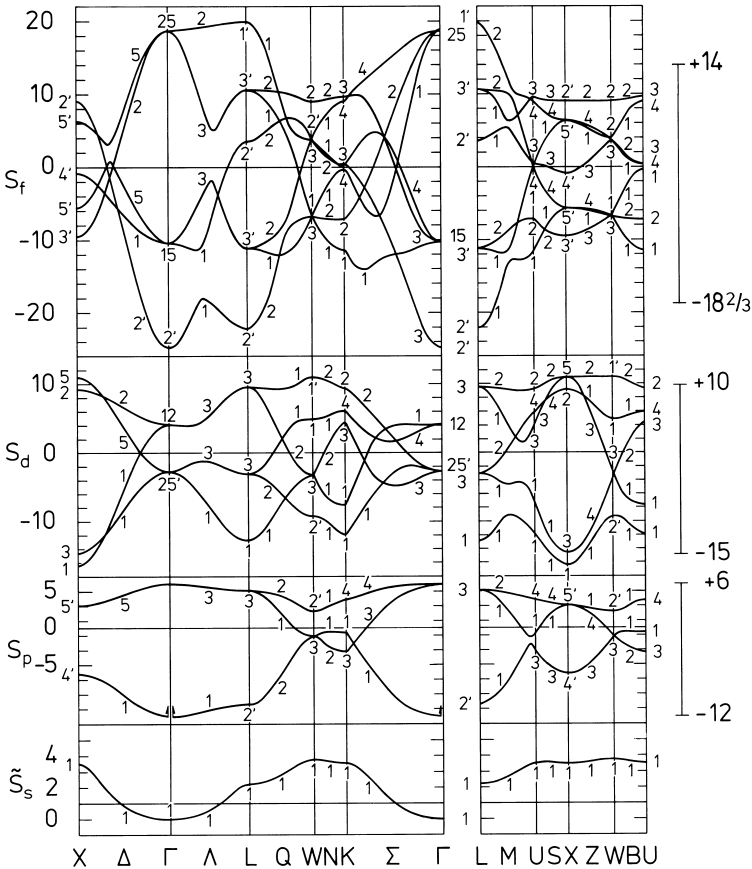


Fig. 1.6. The canonical bands for the fcc structure. The band structure in the metal may be obtained by placing, scaling, and distorting the canonical bands according to the values of the corresponding potential parameters C_{nl} , μ_{nl} , and γ_{nl} , and finally hybridizing them. The extent of the bands, according to the Wigner–Seitz rule, is indicated on the right.

In this determinantal equation for the band structure $\varepsilon_j(\mathbf{k})$, the information about the structure is separated from that on the potential. The structure constants $\mathcal{S}_{l'm',lm}^{\mathbf{k}}$ are canonical in the sense that they depend only on the crystal structure and not, for example, on the lattice constant, as may be seen from the definition (1.3.8), and the potential function $P_l(\varepsilon)$ is determined entirely by the potential within the atomic sphere. We shall consider these two terms in turn.

If we include values of l up to 3, i.e. s, p, d , and f partial waves, the structure constants form a square matrix with 16 rows and columns. The terms with $l = l'$ fall into 4 blocks, and these submatrices may be diagonalized by a unitary transformation from the lm to an lj representation. The $(2l+1)$ diagonal elements $\mathcal{S}_{lj}^{\mathbf{k}}$ of each sub-block are the unhybridized *canonical l bands*. The canonical bands for the fcc structure are shown in Fig. 1.6. If hybridization is neglected, which corresponds to setting to zero the elements of $\mathcal{S}_{l'm',lm}^{\mathbf{k}}$ with $l \neq l'$, eqn (1.3.11) takes the simple form

$$P_l(\varepsilon) = \mathcal{S}_{lj}^{\mathbf{k}}. \quad (1.3.12)$$

Since $P_l(\varepsilon)$ is a monotonically increasing function of energy, as illustrated in Fig. 1.7, the band energies $\varepsilon_{lj}(\mathbf{k})$ for the pure l bands are obtained by a monotonic scaling of the corresponding canonical bands. $P_l(\varepsilon)$ does not, furthermore, depart greatly from a straight line in the energy region over which a band is formed, so the canonical bands resemble the energy bands in the solid quite closely, whence the name.

The potential function $P_l(\varepsilon)$ and the logarithmic-derivative function $D_l(\varepsilon)$ are related to each other through the definition (1.3.10), and this relationship is shown schematically in Fig. 1.7. It is convenient and illuminating to parametrize the potential function, when considering the formation of the energy bands from the canonical bands. The poles of $P_l(\varepsilon)$, which occur when $D_l(\varepsilon) = l$, divide the energy into regions in which lie the corresponding atomic energy-levels ε_{nl} . The energies V_{nl} which separate these regions are defined by

$$D_l(V_{nl}) = l \quad (1.3.13)$$

and, within a particular region, the energy C_{nl} of the centre of the band is fixed by the condition that $P_l(C_{nl}) = 0$, or

$$D_l(C_{nl}) = -(l+1). \quad (1.3.14)$$

The allowed \mathbf{k} -values corresponding to this energy are just those for

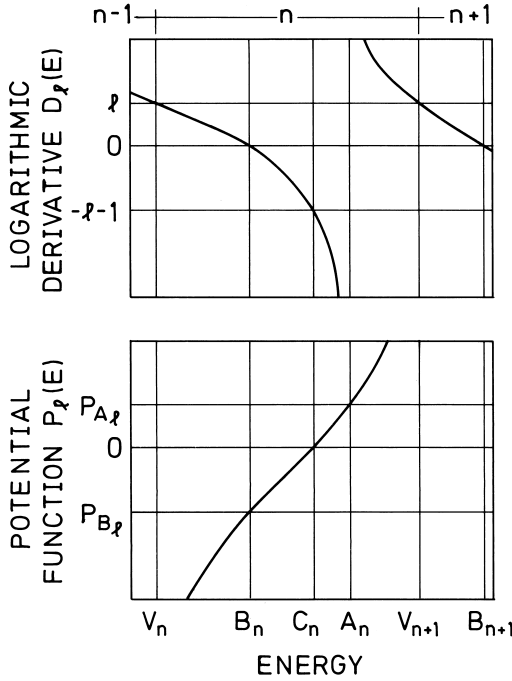


Fig. 1.7. The n th period of the logarithmic derivative function $D_l(\varepsilon)$, and the corresponding potential function $P_l(\varepsilon)$. The bottom, centre, and top of the nl band are defined respectively by $P_l(B_{nl}) = -2(2l+1)(l+1)/l$ ($D_l(B_{nl}) = 0$), $P_l(C_{nl}) = 0$, and $P_l(A_{nl}) = l$ ($D_l(A_{nl}) = -\infty$).

which $\mathcal{S}_{ij}^k = 0$ and, since the average over the Brillouin zone may be shown to vanish, i.e.

$$\sum_{j=1}^{2l+1} \int_{BZ} \mathcal{S}_{ij}^k d\mathbf{k} = 0, \quad (1.3.15)$$

the designation of C_{nl} as the centre of the band is appropriate. Equation (1.3.12) may be satisfied, and energy bands thereby formed, over an energy range around C_{nl} which, to a good approximation, is defined by the Wigner–Seitz rule, which states that, by analogy with molecular binding, the top and bottom of the band occur where the radial wavefunction and its derivative respectively are zero on the atomic sphere. The corresponding energies, defined by

$$D_l(A_{nl}) = -\infty \quad (1.3.16)$$

and

$$D_l(B_{nl}) = 0, \quad (1.3.17)$$

are then known respectively as the top and bottom of the nl band, even though this designation is not precisely accurate.

Over the energy range $A_{nl}-B_{nl}$, the potential function may be parametrized with reasonable accuracy as

$$P_l(\varepsilon) \simeq \frac{1}{\gamma_{nl}} \frac{\varepsilon - C_{nl}}{\varepsilon - V_{nl}}. \quad (1.3.18)$$

It is convenient to define the related mass parameter μ_{nl} by

$$\mu_{nl} S^2 = \left. \frac{dP_l(\varepsilon)}{d\varepsilon} \right|_{C_{nl}} \simeq \frac{1}{\gamma_{nl}(C_{nl} - V_{nl})}. \quad (1.3.19)$$

It is determined by the probability that an electron described by the partial wave $R_l(C_{nl}, r)$ reaches the atomic sphere and, if the wavefunction is normalized within the sphere, it may be shown that

$$\mu_{nl} S^2 = \left[\frac{1}{2} S R_l^2(C_{nl}, S) \right]^{-1}. \quad (1.3.20)$$

For free electrons, $\mu_{nl} \equiv 1$ for all values of n and l .

With this parametrization, we may write down an explicit expression for the unhybridized band energies. From eqns (1.3.12), (1.3.18) and (1.3.19) these are given by

$$\varepsilon_{lj}(\mathbf{k}) = C_{nl} + \frac{1}{\mu_{nl} S^2} \frac{S_{lj}^{\mathbf{k}}}{1 - \gamma_{nl} S_{lj}^{\mathbf{k}}}. \quad (1.3.21)$$

The pure l bands are thus obtained from the corresponding canonical bands by fixing the position with C_{nl} , scaling the bandwidth by $\mu_{nl} S^2$, and distorting them with γ_{nl} .

Hybridization between bands of different l is taken into account by including the structure constants with $l \neq l'$ in (1.3.11), causing a repulsion between energy levels with the same \mathbf{k} and symmetry, as specified by the labels in Fig. 1.6. Bands of the same symmetry are thus not allowed to cross, and *strong hybridization* instead creates an energy gap. In addition, *weak hybridization* gives rise to a mixing and repulsion between bands which do not cross in the absence of hybridization. In order to complete the calculation of the band structure, the inaccuracies due to approximating the atomic polyhedron by a sphere, and to neglecting higher partial waves, may be conveniently treated together by perturbation theory. In practice, the energy bands are not of course calculated step-wise as described above, but all the steps are performed simultaneously on a computer. Nevertheless, the conceptual description of the procedure as a placing, scaling and distortion of the

canonical bands, according to the values of the potential parameters, with a final hybridization between bands of the same symmetry, allows a clear visualization of the way in which the relatively complex band structure is built up from simpler elements, and of the relation between the eigenstates of the atom and those in the solid.

Table 1.3. Electronic parameters for α -Ce.

	6s	6p	5d	4f
A_l (Ry)	2.234	2.698	1.198	0.648
C_l (Ry)	0.620	1.452	0.792	0.628
B_l (Ry)	0.330	0.909	0.409	0.587
μ_l	0.61	0.70	2.18	45.36
n_l	0.509	0.245	2.091	1.154
$N_l(\varepsilon_F)$ (Ry $^{-1}$)	1.81	1.50	6.48	21.11
$\mathcal{P}_l\Omega$ (Ry)	0.195	0.152	-0.219	-0.163

This procedure may be illustrated by considering the construction of the band structure of α -Ce from its component parts. Partial waves in the atomic sphere at the energies of the band-centres, where $P_l(\varepsilon) = 0$, are shown in Fig. 1.5, and the corresponding potential parameters are given in Table 1.3. In this section, we express the energies in Rydbergs, following our general principle of using throughout the book those units which are favoured by practitioners of research in the subject currently under discussion. The s and p effective masses are somewhat below 1, and the relative positions of the band centres correspond quite closely to those of the free-electron gas. Through the influence of the l -dependent centrifugal-potential term in (1.2.12), the d and f states are in contrast constrained to the inner regions of the atomic sphere, with the consequence that the d mass is relatively large (though not as large as in a typical transition metal) and the f mass is extremely large.

The energy bands of Fig. 1.8 were calculated by an iterative procedure, by Skriver (private communication). The electron density $n(\mathbf{r})$ is first estimated by, for example, overlapping *atomic* charge densities situated on the lattice sites, and from it the periodic potential $v_{\text{eff}}(\mathbf{r})$ is constructed, using the local-density approximation (1.2.9). The band structure is then determined for this potential and $n(\mathbf{r})$ recalculated, in analogy with (1.2.6), by summing over occupied states, those beneath the Fermi level. This procedure is repeated until the potential self-consistently reproduces itself, and the energy bands have converged to the desired accuracy. The band structure can be considered as being

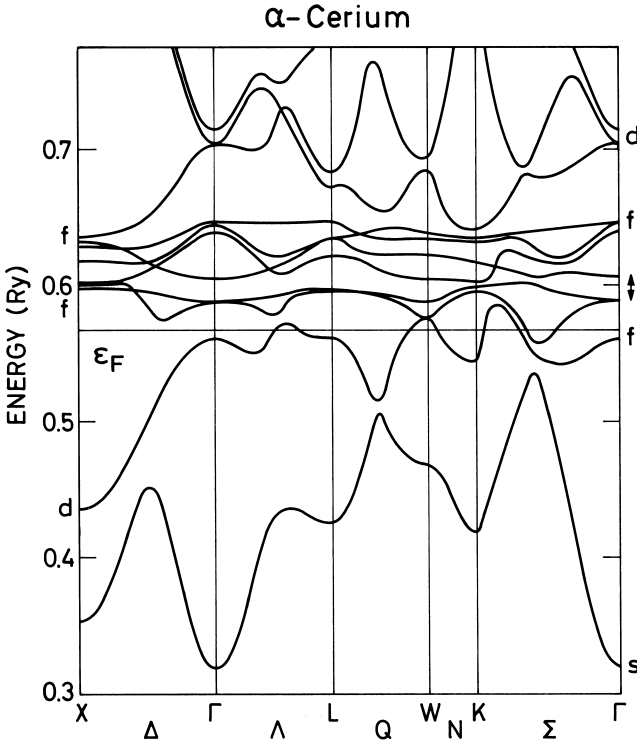


Fig. 1.8. The band structure of fcc α -Ce, calculated by Skriver. The orbital angular momentum of some states at symmetry points in the zone is indicated, including the top and bottom of the narrow bands. The doubleheaded arrow indicates the spin-orbit splitting of a 4f state.

composed of a broad free-electron-like sp band, crossed by and hybridizing both strongly and weakly with the d and f bands. The occupation numbers n_i of the various states given in Table 1.3 make it clear that α -Ce may be classified as both a d - and an f -band transition metal.

The above description of the f states in α -Ce as occupying the bottom of an f band is now generally accepted as valid, but the correct treatment of the f electrons in the rare earth metals, and especially Ce, was a matter of lengthy controversy. According to the standard model, which is generally applicable to rare earth magnetism, an integral number of f electrons are localized on each ion, subject to the same intra-ionic interactions as in the free atom. The Pauling-Zachariasen promotional model for the γ - α phase transition in Ce, which associated the transition with the transfer of a single f electron on each ion to a d state, with a concomitant decrease of about 6% in the fcc lattice

constant, was therefore consistent with the standard model. However the positron-annihilation experiments of Gustafson and Mackintosh (1964) showed that the change in f occupancy, when the transition was induced by a change in temperature, was much less than one, and indeed that the results in both phases were consistent with about one f electron per ion. Similar results were obtained by Gustafson *et al.* (1969) when the transition was driven by pressure, and they concluded that it involves not primarily a change in the f occupancy but rather a change in the f state, from being localized in the γ -phase to being an itinerant band electron in the α -phase. This idea was taken up by Johansson (1974) who, from a consideration of spectroscopic, cohesive and thermodynamic evidence, proposed that the γ - α transition should be considered as a Mott localized-delocalized transition among the f electrons. Glötzel (1978) used density-functional theory to calculate the ground state properties and showed that the equation of state in the α -phase can be accounted for rather satisfactorily by including the f electrons in the band structure, and furthermore that a transition to a spin-polarized state should occur at a lattice constant close to that of γ -Ce, though at a (negative) pressure considerably lower than that deduced from experiment. Eriksson *et al.* (1990) have recently shown that this discrepancy may be substantially reduced by including the l - l coupling, which is responsible for the second of Hund's rules, in the calculation of the $4f$ bands. This leads to a ground state in γ -Ce in which the $4f$ electrons are almost fully polarized, thus occupying the Hund's-rule ground state on each site. Despite the fact that they are described in the band picture, they may thus be considered as *localized*, making very little contribution to the cohesive properties. The calculated atomic volumes in both phases are in good agreement with experiment. Podloucky and Glötzel (1983) found a cohesive energy for α -Ce in accord with the measured value, while that of a 'promotional' state with no f electrons is far too small. They were also able to account for the Compton-scattering experiments of Kornstädt *et al.* (1980), who had verified that the change in f occupancy at the transition is small. Skriver (1985) calculated the crystal structure and equation of state of α -Ce up to high pressures, finding very good agreement with experiment (Staun Olsen *et al.* 1985), provided that the f bands are included, but very poor agreement if the f electrons are promoted to the d bands, or are assumed to be localized, and therefore to make a negligible contribution to the electronic pressure. The relative stability at high pressures of low-symmetry configurations such as the α -U structure, which is observed experimentally, is a strong indicator that there are f electrons in the conduction bands, as in the light actinides, where they play a decisive role in determining the structure (Skriver 1985).

The most powerful experimental technique available for studying the details of the electronic structure in the vicinity of the Fermi level is the de Haas–van Alphen (dHvA) effect (Shoenberg 1983), which allows a precise determination not only of the shape of the Fermi surface, but also of the effective masses of the electrons whose wave-vectors lie on it. Unfortunately, the metallurgical difficulties encountered in attempting to fabricate pure single crystals have so far precluded the observation of the effect in α -Ce, but Johanson *et al.* (1981) studied the related compound CeSn₃, and demonstrated that it contains itinerant f electrons of large mass at low temperatures. More recently, a number of examples of heavy-fermion Ce compounds have been investigated (Reinders *et al.* 1986; Lonzarich 1988) in which the effective masses, as deduced either from the dHvA effect or the low-temperature heat capacity, are enhanced by up to an order of magnitude compared with those deduced from band structure calculations.

There is thus very convincing evidence that the f electrons in Ce and its compounds can form bands and extend in coherent Bloch states throughout the crystal. Photoemission experiments in α -Ce (Wieliczka *et al.* 1982; Mårtensson *et al.* 1982) revealed a structure with two peaks, which may plausibly be associated respectively with an itinerant f hole near the Fermi level, and one localized for a finite time at a particular ionic site (Norman *et al.* 1984; Mackintosh 1985). There are very few indications of itinerant f behaviour in the other rare earth elements, although the above-mentioned double-peaked structure is also observed in γ -Ce and Pr (Wieliczka *et al.* 1984), in both of which the f electrons are normally considered as localized, and as we shall see, there is evidence of an f contribution to the binding energy in some of the light rare earths. After this brief interlude, we will therefore leave the question of f bands and return to the standard model of f electrons localized on the ions, interacting with the surroundings but only indirectly with each other.

Pr, the neighbouring element to Ce, undergoes a phase transition at high pressures (Wittig 1980) which is probably associated with the formation of a band by the f electrons (Skriver 1981; Eriksson *et al.* 1990), but at ambient pressures they are localized and may be considered as part of the ionic core. Indeed, intermultiplet transitions, corresponding to those occurring on Pr ions in insulators, but shifted due to screening by the conduction electrons in the metal, have been observed by Taylor *et al.* (1988), using inelastic neutron-scattering at relatively high energies. The $4f$ states do not therefore appear in the energy bands of Fig. 1.9, which portrays broad sp bands hybridized with a much narrower d band. As will be discussed later, Pr is paramagnetic above about 50 mK, and in zero field the Fermi surface, which is relatively complex, may be deduced from the figure to be composed of 2 electron pockets and 4 open

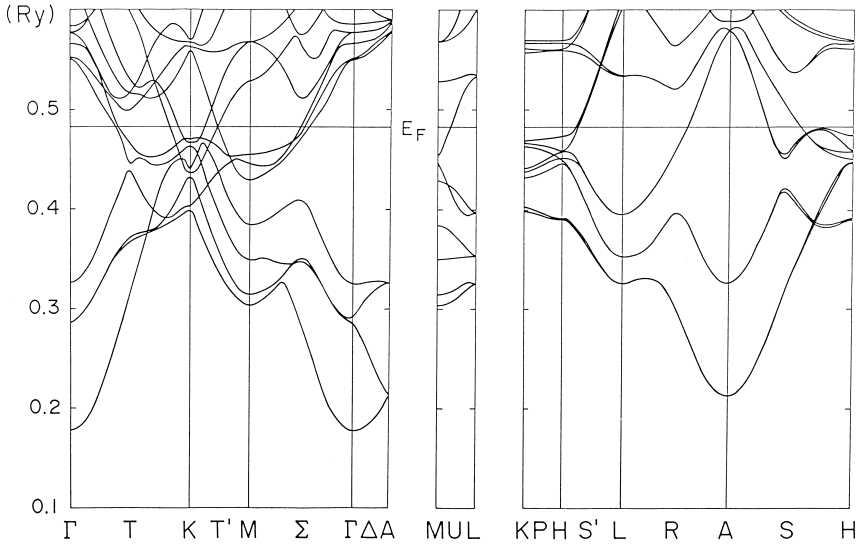


Fig. 1.9. The band structure of dhcp Pr, calculated by Skriver. The energy bands in the vicinity of the Fermi level are predominantly d -like, and the $4f$ states are assumed to be localized and therefore do not appear, in contrast to Fig. 1.8.

hole sheets. However, the dHvA effect is measured in a relatively high magnetic field, and the induced moment modifies the band structure in a way which has been studied in detail by Wulff (1985). The exchange coupling between a conduction-electron spin \mathbf{s} and the $4f$ spins takes the Heisenberg form

$$\mathcal{H}_{\text{sf}} = -2Is \cdot \sum_i \mathbf{S}_i. \quad (1.3.22)$$

In the ground-state manifold, this interaction may from (1.2.29) be written

$$\mathcal{H}_{\text{sf}} = -2(g-1)Is \cdot \sum_i \mathbf{J}_i. \quad (1.3.23)$$

When a magnetic field is applied, the induced moment therefore gives rise to a splitting between the up- and down-spin energy bands. Since Pr is magnetically highly anisotropic, this splitting depends strongly on the direction of the field, but it can readily attain values of several mRy, and hence have drastic effect on the Fermi surface. In particular, the seventh-band minority-spin surface changes its topology at a critical (internal) field of about 40 kOe, as shown in Fig. 1.10,

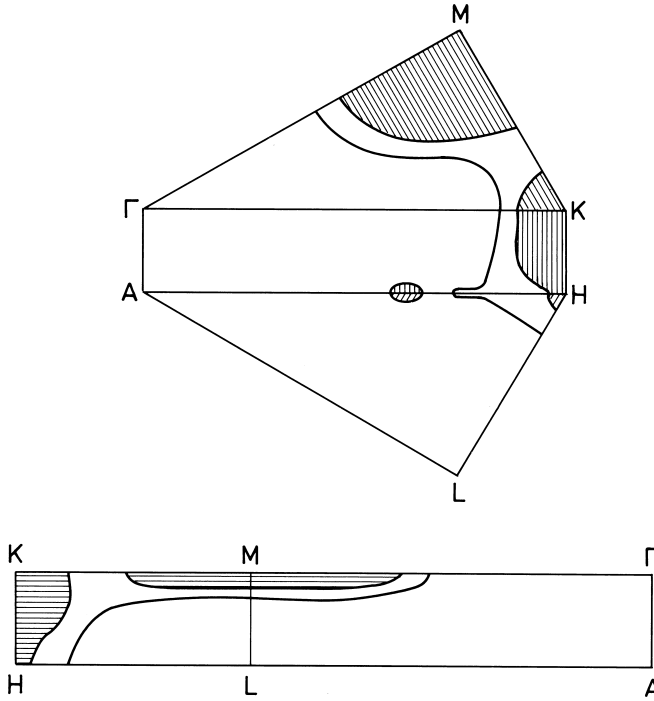


Fig. 1.10. The intersections of the Fermi surfaces, for the two spin states of the seventh band in dhcp Pr, with the faces of the Brillouin zone of Fig. 1.4. The surfaces are generated by a rigid splitting of the energy bands of Fig. 1.9 by 10 mRy. The unshaded majority-spin surface is a single sheet, whereas the exchange splitting modifies the topology of the shaded minority-spin surface, giving rise to a closed lens at M, a small electron pocket, and an irregular tube along HK.

and clear evidence for this transition has been observed in the dHvA effect. The changes of the Fermi surface in a magnetic field, and particularly the enhancement of the effective masses by the interaction with the $4f$ moments (Wulff *et al.* 1988), which we will discuss further in Section 7.3, give an average value of I of about 9 mRy, with a variation of some 30% over different bands and orbits. The agreement between the measured and calculated electron orbits is such that shifts in the energy bands of only a few mRy are required to bring the two into concordance, and this is comparable to typical values for transition metals (Mackintosh and Andersen 1980). The experimental study of the dHvA effect in Pr, which is the most elaborate which has yet been undertaken for a rare earth metal, has thus led to the important conclusion that energy-band

theory gives a realistic description of the conduction electron states, and may therefore be used as a basis for the calculation of properties which depend on the electronic structure.

This conclusion could already be drawn, though with slightly less confidence, from the pioneering measurements of Mattocks and Young (1977) of the dHvA effect in ferromagnetic Gd. Because of the ferromagnetic moment, the exchange interaction (1.3.22) separates the energy bands of different spin even in zero field, and the exchange splitting is essentially independent of field. The results were interpreted in terms of the paramagnetic energy bands, originally calculated by Dimmock and Freeman (1964) and, with relativistic effects, by Keeton and Loucks (1968), taking account of the ferromagnetic structure by a rigid splitting of the bands. The resulting two majority-spin hole surfaces and the minority-spin electron surface could account for all of the observed large orbits, with a value of I close to that later deduced for Pr, and with a comparable variation through the zone. However, many small orbits were observed which could not be explained with this model, nor have subsequent band calculations, culminating in those of Temmerman and Sterne (1990), in which the exchange splitting of the conduction bands was included a priori, fully accounted for the small pieces of the Fermi surface. Although the general features of the electronic structure of Gd may therefore be considered as well understood, a further theoretical effort, taking into account the effect on the band structure of the spin-orbit coupling in the presence of both an exchange field and an external field, would be necessary to explain the finer details.

The positron-annihilation experiments of Williams and Mackintosh (1968), although at a much lower level of resolution, were also in general accord with the calculations of Keeton and Loucks (1968). They studied a number of heavy rare earths in their paramagnetic phases, showing that their Fermi surfaces are highly anisotropic and rather similar to each other. A calculation based upon energy-band theory gave a good account of the experimental results for Y. The distributions of the annihilation photons displayed a feature which is sensitive to the form of the hole surface shown in Fig. 1.11, namely the shape of the 'webbing' which may join the 'toes' on the surface near L. This characteristic is very dependent on the relative positions of the s and d bands, and the calculations indicated that the webbing is absent in Gd, very narrow in Tb, and fully developed, forming a kind of plateau, in the other heavy rare earths. These conclusions were in accordance with the positron-annihilation results, which further indicated that the webbing is destroyed in the magnetically ordered phase of Ho. The relation of these observations to the occurrence of periodic magnetic structures will be discussed in the following section.

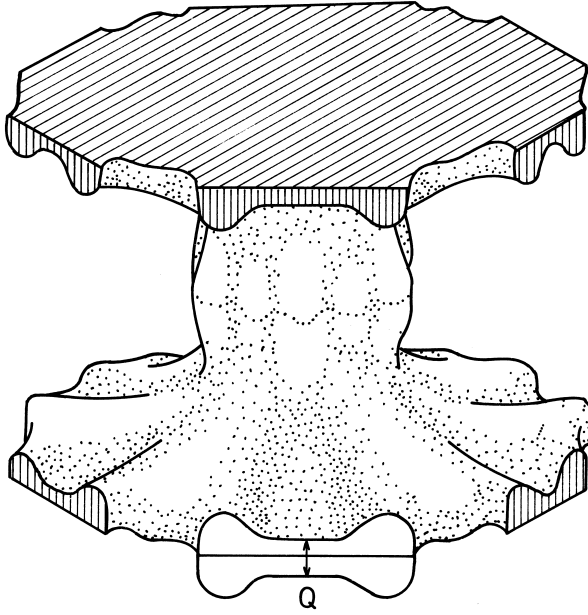


Fig. 1.11. The calculated hole Fermi surface of paramagnetic Tb in the Brillouin zone of Fig. 1.4. The extension of the ‘webbing’ between the ‘toes’ near the zone boundary is believed to give rise to a peak in the conduction-electron susceptibility $\chi(\mathbf{q})$, which determines the \mathbf{Q} -vector characterizing the helical structure.

The Fermi surface of paramagnetic Lu, in which the $4f$ states are all filled, has also been studied by the dHvA effect (Johanson *et al.* 1982) and found to be in semi-quantitative agreement with the calculations of Tibbetts and Harmon (1982). Since the results of band structure calculations have been confirmed experimentally at the Fermi level in widely separated elements in the rare earth series, it is reasonable to suppose that they will also be successful in accounting for other ground-state properties. Characteristic band energies for the trivalent lanthanides, calculated by Skriver (1983) at a common atomic volume close to the equilibrium value for Gd, are shown in Fig. 1.12. In this figure, the effect of the change in potential is thus separated from that of the interatomic spacing. The most notable feature is the fall in energy of the s band relative to the d band with increasing atomic number, which results in a decrease of the occupation of the latter, with consequences, as we shall

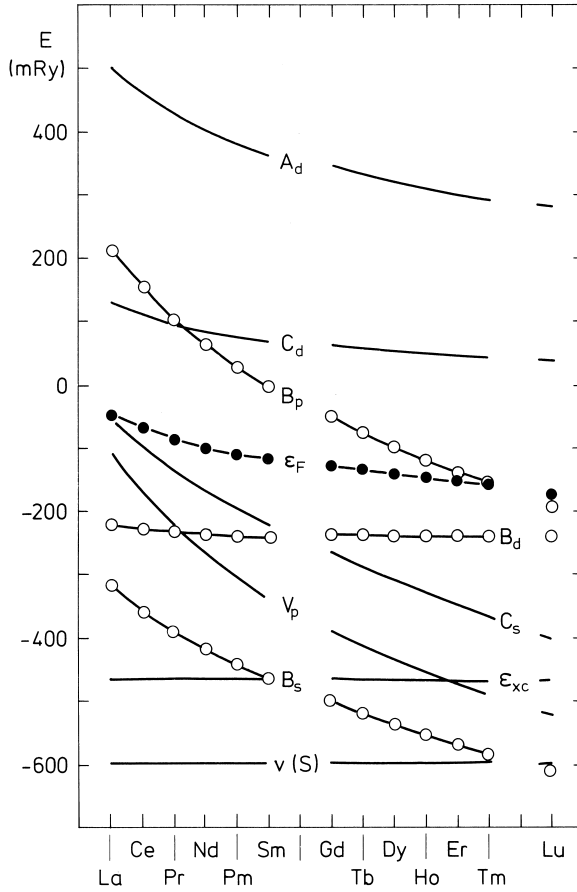


Fig. 1.12. Characteristic band energies for the trivalent lanthanides, for a common value of the atomic radius S , after Skriver (1983). The values of the potential $v(S)$ and the exchange-correlation energy ε_{xc} at the atomic sphere are shown, together with the bottom, B_i , the centre, C_i , and the top, A_i , of the $6s$, $6p$, and $5d$ bands, and the Fermi level ε_F . The relative lowering of the $6s$ band with increasing atomic number reduces the $5d$ occupancy, which in turn changes the crystal structure.

see, for the crystal structure. The reason for the fall in the band energies is the increase of the nuclear charge with atomic number, which is incompletely screened by the additional f electrons. The potential $v_{\text{eff}}(\mathbf{r})$ in (1.2.12) is therefore on average increasingly negative, and in order to maintain an unchanged boundary condition, as expressed by the logarithmic derivative, the band energies must decrease accordingly.

This effect is relatively modest for the d bands, but much greater for the s and p bands. The relative shift of the s and d bands is reduced by the adjustment of the lattice to its equilibrium configuration, but only by a small amount. As may be seen from Fig. 1.12, $(B_d - B_s)$ increases from 101 mRy for La to 373 mRy for Lu at constant S , whereas the corresponding values for the equilibrium atomic volumes are 136 mRy and 380 mRy. The band masses also change across the series; μ_d at constant volume increases from 2.1 in La to 3.0 in Lu, so that the d bands narrow as they fall, while μ_s increases slightly with atomic number, but remains below 1 throughout (Skriver 1983).

The canonical-band theory may be used to calculate the electronic pressure and its partitioning between the different angular momentum components. According to the *force theorem* (see Mackintosh and Andersen 1980) the change in the total energy, due to an infinitesimal change in the lattice constant, may be determined as the difference in the band energies, calculated while maintaining the potential unchanged. We may thus write

$$dU = \delta \int^{\varepsilon_F} \varepsilon N(\varepsilon) d\varepsilon, \quad (1.3.24)$$

where $N(\varepsilon)$ is the total electronic density of states, and δ indicates the restricted variation with a *frozen potential*. The electronic pressure is then given by

$$\mathcal{P} = -\frac{dU}{d\Omega}, \quad (1.3.25)$$

where Ω is the volume of the atomic polyhedron. The expression (1.3.21) for the canonical-band energies then leads to the approximate result for the l partial pressure:

$$3\mathcal{P}_l\Omega = -n_l \frac{\delta C_l}{\delta \ln S} + n_l(\bar{\varepsilon}_l - C_l) \frac{\delta \ln \mu_l S^2}{\delta \ln S}, \quad (1.3.26)$$

where n_l is the occupation number of the l states and

$$\bar{\varepsilon}_l = \frac{1}{n_l} \int^{\varepsilon_F} \varepsilon N_l(\varepsilon) d\varepsilon \quad (1.3.27)$$

is their mean energy. Equation (1.3.26) is useful for purposes of interpretation, but the results which we shall present are based upon a more accurate procedure, involving the fully hybridized self-consistent band structure (Skriver 1983).

The partial occupation numbers, state-densities and electronic pressures for α -Ce, at the equilibrium lattice constant, are given in Table 1.3. The s and p electrons make a positive, repulsive contribution to

the pressure while the d and f states provide the binding, through their negative, attractive partial pressure. This difference is essentially due to the fact that the s and p wavefunctions have a positive curvature at the atomic sphere, over the energy range of the corresponding bands, as illustrated in Fig. 1.5, while the d and f functions have a negative curvature. Consequently, a decrease in volume causes an increase in the logarithmic derivative for the former and a decrease for the latter, and since $D_l(E)$ is a decreasing function of energy, the s and p bands must rise and the d and f bands fall in order to maintain the boundary condition. Equation (1.3.25) then immediately accounts for the signs of the corresponding partial pressures. The attractive f pressure for α -Ce is substantial; if it is removed, the lattice expands to a volume greater than that of γ -Ce. The partial pressures at a constant atomic volume for the trivalent rare earths are shown in Fig. 1.13. As may be seen, it is primarily the decrease in the s and p pressures, which has its origin in the incompletely

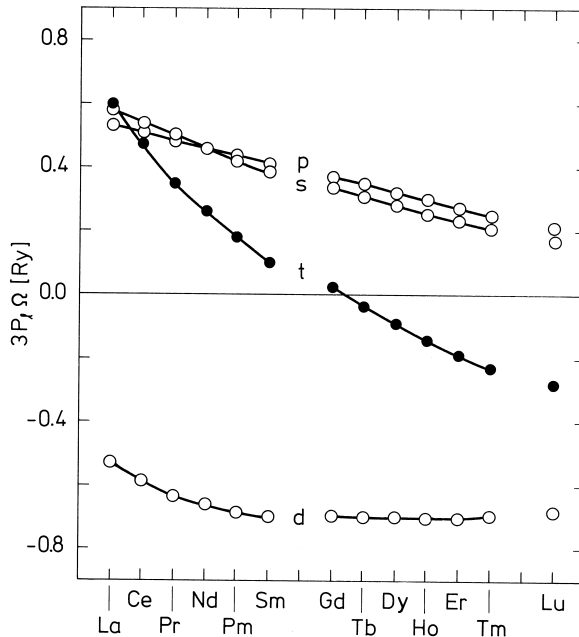


Fig. 1.13. The partial $6s$, $6p$, and $5d$ pressures for the trivalent rare earths, calculated for a common atomic volume close to the equilibrium value for Gd, after Skriver (1983). It is the decrease in the s and p pressures which gives rise to the lanthanide contraction.

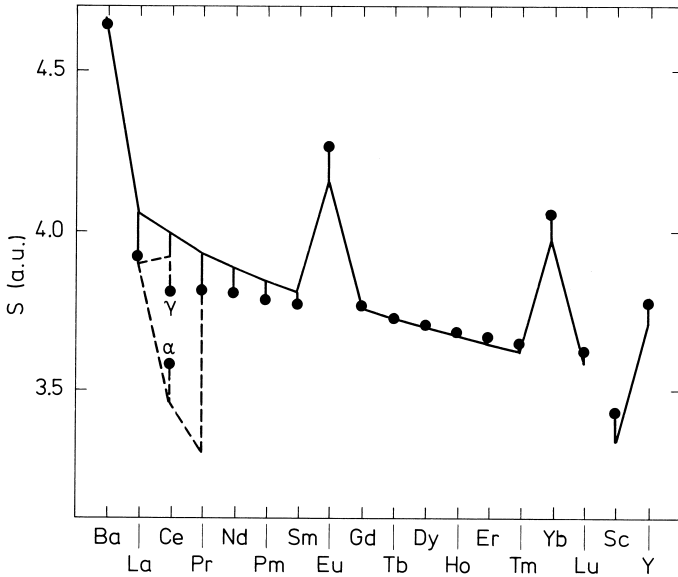


Fig. 1.14. The equilibrium atomic radii for the rare earth metals, after Skriver (1983). The full circles indicate the experimental values. The full line is a calculation including the s , p , and d partial pressures, while the broken line indicates that the f contribution is also taken into account.

screened increase in the nuclear charge, which leads to the lanthanide contraction. This contraction is clearly apparent in the atomic radii shown in Fig. 1.14. The values calculated from the condition that the total pressure is zero agree very well with the experimental observations for the heavy metals, but if the f contribution is neglected, the calculated electronic pressure is increasingly too high as the atomic number decreases. As mentioned earlier, the partial pressure of the f band is essential for understanding α -Ce, and it seems that the interaction of the f electrons with their surroundings makes a contribution to the binding, even in some metals in which the magnetic behaviour strongly indicates that they are localized.

In Eu and Yb, the intra-atomic interactions make it favourable to (half) fill the sub-band by transferring an electron from the conduction bands to an f state, leading to the formation of the divalent cubic structures which strongly resemble the alkaline earth metals. This transfer occurs predominantly at the expense of the d electrons, whose binding contribution to the electronic pressure is thereby reduced, causing

a substantial increase in the atomic volume. The relatively weak binding of the $4f$ states in the divalent rare earths is clearly apparent in the experiments of Lang *et al.* (1981), who used X-ray photoemission to measure the energies required to transfer a $4f$ electron to the Fermi level, throughout the whole series. By inverse photoemission (*Bremsstrahlung Isochromat Spectroscopy*) they were similarly able to deduce the energies required to move an electron from the Fermi level to the unoccupied $4f$ states. Combining the two experiments, the Coulomb correlation energy required to transfer an electron from an occupied level on another site could be deduced. These energies were later calculated by Min *et al.* (1986a) using a supercell method, in which rare earth ions with different f occupancies are considered as distinct species, and the agreement with experiment was generally very satisfactory.

For close-packed structures, the atomic volume is almost independent of the structure, but there are small differences in the electronic contribution to the cohesive energy, which manifest themselves in the common structural sequence $hcp \rightarrow dhcp \rightarrow \text{Sm-structure} \rightarrow fcc$ in the rare earths, as the atomic number is reduced or the pressure is increased. Duthie and Pettifor (1977) proposed that the d -electron occupancy,

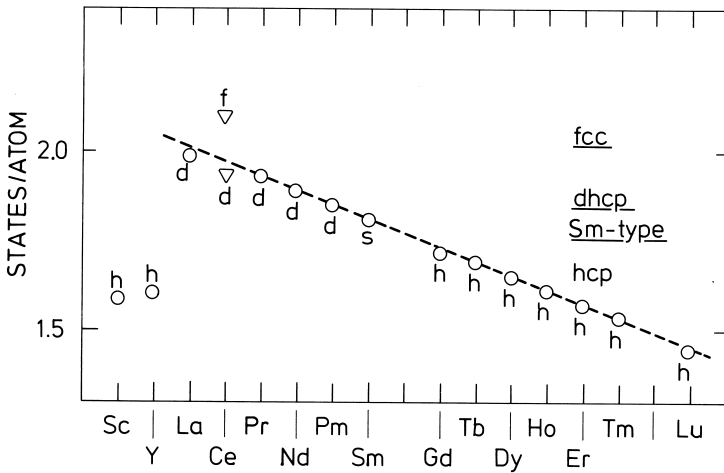


Fig. 1.15. The occupation numbers of the $5d$ states for the trivalent lanthanides, at the observed equilibrium atomic volumes, after Skriver (1983). For Ce, the $4f$ electrons are included in the energy bands. The experimentally observed crystal structures are labelled by h, s, d, and f, for hcp, Sm-structure, dhcp, and fcc, respectively. The empirical d -occupation numbers which separate the different structures are indicated by the lines on the right.

which increases through these structural sequences, is the essential determinant of the structure, and made an approximate calculation of the energy differences using canonical-band theory. The results of Skriver (1983) in Fig. 1.15 show how well the d occupancy indeed correlates with the structure. To complete the picture, Min *et al.* (1986b) demonstrated that increasing the pressure on Lu should produce a series of phase transitions following the above sequence, the first of which has been observed experimentally.

1.4 Magnetic interactions

In the metallic state, the $4f$ electrons on a rare earth ion are subjected to a variety of interactions with their surroundings. These forces may be broadly classified into two categories. The *single-ion interactions* act independently at each ionic site, so that their influence on the state of the $4f$ electrons at a particular site is unaffected by the magnetic state of its neighbours. The corresponding contribution to the Hamiltonian therefore contains sums over terms located at the ionic sites i of the crystal, but without any coupling between different ions. On the other hand, the *two-ion interactions* couple the $4f$ -electron clouds at pairs of ions, giving terms which involve two sites i and j .

The charge distribution around an ion produces an electric field, with the local point-symmetry, which acts on the $4f$ electrons and gives rise to the large magnetic anisotropies which are characteristic of the rare earth metals. This *crystal field* makes a contribution to the potential energy of a $4f$ electron with charge $-e$

$$v_{\text{cf}}(\mathbf{r}) = - \int \frac{e\rho(\mathbf{R})}{|\mathbf{r} - \mathbf{R}|} d\mathbf{R}, \quad (1.4.1)$$

where $\rho(\mathbf{R})$ is the charge density of the surrounding electrons and nuclei. If these do not penetrate the $4f$ charge cloud, $v_{\text{cf}}(\mathbf{r})$ is a solution of Laplace's equation, and may be expanded in spherical harmonics as

$$v_{\text{cf}}(\mathbf{r}) = \sum_{lm} A_l^m r^l Y_{lm}(\hat{\mathbf{r}}), \quad (1.4.2)$$

where

$$A_l^m = -(-1)^m \frac{4\pi}{2l+1} \int \frac{e\rho(\mathbf{R})}{R^{l+1}} Y_{l-m}(\hat{\mathbf{R}}) d\mathbf{R}, \quad (1.4.3)$$

which is a special case of the multipole expansion (1.3.7). We can thus look upon (1.4.2) as arising from the interaction of the multipoles $r^l Y_{lm}(\hat{\mathbf{r}})$ of the $4f$ electrons with the appropriate components of the electric field. If part of the charge which is responsible for the crystal field lies within the $4f$ cloud, $v_{\text{cf}}(\mathbf{r})$ can still be expanded in spherical

harmonics with the appropriate symmetry, but the coefficients are not generally proportional to r^l , nor to (1.4.3).

As the crystal-field energy is small compared to the spin-orbit splitting, its effects on the eigenstates of the system are adequately accounted for by first-order perturbation theory. Since f electrons cannot have multipole distributions with $l > 6$, the properties of the spherical harmonics ensure that the corresponding matrix elements of (1.4.2) vanish. Even so, the calculation of those that remain from the electronic wavefunctions would be a formidable task, even if the surrounding charge distribution were known, if the ubiquitous Wigner-Eckart theorem did not once again come to the rescue. As first pointed out by Stevens (1952), provided that we remain within a manifold of constant J , in this case the ground-state multiplet, the matrix elements of $v_{\text{cf}}(\mathbf{r})$ are proportional to those of operator equivalents, written in terms of the \mathbf{J} operators. We may thus replace (1.4.2) by

$$\mathcal{H}_{\text{cf}} = \sum_i \sum_{lm} A_i^m \alpha_l \langle r^l \rangle \left(\frac{2l+1}{4\pi} \right)^{1/2} \tilde{O}_{lm}(\mathbf{J}_i), \quad (1.4.4)$$

where we have also summed over the ions. The *Stevens factors* α_l depend on the form of the electronic charge cloud through L , S and J , and on l , but not on m . They are frequently denoted α , β , and γ when l is 2, 4, and 6 respectively, and their values for the magnetic rare earth ions are given in Table 1.4. The expectation value $\langle r^l \rangle$ is an average over the $4f$ states. The *Racah operators* $\tilde{O}_{lm}(\mathbf{J})$ are obtained from the spherical harmonics, multiplied by $(4\pi/2l+1)^{1/2}$, by writing them in terms of

Table 1.4. Stevens factors for rare earth ions.

Ion ⁺⁺⁺	$\alpha \times 10^2$	$\beta \times 10^4$	$\gamma \times 10^6$
Ce	-5.714	63.49	0
Pr	-2.101	-7.346	60.99
Nd	-0.6428	-2.911	-37.99
Pm	0.7714	4.076	60.78
Sm	4.127	25.01	0
Tb	-1.0101	1.224	-1.121
Dy	-0.6349	-0.5920	1.035
Ho	-0.2222	-0.3330	-1.294
Er	0.2540	0.4440	2.070
Tm	1.0101	1.632	-5.606
Yb	3.175	-17.32	148.0

Cartesian coordinates and replacing (x, y, z) by (J_x, J_y, J_z) , with an appropriate symmetrization to take account of the non-commutation of the \mathbf{J} operators. They have been tabulated for l -values up to 8 by Lindgård and Danielsen (1974).

Following the customary practice, we shall generally use not the Racah operators, which are tensor operators transforming under rotations like spherical harmonics, but the *Stevens operators* $O_l^m(\mathbf{J})$, which transform like the real *tesseral harmonics* T_{lm} . If we define corresponding operators for m zero or positive as:

$$\begin{aligned} T_{l0} &= \tilde{O}_{l0} \\ T_{lm}^c &= \frac{1}{\sqrt{2}} [\tilde{O}_{l-m} + (-1)^m \tilde{O}_{lm}] \\ T_{lm}^s &= \frac{i}{\sqrt{2}} [\tilde{O}_{l-m} - (-1)^m \tilde{O}_{lm}], \end{aligned} \quad (1.4.5)$$

the Stevens operators for positive and negative m are proportional respectively to T_{lm}^c and $T_{l|m|}^s$. There is some ambiguity in the literature about the proportionality constants, but we have used the standard definitions of the Stevens operators in Table 1.5, see also Hutchings (1964). In terms of these operators, we may write the crystal-field Hamiltonian

$$\mathcal{H}_{\text{cf}} = \sum_i \sum_{lm} B_l^m O_l^m(\mathbf{J}_i). \quad (1.4.6a)$$

The *crystal-field parameters* B_l^m can in principle be calculated from the charge distribution in the metal, but in practice attempts to do so have met with limited success. The difficulties are two-fold. The charge density on the surroundings of an ion is not easy to determine with the necessary accuracy, and the approximations normally used in the calculation of the electronic structure of a metal, in particular the assumption that the charge distribution in the atomic polyhedron is spherically symmetric, are inadequate for the purpose. Furthermore, a redistribution of the charge within the cell can modify the electric fields experienced by the $4f$ electrons, and such shielding effects are again very difficult to estimate. It is therefore necessary to appeal to relatively crude models, such as the instructive but quite unjustified point-charge model, in which an adjustable charge is placed on each lattice site, or alternatively to regard the B_l^m as parameters to be determined from experiment.

Fortunately, the number of such parameters is strongly restricted by symmetry. We shall be concerned almost exclusively with the hexagonal structures of Fig. 1.3, and in defining the Stevens operators, we have used a Cartesian system in which the (x, y, z) -directions are along the

Table 1.5. Stevens operators. $X \equiv J(J + 1)$ and $J_{\pm} \equiv J_x \pm iJ_y$.

O_2^2	$= \frac{1}{2}(J_+^2 + J_-^2)$
O_2^1	$= \frac{1}{2}(J_z J_x + J_x J_z)$
O_2^0	$= 3J_z^2 - X$
O_2^{-1}	$= \frac{1}{2}(J_z J_y + J_y J_z)$
O_2^{-2}	$= \frac{1}{2i}(J_+^2 - J_-^2)$
O_4^4	$= \frac{1}{2}(J_+^4 + J_-^4)$
O_4^2	$= \frac{1}{4}[(7J_z^2 - X - 5)(J_+^2 + J_-^2) + (J_+^2 + J_-^2)(7J_z^2 - X - 5)]$
O_4^0	$= 35J_z^4 - (30X - 25)J_z^2 + 3X^2 - 6X$
O_4^{-2}	$= \frac{1}{4i}[(7J_z^2 - X - 5)(J_+^2 - J_-^2) + (J_+^2 - J_-^2)(7J_z^2 - X - 5)]$
O_4^{-4}	$= \frac{1}{2i}(J_+^4 - J_-^4)$
O_6^0	$= 231J_z^6 - (315X - 735)J_z^4 + (105X^2 - 525X + 294)J_z^2$ $- 5X^3 + 40X^2 - 60X$
O_6^6	$= \frac{1}{2}(J_+^6 + J_-^6)$

crystallographic (a, b, c)-axes specified in the previous section. However, it will later be convenient to rotate the z -axis into the magnetization direction, and instead orient the crystallographic (a, b, c)-axes along the (ξ, η, ζ) -Cartesian directions. For an ion with hexagonal point-symmetry, as in the hcp structure or on the hexagonal sites of the dhcp structure, the crystal field is specified by 4 parameters:

$$\mathcal{H}_{\text{cf}} = \sum_i \left[\sum_{l=2,4,6} B_l^0 O_l^0(\mathbf{J}_i) + B_6^6 O_6^6(\mathbf{J}_i) \right]. \quad (1.4.6b)$$

The Hamiltonian (1.4.6) lifts the degeneracy of the ionic $|JM_J\rangle$ states and, since it is expressed in terms of \mathbf{J} operators, whose matrix elements between these states may be determined by straightforward calculation, it may readily be diagonalized to yield the crystal-field energies and eigenfunctions. The B_l^m may then be used as adjustable parameters to reproduce the available experimental information on these eigenstates. As an example, we show in Fig. 1.16 the splitting of the nine $|4M_J\rangle$ states in Pr by the crystal fields acting on the hexagonal sites. This level scheme was derived from values of the crystal-field parameters adjusted

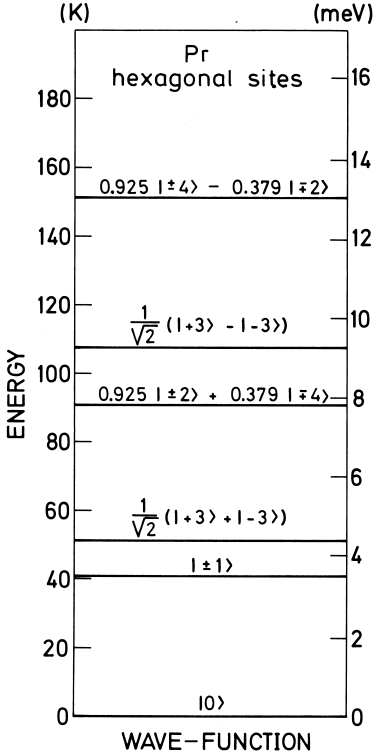


Fig. 1.16. The crystal-field splitting of the nine $|4M_J\rangle$ states on the hexagonal sites in dhcp Pr. The wavefunctions are written in terms of a basis $|M_J\rangle$ corresponding to quantization along the c -direction.

to account for a variety of experimental phenomena (Houmann *et al.* 1979).

If the lattice is strained, the crystal fields, and indeed all the other magnetic interactions which we shall discuss, are modified. In consequence, there is a *magnetoelastic coupling* between the moments and the strain, which can have profound consequences for rare earth magnetism. Magnetoelastic effects are manifested in both single-ion and two-ion terms in the Hamiltonian, though we shall mostly be concerned with the former. The elastic energy is quadratic in the strain, measured relative to the equilibrium configuration in the absence of magnetic interactions. The magnetoelastic energy is linear in the strain and the competition between the two effects may lead to some equilibrium strain or *magnetostriction*. Because of their moderate elastic constants and the large orbital component in their moments, the lanthanide metals display the largest known magnetostrictions.

Following Callen and Callen (1965), it is convenient to develop the theory in terms of the irreducible strains for hexagonal point-symmetry,

which are related to the Cartesian strains as follows:

$$\begin{aligned}
\epsilon_{\alpha 1} &= \epsilon_{11} + \epsilon_{22} + \epsilon_{33} \\
\epsilon_{\alpha 2} &= \frac{1}{3}(2\epsilon_{33} - \epsilon_{11} - \epsilon_{22}) \\
\epsilon_{\gamma 1} &= \frac{1}{2}(\epsilon_{11} - \epsilon_{22}) \\
\epsilon_{\gamma 2} &= \epsilon_{12} \\
\epsilon_{\varepsilon 1} &= \epsilon_{13} \\
\epsilon_{\varepsilon 2} &= \epsilon_{23},
\end{aligned} \tag{1.4.7}$$

where we have adopted the conventional notation of designating the Cartesian axes (ξ, η, ζ) by $(1, 2, 3)$. The α -strains are thus symmetry-conserving dilatations, the γ -strains distort the hexagonal symmetry of the basal plane, and the ε -strains shear the c -axis. The elastic energy may then be written

$$\begin{aligned}
\mathcal{H}_{\text{el}} = N \left[\frac{1}{2}c_{\alpha 1}\epsilon_{\alpha 1}^2 + c_{\alpha 3}\epsilon_{\alpha 1}\epsilon_{\alpha 2} + \frac{1}{2}c_{\alpha 2}\epsilon_{\alpha 2}^2 \right. \\
\left. + \frac{1}{2}c_{\gamma}(\epsilon_{\gamma 1}^2 + \epsilon_{\gamma 2}^2) + \frac{1}{2}c_{\varepsilon}(\epsilon_{\varepsilon 1}^2 + \epsilon_{\varepsilon 2}^2) \right],
\end{aligned} \tag{1.4.8}$$

where we have defined irreducible elastic stiffness constants per ion, related to the five independent Cartesian constants by

$$\begin{aligned}
c_{\alpha 1} &= \frac{1}{9}(2c_{11} + 2c_{12} + 4c_{13} + c_{33})V/N \\
c_{\alpha 2} &= \frac{1}{2}(c_{11} + c_{12} - 4c_{13} + 2c_{33})V/N \\
c_{\alpha 3} &= \frac{1}{3}(-c_{11} - c_{12} + c_{13} + c_{33})V/N \\
c_{\gamma} &= 2(c_{11} - c_{12})V/N \\
c_{\varepsilon} &= 4c_{44}V/N.
\end{aligned} \tag{1.4.9}$$

The contributions to the single-ion magnetoelastic Hamiltonian, corresponding to the different irreducible strains, are

$$\begin{aligned}
\mathcal{H}_{\text{me}}^{\alpha} = - \sum_i \left[\sum_{l=2,4,6} \{B_{\alpha 1}^l \epsilon_{\alpha 1} + B_{\alpha 2}^l \epsilon_{\alpha 2}\} O_l^0(\mathbf{J}_i) \right. \\
\left. + \{B_{\alpha 1}^{66} \epsilon_{\alpha 1} + B_{\alpha 2}^{66} \epsilon_{\alpha 2}\} O_6^6(\mathbf{J}_i) \right]
\end{aligned} \tag{1.4.10}$$

$$\begin{aligned}
\mathcal{H}_{\text{me}}^{\gamma} = - \sum_i \left[\sum_{l=2,4,6} B_{\gamma 2}^l \{O_l^2(\mathbf{J}_i) \epsilon_{\gamma 1} + O_l^{-2}(\mathbf{J}_i) \epsilon_{\gamma 2}\} \right. \\
\left. + \sum_{l=4,6} B_{\gamma 4}^l \{O_l^4(\mathbf{J}_i) \epsilon_{\gamma 1} - O_l^{-4}(\mathbf{J}_i) \epsilon_{\gamma 2}\} \right]
\end{aligned} \tag{1.4.11}$$

$$\begin{aligned}
\mathcal{H}_{\text{me}}^{\varepsilon} = - \sum_i \left[\sum_{l=2,4,6} B_{\varepsilon 1}^l \{O_l^1(\mathbf{J}_i) \epsilon_{\varepsilon 1} + O_l^{-1}(\mathbf{J}_i) \epsilon_{\varepsilon 2}\} \right. \\
\left. + B_{\varepsilon 5} \{O_6^5(\mathbf{J}_i) \epsilon_{\varepsilon 1} - O_6^{-5}(\mathbf{J}_i) \epsilon_{\varepsilon 2}\} \right].
\end{aligned} \tag{1.4.12}$$

The operators in the α -strain term are the same as those in the crystal-field Hamiltonian (1.4.6b), and the associated magnetoelastic effects may thus be considered as a strain-dependent renormalization of the crystal-field parameters, except that these interactions may mediate a dynamical coupling between the magnetic excitations and the phonons. The other two terms may have the same effect, but they also modify the symmetry and, as we shall see, can therefore qualitatively influence both the magnetic structures and excitations.

It is the two-ion couplings which are primarily responsible for cooperative effects and magnetic ordering in the rare earths, and of these the most important is the *indirect exchange*, by which the moments on pairs of ions are coupled through the intermediary of the conduction electrons. The form of this coupling can be calculated straightforwardly, provided that we generalize (1.3.22) slightly to

$$\mathcal{H}_{\text{sf}}(i) = -2 \int I(\mathbf{r} - \mathbf{R}_i) \mathbf{S}_i \cdot \mathbf{s}(\mathbf{r}) d\mathbf{r} = - \int \mathbf{H}_i(\mathbf{r}) \cdot \boldsymbol{\mu}(\mathbf{r}) d\mathbf{r}, \quad (1.4.13)$$

$\mathbf{s}(\mathbf{r})$ is the conduction-electron spin density, and the exchange integral $I(\mathbf{r} - \mathbf{R}_i)$ is determined by the overlap of the $4f$ and conduction-electron charge clouds. This expression, whose justification and limitations will be discussed in Section 5.7, can be viewed as arising from the action of the effective inhomogeneous magnetic field

$$\mathbf{H}_i(\mathbf{r}) = \frac{1}{\mu_B} I(\mathbf{r} - \mathbf{R}_i) \mathbf{S}_i = \frac{1}{\mu_B N} \sum_{\mathbf{q}} I(\mathbf{q}) e^{i\mathbf{q} \cdot (\mathbf{r} - \mathbf{R}_i)} \mathbf{S}_i \quad (1.4.14)$$

on the conduction-electron moment density $\boldsymbol{\mu}(\mathbf{r}) = 2\mu_B \mathbf{s}(\mathbf{r})$. The spin at \mathbf{R}_i generates a moment at \mathbf{r} , whose Cartesian components are given by

$$\mu_{i\alpha}(\mathbf{r}) = \frac{1}{V} \sum_{\beta} \int \chi_{\alpha\beta}(\mathbf{r} - \mathbf{r}') H_{i\beta}(\mathbf{r}') d\mathbf{r}', \quad (1.4.15)$$

where $\bar{\chi}$ is the nonlocal susceptibility tensor for the conduction electrons and V the volume. This induced moment interacts through $\mathcal{H}_{\text{sf}}(j)$ with the spin \mathbf{S}_j , leading to a coupling

$$\mathcal{H}(ij) = -\frac{1}{V} \sum_{\alpha\beta} \iint H_{j\alpha}(\mathbf{r}) \chi_{\alpha\beta}(\mathbf{r} - \mathbf{r}') H_{i\beta}(\mathbf{r}') d\mathbf{r} d\mathbf{r}'. \quad (1.4.16)$$

If we neglect, for the moment, the spin-orbit coupling of the conduction electrons, and the crystal is unmagnetized, $\chi_{\alpha\beta}$ becomes a scalar. The Fourier transform is:

$$\chi(\mathbf{q}) = \frac{1}{V} \int \chi(\mathbf{r}) e^{-i\mathbf{q} \cdot \mathbf{r}} d\mathbf{r} \quad (1.4.17)$$

in terms of which the integrations with respect to \mathbf{r} and \mathbf{r}' in eqn (1.4.16) are calculated straightforwardly. Summing the result over the N lattice sites, counting each interaction once only, we find that the indirect-exchange interaction takes the familiar isotropic Heisenberg form:

$$\begin{aligned} \mathcal{H}_{\text{ff}} &= -\frac{1}{2} \frac{V}{N^2 \mu_B^2} \sum_{ij} \sum_{\mathbf{q}} \chi(\mathbf{q}) I(\mathbf{q}) I(-\mathbf{q}) e^{i\mathbf{q} \cdot (\mathbf{R}_i - \mathbf{R}_j)} \mathbf{S}_i \cdot \mathbf{S}_j \\ &= -\frac{1}{2N} \sum_{\mathbf{q}} \sum_{ij} \mathcal{J}_S(\mathbf{q}) e^{i\mathbf{q} \cdot (\mathbf{R}_i - \mathbf{R}_j)} \mathbf{S}_i \cdot \mathbf{S}_j \\ &= -\frac{1}{2} \sum_{ij} \mathcal{J}_S(ij) \mathbf{S}_i \cdot \mathbf{S}_j, \end{aligned} \quad (1.4.18)$$

where

$$\mathcal{J}_S(ij) = \frac{1}{N} \sum_{\mathbf{q}} \mathcal{J}_S(\mathbf{q}) e^{i\mathbf{q} \cdot (\mathbf{R}_i - \mathbf{R}_j)} \quad (1.4.19)$$

and

$$\mathcal{J}_S(\mathbf{q}) = \sum_j \mathcal{J}_S(ij) e^{-i\mathbf{q} \cdot (\mathbf{R}_i - \mathbf{R}_j)} = \frac{V}{N \mu_B^2} |I(\mathbf{q})|^2 \chi(\mathbf{q}). \quad (1.4.20)$$

In the presence of an orbital moment, it is convenient to express (1.4.18) in terms of \mathbf{J} rather than \mathbf{S} , which we may do within the ground-state multiplet by using (1.2.29) to project \mathbf{S} on to \mathbf{J} , obtaining

$$\mathcal{H}_{\text{ff}} = -\frac{1}{2} \sum_{ij} \mathcal{J}(ij) \mathbf{J}_i \cdot \mathbf{J}_j, \quad (1.4.21)$$

with

$$\mathcal{J}(\mathbf{q}) = (g-1)^2 \left[\mathcal{J}_S(\mathbf{q}) - \frac{1}{N} \sum_{\mathbf{q}'} \mathcal{J}_S(\mathbf{q}') \right], \quad (1.4.22)$$

where we have also subtracted the interaction of the i th moment with itself, as this term only leads to the constant contribution to the Hamiltonian; $-\frac{1}{2}(g-1)^2 N \mathcal{J}_S(ii) J(J+1)$. The origin of the indirect exchange in the polarization of the conduction-electron gas by the spin on one ion, and the influence of this polarization on the spin of a second ion, is apparent in the expression (1.4.20) for $\mathcal{J}_S(\mathbf{q})$. As we shall see, it is the Fourier transform $[\mathcal{J}(\mathbf{q}) - \mathcal{J}(\mathbf{0})]$ which may be directly deduced from measurements of the dispersion relations for the magnetic excitations, and its experimentally determined variation with \mathbf{q} in the c -direction for the heavy rare earths is shown in Fig. 1.17.

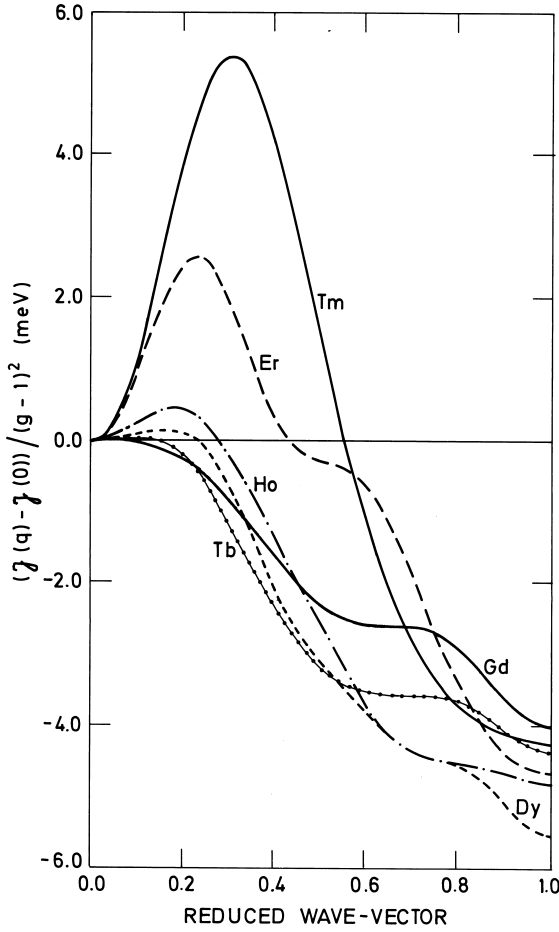


Fig. 1.17. The exchange interaction $\mathcal{J}_S(\mathbf{q}) - \mathcal{J}_S(\mathbf{0})$, determined experimentally in the magnetic heavy rare earth metals. The magnitude of the peak, which stabilizes the observed periodic magnetic structures, increases monotonically with atomic number.

A notable feature is the maximum which, except in Gd, occurs at non-zero \mathbf{q} and, as discussed in the following section, is responsible for stabilizing the periodic magnetic structures in the metals. In the approximation which we have used, the conduction-electron susceptibility is given by

$$\chi(\mathbf{q}) = \frac{2\mu_B^2}{V} \sum_{nn'\mathbf{k}} \frac{f_{n\mathbf{k}} - f_{n'\mathbf{k}-\mathbf{q}}}{\varepsilon_{n'}(\mathbf{k}-\mathbf{q}) - \varepsilon_n(\mathbf{k})}, \quad (1.4.23)$$

where $f_{n\mathbf{k}}$ is the Fermi–Dirac function. It is clear that a large contribution to the sum is made by pairs of electronic states, separated by \mathbf{q} , one of which is occupied and the other empty, and both of which have energies very close to the Fermi level. Consequently, parallel or *nesting* regions of the Fermi surface tend to produce peaks, known as *Kohn anomalies*, at the wave-vector \mathbf{Q} which separates them, and it is believed that the parallel sections of the webbing in the hole surface of Fig. 1.11 give rise to the maxima shown in Fig. 1.17. As we have mentioned, this conjecture is supported by both positron-annihilation experiments and band structure calculations but, despite extensive efforts, first-principles estimates of $\mathcal{J}(\mathbf{q})$ have not proved particularly successful. $\chi(\mathbf{q})$ may be calculated quite readily from the energy bands (Liu 1978), and exhibits the expected peaks, but the exchange matrix elements which determine $I(\mathbf{q})$ are much less tractable. Lindgård *et al.* (1975) obtained the correct general variation with \mathbf{q} for Gd, but the matrix elements were, not surprisingly, far too large when the screening of the Coulomb interaction was neglected.

The Kohn anomalies in $\mathcal{J}(\mathbf{q})$ Fourier transform into *Friedel oscillations* in $\mathcal{J}(\mathbf{R})$, and such oscillations, and the extremely long range of the indirect exchange, are illustrated in the results of Houmann *et al.* (1979) for Pr in Fig. 1.18. As is also shown in this figure, they found that the *anisotropic* component of the coupling is a substantial proportion of the Heisenberg exchange. The anisotropic coupling between the moments on two ions can be written in the general form

$$\mathcal{H}_{JJ} = -\frac{1}{2} \sum_{ij} \sum_{l' m m'} \mathcal{K}_{l' l}^{m m'}(ij) O_l^m(\mathbf{J}_i) O_{l'}^{m'}(\mathbf{J}_j), \quad (1.4.24)$$

where the terms which appear in the sum are restricted by symmetry, but otherwise may exhibit a large variety, depending on their origin. The many possible causes of anisotropy have been summarized by Jensen *et al.* (1975). They are usually associated with the orbital component of the moment and are therefore expected to be relatively large when L is large. In addition to contributions due to the influence of the localized $4f$ orbital moment on the conduction electrons (Kaplan and Lyons 1963), and to the magnetization and spin–orbit coupling of the latter (Levy 1969), direct multipolar interactions and two-ion magnetoelastic couplings, for which the coefficients $\mathcal{K}_{l' l}^{m m'}$ depend explicitly on the strain, may be important. A general two-ion coupling which depends only on the dipolar moments of the $4f$ electrons is

$$\mathcal{H}_{\text{dd}} = -\frac{1}{2} \sum_{ij} \mathcal{J}_{\alpha\beta}(ij) J_{i\alpha} J_{j\beta}. \quad (1.4.25)$$

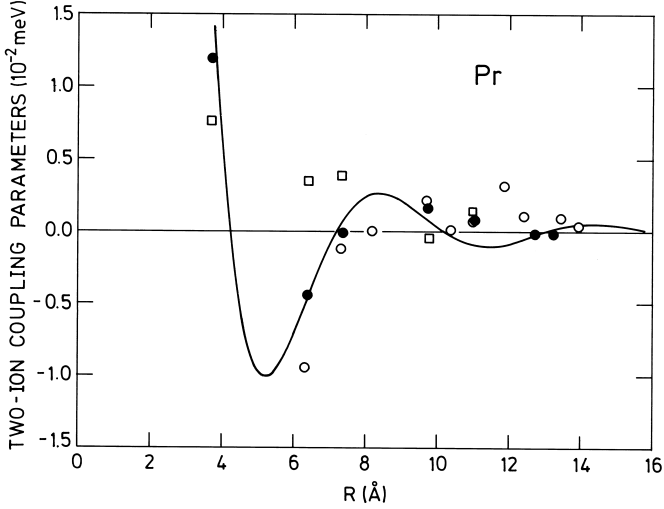


Fig. 1.18. The indirect-exchange interaction between ions on the hexagonal sites in Pr, deduced from measurements of the magnetic excitations at 6 K. The circles represent the isotropic interaction $\mathcal{J}(\mathbf{R})$ between an ion at the origin and those at different sites. The filled symbols are for pairs of ions in the same hexagonal plane, and the open symbols for pairs in different planes. The former are reasonably well described by the simple free-electron model of Section 5.7.1, with an effective value of 1.1 \AA^{-1} for $2k_F$, as shown by the full curve. In addition, the exchange incorporates an anisotropic component $\mathcal{K}(\mathbf{R})$, discussed in Section 2.1.6, which is smaller, but of comparable magnitude. Its values between pairs of ions in the plane are indicated by the squares. The calculated uncertainties in the exchange interactions are, at the most, the size of the points.

The dispersion relations for the magnetic excitations provide extensive evidence for anisotropy of this form. A special case is the classical *dipole-dipole interaction* for which

$$\mathcal{J}_{\alpha\beta}(ij) = (g\mu_B)^2 \frac{3(R_{i\alpha} - R_{j\alpha})(R_{i\beta} - R_{j\beta}) - \delta_{\alpha\beta}|\mathbf{R}_i - \mathbf{R}_j|^2}{|\mathbf{R}_i - \mathbf{R}_j|^5}. \quad (1.4.26)$$

Although it is very weak, being typically one or two orders of magnitude less than the exchange between nearest neighbours, the dipole-dipole coupling is both highly anisotropic and extremely long-ranged, and may therefore have important effects on both magnetic structures and excitations. Apart from this example, the anisotropic two-ion couplings are even more difficult to calculate than are the isotropic components, so the strategy which has generally been adopted to investigate them is to

assume that all terms in (1.4.24) which are not forbidden by symmetry are present, to calculate their influence on the magnetic properties, and to determine their magnitude by judicious experiments.

The *hyperfine interaction* between the $4f$ moment and the nuclear spin \mathbf{I} may be written

$$\mathcal{H}_{\text{hf}} = A \sum_i \mathbf{I}_i \cdot \mathbf{J}_i. \quad (1.4.27)$$

Since A is typically of the order of micro-electron-volts, the coupling to the nuclei normally has a negligible effect on the electronic magnetism in the rare earth metals, but we shall see in Sections 7.3 and 7.4 that it has a decisive influence on the low-temperature ordering in Pr.

1.5 Rare earth magnetism

The interactions discussed in the preceding section are the origin of the characteristic magnetic properties of the rare earth metals. The long-range and oscillatory indirect exchange gives rise to *incommensurable periodic structures*, the crystal fields and anisotropic two-ion coupling induce a *magnetic anisotropy* which may require fields up to hundreds of tesla to overcome, and the magnetoelastic interactions cause *magnetostrictive strains* which may approach one per cent. In the following, we shall give a brief description of some features of rare earth magnetism, as a prelude to a more detailed discussion of selected structures in the next chapter, and as a necessary basis for our later treatment of magnetic excitations. We have emphasized general principles, with appropriate illustrations, and have not attempted an exhaustive description of the magnetic properties of each element. This task has been accomplished by McEwen (1978), following earlier surveys by Rhyne (1972) and Coqblin (1977), and we shall refer to his comprehensive review article for further details, while quoting more recent investigations where appropriate.

Below the critical temperatures, listed in Table 1.6 on page 57, the rare earth metals form magnetically ordered phases. In the heavy elements, the maximum moment of $g\mu_B J$ per ion is approached in moderate fields at low temperatures. As is also apparent from Table 1.6, there is an additional contribution from the conduction electrons, which is almost 10% of the total moment in Gd, and appears to fall with S , as expected from (1.3.23). In their ordered phases, all the moments in a particular plane normal to the c -axis are aligned but, as illustrated in Fig. 1.19, their relative orientations may change from plane to plane. The magnetic structures of the heavy rare earths, which have been thoroughly reviewed by Koehler (1972) and Sinha (1978), derive basically from two different configurations of moments. In the *helix*, the expectation values

of the moments take the form:

$$\begin{aligned}\langle J_{i\xi} \rangle &= \langle J_{\perp} \rangle \cos(\mathbf{Q} \cdot \mathbf{R}_i + \varphi) \\ \langle J_{i\eta} \rangle &= \langle J_{\perp} \rangle \sin(\mathbf{Q} \cdot \mathbf{R}_i + \varphi) \\ \langle J_{i\zeta} \rangle &= 0,\end{aligned}\tag{1.5.1}$$

while the *longitudinal wave*, sometimes known in the heavy rare earths as the *c-axis modulated structure* or CAM, is described by

$$\langle J_{i\zeta} \rangle = \langle J_{\parallel} \rangle \cos(\mathbf{Q} \cdot \mathbf{R}_i + \varphi),\tag{1.5.2}$$

with the two other components being zero. The wave-vectors \mathbf{Q} are along the *c*-axis, and the associated wavelength $2\pi/Q$ does not necessarily bear any simple relationship to the lattice spacing.

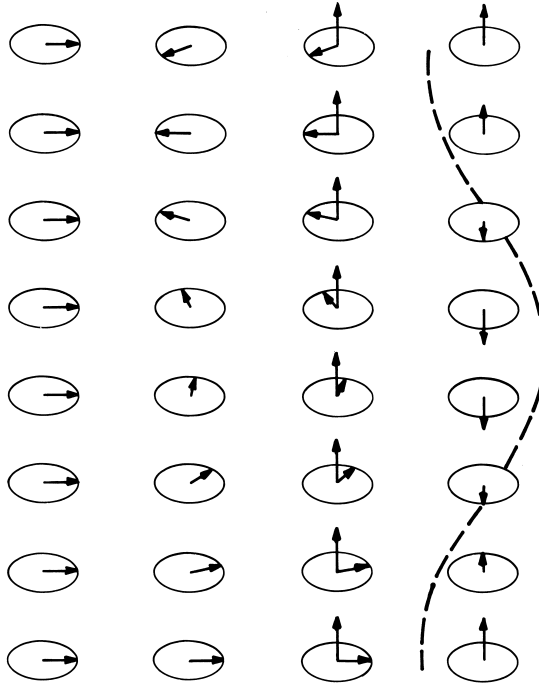


Fig. 1.19. Magnetic structures of the heavy rare earths. The moments in a particular hexagonal layer are parallel, and the relative alignments of different planes are illustrated. From left to right; the basal-plane ferromagnet, the helix, the cone, and the longitudinal-wave structure.

A helix is formed at the Néel temperature in Tb, Dy, and Ho, while the longitudinal-wave structure is preferred in Er and Tm. If the \mathbf{Q} -vectors are zero, a *ferromagnetic structure* results, with the ordered moment along some specified direction. In Tb and Dy at low temperatures, the easy direction of magnetization lies in the plane, while in Gd, which has a very small magnetic anisotropy, it is along the c -axis just below the Curie temperature, but is tilted about 30° towards the b -axis at low temperatures. If a ferromagnetic component in the c -direction is added to the helix, the moments rotate on the surface of a cone with its axis in the c -direction. This *conical structure* is stable in both Ho and Er at the lowest temperatures, but the cone angle between the c -axis and the moments at 4 K is large (about 80°) in the former, and small (about 30°) in the latter. If the plane of the moments in the helix is rotated about an axis in the hexagonal plane, so that its normal makes a non-zero angle with \mathbf{Q} , the structure becomes the *tilted helix*, which may be regarded as a combination of a helix and a longitudinal wave, with the same \mathbf{Q} -vectors. This structure has not been definitively identified in the elements in zero field. The moments in the hexagonal plane of Er do order below 52 K, with the same period as the c -axis modulation, but they are most probably confined to the a - c plane, in an elliptically polarized *cycloidal structure* (Miwa and Yosida 1961; Nagamiya 1967) in the whole temperature interval between 52 K and the transition to the cone (Jensen 1976b). As the temperature is reduced, in the modulated c -axis phases, the moments on the individual sites approach their saturation values, resulting in a squaring of the longitudinal wave which manifests itself in higher odd harmonics. This phenomenon is observed in both Er and Tm and, in the latter, results in a low-temperature ferrimagnetic *square-wave structure* in which alternately four layers of moments point up and three layers point down.

The hexagonal anisotropy B_6^6 tends to distort the helical structure, by deflecting the moments towards the nearest easy axis. In a helix which is *incommensurable* with the lattice periodicity, this effect may be treated by perturbation theory, which predicts a change of the energy in second order. However, in Ho at low temperatures, B_6^6 is so large that the magnetic structure is forced to be *commensurable* with the lattice, so that \mathbf{Q} has the magnitude $\pi/3c$, and the turn angle between the moments in successive planes averages 30° . It was verified experimentally by Koehler *et al.* (1966) that, under these circumstances, the large hexagonal anisotropy causes the helix to distort so that the moments in the plane bunch about the b -directions, as illustrated in Fig. 1.20. This *bunched helix* is described by

$$\begin{aligned} \langle J_{i\xi} \rangle &= \langle J_\perp \rangle (u \sin \mathbf{Q} \cdot \mathbf{R}_i - v \sin 5\mathbf{Q} \cdot \mathbf{R}_i) \\ \langle J_{i\eta} \rangle &= \langle J_\perp \rangle (u \cos \mathbf{Q} \cdot \mathbf{R}_i + v \cos 5\mathbf{Q} \cdot \mathbf{R}_i), \end{aligned} \quad (1.5.3a)$$

where

$$u = \cos(\pi/12 - \phi) \quad ; \quad v = \sin(\pi/12 - \phi), \quad (1.5.3b)$$

and any moment deviates from the nearest b -axis by the *bunching angle* ϕ . At 4 K, ϕ in Ho is 5.8° , and it increases monotonically with temperature towards the value 15° which characterizes the uniform commensurate helix. An increase in temperature also causes an increase in Q , but it was shown by Gibbs *et al.* (1985) that this change does not occur smoothly and continuously. Instead, the magnetic periodicity tends to lock in to values commensurate with the lattice, and they proposed that this is a manifestation of *spin-slip structures*, in which the moments are arranged in a pattern in which one of the planes in regularly spaced members of the bunched doublets of Fig. 1.20 is omitted, while the remaining plane of the pair orients its moments along the adjacent easy axis. We shall discuss such structures in more detail in the next chapter.

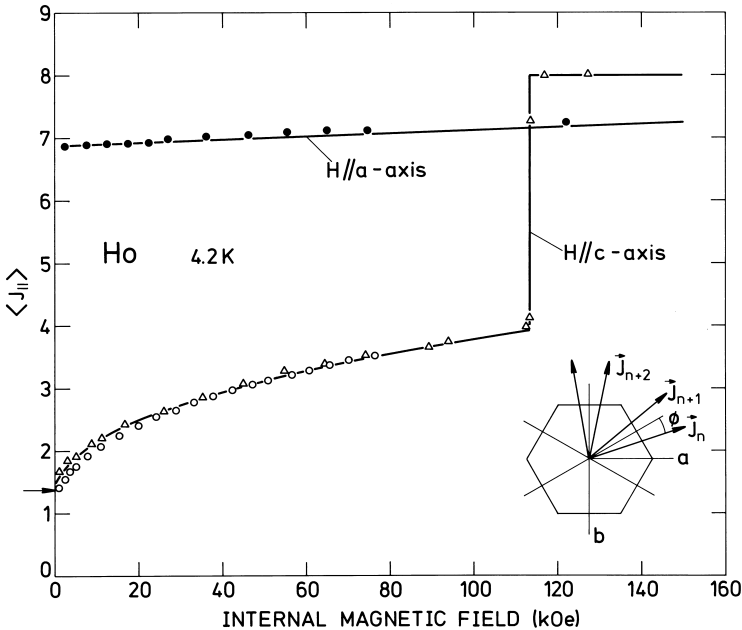


Fig. 1.20. The $4f$ contribution to the magnetization of Ho at 4 K, calculated by a self-consistent mean-field theory and compared with experimental values. The zero-field structure is a bunched cone, comprising the illustrated bunched helix in the plane, and a small moment in the c -direction. The value of the c -axis moment, deduced from neutron-diffraction measurements, is indicated by the arrow.

The aforementioned magnetic structures may readily be understood as the result of the co-operation and competition between the oscillatory indirect exchange, which is relatively strong in the heavy rare earths, because $(g-1)J$ is generally large, and the crystal-field and magnetoelastic anisotropy forces. The origin of the periodic structures can be explained by writing (1.4.21) in the form

$$\mathcal{H}_{\text{ff}} = -\frac{N}{2} \sum_{\mathbf{q}} \mathcal{J}(\mathbf{q}) \mathbf{J}(\mathbf{q}) \cdot \mathbf{J}(-\mathbf{q}), \quad (1.5.4)$$

where the Fourier transform of the magnetic structure is

$$\mathbf{J}(\mathbf{q}) = \frac{1}{N} \sum_i \mathbf{J}_i e^{-i\mathbf{q} \cdot \mathbf{R}_i}. \quad (1.5.5)$$

In order to minimize the energy of the magnetic system, this term will favour a \mathbf{Q} vector which corresponds to the maximum in $\mathcal{J}(\mathbf{q})$. The maxima shown in Fig. 1.17 thus reflect the observed \mathbf{Q} values in the heavy rare earths through their position, and the relative stability of the periodic structures through their magnitude. The isotropic exchange does not in itself specify any orientation of the moments relative to the crystal axes. The normal to a planar helix can, for example, be rotated into an arbitrary direction without altering the exchange energy. This flexibility is realized in Eu, where the crystal-field anisotropy is very small because, like Gd, it has no ionic orbital moment. Neutron-diffraction studies of a single crystal by Millhouse and McEwen (1973) showed a first-order transition to a helical structure, and magnetization measurements indicate that the plane of the helical structure is always normal to the direction of a moderate applied field, even though \mathbf{Q} remains along a four-fold axis of the bcc structure.

It is the magnetic anisotropy which fixes the magnetic structure relative to the crystal axes. As may be seen from eqn (1.4.4), the two-fold axial anisotropy (proportional to J_{ζ}^2) is also proportional to the Stevens factor α . If A_2^0 is negative throughout the heavy rare earths, as we shall see is the case, the values in Table 1.4 immediately explain why Tb and Dy have easy axes in the hexagonal plane, while the moments in Tm are strongly bound to the c -axis. In Ho and Er the higher-order axial anisotropy is important, but the values of α are consistent with the respectively large and small cone angles. Similarly, the alternation in the sign of γ in the series of the heavy elements is reflected in the easy directions of magnetization in the hexagonal plane. The competition between the exchange and the anisotropy is manifested in the low-temperature magnetic structures. In the ferromagnetic phases of Tb and Dy, the

anisotropy and magnetoelastic forces, which are averaged out or ineffective in the helical structure, are strong enough to overcome the relatively weak tendency to periodic ordering. In Tm, on the other hand, a compromise obtains, by which the moments take their maximum value along the c -axis, but alternate in direction so as to take advantage of the large peak in $\mathcal{J}(\mathbf{q})$. In Ho, the balance is so delicate that the weak classical dipolar interaction plays a crucial role, as we shall discuss in Section 2.3.

In order to explain the temperature dependence of the structures, it is necessary to determine the configuration of the moments which minimizes the *free energy*, taking into account the influence of increasing temperature and magnetic disorder on the interactions. Provided that the magnitude $|\langle \mathbf{J}_i \rangle|$ of the ordered moment is the same on all sites, the *entropy* term is independent of the details of the ordering (Elliott 1961), so the stable structure has the minimum *energy*. In exchange-dominated systems, like the heavy rare earths, the ordered moment approaches its saturation value at low temperature. As the temperature is increased, the structure which has the lowest energy may change as the effective interactions *renormalize*. This may occur either through a *second-order* transition, in which some *order-parameter* goes continuously to zero or, more commonly, discontinuously through a *first-order* transition. At elevated temperatures, the entropy may favour a structure, such as the longitudinal wave, in which the degree of order varies from site to site.

A conceptually simple but powerful means of calculating magnetic properties, and their dependence on the temperature, is provided by the molecular-field approximation or *mean-field theory*. We shall describe this method in some detail in the next chapter, but it is convenient to introduce it here in order to establish a few elementary results. The essential feature of the theory is the approximation of the two-ion interactions by effective single-ion terms, by replacing the instantaneous values of the \mathbf{J} operators on the surroundings of any particular ion by their thermal averages. The effect of the exchange interaction (1.4.21) with the surrounding ions on the moment at \mathbf{R}_i may then be written

$$\mathcal{H}_{\text{ff}}(i) \simeq -(\mathbf{J}_i - \frac{1}{2}\langle \mathbf{J}_i \rangle) \cdot \sum_j \mathcal{J}(ij)\langle \mathbf{J}_j \rangle, \quad (1.5.6)$$

which in turn may be written in terms of an effective magnetic field

$$\mathbf{H}_{\text{eff}}(i) = (g\mu_B)^{-1} \sum_j \mathcal{J}(ij)\langle \mathbf{J}_j \rangle, \quad (1.5.7)$$

plus a constant contribution to the energy. If the sum of the applied and effective fields is small, which will generally be true in the paramagnetic

phase (but not if spontaneous ordering occurs), the magnetic moment of the system per unit volume, neglecting the anisotropy, is given by Curie's law (1.2.32):

$$\mathbf{M} = \frac{g^2 \mu_B^2 J(J+1) N}{3k_B T} \frac{1}{V} (\mathbf{H} + \mathbf{H}_{\text{eff}}). \quad (1.5.8)$$

For a uniform system, we may write

$$\mathbf{H}_{\text{eff}} = \frac{1}{g^2 \mu_B^2} \frac{V}{N} \sum_j \mathcal{J}(ij) \mathbf{M} = \frac{\mathcal{J}(\mathbf{0})}{g^2 \mu_B^2} \frac{V}{N} \mathbf{M}, \quad (1.5.9)$$

recalling that

$$\mathcal{J}(\mathbf{q}) = \sum_j \mathcal{J}(ij) e^{-i\mathbf{q} \cdot (\mathbf{R}_i - \mathbf{R}_j)}, \quad (1.5.10)$$

and the susceptibility is therefore

$$\chi_{\text{MF}} = \frac{g^2 \mu_B^2 J(J+1) N}{3k_B T} \frac{1}{V} \left[1 - \frac{\mathcal{J}(\mathbf{0}) J(J+1)}{3k_B T} \right]^{-1} \equiv \frac{C}{T - \theta}, \quad (1.5.11)$$

where C is the Curie constant (1.2.32), and the *paramagnetic Curie temperature* is

$$\theta = \frac{\mathcal{J}(\mathbf{0}) J(J+1)}{3k_B}. \quad (1.5.12)$$

From the *Curie-Weiss law* (1.5.11) it is apparent that, if nothing else happens, the susceptibility diverges at θ , which is therefore also the Curie temperature T_C at which spontaneous ferromagnetism occurs in this model.

The bulk magnetic properties of the rare earths are summarized in Table 1.6, where the moments are given in units of μ_B/ion , and the temperatures in K . The theoretical paramagnetic moments per ion are $\mu = g\{J(J+1)\}^{1/2}\mu_B$, and are compared with values deduced from the linear magnetic susceptibilities in the paramagnetic phases, using (1.5.11). The theoretical saturation moments per ion are $g\mu_B J$, from (1.2.30), and are compared with low-temperature values, in fields high enough essentially to saturate the magnetization, or in the highest fields in which measurements have been made (McEwen *et al.* 1973). θ_{\parallel} and θ_{\perp} are the paramagnetic Curie temperatures, deduced from measurements with a field applied respectively parallel and perpendicular to the c -axis, and using (1.5.11). As we shall see in Section 2.1.1, there are corrections to this expression at finite temperatures, which give rise to a non-linearity in the inverse susceptibility. A simple linear extrapolation

therefore gives values for the paramagnetic Curie temperatures which depend on the highest temperature of the measurements. The fit to the experimental results for Tm illustrated in Fig. 2.1, for example, in which the mean-field corrections are taken into account, gives θ_{\parallel} and θ_{\perp} as respectively 52 K and -3 K, which differ significantly from the values deduced from a linear extrapolation of the same results, given in Table 1.6. A similar analysis for Er yields 69 K and 46 K. The ordering temperatures are determined either from bulk measurements or neutron diffraction. T_N and T_C denote transition temperatures to magnetically-ordered states without and with a net moment respectively, and values are given for sites of both kinds of symmetry, in the light rare earths.

Table 1.6. Magnetic properties of rare earth metals.

Metal	Para. moment		Sat. moment		θ_{\parallel}	θ_{\perp}	T_N		T_C
	μ	Obs.	gJ	Obs.			hex.	cub.	
Ce	2.54	2.51	2.14	0.6			13.7	12.5	
Pr	3.58	2.56	3.20	2.7 ^a			0.05		
Nd	3.62	3.4	3.27	2.2 ^a			19.9	8.2	
Pm	2.68		2.40						
Sm	0.85	1.74	0.71	0.13 ^a			106	14.0	
Eu	7.94	8.48	7.0	5.1 ^a				90.4	
Gd	7.94	7.98	7.0	7.63	317	317			293
Tb	9.72	9.77	9.0	9.34	195	239	230		220
Dy	10.65	10.83	10.0	10.33	121	169	179		89
Ho	10.61	11.2	10.0	10.34	73	88	132		20
Er	9.58	9.9	9.0	9.1	62	33	85		20
Tm	7.56	7.61	7.0	7.14	41	-17	58		32

^a Values measured at 38 tesla.

A straightforward generalization of the above argument (see Section 2.1) gives the response of the ions in the paramagnetic phase to a spatially varying magnetic field with wave-vector \mathbf{q} . The corresponding susceptibility tensor (not to be confused with that for the conduction-electron gas) is

$$\chi_{\text{MF}}(\mathbf{q}) = \frac{g^2 \mu_B^2 J(J+1) N}{3k_B T} \frac{N}{V} \left[1 - \frac{\mathcal{J}(\mathbf{q}) J(J+1)}{3k_B T} \right]^{-1} = \frac{C}{T - T_N}. \quad (1.5.13)$$

Spontaneous ordering is therefore predicted to occur at the wave-vector

\mathbf{Q} for which $\mathcal{J}(\mathbf{q})$ has its maximum value, and the Néel temperature is

$$T_N = \frac{\mathcal{J}(\mathbf{Q})J(J+1)}{3k_B}. \quad (1.5.14)$$

Since, from (1.4.22), $\mathcal{J}(\mathbf{q})$ varies as $(g-1)^2$, the critical temperature is expected to be proportional to the *de Gennes factor* $(g-1)^2J(J+1)$, provided that the susceptibility of the conduction-electron gas is constant. As may be seen from Tables 1.1 and 1.6, this relationship is rather accurately obeyed for the heavy rare earths, though not so well in the light elements. The crystal-field interactions influence the critical temperatures significantly, especially in the light end of the series, and both the electronic susceptibility and the matrix elements of the *sf*-exchange coupling, which together determine the indirect spin-spin interaction $\mathcal{J}_S(\mathbf{q})$, change through the series. The scaling of the critical temperature with the de Gennes factor is therefore more precise than would have been anticipated. The mean-field theory is known to be inadequate in the vicinity of the critical temperature, but as the rare earth metals are three-dimensional systems with long-range interactions, the transition temperature itself is rather well determined by this approximation. The theory is valid at high temperatures, and should describe the static magnetic structures adequately in the low-temperature limit. The discussion of the dynamical behaviour requires a time-dependent generalization of the mean-field, accomplished by the *random-phase approximation*. We shall later describe how low-temperature corrections to the mean-field properties may be derived from the magnetic-excitation spectrum, determined within the random-phase approximation. The discussion of the detailed behaviour close to the critical temperature, i.e. the *critical phenomena*, is however beyond the scope of this book, and we refer instead to the recent introduction to the subject by Collins (1989), and to the specialist literature on the application of statistical mechanics to phase transitions.

In mean-field theory, the exchange energy varies like σ^2 , where the relative magnetization $\sigma(T)$ is $|\langle \mathbf{J} \rangle|/J$. However, the anisotropy energy generally changes more rapidly with magnetization. The crystal-field parameters B_l^m in (1.4.6) are generally assumed to vary only slightly with temperature, but the thermal average $\langle O_l^m(\mathbf{J}) \rangle$ is very dependent on the degree of ordering. By treating the deviation in the direction of the moment on a particular site from the perfectly ordered state as a random walk on a sphere, Zener (1954) showed that

$$\langle O_l^m(\mathbf{J}) \rangle_T = \langle O_l^m(\mathbf{J}) \rangle_{T=0} \sigma^{l(l+1)/2}. \quad (1.5.15)$$

We shall discuss the derivation of this thermal average by mean-field theory in Section 2.2, and show that Zener's result is indeed correct at

low temperatures. Since the anisotropy energy is very small just below the critical temperature, the exchange dominates and gives rise to periodic magnetic structures in the heavy rare earths, except in Gd where the peak in $\mathcal{J}(\mathbf{q})$ occurs at $\mathbf{q} = \mathbf{0}$. As the temperature is lowered, the anisotropy forces become relatively more important, and phase transitions occur to structures in which their influence is apparent. A less obvious but nevertheless important effect is that $\mathcal{J}(\mathbf{q})$ itself changes substantially with temperature. As was mentioned in the last section, the peak reflects a maximum in the conduction-electron $\chi(\mathbf{q})$, which is determined by the form of the Fermi surface. Because of the interaction (1.3.23) between the local moments and the spins of the conduction electrons, the latter experience a potential with a period which is generally different from that of the lattice, and therefore generates extra energy gaps in the band structure. These *magnetic superzone* gaps, which we shall discuss in more detail in Section 5.7, may be of the order of 10 mRy and therefore perturb the energy spectrum of the conduction electrons significantly. In particular, the regions of the Fermi surface responsible for the peak in $\mathcal{J}(\mathbf{q})$ are severely modified, as has been verified through calculations on Tm by Watson *et al.* (1968). The result is that both the *position* of the peak is changed and its *magnitude* is reduced. As a consequence, periodic magnetic structures tend to be self-destructive; as they become established they try to eliminate the characteristic of the exchange which ensures their stability. These effects were studied by Elliott and Wedgwood (1964), who used a free-electron model to explain the variation of \mathbf{Q} in the heavy metals. Although their model is greatly over-simplified, it illustrates the essential features of the problem. We shall see in Chapters 2 and 5 that this variation in $\mathcal{J}(\mathbf{q})$ is necessary to explain the change in both the magnetic structures and excitations with temperature.

Whereas the magnetic structures of the heavy rare earths can be accounted for by recognizing the dominant role of the exchange, and considering the crystal fields and magnetoelastic effects as perturbations, whose essential role is to establish favoured directions for the moments in the lattice, the balance in the light elements is not so clear-cut. Since g is generally close to 1, the exchange is relatively weak, and the larger values of $\langle r^l \rangle$ towards the beginning of the series are expected to make crystal-field effects relatively important. As a result, the latter are able to hinder the moments from attaining their saturation values of $g\mu_B J$, even in high fields at low temperatures, as illustrated in Table 1.6.

The most remarkable manifestation of the influence of the crystal fields is found in Pr, where they are able effectively to frustrate the efforts of the exchange to produce a magnetically ordered state. As illustrated in Fig. 1.16, the ground state on the hexagonal sites is the $|J_C = 0\rangle$

singlet which, in common with all singlet states, carries no moment. The first term in (1.2.24) therefore gives no contribution to the susceptibility, but the mixing of the $|\pm 1\rangle$ excited doublet into the ground state by the field gives a Van Vleck susceptibility at low temperatures which, if we neglect the exchange, has the form

$$\chi = \frac{2g^2\mu_B^2 M_\alpha^2 N}{\Delta V}, \quad (1.5.16)$$

where $M_\alpha^2 = |\langle \pm 1 | J_\alpha | 0 \rangle|^2$ is the square of the matrix element of the component of \mathbf{J} in the field direction, and Δ is the energy separation between the ground state and the first excited state. Since M_α is zero when the field is applied along the c -axis, no moment is initially generated on the hexagonal sites, as confirmed by the neutron diffraction measurements of Lebeck and Rainford (1971), whereas the susceptibility in the basal plane is large. An applied field in the c -direction changes the relative energies of the crystal-field levels however, and at 4.2K a field of 32 tesla induces a first-order *metamagnetic* transition to a phase with a large moment (McEwen *et al.* 1973), as shown in Fig. 7.13. This is believed to be due to the crossing of the ground state by the *second* excited state, as illustrated in Fig. 7.12.

If the exchange is included in the mean-field approximation, the \mathbf{q} -dependent susceptibility becomes, in analogy with (1.5.13),

$$\chi_{\text{MF}}(\mathbf{q}) = g^2\mu_B^2 \frac{N}{V} \left[\frac{\Delta}{2M_\alpha^2} - \mathcal{J}(\mathbf{q}) \right]^{-1}. \quad (1.5.17)$$

From this expression, it is apparent that the susceptibility diverges, corresponding to spontaneous ordering, if

$$\frac{2\mathcal{J}(\mathbf{q})M_\alpha^2}{\Delta} \geq 1. \quad (1.5.18)$$

The magnetic behaviour of such a singlet ground-state system is therefore determined by the balance between the exchange and the crystal field. If the exchange is strong enough, magnetic ordering results; otherwise paramagnetism persists down to the absolute zero. In Pr, the crystal-field splitting is strong enough to preclude magnetic order, but the exchange is over 90% of that required for antiferromagnetism. We shall return to the consequences of this fine balance in Chapter 7.

The remaining close-packed light rare earths Ce, Nd, and Sm, which are amenable to experimental study (radioactive Pm is very intractable), all have an odd number of $4f$ electrons and thus, according to *Kramers' theorem*, crystal-field levels with even degeneracy and a magnetic moment. The crystal fields cannot therefore suppress magnetic ordering,

but they reduce the ordered moment and contribute to the complexity of the magnetic structures (Sinha 1978), which is exacerbated by the two different site-symmetries in each of the metals. The magnetic structure of Ce has not been fully determined, but it now seems (Gibbons *et al.* 1987) that commensurable transverse waves are formed on both the hexagonal and cubic sites, with \mathbf{Q} in a b -direction and the moments pointing along an a -axis in the plane. The magnetic periodicity is twice that of the lattice. This relatively straightforward structure is in marked contrast to that of Nd, which displays an extraordinary complexity. An incommensurable longitudinal wave in a b -direction is formed on the hexagonal sites through a first-order transition at T_N , with a simple antiferromagnetic arrangement of successive hexagonal layers. As the temperature is lowered, a further first-order transition takes place within a degree to a double- \mathbf{Q} structure (McEwen *et al.* 1985). At a still lower temperature, an incommensurable periodic structure in the b -direction is also formed on the cubic sites. At the lowest temperatures, the moments assume an elaborate quadruple- \mathbf{Q} pattern (Forgan *et al.* 1989), which we shall discuss in more detail in Chapter 2. The magnetic structure on the hexagonal sites of Sm comprises pairs of planes with the moments arranged ferromagnetically in the c -direction (Koehler and Moon 1972). Adjacent pairs are coupled antiferromagnetically and separated by the cubic sites. The latter also order antiferromagnetically, with the moments along the c -axis, at low temperatures, but the normal to the ferromagnetic sheets is now in the b - c plane. Although the magnetic structures of the light rare earths are phenomenologically reasonably well described, the explanation of their origin in terms of the crystal-field and exchange interactions is still at a rudimentary stage.

The application of a magnetic field adds to the Hamiltonian a term

$$\mathcal{H}_Z = -g\mu_B \sum_i \mathbf{J}_i \cdot \mathbf{H}. \quad (1.5.19)$$

In a sufficiently large field, the stable configuration is thus an array of moments $g\mu_B J$ pointing along the field direction. The intermediate states between the zero-field structure and the high-field limit may however be very complex. In Fig. 1.20 on page 53 is shown a relatively simple example of the magnetization curves which result when a cone structure undergoes first-order transitions to the almost fully-aligned ferromagnetic state. We will discuss the effect of a magnetic field on periodic magnetic structures in some detail in Section 2.3, and therefore restrict ourselves for the moment to outlining the results of the mean-field treatment of Nagamiya *et al.* (1962) of the helical structure without planar anisotropy, to which a field is applied in the plane. The ferromagnetic

structure is reached at a field

$$H_c = \frac{J[\mathcal{J}(\mathbf{Q}) - \mathcal{J}(\mathbf{0})]}{g\mu_B}, \quad (1.5.20)$$

but there is an intermediate transition, occurring at approximately $H_c/2$, at which the helix transforms abruptly through a first-order transition to a *fan structure*, in which the moments make an angle θ with the field direction, given by

$$\sin \frac{\theta_i}{2} = \left\{ \frac{2g\mu_B(H_c - H)}{J[3\mathcal{J}(\mathbf{Q}) - 2\mathcal{J}(\mathbf{0}) - \mathcal{J}(2\mathbf{Q})]} \right\}^{1/2} \sin \mathbf{Q} \cdot \mathbf{R}_i. \quad (1.5.21)$$

The opening angle of the fan thus goes continuously to zero at the second-order transition to the ferromagnetic phase.

The crystal fields manifest themselves in both microscopic and macroscopic magnetic properties. The macroscopic anisotropy parameters κ_l^m are defined as the coefficients in an expansion of the free energy in spherical harmonics, whose polar coordinates (θ, ϕ) specify the magnetization direction relative to the crystallographic axes. For hexagonal symmetry,

$$F(\theta, \phi) = N[\kappa_0(T) + \kappa_2^0(T)P_2(\cos \theta) + \kappa_4^0(T)P_4(\cos \theta) + \kappa_6^0(T)P_6(\cos \theta) + \kappa_6^6(T)\sin^6 \theta \cos 6\phi], \quad (1.5.22)$$

where $P_l(\cos \theta) = (4\pi/2l + 1)^{1/2}Y_{l0}(\theta, \phi)$ are the Legendre polynomials. Anisotropic two-ion coupling and magnetoelastic strains may introduce additional higher-rank terms of the appropriate symmetry. If the Hamiltonian is written in a representation $\mathcal{H}(\theta, \phi)$ in which the quantization axis is along the magnetization, the macroscopic and microscopic parameters are related by

$$F(\theta, \phi) = -\frac{1}{\beta} \ln \text{Tr}\{e^{-\beta\mathcal{H}(\theta, \phi)}\}. \quad (1.5.23)$$

Transforming the Stevens operators to a coordinate system with the z -axis along the magnetization direction, and assuming that the isotropic exchange is the dominant interaction, we find at absolute zero

$$\begin{aligned} \kappa_2^0(0) &= 2B_2^0 J^{(2)} & \kappa_4^0(0) &= 8B_4^0 J^{(4)} \\ \kappa_6^0(0) &= 16B_6^0 J^{(6)} & \kappa_6^6(0) &= B_6^6 J^{(6)} \end{aligned} \quad (1.5.24)$$

where

$$J^{(n)} \equiv J(J - \frac{1}{2})(J - 1) \cdots (J - \frac{n-1}{2}). \quad (1.5.25)$$

There are a number of different experimental methods for obtaining values for the microscopic and macroscopic anisotropy parameters. The susceptibility in different directions, or equivalently the torque on a crystal in a field, can be measured either in the paramagnetic or magnetically ordered phases and, as we shall discuss in detail later, much information may be obtained from the excitation spectrum and its field dependence. The values of $\kappa_l^m(0)$ obtained from these various sources for the different elements have been reviewed and tabulated by McEwen (1978).

In order to deduce the crystal-field parameters B_l^m in the absence of exchange and magnetoelastic effects, Touborg and his collaborators studied the crystal-field states of dilute alloys of the magnetic rare earths in the non-magnetic hosts Sc, Y, and Lu, utilizing magnetization measurements and, to a limited extent, neutron spectroscopy. Their results for heavy rare earth solutes have been reviewed by Touborg (1977) and, for the light elements, by Touborg *et al.* (1978). Within the uncertainty of the measurements and of the interpretation, and with the exception of Ce in Y, which behaves anomalously, they found that a common set of parameters B_l^m/α_l accounts for the behaviour of all solutes in a particular host. B_4^0/β and B_6^0/γ are roughly 10 K/ion and 15 K/ion respectively in all cases, while B_6^0 is close to the value $-\frac{77}{8}B_6^0$ which the point-charge model would predict. B_2^0/α increases from about 30 K/ion in Sc, to 45 K/ion in Lu, to 100 K/ion in Y, which correlates with the deviation of the c/a ratio of the host metal (1.592 for Sc, 1.584 for Lu, and 1.573 for Y) from the ideal value of 1.633 (Orlov and Jensen 1988). It is noteworthy that the parameters B_l^m/α_l show no obvious correlation with $\langle r^l \rangle$, as would be anticipated from (1.4.4).

The values of B_l^m from these studies of dilute alloys may be compared with those from other sources. In particular, B_2^0 may be estimated for the pure metals by interpolating between the c/a ratios of the non-magnetic hosts. These values may then be compared with those deduced from the difference between the paramagnetic Curie temperatures parallel and perpendicular to the c -axis, which is shown in Section 2.1 to be given by

$$B_2^0 = \frac{5k_B(\theta_\perp - \theta_\parallel)}{6(J - \frac{1}{2})(J + \frac{3}{2})}. \quad (1.5.26)$$

The agreement for the heavy rare earths is in all cases good (McEwen 1978), indicating that the crystal fields measured in dilute alloys are related to those acting in the pure metals. On the other hand, the values deduced from torque and magnetization measurements at low temperatures in the ferromagnetic state show large discrepancies with those in the paramagnetic phase. For Tb and Dy, the former are roughly three times the latter. Despite this discrepancy, which is probably primarily

due to the anisotropic two-ion coupling in the magnetically ordered phases, the axial anisotropy parameter $\kappa_2^0(T) - \frac{5}{2}\kappa_4^0(T) + \frac{35}{8}\kappa_6^0(T)$, where $\kappa_2^0(T)$ is the dominating term, depends on temperature approximately as predicted by (1.5.15), varying roughly as σ^3 in Dy and σ^4 in Tb. We shall return to the question of the anisotropy parameters in the rare earths when we discuss the structures and excitations.

The large magnetoelastic effects have a profound effect on the magnetic properties of the rare earths, making a significant contribution to the anisotropy, playing a decisive role in some instances in determining the structures, and modifying the excitation spectrum. We here consider for illustrative purposes a special example, the basal-plane ferromagnet, exemplified by Tb and Dy. As mentioned previously, the α -strains maintain the symmetry and therefore only have the effect of renormalizing the B_l^m , and if the moments are confined to the plane, the ε -strains vanish. However, the γ -strains are large and symmetry-breaking, and thereby cause qualitative modifications in the magnetic behaviour. From (1.4.8) and (1.4.11), their contribution to the magnetoelastic Hamiltonian may be written

$$\mathcal{H}_\gamma = \sum_i \left[\frac{1}{2}c_\gamma(\epsilon_{\gamma 1}^2 + \epsilon_{\gamma 2}^2) - B_{\gamma 2}\{O_2^2(\mathbf{J}_i)\epsilon_{\gamma 1} + O_2^{-2}(\mathbf{J}_i)\epsilon_{\gamma 2}\} \right. \\ \left. - B_{\gamma 4}\{O_4^4(\mathbf{J}_i)\epsilon_{\gamma 1} - O_4^{-4}(\mathbf{J}_i)\epsilon_{\gamma 2}\} \right], \quad (1.5.27)$$

where we have included only the lowest ranks ($l = 2$ and 4 respectively) of the $\gamma 2$ and $\gamma 4$ terms. As shown in Section 2.2, the condition

$$\partial F / \partial \epsilon_\gamma = 0 \quad (1.5.28)$$

leads to the equilibrium strains

$$\epsilon_{\gamma 1} = \frac{1}{c_\gamma}(B_{\gamma 2}\langle O_2^2 \rangle + B_{\gamma 4}\langle O_4^4 \rangle) \\ \epsilon_{\gamma 2} = \frac{1}{c_\gamma}(B_{\gamma 2}\langle O_2^{-2} \rangle - B_{\gamma 4}\langle O_4^{-4} \rangle). \quad (1.5.29)$$

Transforming the Stevens operators as before, and using (1.5.15) to estimate the magnetization dependence of the thermal averages, we obtain

$$\epsilon_{\gamma 1} = C \cos 2\phi - \frac{1}{2}A \cos 4\phi \\ \epsilon_{\gamma 2} = C \sin 2\phi + \frac{1}{2}A \sin 4\phi, \quad (1.5.30)$$

where

$$C = \frac{1}{c_\gamma}B_{\gamma 2}J^{(2)}\sigma^3 \\ A = -\frac{2}{c_\gamma}B_{\gamma 4}J^{(4)}\sigma^{10} \quad (1.5.31)$$

are the conventional magnetostriction parameters (Mason 1954), and ϕ

is the angle between the a -axis and the magnetization in the plane.

The dominant contribution to the magnetoelastic energy is

$$\langle \mathcal{H}_\gamma \rangle = -\frac{1}{2} N c_\gamma (\epsilon_{\gamma 1}^2 + \epsilon_{\gamma 2}^2) = -\frac{1}{2} N c_\gamma (C^2 + \frac{1}{4} A^2 - C A \cos 6\phi). \quad (1.5.32)$$

The $\cos 6\phi$ term makes a contribution to the hexagonal anisotropy, which is in total, from (1.5.24), (1.5.15), and (1.5.31),

$$\begin{aligned} \kappa_6^6(T) &= B_6^6 J^{(6)} \sigma^{21} + \frac{1}{2} c_\gamma C A \\ &= B_6^6 J^{(6)} \sigma^{21} - \frac{1}{c_\gamma} B_{\gamma 2} J^{(2)} B_{\gamma 4} J^{(4)} \sigma^{13}. \end{aligned} \quad (1.5.33)$$

The hexagonal anisotropy can readily be deduced from the critical field H_c necessary to rotate the moments from an easy direction to a neighbouring hard direction in the plane (respectively a b -axis and an a -axis in Tb), which is given by

$$g\mu_B J \sigma H_c = 36 |\kappa_6^6(T)|. \quad (1.5.34)$$

Values of the critical field for Tb are given as a function of σ in Fig. 1.21.

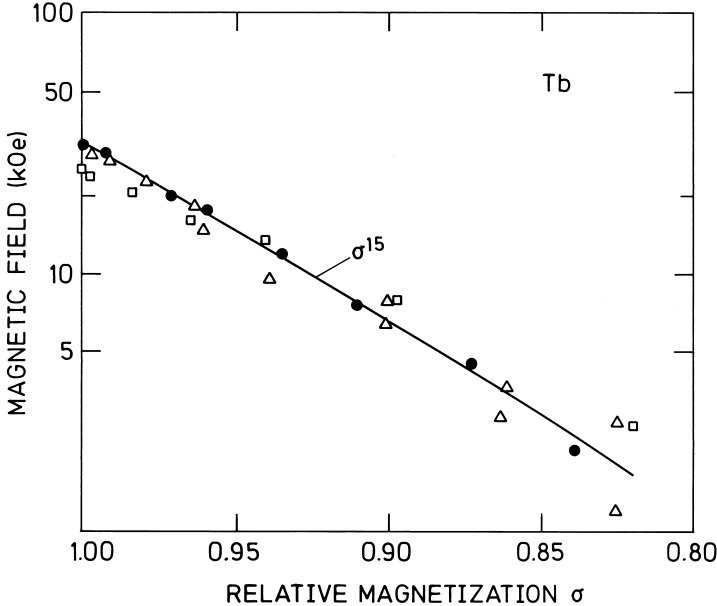


Fig. 1.21. The critical field H_c necessary to rotate the moments from an easy direction to a neighbouring hard direction in the plane in Tb, as a function of the reduced magnetization. The closed circles denote the results of neutron-scattering experiments, and the other signatures are deduced from macroscopic measurements.

The observed σ^{15} dependence on the magnetization indicates that the magnetoelastic term dominates. As illustrated in Fig. 1.22, C and A have been accurately determined by Rhyne and Legvold (1965a) from macroscopic strain-gauge measurements and, since the elastic constant is known (Jensen and Palmer 1979), the relative magnetoelastic and crystal-field contributions to (1.5.33) may readily be determined. At absolute zero, the former is 1.14 K/ion and the latter is -0.60 K/ion, rapidly becoming negligible as the temperature is increased. On account of the sign of the Stevens factor γ for Tb, the crystal-field contribution is expected to be positive, and this may be another indication of the importance of anisotropic two-ion coupling in the magnetically ordered phases.

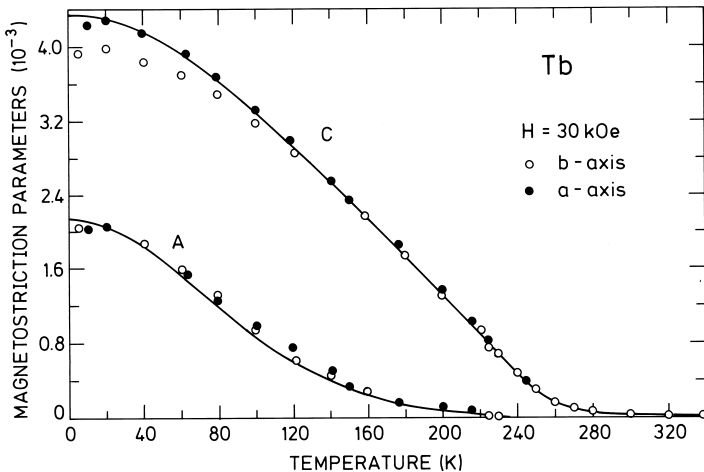


Fig. 1.22. The temperature dependence of the magnetostriction parameters C and A in Tb, after Rhyne and Legvold (1965a). The full lines show the results of the Callen-Callen theory presented in Section 2.2.

The magnetoelastic energy (1.5.32) is substantial in the ferromagnetic phase. In particular the term $-\frac{1}{2}c\gamma C^2$, which results from a magnetoelastic strain of *cylindrical* symmetry, is relatively important at high temperatures, because it renormalizes roughly as σ^4 , and is therefore still about 0.3 K/ion in Dy at 85 K, the temperature at which a first-order transition occurs from the helical to the ferromagnetic phase. The *hexagonally* symmetric contribution proportional to CA is small at all temperatures in Dy, since $A \approx 0$ (Martin and Rhyne 1977). In the helical phase, the lattice is *clamped* (Evenson and Liu 1969), so that the γ -strains are zero, and the magnetoelastic contribution to the stabilization energy is therefore absent. At T_C , this energy, plus a minor

contribution from the crystal-field anisotropy, just balances the difference in exchange energy between the helical and ferromagnetic phases:

$$\Delta U_{\text{ff}} = -\frac{1}{2}NJ^2\sigma^2\{\mathcal{J}_h(\mathbf{Q}) - \mathcal{J}_f(\mathbf{0})\}. \quad (1.5.35)$$

There has been some discussion about the relative importance of the two terms in stabilizing the ferromagnetic phase. From an analysis of the field required to induce the transition above T_C , Cooper (1968a) concluded that the magnetoelastic energy plays the dominant role. This conclusion was, however, based on the implicit assumption that the exchange energy changes little between the phases, and later measurements of the spin waves by Nicklow *et al.* (1971b) demonstrated that this is not the case. The energy difference $-\frac{1}{2}J^2\sigma^2\{\mathcal{J}_h(\mathbf{Q}) - \mathcal{J}_h(\mathbf{0})\}$ is about 2 K/ion in the helical phase, but the corresponding quantity is substantially smaller in the ferromagnetic phase. Del Moral and Lee (1975) reanalysed the data and concluded that the change (1.5.35) in the exchange energy makes the major contribution to driving the transition. Any statement about what drives a *first-order*, as distinct from a *second-order* transition must necessarily be imprecise, since all contributions to the energy change discontinuously at the transition. Immediately below T_N , the exchange dominates and the anisotropy forces are small. As the temperature is lowered, the peak in $\mathcal{J}(\mathbf{Q})$ decreases and moves, as was shown explicitly for the analogous case of Tb by the spin-wave measurements of Bjerrum Møller *et al.* (1967), illustrated in Fig. 6.1. The magnetoelastic forces therefore increase in relative importance, until a balance is reached and the transition to the ferromagnetic phase takes place. At the transition, a large change occurs in the exchange. Without the magnetoelastic term, T_C would be determined by the hexagonal crystal-field anisotropy, and would therefore be much lower. In this sense, the cylindrically-symmetric magnetoelastic forces drive the transition.

MAGNETIC STRUCTURES

The *mean-field theory* introduced in the previous section is used in this chapter as a basis for examining some of the magnetic structures assumed by the rare earth metals. The theory is presented at length in the first section. Beginning with the expression for the free energy, some general results are established for the magnetization, and applied analytically to the calculation of the susceptibility in the *high-temperature* limit. The mean-field approximation is then developed, and a numerical method for solving the resulting equations self-consistently, for magnetic structures which are commensurable with the lattice, is described. The *Landau expansion* of the free energy in terms of the *order parameters* of the magnetic system provides the starting point for a discussion of a number of the periodic magnetic structures which arise as a result of the long range of the indirect-exchange interaction. The ordering temperatures are calculated by analytical means, and the relative stability of different structures compared. In the following section, the important extension by Callen and Callen of the Zener power-law for the temperature dependence of the magnetic anisotropy is derived. The thermal expectation values $\langle O_l^m \rangle$ of the *Stevens operators* are calculated and their dependence on the magnetization determined. From the free energy, the *magnetic anisotropy* and the *magnetoelastic coefficients* are deduced. We conclude with a detailed discussion of some *magnetic structures*, using the aforementioned analytical methods, supplemented by numerical calculations, to help identify those characteristics of the magnetic interactions which lead to the stability of different moment-configurations under various conditions. This account is illustrated by various examples, with emphasis on the the diverse magnetic phases of Ho. Among other structures, we consider the *ferromagnet*, the *cone*, the *helix*, the *longitudinal wave*, the *cycloid*, and commensurable *spin slips*. The effect of a magnetic field in stabilizing *fan* and *helifan* structures, and the ordering of *thin films* and *superlattices*, are also discussed.

2.1 Mean-field theory of magnetic ordering

The simplest form of Hamiltonian which is adequate to explain the occurrence of most of the observed magnetic structures is

$$\mathcal{H} = \sum_i \mathcal{H}_{\text{cf}}(i) - \frac{1}{2} \sum_{ij} \mathcal{J}(ij) \mathbf{J}_i \cdot \mathbf{J}_j + \mathcal{H}_Z, \quad (2.1.1a)$$

where the first sum is the single-ion crystal-field Hamiltonian

$$\mathcal{H}_{\text{cf}}(i) = \sum_{l=2,4,6} B_l^0 O_l^0(\mathbf{J}_i) + B_6^6 O_6^6(\mathbf{J}_i), \quad (2.1.1b)$$

the two-ion term is assumed to be isotropic, and the Zeeman term is

$$\mathcal{H}_Z = - \sum_i \boldsymbol{\mu}_i \cdot \mathbf{H}_i. \quad (2.1.1c)$$

The field may vary spatially, so that we must specify its value on each site, writing $\mathbf{H}_i \equiv \mathbf{H}(\mathbf{R}_i)$, and the magnetic moment on the i th ion is $\boldsymbol{\mu}_i = g\mu_B \mathbf{J}_i$.

The static-susceptibility tensor may be derived as the second derivative of the free energy, and we shall therefore begin by recapitulating a few basic thermodynamic results. The free energy is

$$F = U - TS = -\frac{1}{\beta} \ln Z, \quad (2.1.2)$$

where U is the internal energy, S the entropy, and $\beta = (k_B T)^{-1}$. The partition function is

$$Z = \text{Tr}\{e^{-\beta\mathcal{H}}\} = \sum_p e^{-\beta E_p}. \quad (2.1.3)$$

Tr indicates the trace over a complete set of states, and the final summation may be performed if the eigenvalues E_p of the Hamiltonian are known. The expectation value of an operator A is

$$\langle A \rangle = \frac{1}{Z} \text{Tr}\{Ae^{-\beta\mathcal{H}}\}. \quad (2.1.4)$$

The derivative of the free energy with respect to a variable x is

$$\frac{\partial F}{\partial x} = -\frac{1}{\beta Z} \frac{\partial Z}{\partial x} = \frac{1}{Z} \text{Tr}\left\{\frac{\partial \mathcal{H}}{\partial x} e^{-\beta\mathcal{H}}\right\} = \left\langle \frac{\partial \mathcal{H}}{\partial x} \right\rangle. \quad (2.1.5)$$

This expression is obtained by utilizing the invariance of the trace to the basis used, assuming it to be independent of x and a cyclic permutation of the operators, thus allowing a conventional differentiation of the exponential operator, as may be seen by a Taylor expansion. This result is general, but the exponential operator can only be treated in this simple way in second derivatives if $\partial\mathcal{H}/\partial x$ commutes with the Hamiltonian, which is usually not the case. However, we may be interested only in the leading-order contributions in the limit where β is small, i.e. at *high*

temperatures. Expanding in powers of β , we may use the approximation $\exp\{-\beta\mathcal{H}\} \simeq 1 - \beta\mathcal{H} + \frac{1}{2}\beta^2\mathcal{H}^2$. In this case, we may proceed as above, and the result is

$$\begin{aligned} \frac{\partial^2 F}{\partial x \partial y} = & \left\langle \frac{\partial^2 \mathcal{H}}{\partial x \partial y} \right\rangle + \beta \left(\left\langle \frac{\partial \mathcal{H}}{\partial x} \right\rangle \left\langle \frac{\partial \mathcal{H}}{\partial y} \right\rangle - \left\langle \frac{\partial \mathcal{H}}{\partial x} \frac{\partial \mathcal{H}}{\partial y} \right\rangle \right) \\ & - \frac{\beta^2}{2} \left\langle \left[\frac{\partial \mathcal{H}}{\partial x}, \frac{\partial \mathcal{H}}{\partial y} \right] \mathcal{H} \right\rangle + \mathcal{O}(\beta^3), \end{aligned} \quad (2.1.6)$$

where the second- and higher-order terms vanish if one of the derivatives of \mathcal{H} commutes with \mathcal{H} itself.

In many instances, it is more convenient to consider the angular momentum rather than the magnetic moment, with a corresponding field variable $\mathbf{h}_i = g\mu_B \mathbf{H}_i$, so that the Zeeman term (2.1.1c) becomes

$$\mathcal{H}_Z = - \sum_i \boldsymbol{\mu}_i \cdot \mathbf{H}_i = - \sum_i \mathbf{J}_i \cdot \mathbf{h}_i. \quad (2.1.7)$$

Since the exchange and anisotropy terms in \mathcal{H} do not depend explicitly on the field, $\partial\mathcal{H}/\partial H_{i\alpha} = -\mu_{i\alpha}$ and, using eqn (2.1.5), we have

$$\langle \mu_{i\alpha} \rangle = -\partial F / \partial H_{i\alpha} \quad \text{or} \quad \langle J_{i\alpha} \rangle = -\partial F / \partial h_{i\alpha}. \quad (2.1.8)$$

Next, we define the non-local susceptibilities

$$\chi_{\alpha\beta}^\mu(ij) = \partial \langle \mu_i \rangle / \partial H_{j\beta} = -\partial^2 F / \partial H_{i\alpha} \partial H_{j\beta}, \quad (2.1.9a)$$

and similarly

$$\chi_{\alpha\beta}^J(ij) = (g\mu_B)^{-2} \chi_{\alpha\beta}^\mu(ij) = -\partial^2 F / \partial h_{i\alpha} \partial h_{j\beta}, \quad (2.1.9b)$$

and the corresponding Fourier transforms, e.g.

$$\chi_{\alpha\beta}^J(\mathbf{q}) = \frac{1}{N} \sum_{ij} \chi_{\alpha\beta}^J(ij) e^{-i\mathbf{q} \cdot (\mathbf{R}_i - \mathbf{R}_j)} = \sum_j \chi_{\alpha\beta}^J(ij) e^{-i\mathbf{q} \cdot (\mathbf{R}_i - \mathbf{R}_j)}. \quad (2.1.9c)$$

The final equality only applies in a uniform system. If the field is increased by an infinitesimal amount $\delta\mathbf{H}(\mathbf{q}) \exp(i\mathbf{q} \cdot \mathbf{R}_i)$, the individual moments are changed by

$$\delta \langle \mu_{i\alpha} \rangle = \sum_j \sum_\beta \chi_{\alpha\beta}^\mu(ij) \delta H_\beta(\mathbf{q}) e^{i\mathbf{q} \cdot \mathbf{R}_j}, \quad (2.1.10a)$$

according to (2.1.9). Hence the added harmonically-varying field introduces one Fourier component in the magnetization:

$$\delta M_\alpha(\mathbf{q}) = \frac{1}{V} \sum_i \delta \langle \mu_{i\alpha} \rangle e^{-i\mathbf{q} \cdot \mathbf{R}_i} = \frac{N}{V} \sum_\beta \chi_{\alpha\beta}^\mu(\mathbf{q}) \delta H_\beta(\mathbf{q}), \quad (2.1.10b)$$

proportional to the susceptibility at the wave-vector considered. The usual definition of the susceptibility components (per unit volume), as used in Chapter 1, is $\delta M_\alpha(\mathbf{q})/\delta H_\beta(\mathbf{q})$. The susceptibility used in (2.1.10b) differs from this by the factor V/N , i.e. we are here considering the susceptibility per atom instead of per unit volume. Furthermore, since we shall not make any further use of $\chi_{\alpha\beta}^\mu(\mathbf{q})$, we shall reserve the notation $\chi_{\alpha\beta}(\mathbf{q})$ for the \mathbf{q} -dependent susceptibility $\chi_{\alpha\beta}^{\mathbf{J}}(\mathbf{q})$, introduced in eqn (2.1.9b), throughout the rest of the book. So in terms of the susceptibility per atom, ‘in units of $(g\mu_B)^2$ ’, the above equation may be written

$$\delta\langle J_\alpha(\mathbf{q}) \rangle = \frac{1}{N} \sum_i \delta\langle J_{i\alpha} \rangle e^{-i\mathbf{q}\cdot\mathbf{R}_i} = \sum_\beta \chi_{\alpha\beta}(\mathbf{q}) \delta h_\beta(\mathbf{q}), \quad (2.1.10c)$$

with the upper index \mathbf{J} in $\chi_{\alpha\beta}^{\mathbf{J}}(\mathbf{q})$ being suppressed from now on.

2.1.1 The high-temperature susceptibility

In order to calculate $\bar{\chi}(\mathbf{q})$ in zero field, we shall first use the approximation (2.1.6) to the derivative of the free energy, valid at high temperatures. In this limit $\langle \mathbf{J}_i \rangle = \mathbf{0}$, and only one term in the expansion is non-zero:

$$\chi_{\alpha\beta}(ij) = \beta \text{Tr}\{J_{i\alpha} J_{j\beta} (1 - \beta\mathcal{H})\} / \text{Tr}\{1 - \beta\mathcal{H}\}, \quad (2.1.11)$$

to second order in β . The commutator in the third term on the right-hand side of (2.1.6) is either zero or purely imaginary (if $i = j$ and $\alpha \neq \beta$), showing immediately that the expectation value of this term must vanish in all cases. To first order in β , we obtain from (2.1.11)

$$\chi_{\alpha\beta}(ij) \simeq \beta \text{Tr}\{J_{i\alpha} J_{j\beta}\} / \text{Tr}\{1\} = \frac{1}{3} J(J+1) \beta \delta_{\alpha\beta} \delta_{ij},$$

using the product of the eigenvectors of $J_{i\alpha}$ as the basis, and recalling that

$$\sum m^2 = \frac{1}{3} J(J+1)(2J+1),$$

when m runs from $-J$ to J . In order to calculate the second-order contribution, we shall utilize the general tensor properties of the Stevens operators, which satisfy the orthogonality condition:

$$\text{Tr}\{O_l^m(\mathbf{J}_i) O_{l'}^{m'}(\mathbf{J}_j)\} = \delta_{ij} \delta_{ll'} \delta_{mm'} \text{Tr}\{[O_l^m(\mathbf{J}_i)]^2\} \quad (2.1.12)$$

$$\text{and } \text{Tr}\{O_l^m(\mathbf{J}_i)\} = 0,$$

when l and l' are both non-zero. O_0^0 is just the identity operator. $J_{i\alpha}$ is a linear combination of $O_1^m(\mathbf{J}_i)$, $m = -1, 0, 1$, and (2.1.12) then implies

that the trace of the Hamiltonian (2.1.1) vanishes, and hence that the denominator in (2.1.11) is $\text{Tr}\{1\} = (2J + 1)^N$. For the second-order term in the numerator, we find

$$\begin{aligned} \text{Tr}\{J_{i\alpha}J_{j\beta}\mathcal{H}\} &= \delta_{ij}B_2^0\text{Tr}\{J_{i\alpha}J_{i\beta}O_2^0(\mathbf{J}_i)\} - \mathcal{J}(ij)\text{Tr}\{J_{i\alpha}J_{j\beta}\mathbf{J}_i\cdot\mathbf{J}_j\} \\ &= \delta_{ij}\delta_{\alpha\beta}B_2^0\text{Tr}\{J_{i\alpha}^2[3J_{iz}^2 - J(J+1)]\} - \delta_{\alpha\beta}\mathcal{J}(ij)\text{Tr}\{J_{i\alpha}^2J_{j\alpha}^2\}, \end{aligned}$$

utilizing that $J_{i\alpha}J_{j\beta}$ is a linear combination of second- and lower-rank tensors for $i = j$, and a product of first-rank tensors for $i \neq j$. When $\alpha = z$ (or ζ), we may readily calculate the first trace, using

$$\sum m^4 = \frac{1}{15}J(J+1)(2J+1)(3J^2 + 3J - 1).$$

The traces with $\alpha = x$ or $\alpha = y$ must be equal, and using this equality in the case $\alpha = x$, for instance, we may replace J_x^2 in the trace by $\frac{1}{2}(J_x^2 + J_y^2) \rightarrow \frac{1}{2}J(J+1) - \frac{1}{2}J_z^2$. As the constant term multiplied by $3J_z^2 - J(J+1)$ does not contribute (as $\text{Tr}\{3J_z^2 - J(J+1)\} = 0$), the trace with $\alpha = x$ or y is equal to $-1/2$ times that with $\alpha = z$. Only the single-ion terms contribute to the trace when $i = j$ ($\mathcal{J}(ii)$ is assumed to be zero), and of these only the lowest-rank term B_2^0 appears, to leading order. The two-ion coupling only occurs in the trace, and hence in $\chi_{\alpha\beta}(ij)$, when $i \neq j$, and this contribution may be straightforwardly calculated. To second order in β , the off-diagonal terms are zero, whereas

$$\begin{aligned} \chi_{\alpha\alpha}(ij) &= \delta_{ij}\frac{1}{3}J(J+1)\beta\left[1 - \frac{2}{5}(3\delta_{\alpha\zeta} - 1)B_2^0(J - \frac{1}{2})(J + \frac{3}{2})\beta\right] \\ &\quad + \left[\frac{1}{3}J(J+1)\beta\right]^2\mathcal{J}(ij). \end{aligned}$$

Introducing the Fourier transform of the two-ion coupling,

$$\mathcal{J}(\mathbf{q}) = \sum_j \mathcal{J}(ij)e^{-i\mathbf{q}\cdot(\mathbf{R}_i - \mathbf{R}_j)}, \quad (2.1.13)$$

we find that, to the order considered, the inverse of the \mathbf{q} -dependent susceptibility may be written

$$1/\chi_{\alpha\alpha}(\mathbf{q}) = \frac{3k_B T}{J(J+1)} + (3\delta_{\alpha\zeta} - 1)\frac{6(J - \frac{1}{2})(J + \frac{3}{2})}{5J(J+1)}B_2^0 - \mathcal{J}(\mathbf{q}) + \mathcal{O}(1/T). \quad (2.1.14)$$

The inverse susceptibility in the high-temperature limit thus increases linearly with the temperature, with a slope inversely proportional to the square of the effective paramagnetic moment ($\propto \{J(J+1)\}^{1/2}$). The susceptibilities determined experimentally by magnetization measure-

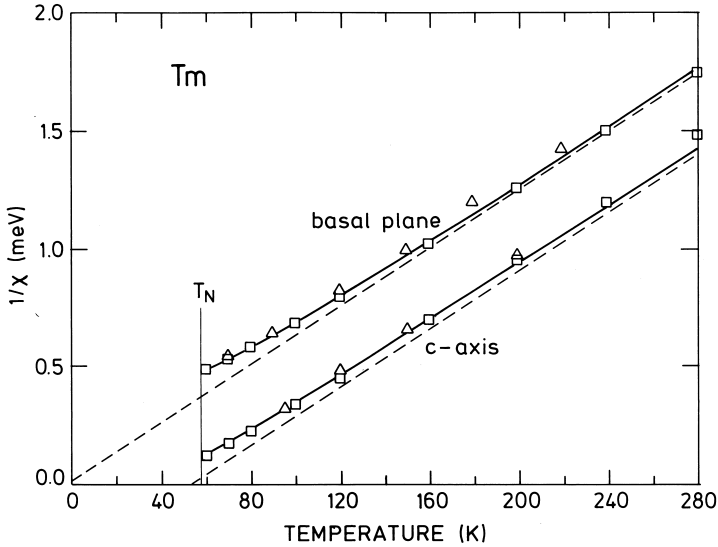


Fig. 2.1. The inverse susceptibility, in atomic units, in Tm above T_N . The full lines depict the results of a mean-field calculation and the dashed lines are extrapolations of the high-temperature limit. Experimental values are also shown. The MF theory predicts a deviation from the high-temperature expression as the ordering temperature is approached from above, because of crystal-field anisotropy effects.

ments are the bulk values at zero wave-vector. The straight lines found at high temperatures for the inverse-susceptibility components $1/\chi_{\alpha\alpha}(\mathbf{0})$ versus temperature may be extrapolated to lower values, as illustrated in Fig. 2.1. The values at which these lines cross the temperature axis are the *paramagnetic Curie temperatures* θ_{\parallel} and θ_{\perp} , determined respectively when the field is parallel and perpendicular to the c -axis (ζ -axis). The high-temperature expansion then predicts these temperatures to be

$$k_B\theta_{\parallel} = \frac{1}{3}J(J+1)\mathcal{J}(\mathbf{0}) - \frac{4}{5}(J - \frac{1}{2})(J + \frac{3}{2})B_2^0, \quad (2.1.15a)$$

and

$$k_B\theta_{\perp} = \frac{1}{3}J(J+1)\mathcal{J}(\mathbf{0}) + \frac{2}{5}(J - \frac{1}{2})(J + \frac{3}{2})B_2^0. \quad (2.1.15b)$$

Hence the paramagnetic Curie temperatures are determined by the lowest-rank interactions in the Hamiltonian, i.e. those terms for which $l+l' = 2$. The difference between the two temperatures depends only on B_2^0 , because of the assumption that the two-ion coupling is an *isotropic*

Heisenberg exchange. The mean temperature $(\theta_{\parallel} + 2\theta_{\perp})/3$ is determined by $\mathcal{J}(\mathbf{0})$ which, from (2.1.13), is the algebraic sum of the isotropic two-ion interactions, and this temperature may be measured directly with a polycrystalline sample. The two basal-plane components are found to be equal. This is not just due to the assumption of high temperatures, but is generally valid as long as there is no ordered moment in the basal-plane. In this case, the c -axis is a three-fold symmetry axis, or effectively a six-fold axis, due to the symmetry of the basal-plane anisotropy B_6^6 in the Hamiltonian. The susceptibility is a second-rank tensor, according to (2.1.9), and it cannot therefore vary under rotation about a three- or six-fold axis.

2.1.2 The mean-field approximation

The high-temperature expansion may be extended to higher order in β , but the calculations rapidly become more complex, so we shall instead adopt another approach, the mean-field approximation. In this method, the correlated fluctuations of the moments around their equilibrium values are neglected. In order to introduce $\langle \mathbf{J}_i \rangle$ into the Hamiltonian, we utilize the identity

$$\mathbf{J}_i \cdot \mathbf{J}_j = (\mathbf{J}_i - \langle \mathbf{J}_i \rangle) \cdot (\mathbf{J}_j - \langle \mathbf{J}_j \rangle) + \mathbf{J}_i \cdot \langle \mathbf{J}_j \rangle + \mathbf{J}_j \cdot \langle \mathbf{J}_i \rangle - \langle \mathbf{J}_i \rangle \cdot \langle \mathbf{J}_j \rangle.$$

The MF approximation then consists in neglecting the first term on the right-hand side, which is associated with two-site fluctuations, since $i \neq j$. The Hamiltonian (2.1.1) is then effectively decoupled into a sum of N independent terms for the single sites; $\mathcal{H} \simeq \sum_i \mathcal{H}_{\text{MF}}(i)$, where

$$\mathcal{H}_{\text{MF}}(i) = \mathcal{H}_{\text{cf}}(i) - \mathbf{J}_i \cdot \mathbf{h}_i - \left(\mathbf{J}_i - \frac{1}{2} \langle \mathbf{J}_i \rangle \right) \cdot \sum_j \mathcal{J}(ij) \langle \mathbf{J}_j \rangle, \quad (2.1.16)$$

in the presence of an external magnetic field $\mathbf{h}_i = g\mu_B \mathbf{H}_i$. Introducing the effective field

$$\mathbf{h}_i^{\text{eff}} = \mathbf{h}_i + \sum_j \mathcal{J}(ij) \langle \mathbf{J}_j \rangle, \quad (2.1.17a)$$

we may write the MF Hamiltonian

$$\mathcal{H}_{\text{MF}}(i) = \mathcal{H}_{\text{cf}}(i) - \mathbf{J}_i \cdot \mathbf{h}_i^{\text{eff}} + \frac{1}{2} \langle \mathbf{J}_i \rangle \cdot (\mathbf{h}_i^{\text{eff}} - \mathbf{h}_i). \quad (2.1.17b)$$

Self-consistent solutions of the MF equations may sometimes be obtained analytically, but numerical methods may be used more generally, provided that the periodicity of the magnetic structure is commensurable with that of the lattice. For an assumed distribution of $\langle \mathbf{J}_j \rangle$, the effective field and hence the MF Hamiltonian for the i th site is calculated.

Diagonalizing this Hamiltonian, we may derive the partition function Z_i , the free energy F_i , and the expectation value $\langle \mathbf{J}_i \rangle$ for this site. The last term in (2.1.17b) just adds a constant contribution to F_i , without affecting $\langle \mathbf{J}_i \rangle$. Performing this calculation for all the different ions, we determine the various values of $\langle \mathbf{J}_j \rangle$, and the total free energy is the sum of the F_i . The derived values of $\langle \mathbf{J}_j \rangle$ are used as the input for a new MF Hamiltonian, and this iterative procedure is repeated until self-consistency is attained. The self-consistent solution of the MF Hamiltonian may be one in which $\langle \mathbf{J}_i \rangle$ is non-zero even in zero field, thus describing the occurrence of a spontaneous ordering of the moments.

Having found the self-consistent solution for the angular momenta, we may proceed to calculate the susceptibility. The MF Hamiltonian for the i th site has been diagonalized, and we shall denote the $(2J+1)$ eigenstates by $|p\rangle$, with corresponding energy eigenvalues E_p . If the effective field is changed by a small amount $\delta h_\beta^{\text{eff}}$, the Zeeman term $-J_{i\beta} \delta h_\beta^{\text{eff}}$ must be added to the Hamiltonian, and $E_p^{(1)} = E_p - \langle p | J_{i\beta} | p \rangle \delta h_\beta^{\text{eff}}$, to first order in the perturbation, provided that $|p\rangle$ is a set which diagonalizes the perturbation within the possibly degenerate subspaces of the zero-field Hamiltonian. The new eigenstates are

$$|p^{(1)}\rangle = |p\rangle - \delta h_\beta^{\text{eff}} \sum_{p'} |p'\rangle \langle p' | J_{i\beta} | p \rangle / (E_p - E_{p'}),$$

where the terms for which $E_p = E_{p'}$ vanish. Using (2.1.3) and (2.1.4), we then have, to first order in $\delta h_\beta^{\text{eff}}$,

$$\begin{aligned} \langle J_{i\alpha}^{(1)} \rangle &= \sum_p \langle p^{(1)} | J_{i\alpha} | p^{(1)} \rangle = n_p^{(1)} = \sum_p \langle p | J_{i\alpha} | p \rangle n_p^{(1)} \\ &\quad - \delta h_\beta^{\text{eff}} \sum_{pp'} \langle p | J_{i\alpha} | p' \rangle \langle p' | J_{i\beta} | p \rangle n_p / (E_p - E_{p'}) \\ &\quad - \delta h_\beta^{\text{eff}} \sum_{pp'} \langle p | J_{i\beta} | p' \rangle \langle p' | J_{i\alpha} | p \rangle n_p / (E_p - E_{p'}), \end{aligned}$$

where the last two sums extend over states for which $E_p \neq E_{p'}$. The population factor of the p th level at $\delta h_\beta^{\text{eff}} = 0$ is $n_p = \exp(-\beta E_p) / Z_i$, and $n_p^{(1)}$ is the corresponding factor at the field $\delta h_\beta^{\text{eff}}$. By differentiation, we find

$$\begin{aligned} \partial n_p^{(1)} / \partial (\delta h_\beta^{\text{eff}}) &= \left\{ \langle p | J_{i\beta} | p \rangle - \sum_{p'} \langle p' | J_{i\beta} | p' \rangle n_{p'} \right\} \beta n_p \\ &= \left\{ \langle p | J_{i\beta} | p \rangle - \langle J_{i\beta} \rangle \right\} \beta n_p. \end{aligned}$$

Introducing this result in the equation above, and interchanging p and

p' in the last sum, we obtain finally:

$$\begin{aligned} \chi_{\alpha\beta}^o(i) = \partial\langle J_{i\alpha} \rangle / \partial h_{i\beta}^{\text{eff}} &= \sum_{pp'}^{E_p \neq E_{p'}} \frac{\langle p | J_{i\alpha} | p' \rangle \langle p' | J_{i\beta} | p \rangle}{E_{p'} - E_p} (n_p - n_{p'}) \\ &+ \beta \sum_{pp'}^{E_p = E_{p'}} \langle p | J_{i\alpha} | p' \rangle \langle p' | J_{i\beta} | p \rangle n_p - \beta \langle J_{i\alpha} \rangle \langle J_{i\beta} \rangle. \end{aligned} \quad (2.1.18)$$

The second summation is transformed in such a way that it is no longer necessary for $J_{i\beta}$ to be diagonal within the degenerate subspaces, as required initially. The first term in the susceptibility is the *Van Vleck* contribution, which becomes constant at zero temperature, whereas the second term, the *Curie* contribution, diverges as $1/T$ in the low-temperature limit. The susceptibility deduced above is that determining the response due to a change of the *effective* field, $\delta\langle \mathbf{J}_i \rangle = \bar{\chi}^o(i) \delta \mathbf{h}_i^{\text{eff}}$, whereas we wish to know the response due to a small change of the *external* field. If a small harmonically-varying field $\delta \mathbf{h}_{\mathbf{q}} \exp(i\mathbf{q} \cdot \mathbf{R}_i)$ is applied, the effective field, according to (2.1.17a), is

$$\delta \mathbf{h}_i^{\text{eff}} = \delta \mathbf{h}_{\mathbf{q}} e^{i\mathbf{q} \cdot \mathbf{R}_i} + \sum_j \mathcal{J}(ij) \bar{\chi}^o(j) \delta \mathbf{h}_j^{\text{eff}}.$$

This equation may be solved by a Fourier transformation if $\bar{\chi}^o(i) = \bar{\chi}^o$ is site-independent, which it is so long as $\langle \mathbf{J}_i \rangle$ is independent of i , as in the high-temperature paramagnetic phase, for example, where $\langle \mathbf{J}_i \rangle = \mathbf{0}$. Neglecting any site-dependence of $\bar{\chi}^o$, and introducing the notation $\delta \mathbf{h}_i^{\text{eff}} = \delta \mathbf{h}_{\mathbf{q}}^{\text{eff}} \exp(i\mathbf{q} \cdot \mathbf{r}_i)$, we get

$$\delta \mathbf{h}_{\mathbf{q}}^{\text{eff}} = \{1 - \bar{\chi}^o \mathcal{J}(\mathbf{q})\}^{-1} \delta \mathbf{h}_{\mathbf{q}},$$

or, by the definition of the susceptibility,

$$\bar{\chi}(\mathbf{q}) = \{1 - \bar{\chi}^o \mathcal{J}(\mathbf{q})\}^{-1} \bar{\chi}^o. \quad (2.1.19a)$$

In the following, we shall assume that the external magnetic field is zero. With this restriction, $\bar{\chi}(\mathbf{q})$ is diagonal in the $(\xi\eta\zeta)$ -coordinate system, and the reciprocal susceptibility, in the MF approximation, may be written

$$1/\chi_{\alpha\alpha}(\mathbf{q}) = 1/\chi_{\alpha\alpha}^o - \mathcal{J}(\mathbf{q}). \quad (2.1.19b)$$

In the degenerate case, (2.1.18) implies that $\chi_{\alpha\alpha}^o = \beta J(J+1)/3$. However, if \mathcal{H}_{cf} is non-zero, the expression (2.1.18) for the susceptibility becomes quite complex. A drastic simplification is achieved by assuming a

small value of β . In this high temperature limit, $\overline{\chi}^o$ may be calculated by a procedure equivalent to that used in deriving (2.1.14), except that $\mathcal{J}(ij) = 0$. Hence, to second order in β , we have

$$\chi_{\alpha\alpha}^o \simeq \frac{1}{3}J(J+1)\beta\left[1 - \frac{2}{5}(3\delta_{\alpha\zeta} - 1)\left(J - \frac{1}{2}\right)\left(J + \frac{3}{2}\right)B_2^0\beta\right]. \quad (2.1.20)$$

Introducing (2.1.20) in (2.1.19), we obtain the same result as previously derived in (2.1.14), demonstrating that the MF approximation is correct in the high-temperature limit. Although the thermal fluctuations increase when the temperature is raised, they also become increasingly uncorrelated. It is the latter effect which is the most pronounced, and the correction to the MF value of the free energy, proportional to the correlation energy of the two-site fluctuations $\mathcal{J}(ij)\{\langle \mathbf{J}_i \cdot \mathbf{J}_j \rangle - \langle \mathbf{J}_i \rangle \cdot \langle \mathbf{J}_j \rangle\}$, decreases with temperature at high temperatures. In the other limit of zero temperature, the correlation effects are much stronger, but the fluctuations themselves are small. We may therefore also expect the MF approximation to be accurate in this limit, and to provide a useful interpolation at intermediate temperatures.

$\overline{\chi}^o$ increases steadily with decreasing temperature. If the crystal-field ground state is degenerate, the second sum in (2.1.18) is non-zero and $\overline{\chi}^o$ diverges in the zero-temperature limit. Because of the Kramers degeneracy, the ground state is always at least doubly degenerate if $2J$ is odd. When J is an integer, the ground state may be a singlet, in which case $\overline{\chi}^o$ saturates at a constant value at zero temperature. Except in this special case, it is always possible to find a temperature where $1/\chi_{\alpha\alpha}(\mathbf{q})$ is zero, corresponding to an infinite $\chi_{\alpha\alpha}(\mathbf{q})$. The largest value of the \mathbf{q} -dependent susceptibility is found at the wave-vector \mathbf{Q} at which $\mathcal{J}(\mathbf{q})$ has its maximum. Of the three non-zero components of $\overline{\chi}(\mathbf{Q})$, the cc -component is the largest if B_2^0 is negative. If B_2^0 is positive, on the other hand, the two equal basal-plane components are the largest. It is the maximum component of the susceptibility at $\mathbf{q} = \mathbf{Q}$ which first diverges when the system is cooled. This divergence signals that the paramagnetic ground-state becomes unstable against the formation of an ordered state in which the moments are modulated with the wave-vector \mathbf{Q} , and point along or perpendicular to the c -direction, depending on whether B_2^0 is respectively negative or positive. Hence, a second-order phase transition takes place at this critical temperature, called the Curie temperature, T_C , or the Néel temperature, T_N , depending on whether $\mathbf{Q} = \mathbf{0}$ or $\mathbf{Q} \neq \mathbf{0}$. Just below T_N , the ordered moment $\langle \mathbf{J}_i \rangle$ is small, and the free energy of the i th ion may be expanded in powers of this moment. In order to establish this expansion, we first consider the Hamiltonian $\mathcal{H}'(i) = \mathcal{H}_{\text{cf}}(i) - \mathbf{J}_i \cdot \mathbf{h}$. The corresponding free energy may be written

$$F'_i = F_0/N - \langle \mathbf{J}_i \rangle \cdot \mathbf{h} + \sum_{\alpha} A_{\alpha} \langle J_{i\alpha} \rangle^2 + \sum_{\alpha\beta} B_{\alpha\beta} \langle J_{i\alpha} \rangle^2 \langle J_{i\beta} \rangle^2 + \dots$$

Except for the field term, this expansion only includes products of components in which the sum of the exponents is even, because of time-reversal symmetry. Using the equilibrium condition $\partial F'_i / \partial \langle J_{i\alpha} \rangle = 0$, and recalling that $\langle J_{i\alpha} \rangle = \chi_{\alpha\alpha}^o(\sigma = 0)h_\alpha$ to leading order, in the zero-field limit, we obtain

$$A_\alpha = \{2\chi_{\alpha\alpha}^o(\sigma = 0)\}^{-1}, \quad (2.1.21a)$$

where $\chi_{\alpha\alpha}^o(\sigma = 0)$ is the MF susceptibility (2.1.18), in the limit of zero magnetization (field). The susceptibility decreases with increasing magnetization (or field), as described by the fourth-order terms. An order-of-magnitude estimate of $B_{\alpha\beta}$ may be obtained by neglecting $\mathcal{H}_{\text{cf}}(i)$. In this case, the magnetization as a function of the field is given by the Brillouin function (1.2.31):

$$\langle J_{i\alpha} \rangle = JB_J(\beta J h_\alpha) \simeq \frac{1}{3}J(J+1)\beta h_\alpha \left\{1 - \frac{1}{15}(J^2 + J + \frac{1}{2})\beta^2 h_\alpha^2\right\},$$

which, in combination with the equilibrium condition for the free energy, determines $B_{\alpha\alpha}$. The off-diagonal terms may be obtained straightforwardly by utilizing the condition that, when $\mathcal{H}_{\text{cf}}(i)$ is neglected, the free energy should be invariant with respect to any rotation of the magnetization vector, implying that all the coefficients $B_{\alpha\beta}$ are equal, or

$$B_{\alpha\beta} \approx \frac{9}{20} \frac{J^2 + J + \frac{1}{2}}{J^3(J+1)^3} k_B T. \quad (2.1.21b)$$

The introduction of the crystal-field terms of course modifies this result, but rather little in the high-temperature limit. Under all circumstances, the effective six-fold symmetry around the c -axis implies that $B_{\alpha\beta}$ is symmetric, $B_{\xi\xi} = B_{\eta\eta} = B_{\xi\eta}$, and $B_{\xi\zeta} = B_{\eta\zeta}$, and it also eliminates the possibility that any other fourth-order terms may contribute. The expansion of the free energy of the total system, when the external field is zero, is obtained from the expansion of F'_i , summed over i , by substituting the *exchange* field $\mathbf{h}_i^{\text{eff}} = \sum_j \mathcal{J}(ij) \langle \mathbf{J}_j \rangle$ for \mathbf{h} , and adding the ‘constant’ $\frac{1}{2} \langle \mathbf{J}_i \rangle \cdot \mathbf{h}_i^{\text{eff}}$, so that

$$F = F_0 - \frac{1}{2} \sum_{ij} \mathcal{J}(ij) \langle \mathbf{J}_i \rangle \cdot \langle \mathbf{J}_j \rangle + \sum_i \left[\sum_\alpha A_\alpha \langle J_{i\alpha} \rangle^2 + \sum_{\alpha\beta} B_{\alpha\beta} \langle J_{i\alpha} \rangle^2 \langle J_{i\beta} \rangle^2 \right] \quad (2.1.22)$$

to fourth order in the magnetization. This expansion of the free energy in terms of the *order parameter(s)* is called the *Landau expansion*.

Assuming the ordered phase to be described by a single wave-vector, we may write

$$\langle J_{i\alpha} \rangle = J\sigma_\alpha \cos(\mathbf{q} \cdot \mathbf{R}_i + \varphi_\alpha), \quad (2.1.23)$$

where $\sigma_\alpha = \sigma_\alpha(\mathbf{q})$ is the relative magnetization at the wave-vector \mathbf{q} . Introducing this into the free-energy expression, and utilizing the condition that $\sum_i \cos(\mathbf{q}' \cdot \mathbf{R}_i + \varphi) = 0$, if \mathbf{q}' is not a reciprocal lattice vector, we find

$$f = (F - F_0)/N = \frac{1}{4} J^2 \sum_{\alpha} \{2A_\alpha - \mathcal{J}(\mathbf{q})\} \sigma_\alpha^2 + \frac{1}{8} J^4 \sum_{\alpha\beta} B_{\alpha\beta} \{2 + \cos 2(\varphi_\alpha - \varphi_\beta)\} \sigma_\alpha^2 \sigma_\beta^2, \quad (2.1.24)$$

if $4\mathbf{q}$ is different from a reciprocal lattice vector. The coefficients of the second power are thus $\propto \{2A_\alpha - \mathcal{J}(\mathbf{q})\} = 1/\chi_{\alpha\alpha}(\mathbf{q}, \sigma = 0)$, where the susceptibility is evaluated at zero magnetization. As long as all the second-order coefficients are positive, at any value of \mathbf{q} , the free energy is at its minimum when $\sigma_\alpha = 0$, i.e. the system is paramagnetic. The smallest of these coefficients are those at $\mathbf{q} = \mathbf{Q}$, where $\mathcal{J}(\mathbf{q})$ has its maximum. In the heavy rare earths, with the exception of Gd, \mathbf{Q} is non-zero and is directed along the c -axis. Depending on the sign of B_2^0 , the magnetic structures occurring in the heavy rare earths may be divided into two classes, which we will discuss in turn.

2.1.3 Transversely ordered phases

When $B_2^0 > 0$, as in Tb, Dy, and Ho, the two basal-plane components of $\bar{\chi}(\mathbf{Q})$ both diverge at the same critical temperature T_N . Using the approximate high-temperature value (2.1.20) for the susceptibility, we find that $1/\chi_{\xi\xi}(\mathbf{Q}, \sigma = 0) = 1/\chi_{\eta\eta}(\mathbf{Q}, 0) = 2A_\xi - \mathcal{J}(\mathbf{Q})$ vanishes at the temperature determined by

$$k_B T_N \simeq \frac{1}{3} J(J+1) \mathcal{J}(\mathbf{Q}) \left[1 + \frac{2}{5} \left(J - \frac{1}{2} \right) \left(J + \frac{3}{2} \right) B_2^0 / k_B T_N \right]. \quad (2.1.25)$$

Below T_N , both σ_ξ and σ_η are generally non-zero at the wave-vector \mathbf{Q} , and the free energy f , given by (2.1.24) with $\sigma_\zeta = 0$, is minimized when $\sigma_\xi(\mathbf{Q}) = \sigma_\eta(\mathbf{Q}) = \sigma_{\mathbf{Q}}$, and

$$\sigma_{\mathbf{Q}} = \left(\frac{\mathcal{J}(\mathbf{Q}) - 2A_\xi}{4J^2 B_{\xi\xi}} \right)^{1/2} \quad ; \quad \varphi_\xi - \varphi_\eta = \pm \frac{\pi}{2}, \quad (2.1.26a)$$

corresponding to the helical ordering:

$$\begin{aligned} \langle J_{i\xi} \rangle &= J \sigma_{\mathbf{Q}} \cos(\mathbf{Q} \cdot \mathbf{R}_i + \varphi) \\ \langle J_{i\eta} \rangle &= \pm J \sigma_{\mathbf{Q}} \sin(\mathbf{Q} \cdot \mathbf{R}_i + \varphi). \end{aligned} \quad (2.1.26b)$$

The length of the angular-momentum vector is $J\sigma_{\mathbf{Q}}$, independent of the site considered. There are two energetically-degenerate configurations,

a right- or a left-handed screw, depending on the choice of sign. From the condition $1/\chi_{\xi\xi}(\mathbf{Q}, 0) \propto (T - T_N)$, sufficiently close to T_N , we get the usual MF result that the order parameter $\sigma_{\mathbf{Q}} \propto (T_N - T)^{1/2}$. Although $1/\chi_{\xi\xi}(\mathbf{Q}, 0)$ becomes negative below T_N , the inverse of the actual susceptibility, $1/\chi_{\xi\xi}(\mathbf{Q}) = 1/\chi_{\xi\xi}(\mathbf{Q}, \sigma_{\mathbf{Q}})$, does not. Analogously to the derivation of A_α in (2.1.21a), it may be seen that $1/\chi_{\xi\xi}(\mathbf{Q})$ is a second derivative of the free energy, i.e.

$$\begin{aligned} 1/\chi_{\xi\xi}(\mathbf{Q}) &= \partial^2 f / \partial (J\sigma_{\mathbf{Q}})^2 \\ &\simeq 1/\chi_{\xi\xi}(\mathbf{Q}, \sigma = 0) + 12J^2 B_{\xi\xi} \sigma_{\mathbf{Q}}^2 = -2/\chi_{\xi\xi}(\mathbf{Q}, \sigma = 0). \end{aligned}$$

Hence, $1/\chi_{\xi\xi}(\mathbf{Q})$ is non-negative, as it must be to ensure that the system is stable, as is also the case for any other component of the susceptibility.

Because $|\langle \mathbf{J}_i \rangle|$ is constant, the *umklapp* contributions to the free energy in (2.1.24), for which $4Q$ is a multiple of the reciprocal-lattice parameter $4\pi/c$, cancel. The free energy of the helix is therefore independent of the lattice, at least to the fourth power in the magnetization. If the anisotropy terms in \mathcal{H}_{cf} can be neglected, the helix is the most stable configuration satisfying the condition that $|\langle \mathbf{J}_i \rangle| = J\sigma$ is constant. With this constraint, only the two-ion interaction term in the free energy (2.1.22) may vary, and this may be minimized by the method of Lagrange multipliers (Nagamiya 1967). We will begin with the weaker constraint; $\sum_i \langle \mathbf{J}_i \rangle^2 = N(J\sigma)^2$ is constant, which means that we have to minimize the energy expression

$$\begin{aligned} U &= -\frac{1}{2} \sum_{ij} \mathcal{J}(ij) \langle \mathbf{J}_i \rangle \cdot \langle \mathbf{J}_j \rangle + \lambda \sum_i (\langle \mathbf{J}_i \rangle^2 - (J\sigma)^2) \\ &= N \sum_{\mathbf{q}} \left\{ -\frac{1}{2} \mathcal{J}(\mathbf{q}) + \lambda \right\} \langle \mathbf{J}(\mathbf{q}) \rangle \cdot \langle \mathbf{J}(-\mathbf{q}) \rangle - N\lambda (J\sigma)^2, \end{aligned} \quad (2.1.27a)$$

where the introduction of $\langle \mathbf{J}_i \rangle = \sum_{\mathbf{q}} \langle \mathbf{J}(\mathbf{q}) \rangle \exp(i\mathbf{q} \cdot \mathbf{R}_i)$, as in (2.1.10c), yields the second form. Minimizing this expression with respect to $\langle \mathbf{J}(-\mathbf{q}) \rangle$, we obtain the following equation:

$$\partial U / \partial \langle \mathbf{J}(-\mathbf{q}) \rangle = N \{ -\mathcal{J}(\mathbf{q}) + 2\lambda \} \langle \mathbf{J}(\mathbf{q}) \rangle = 0,$$

assuming $\mathcal{J}(-\mathbf{q}) = \mathcal{J}(\mathbf{q})$. For a given value of λ , this condition is only satisfied if either $\langle \mathbf{J}(\mathbf{q}) \rangle = \mathbf{0}$, or if $\mathbf{q} = \mathbf{q}_\lambda$, where $\mathcal{J}(\mathbf{q}_\lambda) = 2\lambda$, which implies that only $\langle \mathbf{J}(\mathbf{q}_\lambda) \rangle$ may be non-zero. Introducing this condition in U , we find

$$U = -N\lambda (J\sigma)^2 = -\frac{1}{2} N \mathcal{J}(\mathbf{q}_\lambda) (J\sigma)^2, \quad (2.1.27b)$$

which is then minimized with respect to \mathbf{q} when $\mathbf{q}_\lambda = \mathbf{Q}$, at which wave-vector $\mathcal{J}(\mathbf{q})$ has its maximum. Hence the two-ion energy attains its minimum when only the two Fourier components $\langle \mathbf{J}_i(\pm \mathbf{Q}) \rangle$ are non-zero. The stronger constraint that $|\langle \mathbf{J}_i \rangle|$ should be constant is then met only by the helix (2.1.26). In the zero-temperature limit, this constraint derives from the fact that the moments attain their saturation value, $|\langle \mathbf{J}_i \rangle| = J$, immediately the exchange field is not identically zero, since $\chi_{\alpha\alpha}^o(\sigma = 0)$ diverges in this limit when $\mathcal{H}_{\text{cf}} = 0$. At elevated temperatures, it is clear that the sum of the single-ion terms in the free energy (the A - and B -terms in (2.1.22)) is most effectively minimized if the minimum condition is the same for all the ions. When $\mathcal{H}_{\text{cf}} = 0$, there are no restrictions on the plane in which the moments spiral; it may be rotated freely, without change in energy, as long as $|\mathbf{J}_i|$ is constant and all the components vary with the wave-vector \mathbf{Q} . This behaviour is analogous to that of the Heisenberg ferromagnet, which may be considered as a helically ordered system with $\mathbf{Q} = \mathbf{0}$. If \mathbf{Q} is not perpendicular to the plane in which the moments lie, the structure is called the *tilted helix* (Elliott 1971; Sherrington 1972) and the extreme case, with \mathbf{Q} in the plane of the moments, is the *cycloidal structure*. When $B_2^0 > 0$, the orientation of the plane is stabilized to be perpendicular to the c -axis, and with \mathbf{Q} along this axis we obtain the true helical structure.

If $B_2^0 > 0$ is the only crystal-field parameter of importance, the regular helix is the stable structure in the whole temperature interval between zero and T_N . If the Landau expansion (2.1.22) is continued to the sixth power in the magnetization, a term appears proportional to B_6^6 , distinguishing between the a - and b -directions in the basal-plane. Instead of using this expansion, we shall consider the alternative expression for the free energy, to leading order in B_6^6 ,

$$\begin{aligned} F &\simeq F_1 - \frac{1}{2} \sum_{ij} \mathcal{J}(ij) \langle \mathbf{J}_i \rangle \cdot \langle \mathbf{J}_j \rangle + \sum_i B_6^6 \langle O_6^6(\mathbf{J}_i) \rangle \\ &= F_1 - \frac{1}{2} \sum_{ij} (J\sigma)^2 \mathcal{J}(ij) \cos(\phi_i - \phi_j) + \sum_i \kappa_6^6 \cos 6\phi_i, \end{aligned} \quad (2.1.28)$$

where $\mathbf{J}_i = J\sigma(\cos \phi_i, \sin \phi_i, 0)$ and F_1 is the part independent of ϕ_i . The expectation values are those obtained in the limit $B_6^6 = 0$, i.e. σ and κ_6^6 are assumed to be independent of the angle ϕ_i . The presence of the six-fold anisotropy term distorts the helix. In order to solve the equilibrium equation

$$\partial F / \partial \phi_i = (J\sigma)^2 \sum_j \mathcal{J}(ij) \sin(\phi_i - \phi_j) - 6\kappa_6^6 \sin 6\phi_i = 0,$$

we introduce the expansion

$$\phi_i = u_i + \gamma \sin 6u_i + \cdots \quad ; \quad u_i = \mathbf{Q} \cdot \mathbf{R}_i, \quad (2.1.29a)$$

using the series

$$\begin{aligned} & \exp[i(u + \gamma \sin 6u)] \\ &= J_0(\gamma)e^{iu} + J_1(\gamma)(e^{i7u} - e^{-i5u}) + J_2(\gamma)(e^{i13u} + e^{-i11u}) + \dots \\ &\simeq e^{iu} + \frac{\gamma}{2}(e^{i7u} - e^{-i5u}), \end{aligned} \quad (2.1.29b)$$

where $J_n(x)$ are the Bessel functions. To leading order in γ , the equilibrium equation then gives

$$\gamma = \frac{12\kappa_6^6}{(J\sigma)^2\{2\mathcal{J}(\mathbf{Q}) - \mathcal{J}(5\mathbf{Q}) - \mathcal{J}(7\mathbf{Q})\}}, \quad (2.1.30a)$$

and the free energy is reduced proportionally to γ^2 :

$$F/N = F_1/N - \frac{1}{2}(J\sigma)^2 \mathcal{J}(\mathbf{Q}) - \frac{1}{8}(J\sigma)^2 \{2\mathcal{J}(\mathbf{Q}) - \mathcal{J}(5\mathbf{Q}) - \mathcal{J}(7\mathbf{Q})\} \gamma^2. \quad (2.1.30b)$$

The hexagonal anisotropy introduces harmonics, of equal magnitude, in the basal-plane moments at the wave-vectors $6\mathbf{Q} \pm \mathbf{Q}$ and, in higher order, at the wave-vectors $6m\mathbf{Q} \pm \mathbf{Q}$. If κ_6^6 , and thus also γ , are negative, the easy directions in the plane are the a -axes. In the special case where the angle $u_i = \pi/12$, i.e. the unperturbed i th moment is half-way between an easy and a hard direction, the largest change $\phi_i - u_i = \gamma$ occurs in the orientation of the moments, and the angle to the nearest easy direction is reduced, since u_i lies between 0 and $\pi/6$, and κ_6^6 is negative. The moments in the helix are therefore distorted so that they bunch around the easy axes.

The above calculation is not valid if Q is 0 or $2\pi/c$, when the hexagonal anisotropy may be minimized without increasing the exchange energy, as it may also if the (average) turn angle ω of the moments from one hexagonal plane to the next is a multiple of 60° , so that $6Q$ is an integer times $4\pi/c$. The products of the fifth and seventh harmonics introduce additional umklapp contributions to the free energy if $12Q$ is a multiple of the *effective* reciprocal-lattice spacing $4\pi/c$, implying that the cases where ω is $p30^\circ$ and $p = 1, 3, 5$ are also special. In higher order, corrections appear whenever $m12Q = p4\pi/c$, where m and p are integers and $0 \leq p \leq 6m$, i.e. at any commensurable value of Q , but the corrections decrease rapidly with m , excluding cases where m and p have common factors. In contrast to the result found above, the commensurable contributions depend on the absolute phase φ in (2.1.26b), and an adjustment of this phase will quite generally allow the system to reduce the anisotropy energy through the umklapp terms. This change in energy may compensate for the increase in the exchange energy when the ordering wave-vector \mathbf{Q} is changed from its value $\mathbf{Q} = \mathbf{Q}_0$, at which

$\mathcal{J}(\mathbf{q})$ has its maximum, to a nearby commensurable value \mathbf{Q}_c . Hence the hexagonal anisotropy couples the helical magnetic structure to the lattice, and it may induce continuous or abrupt changes of the ordering wave-vector as a function of temperature, as discussed, for instance, by Bak (1982). In Ho, $12Q_0$ is close to $4\pi/c$, and the hexagonal anisotropy is large at low temperatures. Experimental investigations have shown that a number of commensurable values of \mathbf{Q} are stabilized in this system, as we shall discuss in more detail in the last section of this chapter.

2.1.4 Longitudinally ordered phases

When B_2^0 is negative, as in Er and Tm, $\chi_{\zeta\zeta}(\mathbf{Q})$ is the component of the susceptibility which diverges at the highest temperature, and the high-temperature expansion predicts that $2A_\zeta - \mathcal{J}(\mathbf{Q})$ vanishes at a critical temperature determined by

$$k_B T_N \simeq \frac{1}{3} J(J+1) \mathcal{J}(\mathbf{Q}) \left[1 - \frac{4}{5} \left(J - \frac{1}{2} \right) \left(J + \frac{3}{2} \right) B_2^0 / k_B T_N \right]. \quad (2.1.31)$$

Just below this temperature, only the component σ_ζ at the wave-vector \mathbf{Q} is non-zero and, from the free energy expansion (2.1.24), $\partial f / \partial \sigma_\zeta = 0$ determines the relative magnetization as

$$\sigma_\zeta(\mathbf{Q}) = \sigma_{\mathbf{Q}} = \left(\frac{\mathcal{J}(\mathbf{Q}) - 2A_\zeta}{3J^2 B_{\zeta\zeta}} \right)^{1/2}. \quad (2.1.32)$$

The free energy is independent of the phase $\varphi = \varphi_\zeta$, so we set $\varphi = 0$. If we add another Fourier component with $\mathbf{q} \neq \pm\mathbf{Q}$:

$$\langle J_{i\zeta} \rangle = J \sigma_{\mathbf{Q}} \cos(\mathbf{Q} \cdot \mathbf{R}_i) + J \sigma_{\mathbf{q}} \cos(\mathbf{q} \cdot \mathbf{R}_i + \varphi') \quad (2.1.33)$$

then, if $m\mathbf{Q} \pm n\mathbf{q}$ is different from a reciprocal lattice vector, where m and n are integers and $m+n = \pm 4$, the free energy is

$$f = \frac{1}{4} J^2 [\{2A_\zeta - \mathcal{J}(\mathbf{Q})\} \sigma_{\mathbf{Q}}^2 + \{2A_\zeta - \mathcal{J}(\mathbf{q})\} \sigma_{\mathbf{q}}^2] + \frac{1}{8} J^4 B_{\zeta\zeta} [3\sigma_{\mathbf{Q}}^4 + 3\sigma_{\mathbf{q}}^4 + 12\sigma_{\mathbf{Q}}^2 \sigma_{\mathbf{q}}^2 + 4\sigma_{\mathbf{Q}}^3 \sigma_{\mathbf{q}} \delta_{\mathbf{q}, \pm 3\mathbf{Q}} \cos \varphi' + 4\sigma_{\mathbf{Q}} \sigma_{\mathbf{q}}^3 \delta_{3\mathbf{q}, \pm \mathbf{Q}} \cos 3\varphi']. \quad (2.1.34)$$

This result shows that, if $\mathbf{q} = 3\mathbf{Q}$ or $\mathbf{q} = \frac{1}{3}\mathbf{Q}$, there is an extra fourth-order contribution to the free energy ($\mathbf{q} \rightarrow -\mathbf{q}$ represents the same structure with $\varphi' \rightarrow -\varphi'$). Of these two special cases, the one where $\mathbf{q} = 3\mathbf{Q}$ is the most interesting, because the extra term is linear in $\sigma_{3\mathbf{Q}}$. This means that the third harmonic appears simultaneously with the basic Fourier component at \mathbf{Q} . Minimizing the free energy given by (2.1.34), we find

$$\sigma_{3\mathbf{Q}} = \frac{J^2 B_{\zeta\zeta}}{\mathcal{J}(\mathbf{Q}) - \mathcal{J}(3\mathbf{Q})} \sigma_{\mathbf{Q}}^3 \quad ; \quad \varphi' = \varphi + \pi, \quad (2.1.35a)$$

neglecting a term proportional to $\sigma_{\mathbf{Q}}^2$ in the denominator. The $3\mathbf{Q}$ -component is thus proportional to $\sigma_{\mathbf{Q}}^3$, and hence to $(T_N - T)^{3/2}$. Denoting the wave-vector at which $\mathcal{J}(\mathbf{q})$ has its maximum by \mathbf{Q}_0 , we conclude that the appearance of the third harmonic implies that f has its minimum at a value of \mathbf{Q} slightly different from \mathbf{Q}_0 . Minimizing the free energy with respect to \mathbf{Q} along the c -axis, by requiring $\partial f / \partial Q = 0$, we obtain to leading order

$$Q = Q_0 - 3 \frac{\mathcal{J}'(3\mathbf{Q}_0)}{\mathcal{J}''(\mathbf{Q}_0)} \left(\frac{\sigma_{3\mathbf{Q}}}{\sigma_{\mathbf{Q}}} \right)^2. \quad (2.1.35b)$$

$\mathcal{J}''(\mathbf{Q}_0)$ is negative, so the shift $Q - Q_0$ has the same sign as $\mathcal{J}'(3\mathbf{Q}_0)$ and is proportional to $(T_N - T)^2$. The other special case, $3\mathbf{q} = \mathbf{Q}$, reflects the possibility that, if $\mathcal{J}(\mathbf{Q}_0/3)$ is close to $\mathcal{J}(\mathbf{Q}_0)$, the system may reduce its energy by making a *first order* transition to a state where $\mathbf{Q} \simeq \mathbf{Q}_0/3$ is the fundamental wave-vector, with the third harmonic being close to \mathbf{Q}_0 . The presence of a term in the free energy cubic in the order parameter, $\sigma_{\mathbf{Q}/3}$ in this case, implies that the transition becomes of first order, so that the order parameter changes discontinuously from zero to a finite value. The $\mathbf{Q}_0/3$ -transition appears to be of no importance in real systems, so we shall return to the discussion of the other case. If the free energy is expanded to higher (even) powers in the relative magnetization, it is clear that the $(2n + 2)$ -power term leads to a contribution proportional to $\sigma_{(2n+1)\mathbf{Q}} \sigma_{\mathbf{Q}}^{2n+1}$ which, in combination with the term quadratic in $\sigma_{(2n+1)\mathbf{Q}}$, implies that the ordering at the fundamental wave-vector \mathbf{Q} induces a $(2n + 1)$ -harmonic proportional to $\sigma_{\mathbf{Q}}^{2n+1} \propto (T_N - T)^{(2n+1)/2}$. Starting as a pure sinusoidally modulated wave at T_N , the moments approach the *square wave*

$$\langle J_{i\zeta} \rangle = \frac{4J}{\pi} \left(\cos x - \frac{1}{3} \cos 3x + \frac{1}{5} \cos 5x - \frac{1}{7} \cos 7x + \dots \right)_{x=\mathbf{Q} \cdot \mathbf{R}_i + \varphi}, \quad (2.1.36a)$$

in the limit of zero temperature where $\langle J_{i\zeta} \rangle = \pm J$, neglecting strong anisotropy effects. Although the behaviour of the angular momentum is simple, the dependence of the free energy on the wave-vector is complicated. It is only when the ordering is incommensurable, i.e. mQ is different from any multiple of the length $4\pi/c$ of the reciprocal-lattice vector along the c -axis, that the energy of the square-wave structure at $T = 0$ is

$$f(0) = \langle \mathcal{H}_{\text{cf}} \rangle - \frac{4J^2}{\pi^2} \left\{ \mathcal{J}(\mathbf{Q}) + \frac{1}{9} \mathcal{J}(3\mathbf{Q}) + \frac{1}{25} \mathcal{J}(5\mathbf{Q}) + \dots \right\}. \quad (2.1.36b)$$

An infinitesimal change of the ordering wave-vector from \mathbf{Q} , which minimizes $f(0)$, to \mathbf{Q}_c may make it commensurable with the lattice, so that

$mQ_c = p(4\pi/c)$ and additional umklapp terms contribute to the free energy. Again these contributions depend on the absolute phase φ , and there will always be values of Q_c close to Q leading to a lower free energy than that obtained in the incommensurable case. In the low-temperature limit, the modulation of the c -axis moment is therefore locked to the lattice periodicity. This tendency is already apparent close to T_N . In the expansion of the free energy considered above for $m = 4$, umklapp terms modify the fourth-power coefficient, and analogous effects occur in higher powers of the magnetization. This indicates that the system may stay commensurable even near T_N although, in the close neighbourhood of T_N , the critical fluctuations neglected here may oppose this tendency. The optimal value of Q_c may change as a function of temperature, in which case the system will exhibit a number of first-order, or possibly continuous, transitions from one commensurable structure to another. Of these structures, those for which $Q_c = 3Q_c = 5Q_c = \dots$, i.e. $Q_c = 0$ or $2\pi/c$, are particularly stable, as they only involve one wave-vector, so that $f(0) = \langle \mathcal{H}_{cf} \rangle - \frac{1}{2}J^2 \mathcal{J}(\mathbf{Q}_c)$ (in this connection, we note that $1 + \frac{1}{9} + \frac{1}{25} + \dots = \pi^2/8$). The anisotropic Ising-model with competing interactions, the so-called *ANNNI* model, is a simplified version of the above, and it shows a rich variety of different incommensurable, commensurable, and chaotic ordered structures as a function of temperature and the coupling parameters (Bak 1982).

2.1.5 Competing interactions and structures

The complex behaviour of the longitudinally ordered phase is a consequence of the competition between the single-ion part of the free energy, which favours a structure in which the magnitude of the moments varies as little as possible, particularly at low temperature, and the two-ion contributions, which prefer a single- \mathbf{Q} ordering. When B_2^0 is positive, helical ordering satisfies both tendencies without conflict. This points to another alternative which the longitudinal system may choose. Although $\chi_{\zeta\zeta}(\mathbf{Q})$ decreases below T_N , the two perpendicular components continue to increase, and they may therefore diverge at a lower temperature T'_N . Assuming the expansion (2.1.24) of the free energy still to be valid at T'_N , and neglecting the third and higher harmonics of $\langle J_{i\zeta} \rangle$, we may write it:

$$f = f(\sigma_{\mathbf{Q}}) + \frac{1}{4}J^2 \sum_{\alpha=\xi,\eta} [2A_{\xi} - \mathcal{J}(\mathbf{Q}) + B_{\xi\zeta}(J\sigma_{\mathbf{Q}})^2 \{2 + \cos 2(\varphi_{\alpha} - \varphi)\}] \sigma_{\alpha}^2 + \frac{1}{8}J^4 B_{\xi\xi} [3\sigma_{\xi}^4 + 3\sigma_{\eta}^4 + 2\{2 + \cos 2(\varphi_{\xi} - \varphi_{\eta})\} \sigma_{\xi}^2 \sigma_{\eta}^2]. \quad (2.1.37)$$

The effective coefficient of σ_{α}^2 ($\alpha = \xi$ or η) is smallest when $\varphi_{\alpha} = \varphi \pm \frac{\pi}{2}$, meaning that the basal-plane moments appearing just below T'_N , where

this coefficient vanishes, are locked to be out of phase by 90° with the c -axis component. This phase difference arises because the transverse MF susceptibility $\chi_{\xi\xi}^o$ for the single sites increases as the c -axis exchange field falls. Using the estimate (2.1.21b) for the B -tensor, and the high-temperature value for A_ξ , we find the transition temperature to be

$$k_B T'_N \simeq \frac{1}{3} J(J+1) \mathcal{J}(\mathbf{Q}) \left[1 + \frac{2}{5} (J - \frac{1}{2})(J + \frac{3}{2}) B_2^0 / k_B T'_N \right. \\ \left. - \frac{3}{20} \{ 1 + \frac{1}{2} (J+1)^{-2} \} \sigma_{\mathbf{Q}}^2 \right]. \quad (2.1.38)$$

A slightly better estimate may be obtained by calculating the MF value of the transverse susceptibility directly, in the presence of a non-zero exchange field, which just causes the replacement of $\sigma_{\mathbf{Q}}$ in (2.1.38) by $3\sigma_{\mathbf{Q}} \mathcal{J}(\mathbf{Q}) / [J(J+1)k_B T'_N]$ (Miwa and Yosida 1961). However, both results are based on the high-temperature expansion, which ceases to be valid at low temperatures. In the zero-temperature limit, $\chi_{\xi\xi}^o$ of the i th site remains finite, being of the order $J/h_{i\xi}^{\text{eff}}$. This saturation implies that the transition does not necessarily occur. If the c -axis is favoured too strongly by the anisotropy terms, the basal-plane components remain disordered at low temperatures, as is observed in Tm. When the basal-plane moments order, as in Er, eqn (2.1.38) may give a reasonable estimate of the transition temperature. As mentioned previously, the modulation of the basal-plane moments, just below T'_N , is locked at 90° out of phase with that of the c -axis component. Since this applies to both components, only a linearly-polarized moment can develop at the transition temperature, with a relative magnitude $\sigma_{\perp} = (\sigma_{\xi}^2 + \sigma_{\eta}^2)^{1/2}$, in a specified but arbitrary direction in the plane. If the sixth-power terms are included in the free energy, B_6^0 favours either the a - or the b -directions, but there are still six equivalent but different directions of the moments in the basal plane with equal energies. To be specific, we may assume that B_6^0 is negative and that the ordered moments in the basal plane establish themselves along the ξ -axis. In this case, the moments all lie in the ξ - ζ plane in an elliptic cycloidal structure. Displaced to a common origin, the hodograph of the moments is an ellipse, with its principal axes along the ξ - and ζ -axes, as is illustrated, in connection with our discussion of Er, in Fig. 2.6 on page 120. The c -axis moments will still show a strong tendency towards squaring up with decreasing temperature, as long as they are large compared with the basal-plane moments. Because of the phase-locking between the components, the higher odd-harmonics in the modulation of the c -axis moments will also be reflected in the basal-plane.

At high temperatures, B_2^0 is the dominant anisotropy parameter, and its sign determines whether the system orders in a helically or longitudinally polarized structure, when \mathbf{Q}_0 is along the c -axis. If B_2^0 is still

the most important axial-anisotropy parameter in the low-temperature limit, the helix is still a stable structure at $T = 0$ whereas, in the longitudinally polarized case, the tendency to minimize the variation of the lengths of the moments may result in two different paths. Either the system stays in the longitudinally polarized phase, ending up as a (commensurable) square-wave structure at $T = 0$, or it goes through a transition to an elliptic cycloidal structure. The path which is chosen depends on the magnitude of B_2^0 ; if the effective axial anisotropy $-B_2^0 \langle O_2^0 \rangle$ is sufficiently large, the ordering of the basal-plane moments is quenched. It has already been mentioned in Section 1.5 that this anisotropy depends on the magnetization, being proportional approximately to σ^3 . We shall discuss this renormalization in more detail in the next section, but it is worth mentioning here that this behaviour of the effective anisotropy-parameter means that there is an intermediate range of B_2^0 for which the system makes a transition to the elliptic cycloidal structure, but leaves it again at a lower temperature, by returning to the longitudinally polarized phase when $-B_2^0 \langle O_2^0 \rangle$ becomes large enough. When B_4^0 and B_6^0 are included, a more realistic situation may occur, in which the low-temperature anisotropy favours an orientation of the moments making an angle θ with the c -axis, which is neither 0 or $\pi/2$ but some, temperature-dependent, intermediate value. In the case of the helix, this means that there will be a critical temperature T'_N (below T_N) where the effective axial anisotropy parameter vanishes, and below which the c -axis moments are ordered. If the ordering wave-vector for the c -axis component is the same as the helical wave-vector, the structure adopted is the tilted helix. However the two-ion coupling between the c -axis moments, $\mathcal{J}_{\parallel}(\mathbf{q})$ with $\mathbf{q} \parallel c$ -axis, is not restricted by any symmetry argument to be equal to the coupling between the basal-plane moments, $\mathcal{J}_{\perp}(\mathbf{q}) = \mathcal{J}(\mathbf{q})$ with its maximum at $\mathbf{q} = \mathbf{Q}_0$. If the maximum of $\mathcal{J}_{\parallel}(\mathbf{q})$ lies at a $\mathbf{q} \neq \mathbf{Q}_0$, the c -component will order at this wave-vector and not at \mathbf{Q}_0 , as the extra energy gained by the c -component by locking to the basal-plane moments is very small, being proportional to $\{B_6^0 \langle O_6^0 \rangle / (J\sigma)^2 \mathcal{J}(\mathbf{Q})\}^2$. When B_2^0 is negative, a non-zero value of θ favours the elliptic cycloidal structure, compared to the longitudinally polarized phase. If the system is already in the cycloidal phase, it may undergo a new second-order transition, in which the plane of the ellipse starts to tilt away from the ξ - ζ plane, in close correspondence with the behaviour of the helix. Referring back to eqn (2.1.37), we observe that this transition occurs when the coefficient of σ_{η}^2 , with $\varphi_{\eta} = \varphi(+\pi) = \varphi_{\xi} \pm \pi/2$, becomes zero. The phase-locking energy, comprising the terms in (2.1.37) involving φ_{η} , is more important in this case than in the helix, but it is nevertheless possible that the third component may order at a wave-vector different from that of the other

two. If the η -component is locked at the same wave-vector as the two other components, and if the ellipse is tilted just such an amount that $\sigma_\eta = \sigma_\xi$, the structure is a helix superimposed on a modulated c -axis moment. If a transition to the tilted cycloidal structure has occurred, and the hexagonal anisotropy is small, it might be favourable for the system at a lower temperature to pass directly, via a first-order transition, to this helical structure in which the c -axis component is no longer phase-locked to the basal-plane moments.

Instead of basing our analysis on the Hamiltonian (2.1.1), we may use symmetry arguments for deriving the most general behaviour of the magnetic ordering in hcp crystals. We have already indicated that $\mathcal{J}_\parallel(\mathbf{q})$ may differ from $\mathcal{J}_\perp(\mathbf{q})$ and mentioned some of the consequences. The assumption that the c -axis is effectively a six-fold axis of the lattice leads to the strong restriction that the expansion of the free energy, (2.1.22) or (2.1.24), only involves even powers of each of the Cartesian components, when \mathbf{q} is along this axis. This has the consequence, for example, that all the main transitions, at T_N or T'_N , are predicted to be of second order, excluding those involving changes of the same component, i.e. transitions between different commensurable structures. However, there are two-ion terms which reflect the fact that the c -axis is only a three-fold axis. The term of lowest rank has the form

$$\begin{aligned} \mathcal{H}_3(i \in s\text{'th plane}) = & (-1)^s K_3 \left[(J_{i\zeta} - \frac{1}{2}\langle J_{i\zeta} \rangle) \langle O_3^{-3}(\mathbf{J}_{s+1}) - O_3^{-3}(\mathbf{J}_{s-1}) \rangle \right. \\ & \left. + (O_3^{-3}(\mathbf{J}_i) - \frac{1}{2}\langle O_3^{-3}(\mathbf{J}_i) \rangle) \langle J_{s+1,\zeta} - J_{s-1,\zeta} \rangle \right], \quad (2.1.39) \end{aligned}$$

in the MF approximation, where only interactions between neighbouring planes are included. $O_3^{-3} = (J_+^3 - J_-^3)/2i$, and $\mathbf{J}_{s\pm 1}$ denotes a moment in the $(s\pm 1)$ th plane. The contribution of this coupling to the expansion (2.1.22) of the free energy to the fourth power is found by adding $\sum_i \langle \mathcal{H}_3 \rangle$ to F , using the approximation $\langle O_3^{-3}(\mathbf{J}_i) \rangle \propto \langle J_{i\eta} \rangle (3\langle J_{i\xi} \rangle^2 - \langle J_{i\eta} \rangle^2) = \langle J_\perp \rangle^3 \sin 3\phi_i$. One remarkable effect is that this coupling introduces a term linear in $\langle J_{i\zeta} \rangle$ in the helix. If the basal-plane moments are ordered with the wave-vector \mathbf{Q} , they induce a c -axis moment modulated with a wave-vector along the c -axis of length $2\pi/c - 3Q$, provided that $6\mathbf{Q}$ is not a reciprocal lattice vector. In the elliptic cycloidal structure, this coupling induces an ordering of the η -component at the two wave-vectors of length $2\pi/c - Q$ and $2\pi/c - 3Q$, when the ellipse is assumed to lie in the ξ - ζ plane and only the fundamental at Q is considered. Although this additional coupling may not change the nature of the transitions at T_N or T'_N , it has qualitative consequences for the magnetic structures, and it may introduce new effects associated with commensurability. For instance, the three-fold symmetrical interaction will favour the commensurable structure with $Q = \pi/2c$ (an average turn angle of 45°). In the

case of a helix with this particular period, the coupling induces a modulation of the c -axis moments with the same wave-vector, $2\pi/c - 3Q = Q$, causing a tilting of the plane of the helix.

2.1.6 Multiply periodic structures

We have so far only considered order parameters which are specified by two \mathbf{Q} -vectors ($\pm\mathbf{Q}$), or one \mathbf{Q} plus a phase. This is a consequence of the assumption that \mathbf{Q} is along the c -axis. If \mathbf{Q} is in the basal-plane, as in the light rare earths Pr and Nd, there are six equivalent ordering wave-vectors, $\pm\mathbf{Q}_1$, $\pm\mathbf{Q}_2$, and $\pm\mathbf{Q}_3$, where the three vectors make an angle of 120° with each other. This leads to the possibility that the ordered structure is a *multiple-Q structure*, where

$$\langle \mathbf{J}_i \rangle = \mathbf{J}_1 \cos(\mathbf{Q}_1 \cdot \mathbf{R}_i + \varphi_1) + \mathbf{J}_2 \cos(\mathbf{Q}_2 \cdot \mathbf{R}_i + \varphi_2) + \mathbf{J}_3 \cos(\mathbf{Q}_3 \cdot \mathbf{R}_i + \varphi_3) \quad (2.1.40)$$

referred to as *single-*, *double-*, or *triple-Q* ordering, depending on the number of vectors \mathbf{J}_p which are non-zero. The transition at T_N will generally involve only a single real vector \mathbf{J}_p for each \mathbf{Q}_p , as implicitly assumed in (2.1.40). We will not therefore consider multiple- \mathbf{Q} cycloidal/helical structures, but restrict the discussion to configurations which correspond to the type observed in Pr or Nd. We furthermore neglect the complications due to the occurrence of different sublattices in the dhcp crystals, by assuming the lattice to be primitive hexagonal. This simplification does not affect the description of the main features of the magnetic structures. On the hexagonal sites of Pr and Nd, the ordered moments below T_N lie in the basal plane. This confinement is not primarily determined by the sign of B_2^0 , but is decisively influenced by the anisotropic two-ion coupling

$$\mathcal{H}_{\text{an}} = \frac{1}{2} \sum_{ij} \mathcal{K}(ij) [(J_{i\xi} J_{j\xi} - J_{i\eta} J_{j\eta}) \cos 2\phi_{ij} + (J_{i\xi} J_{j\eta} + J_{i\eta} J_{j\xi}) \sin 2\phi_{ij}], \quad (2.1.41)$$

where ϕ_{ij} is the angle between the ξ -axis and the projection of $\mathbf{R}_i - \mathbf{R}_j$ on the basal plane. This anisotropic coupling, which includes a minor contribution from the classical dipole-dipole interaction, is known from the excitation spectrum to be of the same order of magnitude as the isotropic coupling in Pr, as we shall discuss in Chapter 7, and must be of comparable importance in Nd. We define the coupling parameter $\mathcal{K}(\mathbf{q}) = \mathcal{K}_0(q) + \mathcal{K}_6(q) \cos 6\psi_q$, where ψ_q is the angle between \mathbf{q} (in the basal plane) and the ξ -axis, and $\mathcal{K}_0(q) \pm \mathcal{K}_6(q)$ is the Fourier transform of $\pm\mathcal{K}(ij) \cos 2\phi_{ij}$ when \mathbf{q} is respectively parallel or perpendicular to the ξ -axis. Introducing $\mathbf{J}_p = J\boldsymbol{\sigma}_p$, and assuming the moments to be perpendicular to the c -axis, we find the mean-field free energy of second

order in σ_p to be

$$f_2(\sigma_p) = \frac{1}{4}J^2 \sum_p [\{2A_\xi - \mathcal{J}(\mathbf{Q}_p)\}\sigma_p^2 + \mathcal{K}(\mathbf{Q}_p)\{2(\sigma_p \cdot \hat{\mathbf{Q}}_p)^2 - \sigma_p^2\}], \quad (2.1.42)$$

where $\hat{\mathbf{Q}}_p = \mathbf{Q}_p/Q_p$. In Pr and Nd, the maximum of $\mathcal{J}(\mathbf{q}) \pm \mathcal{K}(\mathbf{q})$ is found at $\mathbf{q} = \mathbf{Q}$ along the η -axis, or the other equivalent b -axes, with Q being about one fourth of the distance to the Brillouin-zone boundary, and $\mathcal{K}(\mathbf{Q})$ is negative. The transition between the paramagnetic phase and a phase described by (2.1.40), with \mathbf{J}_p lying in the hexagonal plane, then occurs when the coefficient $2A_\xi - \mathcal{J}(\mathbf{Q}) + \mathcal{K}(\mathbf{Q})$ vanishes, at which temperature the corresponding factor for the c -component of the moments, $2A_\zeta - \mathcal{J}(\mathbf{Q})$, is still positive in Pr and Nd. Besides confining the moments to the hexagonal planes, $\mathcal{K}(\mathbf{Q})$ also removes the degeneracy between the two states in which \mathbf{J}_p is parallel or perpendicular to \mathbf{Q}_p . With a negative $\mathcal{K}(\mathbf{Q})$, the anisotropic coupling favours a longitudinal ordering of the moments at T_N , with \mathbf{J}_p parallel to \mathbf{Q}_p . Just below T_N , the magnitude of the ordered moments is determined by $f_2(\sigma_p)$, together with the fourth-order contributions. When the moments lie in the basal plane ($B = B_{\xi\xi} = B_{\eta\eta} = B_{\xi\eta}$), we obtain, from eqn (2.1.22),

$$\begin{aligned} f_4(\sigma_p) &= B \frac{1}{N} \sum_i (\langle \mathbf{J}_i \rangle \cdot \langle \mathbf{J}_i \rangle)^2 \\ &= BJ^4 \left[\frac{3}{8} \sum_p \sigma_p^4 + \frac{1}{4} \sum_{p \neq p'} \{ \sigma_p^2 \sigma_{p'}^2 + 2(\sigma_p \cdot \sigma_{p'})^2 \} \right]. \end{aligned} \quad (2.1.43)$$

Introducing the effective order parameter σ , defined by $\sigma^2 = \sum_p \sigma_p^2$, we obtain further:

$$f \simeq f_2(\sigma_p) + f_4(\sigma_p) = \frac{1}{4}J^2 \{ 2A_\xi - \mathcal{J}(\mathbf{Q}) + \mathcal{K}(\mathbf{Q}) \} \sigma^2 + \frac{3}{8}J^4 B \sigma^4, \quad (2.1.44)$$

assuming \mathbf{J}_p parallel to \mathbf{Q}_p along the three b -axes making an angle of 120° with each other ($\hat{\mathbf{Q}}_p \cdot \hat{\mathbf{Q}}_{p'} = -1/2$ when $p \neq p'$). Hence the free energy, in this approximation, is independent of whether the ordering is single-, double- or triple- \mathbf{Q} . Instead of utilizing (2.1.22), we may appeal to symmetry arguments, by which the fourth-order term may readily be seen to have the general form

$$f_4(\sigma_p) = u \sum_p \sigma_p^4 + \frac{1}{2}v \sum_{p \neq p'} \sigma_p^2 \sigma_{p'}^2, \quad (2.1.45a)$$

as long as the angles between the different σ_p vectors remain at 120° (Bak and Lebeck 1978). Introducing the parameter $w \equiv v - 2u$, we may write this:

$$f_4(\sigma_p) = u \left(\sum_p \sigma_p^2 \right)^2 + \frac{1}{2}w \sum_{p \neq p'} \sigma_p^2 \sigma_{p'}^2 = (u + \gamma w) \sigma^4, \quad (2.1.45b)$$

where $\gamma = 0, 1/4,$ or $1/3$ respectively, in a single-, double-, or triple- \mathbf{Q} structure. If only an isotropic two-ion coupling and the crystal-field terms are included, $2u = v$ or $w = 0$, and the different multiple- \mathbf{Q} structures are degenerate to the fourth power of the order parameter. This situation is not changed by the anisotropic dipole coupling $\mathcal{K}(\mathbf{q})$ introduced above (as long as $\boldsymbol{\sigma}_p$ is parallel to \mathbf{Q}_p). However, two-ion quadrupole couplings may remove the degeneracy. For example, the coupling $\mathcal{K}_2(ij)J_{i+}^2 J_{j-}^2$ makes a contribution proportional to

$$w \sim 3\mathcal{K}_2(\mathbf{0}) + \mathcal{K}_2(2\mathbf{Q}) - 2\mathcal{K}_2(\mathbf{Q}) - 2\mathcal{K}_2(\mathbf{Q}_1 - \mathbf{Q}_2). \quad (2.1.46)$$

Depending on the detailed \mathbf{q} -dependence of this coupling, it may lead to a positive or a negative contribution to w . If w is positive, the single- \mathbf{Q} structure is stable, and conversely a negative w leads to a triple- \mathbf{Q} structure just below T_N . The Landau expansion for this case has been discussed by Forgan (1982), Walker and McEwen (1983) and McEwen and Walker (1986), who all take the possible contributions to w as being of magnetoelastic origin. In Pr, the dominating magnetoelastic interaction is known to be due to the γ -strain coupling, and a rough estimate (including both the uniform and modulated γ -strain) indicates that v is unaffected, whereas the reduction of u proportional to $B_{\gamma 2}^2/c_\gamma$, with the parameters of (1.5.27), is about 10%, corresponding to a *positive* contribution to w of about $0.2u$, or to an energy difference between the single- and double- \mathbf{Q} structures of $\sim 0.05u\sigma^4$. If the other quadrupolar contributions are unimportant, as is indicated by the behaviour of the excitations in Pr (Houmann *et al.* 1979), we should expect the single- \mathbf{Q} structure to be favoured in Pr and Nd, at least close to T_N .

If w is relatively small, the single- or triple- \mathbf{Q} structures may only be stable in a narrow temperature range below T_N , because the sixth-order contributions may assume a decisive influence. A number of new effects appear in this order, but the most important stems from the possibility that the moments and the wave-vectors may rotate away from the b -directions, as first considered by Forgan (1982). The $(\boldsymbol{\sigma}_p \cdot \boldsymbol{\sigma}_{p'})^2$ -term in (2.1.43) may drive such a rotation, because it favours an orthogonal configuration of the different $\boldsymbol{\sigma}_p$ vectors, since B is positive. This term does not appear in the single- \mathbf{Q} structure, whereas in the triple- \mathbf{Q} case, $f_4(\boldsymbol{\sigma}_p)$ is reduced quadratically with θ_p , where θ_p is the angle between \mathbf{J}_p and the nearest b -direction. However, the much larger quadratic increase of $f_2(\boldsymbol{\sigma}_p)$, due to $\mathcal{K}(\mathbf{Q})$, will eliminate any tendency for θ_p to become non-zero. In contrast, $f_4(\boldsymbol{\sigma}_p)$ depends linearly on θ_p in the double- \mathbf{Q} structure, and the free energy can always be reduced by allowing the two components $\boldsymbol{\sigma}_1$ and $\boldsymbol{\sigma}_2$ (with $\boldsymbol{\sigma}_3 = \mathbf{0}$) to rotate towards each other. Defining $\mathcal{J}_6(Q)$ equivalently to $\mathcal{K}_6(Q)$, i.e. $\mathcal{J}(\mathbf{Q}) = \mathcal{J}_0(Q) + \mathcal{J}_6(Q) \cos 6\psi_Q$, and using the constraint that the change of ψ_Q for the p th component must

have the same sign as θ_p , we may write the angular-dependent part of the free energy, to the fourth power of the magnetization, as

$$\begin{aligned} f(\theta, \psi) = & \frac{1}{4}J^2 \left[-\mathcal{J}_6(Q) + \mathcal{K}_6(Q) \cos 2(\theta - \psi) \right] \\ & \times \{ \sigma_1^2 \cos(\pi + 6\psi) + \sigma_2^2 \cos(5\pi - 6\psi) \} \\ & + \frac{1}{4}J^2 \mathcal{K}_0(Q) (\sigma_1^2 + \sigma_2^2) \cos 2(\theta - \psi) + BJ^4 \sigma_1^2 \sigma_2^2 \cos^2(2\pi/3 - 2\theta). \end{aligned} \quad (2.1.47a)$$

For definiteness, we have chosen the case where the angle between the ξ -axis and σ_1 or σ_2 is respectively $\pi/6 + \theta$ and $5\pi/6 - \theta$ (by symmetry $\theta = \theta_1 = -\theta_2$). Analogously to θ , ψ is the angle between \mathbf{Q}_p and the nearest b -axis. Introducing $\sigma^2 = 2\sigma_1^2 = 2\sigma_2^2$, and expanding $f(\theta, \psi)$ to second order in the small angles, we obtain

$$\begin{aligned} f(\theta, \psi) = & f_0 - \frac{9}{2}(J\sigma)^2 \{ \mathcal{J}_6(Q) - \mathcal{K}_6(Q) \} \psi^2 - \frac{1}{2}(J\sigma)^2 \mathcal{K}(\mathbf{Q})(\theta - \psi)^2 \\ & - \frac{1}{4}(J\sigma)^4 B(\sqrt{3}\theta - 2\psi^2). \end{aligned} \quad (2.1.47b)$$

We note that, with the chosen sign conventions, $\mathcal{K}(\mathbf{Q}) = \mathcal{K}_0(Q) - \mathcal{K}_6(Q)$ and $\mathcal{J}_6(Q) - \mathcal{K}_6(Q)$ are both negative. The additional contribution to the free energy of the double- \mathbf{Q} structure is minimized when

$$\theta = \frac{\sqrt{3}B(J\sigma)^2}{4|\mathcal{K}(\mathbf{Q})|} + \psi \quad ; \quad \psi = \frac{\sqrt{3}B(J\sigma)^2}{36|\mathcal{J}_6(Q) - \mathcal{K}_6(Q)|}, \quad (2.1.48a)$$

neglecting the small term proportional to $B\theta^2$, in which case

$$\Delta f = -\frac{3}{32}B^2(J\sigma)^6 \left(-\frac{1}{\mathcal{K}(\mathbf{Q})} - \frac{1}{9} \frac{1}{\mathcal{J}_6(Q) - \mathcal{K}_6(Q)} \right). \quad (2.1.48b)$$

Introducing $A = A_\xi(T = T_N)$, i.e. $\mathcal{J}(\mathbf{Q}) - \mathcal{K}(\mathbf{Q}) = 2A$, then for Pr we have: $\mathcal{K}(\mathbf{Q}) \simeq -0.24A$, $\mathcal{J}_6(Q) - \mathcal{K}_6(Q) \simeq -0.05A$, and $BJ^2 \simeq 0.35A$. These values may also provide a reasonable estimate in the case of Nd. Inserting them in (2.1.48), we find that $\theta \simeq 3\psi \simeq 1.0\sigma^2$, and $\Delta f \simeq -0.2BJ^4\sigma^6 \simeq -0.5u\sigma^6$. So, even though Δf is of sixth order in σ , it outweighs the small fourth-order energy difference of $w\sigma^4/4$ between the single- and the double- \mathbf{Q} structure when $\sigma^2 \approx 0.1$, if $w \simeq 0.2u$ as estimated above. The temperature T'_N at which this occurs is $\sim 0.97 T_N$, i.e. ~ 0.9 K below T_N in Nd. Hence, if w is positive and has the estimated small magnitude, the system will first undergo a second-order transition from the paramagnetic phase to a single- \mathbf{Q} structure, which will only be stable as long as σ^2 is small. At T'_N , slightly below T_N , the system will make a first-order transition to a double- \mathbf{Q} structure, in which the moments \mathbf{J}_1 and \mathbf{J}_2 are rotated slightly towards each other and away from the symmetry axes, as also are the ordering wave-vectors \mathbf{Q}_1 and \mathbf{Q}_2 . These rotations are proportional to σ^2 .

The explicitly sixth-order contribution to the free energy, proportional to $(1/N) \sum_i (\langle \mathbf{J}_i \rangle \cdot \langle \mathbf{J}_i \rangle)^3$, is somewhat smaller than the estimated value of Δf , and it leads to energy differences between the different multiple- \mathbf{Q} structures which are a further order of magnitude smaller. The hexagonal-anisotropy term, which also appears in this order, is minute compared to the anisotropy introduced by $\mathcal{K}(\mathbf{Q})$ in Pr and Nd, and its influence on the turn angles ψ and θ should be negligible. The only other new effect in this order is the appearance of higher harmonics. The mechanism is identical to that discussed in Section 2.1.4 for the longitudinally-polarized phase, but in addition to the occurrence of third harmonics at the wave-vectors $3\mathbf{Q}_p$, equivalently to (2.1.35a), they also appear at all possible combinations of $2\mathbf{Q}_p \pm \mathbf{Q}_{p'}$ ($p \neq p'$) in the multiple- \mathbf{Q} structures. In the triple- \mathbf{Q} structure, one might expect third harmonics also at $\mathbf{Q}_1 \pm \mathbf{Q}_2 \pm \mathbf{Q}_3$, but the new wave-vectors derived from this condition are either $\mathbf{0}$, which changes the symmetry class of the system, or twice one of the fundamental wave-vectors, which are energetically unfavourable because they do not contribute to the ‘squaring up’. These extra possibilities in the triple- \mathbf{Q} case are not therefore realized. The appearance of the higher ‘odd’ harmonics is not important for the energy differences between the different multiple- \mathbf{Q} structures, but they may provide an experimental method for differentiating between the various possibilities (Forgan *et al.* 1989). In a neutron-diffraction experiment, the scattering intensity at the fundamental wave-vectors in a multi-domain single- \mathbf{Q} structure, with an equal distribution of the domains, is the same as that produced by a triple- \mathbf{Q} structure. These structures may then be distinguished either by removing some of the domains by applying an external field, or by using scattering peaks at, for instance, $2\mathbf{Q}_1 \pm \mathbf{Q}_2$ to exclude the possibility of a single- \mathbf{Q} structure.

The discussion of this section has been based exclusively on the MF approximation, which neglects the important dynamical feature that a system close to a second-order phase-transition will show strong correlated fluctuations in the components which order at the transition. A discussion of the effects of the *critical fluctuations* is beyond the scope of this book, and we refer instead to the recent introduction to the field by Collins (1989), in which references may be found to the copious literature on the subject. Although the MF approximation does not take into account the contributions to the free energy from the critical fluctuations, it gives a reasonable estimate of the transition temperatures in the rare earth metals, which can all be characterized as three-dimensional systems with long-range interactions. The fluctuations contribute to the free energy on both sides of the transition, and they only suppress the transition temperature by a few per cent in such systems. The Landau expansion considered above does not predict the right *critical*

exponents, but it is nevertheless decisive for which *universality classes* the phase transitions belong to. The transitions which are predicted to be continuous by the MF theory, i.e. all those considered above which are not accompanied by a change of \mathbf{Q} to a commensurable value, may be driven into (weak) first-order behaviour by the fluctuations. An important parameter for determining the nature of the phase transition is the product (n) of the number of components of the order parameter, and of the star of the wave-vector (Mukamel and Krinsky 1976; Bak and Mukamel 1976), the latter being two, corresponding to $\pm\mathbf{Q}$, for the periodically-ordered heavy rare earths. If $n \leq 3$, the transition is expected to remain continuous, which is in accord with the observation by Habenschuss *et al.* (1974) of a second-order transition in Er, since $n = 2$ for the transition between the paramagnetic and the longitudinally ordered phase. The transition from the paramagnet to the helix is less clear-cut, since it belongs to the class $n = 4$, and a theoretical analysis by Barak and Walker (1982) suggested that it might be discontinuous. The bulk of the experimental evidence points towards a continuous transition (Brits and du Plessis 1988) but some measurements, especially by Zochowski *et al.* (1986) on pure Dy, indicate a very weak discontinuity. In the case of the multiple- \mathbf{Q} structures, the fluctuations may drive the transition to the single- \mathbf{Q} structure to be discontinuous, whereas that to the triple- \mathbf{Q} structure, if it is stable, should stay continuous (Bak and Lebech 1978). In Nd, for example, a single- \mathbf{Q} state is formed at T_N and the transition is found to be weakly discontinuous (Zochowski and McEwen 1986). In accordance with the MF analysis above, a first-order transition leads to a double- \mathbf{Q} structure less than a degree below T_N (McEwen *et al.* 1985).

2.2 The magnetic anisotropy

In this section, we shall discuss the thermal expectation-values of the Stevens operators of the single ions when their moments are non-zero, so that $|\langle \mathbf{J}_i \rangle| = \sigma J$. We shall then consider the contribution which the single-ion terms in the Hamiltonian make to the free energy, and thereby derive the relationship between the microscopic parameters and the macroscopic magnetic-anisotropy and magnetoelastic coefficients.

2.2.1 Temperature dependence of the Stevens operators

In a ferromagnet, the Zener power-law (1.5.15) for the expectation values of the Stevens operators is valid only at the lowest temperatures. Callen and Callen (1960, 1965) have derived $\langle O_l^m \rangle$ in exchange-dominated systems and obtained results which are useful over a much wider temperature range than the Zener expression. They begin with the density matrix for a single site in the MF approximation, including only the

exchange and Zeeman energies,

$$\rho_{\text{MF}}(x) = \frac{1}{Z} \exp(xJ_z/J) \quad ; \quad x = \beta\{\mathcal{J}(\mathbf{0})J^2\sigma + g\mu_B JH\}, \quad (2.2.1)$$

where $\sigma = M/M_0$ is the relative magnetization, the direction of which is assumed to be parallel to the field. In this case the n th moment of J_z is determined as

$$\sigma_n = \langle (J_z/J)^n \rangle = \frac{1}{Z} \sum_{p=-J}^J \left(\frac{p}{J}\right)^n \exp(xp/J). \quad (2.2.2)$$

This equation offers the possibility of relating the higher moments σ_n to the first moment, which is the relative magnetization $\sigma_1 = \sigma$, without referring explicitly to the MF value of x in eqn (2.2.1). According to the analysis of Callen and Shtrikman (1965), the functional dependence of σ_n on σ has a wider regime of validity than the MF approximation, because it only utilizes the exponential form of the density matrix, which is still valid when correlation effects are included in the random-phase approximation, where the excitations are collective spin-waves, as we shall discuss in Section 3.5. Furthermore, they found that the functions $\sigma_n = \sigma_n(\sigma)$; $n \geq 2$, derived from (2.2.2), only depend very weakly on the actual value of J , and for increasing values these functions rapidly converge towards the results obtained in the limit of infinite J (Callen and Callen 1965). In this limit, the sums in (2.2.2) are replaced by integrals, and the reduced diagonal matrix-elements of the Stevens operators are

$$(1/J^{(l)}) \langle J_z = p | O_l^m | J_z = p \rangle \Big|_{J \rightarrow \infty} = \delta_{m0} c_l P_l(u = p/J), \quad (2.2.3)$$

where the $J^{(l)}$ are defined by eqn (1.5.25), $P_l(u)$ are the Legendre polynomials, and c_l are constants. Multiplying the terms in the sum in (2.2.2) by $\Delta p = J\Delta u = 1$, and then taking the limit $J \rightarrow \infty$, we obtain

$$\frac{1}{c_l J^{(l)}} \langle O_l^0 \rangle = \int_{-1}^1 P_l(u) e^{xu} du \Big/ \int_{-1}^1 e^{xu} du = I_{l+\frac{1}{2}}(x) / I_{\frac{1}{2}}(x) = \hat{I}_{l+\frac{1}{2}}(x). \quad (2.2.4)$$

$\hat{I}_{l+\frac{1}{2}}(x)$ is the usual shorthand notation for the ratio of $I_{l+\frac{1}{2}}(x)$ to $I_{\frac{1}{2}}(x)$, and the functions $I_{l+\frac{1}{2}}(x) = (-i)^{l+\frac{1}{2}} J_{l+\frac{1}{2}}(ix)$ are the modified spherical (or hyperbolic) Bessel functions. The relative magnetization

$$\sigma = \hat{I}_{\frac{3}{2}}(x) = \coth x - \frac{1}{x}$$

is the familiar Langevin function $\mathcal{L}(x)$ and, eliminating x in (2.2.4) by writing $x = \mathcal{L}^{-1}(\sigma)$, we finally arrive at

$$\langle O_l^m(\sigma) \rangle = \delta_{m0} c_l J^{(l)} \hat{I}_{l+\frac{1}{2}}[\sigma] \quad \text{with} \quad \hat{I}_{l+\frac{1}{2}}[\sigma] = \hat{I}_{l+\frac{1}{2}}(\mathcal{L}^{-1}(\sigma)), \quad (2.2.5)$$

for the thermal average of the Stevens operators as functions of $\sigma = \sigma(T, H)$, where $c_2 = 2$, $c_4 = 8$, and $c_6 = 16$. This result has turned out to be very useful for analysing the variation of the magnetic anisotropies and the magnetoelastic strains with temperature and magnetic field. In order to take full advantage of the theory, σ in eqn (2.2.5) is usually taken as the experimental value. If this is not available, it is a better approximation to use the correct MF value for it, rather than the Langevin-function, i.e. $\sigma = B_J(x)$ where $B_J(x)$ is the Brillouin function (1.2.31), determined directly from (2.2.2), because the actual value of J has some influence on the magnitude of σ . This is particularly true for the change of σ with magnetic field. In the limit of infinite J , $\partial\sigma/\partial(JH) \simeq (1 - \sigma)g\mu_B/(J^2\mathcal{J}(\mathbf{0}))$ at low temperatures, which is just a factor of three smaller than the MF value for $J = 6$, which agrees reasonably well with experiments on Tb.

The functions $\hat{I}_{l+\frac{1}{2}}(x)$, for $l = 2, 3, \dots$ are most easily calculated from the recurrence relation

$$\hat{I}_{l+\frac{3}{2}}(x) = \hat{I}_{l-\frac{1}{2}}(x) - \frac{2l+1}{x}\hat{I}_{l+\frac{1}{2}}(x). \quad (2.2.6)$$

At low temperatures, where $x \gg 1$ and $\sigma \simeq 1 - \frac{1}{x}$, it may easily be shown from (2.2.6) that $\hat{I}_{l+\frac{1}{2}}[\sigma] \simeq \sigma^{l(l+1)/2}$ (differences appear only in the third order of $m = 1 - \sigma$). Hence the result (2.2.5) of the Callen–Callen theory agrees with the Zener power-law in the low-temperature limit. With increasing temperature, as x becomes comparable to 1, the exponential terms in the expansion of $\sigma \simeq 1 - \frac{1}{x} + 2\exp(-2x) + \dots$, which have no counterpart in the classical Zener power-law, start to be important. In Chapter 5, we shall develop a detailed description of the excitations in the ferromagnet, the spin-waves. The thermal population of the spin-wave states is described by Bose statistics, assuming the availability of an infinite number of states of the single angular-momentum operators. The spin-wave theory reproduces the result of the Callen–Callen theory, in an expansion in powers of $m = 1 - \sigma$, but only if the exponential corrections above are negligible. The appearance of these terms at high temperatures signals the breakdown of the Bose approximation for the spin-wave excitations, which occurs because the actual number of states is not unlimited. As would be anticipated, this limitation in the number of states (or bandwidth if J is infinite) begins to be effective when the population of the uppermost level, which in the MF approximation is just proportional to $\exp(-2x)$, becomes significant. In the limit of a small relative magnetization, where $x \ll 1$, the Zener power-law and the spin-wave theory are both inadequate, whereas the Callen–Callen theory may still be applicable. In this limit, we may use the approximation

$$\hat{I}_{l+\frac{1}{2}}[\sigma] = \frac{3^l}{(2l+1)!!}\sigma^l \quad ; \quad \sigma \ll 1. \quad (2.2.7)$$

One of the advantages of the Callen–Callen theory is that the results only depend on the one parameter σ , but not explicitly on the Hamiltonian. The relative magnetization may then be determined either by experiment, or by MF or more accurate theories, which result in a σ which depends on the actual Hamiltonian employed. The simplicity of this result may be impaired if the magnetic anisotropy of the system is substantial, so that the exchange interaction is no longer the dominant term in the density matrix. We shall be mostly concerned with the applicability of the theory at low temperatures, and the introduction of an axial-anisotropy term, such as $B_2^0 O_2^0(\mathbf{J}_i)$, is not inimical to the theory in this regime, provided that the magnetization is along the anisotropy c -axis, i.e. if B_2^0 is negative. Since only the lowest states are important at low temperatures and, in the MF approximation, these are still reasonably well accounted for by the density matrix in eqn (2.2.1), only the value of x is changed, with no direct consequences for the result. There are however noticeable effects if the anisotropy destroys the rotational symmetry about the magnetization axis. This is the case if B_2^0 is positive and forces the moments to lie in the basal plane, so that it requires a magnetic field to pull them out of it, whereas they may rotate much more freely within the plane, since B_6^6 is unimportant compared to the axial anisotropy. As we shall discuss in detail in Chapter 5, the ground state in this situation is no longer the fully-polarized state, the expectation value of J_z is slightly smaller than J at zero temperature, and the lower symmetry of the anisotropy field has direct consequences for the nature of the elementary spin-wave excitations, and thus for the form of the density matrix. The necessary modification of the Callen–Callen theory may be developed in two ways. One is to analyse the influence of the anisotropy on the low-temperature elementary excitations, and thereby derive the density matrix, as is done in Chapter 5. The other approach is numerical and involves the construction of a Hamiltonian which has the right transition temperature and the correct anisotropy fields, in the MF approximation. ρ_{MF} may then be calculated as a function of temperature, and results corresponding to (2.2.5), relating the expectation values of the various Stevens operators to the relative magnetization, may be obtained numerically. By the same argumentation as that used by Callen and Shtrikman (1965), these results may be expected to be insensitive to the actual model Hamiltonian used for describing the system. In the low temperature limit, the spin-wave theory supports this point of view, as its results are described in terms of only two parameters. One is the relative magnetization σ , as before, while the other, \tilde{b} or $\eta_{\pm} = (1 \pm \tilde{b})(1 - \frac{1}{2}\tilde{b}^2)$, measures the eccentricity of the anisotropic potential about the axis of magnetization.

In our discussion of the Callen–Callen theory, we have assumed

that the quantization axis (z -axis), defining the Stevens operators, coincides with the direction of magnetization. We shall continue to use this convention, but must then take account of the difficulty that the crystal-field Hamiltonian in the hcp metals only has the simple form of eqn (1.4.6b) if the quantization axis is chosen to be along the c - or ζ -direction. In order to distinguish between the two systems, we shall denote the Stevens operators in the Hamiltonian defined with respect to the crystallographic axes, i.e. in the (ξ, η, ζ) -coordinate system, by $Q_l^m(\mathbf{J})$. The direction of magnetization, the z -axis, is specified by the polar angles (θ, ϕ) in the (ξ, η, ζ) -coordinate system, and we must introduce the following transformation of the angular momentum operators in $Q_l^m(\mathbf{J})$:

$$\begin{aligned} J_\xi &= J_z \sin \theta \cos \phi - J_x \cos \theta \cos \phi + J_y \sin \phi \\ J_\eta &= J_z \sin \theta \sin \phi - J_x \cos \theta \sin \phi - J_y \cos \phi \\ J_\zeta &= J_z \cos \theta + J_x \sin \theta, \end{aligned} \quad (2.2.8)$$

choosing the y -axis to lie in the basal-plane. By this transformation, Q_l^m is expressed as a linear combination of the Stevens operators $O_l^{m'}$, with the same l but various m' -values. For instance, we have

$$\begin{aligned} Q_2^0 &= 3J_\zeta^2 - J(J+1) \\ &= 3J_z^2 \cos^2 \theta + 3J_x^2 \sin^2 \theta + \frac{3}{2}(J_z J_x + J_x J_z) \sin 2\theta - J(J+1) \\ &= \frac{1}{2}O_2^0(3 \cos^2 \theta - 1) + \frac{3}{2}O_2^2 \sin^2 \theta + 3O_2^1 \sin 2\theta. \end{aligned} \quad (2.2.9)$$

Carrying out the same transformation on Q_2^2 we find the following relations:

$$\begin{aligned} Q_2^0 &= \frac{1}{2}(-O_2^0 + 3O_2^2) \\ Q_2^2 &= \frac{1}{2}(O_2^0 + O_2^2) \quad ; \quad \phi = p\pi, \end{aligned} \quad (2.2.10)$$

when the moment is in the basal-plane ($\theta = \pi/2$). The expectation value of Q_2^2 is relevant for determining the γ -strain $\epsilon_{\gamma 1}$, as shown in (1.5.29). According to the result (2.2.5) of Callen and Callen, $\langle O_2^2 \rangle$ should vanish, but in a basal-plane ferromagnet this may not occur. The eccentricity parameter mentioned above is just defined as

$$\tilde{b} = \langle O_2^2 \rangle / \langle O_2^0 \rangle, \quad (2.2.11)$$

which is zero, by definition, only if the anisotropy is invariant with respect to a rotation about the z -axis.

The numerical programme sketched above has been carried through for a model corresponding to Tb. The effective basal-plane anisotropy is about a factor of 10 smaller than the axial anisotropy, so that \tilde{b} is

about -0.03 at zero temperature. The negative sign of \tilde{b} shows that the fluctuations of the moments within the plane are larger than those out of the plane, as measured respectively by $\langle J_y^2 \rangle$ and $\langle J_x^2 \rangle$, since $O_2^2 = J_x^2 - J_y^2$. In Fig. 2.2 the numerical results for $\langle O_2^0 \pm O_2^2 \rangle / J^{(2)}$ are compared with the predictions of the Callen–Callen theory, and of the linear spin-wave theory developed in Chapter 5, in which the MF values (5.3.23) of m_o and b_o are used, instead of (5.3.18). The Callen–Callen theory predicts that both thermal averages vary like $\hat{I}_{5/2}(\sigma)$, which is not consistent with a \tilde{b} different from zero. Furthermore, the effective power-laws in the zero-temperature limit are changed from σ^3 to $\langle O_2^0 - O_2^2 \rangle \propto \sigma^{2.65}$, and $\langle O_2^0 + O_2^2 \rangle \propto \sigma^{3.3}$. The predictions of the spin-wave theory are consistent with the numerical results at low temperatures, both with respect to the absolute magnitude of the expectation values and to the effective power-laws, and it appears to give a reasonably correct description of

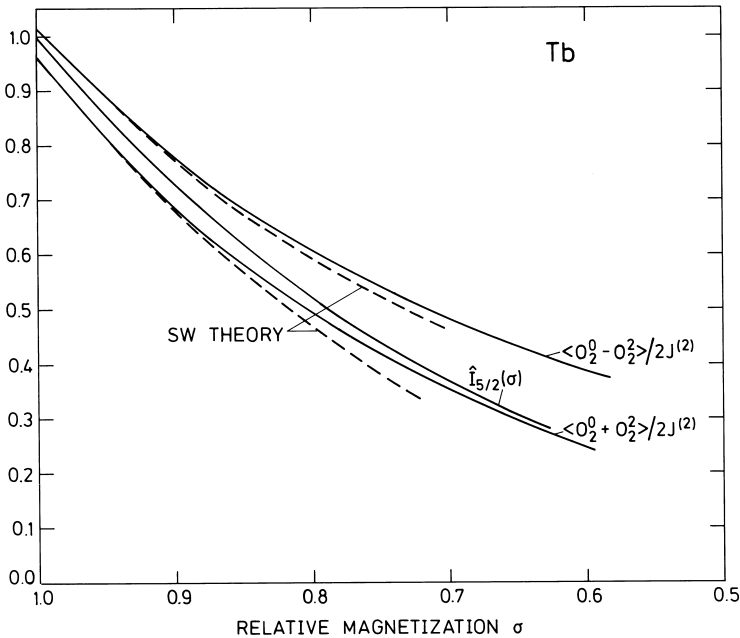


Fig. 2.2. Calculations of the dependence of the expectation values of the Stevens operators $\langle O_2^0 \pm O_2^2 \rangle$ on the relative magnetization in Tb. The numerical calculations described in the text differ from the Callen–Callen result $\hat{I}_{5/2}(\sigma)$, but agree at low temperatures with the predictions of spin-wave theory.

the system as long as σ is greater than about 0.8. The same picture holds true for other combinations of Stevens operators, but the discrepancies between the different theories are accentuated as the rank increases. Figure 2.3 shows the example of $\langle Q_6^6 \rangle$. The absolute magnitude of this quantity is reduced by nearly 40% in the zero-temperature limit, as compared with the Callen–Callen theory, and the slope of the numerical calculation, in the semi-logarithmic plot, changes with σ , leading to an effective power-law depending on the interval over which it is measured. In the zero-temperature limit, $\langle Q_6^6 \rangle$ is proportional to approximately σ^{26} , instead of the Callen–Callen result σ^{21} .

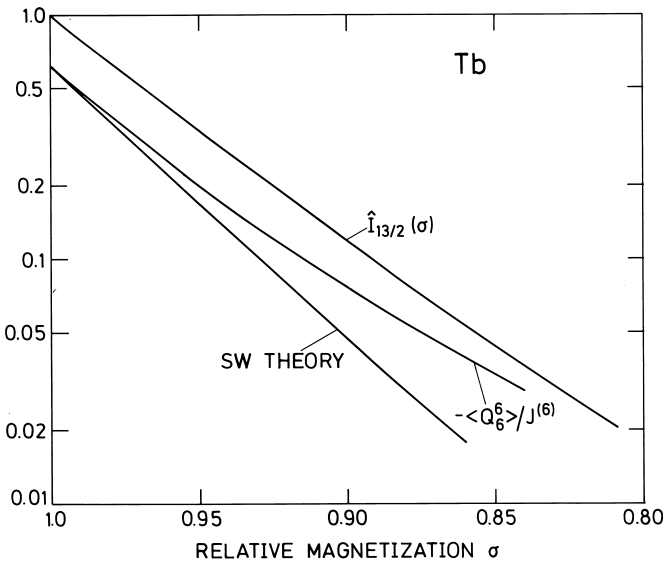


Fig. 2.3. The dependence on the relative magnetization of the expectation value of the Stevens operator $\langle Q_6^6 \rangle$, which determines the hexagonal magnetic anisotropy, in Tb. The numerical calculations and the spin-wave theory both predict a large reduction in this quantity at low temperatures, compared with the Callen–Callen theory.

The numerical results are expected to be sensitive to the magnitude of the anisotropy, rather than to the actual parameters which determine the anisotropy, and the spin-wave theory indicates that this expectation is fulfilled, at least at low temperatures. However, in order to obtain the right variation of the anisotropy fields with temperature, i.e. of \tilde{b} compared to σ , it is necessary to select appropriate linear combinations of Stevens operators of various ranks for the modelling of the different anisotropy terms. At high temperatures, for instance, \tilde{b} is determined

by the low-rank terms alone, i.e. by B_2^0 if anisotropic dipole–dipole coupling is neglected. Using $\beta = (k_B T)^{-1}$ as an expansion parameter, and assuming the magnetization to lie in the basal plane, we find, to leading order in the crystal-field parameters introduced in eqn (1.4.6b),

$$\langle Q_2^2 \rangle = \frac{3}{5} J^{(2)} \sigma^2 \frac{J + \frac{3}{2}}{J + 1} \simeq J^{(2)} \hat{I}_{5/2}[\sigma], \quad (2.2.12a)$$

using (2.2.7) and neglecting the small $1/J$ corrections, whereas

$$\langle Q_2^0 \rangle = -\langle Q_2^2 \rangle - \frac{4}{5} J^{(2)} (J + 1) (J + \frac{3}{2}) \beta B_2^0, \quad (2.2.12b)$$

which depends on the anisotropy, but only on the term of lowest rank. Considering the *field* dependence of the two expectation values, as determined by their dependence on σ , we observe that the Callen–Callen theory leads to the right result in this high-temperature limit. The two relations above explain the behaviour of $\langle O_2^0 \pm O_2^2 \rangle$ in Fig. 2.2, when σ becomes small, as $\langle O_2^0 + O_2^2 \rangle / 2J^{(2)}$ should approach $\hat{I}_{5/2}(\sigma)$ at small values of σ , and go to zero at the transition temperature. $\langle O_2^0 - O_2^2 \rangle / 2J^{(2)}$, on the other hand, should still be non-zero (about 0.23 as determined by $T_N \simeq 229$ K and the value $B_2^0 = 0.18$ meV used in the model) when T_N is approached from below and σ vanishes.

2.2.2 Anisotropic contributions to the free energy

The anisotropy of a magnetic system is determined by those contributions to the free energy which depend on the polar angles (θ, ϕ) , which specify locally the direction of the moments. Restricting ourselves to the case of a ferromagnet in a uniform field, we may expand the free energy in terms of functions proportional to the spherical harmonics, as in eqn (1.5.22). To relate this expansion to the Hamiltonian (2.1.1), we may use (2.1.5), which states that any change in the free energy due to a change of the angles is given by $\delta \tilde{F} = \langle \delta \mathcal{H} \rangle$. The field is the independent variable in \tilde{F} but, as in (2.1.22), we wish the magnetization to be the independent variable. To obtain this free energy $F(\theta, \phi)$, we subtract the Zeeman energy, so that $F(\theta, \phi) = \tilde{F} - \langle \mathcal{H}_Z \rangle$, where the field needed for establishing the specified angles is determined from the equilibrium condition $\delta \tilde{F} = 0$. In the ferromagnet, the moments all point in the same direction, and any contributions from the isotropic-exchange coupling cancel out in $\delta \mathcal{H}$. The free-energy function $F(\theta, \phi)$ is thus determined by

$$\delta F(\theta, \phi) = \langle \delta(\mathcal{H}_{\text{cf}} + \mathcal{H}_Z) \rangle - \delta \langle \mathcal{H}_Z \rangle. \quad (2.2.13)$$

Introducing the angle variables in the Hamiltonian by the transformation (2.2.8), we find that the operators of rank l become angle-dependent

linear combinations of the l -rank Stevens operators, which have their polar axis along the z -axis defined by the direction of the moments. The variational expression for the free energy then involves the calculation of the expectation values of these Stevens operators. To leading order in the crystal-field parameters, we may neglect the influence of the anisotropy terms on the thermal averages in (2.2.13). This is the approximation used by Callen and Callen, and we may utilize their result, eqn (2.2.5). This has the consequence that, in the various linear combinations of Stevens operators, only those terms in which $m = 0$ contribute to the free energy, to leading order in the anisotropy parameters. From the expansion (2.2.9) of Q_2^0 , we find the following result:

$$\langle \delta(Q_2^0) \rangle \simeq \langle O_2^0 \rangle \delta \left\{ \frac{1}{2} (3 \cos^2 \theta - 1) \right\}$$

and, repeating this calculation for the other operators, we have in general

$$\langle \delta(Q_l^0) \rangle \simeq \langle O_l^0 \rangle \delta P_l(\cos \theta) \quad ; \quad \langle \delta(Q_6^0) \rangle \simeq \frac{1}{16} \langle O_6^0 \rangle \delta \left\{ \sin^6 \theta \cos 6\phi \right\}. \quad (2.2.14)$$

Because $\langle J_x \rangle = \langle J_y \rangle = 0$, the Zeeman terms in (2.2.13) cancel within this approximation, and an integration of $\delta F(\theta, \phi)$ leads to

$$F(\theta, \phi)/N \simeq f_0 + \sum_l B_l^0 \langle O_l^0 \rangle P_l(\cos \theta) + \frac{1}{16} B_6^0 \langle O_6^0 \rangle \sin^6 \theta \cos 6\phi. \quad (2.2.15)$$

Comparing this result with the free energy expression (1.5.22), and introducing the anisotropy parameters $\kappa_l^m(T)$, we obtain to a first approximation

$$\kappa_l^0(T) = c_l B_l^0 J^{(l)} \hat{I}_{l+\frac{1}{2}}[\sigma] \quad ; \quad \kappa_6^6(T) = B_6^0 J^{(6)} \hat{I}_{13/2}[\sigma], \quad (2.2.16)$$

with $\sigma = \sigma(T)$, which leads to eqn (1.5.24) at zero temperature ($\sigma = 1$).

The equilibrium values of the angles in zero field are determined by $\partial F(\theta, \phi)/\partial \theta = \partial F(\theta, \phi)/\partial \phi = 0$. In the above result for the free energy, the ϕ -dependence is determined exclusively by B_6^0 , the sign of which then determines whether the a - or b -directions are the magnetically easy or hard axes in the basal-plane ($\phi_0 = p\pi/3$ or $\pi/2 + p\pi/3$). Because B_6^0 is a sixth-rank coupling parameter, the importance of this anisotropy decreases rapidly with the magnetization; $\hat{I}_{13/2}[\sigma] \propto \sigma^{21}$ at low temperatures, or σ^6 when σ is small. The axial anisotropy derives from all four parameters, and the equilibrium value θ_0 is determined by minimizing

$$\begin{aligned} f(u = \cos \theta) &= F(\theta, \phi_0)/N - f_0 \\ &= \frac{1}{2} \kappa_2^0 (3u^2 - 1) + \frac{1}{8} \kappa_4^0 (35u^4 - 30u^2 + 3) \\ &\quad + \frac{1}{16} \kappa_6^0 (231u^6 - 315u^4 + 105u^2 - 5) - |\kappa_6^6| (1 - u^2)^3. \end{aligned} \quad (2.2.17)$$

Equation (2.2.16) shows that the various anisotropy parameters depend differently on temperature. At high temperatures, κ_2^0 dominates and its sign determines whether the moments are parallel or perpendicular to the c -axis. As the temperature is decreased, the importance of the higher-rank terms grows, putting increasing weight on the terms of fourth and sixth power in $\cos\theta$. The equilibrium value $\theta_0(T)$ of θ may therefore change as a function of temperature, as occurs in Ho and Er, and also in Gd where, however, the theory of this section is not immediately applicable.

The coefficients in the expansion for the free energy may be obtained from experimental studies of the magnetization as a function of the magnitude and direction of an applied magnetic field. The axial part of the anisotropy is predominantly determined by the three κ_l^0 -parameters, and it is not usually easy to separate their contributions. At low temperatures, where the higher-rank terms become relatively important, the axial anisotropy in the heavy rare earths is frequently so strong that it is only possible to change θ by a few degrees from its equilibrium value. Under these circumstances, it is only possible to measure the components of the susceptibility, allowing a determination of the second derivatives of $F(\theta, \phi)$ in the equilibrium state $(\theta, \phi) = (\theta_0, \phi_0)$. The x -axis lies in the symmetry z - ζ plane and the transverse part of the susceptibility tensor is diagonal with respect to the (x, y) -axes. With a field h_x applied in the x -direction, the moments rotate through an angle $\delta\theta = \theta - \theta_0$, giving a component $\langle J_x \rangle = -\langle J_z \rangle \delta\theta = \chi_{xx} h_x$. Introducing the notation $F_{\theta\theta} \equiv \partial^2 F(\theta, \phi) / \partial \theta^2$ at $(\theta, \phi) = (\theta_0, \phi_0)$, and similarly for the other second derivatives, we may write

$$F = F(\theta_0, \phi_0) + \frac{1}{2} F_{\theta\theta} (\delta\theta)^2 + \frac{1}{2} F_{\phi\phi} (\delta\phi)^2 + N \langle J_z \rangle \delta\theta h_x,$$

in the limit where the field goes to zero. The term $F_{\theta\phi} = 0$, because $\sin 6\phi_0 = 0$. At equilibrium, $\delta\theta = -N \langle J_z \rangle h_x / F_{\theta\theta}$, which determines the susceptibility. When the field is applied in the y -direction, i.e. along the direction $(-\sin \phi_0, \cos \phi_0, 0)$, the Zeeman contribution to F is

$$N \langle J_z \rangle h_y \sin \theta \sin(\phi - \phi_0) = N \langle J_z \rangle h_y \sin \theta_0 \delta\phi,$$

with $\langle J_y \rangle = -\langle J_z \rangle \sin \theta_0 \delta\phi = \chi_{yy} h_y$. Minimizing the free energy in the presence of a field along the y -axis, we may derive the other susceptibility component, obtaining

$$\chi_{xx} = N \langle J_z \rangle^2 / F_{\theta\theta} \quad ; \quad \chi_{yy} = N \langle J_z \rangle^2 \sin^2 \theta_0 / F_{\phi\phi}. \quad (2.2.18)$$

In calculating χ_{yy} , we have assumed that $\theta_0 \neq 0$; if $\theta_0 = 0$ then $\chi_{yy} = \chi_{xx}$. Equation (2.2.18) is also valid in the presence of an external field, provided that the effects due to the Zeeman contribution,

$F_Z = -Ng\mu_B \mathbf{H} \cdot \langle \mathbf{J} \rangle$, are included explicitly in $F(\theta_0, \phi_0)$ and its derivatives. Introducing the expression (2.2.17) for the free energy, in the two cases where the moments are either parallel or perpendicular to the c -axis, we find

$$1/\chi_{xx} = 1/\chi_{yy} = -(3\kappa_2^0 + 10\kappa_4^0 + 21\kappa_6^0)/(\sigma J)^2 \quad ; \quad \theta_0 = 0, \quad (2.2.19a)$$

or

$$\begin{aligned} 1/\chi_{xx} &= (3\kappa_2^0 - \frac{15}{2}\kappa_4^0 + \frac{105}{8}\kappa_6^0 + 6|\kappa_6^6|)/(\sigma J)^2 \\ 1/\chi_{yy} &= 36|\kappa_6^6|/(\sigma J)^2 \end{aligned} \quad ; \quad \theta_0 = \frac{\pi}{2}, \quad (2.2.19b)$$

which must be positive if the structure is to be stable. In order to determine the higher derivatives of the free energy, a transverse field greater than that corresponding to the linear regime described by the (zero-field) susceptibility must be applied. The application of a large magnetic field perpendicular to the magnetization axis, in a strongly anisotropic system, creates a large mechanical torque, which may cause practical problems with maintaining the orientation of the crystal. If the experimental facilities do not allow the determination of the higher derivatives, the different temperature dependences of the various anisotropy parameters may yield a rough separation of their contributions to the total axial anisotropy. However the Callen–Callen theory is an approximation, the corrections to which are important if the anisotropy is large, and there are other contributions to the free energy than those which we have considered above.

The results derived above are only valid if the anisotropy energies are small compared to the exchange energy. In order to demonstrate the kind of modifications which may appear in higher order, we shall consider the simplest possible case, where only B_2^0 is non-zero, and we shall only calculate the free energy at zero temperature in the MF approximation, i.e. the ground-state energy of a single site subjected to the exchange field $h_{\text{ex}} = \langle J_z \rangle \mathcal{J}(\mathbf{0})$, with $\langle J_z \rangle = \sigma J$. In this case, the MF Hamiltonian (2.1.16) is

$$\begin{aligned} \mathcal{H} &= -(J_z - \frac{1}{2}\sigma J)\sigma J \mathcal{J}(\mathbf{0}) - h(J_z \cos \theta + J_x \sin \theta) \\ &+ B_2^0 [3J_z^2 \cos^2 \theta + 3J_x^2 \sin^2 \theta + \frac{3}{2}(J_z J_x + J_x J_z) \sin 2\theta - J(J+1)], \end{aligned} \quad (2.2.20)$$

in an applied field h along the ζ -axis. With the J_z -eigenstates as the basis, the leading-order ground-state energy is

$$E_0^0 = \langle J | \mathcal{H} | J \rangle = -(1 - \frac{1}{2}\sigma) \sigma J^2 \mathcal{J}(\mathbf{0}) - hJ \cos \theta + B_2^0 J^{(2)} (3 \cos^2 \theta - 1).$$

The off-diagonal matrix elements involving the ground state are

$$\begin{aligned}\langle J-1 | \mathcal{H} | J \rangle &= \left\{ 6\left(J - \frac{1}{2}\right) B_2^0 \cos \theta - h \right\} (J/2)^{1/2} \sin \theta \\ \langle J-2 | \mathcal{H} | J \rangle &= \frac{3}{2} \{ 2J^{(2)} \}^{1/2} B_2^0 \sin^2 \theta.\end{aligned}$$

We shall only be concerned with terms up to second order in B_2^0 and h , so that we may use second-order perturbation theory, and it is sufficiently accurate to approximate the energy differences between the ground state and the first and second excited-states by respectively $\Delta_1 = J\mathcal{J}(\mathbf{0})$ and $\Delta_2 = 2J\mathcal{J}(\mathbf{0})$. Because of the mixing of the states, $\sigma = \langle J_z \rangle / J = 1 - m$ becomes slightly smaller than 1, but this only affects the exchange contribution quadratic in m , as $(1 - \frac{1}{2}\sigma)\sigma = \frac{1}{2}(1 - m^2)$. To second order, the ground-state energy is found to be

$$\begin{aligned}E_0(h) &= -\frac{1}{2}J^2\mathcal{J}(\mathbf{0}) - hJ \cos \theta + B_2^0 J^{(2)} (3 \cos^2 \theta - 1) \\ &\quad - \frac{1}{2} \left\{ 6\left(J - \frac{1}{2}\right) B_2^0 \cos \theta - h \right\}^2 \sin^2 \theta / \mathcal{J}(\mathbf{0}) - \frac{9}{4} \left(J - \frac{1}{2}\right) (B_2^0)^2 \sin^4 \theta / \mathcal{J}(\mathbf{0}).\end{aligned}\tag{2.2.21}$$

The minimum condition $\partial E_0 / \partial \theta = 0$ leads to

$$h = h_0 = 6\left(J - \frac{1}{2}\right) B_2^0 \left[1 + 3B_2^0 \sin^2 \theta / \{ 2J\mathcal{J}(\mathbf{0}) \} \right] \cos \theta \quad \text{or} \quad \sin \theta = 0,$$

to second order in B_2^0 . The free energy $F(\theta, \phi)$ at zero temperature is then, in both cases,

$$\begin{aligned}F(\theta, \phi) / N &= E_0(h_0) + h_0 J \sigma \cos \theta \\ &= -\frac{1}{2}J^2\mathcal{J}(\mathbf{0}) + \frac{1}{2}\tilde{\kappa}_2^0 (3 \cos^2 \theta - 1) + \frac{3}{4}b\tilde{\kappa}_2^0 \sin^4 \theta,\end{aligned}$$

with

$$\tilde{\kappa}_2^0 = 2B_2^0 J^{(2)} \quad ; \quad b = -3B_2^0 / \{ 2J\mathcal{J}(\mathbf{0}) \},\tag{2.2.22a}$$

and the relative magnetization is $\sigma = 1 - (J - \frac{1}{2})b^2 \sin^4 \theta$. The b -parameter introduced here is the leading order contribution to \tilde{b} , defined in (2.2.11), when $\theta = \pi/2$. One important feature illustrated by this calculation is that the O_2^m -term in Q_2^0 , with m odd, is cancelled by the Zeeman contribution, to second order in B_2^0 . This is a consequence of the freedom to replace the equilibrium condition $\partial F / \partial \theta = 0$ by the requirement that $\langle J_x \rangle$ (and $\langle J_y \rangle$) should vanish, by definition, with the implication that the matrix-element $\langle J-1 | \mathcal{H} | J \rangle$ must be zero within the present approximation. Bowden (1977) did not take the Zeeman effect into account, and therefore obtained an erroneously strong renormalization of the anisotropy. The second derivatives of $F(\theta, \phi)$ are $F_{\phi\phi} = 0$, and

$$F_{\theta\theta} / N = -3\tilde{\kappa}_2^0 (1 - b \sin^2 \theta) \cos 2\theta + \frac{3}{2}\tilde{\kappa}_2^0 b \sin^2 2\theta.\tag{2.2.22b}$$

There is no change in the axial susceptibility in the axial ferromagnet, for which $\theta = 0$, but the higher derivatives are affected by the modifications $\kappa_2^0(0) = \tilde{\kappa}_2^0(1 - \frac{4}{7}b)$ and $\kappa_4^0(0) = \frac{6}{35}b\tilde{\kappa}_2^0$. The correction to the Callen–Callen theory is proportional to b , which is of the order $1/J$ times the ratio between the anisotropy and the exchange energy ($\propto B_2^0 J^{(2)}/J^2 \mathcal{J}(\mathbf{0})$), and hence becomes smaller for larger values of J . This calculation may be extended to higher order and to non-zero temperatures, but the complications are much reduced by the application of the *Holstein–Primakoff transformation* which utilizes directly the factor $1/J$ in the expansion, as we shall see in the discussion of the spin-wave theory in Chapter 5.

In the ferromagnetic phase, the ordered moments may distort the lattice, due to the magnetoelastic couplings, and this gives rise to additional contributions to $F(\theta, \phi)$. We shall first consider the effects of the γ -strains by including the magnetoelastic Hamiltonian, incorporating (1.4.8) and (1.4.11),

$$\mathcal{H}_\gamma = \sum_i \left[\frac{1}{2} c_\gamma (\epsilon_{\gamma 1}^2 + \epsilon_{\gamma 2}^2) - B_{\gamma 2} \{ Q_2^2(\mathbf{J}_i) \epsilon_{\gamma 1} + Q_2^{-2}(\mathbf{J}_i) \epsilon_{\gamma 2} \} \right. \\ \left. - B_{\gamma 4} \{ Q_4^4(\mathbf{J}_i) \epsilon_{\gamma 1} - Q_4^{-4}(\mathbf{J}_i) \epsilon_{\gamma 2} \} \right], \quad (2.2.23)$$

retaining only the lowest-rank couplings ($l = 2$ and 4 of respectively the γ_2 and γ_4 terms). The equilibrium condition

$$\partial F / \partial \epsilon_{\gamma 1} = \langle \partial \mathcal{H}_\gamma / \partial \epsilon_{\gamma 1} \rangle = 0, \quad (2.2.24)$$

and similarly for $\epsilon_{\gamma 2}$, leads to the equilibrium strains

$$\epsilon_{\gamma 1} = (B_{\gamma 2} \langle Q_2^2 \rangle + B_{\gamma 4} \langle Q_4^4 \rangle) / c_\gamma \\ \epsilon_{\gamma 2} = (B_{\gamma 2} \langle Q_2^{-2} \rangle - B_{\gamma 4} \langle Q_4^{-4} \rangle) / c_\gamma. \quad (2.2.25)$$

The conventional magnetostriction parameters C and A are introduced via the equations

$$\epsilon_{\gamma 1} = C \sin^2 \theta \cos 2\phi - \frac{1}{2} A \sin^4 \theta \cos 4\phi \\ \epsilon_{\gamma 2} = C \sin^2 \theta \sin 2\phi + \frac{1}{2} A \sin^4 \theta \sin 4\phi \quad (2.2.26a)$$

(Mason 1954). Expressing Q_l^m in terms of O_l^m , and retaining only the terms with $m = 0$, we may derive these parameters from (2.2.25), obtaining

$$C = \frac{1}{c_\gamma} B_{\gamma 2} J^{(2)} \hat{I}_{5/2}[\sigma] \\ A = -\frac{2}{c_\gamma} B_{\gamma 4} J^{(4)} \hat{I}_{9/2}[\sigma]. \quad (2.2.26b)$$

Within this approximation, the γ -strain contribution $F_\gamma(\theta, \phi)$ to the free energy is

$$\begin{aligned} F_\gamma(\theta, \phi) &= \langle \mathcal{H}_\gamma \rangle = -\frac{1}{2}c_\gamma(\epsilon_{\gamma 1}^2 + \epsilon_{\gamma 2}^2)N \\ &= -\frac{1}{2}c_\gamma\left(C^2 \sin^4 \theta + \frac{1}{4}A^2 \sin^8 \theta - CA \sin^6 \theta \cos 6\phi\right)N, \end{aligned} \quad (2.2.27)$$

showing that these strains affect the axial-anisotropy parameters $\kappa_l^0(T)$, introducing effects of higher rank than $l = 6$, and that the six-fold anisotropy in the basal plane is now

$$\kappa_6^0(T) = B_6^0 J^{(6)} \hat{I}_{15/2}[\sigma] + \frac{1}{2}c_\gamma CA. \quad (2.2.28)$$

When both C and A are non-zero, the maximum area-conserving elongation of the hexagonal planes varies between $|C + \frac{1}{2}A|$ and $|C - \frac{1}{2}A|$, which results in a ϕ -dependent magnetoelastic energy, and thus a contribution to κ_6^0 . The γ -strain hexagonal anisotropy decreases more slowly (like σ^{13} at low temperatures) than the B_6^0 term, as σ decreases, and therefore dominates at sufficiently high temperatures.

The ε -strains may be included in a similar way. Retaining only the lowest-rank coupling $B_{\varepsilon 1} \equiv B_{\varepsilon 1}^{(l=2)}$ in eqn (1.4.12), we have

$$\mathcal{H}_\varepsilon = \sum_i \left[\frac{1}{2}c_\varepsilon(\epsilon_{\varepsilon 1}^2 + \epsilon_{\varepsilon 2}^2) - B_{\varepsilon 1} \{Q_2^1(\mathbf{J}_i)\epsilon_{\varepsilon 1} + Q_2^{-1}(\mathbf{J}_i)\epsilon_{\varepsilon 2}\} \right]. \quad (2.2.29)$$

Introducing the magnetostriction parameter H_ε of Mason (1954) (the index ε should prevent any confusion with the magnetic field) by

$$\epsilon_{\varepsilon 1} = \frac{1}{4}H_\varepsilon \sin 2\theta \cos \phi \quad ; \quad \epsilon_{\varepsilon 2} = \frac{1}{4}H_\varepsilon \sin 2\theta \sin \phi, \quad (2.2.30a)$$

we obtain within the Callen–Callen theory

$$H_\varepsilon = \frac{2}{c_\varepsilon} B_{\varepsilon 1} J^{(2)} \hat{I}_{5/2}[\sigma], \quad (2.2.30b)$$

and the ε -strain contribution to the free energy

$$F_\varepsilon(\theta, \phi) = -\frac{1}{32}N c_\varepsilon H_\varepsilon^2 \sin^2 2\theta. \quad (2.2.31)$$

The α -strains (1.4.10) do not influence the symmetry of the system, but they do make a contribution, essentially proportional to $\langle Q_2^0 \rangle$, to the anisotropy, the effects of which may be derived in the same way as those of the γ - and ε -strains. The magnetoelastic contributions to the free energy can be estimated experimentally if the elastic constants are known, by a determination of the strains as a function of the magnetization. The

knowledge of the equilibrium strains may also be used for a reasonable estimate of the magnetoelastic modifications of the second derivatives, provided that the additional assumption is made that the couplings of lowest rank are dominant. For example, the higher-rank γ -strains in the basal-plane magnet make contributions to the axial anisotropy which cannot be written in terms of C and A in eqn (2.2.27). A more direct estimate of the contributions to the second derivatives requires an experimental determination of how the strains behave when the direction of the magnetization is changed. In basal-plane ferromagnets, such as Tb and Dy, it may be possible to observe the ϕ -dependence of the strains (Rhyne and Legvold 1965a), whereas if the axial anisotropy is large, it may be very difficult to determine the variation of the strains with θ . In the case of the α -strains, the argument that the ($l = 2$) couplings are dominant is not sufficient for a determination of their effect on the axial anisotropy. The reason is that the *two-ion magnetoelastic couplings* of lowest rank, i.e. the dipolar interactions

$$\begin{aligned} \Delta\mathcal{H}_{\text{me}}^{\alpha} = - \sum_{ij} & \left[\{D_{10}(ij)\epsilon_{\alpha 1} + D_{20}(ij)\epsilon_{\alpha 2}\} \mathbf{J}_i \cdot \mathbf{J}_j \right. \\ & \left. + \{D_{13}(ij)\epsilon_{\alpha 1} + D_{23}(ij)\epsilon_{\alpha 2}\} J_{i\zeta} J_{j\zeta} \right], \end{aligned} \quad (2.2.32)$$

may be important. This is the case in Tb and Dy, as shown by the analysis of the stress-dependence of the Néel temperatures (Bartholin *et al.* 1971). These interactions affect the α -strains, but they contribute differently to the axial anisotropy from the ($l = 2$)-terms in the single-ion magnetoelastic Hamiltonian (1.4.10).

The simplifications introduced in the above discussion of the ferromagnet may also be utilized in non-uniform systems, because the MF approximation allows the individual ions to be treated separately. However, the isotropic two-ion contributions no longer cancel in $\delta F(\theta, \phi)$ in (2.2.13), since the direction of the exchange field depends on the site considered. We consider as an example the helically ordered phase. If we neglect the bunching effect due to the hexagonal anisotropy, the axial anisotropy is independent of the site considered. Treating the ions as isolated, but subject to a constant exchange-field, we may calculate $F_{\theta\theta}^0$, corresponding to $1/\chi_{xx}^0$, and then use (2.1.19) to account for the induced exchange-field due to an applied field in the x - or c -direction, modulated with a wave-vector \mathbf{q} along the c -axis. If the two-ion coupling between the moments is allowed to be anisotropic, the leading order result is

$$1/\chi_{xx}(\mathbf{q}) = \mathcal{J}_{\perp}(\mathbf{Q}) - \mathcal{J}_{\parallel}(\mathbf{q}) + (3\kappa_2^0 - \frac{15}{2}\kappa_4^0 + \frac{105}{8}\kappa_6^0)/(\sigma J)^2. \quad (2.2.33)$$

This is the anisotropy parameter which determines the plane in which the moments spiral, and it vanishes at the temperature T'_N at which

the c -axis moments begin to order. Just below T'_N , the c -component is modulated with the wave-vector \mathbf{Q}' at which $\mathcal{J}_{\parallel}(\mathbf{q})$ has its maximum, and only if $\mathbf{Q}' = \mathbf{Q}$ is the structure the tilted helix. If $\mathbf{Q}' = \mathbf{0}$, so that the c -axis moments are ferromagnetically ordered, the resulting structure is the *cone*.

The magnetoelastic contributions require special treatment when the structures are modulated, because of the limited ability of the lattice to adapt to various strain configurations, when the strains are spatially modulated. The magnetoelastic Hamiltonians considered above are only strictly valid in the uniform case, but they may be generalized to non-uniform structures by replacing the strains by their local values $\epsilon_{\alpha\beta}(i)$, at least in the limit where the wavelength of the modulation is much longer than the range of the interactions. At shorter wavelengths, the form of the magnetoelastic-interaction Hamiltonian may still be applicable, but the effective coupling parameters may depend on the wave-vector. This suggests that the above discussion may be largely unchanged if the magnetic structure is modulated, provided that we take account of the new constraints which we shall now examine. The displacement of the i th ion, $\mathbf{u}(\mathbf{R}_i) = \tilde{\mathbf{R}}_i - \mathbf{R}_i$, from its equilibrium position \mathbf{R}_i may be divided into a uniform and a non-uniform component, and the non-uniform part may be written as a linear combination of contributions from the *normal phonon modes* at various wave-vectors. It follows from this that a displacement of the ions which varies with a certain wave-vector should be describable in terms of the normal phonon modes at that particular wave-vector, in order to ensure that such a displacement is compatible with the lattice.

To be more specific, we shall consider the wave-vector to be along the c -axis in the hcp lattice. In the *double-zone representation*, which neglects the two different displacements of the hexagonal layers, there are only three normal modes; one longitudinal and two energetically-degenerate transverse modes. All three modes correspond to rigid displacements of the hexagonal layers. The γ -strains describe an elongation of these layers along a certain direction in the plane. If the γ -strains are uniform within each hexagonal layer, the magnitude or the direction of the elongation cannot be allowed to vary from one layer to the next, as this would destroy the crystal. Hence, even though $\langle Q_2^2(\mathbf{J}_i) \rangle$ in the equilibrium equation for $\epsilon_{\gamma 1}(i)$, corresponding to eqn (2.2.25), varies in a well-defined way in a helical structure with \mathbf{Q} along the c -axis, $\epsilon_{\gamma 1}(i)$ is forced to stay constant. The site-dependent version of (2.2.25) is only valid when the right-hand sides are replaced by their averages with respect to any variation along the c -axis, and these averages vanish in the helix. This phenomenon was named the *lattice clamping effect* by Cooper (1967), and further discussed by Evenson and Liu (1969). One

of its consequences is that the γ -strain contributions (2.2.27) to the free energy cancel out in the helical phase. This behaviour of the γ -strains therefore enhances the tendency of the wave-vector of the helix to jump to one of the two commensurable values $Q = 0$ or $2\pi/c$, or may increase the stability of other commensurable structures which have a net moment in the basal-plane.

The only strain modes which are allowed to vary along the c -axis are those deriving from the transverse modes, which are $\epsilon_{\varepsilon 1}(i)$ and $\epsilon_{\varepsilon 2}(i)$, and the longitudinal component $\epsilon_{33}(i)$. Like the γ -strains, the α -strains $\epsilon_{11}(i)$ and $\epsilon_{22}(i)$ must remain constant. In the longitudinally polarized phase, the ε -strains are not affected by the ordered moment. The uniform α -strains are determined by the average of $\langle Q_l^0(\mathbf{J}_i) \rangle$ and, in addition, the c -axis moments induce a non-uniform longitudinal-strain mode $\epsilon_{33}(i) \propto \langle J_{i\zeta} \rangle^2$ at the wave-vector $2\mathbf{Q}$, twice the ordering wave-vector. The amplitude $\epsilon_{2\mathbf{Q}}$, in $\epsilon_{33}(i) = \epsilon_{2\mathbf{Q}} \cos(2Q R_{i\zeta})$, may be determined by the equilibrium conditions for the single sites, with the magnetoelastic-coupling parameters replaced by those corresponding to $2\mathbf{Q}$. The longitudinal strain at site i is directly related to the displacement of the ion along the ζ -axis; $\epsilon_{33}(i) = \partial u_\zeta / \partial R_{i\zeta}$ and hence $u_\zeta(\mathbf{R}_i) = (2Q)^{-1} \epsilon_{2\mathbf{Q}} \sin(2\mathbf{Q} \cdot \mathbf{R}_i)$. Below T'_N , where $\langle J_{i\xi} \rangle$ becomes non-zero, the cycloidal ordering induces an $\epsilon_{\varepsilon 1}$ -strain, modulated with the wave-vector $2\mathbf{Q}$. The presence of a (static) transverse phonon mode polarized along the ξ -direction corresponds to $\partial u_\xi / \partial R_{i\zeta} = \epsilon_{13}(i) + \omega_{13}(i) \neq 0$, whereas $\partial u_\zeta / \partial R_{i\xi} = \epsilon_{13}(i) - \omega_{13}(i) = 0$. Hence it is $\epsilon_{\varepsilon 1}(i) + \omega_{13}(i)$, with $\omega_{13}(i) = \epsilon_{\varepsilon 1}(i)$, which becomes non-zero, and not just $\epsilon_{13}(i) = \epsilon_{\varepsilon 1}(i)$. In these expressions, $\omega_{13}(i)$ is the antisymmetric part of the strain tensor, which in the long-wavelength limit describes a rigid rotation of the system around the η -axis. Because such a rotation, in the absence of external fields, does not change the energy in this limit, the magnetoelastic Hamiltonian may still be used for determining $\epsilon_\varepsilon(i)$. Only when the relation between the strains and the transverse displacements is considered, is it important to include the antisymmetric part. In helically-ordered systems, the γ -strains are zero, due to the clamping effect, as are the ε -strains, because the moments are perpendicular to the c -axis. Only the α -strains may be non-zero, and because $\langle Q_l^0(\mathbf{J}_i) \rangle$ are independent of the direction of the basal-plane moments, the α -strains are the same as in the ferromagnet (we neglect the possible six-fold modification due to B_α^{66} in (1.4.10)). Their contributions to the axial anisotropy (2.2.33), to be included in κ_l^0 , are also the same as in the ferromagnetic case. In the basal-plane ferromagnet, the ε strains contribute to the axial anisotropy $1/\chi_{xx}$ in eqn (2.2.19b):

$$\Delta(1/\chi_{xx}) = \frac{1}{N(\sigma J)^2} \partial^2 F_\varepsilon / \partial \theta^2 = -\frac{1}{4} c_\varepsilon H_\varepsilon^2 / (\sigma J)^2 \quad ; \quad \theta_0 = \frac{\pi}{2}, \quad (2.2.34)$$

as derived from (2.2.31). It is straightforward to see that we get the equivalent contribution in the helix at $\mathbf{q} = \mathbf{0}$ in eqn (2.2.33), except that the coupling parameters in (2.2.34) should have the effective values at the wave-vector \mathbf{Q} . In the conical phase, both $\epsilon_{\varepsilon_1}(i)$ and $\epsilon_{\varepsilon_2}(i)$ become non-zero, 90° out of phase with each other, corresponding to a transverse displacement of the planes, in a direction which follows the orientation of the moments in the basal plane.

2.3 Magnetic structures of the elements

As we have seen, the ‘exotic spin configurations’ first observed by Koehler and his colleagues in the heavy rare earths may be understood as the result of a compromise between the competing magnetic interactions to which the moments are subjected. The complex changes which occur as the temperature is varied stem primarily from the temperature dependence of the expectation values of the terms in the MF Hamiltonian (2.1.16). The *crystal-field parameters* B_l^m are expected to change little with temperature but, as shown in the previous section, the variation of the expectation values $\langle O_l^m \rangle$ of the *Stevens operators* may give rise to a very pronounced temperature dependence of the anisotropy forces, including the magnetoelastic effects. The contribution from the *two-ion coupling* generally varies more slowly, since the exchange field is proportional to $\langle \mathbf{J}_j \rangle$ or σ , but changes in the magnitude and orientation of the ordered moments alter the band structure of the conduction electrons, which in turn modifies the *indirect exchange* $\mathcal{J}(ij)$. Hence the Fourier transform $\mathcal{J}(\mathbf{q})$, and in particular the value \mathbf{Q} at which it attains its maximum, may change with temperature in the ordered phase. In addition, the possibility that *anisotropic two-ion coupling* may be of importance implies that the effective parameters of the simple MF Hamiltonian (2.1.16) may all depend on the magnitude and orientation of the moments.

The anisotropy forces favour a set of crystallographic directions, related by a rotational symmetry operator, along which the moments tend to align themselves. In particular, the low-order crystal-field term $B_2^0 \langle O_2^0(\mathbf{J}) \rangle$ gives rise to an *axial anisotropy*, which strives to confine the magnetization either to the basal plane or along the *c*-axis, and declines relatively slowly with temperature. Except for Gd, the rare earth elements all have a $\mathcal{J}(\mathbf{q})$ with a maximum at $\mathbf{Q} \neq \mathbf{0}$, reflecting the complexities of the Fermi surface and corresponding to a periodicity which is not generally commensurate with the lattice. Transverse and longitudinal magnetic structures can accommodate both the anisotropy and the periodicity constraints at high temperatures, with respectively uniform helical or longitudinal-wave configurations of the moments, characterized by a single wave-vector. As the temperature is lowered, however,

conditions develop which favour commensurable structures, including the ferromagnet. The *hexagonal anisotropy* distorts the helical structure, while the development of higher harmonics, assisted by the axial-anisotropy forces, favours commensurability in the longitudinal structure. The *higher-order axial-anisotropy terms* may also tend to pull the moments away from their planar or axial orientations. The application of a *magnetic field* requires further compromises, until it is so great that it coerces all the moments into alignment.

The variation of temperature and field thus reveals a rich variety of intermediate phase transitions to different structures. Most of these transitions are discontinuous, but occasionally a second-order transition is observed. In the following, we will discuss the relation between the *interactions*, and their variation, and the *magnetic structures* in the rare earths. We shall give a summary of the rather complete understanding which has been attained of the heavy elements, followed by a brief discussion of the complex structures of Nd, which is the only light rare earth which has been studied in comparable detail. The effect of a magnetic field will be exemplified by a description of the magnetization of Ho. Finally we will consider the new features which emerge when one dimension of the magnetic lattice is bounded, illustrated by some of the results from the rapidly developing study of thin films and superlattices.

2.3.1 Bulk magnetic structures

The manner in which the competing interactions express themselves is very well illustrated by the heavy hcp rare earths. In their magnetically ordered phases, all the moments in a particular plane normal to the c -axis are aligned, but their relative orientations may change from plane to plane. Fig. 1.19 illustrates some of the simpler of these structures, while the transition temperatures T_N and T_C to ordered states, respectively without and with a net moment, are given in Table 1.6.

Gd is magnetically by far the simplest of the rare earths. The exchange favours ferromagnetism and the $4f$ charge-cloud is spherically symmetric, so that the crystal-field interactions (1.4.4) are zero. However there is a residual magnetic anisotropy, which causes the moments to point preferentially along the c -axis just below T_C . At lower temperatures, the easy axis begins to deviate towards the basal plane, reaching a maximum tilt angle of 60° at 180 K before decreasing to just below 30° at 4.2 K (Corner and Tanner 1976). The anisotropy parameters are typically two or three orders of magnitude smaller than those of the other heavy rare earths (Mishima *et al.* 1976). Since the c/a ratio of Table 1.2 is less than the ideal value, the dipolar coupling induces an anisotropy, discussed in Section 5.5.1, which tends to hold the moments along the c -direction and has roughly the observed magnitude (Brooks and Good-

ings 1968). There is in addition a competing anisotropy, which has its origin in the spin-orbit coupling (1.2.13) of the conduction electron gas, which restricts the free rotation of the spins relative to the lattice. The indirect-exchange interaction then ensures that the localized spins are correspondingly constrained. The magnitude of this effect could in principle be calculated from the electronic structure, at least at absolute zero, but no serious attempts have yet been made to do so.

The small anisotropy of Gd leads to an unusual sequence of structures when it is diluted with Y. The latter has a very strong tendency to impose a periodic magnetic structure on dissolved rare earth moments (Rainford *et al.* 1988a; Caudron *et al.* 1990) and, in a concentration above about 30% in Gd, induces a helical structure below T_N . The magnetic behaviour of these alloys is completely dominated by the exchange, and the transition to the ferromagnetic structure, both with increasing Gd concentration and, as occurs if the Y concentration is not too high, with decreasing temperature, takes place by a continuous reduction of the turn angle of the helix (Palmer *et al.* 1986), as the peak in $\mathcal{J}(\mathbf{q})$ moves smoothly to the origin. At higher Y concentrations, a longitudinal wave is also formed along the c -axis, over a temperature range and with a wave-vector which are different from those of the helix. As discussed in Section 2.1.5, this behaviour shows explicitly that the exchange must be anisotropic. Furthermore, at Y concentrations just above the critical value for the formation of a helix, a ferromagnetic structure, with the easy direction along the c -axis, forms at T_C , is transformed into a basal-plane helix through a first-order transition at a lower temperature T_N , and at an even lower temperature transforms back into the aforementioned ferromagnetic structure, with the moments canted away from the c -direction.

Tb and Dy both have large axial anisotropies which confine the moments to their basal planes, and the peaks in $\mathcal{J}(\mathbf{q})$, illustrated in Fig. 1.17, induce helical structures at the respective Néel temperatures. In Tb, this peak is very small, and the spin-wave measurements illustrated in Fig. 6.1 indicate that it becomes even smaller as the helical phase is established and the superzone energy-gaps grow. Simultaneously, the (negative) anisotropy energy in the ferromagnetic phase increases, particularly the cylindrically-symmetric magnetoelastic term proportional to C^2 in (2.2.27), which makes no contribution in the helical phase because of lattice clamping. Consequently, this anisotropy energy overwhelms the exchange-energy difference (1.5.35) only ten degrees below T_N , and a first-order transition occurs to a ferromagnetic structure. The peak in the exchange function in Dy is more robust, and the helical phase correspondingly more stable but, as we have discussed in Section 1.5, a ferromagnetic transition ultimately takes place at 85 K.

An instructive example of competing anisotropy forces has been observed in a $\text{Tb}_{0.5}\text{Dy}_{0.5}$ crystal (Spano *et al.* 1988). This alloy, as would be anticipated, forms a helical structure at 206 K, and transforms into a ferromagnet at 152 K. At this temperature, the predominant anisotropy is due to the Tb magnetoelastic forces in (2.2.28), since the coefficient A is almost zero for Dy (Martin and Rhyne 1977), and the hexagonal crystal-field anisotropy for both types of ion has renormalized to a very small value. Consequently, the easy axis of magnetization is the b -axis, as in pure Tb. As the temperature is further reduced, however, the crystal-field contribution grows, roughly as σ^{21} , and since it is much greater for Dy than Tb, the easy axis switches at about 100 K to the a -direction, as in pure Dy.

Table 2.1. Crystal-field parameters (meV).

	B_2^0	B_4^0	B_6^0	B_6^6
Ho	0.024	0.0	$-9.6 \cdot 10^{-7}$	$9.2 \cdot 10^{-6}$
Er	-0.027	$-0.3 \cdot 10^{-4}$	$1.3 \cdot 10^{-6}$	$-9.0 \cdot 10^{-6}$
Tm	-0.096	0.0	$-9.2 \cdot 10^{-6}$	$8.9 \cdot 10^{-5}$

Compared with these relatively straightforward systems, the behaviour of the remainder of the magnetic heavy rare earth series, Ho, Er, and Tm, is more intriguing. As illustrated in Fig. 1.17, the peaks in $\mathcal{J}(\mathbf{q})$ are large, so that periodic structures are stabilized down to low temperatures. The crystal-field anisotropy also allows the moments to move out of the plane. In Table 2.1 are given the anisotropy parameters deduced from studies of the magnetic structures and excitations. Although these must to some extent be considered as effective values, assuming for example the effects of two-ion and magnetoelastic anisotropy, they are among the best estimates which we have for the crystal fields in the rare earths, and they correlate well with the Stevens factors of Table 1.4.

Ho demonstrates the interplay of the various interactions in an exemplary manner. The positive value of B_2^0 and the peak in the exchange function again stabilize the helix at T_N . The peak value $\mathcal{J}(\mathbf{Q})$ is now so large, however, that the cylindrically-symmetric magnetoelastic energy, which is substantially smaller than that of Dy, is unable to induce a ferromagnetic transition. On the other hand, the hexagonal crystal-field anisotropy is nearly three times as big as in Dy, and distorts the helix drastically when the temperature is reduced, as revealed by the appear-

ance of higher harmonics in neutron diffraction (Koehler *et al.* 1966). As illustrated in Fig. 2.4, the peak in $\mathcal{J}(\mathbf{q})$ simultaneously moves to smaller values of \mathbf{q} , and the \mathbf{Q} of the magnetic structure decreases correspondingly. However this change does not occur uniformly with temperature, but rather a series of *commensurable* wave-vectors is traversed, with apparently discontinuous jumps between them (Gibbs *et al.* 1985). At 20 K, a second-order transition to a shallow cone structure, with an opening angle which decreases continuously towards 80° as the temperature is lowered, is observed. The helical component is commensurable with the lattice, with an average turn angle of 30° , but the moments are strongly bunched around the easy b -axes, as shown in Fig. 1.20.

To interpret this rich variety of phenomena, we will use the model of Larsen *et al.* (1987). The Hamiltonian which they constructed has

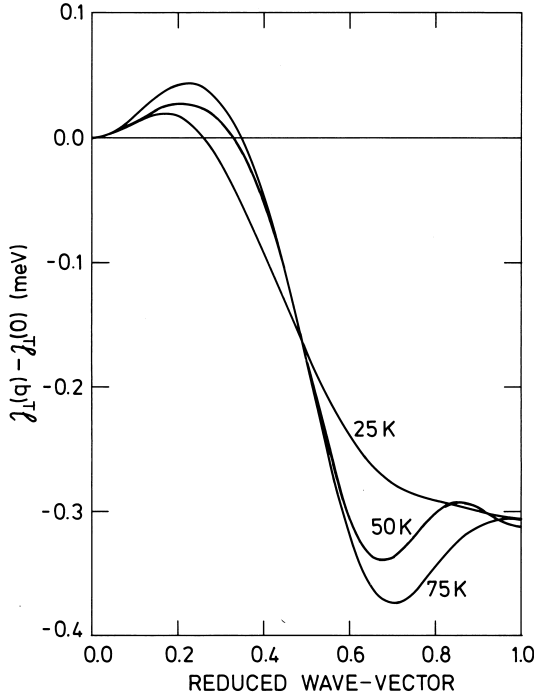


Fig. 2.4. The Fourier transform, for wave-vectors in the c -direction, of the indirect-exchange interaction in Ho at different temperatures, deduced from the magnetic excitations and used in the calculation of the structures. The maximum in $\mathcal{J}_\perp(\mathbf{q})$ increases in magnitude and moves to larger wave-vectors as the temperature is increased, leading to a decrease in the repeat distance of the periodic structures.

the form of (2.1.1), augmented by the magnetic dipole–dipole interaction (1.4.26) which, as we shall see, is of crucial importance. The crystal-field parameters B_l^m were determined primarily from a fit to the magnetic structures and magnetization curves at low temperatures, shown in Fig. 1.20, and the temperature dependence of these parameters was assumed to be negligible. The initial values for the isotropic Heisenberg exchange were taken from an analysis of the spin waves in Ho (Jensen 1988a), and depend explicitly on the temperature, as shown in Fig. 2.4. They were adjusted slightly (Mackintosh and Jensen 1990) to reproduce correctly the transition fields from the helical phase, but remain consistent with the spin-wave data, within the experimental error. The magnetic properties are calculated by means of the method described in Section 2.1.2, assuming an initial distribution $\langle \mathbf{J}_i \rangle$ of the moments at a given temperature. The structure is taken to be commensurate, with a repeat distance, deduced from experimental data, which may be as high as 50–100 atomic layers for the more complex configurations. The assumed values of $\langle \mathbf{J}_i \rangle$ are inserted into the Hamiltonian and a new set of moments calculated, using the mean-field method to reduce the two-ion term to the single-ion form. This procedure is repeated until self-consistency is attained. The free energy and the moments on the different sites can then readily be calculated for the self-consistent structure.

The results of such self-consistent calculations for different temperatures and commensurate periodicities are shown in Fig. 2.5. The data indicate that B_4^0 is zero, to within the experimental error, whereas B_6^0 has the opposite sign to B_2^0 . As the temperature is reduced in the helical phase and $B_6^0 \langle O_6^0 \rangle$ increases, this term tends to pull the moments out of the plane. If the only two-ion coupling were the isotropic exchange, this would give rise to a continuous transition to a tilted helix, which reduces the exchange energy more effectively than the cone (Elliott 1971, Sherrington 1972). However, the dipolar interaction strongly favours a ferromagnetic orientation of the c -axis moments, because the dipolar energy associated with a longitudinal wave is very high, as we discuss in detail in Section 5.5.1. Consequently, the dipolar contribution shifts the position of the maximum in $\mathcal{J}_{\parallel}(\mathbf{q})$ from $\mathbf{q} = \mathbf{Q}$ to zero wave-vector, as illustrated in Fig. 5.7, and the vanishing of the axial anisotropy (2.2.33) at $\mathbf{q} = \mathbf{0}$ leads to a second-order transition at T'_N to the cone phase. In this special case, we can therefore conclude that it is the temperature dependence of $B_6^0 \langle O_6^0 \rangle$ which drives the helix into instability, and that the dipolar interaction chooses the cone, rather than the tilted helix, as the stable low-temperature phase.

At 4 K, in the cone phase, the large hexagonal anisotropy causes the helical component of the moments to bunch around the easy directions of magnetization, in the twelve-layer structure described by eqn (1.5.3),

so that the constant angle ϕ in the plane between any moment and the nearest b -axis is only 5.8° , as shown in Fig. 2.5(a), compared with the 15° which corresponds to a uniform helix. As the temperature is increased, the expectation value $\langle O_6^6 \rangle$ decreases with the relative magnetization, roughly like σ^{21} , and ϕ increases correspondingly. Simultaneously Q tends to increase, reflecting the change in the position of the maximum

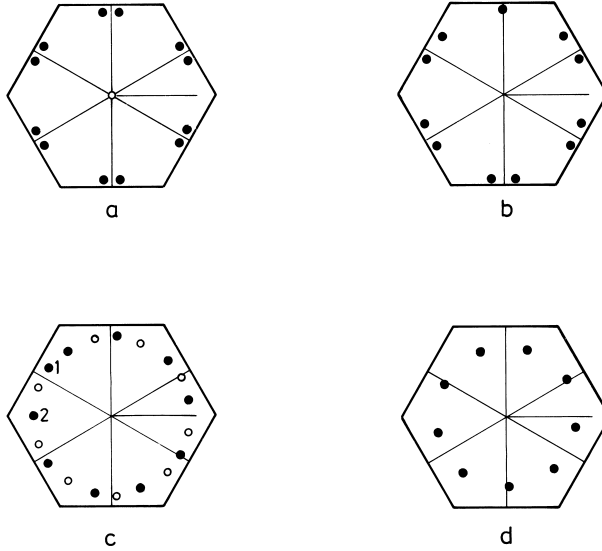


Fig. 2.5. The self-consistent periodic structures in Ho, calculated at different temperatures. Each circle represents the magnitude and direction of the ordered moment in a specific plane, relative to the size of the moment at absolute zero ($10 \mu_B$), indicated by the length of the horizontal lines. The orientation of moments in adjacent planes is depicted by the positions of neighbouring circles.

(a) The 12-layer zero-spin-slip structure at 4 K. The open circle in the centre indicates the ferromagnetic component in the cone structure.

(b) The 11-layer one-spin-slip structure at 25 K. The bunched pairs of moments are disposed unsymmetrically with respect to the easy axis in the vicinity of the spin slip.

(c) The 19-layer structure at 50 K. The orientation of the moments in successive layers is determined by following first the filled circles in an anticlockwise direction, as indicated, and then the open circles.

(d) The 9-layer trigonal structure at 75 K. This may be looked upon as a three-spin-slip structure, but the bunching is so slight that it is more useful to regard it as an almost regular helix, in which every third plane aligns its moments close to an easy axis, in order to reduce the anisotropy energy.

in $\mathcal{J}(\mathbf{q})$, so that the structure at 25 K has reduced its periodicity to 11 layers by introducing a regularly-spaced series of *spin slips*, at which one plane of a bunched doublet is omitted while the remaining member orients its moments along the adjacent easy axis. The configuration of Fig. 2.5(b), in which one spin slip is introduced for each repeat distance of the perfect commensurable structure, is the primordial spin-slip structure and has a number of interesting features. It is particularly stable, existing over a range of temperature (Gibbs *et al.* 1985), possesses a net moment, and the bunching angle is still rather small. Although the angle 2ϕ between two bunched planes is almost constant, the exchange interaction distorts the structure near the spin slips so that the moments are not symmetrically disposed around the easy axis. As the temperature is increased further, the bunching decreases and the concept of spin slips becomes less useful. Thus the configuration of Fig. 2.5(d) can be considered as a distorted three spin-slip structure, but it is simpler to regard it as a commensurable, almost regular helix in which every third plane aligns its moments close to an easy axis in order to reduce the anisotropy energy.

The spin-slip structures of Ho have been subjected to a careful and extensive neutron-diffraction study by Cowley and Bates (1988). They interpreted their results in terms of three parameters:

b - the number of lattice planes between spin slips,

2α - the average angle between the moments in a bunched pair,

σ_G - a Gaussian-broadening parameter for α .

In a perfect, undistorted structure, $\alpha = \phi$ and $\sigma_G = 0$. The parameter σ_G takes into account two effects; the distortions which occur in perfect periodic structures such as that illustrated in Fig. 2.5(b), and possible irregularities in the positions of the spin-slip planes. The former is in principle included in the calculations, whereas the latter is not. From the calculated magnetic structures, such as those illustrated in Fig. 2.5, it is possible to deduce the corresponding neutron-diffraction patterns and hence, by fitting the peak intensities, determine the values for α and σ_G (Mackintosh and Jensen 1990). The parametrization suggested by Cowley and Bates is in practice rather satisfactory; it allows a fit of all the calculated neutron-diffraction intensities, which vary over about five orders of magnitude, with a relative error of in all cases of less than 20%. Furthermore, the parameter α is close to the average values of the angle ϕ determined directly from the calculated structures. The measured and calculated values of α are in good agreement, taking into account the experimental uncertainties, but there are some discrepancies in σ_G . It is noteworthy that the agreement between the predicted and observed neutron-diffraction intensities is very good for the $b = 11$, one-spin-slip structure, but that the experimental values of σ_G otherwise

lie consistently above the theoretical. This may indicate that the perfect periodicity of the less stable spin-slip structures is more effectively disturbed by imperfections.

As may be seen from Table 2.1, the easy direction in Er is the c -axis at high temperature, so the moments order in a longitudinal-wave structure at T_N . As the temperature is reduced, the structure squares up, as discussed in Section 2.1.4. The basic wave-vector \mathbf{Q} describing the magnetic ordering increases approximately linearly just below T_N (Atoji 1974; Habenschuss *et al.* 1974). This is not in accord with the quadratic dependence predicted by (2.1.35b) and furthermore, since $\mathcal{J}'(3\mathbf{Q})$ is probably negative, the predicted change in \mathbf{Q} also has the opposite sign to that observed. This behaviour can only be accounted for if $\mathcal{J}(\mathbf{q})$ is temperature dependent, as is indicated even more clearly at lower temperatures, where \mathbf{Q} starts to decrease quite rapidly. At $T'_N \simeq 52$ K, a basal-plane component begins to order, through the mechanism described in Section 2.1.5. When the temperature is lowered further, \mathbf{Q} continues to decrease, exhibiting a number of plateaux, and a rich harmonic structure is observed (Atoji 1974; Habenschuss *et al.* 1974; Gibbs *et al.* 1986). Very detailed neutron-diffraction measurements by Cowley (1991) have revealed a whole sequence of commensurable structures with decreasing temperature, with $Q = 2/7, 3/11, 7/26, 4/15, 5/19, 6/23,$ and $1/4$, in units of $2\pi/c$. At 18 K, a first-order transition to a steep cone, with an opening angle of 30° and a wave-vector of $\sim 5/21$, is observed.

To explain these results, we may employ a modified version of the model of Jensen (1976b), in which crystal fields, isotropic exchange, and dipolar interactions are included. In addition, the anisotropic two-ion coupling, which is required by the observed excitation spectrum and discussed in Section 6.1, is also taken into account. Mean-field calculations then predict that the structure in the intermediate temperature range is an elliptic cycloid, the hodograph of which at 48 K, just below the transition temperature, is shown in Fig. 2.6. As discussed in Section 2.1.5, an additional second-order transition may occur below T'_N , to a phase with a non-collinear, elliptical ordering of the basal-plane moments. In the presence of random domains, the neutron-diffraction patterns from the two structures are essentially indistinguishable, and if this transition occurs in Er, the fluctuations expected near a second-order transition may also be suppressed, because it is then likely that it coincides with one of the first-order commensurable transitions. The model calculations indicate that the non-collinear component in the basal plane is close to becoming stable when the cycloidal phase is disrupted by the first-order transition to the cone phase. Hence it is most probable that the moments in Er are ordered in a planar elliptic-cycloidal structure in the

whole interval between T_C and T'_N , but it is possible that a non-collinear basal-plane component is present in some of the commensurable structures just above T_C .

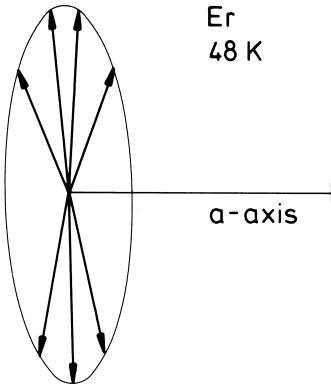


Fig. 2.6. The calculated magnetic structure in Er at 48 K. Each arrow represents the magnitude and orientation, in the a - c plane, of the ordered moment in a specific plane normal to the c -axis, relative to the magnitude of the moment at absolute zero ($9\mu_B$), indicated by the length of the line along the a -axis. The hodograph is very close to an ellipse, with semi-axes of length 6.5 and $2.2\mu_B$, and this structure can be considered as comprising four planes of moments with a positive component along the c -axis, followed by three with a negative moment, with the designation (43).

The structure shown in Fig. 2.6 comprises four planes of moments with a positive component along the c -axis, followed by three with a negative moment. The basic wave-vector is therefore $2/7$, and we may describe the structure as (43). The other commensurable structures listed above are then respectively $2\times(443)$, $2\times(4434443)$, (4443), $2\times(44443)$, (444443), and (44) where, in each case, blocks of n moments with a positive component along the c -axis alternate with negative blocks, and the doubling is necessary to ensure periodicity if the number of blocks is odd. These calculations give a good account of the neutron-diffraction results of Cowley (1991). The lattice strains associated with a number of these structures have been studied with synchrotron X-rays by Gibbs *et al.* (1986). The fundamental wave-vector for the oscillating c -axis strain in a structure like (44), which has inversion symmetry, is twice that of the magnetic structure. However, the other examples above do not have inversion symmetry, so charge-scattering of X-rays may occur at the fundamental magnetic wave-vector. In the cone phase, the X-ray scattering at the fundamental wave-vector of the helical component is anomalously large, even though the longitudinal lattice-strain must be very small. There is however also a contribution from charge scattering associated with a *transverse* strain, discussed at the end of the previous section, which may arise when the mirror symmetry normal to the c -axis is broken, as it is in this structure. The hexagonal symmetry of a

particular plane is then maintained, but it suffers a lateral displacement which follows the direction of the helical component of the moment.

The transition from the cycloidal to the cone structure in Er at 18 K reflects a shift in the balance between a number of competing effects. At this low temperature, the entropy is not important, since most of the moments are close to their saturation value near T_C , nor does the difference between the single-ion crystal-field anisotropy energy in the two phases play a significant role. Because of cancellation among the three contributions, the axial anisotropy is relatively insensitive to the angle between the c -axis and the moments, the average value of which does not, in any case, change much at the transition. The small amplitude of the basal-plane components ensures that the hexagonal-anisotropy energy also has only a minor influence. Hence the choice between the two phases is dominated by the two-ion contributions to the energy. From the spin-wave dispersion relation, discussed in Section 6.1, the difference $\mathcal{J}_\perp(\mathbf{Q}) - \mathcal{J}_\perp(\mathbf{0})$ is estimated to be about 0.07–0.1 meV, strongly favouring a modulated structure. The tendency towards a modulation of the c -axis component is opposed by three effects. Firstly, the anisotropy of the classical dipole–dipole contribution reduces $\mathcal{J}_\parallel(\mathbf{Q}) - \mathcal{J}_\parallel(\mathbf{0})$ by 0.03 meV to about 0.04–0.07 meV. Secondly, the modulated ordering of the c -axis component cannot take full advantage of the large value of $\mathcal{J}_\parallel(\mathbf{Q})$, because of the squaring up which occurs as the temperature is decreased. The energy due to the coupling of the longitudinal component of the moments is

$$U_{\zeta\zeta} = -\frac{1}{4}N \sum_{n \text{ odd}} \mathcal{J}_\parallel(n\mathbf{Q}) \langle J_\zeta(n\mathbf{Q}) \rangle^2 = -\frac{1}{2}N \overline{\mathcal{J}}_\parallel(\mathbf{Q}) \langle |J_\zeta| \rangle^2, \quad (2.3.1a)$$

introducing the effective coupling parameter $\overline{\mathcal{J}}_\parallel(\mathbf{Q})$. At high temperatures, close to T_N , the two coupling parameters $\overline{\mathcal{J}}_\parallel(\mathbf{Q})$ and $\mathcal{J}_\parallel(\mathbf{Q})$ are equal, but as the higher odd harmonics gradually develop, $\overline{\mathcal{J}}_\parallel(\mathbf{Q})$ decreases, and when the structure is close to the square wave, we find from (2.1.36) that

$$\overline{\mathcal{J}}_\parallel(\mathbf{Q}) \simeq \frac{8}{\pi^2} \left\{ \mathcal{J}_\parallel(\mathbf{Q}) + \frac{1}{9} \mathcal{J}_\parallel(3\mathbf{Q}) + \dots \right\}. \quad (2.3.1b)$$

Just above the cone transition, the model calculations indicate that $\overline{\mathcal{J}}_\parallel(\mathbf{Q})$ is reduced by 0.02–0.03 meV, compared to $\mathcal{J}_\parallel(\mathbf{Q})$, which in combination with the dipolar term removes most of the energy difference between the modulated and ferromagnetic ordering of the c -axis component. The final contribution, which tips the balance into the cone phase below T_C , is the magnetoelastic energy associated with the α -strains

$$U_{\text{me}}^\alpha = -\frac{1}{2}(c_{11} - c_{66})(\epsilon_{11} + \epsilon_{22})^2 - \frac{1}{2}c_{33}\epsilon_{33}^2 - c_{13}(\epsilon_{11} + \epsilon_{22})\epsilon_{33}. \quad (2.3.2)$$

The abrupt change in the uniform α -strains (Rhyne and Legvold 1965b) at the transition to the cone phase reduces this energy by 0.19 meV/ion (Rosen *et al.* 1973), corresponding to an increase of $\mathcal{J}(\mathbf{0})$ by about 0.01 meV. In the cycloidal phase, there is also a longitudinal-strain mode at wave-vector $2\mathbf{Q}$, which disappears in the cone phase, but the energy gained by this distortion is estimated to be very small. Since the c -axis moment is substantially squared up in the cycloidal phase just above the transition, the change of the α -strains cannot have its origin in the single-ion magnetoelastic coupling, which does not distinguish between positive and negative moments. It must rather be caused by the strain-dependence of the two-ion interaction

$$\Delta\mathcal{H}_{\text{me}} = - \sum_{ij} [I_1(ij)\{\epsilon_{11}(i) + \epsilon_{22}(i)\} + I_3(ij)\epsilon_{33}(i)] J_{i\zeta} J_{j\zeta}, \quad (2.3.3)$$

which is that part of eqn (2.2.32) which changes at the transition. If the basal-plane moments and the single-ion magnetoelastic terms are assumed to be the same immediately above and below T_C , $\Delta\mathcal{H}_{\text{me}}$ gives rise to the following changes at the transition:

$$\begin{aligned} (c_{11} - c_{66})\Delta(\epsilon_{11} + \epsilon_{22}) + c_{13}\Delta\epsilon_{33} &= N\{I_1(\mathbf{0}) - \bar{I}_1(\mathbf{Q})\}\langle|J_\zeta|\rangle^2 \\ c_{13}\Delta(\epsilon_{11} + \epsilon_{22}) + c_{33}\Delta\epsilon_{33} &= N\{I_3(\mathbf{0}) - \bar{I}_3(\mathbf{Q})\}\langle|J_\zeta|\rangle^2, \end{aligned} \quad (2.3.4)$$

where the bars denote effective coupling parameters, as in (2.3.1), and $\Delta\epsilon_{\alpha\alpha} = \epsilon_{\alpha\alpha}(\text{cone}) - \epsilon_{\alpha\alpha}(\text{cycloid})$. Since the elastic constants are known, and the strains are $\Delta\epsilon_{33} = 3.1 \cdot 10^{-3}$ and $\Delta(\epsilon_{11} + \epsilon_{22}) = -2.4 \cdot 10^{-3}$, the two-ion magnetoelastic-coupling parameters may be determined from this equation. The nature of this magnetoelastic contribution implies that it should be possible to suppress the cone phase in Er by applying hydrostatic pressure. In the zero-temperature limit, the energy difference between the two phases is estimated to be only about 0.033 meV/ion, so a hydrostatic pressure of about 2.5 kbar, or alternatively a uniaxial pressure along the c -axis of only about half this amount, should be sufficient to quench the cone. The application of this modest pressure should then allow experimental studies of the cycloidal phase in Er below 18 K, to ascertain, for example, whether the transition to the phase with an elliptical ordering of the basal-plane moments occurs. We shall return to this two-ion magnetoelastic interaction when we discuss Er films and superlattices.

The negative value of B_2^0 in Tm is large and B_6^0 is also negative, as may be seen in Table 2.1, so that the moments are firmly anchored to the c -direction, and no ordered basal-plane component appears at any temperature. A longitudinal-wave structure forms at 56 K, and starts to square up at about 40 K, as the amplitude approaches the free-ion

moment of $7.0 \mu_B$. At 32 K, there is a first-order transition to a commensurate state, with a seven-layer repeat distance, which has a ferromagnetic component (Brun *et al.* 1970). At the lowest temperatures, this has developed into a *ferrimagnetic* square-wave structure, comprising a repeating pattern of four layers of positive moments followed by three of negative moments. These structures, the susceptibility curves of Fig. 2.1, and the excitation spectrum have been used to determine the parameters of a model for Tm with the usual basic ingredients of isotropic exchange, crystal fields, and dipolar interactions (McEwen *et al.* 1991). As shown in Fig. 2.7, the observed squaring-up process is very well accounted for by mean-field calculations based on this model. The principal discrepancy with experiment is in the magnitude of the field along the *c*-axis which is required to form a ferromagnetic structure, where the calculation gives a value about 50% above the observed 28 kOe. This may indicate that the form of $\mathcal{J}(\mathbf{q})$ in Tm which, as illustrated in Fig. 1.17, has the largest peak in the whole heavy rare earth series, changes substantially at this first-order transition.

The magnetic structures of the light rare earths have not generally been described in the same detail as those of the hcp metals, with the exception of Nd, which has been intensively studied for several decades.

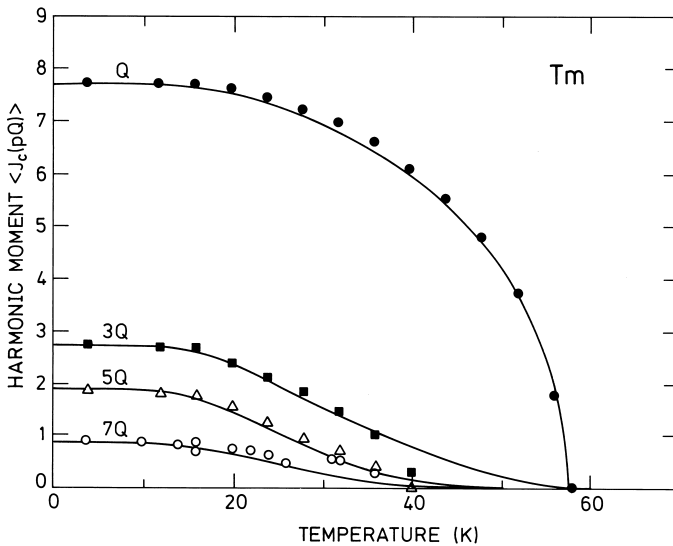


Fig. 2.7. The calculated harmonics of the *c*-axis moment in Tm as a function of temperature, compared with the results of neutron diffraction measurements, and the ferromagnetic moment ($7Q$).

Such is the complexity of the observed neutron diffraction patterns, however, that it is only recently that a reasonably complete delineation of the ordered moments has been attained (Zochowski *et al.* 1991). At the Néel temperature of 19.9 K, a weakly first-order transition leads to a longitudinal-wave structure propagating in a b -direction on the hexagonal sites of the dhcp structure, with an incommensurable periodicity given by $\mathbf{Q}_h = 0.13\mathbf{b}_1$. The moments on neighbouring hexagonal layers are ordered antiferromagnetically. Simultaneously, a c -axis moment (plus a small component in the basal plane) with the same \mathbf{Q} is induced on the cubic sites by the anisotropic two-ion coupling. The moments on neighbouring cubic layers are also ordered antiferromagnetically. As the temperature is further lowered, another first-order transition at 19.2 K establishes a double- \mathbf{Q} structure, with wave-vectors \mathbf{Q}_1 and \mathbf{Q}_2 aligned approximately along a pair of b -axes but canted slightly, so that the angle between them is somewhat less than 120° . The polarization vectors of the moments in the two waves are also canted away from the corresponding b -axes and towards each other, but by a different amount from the wave-vectors, so that the waves are no longer purely longitudinal. Compared with the single- \mathbf{Q} structure, this arrangement increases the average ordered moment, which is further augmented, as the temperature is lowered, by a squaring-up of the structure, which generates harmonics in the neutron-diffraction pattern. Simultaneously, the period gradually increases. At 8.2 K, the planar components of the moments on the cubic sites begin to order, and after undergoing a number of phase transitions, the structure at low temperatures is characterized by the four \mathbf{Q} -vectors illustrated in Fig. 2.8. Although all four periodicities are present on each type of site, \mathbf{Q}_1 and \mathbf{Q}_2 , which are now aligned precisely along b -axes, but have different magnitudes $0.106b_1$ and $0.116b_1$, generate the dominant structures on the hexagonal sites, while \mathbf{Q}_3 and \mathbf{Q}_4 , which have lengths $0.181b_1$ and $0.184b_1$ and are canted towards each other, predominate on the cubic sites. The different types of \mathbf{Q} -vector are interrelated; within the experimental uncertainty $\mathbf{Q}_3 + \mathbf{Q}_4 = 2\mathbf{Q}_1$, and the canting of \mathbf{Q}_3 and \mathbf{Q}_4 is related to the difference in length between \mathbf{Q}_1 and \mathbf{Q}_2 .

The explanation of these structures from first principles in terms of the elementary magnetic interactions is clearly a formidable task but, as we have seen in Section 2.1.6, the ordering on the hexagonal sites at high temperatures can be satisfactorily accounted for by a phenomenological Landau expansion of the free energy in terms of the order parameters, and the role of the different interactions thereby clarified. The anisotropic two-ion coupling between the dipoles confines the moments to the basal plane and tends to favour the longitudinal-wave structure. Two-ion coupling between the quadrupoles, proba-

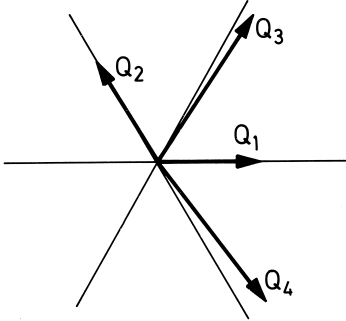


Fig. 2.8. The relative orientations and magnitudes of the fundamental wave-vectors which describe the quadruple- \mathbf{Q} magnetic structure of Nd at low temperatures. All four periodicities are present on each type of site, but \mathbf{Q}_1 and \mathbf{Q}_2 generate the dominant structures on the hexagonal sites, while \mathbf{Q}_3 and \mathbf{Q}_4 predominate on the cubic sites.

bly of magnetoelastic origin, lifts the degeneracy between the different multiple- \mathbf{Q} structures and stabilizes the single- \mathbf{Q} state just below T_N . The Landau expansion can also explain the rotation of the wave-vectors and moments away from the b -axes, with the consequent stabilization of the double- \mathbf{Q} configuration, and account for the observed harmonics in this structure. A similar analysis for the quadruple- \mathbf{Q} structure in the low-temperature region would provide the basis for understanding the even more complicated phenomena which are observed when a magnetic field is applied to Nd (Zochowski *et al.* 1991).

2.3.2 The magnetization of Holmium

The analytical mean-field treatment by Nagamiya *et al.* (1962) of the effect of a magnetic field applied in the plane of a helical structure was mentioned in Section 1.5. As the field is increased, the helix first distorts, giving rise to a moment along \mathbf{H} , and then undergoes a first-order transition to a fan structure, in which the moments oscillate about the field direction. A further increase in the field reduces the opening angle of the fan which, in the absence of magnetic anisotropy, goes continuously to zero, establishing a ferromagnetic phase at a second-order transition. Hexagonal anisotropy may modify this process by inducing a first-order transition or, if it is large enough, eliminate the fan phase entirely.

The magnetization curves measured by Strandburg *et al.* (1962) and Féron (1969) behaved in accordance with this description at low temperatures, but above about 40 K when the fan phase was first observed, a further phase also appeared, manifested by a plateau corresponding to a moment about one half of that attained in the fan phase. This extra phase was clearly apparent in the magnetoresistance measurements of Mackintosh and Spanel (1964), and later experiments by Akhavan and Blackstead (1976), in which the field was changed continuously, revealed

as many as five different phases at some temperatures. The structures in a magnetic field were investigated with neutron diffraction by Koehler *et al.* (1967), who identified two intermediate phases which they called fans and characterized by the intensity distribution of the Bragg peaks.

These phenomena have been elucidated by means of calculations of the effect of a magnetic field on the commensurable structures of Fig. 2.5 (Jensen and Mackintosh 1990). At low temperatures, the hexagonal anisotropy has a decisive influence on the magnetic structures, ensuring that a first-order transition occurs from the helix or cone to the ferromagnet, without any intermediate phases. Below about 20 K, where the cone is the stable structure in zero field, the cone angle is almost independent of the applied field in the basal plane, but at the transition to the ferromagnet, the c -axis moment disappears. When the field is applied in the hard direction at these temperatures, the moments just above the ferromagnetic transition do not point along the field direction, but are aligned very closely with the nearest easy axis, so that $\langle J_{\parallel} \rangle \simeq 8 \cdot \sqrt{3}/2$, as illustrated in Fig. 1.20. As the field is further increased, they turn towards it, becoming fully aligned through a second-order phase transition at a critical field which is estimated from B_0^G to be about 460 kOe at absolute zero. At low temperatures, the hexagonal anisotropy also hinders the smooth distortion of the helix in a field. The moments jump discontinuously past the hard directions as the field is increased, giving first-order transitions which may have been observed, for example, as low-field phase boundaries below 20 K in the measurements of Akhavan and Blackstead (1976).

Above about 40 K, when the hexagonal anisotropy is not so dominant, intermediate stable phases appear between the helix and the ferromagnet. The nature of these phases may be appreciated by noting that the helix can be considered as blocks of moments with components alternately parallel and antiparallel to the field, as is apparent from the structures illustrated in Fig. 2.5. If we write this pattern schematically as $(+ - + -)$, then the fan structure may be described as $(+ + + +)$. The intermediate structures, the helifans, then correspond to patterns of the type specified in Table 2.2. The notation $\text{helifan}(p)$ is used to designate a structure whose fundamental period is p times that of the helix (the single number p is not generally adequate for discriminating between the different helifans). It is clear that these structures represent compromises between the demands of the exchange for a periodic structure, and the field for a complete alignment of the moments. They are not due to the hexagonal anisotropy which, on the contrary, tends to suppress them, and occur both when the field is applied along the easy and hard directions in the plane. The free energies of the various magnetic phases as a function of magnetic field in the easy direction at

Table 2.2. The arrangement of blocks of spins in the helifan structures. The first row shows the relative number of $(-)$ blocks in the different structures.

Helix	Helifan				Fan
	(4)	(3)	(3/2)	(2)	
1/2	3/8	1/3	1/3	1/4	0
+	+	+	+	+	+
-	+	+	+	+	+
+	+	+	-	+	+
-	-	-	+	-	+
+	+	+	+	+	+
-	-	+	+	-	+
+	+	+	-	+	+
-	+	-	+	+	+
+	+	+	+	+	+
-	-	-	-	-	+

50K are shown in Fig. 2.9. In these calculations, the wave-vector \mathbf{Q} was allowed to vary in small, discrete steps, by changing the repeat distance, and the absolute minimum in the free energy for the structure thereby determined, as illustrated in the insert to Fig. 2.9, leading to the prediction that the stable magnetic structures follow the sequence helix \rightarrow helifan(3/2) \rightarrow fan \rightarrow ferromagnet as the field is increased. The helifan(3/2) is depicted in Fig. 2.10. In a narrow interval between the helix and the helifan(3/2), other stable phases appear, e.g. the helifan(4') (+ + - + + - + -), and similarly a sequence of helifans with m (+) blocks followed by a $(-)$ ($m \geq 3$) occurs in the close neighbourhood of the fan phase. The various structures are associated with characteristic neutron-diffraction patterns. An examination of the neutron-diffraction intensities which Koehler *et al.* (1967) associate with the phase which they designate as 'Fan I' reveals a striking correspondence with the helifan(3/2) pattern, with a very weak fundamental at $\mathbf{Q}_0/3$, where \mathbf{Q}_0 is approximately the wave-vector of the helix, strong second and third harmonics, and a weak fourth harmonic. The basic periodicities of this structure are $2\mathbf{Q}_0/3$ for the component of the moments parallel to the field, and \mathbf{Q}_0 for the perpendicular component; the weak $\mathbf{Q}_0/3$ peak arises as the result of interference between them. Similar but more detailed neutron-diffraction results have more recently been obtained by Axe *et al.* (1991). The changes in the basic wave-vector are substantial,

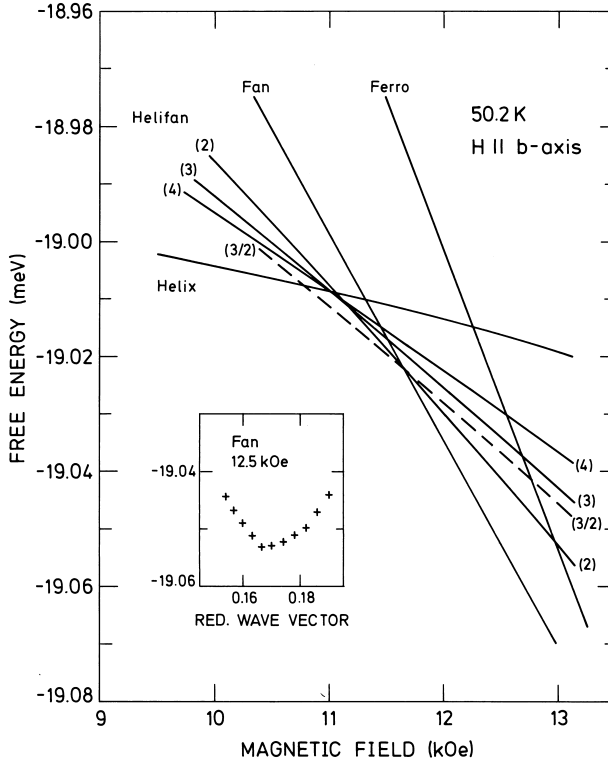


Fig. 2.9. Mean-field calculation of the free energy per ion for different magnetic structures in Ho at 50 K, as a function of the magnetic field along an easy b -axis. The free energy is in each case minimized with respect to the wave-vector which characterizes the structure, as illustrated for the fan phase in the insert.

even though the underlying exchange function is constant, and they agree very well with those observed by neutron diffraction. For the helix, fan and helifan(3/2) structures, the experimental (theoretical) values of Q are respectively 0.208 (0.211), 0.170 (0.168), and 0.063 (0.066), times $2\pi/c$. The period of the fan phase increases relative to that of the helix because of the resulting increase in the opening angle of the fan, expressed by the relation (1.5.21). This allows a decrease in the exchange energy which is greater than the concomitant increase of the Zeeman energy. The change in Q in the various helifan phases is therefore to a very good approximation proportional to their magnetization.

Helifan (3/2)

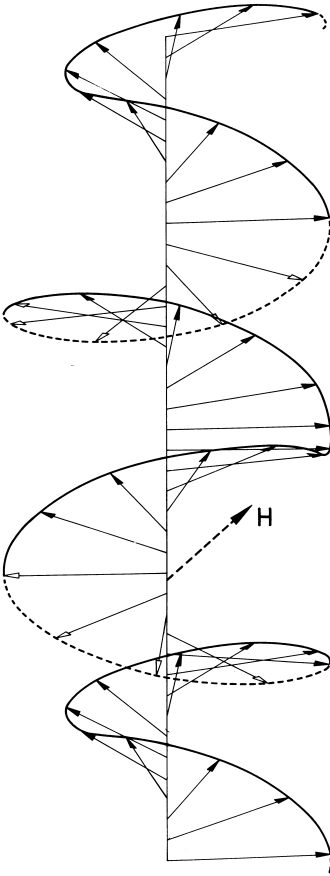


Fig. 2.10. The helifan(3/2) structure in Ho at 50 K. The moments lie in planes normal to the c -axis and their relative orientations are indicated by arrows. A magnetic field of 11 kOe is applied in the basal plane, and moments with components respectively parallel and antiparallel to the field are designated by filled and open arrow-heads. This component of the moments has a periodicity which is 3/2 that of the corresponding helix, and the helicity of the structure changes regularly.

A detailed consideration (Mackintosh and Jensen 1990) of the magnetization curves measured in Ho indicates that the metastable helifan(2) may replace or co-exist with the stable (3/2)-structure, if the measurements are made so rapidly that complete thermodynamic equilibrium is not attained. Other stable or metastable helifans may be involved in the five phases observed by Akhavan and Blackstead (1976). In addition, the very pronounced hysteresis which they observed is consistent with the existence of a large number of phases which have almost the same energy, but are not easily transformed into each other.

The stability of the various periodic structures is determined by the form of the two-ion coupling, especially the long-range component. If

the exchange is sufficiently short-range, the helix, helifans and fan are almost degenerate at the critical field; it is the interaction between the blocks which differentiates between these structures. One of the most remarkable features of the helifans is the large number of hexagonal layers involved in a single period, a characteristic which they share with the commensurate structures observed in zero field in Ho and Er, which were discussed in the preceding sub-section.

Helifans, or analogous structures, may also occur in other rare earth systems where periodic ordering is observed. For example, the modulated structures in Nd discussed previously may be described as $(+ - + - + - + -)$, indicating blocks of moments with a component parallel or antiparallel to a magnetic field applied in the basal plane. A periodic reversal of $(-)$ blocks will then generate subharmonics of the basic \mathbf{Q} -vector. Thus the sequence $(+ + + - + - + -)$ generates $\mathbf{Q}/4$, and $(+ + + - + + + -)$ gives $\mathbf{Q}/2$, both of which have been observed by neutron diffraction in a magnetic field (Zochowski *et al.* 1991).

2.3.3 Films and superlattices

The development of the technique of *molecular-beam epitaxy* has allowed the fabrication on a substrate of films of rare earth metals, with thicknesses ranging from a few to thousands of atomic planes. In addition, *superlattices*, or *multilayers*, of the form $[A_l|B_m]_n$ may be produced, in which blocks comprising l planes of element A, followed by m planes of element B, are replicated n times. It is clear that an endless variety of such systems may be constructed, and the field is in a stage of rapid development. We will restrict ourselves to a discussion of some of the new physical principles involved in understanding the magnetic properties of such structures, illustrated by a few specific examples.

The essential difference between these structures and a bulk crystal lies, of course, in the boundary conditions. Films and superlattices are *finite* in one dimension, whereas a bulk crystal is assumed to be essentially unbounded, and the magnetic layers are terminated by a medium which may have very different magnetic properties, be it a vacuum, a rare earth with quite different moments and interactions, or a nominally non-magnetic metal such as Y, which is a very popular choice for the intermediate layers in superlattices.

The influence of the finite size on the orientation of the ordered moments is illustrated in Fig. 2.11, which depicts the results of a mean-field calculation, based on the model of Larsen *et al.* (1987), for a 15-plane slab of Ho at 4K. The bunched commensurate helix encompassing the inner 12 planes is enclosed by a single and a double plane, aligned almost ferromagnetically with the respective outer planes. These ferromagnetic clusters distort the adjacent bunched pairs in a manner reminiscent of

spin slips. Such ferromagnetic terminations at the surfaces of slabs containing planes of rotating moments are a general feature, reflecting the predominantly ferromagnetic interaction between closely neighbouring planes in the magnetic rare earths. This coupling normally gives rise to a net moment in the slab, and is calculated to stabilize ferromagnetic ordering at 4 K in samples thinner than about nine atomic planes (Bohr *et al.* 1989).

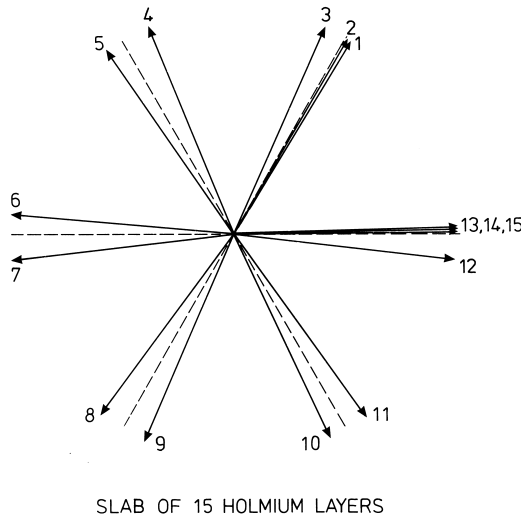


Fig. 2.11. Mean-field calculation of the orientation of the magnetic moments in a 15-plane slab of Ho at 4 K. The inner planes are close to a bunched commensurate helix, but there is a strong tendency to ferromagnetism near the surfaces.

The effect of the epitaxial strain is strikingly illustrated by the behaviour of thin films and superlattices of Dy and Er grown on Y, in both of which ferromagnetism is suppressed, by somewhat different mechanisms, in favour of periodic magnetic ordering. In 16-plane Dy films embedded in Y in a variety of $[\text{Dy}_{16}|\text{Y}_m]$ multilayers, with the c -axis normal to the plane of the slab, Rhyne *et al.* (1989) found that the helix persists to the lowest temperatures, and the ferromagnetic state is only induced if a field of the order of 10 kOe is applied in the easy direction. An obvious mechanism for this quenching of ferromagnetism is the constraint which the Y slabs impose on the Dy layers, so that the γ -strains which provide the principal driving force for the transition cannot be fully developed.

The ferromagnetic ordering of the axial moment is also suppressed

in c -axis films and superlattices of Er (Borchers *et al.* 1988), but the explanation in this case is not quite so evident. The dipolar energies are unchanged in the films, nor is it likely that the anisotropy and exchange contributions are decisively different. The strain-dependence of the exchange energy, expressed in eqn (2.3.3), can however provide a mechanism. Y has a planar lattice-constant a of 3.648 Å, which is over two per cent greater than that of Er, and the Y substrate therefore imposes a strain on the Er film, which is measured to be $\epsilon_{11} = \epsilon_{22} \simeq 6 \times 10^{-3}$. If the atomic volume is assumed to be unchanged in the film, $\epsilon_{33} \simeq -12 \times 10^{-3}$. The difference in exchange energy between the solid and a thin film may then be found from (2.3.4), and is equivalent to a field of 13 kOe acting on the c -axis moment of about $8\mu_B$. The above estimate of ϵ_{33} is probably too great, so this calculation may be considered in reasonably good agreement with the observation that Er films with thicknesses between 860 Å and 9500 Å require fields varying linearly between 8 kOe and 3 kOe to establish a ferromagnetic state at 10 K. It is noteworthy that, since Lu has a significantly smaller basal-plane lattice-constant than Er, the cone structure should be favoured in a c -axis epitaxial film grown on Lu.

Many of the characteristic features of rare earth superlattices are demonstrated by the aforementioned [Dy|Y] systems, which are observed to form helical structures over the whole temperature range of magnetic ordering. When the c -axis is normal to the plane of the film, a coherent magnetic structure may be formed, in which the phase and chirality of the helix are maintained over many bilayers, provided that the slabs of non-magnetic Y are not too thick. The coherence length may be estimated from the widths of the neutron-diffraction peaks, and corresponds to more than 10 bilayers if the Y layers are less than about 10 planes thick. If the thickness is increased to about 35 planes, however, the coherence length, which is inversely proportional to the width of the Y layers, is less than the bilayer thickness, so that the helix in one Dy layer is uncorrelated with that in the next. In the long-range coherent structures, the phase change of the helix across the Dy layers corresponds to a turn angle which varies with temperature and shows a tendency to lock in to 30° , with associated bunching. The phase change across the Y layers, on the other hand, is independent of temperature and the turn angle takes the much larger value of about 50° , which is characteristic of the periodic structures formed by dilute alloys of magnetic rare earths in bulk Y. It therefore appears that the magnetic order is propagated through the Y layers by a spin-density wave, which is incipient in the unperturbed metal, and is associated with the very large susceptibility $\chi(\mathbf{Q})$ of the conduction electrons. The helical ordering in the Dy layers of the c -axis superlattice is disturbed by edge effects of the type illustrated for the Ho film in Fig. 2.11. Consequently, the ordered helical

moment falls below the saturation value of $10\mu_B$ at low temperatures, even though the total integrated magnetic scattering corresponds to the fully saturated moment. At higher temperatures, the coupling of the net ferromagnetic moment in a Dy layer to an applied magnetic field breaks the coherence of the helical structure between the layers well before the transition to the true ferromagnetic phase occurs. A b -axis superlattice, on the other hand, fails to form a coherent magnetic structure even when the Y layer is as thin as 9 planes, since the static susceptibility at $\mathbf{q} = \mathbf{0}$, which is required to propagate the ferromagnetic coupling between the basal planes of the Dy layers through the Y, is not particularly high. The Dy layers therefore form helical magnetic structures with wave-vectors in the plane of the layers, but no coherence of phase or chirality between the layers.

LINEAR RESPONSE THEORY

This chapter is devoted to a concise presentation of linear response theory, which provides a general framework for analysing the dynamical properties of a condensed-matter system close to thermal equilibrium. The dynamical processes may either be spontaneous fluctuations, or due to external perturbations, and these two kinds of phenomena are interrelated. Accounts of linear response theory may be found in many books, for example, des Cloizeaux (1968), Marshall and Lovesey (1971), and Lovesey (1986), but because of its importance in our treatment of magnetic excitations in rare earth systems and their detection by inelastic neutron scattering, the theory is presented below in adequate detail to form a basis for our later discussion.

We begin by considering the dynamical or *generalized susceptibility*, which determines the response of the system to a perturbation which varies in space and time. The *Kramers–Kronig relation* between the real and imaginary parts of this susceptibility is deduced. We derive the *Kubo formula* for the *response function* and, through its connection to the dynamic *correlation function*, which determines the results of a scattering experiment, the *fluctuation–dissipation theorem*, which relates the spontaneous fluctuations of the system to its response to an external perturbation. The energy absorption by the perturbed system is deduced from the susceptibility. The *Green function* is defined and its equation of motion established. The theory is illustrated through its application to the simple Heisenberg ferromagnet. We finally consider the calculation of the susceptibility in the *random-phase approximation*, which is the method generally used for the quantitative description of the magnetic excitations in the rare earth metals in this book.

3.1 The generalized susceptibility

A response function for a macroscopic system relates the change of an ensemble-averaged physical observable $\langle \hat{B}(t) \rangle$ to an external force $f(t)$. For example, $\hat{B}(t)$ could be the angular momentum of an ion, or the magnetization, and $f(t)$ a time-dependent applied magnetic field. As indicated by its name, the applicability of linear response theory is restricted to the regime where $\langle \hat{B}(t) \rangle$ changes linearly with the force. Hence we suppose that $f(t)$ is sufficiently weak to ensure that the response is linear. We further assume that the system is in thermal equilibrium *before*

the external force is applied.

When the system is in thermal equilibrium, it is characterized by the density operator

$$\rho_0 = \frac{1}{Z} e^{-\beta \mathcal{H}_0} \quad ; \quad Z = \text{Tr} e^{-\beta \mathcal{H}_0}, \quad (3.1.1)$$

where \mathcal{H}_0 is the (effective) Hamiltonian, Z is the (grand) partition function, and $\beta = 1/k_B T$. Since we are only interested in the linear part of the response, we may assume that the weak external disturbance $f(t)$ gives rise to a linear time-dependent perturbation in the total Hamiltonian \mathcal{H} :

$$\mathcal{H}_1 = -\hat{A} f(t) \quad ; \quad \mathcal{H} = \mathcal{H}_0 + \mathcal{H}_1, \quad (3.1.2)$$

where \hat{A} is a constant operator, as for example $\sum_i J_{zi}$, associated with the Zeeman term when $f(t) = g\mu_B H_z(t)$ (the circumflex over A or B indicates that these quantities are quantum mechanical operators). As a consequence of this perturbation, the density operator $\rho(t)$ becomes time-dependent, and so also does the ensemble average of the operator \hat{B} :

$$\langle \hat{B}(t) \rangle = \text{Tr}\{\rho(t) \hat{B}\}. \quad (3.1.3)$$

The linear relation between this quantity and the external force has the form

$$\langle \hat{B}(t) \rangle - \langle \hat{B} \rangle = \int_{-\infty}^t \phi_{BA}(t-t') f(t') dt', \quad (3.1.4)$$

where $\langle \hat{B} \rangle = \langle \hat{B}(t = -\infty) \rangle = \text{Tr}\{\rho_0 \hat{B}\}$; here $f(t)$ is assumed to vanish for $t \rightarrow -\infty$. This equation expresses the condition that the differential change of $\langle \hat{B}(t) \rangle$ is proportional to the external disturbance $f(t')$ and the duration of the perturbation $\delta t'$, and further that disturbances at different times act independently of each other. The latter condition implies that the *response function* ϕ_{BA} may only depend on the time difference $t-t'$. In (3.1.4), the response is independent of any future perturbations. This causal behaviour may be incorporated in the response function by the requirement

$$\phi_{BA}(t-t') = 0 \quad \text{for } t' > t, \quad (3.1.5)$$

in which case the integration in eqn (3.1.4) can be extended from t to $+\infty$.

Because ϕ_{BA} depends only on the time difference, eqn (3.1.4) takes a simple form if we introduce the Fourier transform

$$f(\omega) = \int_{-\infty}^{\infty} f(t) e^{i\omega t} dt, \quad (3.1.6a)$$

and the reciprocal relation

$$f(t) = \frac{1}{2\pi} \int_{-\infty}^{\infty} f(\omega) e^{-i\omega t} d\omega. \quad (3.1.6b)$$

In order to take advantage of the causality condition (3.1.5), we shall consider the Laplace transform of $\phi_{BA}(t)$ (the usual s is replaced by $-iz$):

$$\chi_{BA}(z) = \int_0^{\infty} \phi_{BA}(t) e^{izt} dt. \quad (3.1.7a)$$

$z = z_1 + iz_2$ is a complex variable and, if $\int_0^{\infty} |\phi_{BA}(t)| e^{-\epsilon t} dt$ is assumed to be finite in the limit $\epsilon \rightarrow 0^+$, the converse relation is

$$\phi_{BA}(t) = \frac{1}{2\pi} \int_{-\infty+i\epsilon}^{\infty+i\epsilon} \chi_{BA}(z) e^{-izt} dz \quad ; \quad \epsilon > 0. \quad (3.1.7b)$$

When $\phi_{BA}(t)$ satisfies the above condition and eqn (3.1.5), it can readily be shown that $\chi_{BA}(z)$ is an analytic function in the upper part of the complex z -plane ($z_2 > 0$).

In order to ensure that the evolution of the system is uniquely determined by $\rho_0 = \rho(-\infty)$ and $f(t)$, it is necessary that the external perturbation be turned on in a smooth, adiabatic way. This may be accomplished by replacing $f(t')$ in (4) by $f(t') e^{\epsilon t'}$, $\epsilon > 0$. This force vanishes in the limit $t' \rightarrow -\infty$, and any unwanted secondary effects may be removed by taking the limit $\epsilon \rightarrow 0^+$. Then, with the definition of the 'generalized' Fourier transform

$$\langle \hat{B}(\omega) \rangle = \lim_{\epsilon \rightarrow 0^+} \int_{-\infty}^{\infty} (\langle \hat{B}(t) \rangle - \langle \hat{B} \rangle) e^{i\omega t} e^{-\epsilon t} dt, \quad (3.1.8)$$

eqn (3.1.4) is transformed into

$$\langle \hat{B}(\omega) \rangle = \chi_{BA}(\omega) f(\omega), \quad (3.1.9a)$$

where $\chi_{BA}(\omega)$ is the boundary value of the analytic function $\chi_{BA}(z)$ on the real axis:

$$\chi_{BA}(\omega) = \lim_{\epsilon \rightarrow 0^+} \chi_{BA}(z = \omega + i\epsilon). \quad (3.1.9b)$$

$\chi_{BA}(\omega)$ is called the frequency-dependent or *generalized susceptibility* and is the Fourier transform, as defined by (3.1.8), of the response function $\phi_{BA}(t)$.

The mathematical restrictions (3.1.5) and (3.1.7) on $\phi_{BA}(t)$ have the direct physical significance that the system is respectively causal and stable against a small perturbation. The two conditions ensure that

$\chi_{BA}(z)$ has no poles in the upper half-plane. If this were not the case, the response $\langle \hat{B}(t) \rangle$ to a small disturbance would diverge exponentially as a function of time.

The absence of poles in $\chi_{BA}(z)$, when z_2 is positive, leads to a relation between the real and imaginary part of $\chi_{BA}(\omega)$, called the *Kramers–Kronig dispersion relation*. If $\chi_{BA}(z)$ has no poles within the contour \mathcal{C} , then it may be expressed in terms of the Cauchy integral along \mathcal{C} by the identity

$$\chi_{BA}(z) = \frac{1}{2\pi i} \int_{\mathcal{C}} \frac{\chi_{BA}(z')}{z' - z} dz'.$$

The contour \mathcal{C} is chosen to be the half-circle, in the upper half-plane, centred at the origin and bounded below by the line parallel to the z_1 -axis through $z_2 = \epsilon'$, and z is a point lying within this contour. Since $\phi_{BA}(t)$ is a bounded function in the domain $\epsilon' > 0$, then $\chi_{BA}(z')$ must go to zero as $|z'| \rightarrow \infty$, whenever $z'_2 > 0$. This implies that the part of the contour integral along the half-circle must vanish when its radius goes to infinity, and hence

$$\chi_{BA}(z) = \lim_{\epsilon' \rightarrow 0^+} \frac{1}{2\pi i} \int_{-\infty + i\epsilon'}^{\infty + i\epsilon'} \frac{\chi_{BA}(\omega' + i\epsilon')}{\omega' + i\epsilon' - z} d(\omega' + i\epsilon').$$

Introducing $z = \omega + i\epsilon$ and applying ‘Dirac’s formula’:

$$\lim_{\epsilon \rightarrow 0^+} \frac{1}{\omega' - \omega - i\epsilon} = \mathcal{P} \frac{1}{\omega' - \omega} + i\pi \delta(\omega' - \omega),$$

in taking the limit $\epsilon \rightarrow 0^+$, we finally obtain the Kramers–Kronig relation (\mathcal{P} denotes the principal part of the integral):

$$\chi_{BA}(\omega) = \frac{1}{i\pi} \mathcal{P} \int_{-\infty}^{\infty} \frac{\chi_{BA}(\omega')}{\omega' - \omega} d\omega', \quad (3.1.10)$$

which relates the real and imaginary components of $\chi(\omega)$.

3.2 Response functions

In this section, we shall deduce an expression for the response function $\phi_{BA}(t)$, in terms of the operators \hat{B} and \hat{A} and the unperturbed Hamiltonian \mathcal{H}_0 . In the preceding section, we assumed implicitly the use of the Schrödinger picture. If instead we adopt the Heisenberg picture, the wave functions are independent of time, while the operators become time-dependent. In the Heisenberg picture, the operators are

$$\hat{B}(t) = e^{i\mathcal{H}t/\hbar} \hat{B} e^{-i\mathcal{H}t/\hbar}, \quad (3.2.1)$$

corresponding to the equation of motion

$$\frac{d}{dt}\hat{B}(t) = \frac{i}{\hbar}[\mathcal{H}, \hat{B}(t)] \quad (3.2.2)$$

(assuming that \hat{B} does not depend explicitly on time). Because the wave functions are independent of time, in the Heisenberg picture, the corresponding density operator ρ_H must also be. Hence we may write (3.1.3)

$$\langle \hat{B}(t) \rangle = \text{Tr}\{\rho(t)\hat{B}\} = \text{Tr}\{\rho_H \hat{B}(t)\}. \quad (3.2.3)$$

Introducing (3.2.1) into this expression, and recalling that the trace is invariant under a cyclic permutation of the operators within it, we obtain

$$\rho(t) = e^{-i\mathcal{H}t/\hbar} \rho_H e^{i\mathcal{H}t/\hbar},$$

or

$$\frac{d}{dt}\rho(t) = -\frac{i}{\hbar}[\mathcal{H}, \rho(t)]. \quad (3.2.4)$$

The equation of motion derived for the density operator, in the Schrödinger picture, is similar to the Heisenberg equation of motion above, except for the change of sign in front of the commutator.

The density operator may be written as the sum of two terms:

$$\rho(t) = \rho_0 + \rho_1(t) \quad \text{with} \quad [\mathcal{H}_0, \rho_0] = 0, \quad (3.2.5)$$

where ρ_0 is the density operator (3.1.1) of the thermal-equilibrium state which, by definition, must commute with \mathcal{H}_0 , and the additional contribution due to $f(t)$ is assumed to vanish at $t \rightarrow -\infty$. In order to derive $\rho_1(t)$ to leading order in $f(t)$, we shall first consider the following density operator, in the *interaction picture*,

$$\rho_I(t) \equiv e^{i\mathcal{H}_0 t/\hbar} \rho(t) e^{-i\mathcal{H}_0 t/\hbar}, \quad (3.2.6)$$

for which

$$\begin{aligned} \frac{d}{dt}\rho_I(t) &= e^{i\mathcal{H}_0 t/\hbar} \left\{ \frac{i}{\hbar}[\mathcal{H}_0, \rho(t)] + \frac{d}{dt}\rho(t) \right\} e^{-i\mathcal{H}_0 t/\hbar} \\ &= -\frac{i}{\hbar} e^{i\mathcal{H}_0 t/\hbar} [\mathcal{H}_1, \rho(t)] e^{-i\mathcal{H}_0 t/\hbar}. \end{aligned}$$

Because \mathcal{H}_1 is linear in $f(t)$, we may replace $\rho(t)$ by ρ_0 in calculating the linear response, giving

$$\frac{d}{dt}\rho_I(t) \simeq -\frac{i}{\hbar} [e^{i\mathcal{H}_0 t/\hbar} \mathcal{H}_1 e^{-i\mathcal{H}_0 t/\hbar}, \rho_0] = \frac{i}{\hbar} [\hat{A}_0(t), \rho_0] f(t),$$

using (3.2.5) and defining

$$\hat{A}_0(t) = e^{i\mathcal{H}_0 t/\hbar} \hat{A} e^{-i\mathcal{H}_0 t/\hbar}.$$

According to (3.2.6), taking into account the boundary condition, the time-dependent density operator is

$$\begin{aligned} \rho(t) &= e^{-i\mathcal{H}_0 t/\hbar} \left(\int_{-\infty}^t \frac{d}{dt'} \rho_I(t') dt' + \rho_0 \right) e^{i\mathcal{H}_0 t/\hbar} \\ &= \rho_0 + \frac{i}{\hbar} \int_{-\infty}^t [\hat{A}_0(t' - t), \rho_0] f(t') dt', \end{aligned} \quad (3.2.7)$$

to first order in the external perturbations. This determines the time dependence of, for example, \hat{B} as

$$\begin{aligned} \langle \hat{B}(t) \rangle - \langle \hat{B} \rangle &= \text{Tr} \{ (\rho(t) - \rho_0) \hat{B} \} \\ &= \frac{i}{\hbar} \text{Tr} \left\{ \int_{-\infty}^t [\hat{A}_0(t' - t), \rho_0] \hat{B} f(t') dt' \right\} \end{aligned}$$

and, utilizing the invariance of the trace under cyclic permutations, we obtain, to leading order,

$$\begin{aligned} \langle \hat{B}(t) \rangle - \langle \hat{B} \rangle &= \frac{i}{\hbar} \int_{-\infty}^t \text{Tr} \{ \rho_0 [\hat{B}, \hat{A}_0(t' - t)] \} f(t') dt' \\ &= \frac{i}{\hbar} \int_{-\infty}^t \langle [\hat{B}_0(t), \hat{A}_0(t')] \rangle_0 f(t') dt'. \end{aligned} \quad (3.2.8)$$

A comparison of this result with the definition (3.1.4) of the response function then gives

$$\phi_{BA}(t - t') = \frac{i}{\hbar} \theta(t - t') \langle [\hat{B}(t), \hat{A}(t')] \rangle, \quad (3.2.9)$$

where the unit step function, $\theta(t) = 0$ or 1 when $t < 0$ or $t > 0$ respectively, is introduced in order to ensure that ϕ_{BA} satisfies the causality principle (3.1.5). In this final result, and below, we suppress the index 0, but we stress that both the variations with time and the ensemble average are thermal-equilibrium values determined by \mathcal{H}_0 , and are unaffected by the external disturbances. This expression in terms of microscopic quantities, is called *the Kubo formula* for the response function (Kubo 1957, 1966).

The expression (3.2.9) is the starting point for introducing a number of useful functions:

$$K_{BA}(t) = \frac{i}{\hbar} \langle [\hat{B}(t), \hat{A}] \rangle = \frac{i}{\hbar} \langle [\hat{B}, \hat{A}(-t)] \rangle \quad (3.2.10)$$

is also called a response function. \hat{A} is a shorthand notation for $\hat{A}(t=0)$. The inverse response function $K_{AB}(t)$, which determines $\langle \hat{A}(t) \rangle$ caused by the perturbation $\mathcal{H}_1 = -f(t)\hat{B}$, is

$$K_{AB}(t) = \frac{i}{\hbar} \langle [\hat{A}(t), \hat{B}] \rangle = -K_{BA}(-t),$$

and $K_{BA}(t)$ can be expressed in terms of the corresponding causal response functions as

$$K_{BA}(t) = \begin{cases} \phi_{BA}(t) & \text{for } t > 0 \\ -\phi_{AB}(-t) & \text{for } t < 0. \end{cases}$$

The susceptibility is divided into two terms, the reactive part

$$\chi'_{BA}(z) = \chi'_{AB}(-z^*) \equiv \frac{1}{2} \{ \chi_{BA}(z) + \chi_{AB}(-z^*) \}, \quad (3.2.11a)$$

and the absorptive part

$$\chi''_{BA}(z) = -\chi''_{AB}(-z^*) \equiv \frac{1}{2i} \{ \chi_{BA}(z) - \chi_{AB}(-z^*) \}, \quad (3.2.11b)$$

so that

$$\chi_{BA}(z) = \chi'_{BA}(z) + i\chi''_{BA}(z) \quad (3.2.11c)$$

and, according to the Kramers–Kronig relation (3.1.10),

$$\chi'_{BA}(\omega) = \frac{1}{\pi} \mathcal{P} \int_{-\infty}^{\infty} \frac{\chi''_{BA}(\omega')}{\omega' - \omega} d\omega' \quad ; \quad \chi''_{BA}(\omega) = -\frac{1}{\pi} \mathcal{P} \int_{-\infty}^{\infty} \frac{\chi'_{BA}(\omega')}{\omega' - \omega} d\omega'. \quad (3.2.11d)$$

In these equations, $\chi_{AB}(-\omega)$ is the boundary value obtained by taking $z = \omega + i\epsilon$, i.e. as $\lim_{\epsilon \rightarrow 0^+} \chi_{AB}(-z^* = -\omega + i\epsilon)$, corresponding to the condition that $\chi_{AB}(-z^*)$, like $\chi_{AB}(z)$, is analytic in the upper half-plane. The appropriate Laplace transform of $K_{BA}(t)$ with this property is

$$\begin{aligned} K_{BA}(z) &= \int_{-\infty}^{\infty} K_{BA}(t) e^{i(z_1 t + i z_2 |t|)} dt \\ &= \int_0^{\infty} \phi_{BA}(t) e^{izt} dt - \int_0^{\infty} \phi_{AB}(t) e^{-iz^* t} dt. \end{aligned}$$

Hence

$$K_{BA}(z) = 2i \chi''_{BA}(z). \quad (3.2.12)$$

Next we introduce the dynamic *correlation function*, sometimes referred to as the *scattering function*. It is defined as follows:

$$S_{BA}(t) \equiv \langle \hat{B}(t) \hat{A} \rangle - \langle \hat{B} \rangle \langle \hat{A} \rangle = \langle \hat{B} \hat{A}(-t) \rangle - \langle \hat{B} \rangle \langle \hat{A} \rangle, \quad (3.2.13)$$

and is related to the response function introduced earlier by

$$K_{BA}(t) = \frac{i}{\hbar} \{S_{BA}(t) - S_{AB}(-t)\}. \quad (3.2.14)$$

The different response functions obey a number of symmetry relations, due to the invariance of the trace under a cyclic permutation of the operators. To derive the first, we recall that the Hermitian conjugate of an operator is defined by

$$\langle \alpha | \hat{B} | \alpha' \rangle^* = \langle \alpha' | \hat{B}^\dagger | \alpha \rangle.$$

If we assume that a certain set of state vectors $|\alpha\rangle$ constitutes a diagonal representation, i.e. $\mathcal{H}_0|\alpha\rangle = E_\alpha|\alpha\rangle$, then it is straightforward to show that

$$\langle \hat{B}(t) \hat{A} \rangle^* = \langle \hat{A}^\dagger(-t) \hat{B}^\dagger \rangle,$$

leading to the symmetry relations

$$K_{BA}^*(t) = K_{B^\dagger A^\dagger}(t)$$

and

$$\chi_{BA}^*(z) = \chi_{B^\dagger A^\dagger}(-z^*). \quad (3.2.15)$$

Another important relation is derived as follows:

$$\begin{aligned} \langle \hat{B}(t) \hat{A} \rangle &= \frac{1}{Z} \text{Tr} \left\{ e^{-\beta \mathcal{H}_0} e^{i \mathcal{H}_0 t / \hbar} \hat{B} e^{-i \mathcal{H}_0 t / \hbar} \hat{A} \right\} \\ &= \frac{1}{Z} \text{Tr} \left\{ e^{i \mathcal{H}_0 (t + i \beta \hbar) / \hbar} \hat{B} e^{-i \mathcal{H}_0 (t + i \beta \hbar) / \hbar} e^{-\beta \mathcal{H}_0} \hat{A} \right\} \\ &= \frac{1}{Z} \text{Tr} \left\{ e^{-\beta \mathcal{H}_0} \hat{A} \hat{B}(t + i \beta \hbar) \right\} = \langle \hat{A} \hat{B}(t + i \beta \hbar) \rangle, \end{aligned}$$

implying that

$$S_{BA}(t) = S_{AB}(-t - i \beta \hbar). \quad (3.2.16)$$

In any realistic system which, rather than being isolated, is in contact with a thermal bath at temperature T , the correlation function $S_{BA}(t)$ vanishes in the limits $t \rightarrow \pm\infty$, corresponding to the condition $\langle \hat{B}(t = \pm\infty) \hat{A} \rangle = \langle \hat{B} \rangle \langle \hat{A} \rangle$. If we further assume that $S_{BA}(t)$ is an analytic function in the interval $|t_2| \leq \beta$ of the complex t -plane, then the Fourier transform of (3.2.16) is

$$S_{BA}(\omega) = e^{\beta \hbar \omega} S_{AB}(-\omega), \quad (3.2.17)$$

which is usually referred to as being the *condition of detailed balance*. Combining this condition with the expressions (3.2.12) and (3.2.14), we

get the following important relation between the correlation function and the susceptibility:

$$S_{BA}(\omega) = 2\hbar \frac{1}{1 - e^{-\beta\hbar\omega}} \chi''_{BA}(\omega), \quad (3.2.18)$$

which is called the *fluctuation-dissipation theorem*. This relation expresses explicitly the close connection between the spontaneous fluctuations in the system, as described by the correlation function, and the response of the system to external perturbations, as determined by the susceptibility.

The calculations above do not depend on the starting assumption that \hat{B} (or \hat{A}) is a physical observable, i.e. that \hat{B} should be equal to \hat{B}^\dagger . This has the advantage that, if the Kubo formula (3.2.9) is taken to be the starting point instead of eqn (3.1.4), the formalism applies more generally.

3.3 Energy absorption and the Green function

In this section, we first present a calculation of the energy transferred to the system by the external perturbation $\mathcal{H}_1 = -\hat{A}f(t)$ in (3.1.2), incidentally justifying the names of the two susceptibility components in (3.2.11). The energy absorption can be expressed in terms of $\chi_{AA}(\omega)$ and, without loss of generality, \hat{A} may here be assumed to be a Hermitian operator, so that $\hat{A} = \hat{A}^\dagger$. In this case, $f(t)$ is real, and considering a harmonic variation

$$f(t) = f_0 \cos(\omega_0 t) = \frac{1}{2} f_0 (e^{i\omega_0 t} + e^{-i\omega_0 t}) \quad \text{with} \quad f_0^* = f_0,$$

then

$$f(\omega) = \pi f_0 \{\delta(\omega - \omega_0) + \delta(\omega + \omega_0)\}, \quad \text{as} \quad \int_{-\infty}^{\infty} e^{i(\omega - \omega_0)t} dt = 2\pi \delta(\omega - \omega_0),$$

and we have

$$\langle \hat{A}(t) \rangle - \langle \hat{A} \rangle = \frac{1}{2} f_0 \{ \chi_{AA}(-\omega_0) e^{i\omega_0 t} + \chi_{AA}(\omega_0) e^{-i\omega_0 t} \}.$$

The introduction of $\hat{A} = \hat{B} = \hat{A}^\dagger$ in (3.2.15), and in the definition (3.2.11), yields

$$\begin{aligned} \chi'_{AA}(\omega)^* &= \chi'_{AA}(\omega) = \chi'_{AA}(-\omega) \\ \chi''_{AA}(\omega)^* &= \chi''_{AA}(\omega) = -\chi''_{AA}(-\omega), \end{aligned} \quad (3.3.1)$$

and these symmetry relations allow us to write

$$\langle \hat{A}(t) \rangle - \langle \hat{A} \rangle = f_0 \{ \chi'_{AA}(\omega_0) \cos(\omega_0 t) + \chi''_{AA}(\omega_0) \sin(\omega_0 t) \}.$$

The part of the response which is in phase with the external force is proportional to $\chi'_{AA}(\omega_0)$, which is therefore called the reactive component. The rate of energy absorption due to the field is

$$Q = \frac{d}{dt} \langle \mathcal{H} \rangle = \langle \partial \mathcal{H} / \partial t \rangle = - \langle \hat{A}(t) \rangle \partial f / \partial t,$$

which shows that the *mean* dissipation rate is determined by the out-of-phase response proportional to $\chi''_{AA}(\omega)$:

$$\bar{Q} = \frac{1}{2} f_0^2 \omega_0 \chi''_{AA}(\omega_0) \quad (3.3.2)$$

and $\chi''_{AA}(\omega)$ is therefore called the absorptive part of the susceptibility.

If the eigenvalues E_α and the corresponding eigenstates $|\alpha\rangle$ for the Hamiltonian $\mathcal{H}(= \mathcal{H}_0)$ are known, it is possible to derive an explicit expression for $\chi_{BA}(\omega)$. According to the definition (3.2.10),

$$\begin{aligned} K_{BA}(t) &= \frac{i}{\hbar} \frac{1}{Z} \text{Tr} \left\{ e^{-\beta \mathcal{H}} \left[e^{i\mathcal{H}t/\hbar} \hat{B} e^{-i\mathcal{H}t/\hbar}, \hat{A} \right] \right\} = \\ &= \frac{i}{\hbar} \frac{1}{Z} \sum_{\alpha\alpha'} e^{-\beta E_\alpha} \left\{ e^{iE_\alpha t/\hbar} \langle \alpha | \hat{B} | \alpha' \rangle e^{-iE_{\alpha'} t/\hbar} \langle \alpha' | \hat{A} | \alpha \rangle \right. \\ &\quad \left. - \langle \alpha | \hat{A} | \alpha' \rangle e^{iE_{\alpha'} t/\hbar} \langle \alpha' | \hat{B} | \alpha \rangle e^{-iE_\alpha t/\hbar} \right\}. \end{aligned}$$

Interchanging α and α' in the last term, and introducing the population factor

$$n_\alpha = \frac{1}{Z} e^{-\beta E_\alpha} \quad ; \quad Z = \sum_{\alpha'} e^{-\beta E_{\alpha'}}, \quad (3.3.3a)$$

we get

$$K_{BA}(t) = \frac{i}{\hbar} \sum_{\alpha\alpha'} \langle \alpha | \hat{B} | \alpha' \rangle \langle \alpha' | \hat{A} | \alpha \rangle (n_\alpha - n_{\alpha'}) e^{i(E_\alpha - E_{\alpha'})t/\hbar}, \quad (3.3.3b)$$

and hence

$$\begin{aligned} \chi_{BA}(\omega) &= \lim_{\epsilon \rightarrow 0^+} \int_0^\infty K_{BA}(t) e^{i(w+i\epsilon)t} dt \\ &= \lim_{\epsilon \rightarrow 0^+} \sum_{\alpha\alpha'} \frac{\langle \alpha | \hat{B} | \alpha' \rangle \langle \alpha' | \hat{A} | \alpha \rangle}{E_{\alpha'} - E_\alpha - \hbar\omega - i\hbar\epsilon} (n_\alpha - n_{\alpha'}), \end{aligned} \quad (3.3.4a)$$

or equivalently

$$\begin{aligned}\chi_{AB}(-\omega) &= \lim_{\epsilon \rightarrow 0^+} \chi_{AB}(-\omega + i\epsilon) \\ &= \lim_{\epsilon \rightarrow 0^+} \sum_{\alpha\alpha'} \frac{\langle \alpha | \hat{A} | \alpha' \rangle \langle \alpha' | \hat{B} | \alpha \rangle}{E_{\alpha'} - E_{\alpha} + \hbar\omega - i\hbar\epsilon} (n_{\alpha} - n_{\alpha'}). \end{aligned} \quad (3.3.4b)$$

An interchange of α and α' shows this expression to be the same as (3.3.4a), with ϵ replaced by $-\epsilon$. The application of Dirac's formula then yields the absorptive part of the susceptibility (3.2.11b) as

$$\chi''_{BA}(\omega) = \pi \sum_{\alpha\alpha'} \langle \alpha | \hat{B} | \alpha' \rangle \langle \alpha' | \hat{A} | \alpha \rangle (n_{\alpha} - n_{\alpha'}) \delta(\hbar\omega - (E_{\alpha'} - E_{\alpha})) \quad (3.3.5)$$

(equal to $K_{BA}(\omega)/2i$ in accordance with (3.2.12)), whereas the reactive part (3.2.11a) is

$$\chi'_{BA}(\omega) = \sum_{\alpha\alpha'}^{E_{\alpha} \neq E_{\alpha'}} \frac{\langle \alpha | \hat{B} | \alpha' \rangle \langle \alpha' | \hat{A} | \alpha \rangle}{E_{\alpha'} - E_{\alpha} - \hbar\omega} (n_{\alpha} - n_{\alpha'}) + \chi'_{BA}(e\ell) \delta_{\omega 0}, \quad (3.3.6a)$$

where

$$\delta_{\omega 0} \equiv \lim_{\epsilon \rightarrow 0^+} \frac{i\epsilon}{\omega + i\epsilon} = \begin{cases} 1 & \text{if } \omega = 0 \\ 0 & \text{if } \omega \neq 0, \end{cases}$$

and the elastic term $\chi'_{BA}(e\ell)$, which only contributes in the static limit $\omega = 0$, is

$$\chi'_{BA}(e\ell) = \beta \left\{ \sum_{\alpha\alpha'}^{E_{\alpha} = E_{\alpha'}} \langle \alpha | \hat{B} | \alpha' \rangle \langle \alpha' | \hat{A} | \alpha \rangle n_{\alpha} - \langle \hat{B} \rangle \langle \hat{A} \rangle \right\}. \quad (3.3.6b)$$

We remark that $\chi'_{BA}(\omega)$ and $\chi''_{BA}(\omega)$ are often referred to respectively as the real and the imaginary part of $\chi_{BA}(\omega)$. This terminology is not valid in general, but only if the matrix-element products are real, as they are if, for instance, $\hat{B} = \hat{A}^{\dagger}$. The presence of the elastic term in the reactive response requires some additional consideration. There are no elastic contributions to $K_{BA}(t)$, nor hence to $\chi''_{BA}(\omega)$, because $n_{\alpha} - n_{\alpha'} \equiv 0$ if $E_{\alpha} = E_{\alpha'}$. Nevertheless, the appearance of an extra contribution at $\omega = 0$, not obtainable directly from $K_{BA}(t)$, is possible because the energy denominator in (3.3.4) vanishes in the limit $|\omega + i\epsilon| \rightarrow 0$, when $E_{\alpha} = E_{\alpha'}$. In order to derive this contribution, we consider the equal-time correlation function

$$\begin{aligned}S_{BA}(t=0) &= \langle (\hat{B} - \langle \hat{B} \rangle) (\hat{A} - \langle \hat{A} \rangle) \rangle \\ &= \sum_{\alpha\alpha'} \langle \alpha | \hat{B} | \alpha' \rangle \langle \alpha' | \hat{A} | \alpha \rangle n_{\alpha} - \langle \hat{B} \rangle \langle \hat{A} \rangle \end{aligned} \quad (3.3.7a)$$

which, according to the fluctuation–dissipation theorem (3.2.18), should be

$$S_{BA}(t=0) = \frac{1}{2\pi} \int_{-\infty}^{\infty} S_{BA}(\omega) d\omega = \frac{1}{\pi} \int_{-\infty}^{\infty} \frac{1}{1 - e^{-\beta\hbar\omega}} \chi''_{BA}(\omega) d(\hbar\omega). \quad (3.3.7b)$$

Introducing (3.3.5), the integration is straightforward, except in a narrow interval around $\omega = 0$, and we obtain

$$S_{BA}(t=0) = \sum_{\alpha\alpha'}^{E_\alpha \neq E_{\alpha'}} \langle \alpha | \hat{B} | \alpha' \rangle \langle \alpha' | \hat{A} | \alpha \rangle n_\alpha + \lim_{\gamma \rightarrow 0^+} \int_{-\gamma}^{\gamma} \frac{\chi''_{BA}(\omega)}{\pi\beta\omega} d\omega$$

after replacing $1 - e^{-\beta\hbar\omega}$ with $\beta\hbar\omega$ in the limit $\omega \rightarrow 0$. A comparison of this expression for $S_{BA}(t=0)$ with (3.3.7a) shows that the last integral has a definite value:

$$\lim_{\gamma \rightarrow 0^+} \int_{-\gamma}^{\gamma} \frac{\chi''_{BA}(\omega)}{\pi\beta\omega} d\omega = \sum_{\alpha\alpha'}^{E_\alpha = E_{\alpha'}} \langle \alpha | \hat{B} | \alpha' \rangle \langle \alpha' | \hat{A} | \alpha \rangle n_\alpha - \langle \hat{B} \rangle \langle \hat{A} \rangle. \quad (3.3.8)$$

The use of the Kramers–Kronig relation (3.1.10), in the form of (3.2.11d), for calculating $\chi'_{BA}(0)$ then gives rise to the extra contribution

$$\chi'_{BA}(el) = \lim_{\gamma \rightarrow 0^+} \frac{1}{\pi} \int_{-\gamma}^{\gamma} \frac{\chi''_{BA}(\omega)}{\omega} d\omega \quad (3.3.9)$$

to the reactive susceptibility at zero frequency, as anticipated in (3.3.6b). The zero-frequency result, $\chi_{BA}(0) = \chi'_{BA}(0)$, as given by (3.3.6), is the same as the conventional isothermal susceptibility (2.1.18) for the magnetic moments, where the elastic and inelastic contributions are respectively the Curie and the Van Vleck terms. This elastic contribution is discussed in more detail by, for instance, Suzuki (1971).

The results (3.3.4–6) show that, if the eigenstates of the Hamiltonian are discrete and the matrix-elements of the operators \hat{B} and \hat{A} between these states are well-defined, the poles of $\chi_{BA}(z)$ all lie on the real axis. This has the consequence that the absorptive part $\chi''_{BA}(\omega)$ (3.3.5) becomes a sum of δ -functions, which are only non-zero when $\hbar\omega$ is equal to the *excitation* energies $E_{\alpha'} - E_\alpha$. In such a system, no spontaneous transitions occur. In a real macroscopic system, the distribution of states is continuous, and only the ground state may be considered as a well-defined discrete state. At non-zero temperatures, the parameters of the system are subject to fluctuations in space and time. The introduction of a non-zero probability for a spontaneous transition between the ‘levels’ α and α' can be included in a phenomenological way by replacing the energy difference $E_{\alpha'} - E_\alpha$ in (3.3.4) by $(E_{\alpha'} - E_\alpha) - i\Gamma_{\alpha'\alpha}(\omega)$,

where the parameters, including the energy difference, usually depend on ω . According to the general stability and causality requirements, the poles of $\chi_{BA}(z)$ at $z = z_{\alpha'\alpha} = (E_{\alpha'} - E_{\alpha}) - i\Gamma_{\alpha'\alpha}$ must lie in the lower half-plane, implying that $\Gamma_{\alpha'\alpha}$ has to be positive (or zero). In the case where $|E_{\alpha'} - E_{\alpha}| \gg \Gamma_{\alpha'\alpha}$, the ω -dependence of these parameters is unimportant, and the δ -function in (3.3.5) is effectively replaced by a *Lorentzian*:

$$\begin{aligned} \chi''_{BA}(\omega) \simeq & \sum_{\alpha\alpha'} \frac{\langle \alpha | \hat{B} | \alpha' \rangle \langle \alpha' | \hat{A} | \alpha \rangle}{(E_{\alpha'} - E_{\alpha} - \hbar\omega)^2 + \Gamma_{\alpha'\alpha}^2} \Gamma_{\alpha'\alpha} (n_{\alpha} - n_{\alpha'}) \\ & + \frac{\hbar\omega\Gamma_0}{(\hbar\omega)^2 + \Gamma_0^2} \chi'_{BA}(el), \end{aligned} \quad (3.3.10)$$

with a *linewidth*, or more precisely FWHM (full width at half maximum), of $2\Gamma_{\alpha'\alpha}$. In (3.3.10), we have added the *quasi-elastic* response due to a pole at $z = -i\Gamma_0$, which replaces the one at $z = 0$. The corresponding reactive part of the susceptibility is

$$\begin{aligned} \chi'_{BA}(\omega) \simeq & \sum_{\alpha\alpha'} \frac{\langle \alpha | \hat{B} | \alpha' \rangle \langle \alpha' | \hat{A} | \alpha \rangle}{(E_{\alpha'} - E_{\alpha} - \hbar\omega)^2 + \Gamma_{\alpha'\alpha}^2} (E_{\alpha'} - E_{\alpha} - \hbar\omega) (n_{\alpha} - n_{\alpha'}) \\ & + \frac{\Gamma_0^2}{(\hbar\omega)^2 + \Gamma_0^2} \chi'_{BA}(el). \end{aligned} \quad (3.3.11)$$

The non-zero linewidth corresponds to an exponential decay of the oscillations in the time dependence of, for instance, the correlation function:

$$S_{BA}(t) \sim e^{-iz_{\alpha'\alpha}t/\hbar} = e^{-i(E_{\alpha'} - E_{\alpha})t/\hbar} e^{-\Gamma_{\alpha'\alpha}t/\hbar}.$$

The absorption observed in a *resonance* experiment is proportional to $\chi''_{AA}(\omega)$. A peak in the absorption spectrum is interpreted as an *elementary* or *quasi-particle excitation*, or as a *normal mode* of the dynamic variable \hat{A} , with a *lifetime* $\tau = \hbar/\Gamma_{\alpha'\alpha}$. A pole at $z = -i\Gamma_0$ is said to represent a *diffusive mode*. Such a pole is of particular importance for those transport coefficients determined by the low-frequency or hydrodynamic properties of the system. Kubo (1957, 1966) gives a detailed discussion of this subject. As we shall see later, the differential scattering cross-section of, for example, neutrons in the Born-approximation is proportional to a correlation function, and hence to $\chi''(\omega)$. This implies that the presence of elementary excitations in the system leads to peaks in the intensity of scattered neutrons as a function of the energy transfer. Finally, the dynamic correlation-functions are related directly to various thermodynamic second-derivatives, such as the compressibility and the

magnetic susceptibility, and thereby indirectly to the corresponding first-derivatives, like the specific heat and the magnetization. Consequently, most physical properties of a macroscopic system near equilibrium may be described in terms of the correlation functions.

As a supplement to the response function $\phi_{BA}(t-t')$, we now introduce the *Green function*, defined as

$$\begin{aligned} G_{BA}(t-t') &\equiv \langle\langle \hat{B}(t); \hat{A}(t') \rangle\rangle \\ &\equiv -\frac{i}{\hbar} \theta(t-t') \langle [\hat{B}(t), \hat{A}(t')] \rangle = -\phi_{BA}(t-t'). \end{aligned} \quad (3.3.12)$$

This Green function is often referred to as the *double-time* or the *retarded* Green function (Zubarev 1960), and it is simply our previous response function, but with the opposite sign. Introducing the Laplace transform $G_{BA}(z)$ according to (3.1.7), we find, as before, that the corresponding Fourier transform is

$$\begin{aligned} G_{BA}(\omega) &\equiv \langle\langle \hat{B}; \hat{A} \rangle\rangle_{\omega} = \lim_{\epsilon \rightarrow 0^+} G_{BA}(z = \omega + i\epsilon) \\ &= \lim_{\epsilon \rightarrow 0^+} \int_{-\infty(0)}^{\infty} G_{BA}(t) e^{i(\omega+i\epsilon)t} dt = -\chi_{BA}(\omega). \end{aligned} \quad (3.3.13)$$

We note that, if \hat{A} and \hat{B} are dimensionless operators, then $G_{BA}(\omega)$ or $\chi_{BA}(\omega)$ have the dimensions of inverse energy.

If $t' = 0$, the derivative of the Green function with respect to t is

$$\begin{aligned} \frac{d}{dt} G_{BA}(t) &= -\frac{i}{\hbar} \left(\delta(t) \langle [\hat{B}(t), \hat{A}] \rangle + \theta(t) \langle [d\hat{B}(t)/dt, \hat{A}] \rangle \right) \\ &= -\frac{i}{\hbar} \left(\delta(t) \langle [\hat{B}, \hat{A}] \rangle - \frac{i}{\hbar} \theta(t) \langle [[\hat{B}(t), \mathcal{H}], \hat{A}] \rangle \right). \end{aligned}$$

A Fourier transformation of this expression then leads to the *equation of motion* for the Green function:

$$\hbar\omega \langle\langle \hat{B}; \hat{A} \rangle\rangle_{\omega} - \langle\langle [\hat{B}, \mathcal{H}]; \hat{A} \rangle\rangle_{\omega} = \langle [\hat{B}, \hat{A}] \rangle. \quad (3.3.14a)$$

The suffix ω indicates the Fourier transforms (3.3.13), and $\hbar\omega$ is shorthand for $\hbar(\omega + i\epsilon)$ with $\epsilon \rightarrow 0^+$. In many applications, \hat{A} and \hat{B} are the same (Hermitian) operator, in which case the r.h.s. of (3.3.14a) vanishes and one may proceed to the second derivative. With the condition that $\langle\langle [[[\hat{A}(t), \mathcal{H}], \mathcal{H}], \hat{A}] \rangle\rangle$ is $-\langle\langle [[[\hat{A}(t), \mathcal{H}], [\hat{A}, \mathcal{H}]]] \rangle\rangle$, the equation of motion for the Green function $\langle\langle [\hat{A}, \mathcal{H}]; \hat{A} \rangle\rangle_{\omega}$ leads to

$$(\hbar\omega)^2 \langle\langle \hat{A}; \hat{A} \rangle\rangle_{\omega} + \langle\langle [\hat{A}, \mathcal{H}]; [\hat{A}, \mathcal{H}] \rangle\rangle_{\omega} = \langle\langle [[\hat{A}, \mathcal{H}], \hat{A}] \rangle\rangle. \quad (3.3.14b)$$

The pair of equations (3.3.14) will be the starting point for our application of linear response theory.

According to the definition (3.2.10) of $K_{BA}(t)$, and eqn (3.2.12),

$$K_{BA}(\omega) = 2i\chi''_{BA}(\omega) = -2iG''_{BA}(\omega).$$

We may write

$$\frac{i}{\pi} \int_{-\infty}^{\infty} \chi''_{BA}(\omega) e^{-i\omega t} d\omega = \frac{i}{\hbar} \langle [\hat{B}(t), \hat{A}] \rangle \quad (3.3.15)$$

and, setting $t = 0$, we obtain the following *sum rule*:

$$\frac{\hbar}{\pi} \int_{-\infty}^{\infty} \chi''_{BA}(\omega) d\omega = \langle [\hat{B}, \hat{A}] \rangle, \quad (3.3.16)$$

which may be compared with the value obtained for the equal-time correlation function $\langle \hat{B} \hat{A} \rangle - \langle \hat{B} \rangle \langle \hat{A} \rangle$, (3.3.7). The Green function in (3.3.14a) must satisfy this sum rule, and we note that the thermal averages in (3.3.14a) and (3.3.16) are the same. Equation (3.3.16) is only the first of a whole series of sum rules.

The n th time-derivative of $\hat{B}(t)$ may be written

$$\frac{d^n}{dt^n} \hat{B}(t) = \left(\frac{i}{\hbar} \right)^n \mathcal{L}^n \hat{B}(t) \quad \text{with} \quad \mathcal{L} \hat{B}(t) \equiv [\mathcal{H}, \hat{B}(t)].$$

Taking the n th derivative on both sides of eqn (3.3.15), we get

$$\frac{i}{\pi} \int_{-\infty}^{\infty} (-i\omega)^n \chi''_{BA}(\omega) e^{-i\omega t} d\omega = \left(\frac{i}{\hbar} \right)^{n+1} \langle [\mathcal{L}^n \hat{B}(t), \hat{A}] \rangle.$$

Next we introduce the normalized *spectral weight function*

$$F_{BA}(\omega) = \frac{1}{\chi'_{BA}(0)} \frac{1}{\pi} \frac{\chi''_{BA}(\omega)}{\omega}, \quad \text{where} \quad \int_{-\infty}^{\infty} F_{BA}(\omega) d\omega = 1. \quad (3.3.17a)$$

The normalization of $F_{BA}(\omega)$ is a simple consequence of the Kramers-Kronig relation (3.2.11d). The n th order moment of ω , with respect to the spectral weight function $F_{BA}(\omega)$, is then defined as

$$\langle \omega^n \rangle_{BA} = \int_{-\infty}^{\infty} \omega^n F_{BA}(\omega) d\omega, \quad (3.3.17b)$$

which allows the relation between the n th derivatives at $t = 0$ to be written

$$\chi'_{BA}(0) \langle (\hbar\omega)^{n+1} \rangle_{BA} = (-1)^n \langle [\mathcal{L}^n \hat{B}, \hat{A}] \rangle. \quad (3.3.18a)$$

These are the sum rules relating the spectral frequency-moments with the thermal expectation-values of operators obtainable from \hat{B} , \hat{A} , and \mathcal{H} . If $\hat{B} = \hat{A} = \hat{A}^\dagger$, then (3.3.1) shows that $F_{BA}(\omega)$ is even in ω , and all the odd moments vanish. In this case, the even moments are

$$\chi'_{AA}(0) \langle (\hbar\omega)^{2n} \rangle_{AA} = -\langle [\mathcal{L}^{2n-1} \hat{A}, \hat{A}] \rangle. \quad (3.3.18b)$$

3.4 Linear response of the Heisenberg ferromagnet

In this section, we shall illustrate the use of linear response theory by applying it to the case of the three-dimensional Heisenberg ferromagnet, with the Hamiltonian

$$\mathcal{H} = -\frac{1}{2} \sum_{i \neq j} \mathcal{J}(ij) \mathbf{S}_i \cdot \mathbf{S}_j, \quad (3.4.1)$$

where \mathbf{S}_i is the spin on the i th ion, placed in a Bravais lattice at the position \mathbf{R}_i . The spatial Fourier transform of the exchange coupling, with the condition $\mathcal{J}(ii) \equiv 0$, is

$$\mathcal{J}(\mathbf{q}) = \frac{1}{N} \sum_{ij} \mathcal{J}(ij) e^{-i\mathbf{q} \cdot (\mathbf{R}_i - \mathbf{R}_j)} = \sum_j \mathcal{J}(ij) e^{-i\mathbf{q} \cdot (\mathbf{R}_i - \mathbf{R}_j)}, \quad (3.4.2a)$$

and conversely

$$\mathcal{J}(ij) = \frac{1}{N} \sum_{\mathbf{q}} \mathcal{J}(\mathbf{q}) e^{i\mathbf{q} \cdot (\mathbf{R}_i - \mathbf{R}_j)} = \frac{V}{N(2\pi)^3} \int \mathcal{J}(\mathbf{q}) e^{i\mathbf{q} \cdot (\mathbf{R}_i - \mathbf{R}_j)} d\mathbf{q}, \quad (3.4.2b)$$

depending on whether \mathbf{q} , defined within the primitive Brillouin zone, is considered to be a discrete or a continuous variable (we shall normally assume it to be discrete). N is the total number of spins, V is the volume, and the inversion symmetry of the Bravais lattice implies that $\mathcal{J}(\mathbf{q}) = \mathcal{J}(-\mathbf{q}) = \mathcal{J}^*(\mathbf{q})$. The maximum value of $\mathcal{J}(\mathbf{q})$ is assumed to be $\mathcal{J}(\mathbf{q} = \mathbf{0})$, in which case the equilibrium state at zero temperature, i.e. the ground state, is the ferromagnet:

$$\langle \mathbf{S}_i \rangle = S \hat{\mathbf{z}} \quad \text{at } T = 0, \quad (3.4.3)$$

where $\hat{\mathbf{z}}$ is a unit vector along the z -axis, which is established as the direction of magnetization by an infinitesimal magnetic field. This result is exact, but as soon as the temperature is increased above zero, it is necessary to make a number of approximations. As a first step, we

introduce the thermal expectation-values $\langle \mathbf{S}_i \rangle = \langle \mathbf{S} \rangle$ in the Hamiltonian which, after a simple rearrangement of terms, can be written

$$\mathcal{H} = \sum_i \mathcal{H}_i - \frac{1}{2} \sum_{i \neq j} \mathcal{J}(ij) (\mathbf{S}_i - \langle \mathbf{S} \rangle) \cdot (\mathbf{S}_j - \langle \mathbf{S} \rangle), \quad (3.4.4a)$$

with

$$\mathcal{H}_i = -S_i^z \mathcal{J}(\mathbf{0}) \langle S^z \rangle + \frac{1}{2} \mathcal{J}(\mathbf{0}) \langle S^z \rangle^2, \quad (3.4.4b)$$

and $\langle \mathbf{S} \rangle = \langle S^z \rangle \hat{\mathbf{z}}$. In the mean-field approximation, discussed in the previous chapter, the dynamic correlation between spins on different sites is neglected. This means that the second term in (3.4.4a) is disregarded, reducing the original many-spin Hamiltonian to a sum of N independent single-spin Hamiltonians (3.4.4b). In this approximation, $\langle S^z \rangle$ is determined by the self-consistent equation

$$\langle S^z \rangle = \frac{\sum_{M=-S}^{+S} M e^{\beta M \mathcal{J}(\mathbf{0}) \langle S^z \rangle}}{\sum_{M=-S}^{+S} e^{\beta M \mathcal{J}(\mathbf{0}) \langle S^z \rangle}} \quad (3.4.5a)$$

(the last term in (3.4.4b) does not influence the thermal average) which, in the limit of low temperatures, is

$$\langle S^z \rangle \simeq S - e^{-\beta S \mathcal{J}(\mathbf{0})}. \quad (3.4.5b)$$

In order to incorporate the influence of two-site correlations, to leading order, we consider the Green function

$$G^\pm(ii', t) = \langle \langle S_i^+(t); S_{i'}^- \rangle \rangle. \quad (3.4.6)$$

According to (3.3.14a), the variation in time of $G^\pm(ii', t)$ depends on the operator

$$[S_i^+, \mathcal{H}] = -\frac{1}{2} \sum_j \mathcal{J}(ij) (-2S_i^+ S_j^z + 2S_i^z S_j^+).$$

The introduction of this commutator in the equation of motion (3.3.14a) leads to a relation between the original Green function and a new, more elaborate Green function. Through its equation of motion, this new function may be expressed in terms of yet another. The power of the exchange coupling in the Green functions which are generated in this way is raised by one in each step, and this procedure leads to an infinite hierarchy of coupled functions. An approximate solution may be obtained by utilizing the condition that the expectation value of S_i^z is close to its saturation value at low temperatures. Thus, in this limit,

S_i^z must be nearly independent of time, i.e. $S_i^z \simeq \langle S^z \rangle$. In this *random-phase approximation* (RPA) the commutator reduces to

$$[S_i^+, \mathcal{H}] \simeq - \sum_j \mathcal{J}(ij) \langle S^z \rangle (S_j^+ - S_i^+),$$

and the equations of motion lead to the following linear set of equations:

$$\begin{aligned} \hbar\omega G^\pm(ii', \omega) + \sum_j \mathcal{J}(ij) \langle S^z \rangle \{G^\pm(ji', \omega) - G^\pm(ii', \omega)\} \\ = \langle [S_i^+, S_{i'}^-] \rangle = 2\langle S^z \rangle \delta_{ii'}. \end{aligned} \quad (3.4.7)$$

The infinite set of RPA equations is diagonal in reciprocal space. Introducing the Fourier transform

$$G^\pm(\mathbf{q}, \omega) = \sum_{i'} G^\pm(ii', \omega) e^{-i\mathbf{q} \cdot (\mathbf{R}_i - \mathbf{R}_{i'})}, \quad (3.4.8)$$

we obtain

$$\hbar\omega G^\pm(\mathbf{q}, \omega) + \langle S^z \rangle \{ \mathcal{J}(\mathbf{q}) G^\pm(\mathbf{q}, \omega) - \mathcal{J}(\mathbf{0}) G^\pm(\mathbf{q}, \omega) \} = 2\langle S^z \rangle,$$

or

$$G^\pm(\mathbf{q}, \omega) = \lim_{\epsilon \rightarrow 0^+} \frac{2\langle S^z \rangle}{\hbar\omega + i\hbar\epsilon - E_{\mathbf{q}}}, \quad (3.4.9)$$

where the *dispersion relation* is

$$E_{\mathbf{q}} = \langle S^z \rangle \{ \mathcal{J}(\mathbf{0}) - \mathcal{J}(\mathbf{q}) \}. \quad (3.4.10)$$

Introducing the susceptibility $\chi_{+-}(\mathbf{q}, \omega) = -G^\pm(\mathbf{q}, \omega)$, we obtain

$$\chi_{+-}(\mathbf{q}, \omega) = \frac{2\langle S^z \rangle}{E_{\mathbf{q}} - \hbar\omega} + i\pi 2\langle S^z \rangle \delta(\hbar\omega - E_{\mathbf{q}}). \quad (3.4.11a)$$

Defining $\chi_{-+}(\mathbf{q}, \omega)$ analogously to $\chi_{+-}(\mathbf{q}, \omega)$, but with S^+ and S^- interchanged, we obtain similarly, or by the use of the symmetry relation (3.2.15),

$$\chi_{-+}(\mathbf{q}, \omega) = \frac{2\langle S^z \rangle}{E_{\mathbf{q}} + \hbar\omega} - i\pi 2\langle S^z \rangle \delta(\hbar\omega + E_{\mathbf{q}}), \quad (3.4.11b)$$

so that the absorptive susceptibility is

$$\chi''_{+-}(\mathbf{q}, \omega) = -\chi''_{-+}(\mathbf{q}, -\omega) = 2\pi \langle S^z \rangle \delta(\hbar\omega - E_{\mathbf{q}}). \quad (3.4.11c)$$

The above susceptibilities do not correspond directly to physical observables but, for instance, $\chi_{xx}(\mathbf{q}, \omega)$ (where S^+ and S^- are both replaced by S_x) does. It is straightforward to see (by symmetry or by direct verification) that $\chi_{++}(\mathbf{q}, \omega) = \chi_{--}(\mathbf{q}, \omega) \equiv 0$, and hence

$$\chi_{xx}(\mathbf{q}, \omega) = \chi_{yy}(\mathbf{q}, \omega) = \frac{1}{4} \{ \chi_{+-}(\mathbf{q}, \omega) + \chi_{-+}(\mathbf{q}, \omega) \}.$$

The presence of two-site correlations influences the thermal average $\langle S^z \rangle$. A determination of the correction to the MF result (3.4.5b) for $\langle S^z \rangle$, leading to a *self-consistent RPA* result for the transverse susceptibility, requires a relation between $\langle S^z \rangle$ and the susceptibility functions deduced above. The spin commutator-relation, $[S_i^+, S_{i'}^-] = 2S^z \delta_{ii'}$, turns out to be satisfied identically, and thus leads to no additional conditions. Instead we consider the *Wortis expansion*

$$S_i^z = S - \frac{1}{2S} S_i^- S_i^+ - \frac{1}{8S^2 (S - \frac{1}{2})} (S_i^-)^2 (S_i^+)^2 - \dots \quad (3.4.12)$$

for which the matrix elements between the p lowest single-spin (or MF) levels are correct, where $p \leq 2S + 1$ is the number of terms in the expansion. Using (3.4.11), we find from the fluctuation-dissipation theorem (3.2.18):

$$\begin{aligned} \langle S_i^- S_i^+ \rangle &= \frac{1}{N} \sum_{\mathbf{q}} S_{-\mathbf{q}}(\mathbf{q}, t=0) \\ &= \frac{1}{N} \sum_{\mathbf{q}} \frac{1}{\pi} \int_{-\infty}^{\infty} \frac{1}{1 - e^{-\beta \hbar \omega}} \chi''_{-\mathbf{q}}(\mathbf{q}, \omega) d(\hbar \omega) = 2 \langle S^z \rangle \Phi, \end{aligned} \quad (3.4.13a)$$

with

$$\Phi = \frac{1}{N} \sum_{\mathbf{q}} n_{\mathbf{q}} \quad ; \quad n_{\mathbf{q}} = \frac{1}{e^{\beta E_{\mathbf{q}}} - 1}, \quad (3.4.13b)$$

where $n_{\mathbf{q}}$ is the population factor for bosons of energy $E_{\mathbf{q}}$. If $S = \frac{1}{2}$, then S^z is determined by the two first terms of (3.4.12), and

$$\langle S^z \rangle = S - \Phi \langle S^z \rangle / S,$$

or

$$\langle S^z \rangle = S^2 / (S + \Phi) \simeq \frac{1}{2} - \Phi + 2\Phi^2 - \dots$$

In general one may use a ‘Hartree-Fock decoupling’, $\langle (S_i^-)^2 (S_i^+)^2 \rangle \simeq 2 \langle (S_i^- S_i^+)^2 \rangle$, of the higher-order terms in (3.4.13) in order to show that

$$\langle S^z \rangle = S - \Phi + (2S + 1)\Phi^{2S+1} - \dots \simeq S - \frac{1}{N} \sum_{\mathbf{q}} n_{\mathbf{q}}, \quad (3.4.14)$$

where the *kinematic correction*, of the order Φ^{2S+1} , due to the limited number of single-spin states, which is neglected in this expression, is unimportant when $S \geq 1$. Utilizing the Hartree–Fock decoupling once more to write $\langle S_i^z S_j^z \rangle_{(i \neq j)} \simeq \langle S^z \rangle^2 \simeq S^2 - 2\langle S^z \rangle \Phi$, we find the internal energy to be

$$\begin{aligned} U = \langle \mathcal{H} \rangle &= -\frac{1}{2}N\mathcal{J}(\mathbf{0})S^2 + \sum_{\mathbf{q}} E_{\mathbf{q}} n_{\mathbf{q}} \\ &= -\frac{1}{2}N\mathcal{J}(\mathbf{0})S(S+1) + \sum_{\mathbf{q}} E_{\mathbf{q}}(n_{\mathbf{q}} + \frac{1}{2}). \end{aligned} \quad (3.4.15)$$

The second form, expressing the effect of the zero-point motion, is derived using $\mathcal{J}(ii) = \frac{1}{N} \sum_{\mathbf{q}} \mathcal{J}(\mathbf{q}) \equiv 0$.

The thermodynamic properties of the Heisenberg ferromagnet are determined by (3.4.10), (3.4.14), and (3.4.15), which are all valid at low temperatures. In a cubic crystal, the energy dispersion $E_{\mathbf{q}}$ is isotropic and proportional to q^2 in the long wavelength limit, and (3.4.14) then predicts that the magnetization $\langle S^z \rangle$ decreases from its saturation value as $T^{3/2}$. The specific heat is also found to be proportional to $T^{3/2}$. The thermodynamic quantities have a very different temperature dependence from the exponential behaviour (3.4.5b) found in the MF approximation. This is due to the presence of elementary excitations, which are easily excited thermally in the long wavelength limit, since $E_{\mathbf{q}} \rightarrow 0$ when $\mathbf{q} \rightarrow \mathbf{0}$ in the RPA. These normal modes, which are described as *spin waves*, behave in most aspects (disregarding the kinematic effects) as non-conserved Bose-particles, and they are therefore also called *magnons*.

We shall not present a detailed discussion of the low-temperature properties of the Heisenberg ferromagnet. Further details may be found in, for instance, Marshall and Lovesey (1971), and a quite complete treatment is given by Tahir-Kheli (1976). The RPA model is correct at $T = 0$ where $\langle S^z \rangle = S$, but as soon as the temperature is increased, the magnons start to interact with each other, giving rise to finite lifetimes, and the temperature dependence of the excitation energies is modified (or *renormalized*). The temperature dependence of $E_{\mathbf{q}} = E_{\mathbf{q}}(T)$ is responsible for the leading order ‘dynamic’ corrections to $\langle S^z \rangle$ and to the heat capacity. A more accurate calculation, which we will present in Section 5.2, adds an extra term to the dispersion:

$$E_{\mathbf{q}} = \langle S^z \rangle \{ \mathcal{J}(\mathbf{0}) - \mathcal{J}(\mathbf{q}) \} + \frac{1}{N} \sum_{\mathbf{k}} \{ \mathcal{J}(\mathbf{k}) - \mathcal{J}(\mathbf{k} + \mathbf{q}) \} n_{\mathbf{k}}, \quad (3.4.16)$$

from which the heat capacity of this non-interacting Bose-gas can be determined as

$$C = \partial U / \partial T = \sum_{\mathbf{q}} E_{\mathbf{q}} dn_{\mathbf{q}} / dT. \quad (3.4.17)$$

We note that there are corrections to U , given by (3.4.15), of second order in Φ . The low-temperature properties, as determined by (3.4.14), (3.4.16), and (3.4.17), agree with the systematic expansion performed by Dyson (1956), including the leading-order dynamical correction of fourth power in T (in the cubic case), except for a minor kinematic correction which is negligible for $S \geq 1$.

3.5 The random-phase approximation

Earlier in this chapter, we have demonstrated that many experimentally observable properties of solids can be expressed in terms of two-particle correlation functions. Hence it is of great importance to be able to calculate these, or the related Green functions, for realistic systems. We shall therefore consider the determination of the generalized susceptibility for rare earth magnets, using the random-phase approximation which was introduced in the last section, and conclude the chapter by applying this theory to the simple Heisenberg model, in which the single-ion anisotropy is neglected.

3.5.1 The generalized susceptibility in the RPA

The starting point for the calculation of the generalized susceptibility is the (effective) Hamiltonian for the angular momenta which, as usual, we write as a sum of single- and two-ion terms:

$$\mathcal{H} = \sum_i \mathcal{H}_J(\mathbf{J}_i) - \frac{1}{2} \sum_{i \neq j} \mathcal{J}(ij) \mathbf{J}_i \cdot \mathbf{J}_j. \quad (3.5.1)$$

For our present purposes, it is only necessary to specify the two-ion part and, for simplicity, we consider only the Heisenberg interaction. As in Section 2.2, we introduce the thermal expectation values $\langle \mathbf{J}_i \rangle$ in the Hamiltonian, which may then be written

$$\mathcal{H} = \sum_i \mathcal{H}_{\text{MF}}(i) - \frac{1}{2} \sum_{i \neq j} \mathcal{J}(ij) (\mathbf{J}_i - \langle \mathbf{J}_i \rangle) \cdot (\mathbf{J}_j - \langle \mathbf{J}_j \rangle), \quad (3.5.2)$$

where

$$\mathcal{H}_{\text{MF}}(i) = \mathcal{H}_J(\mathbf{J}_i) - (\mathbf{J}_i - \frac{1}{2} \langle \mathbf{J}_i \rangle) \cdot \sum_j \mathcal{J}(ij) \langle \mathbf{J}_j \rangle. \quad (3.5.3)$$

From the mean-field Hamiltonians $\mathcal{H}_{\text{MF}}(i)$, we may calculate $\langle \mathbf{J}_i \rangle$ as before. The Hamiltonian (3.5.3) also determines the dynamic susceptibility of the i th ion, in the form of a Cartesian tensor $\bar{\chi}_i^o(\omega)$, according to eqns (3.3.4–6), with \hat{A} and \hat{B} set equal to the angular-momentum components $J_{i\alpha}$. We wish to calculate the linear response $\langle \mathbf{J}_i(t) \rangle$ of

the system to a small perturbative field $\mathbf{h}_j(t) = g\mu_B \mathbf{H}_j(t)$ (the Zeeman term due to a stationary field is taken as included in $\mathcal{H}_j(\mathbf{J}_i)$). From (3.5.2), we may extract all terms depending on \mathbf{J}_i and collect them in an effective Hamiltonian \mathcal{H}_i , which determines the time-dependence of \mathbf{J}_i . Transformed to the Heisenberg picture, this Hamiltonian is

$$\mathcal{H}_i(t) = \mathcal{H}_{\text{MF}}(i, t) - (\mathbf{J}_i(t) - \langle \mathbf{J}_i \rangle) \cdot \left(\sum_j \mathcal{J}(ij) (\mathbf{J}_j(t) - \langle \mathbf{J}_j \rangle) + \mathbf{h}_i(t) \right). \quad (3.5.4)$$

We note that a given site i appears twice in the second term of (3.5.2), and that the additional term $\langle \mathbf{J}_i \rangle \cdot \mathbf{h}_i$ has no consequences in the limit when \mathbf{h}_i goes to zero. The differences $\mathbf{J}_j(t) - \langle \mathbf{J}_j(t) \rangle$ fluctuate in a virtually uncorrelated manner from ion to ion, and their contribution to the sum in (3.5.4) is therefore small. Thus, to a good approximation, these fluctuations may be neglected, corresponding to replacing $\mathbf{J}_j(t)$ in (3.5.4) by $\langle \mathbf{J}_j(t) \rangle$ (when $j \neq i$). This is just the random-phase approximation (RPA), introduced in the previous section, and so called on account of the assumption that $\mathbf{J}_j(t) - \langle \mathbf{J}_j(t) \rangle$ may be described in terms of a random phase-factor. It is clearly best justified when the fluctuations are small, i.e. at low temperatures, and when many sites contribute to the sum, i.e. in three-dimensional systems with long-range interactions. The latter condition reflects the fact that an increase in the number of (nearest) neighbours improves the resemblance of the sum in (3.5.4) to an ensemble average. If we introduce the RPA in eqn (3.5.4), the only dynamical variable which remains is $\mathbf{J}_i(t)$, and the Hamiltonian becomes equivalent to $\mathcal{H}_{\text{MF}}(i)$, except that the probing field $\mathbf{h}_i(t)$ is replaced by an effective field $\mathbf{h}_i^{\text{eff}}(t)$. With $\langle \mathbf{J}_i(\omega) \rangle$ defined as the Fourier transform of $\langle \mathbf{J}_i(t) \rangle - \langle \mathbf{J}_i \rangle$, then, according to eqn (3.1.9),

$$\langle \mathbf{J}_i(\omega) \rangle = \overline{\overline{\chi}}_i^o(\omega) \mathbf{h}_i^{\text{eff}}(\omega),$$

where the effective field is

$$\mathbf{h}_i^{\text{eff}}(\omega) = \mathbf{h}_i(\omega) + \sum_j \mathcal{J}(ij) \langle \mathbf{J}_j(\omega) \rangle. \quad (3.5.5)$$

This may be compared with the response determined by the two-ion susceptibility functions of the system, defined such that

$$\langle \mathbf{J}_i(\omega) \rangle = \sum_j \overline{\overline{\chi}}(ij, \omega) \mathbf{h}_j(\omega). \quad (3.5.6)$$

The two ways of writing the response should coincide for all $\mathbf{h}_j(\omega)$, which implies that, within the RPA,

$$\overline{\overline{\chi}}(ij, \omega) = \overline{\overline{\chi}}_i^o(\omega) \left(\delta_{ij} + \sum_{j'} \mathcal{J}(ij') \overline{\overline{\chi}}(j'j, \omega) \right). \quad (3.5.7)$$

This self-consistent equation may be solved under various conditions. For convenience, we shall consider here only the uniform case of a ferromagnet or paramagnet, where $\mathcal{H}_{\text{MF}}(i)$ is the same for all the ions, i.e. $\langle \mathbf{J}_i \rangle = \langle \mathbf{J} \rangle$ and $\overline{\chi}_i^o(\omega) = \overline{\chi}^o(\omega)$, in which case we get the final result

$$\overline{\chi}(\mathbf{q}, \omega) = \{1 - \overline{\chi}^o(\omega) \mathcal{J}(\mathbf{q})\}^{-1} \overline{\chi}^o(\omega). \quad (3.5.8)$$

Here 1 is the unit matrix, and we have used the Fourier transform (3.4.2) of $\mathcal{J}(ij)$

$$\mathcal{J}(\mathbf{q}) = \sum_j \mathcal{J}(ij) e^{-i\mathbf{q} \cdot (\mathbf{R}_i - \mathbf{R}_j)}. \quad (3.5.9)$$

In the RPA, the effects of the surrounding ions are accounted for by a time-dependent molecular field, which self-consistently enhances the response of the isolated ions. The above results are derived from a kind of hybrid MF-RPA theory, as the single-ion susceptibility $\overline{\chi}_i^o(\omega)$ is still determined in terms of the MF expectation values. A self-consistent RPA theory might be more accurate but, as we shall see, gives rise to further problems. At high temperatures (or close to a phase transition), the description of the dynamical behaviour obtained in the RPA is incomplete, because the thermal fluctuations introduce damping effects which are not included. However, the static properties may still be described fairly accurately by the above theory, because the MF approximation is correct to leading order in $\beta = 1/k_B T$.

The RPA, which determines the excitation spectrum of the many-body system to leading order in the two-ion interactions, is simple to derive and is of general utility. Historically, its applicability was appreciated only gradually, in parallel with the experimental study of a variety of systems, and results corresponding to eqn (3.5.8) were presented independently several times in the literature in the early 1970s (Fulde and Perschel 1971, 1972; Haley and Erdős 1972; Purwins *et al.* 1973; Holden and Buyers 1974). The approach to this problem in the last three references is very similar, and we will now present it, following most closely the account given by Bak (1974).

We start by considering the MF Hamiltonian defined by (3.5.3). The basis in which $\mathcal{H}_{\text{MF}}(i)$ is diagonal is denoted $|\nu_i \rangle$; $\nu = 0, 1, \dots, 2J$, and we assume that $\mathcal{H}_{\text{MF}}(i)$ is the same for all the ions:

$$\mathcal{H}_{\text{MF}}(i) |\nu_i \rangle = E_\nu |\nu_i \rangle, \quad (3.5.10)$$

with E_ν independent of the site index i . The eigenvalue equation defines the *standard-basis* operators

$$a_{\nu\mu}(i) = |\nu_i \rangle \langle \mu_i|, \quad (3.5.11)$$

in terms of which $\mathcal{H}_{\text{MF}}(i) = \sum_{\nu} E_{\nu} a_{\nu\nu}(i)$. Defining the matrix-elements

$$\mathbf{M}_{\nu\mu} = \langle \nu_i | \mathbf{J}_i - \langle \mathbf{J}_i \rangle | \mu_i \rangle, \quad (3.5.12)$$

we may write

$$\mathbf{J}_i - \langle \mathbf{J}_i \rangle = \sum_{\nu\mu} \mathbf{M}_{\nu\mu} a_{\nu\mu}(i),$$

and hence

$$\mathcal{H} = \sum_i \sum_{\nu} E_{\nu} a_{\nu\nu}(i) - \frac{1}{2} \sum_{ij} \sum_{\nu\mu} \sum_{\nu'\mu'} \mathcal{J}(ij) \mathbf{M}_{\nu\mu} \cdot \mathbf{M}_{\nu'\mu'} a_{\nu\mu}(i) a_{\nu'\mu'}(j). \quad (3.5.13)$$

We have expressed \mathcal{H} in terms of the standard-basis operators, as we now wish to consider the Green functions $G_{\nu\mu,rs}(ii',\omega) = \langle\langle a_{\nu\mu}(i); a_{rs}(i') \rangle\rangle$. According to (3.3.14), their equations of motion are

$$\hbar\omega G_{\nu\mu,rs}(ii',\omega) - \langle\langle [a_{\nu\mu}(i), \mathcal{H}]; a_{rs}(i') \rangle\rangle = \langle [a_{\nu\mu}(i), a_{rs}(i')] \rangle. \quad (3.5.14)$$

The MF basis is orthonormal, and the commutators are

$$[a_{\nu\mu}(i), a_{rs}(i')] = \delta_{ii'} \{ \delta_{\mu r} a_{\nu s}(i) - \delta_{s\nu} a_{r\mu}(i) \},$$

so we obtain

$$\begin{aligned} & \{ \hbar\omega - (E_{\mu} - E_{\nu}) \} G_{\nu\mu,rs}(ii',\omega) \\ & + \sum_j \mathcal{J}(ij) \sum_{\xi\nu'\mu'} \langle\langle \{ a_{\nu\xi}(i) \mathbf{M}_{\mu\xi} - a_{\xi\mu}(i) \mathbf{M}_{\xi\nu} \} \cdot \mathbf{M}_{\nu'\mu'} a_{\nu'\mu'}(j); a_{rs}(i') \rangle\rangle \\ & = \delta_{ii'} \{ \delta_{\mu r} a_{\nu s}(i) - \delta_{s\nu} a_{r\mu}(i) \}. \end{aligned} \quad (3.5.15)$$

In order to solve these equations, we make an *RPA decoupling* of the higher-order Green functions:

$$\begin{aligned} & \langle\langle a_{\nu\xi}(i) a_{\nu'\mu'}(j); a_{rs}(i') \rangle\rangle_{i \neq j} \simeq \\ & \langle a_{\nu\xi}(i) \rangle \langle\langle a_{\nu'\mu'}(j); a_{rs}(i') \rangle\rangle + \langle a_{\nu'\mu'}(j) \rangle \langle\langle a_{\nu\xi}(i); a_{rs}(i') \rangle\rangle. \end{aligned} \quad (3.5.16)$$

This equation is correct in the limit where two-ion correlation effects can be neglected, i.e. when the ensemble averages are determined by the MF Hamiltonian. The decoupling is equivalent to the approximation made above, when $\mathbf{J}_j(t)$ in (3.5.4) was replaced by $\langle \mathbf{J}_j(t) \rangle$. The thermal expectation value of a single-ion quantity $\langle a_{\nu\mu}(i) \rangle$ is independent of i , and to leading order it is determined by the MF Hamiltonian:

$$\langle a_{\nu\mu} \rangle \simeq \langle a_{\nu\mu} \rangle_0 = \frac{1}{Z} \text{Tr} \left\{ e^{-\beta \mathcal{H}(\text{MF})} a_{\nu\mu} \right\} = \delta_{\nu\mu} n_{\nu}, \quad (3.5.17)$$

and correspondingly $\langle \mathbf{J} \rangle$ in (3.5.12) is assumed to take the MF value $\langle \mathbf{J} \rangle_0$. Here Z is the partition function of the MF Hamiltonian, and thus n_ν is the population factor of the ν th MF level. With the two approximations (3.5.16) and (3.5.17), and the condition that $\sum_{\nu'\mu'} \langle \mathbf{M}_{\nu'\mu'} a_{\nu'\mu'}(j) \rangle_0 = \langle \mathbf{J}_j - \langle \mathbf{J}_j \rangle_0 \rangle_0 = 0$ by definition, (3.5.15) is reduced to a closed set of equations by a Fourier transformation:

$$\begin{aligned} & \{ \hbar\omega - (E_\mu - E_\nu) \} G_{\nu\mu,rs}(\mathbf{q}, \omega) \\ & + \sum_{\nu'\mu'} \mathcal{J}(\mathbf{q})(n_\nu - n_\mu) \mathbf{M}_{\mu\nu} \cdot \mathbf{M}_{\nu'\mu'} G_{\nu'\mu',rs}(\mathbf{q}, \omega) = (n_\nu - n_\mu) \delta_{\mu r} \delta_{\nu s}. \end{aligned} \quad (3.5.18)$$

We now show that these equations lead to the same result (3.5.8) as found before. The susceptibility, expressed in terms of the Green functions, is

$$\bar{\chi}(\mathbf{q}, \omega) = - \sum_{\nu\mu,rs} \mathbf{M}_{\nu\mu} \mathbf{M}_{rs} G_{\nu\mu,rs}(\mathbf{q}, \omega). \quad (3.5.19)$$

$\mathbf{M}_{\nu\mu} \mathbf{M}_{rs}$ is the dyadic vector-product, with the $(\alpha\beta)$ -component given by $(\mathbf{M}_{\nu\mu} \mathbf{M}_{rs})_{\alpha\beta} = (M_{\nu\mu})_\alpha (M_{rs})_\beta$. Further, from eqns (3.3.4-6), the MF susceptibility is

$$\bar{\chi}^o(\omega) = \sum_{\nu\mu}^{E_\nu \neq E_\mu} \frac{\mathbf{M}_{\nu\mu} \mathbf{M}_{\mu\nu}}{E_\mu - E_\nu - \hbar\omega} (n_\nu - n_\mu) + \sum_{\nu\mu}^{E_\nu = E_\mu} \mathbf{M}_{\nu\mu} \mathbf{M}_{\mu\nu} \beta n_\nu \delta_{\omega 0}. \quad (3.5.20)$$

Multiplying (3.5.18) by $\mathbf{M}_{\nu\mu} \mathbf{M}_{rs} / (E_\mu - E_\nu - \hbar\omega)$, and summing over $(\nu\mu, rs)$, we get (for $\omega \neq 0$)

$$\bar{\chi}(\mathbf{q}, \omega) - \bar{\chi}^o(\omega) \mathcal{J}(\mathbf{q}) \bar{\chi}(\mathbf{q}, \omega) = \bar{\chi}^o(\omega), \quad (3.5.21)$$

in accordance with (3.5.8). Special care must be taken in the case of degeneracy, $E_\mu = E_\nu$, due to the resulting singular behaviour of (3.5.18) around $\omega = 0$. For $\omega \neq 0$, $G_{\nu\mu,rs}(\mathbf{q}, \omega)$ vanishes identically if $E_\mu = E_\nu$, whereas $G_{\nu\mu,rs}(\mathbf{q}, \omega = 0)$ may be non-zero. The correct result, in the zero frequency limit, can be found by putting $E_\mu - E_\nu = \delta$ in (3.5.18), so that $n_\nu - n_\mu = n_\nu(1 - e^{-\beta\delta}) \simeq \beta n_\nu \delta$. Dividing (3.5.18) by δ , and taking the limit $\delta \rightarrow 0$, we obtain in the degenerate case $E_\nu = E_\mu$:

$$-G_{\nu\mu,rs}(\mathbf{q}, 0) - \beta \sum_{\nu'\mu'} \mathcal{J}(\mathbf{q}) n_\nu \mathbf{M}_{\nu\mu} \cdot \mathbf{M}_{\nu'\mu'} G_{\nu'\mu',rs}(\mathbf{q}, 0) = \beta n_\nu \delta_{\mu r} \delta_{\nu s}. \quad (3.5.22)$$

Since $\bar{\chi}(\mathbf{q}, \omega)$ does not depend on the specific choice of state-vectors in the degenerate case, (3.5.22) must also apply for a single level, i.e. when $\mu = \nu$. It then follows that (3.5.18), when supplemented with (3.5.22),

ensures that (3.5.21) is also valid at $\omega = 0$, as (3.5.22) accounts for the elastic contributions due to $\overline{\chi}^o(\omega)$, proportional to $\delta_{\omega 0}$. This zero-frequency modification of the equations of motion was derived in this context in a slightly different way by Lines (1974a).

Although eqns (3.5.18) and (3.5.22) only lead to the result (3.5.8), derived previously in a simpler manner, the equations of motion clarify more precisely the approximations made, and they contain more information. They allow us to keep track in detail of the different transitions between the MF levels, which may be an advantage when performing actual calculations. Furthermore, the set of Green functions $G_{\nu\mu,rs}(\mathbf{q},\omega)$ is complete, and hence any magnetic single- or two-ion response function may be expressed as a linear combination of these functions.

In the derivation of the RPA result, we utilized two approximate equations, (3.5.16) and (3.5.17). The two approximations are consistent, as both equations are correct if two-ion correlation effects are negligible. However, the RPA Green functions contain implicitly two-ion correlations and, according to (3.3.7), we have in the linear response theory:

$$\begin{aligned} \langle a_{\nu\mu}(i) a_{rs}(j) \rangle - \langle a_{\nu\mu}(i) \rangle \langle a_{rs}(j) \rangle = \\ \frac{1}{N} \sum_{\mathbf{q}} e^{i\mathbf{q}\cdot(\mathbf{R}_i - \mathbf{R}_j)} \frac{1}{\pi} \int_{-\infty}^{\infty} \frac{-1}{1 - e^{-\beta\hbar\omega}} G''_{\nu\mu,rs}(\mathbf{q},\omega) d(\hbar\omega), \end{aligned} \quad (3.5.23)$$

where, by the definition (3.2.11b),

$$G''_{\nu\mu,rs}(\mathbf{q},\omega) = \frac{1}{2i} \lim_{\epsilon \rightarrow 0^+} \{ G_{\nu\mu,rs}(\mathbf{q},\omega + i\epsilon) - G_{rs,\nu\mu}(-\mathbf{q}, -\omega + i\epsilon) \}.$$

Equation (3.5.23), with $i = j$, might be expected to give a better estimate of the single-ion average $\langle a_{\nu\mu} \rangle$ than that afforded by the MF approximation used in (3.5.17). If this were indeed the case, the accuracy of the theory could be improved by using this equation, in a self-consistent fashion, instead of (3.5.17), and this improvement would maintain most of the simplicity and general utility of the RPA theory. Unfortunately, such an improvement seems to occur only for the Heisenberg ferromagnet discussed previously, and the nearly-saturated anisotropic ferromagnet, which we will consider later. Equation (3.5.23) allows different choices of the Green functions $G_{\nu\mu,rs}(\mathbf{q},\omega)$ for calculating $\langle a_{\nu\mu} \rangle$, and the results in general depend on this choice. Furthermore, (3.5.23) may lead to non-zero values for $\langle a_{\nu\mu}(i) a_{rs}(i) \rangle$, when $\mu \neq r$, despite the fact that $\langle \mu_i | r_i \rangle = 0$ by definition. The two-ion correlation effects which are neglected by the RPA decoupling in (3.5.18) might be as important, when using eqn (3.5.23) with $i = j$, as those effects which are accounted for by the RPA. Nevertheless, it might be possible that certain choices

of the Green functions, or a linear combination of them, would lead to an accurate determination of $\langle a_{\nu\nu} \rangle$ (the most natural choice would be to use $G''_{\nu 0, 0\nu}(\mathbf{q}, \omega)$). However, a stringent justification of a specific choice would require an analysis of the errors introduced by the RPA decoupling. We conclude that a reliable improvement of the theory can only be obtained by a more accurate treatment of the higher-order Green functions than that provided by the RPA. General programs for accomplishing this have been developed, but they have only been carried through in the simplest cases, and we reserve the discussion of these analyses to subsequent sections, where a number of specific systems are considered.

3.5.2 MF-RPA theory of the Heisenberg ferromagnet

We conclude this chapter by applying the RPA to the Heisenberg model, thereby demonstrating the relation between (3.5.8) and the results presented in the previous section. In order to do this, we must calculate $\bar{\chi}^o(\omega)$. The eigenstates of the MF Hamiltonian (3.4.4b) are $|S^z = M\rangle$, with $M = -S, -S + 1, \dots, S$, and we neglect the constant contribution to the eigenvalues

$$E_M = -M\mathcal{J}(\mathbf{0})\langle S^z \rangle_0 = -M\Delta \quad \text{with} \quad \Delta = \mathcal{J}(\mathbf{0})\langle S^z \rangle_0,$$

denoting the MF expectation-value (3.4.5a) of S^z by $\langle S^z \rangle_0$. According to (3.3.4a), we then have (only terms with $\alpha = M + 1$ and $\alpha' = M$ contribute):

$$\begin{aligned} \chi_{+-}^o(\omega) &= \sum_{M=-S}^{S-1} \frac{\langle M+1|S^+|M\rangle \langle M|S^-|M+1\rangle}{E_M - E_{M+1} - \hbar\omega} (n_{M+1} - n_M) \\ &= \frac{1}{Z} \sum_{-S}^{S-1} \frac{S(S+1) - M(M+1)}{\Delta - \hbar\omega} \left(e^{\beta(M+1)\Delta} - e^{\beta M\Delta} \right) \\ &= \frac{1}{\Delta - \hbar\omega} \frac{1}{Z} \left(\sum_{-S+1}^S \{S(S+1) - (M-1)M\} e^{\beta M\Delta} \right. \\ &\quad \left. - \sum_{-S}^{S-1} \{S(S+1) - M(M+1)\} e^{\beta M\Delta} \right) \\ &= \frac{1}{\Delta - \hbar\omega} \frac{1}{Z} \sum_{-S}^S 2M e^{\beta M\Delta} = \frac{2\langle S^z \rangle_0}{\Delta - \hbar\omega}, \end{aligned}$$

as all the sums may be taken as extending from $-S$ to S . Similarly $\chi_{-+}^o(\omega) = \chi_{+-}^o(-\omega)$, whereas $\chi_{++}^o(\omega) = \chi_{--}^o(\omega) = 0$, from which we

obtain

$$\chi_{xx}^o(\omega) = \chi_{yy}^o(\omega) = \frac{1}{4} \{ \chi_{+-}^o(\omega) + \chi_{-+}^o(\omega) \} = \frac{\Delta \langle S^z \rangle_0}{\Delta^2 - (\hbar\omega)^2}, \quad (3.5.24a)$$

and

$$\chi_{xy}^o(\omega) = -\chi_{yx}^o(\omega) = \frac{i}{4} \{ \chi_{+-}^o(\omega) - \chi_{-+}^o(\omega) \} = \frac{i\hbar\omega \langle S^z \rangle_0}{\Delta^2 - (\hbar\omega)^2}. \quad (3.5.24b)$$

We note here that $\chi_{xy}^o{}'(\omega)$ and $\chi_{xy}^o{}''(\omega)$, obtained by replacing ω by $\omega + i\epsilon$ and letting $\epsilon \rightarrow 0^+$, are both purely imaginary. Of the remaining components in $\overline{\chi}^o(\omega)$, only $\chi_{zz}^o(\omega)$ is non-zero, and it comprises only an elastic contribution

$$\chi_{zz}^o(\omega) = \beta (\delta S^z)^2 \delta_{\omega 0}, \quad \text{with} \quad (\delta S^z)^2 \equiv \langle (S^z)^2 \rangle_0 - \langle S^z \rangle_0^2. \quad (3.5.25)$$

Because $\chi_{\pm z}^o(\omega) = 0$, the RPA equation (3.5.8) factorizes into a 2×2 (xy)-matrix equation and a scalar equation for the zz -component. Inverting the (xy)-part of the matrix $\{1 - \overline{\chi}^o(\omega) \mathcal{J}(\mathbf{q})\}$, we find

$$\chi_{xx}(\mathbf{q}, \omega) = \frac{\chi_{xx}^o(\omega) - |\overline{\chi}^o(\omega)| \mathcal{J}(\mathbf{q})}{1 - \{ \chi_{xx}^o(\omega) + \chi_{yy}^o(\omega) \} \mathcal{J}(\mathbf{q}) + |\overline{\chi}^o(\omega)| \mathcal{J}^2(\mathbf{q})},$$

where the determinant is

$$|\overline{\chi}^o(\omega)| = \chi_{xx}^o(\omega) \chi_{yy}^o(\omega) - \chi_{xy}^o(\omega) \chi_{yx}^o(\omega) = \frac{\langle S^z \rangle_0^2}{\Delta^2 - (\hbar\omega)^2}.$$

By a straightforward manipulation, this leads to

$$\chi_{xx}(\mathbf{q}, \omega) = \frac{E_{\mathbf{q}}^0 \langle S^z \rangle_0}{(E_{\mathbf{q}}^0)^2 - (\hbar\omega)^2}, \quad (3.5.26a)$$

with

$$E_{\mathbf{q}}^0 = \Delta - \langle S^z \rangle_0 \mathcal{J}(\mathbf{q}) = \langle S^z \rangle_0 \{ \mathcal{J}(\mathbf{0}) - \mathcal{J}(\mathbf{q}) \}. \quad (3.5.26b)$$

The same result is obtained for $\chi_{yy}(\mathbf{q}, \omega)$. We note that (3.5.26a) should be interpreted as

$$\chi_{xx}(\mathbf{q}, \omega) = \frac{1}{2} \langle S^z \rangle_0 \lim_{\epsilon \rightarrow 0^+} \left(\frac{1}{E_{\mathbf{q}}^0 - \hbar\omega - i\hbar\epsilon} + \frac{1}{E_{\mathbf{q}}^0 + \hbar\omega + i\hbar\epsilon} \right).$$

This result is nearly the same as that deduced before, eqns (3.4.10–11), except that the RPA expectation-value $\langle S^z \rangle$ is replaced by its MF

value $\langle S^z \rangle_0$, reflecting the lack of self-consistency in this analysis. As a supplement to the previous results, we find that

$$\chi_{zz}(\mathbf{q}, \omega) = \frac{\chi_{zz}^o(\omega)}{1 - \chi_{zz}^o(\omega) \mathcal{J}(\mathbf{q})} = \frac{\beta(\delta S^z)^2}{1 - \beta(\delta S^z)^2 \mathcal{J}(\mathbf{q})} \delta_{\omega 0}, \quad (3.5.27a)$$

and the corresponding correlation function is

$$S_{zz}(\mathbf{q}, \omega) = 2\pi\hbar \frac{(\delta S^z)^2}{1 - \beta(\delta S^z)^2 \mathcal{J}(\mathbf{q})} \delta(\hbar\omega). \quad (3.5.27b)$$

The zz -response vanishes in the zero-temperature limit and, in this approximation, it is completely elastic, since $(\delta S^z)^2$ is assumed independent of time. However, this assumption is violated by the dynamic correlation-effects due to the spin waves. For instance, the ($n = 1$)-sum-rule (3.3.18b) indicates that the second moment $\langle (\hbar\omega)^2 \rangle_{zz}$ is non-zero, when $\mathbf{q} \neq \mathbf{0}$ and $T > 0$, which is not consistent with a spectral function proportional to $\delta(\hbar\omega)$.

Although this procedure leads to a less accurate analysis of the Heisenberg ferromagnet than that applied previously, it has the advantage that it is easily generalized, particularly by numerical methods, to models with single-ion anisotropy, i.e. where $\mathcal{H}_J(\mathbf{J}_i)$ in (3.5.1) is non-zero. The simplicity of the RPA result (3.5.8), or of the more general expression (3.5.7), furthermore makes it suitable for application to complex systems. As argued above, its validity is limited to low temperatures in systems with relatively large coordination numbers. However, these limitations are frequently of less importance than the possibility of making quantitative predictions of reasonable accuracy under realistic circumstances. Its utility and effectiveness will be amply demonstrated in subsequent chapters.

MAGNETIC SCATTERING OF NEUTRONS

The scattering of low-energy neutrons provides an extremely powerful experimental technique for studying the properties of solids. The neutron has a number of special characteristics, on which its utility as a tool for examining magnetic materials depends. Because it is a neutral particle, it can penetrate deeply into most crystals, interacting through its magnetic moment with the electronic moments strongly enough to be measurably scattered, but without disturbing the magnetic system too severely. As a consequence, the great majority of neutrons participate in at most one scattering event, and they sense the properties of the unperturbed crystal. *Thermal neutrons*, with energies of the order of 25 meV, corresponding to wavelengths of the order of 2 Å, match both the interatomic spacings and the energies and momenta of the magnetic excitations, and are generated with adequate intensity by research reactors. *Cold neutrons*, with energies around 5 meV and wavelengths about 4 Å, which are emitted from cooled moderators in reactors, may be even more ideally suited for studying the spatial arrangement and the dynamics of the magnetic moments.

The neutron-scattering cross-section contains precisely that information which is needed to characterize a magnetic material, and to make a stringent comparison with theoretical calculations of its properties. The elastic *Bragg scattering* or *neutron diffraction* provides a systematic procedure for determining the magnetic structure, or the mean values of the magnetic-moment vectors on the different atomic sites. *Inelastic neutron scattering* may be looked upon in three complementary ways. Through conservation of energy and momentum, the scattered neutrons measure the *dispersion relation* of the magnetic excitations. The scattering cross-section is also directly related to the *time-dependent pair-correlation function*, which describes the evolution in space and time of the system of moments. Finally, through the fluctuation–dissipation theorem presented in the last chapter, the cross-section may be expressed in terms of the *generalized susceptibility* of the magnetic crystal, the function describing the dynamics of the moments which is most readily calculated theoretically. No other experimental technique can aspire to providing such detailed microscopic information about magnetic systems.

This chapter does not pretend to be a complete exposition of the theory of magnetic neutron scattering. We shall rather, by elementary

means, derive the magnetic cross-section for unpolarized neutrons in the simple *dipole approximation*, which is normally adequate for scattering by rare earth ions, and will therefore suffice in our further discussion. A neutron interacts with the nuclei in a solid through the nuclear force and, through its magnetic moment, with the magnetic field due to the electrons. In solids with unpaired electrons, the two kinds of scattering mechanism lead to cross-sections of the same order of magnitude. The magnetic field of the electrons may be described by a multipole expansion, and the first term in this series, the dipole term, leads to the dominating contribution to the cross-section at small scattering vectors. We use this approximation in a derivation from first principles of a general expression for the *differential cross-section* (Trammel 1953), which we then separate into *elastic* and *inelastic* components. Using linear response theory, we derive the different forms which the inelastic part may exhibit, and illustrate some of the results by means of the Heisenberg ferromagnet. A detailed treatment of both the nuclear and magnetic scattering of neutrons may be found in Marshall and Lovesey (1971), and Lovesey (1984), while a brief review of some of the salient features of magnetic neutron scattering and its application to physical problems has been given by Mackintosh (1983).

4.1 The differential cross-section in the dipole approximation

A neutron-scattering experiment is performed by allowing a collimated beam of monochromatic (monoenergetic) neutrons to impinge upon a sample, and then measuring the energy distribution of neutrons scattered in different directions. As illustrated in Fig. 4.1, a uniform ensemble of neutrons in the initial state $|\mathbf{k}\mathbf{s}_n\rangle$ is created, typically by utilizing Bragg-reflection in a large single-crystal monochromator, plus suitable shielding by collimators. We may write the state vector for this initial plane-wave state

$$|\mathbf{k}\mathbf{s}_n\rangle = V^{-1/2} \exp(i\mathbf{k} \cdot \mathbf{r}_n) |\mathbf{s}_n\rangle,$$

representing free neutrons with an energy $(\hbar k)^2/2M$ and a flux $\mathbf{j}(\mathbf{k}\mathbf{s}_n) = V^{-1}\hbar\mathbf{k}/M$. When passing through the target, the probability per unit time that a neutron makes a transition from its initial state to the state $|\mathbf{k}'\mathbf{s}'_n\rangle$ is determined by *Fermi's Golden Rule*:

$$W(\mathbf{k}\mathbf{s}_n, \mathbf{k}'\mathbf{s}'_n) = \frac{2\pi}{\hbar} \sum_{if} P_i |\langle \mathbf{k}\mathbf{s}_n; i | \mathcal{H}_{\text{int}} | \mathbf{k}'\mathbf{s}'_n; f \rangle|^2 \delta(\hbar\omega + E_i - E_f). \quad (4.1.1)$$

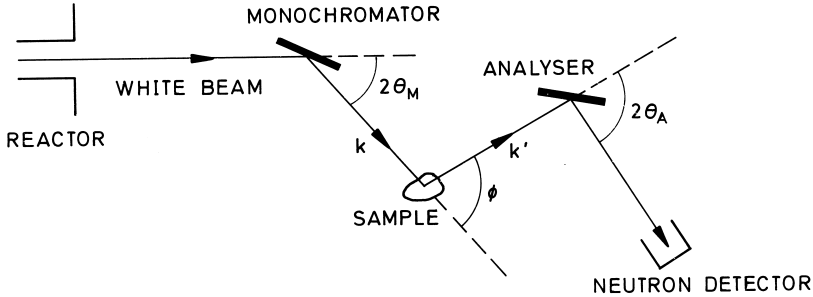


Fig. 4.1. The principle of a neutron-scattering experiment, carried out on a *triple-axis spectrometer*. An incident beam of neutrons, with well-defined momenta, is selected from the continuous reactor spectrum by the monochromator crystal, and scattered from the sample. The intensity of the scattered beam of neutrons, with generally different momenta defined by the analyser crystal, is measured by the detector. The scattered intensity, proportional to the scattering cross-section, is thus determined as a function of the energy transfer $\hbar\omega$ and the momentum transfer $\hbar\boldsymbol{\kappa}$ to the sample, whose orientation relative to $\boldsymbol{\kappa}$ can be varied by rotating the sample table.

\mathcal{H}_{int} is the Hamiltonian describing the interaction between the neutrons and the sample, and the sum extends over all possible scattering processes. It comprises a summation over all possible final states $|f\rangle$ of the sample, and an average over all initial states $|i\rangle$, which occur with the probability P_i . Energy conservation requires that the energy difference between the final and initial states of the sample, $E_f - E_i$, must be equal to the energy transferred from the neutron to it:

$$\hbar\omega = \frac{(\hbar k)^2}{2M} - \frac{(\hbar k')^2}{2M}. \quad (4.1.2)$$

The linear momentum transferred to the sample is $\hbar\boldsymbol{\kappa} = \hbar\mathbf{k} - \hbar\mathbf{k}'$, where $\boldsymbol{\kappa}$ is the *scattering vector*,

$$\boldsymbol{\kappa} = \mathbf{k} - \mathbf{k}'. \quad (4.1.3)$$

The information about the sample is obtained by measuring the scattered intensity as a function of the natural variables of the experiment, the *energy transfer* $\hbar\omega$ and the *momentum transfer* $\hbar\boldsymbol{\kappa}$.

The scattered neutrons with momenta lying in a narrow range around $\hbar\mathbf{k}'$ are counted by placing a detector in a direction along \mathbf{k}' , subtending a small element of solid angle $d\Omega$. The value of k' , or the final

neutron energy, is determined by again making use of Bragg-reflection in a single-crystal analyser, so that only neutrons with energies in a small interval dE around $(\hbar k')^2/2M$ strike the counter. The number of neutrons in this range, corresponding to a state vector $|\mathbf{k}'\mathbf{s}'_n\rangle$ for the scattered neutrons, is

$$\delta N = V(2\pi)^{-3}(k')^2 dk' d\Omega = V(2\pi)^{-3}(Mk'/\hbar^2)dEd\Omega.$$

The number of neutrons arriving at the counter per unit time and per incident neutron is proportional to the scattering area $d\sigma = |\mathbf{j}(\mathbf{k}\mathbf{s}_n)|^{-1} \times W(\mathbf{k}\mathbf{s}_n, \mathbf{k}'\mathbf{s}'_n)\delta N$, or to the *differential scattering cross-section*

$$\frac{d^2\sigma}{dEd\Omega} = \frac{k'}{k} \left(\frac{M}{2\pi\hbar^2} \right)^2 \sum_{if} P_i |\langle \mathbf{s}_n; i | \mathcal{H}_{\text{int}}(\boldsymbol{\kappa}) | \mathbf{s}'_n; f \rangle|^2 \delta(\hbar\omega + E_i - E_f), \quad (4.1.4a)$$

where

$$\mathcal{H}_{\text{int}}(\boldsymbol{\kappa}) = \int \mathcal{H}_{\text{int}} e^{-i\boldsymbol{\kappa}\cdot\mathbf{r}_n} d\mathbf{r}_n. \quad (4.1.4b)$$

This result of time-dependent perturbation theory, in the first Born approximation, is accurate because of the very weak interaction between the neutrons and the constituents of the sample.

In order to proceed further, it is necessary to specify the interaction Hamiltonian \mathcal{H}_{int} . The magnetic moment of the neutron is

$$\boldsymbol{\mu}_n = -g_n\mu_N\mathbf{s}_n \quad ; \quad g_n = 3.827 \quad ; \quad \mu_N = \frac{m}{M}\mu_B = \frac{e\hbar}{2Mc},$$

with $s_n = \frac{1}{2}$. In this chapter, in the interest of conformity with the rest of the literature, we do not reverse the signs of the electronic angular-momentum vectors, which are therefore antiparallel to the corresponding magnetic moments, as is also the case for the neutron.

This magnetic dipole moment at \mathbf{r}_n gives rise to a vector potential, at the position \mathbf{r}_e ,

$$\mathbf{A}_n(\mathbf{r}_e, \mathbf{r}_n) = \mathbf{A}_n(\mathbf{r} = \mathbf{r}_e - \mathbf{r}_n) = \boldsymbol{\mu}_n \times \mathbf{r}/r^3,$$

with $r = |\mathbf{r}|$. The magnetic-interaction Hamiltonian for a neutron at \mathbf{r}_n with a single electron of charge $-e$, with coordinate \mathbf{r}_e , momentum \mathbf{p} , and spin \mathbf{s} is

$$\begin{aligned} \mathcal{H}_{\text{int}}(\mathbf{r}_e, \mathbf{r}_n) &= \frac{1}{2m} \left(\mathbf{p} + \frac{e}{c}(\mathbf{A}_n + \mathbf{A}_e) \right)^2 - \frac{1}{2m} \left(\mathbf{p} + \frac{e}{c}\mathbf{A}_e \right)^2 + 2\mu_B \mathbf{s} \cdot \mathbf{B}_n \\ &= 2\mu_B \left(\frac{1}{\hbar} \mathbf{A}_n \cdot \mathbf{p}' + \mathbf{s} \cdot (\nabla \times \mathbf{A}_n) \right), \end{aligned} \quad (4.1.5)$$

neglecting the diamagnetic term of second order in μ_N . \mathbf{A}_e denotes the additional contribution to the total vector potential from the surrounding electrons, or an external magnetic field. The prime on \mathbf{p} only plays a role if \mathbf{A}_e is non-zero, in which case $\mathbf{p}' = \mathbf{p} + \frac{e}{c}\mathbf{A}_e$. We note that \mathbf{A}_n commutes with \mathbf{p}' , because $\nabla_e \cdot \mathbf{A}_n = \nabla \cdot \mathbf{A}_n$ and

$$\nabla \cdot \mathbf{A}_n(\mathbf{r}) = \nabla \cdot \left\{ -\boldsymbol{\mu}_n \times \nabla\left(\frac{1}{r}\right) \right\} = \boldsymbol{\mu}_n \cdot \nabla \times \nabla\left(\frac{1}{r}\right) = 0,$$

recalling that $\mathbf{r}/r^3 = -\nabla\left(\frac{1}{r}\right)$.

The Fourier transform of \mathbf{A}_n with respect to the neutron coordinate, defining $\mathbf{x} = \mathbf{r}_n - \mathbf{r}_e$, is

$$\begin{aligned} \int \mathbf{A}_n(\mathbf{r}_e - \mathbf{r}_n) e^{-i\boldsymbol{\kappa} \cdot \mathbf{r}_n} d\mathbf{r}_n &= e^{-i\boldsymbol{\kappa} \cdot \mathbf{r}_e} \int \mathbf{A}_n(-\mathbf{x}) e^{-i\boldsymbol{\kappa} \cdot \mathbf{x}} d\mathbf{x} \\ &= -e^{-i\boldsymbol{\kappa} \cdot \mathbf{r}_e} \int (\boldsymbol{\mu}_n \times \mathbf{x}) x^{-3} e^{-i\boldsymbol{\kappa} \cdot \mathbf{x}} d\mathbf{x} = -e^{-i\boldsymbol{\kappa} \cdot \mathbf{r}_e} \frac{4\pi}{i\boldsymbol{\kappa}} \boldsymbol{\mu}_n \times \hat{\boldsymbol{\kappa}}, \end{aligned}$$

where $\hat{\boldsymbol{\kappa}}$ is a unit vector along $\boldsymbol{\kappa}$ (the integration is performed straightforwardly in spherical coordinates). Applying Green's theorem and assuming V to be a sphere of radius r ,

$$\int \nabla \times (e^{-i\boldsymbol{\kappa} \cdot \mathbf{x}} \mathbf{A}_n(\mathbf{x})) d\mathbf{x} \propto (\boldsymbol{\kappa} r)^{-1} \rightarrow 0 \quad \text{for } r \rightarrow \infty,$$

from which we deduce

$$\begin{aligned} \int (\nabla \times \mathbf{A}_n(\mathbf{x})) e^{-i\boldsymbol{\kappa} \cdot \mathbf{x}} d\mathbf{x} &= - \int (\nabla e^{-i\boldsymbol{\kappa} \cdot \mathbf{x}}) \times \mathbf{A}_n(\mathbf{x}) d\mathbf{x} \\ &= i\boldsymbol{\kappa} \times \int e^{-i\boldsymbol{\kappa} \cdot \mathbf{x}} \mathbf{A}_n(\mathbf{x}) d\mathbf{x} = 4\pi \hat{\boldsymbol{\kappa}} \times \boldsymbol{\mu}_n \times \hat{\boldsymbol{\kappa}} \end{aligned}$$

(we note that $\nabla \times \mathbf{A}_n(\mathbf{r}) = \nabla_{(\mathbf{x})} \times \mathbf{A}_n(\mathbf{x})$). From these results, we obtain

$$\begin{aligned} \mathcal{H}_{\text{int}}(\boldsymbol{\kappa}) &= \int \mathcal{H}_{\text{int}}(\mathbf{r}_e, \mathbf{r}_n) e^{-i\boldsymbol{\kappa} \cdot \mathbf{r}_n} d\mathbf{r}_n \\ &= 2\mu_B e^{-i\boldsymbol{\kappa} \cdot \mathbf{r}_e} 4\pi \left(\frac{i}{\hbar\boldsymbol{\kappa}} \boldsymbol{\mu}_n \times \hat{\boldsymbol{\kappa}} \cdot \mathbf{p}' + \mathbf{s} \cdot (\hat{\boldsymbol{\kappa}} \times \boldsymbol{\mu}_n \times \hat{\boldsymbol{\kappa}}) \right), \end{aligned}$$

or

$$\mathcal{H}_{\text{int}}(\boldsymbol{\kappa}) = 8\pi\mu_B \boldsymbol{\mu}_n \cdot \left(\frac{i}{\hbar\boldsymbol{\kappa}} \hat{\boldsymbol{\kappa}} \times \mathbf{p}' + \hat{\boldsymbol{\kappa}} \times \mathbf{s} \times \hat{\boldsymbol{\kappa}} \right) e^{-i\boldsymbol{\kappa} \cdot \mathbf{r}_e}. \quad (4.1.6)$$

$\hat{\boldsymbol{\kappa}} \times \mathbf{p}'$ commutes with $\boldsymbol{\kappa} \cdot \mathbf{r}_e$ and therefore also with $\exp(-i\boldsymbol{\kappa} \cdot \mathbf{r}_e)$, and we have made use of the identity $\hat{\boldsymbol{\kappa}} \times \mathbf{a} \times \hat{\boldsymbol{\kappa}} = \mathbf{a} - (\hat{\boldsymbol{\kappa}} \cdot \mathbf{a})\hat{\boldsymbol{\kappa}}$.

For discussing the rare earths, we may restrict ourselves to the case of electrons localized around the lattice sites in a crystal. Further, we define $\mathbf{r}_e = \tilde{\mathbf{R}}_j + \mathbf{r}$, with \mathbf{r} now being the relative position of the electron belonging to the j th atom at the position $\tilde{\mathbf{R}}_j$. Equation (4.1.6) may then be written

$$\mathcal{H}_{\text{int}}(\boldsymbol{\kappa}) = 8\pi\mu_B \boldsymbol{\mu}_n \cdot (\mathbf{Q}_p + \mathbf{Q}_s) e^{-i\boldsymbol{\kappa} \cdot \tilde{\mathbf{R}}_j}, \quad (4.1.7a)$$

introducing

$$\mathbf{Q}_p = \frac{i}{\hbar\kappa} \hat{\boldsymbol{\kappa}} \times \mathbf{p}' e^{-i\boldsymbol{\kappa} \cdot \mathbf{r}} \quad ; \quad \mathbf{Q}_s = \hat{\boldsymbol{\kappa}} \times \mathbf{s} \times \hat{\boldsymbol{\kappa}} e^{-i\boldsymbol{\kappa} \cdot \mathbf{r}}. \quad (4.1.7b)$$

In order to calculate the matrix element $\langle i | \mathbf{Q}_{p,s} | f \rangle$, the factor $\exp(-i\boldsymbol{\kappa} \cdot \mathbf{r})$ is expanded in spherical Bessel functions $j_n(\rho)$, and with $\rho = \kappa r$ and $\cos\theta = \boldsymbol{\kappa} \cdot \mathbf{r}/\rho$,

$$\begin{aligned} e^{-i\boldsymbol{\kappa} \cdot \mathbf{r}} &= \sum_{n=0}^{\infty} (2n+1) (-i)^n j_n(\rho) P_n(\cos\theta) \\ &\simeq j_0(\rho) - 3i j_1(\rho) \cos\theta = j_0(\rho) - i\boldsymbol{\kappa} \cdot \mathbf{r} \{j_0(\rho) + j_2(\rho)\}, \end{aligned} \quad (4.1.8)$$

using $j_n(\rho) = \rho\{j_{n-1}(\rho) + j_{n+1}(\rho)\}/(2n+1)$. The truncation of the series is valid for small values of ρ , where

$$j_n(\rho) = (\rho^n/(2n+1)!!)\{1 - \rho^2/(4n+6) + \dots\}.$$

We note that, although $\boldsymbol{\kappa} \times \mathbf{p}'$ commutes with $\exp(-i\boldsymbol{\kappa} \cdot \mathbf{r})$, it does not commute with the individual terms in (4.1.8). Introducing this expansion in the expression for \mathbf{Q}_p , we find

$$\mathbf{Q}_p = \hat{\boldsymbol{\kappa}} \times \left(\frac{i}{\hbar\kappa} j_0(\rho) \mathbf{p}' + \frac{1}{\hbar} \{j_0(\rho) + j_2(\rho)\} (\hat{\boldsymbol{\kappa}} \cdot \mathbf{r}) \mathbf{p}' + \dots \right),$$

which can be rearranged to read

$$\mathbf{Q}_p = \frac{1}{2} \{j_0(\rho) + j_2(\rho)\} \hat{\boldsymbol{\kappa}} \times \mathbf{l}' \times \hat{\boldsymbol{\kappa}} + \mathbf{Q}'_p. \quad (4.1.9a)$$

We have defined

$$\mathbf{Q}'_p = \hat{\boldsymbol{\kappa}} \times \left(\frac{i}{\hbar\kappa} j_0(\rho) \mathbf{p}' + \frac{1}{2\hbar} \{j_0(\rho) + j_2(\rho)\} \{(\hat{\boldsymbol{\kappa}} \cdot \mathbf{r}) \mathbf{p}' + (\hat{\boldsymbol{\kappa}} \cdot \mathbf{p}') \mathbf{r}\} + \dots \right), \quad (4.1.9b)$$

where the orbital momentum $\hbar\mathbf{l} = \mathbf{r} \times \mathbf{p}$ and $\hbar\mathbf{l}' = \hbar\mathbf{l} + \frac{e}{c} \mathbf{r} \times \mathbf{A}_e$, and used

$$\hat{\boldsymbol{\kappa}} \times \hbar\mathbf{l}' \times \hat{\boldsymbol{\kappa}} = -\hat{\boldsymbol{\kappa}} \times \{\hat{\boldsymbol{\kappa}} \times (\mathbf{r} \times \mathbf{p}')\} = \hat{\boldsymbol{\kappa}} \times \{(\hat{\boldsymbol{\kappa}} \cdot \mathbf{r}) \mathbf{p}' - (\hat{\boldsymbol{\kappa}} \cdot \mathbf{p}') \mathbf{r}\},$$

where $[\mathbf{l}', j_n(\rho)] = \mathbf{0}$ and $[\hat{\boldsymbol{\kappa}} \times \mathbf{r}, \hat{\boldsymbol{\kappa}} \cdot \mathbf{p}'] = \mathbf{0}$.

If \mathcal{H} is defined to be the Hamiltonian for the electron, then

$$\mathbf{p}' = \mathbf{p} + \frac{e}{c} \mathbf{A}_e = m \, d\mathbf{r}/dt = m \frac{i}{\hbar} [\mathcal{H}, \mathbf{r}],$$

and \mathbf{Q}'_p may be written

$$\mathbf{Q}'_p = \frac{m}{\hbar^2 \kappa} \hat{\boldsymbol{\kappa}} \times \left(-j_0(\rho) [\mathcal{H}, \mathbf{r}] + \frac{i\kappa}{2} \{j_0(\rho) + j_2(\rho)\} [\mathcal{H}, (\hat{\boldsymbol{\kappa}} \cdot \mathbf{r})\mathbf{r}] + \dots \right). \quad (4.1.10)$$

Considering an arbitrary operator \hat{A} , we have

$$\langle i | [\mathcal{H}, \hat{A}] | f \rangle = \langle i | \mathcal{H}\hat{A} - \hat{A}\mathcal{H} | f \rangle = (E_i - E_f) \langle i | \hat{A} | f \rangle,$$

which implies that \mathbf{Q}'_p does not contribute to the cross-section (4.1.4) in the limit $\boldsymbol{\kappa} \rightarrow \mathbf{0}$. In this limit, $j_n(0) = \delta_{n0}$ and, utilizing the energy δ -function in (4.1.4), the contribution to the cross section due to \mathbf{Q}'_p is seen to be proportional to

$$\left| \frac{m}{\hbar^2 \kappa} \hbar\omega \hat{\boldsymbol{\kappa}} \times \langle i | \mathbf{r} | f \rangle \right|^2 \rightarrow 0 \quad \text{for } \kappa \rightarrow 0,$$

since $|\hbar\omega| \leq (\hbar\kappa)^2/2M$. Introducing the vector operator $\mathbf{K}(\boldsymbol{\kappa})$, defined so that

$$\langle i | \hat{\boldsymbol{\kappa}} \times \mathbf{K} \times \hat{\boldsymbol{\kappa}} | f \rangle = \langle i | \mathbf{Q}_p + \mathbf{Q}_s | f \rangle, \quad (4.1.11)$$

we find, neglecting \mathbf{Q}'_p in the limit $\kappa \rightarrow 0$,

$$2\mu_B \mathbf{K}(\mathbf{0}) = \mu_B \left(\mathbf{1} + \frac{e}{\hbar c} \mathbf{r} \times \mathbf{A}_e + 2\mathbf{s} \right) \equiv -\boldsymbol{\mu}_e, \quad (4.1.12a)$$

or

$$\mathcal{H}_{\text{int}}(\mathbf{0}) = -4\pi \boldsymbol{\mu}_n \cdot (\hat{\boldsymbol{\kappa}} \times \boldsymbol{\mu}_e \times \hat{\boldsymbol{\kappa}}), \quad (4.1.12b)$$

implying that the magnetic cross-section (4.1.4), in the limit where the scattering vector approaches zero, is determined by the magnetic dipole moment $\boldsymbol{\mu}_e$ of the electron. In the treatment given above, we have included the diamagnetic contribution to $\boldsymbol{\mu}_e$, induced by external fields $\propto \mathbf{A}_e$. This term may however normally be neglected, as we shall do from now on.

At non-zero κ , we cannot employ directly the above procedure for obtaining an upper bound on the \mathbf{Q}'_p matrix-element, because $j_n(\rho)$ does not commute with \mathcal{H} . However, if we restrict ourselves to scattering processes in which the l quantum number is conserved, the matrix element of the first term in (4.1.10) vanishes identically, because $j_0(\rho)$ and \mathcal{H}

are both diagonal with respect to l , whereas \mathbf{r} has no diagonal elements (cf. the electric-dipole selection rule $\Delta l = \pm 1$). In the second term of (4.1.10) we can, to leading order, replace \mathcal{H} by the kinetic-energy operator and, if we also make the assumption $\Delta l = 0$, this term transforms like a second-rank tensor and so is quadrupolar. Symmetrizing \mathbf{Q}'_p with respect to the expansion in spherical Bessel functions, and taking $(\hat{\boldsymbol{\kappa}} \cdot \hat{\mathbf{r}})\hat{\mathbf{r}}$ outside the commutator, which is allowed because $\Delta l = 0$, we can write the second term in (4.1.10) as

$$(\hat{\boldsymbol{\kappa}} \times \hat{\mathbf{r}})(\hat{\boldsymbol{\kappa}} \cdot \hat{\mathbf{r}}) Q_r,$$

with $\hat{\mathbf{r}} = \mathbf{r}/r$ and

$$Q_r = Q_r^\dagger = -\frac{i}{8} \left(\{j_0(\rho) + j_2(\rho)\} [\nabla^2, r^2] + [\nabla^2, r^2] \{j_0(\rho) + j_2(\rho)\} \right).$$

Thus the second term is a product of an angular and a radial operator, which are both Hermitian. Our next assumption is that the radial part of the wavefunction, as specified by the principal quantum number \tilde{n} , and by l , is the same in the initial and the final state, i.e. that both \tilde{n} and l are unchanged. In this case, $\langle i | Q_r | f \rangle = \langle \tilde{n}l | Q_r | \tilde{n}l \rangle$ vanishes identically, because Q_r is an imaginary Hermitian operator; $Q_r = Q_r^\dagger = -Q_r^*$. If the radial part of the wavefunction is changed in the scattering process, or if \mathcal{H} is not diagonal in l , then the quadrupole moment leads to an imaginary contribution to $\mathbf{K}(\boldsymbol{\kappa})$, and gives a contribution to the cross-section proportional to κ^2 . In most cases of interest, however, this term is very small.

The assumption that $|i\rangle$ and $|f\rangle$ are linear combinations of the states $|(\tilde{n}ls)m_l m_s\rangle$, where $(\tilde{n}ls)$ is constant, implies that the two lowest-order terms in the expansion of Q'_p in (4.1.9b) or (4.1.10) can be neglected. Furthermore, the radial and angular dependences are then factorized, both in the expansion of the operators and in the wavefunctions, so that the radial part of the matrix elements may be calculated separately. Hence the orbital contribution \mathbf{K}_p to \mathbf{K} is approximately

$$\mathbf{K}_p(\boldsymbol{\kappa}) = \frac{1}{2} \{ \langle j_0(\kappa) \rangle + \langle j_2(\kappa) \rangle \} \mathbf{1}, \quad (4.1.13a)$$

with

$$\langle j_n(\kappa) \rangle = \int_0^\infty r^2 R^2(r) j_n(\kappa r) dr \quad ; \quad \int_0^\infty r^2 R^2(r) dr = 1, \quad (4.1.13b)$$

where $R(r)$ is the normalized radial wavefunction. The assumption that the final and initial states have the same parity implies that only the terms in the expansion (4.1.8) for which n is odd may contribute to \mathbf{K}_p . By the same argument, the spin part \mathbf{K}_s of \mathbf{K} only involves the terms

in (4.1.8) with n even. Neglecting the ($n = 2$)-term in \mathbf{K}_s , proportional to \mathbf{s} times an orbital quadrupole moment, we have $\mathbf{K}_s(\boldsymbol{\kappa}) \simeq \langle j_0(\kappa) \rangle \mathbf{s}$, or

$$\mathbf{K}(\boldsymbol{\kappa}) = \mathbf{K}(\kappa) = \frac{1}{2} \langle j_0(\kappa) \rangle (\mathbf{1} + 2\mathbf{s}) + \frac{1}{2} \langle j_2(\kappa) \rangle \mathbf{l}. \quad (4.1.14)$$

This result for $\mathbf{K}(\boldsymbol{\kappa})$ is the basis of the dipole approximation for the scattering cross-section. Within this approximation, it is straightforwardly generalized to the case of more than one electron per atom, as the contributions are additive, in the sense that \mathbf{l} and \mathbf{s} are replaced by $\mathbf{L} = \sum \mathbf{l}$ and $\mathbf{S} = \sum \mathbf{s}$, and $R^2(r)$ by the normalized distribution for all unpaired electrons belonging to the atom at $\tilde{\mathbf{R}}_j$.

The orbital contribution is important in the case of rare earth or actinide ions. In transition-metal ions, the orbital momentum is frequently quenched, and \mathbf{K}_p may then be neglected to leading order. In the rare earths, the spin-orbit coupling is strong and only matrix elements within the ground-state multiplet of $\mathbf{J}^2 = (\mathbf{L} + \mathbf{S})^2$ contribute. In this case, as discussed in Section 1.2, $\mathbf{L} + 2\mathbf{S} = g\mathbf{J}$ and $\mathbf{L} = (2 - g)\mathbf{J}$, where g is the Landé factor, and we have

$$\mathbf{K}(\boldsymbol{\kappa}) = \frac{1}{2} \langle j_0(\kappa) \rangle (\mathbf{L} + 2\mathbf{S}) + \frac{1}{2} \langle j_2(\kappa) \rangle \mathbf{L} = \frac{1}{2} g F(\kappa) \mathbf{J}, \quad (4.1.15a)$$

where $F(\kappa)$ is the *form factor*

$$F(\kappa) = \langle j_0(\kappa) \rangle + \frac{1}{g} (2 - g) \langle j_2(\kappa) \rangle, \quad (4.1.15b)$$

defined so that $F(0) = 1$. When the spin-orbit interaction is introduced, the ($n = 2$)-term in the expansion of \mathbf{K}_s gives a contribution to the dipolar part of $\mathbf{K}(\boldsymbol{\kappa})$ proportional to $\langle j_2(\kappa) \rangle$, but this is an order of magnitude smaller than the orbital term in (4.1.14). A more systematic approach, making extensive use of Racah tensor-algebra, is required to calculate this term and to include the contributions of the higher-rank multipoles produced by the expansion of $\exp(-i\boldsymbol{\kappa} \cdot \mathbf{r})$. This analysis may be found in Marshall and Lovesey (1971), Stassis and Deckman (1975, 1976), and references therein. Within the present approximation, only tensors of *odd* rank give a contribution to \mathbf{K} , proportional to $\kappa^{\tau-1}$, where τ is the rank of the tensors (terms with $\tau = 3$ appear already in order κ^2). In contrast to the dipole contributions, the higher-rank tensor couplings give rise to an angular dependence of $\mathbf{K} = \mathbf{K}(\boldsymbol{\kappa})$. The smaller the scattering wavelength $\lambda = 2\pi/\kappa$, the more the neutron senses the details of the spin and current distributions within the atom, but as long as λ is larger than approximately the mean radius $\langle r \rangle$ of the unpaired electrons, only the dipolar scattering is important. For rare earth ions, $\langle r \rangle \approx 0.6 \text{ \AA}$, indicating that (4.1.15) is a valid approximation as long as κ is smaller than about 6 \AA^{-1} .

Experimental studies of the form factor and the associated moment densities have been reviewed by Sinha (1978). For an accurate interpretation of the data, it is generally necessary to proceed beyond the dipole approximation. In the heavy rare earths, the deduced $4f$ densities are in good agreement with atomic calculations, provided that relativistic effects are included, but the conduction-electron distributions are much less certain. In the light elements, crystal-field effects become important, as observed for example in Pr and Nd by Lebeck *et al.* (1979). Of especial interest is Sm, where the opposition of spin and orbital moments leads to a form factor which has its maximum at a non-zero κ , and the conduction-electron polarization seems to be very strong (Koehler and Moon 1972).

Labelling quantities pertaining to the j th atom with the index j , and summing over all the atoms in the sample, we find that the total $\mathcal{H}_{\text{int}}(\boldsymbol{\kappa})$ (4.1.7), in the dipole approximation, is given by

$$\mathcal{H}_{\text{int}}(\boldsymbol{\kappa}) = 8\pi\mu_B \sum_j \left\{ \frac{1}{2} g F(\kappa) \right\}_j e^{-i\boldsymbol{\kappa} \cdot \tilde{\mathbf{R}}_j} \boldsymbol{\mu}_n \cdot (\hat{\boldsymbol{\kappa}} \times \mathbf{J}_j \times \hat{\boldsymbol{\kappa}}).$$

The squared matrix element in (4.1.4) may furthermore be written

$$\langle \mathbf{s}_n; i | \mathcal{H}_{\text{int}}(\boldsymbol{\kappa}) | \mathbf{s}'_n; f \rangle \langle \mathbf{s}'_n; f | \mathcal{H}_{\text{int}}(-\boldsymbol{\kappa}) | \mathbf{s}_n; i \rangle.$$

We shall only consider the cross-section for unpolarized neutrons, so that we sum over all the spin states $|\mathbf{s}'_n\rangle$ of the scattered neutrons, and average over the spin-states $|\mathbf{s}_n\rangle$, with the distribution P_s , of the incoming neutrons. With an equal distribution of up and down spins, $P_s = \frac{1}{2}$, and introducing $\mathbf{Q}_j = \hat{\boldsymbol{\kappa}} \times \mathbf{J}_j \times \hat{\boldsymbol{\kappa}}$, we find that the cross-section is proportional to

$$\begin{aligned} & \sum_{\mathbf{s}_n \mathbf{s}'_n} P_s \langle \mathbf{s}_n | \boldsymbol{\mu}_n \cdot \mathbf{Q}_j | \mathbf{s}'_n \rangle \langle \mathbf{s}'_n | \boldsymbol{\mu}_n \cdot \mathbf{Q}_{j'} | \mathbf{s}_n \rangle \\ &= \sum_{\mathbf{s}} P_s \langle \mathbf{s}_n | (\boldsymbol{\mu}_n \cdot \mathbf{Q}_j) (\boldsymbol{\mu}_n \cdot \mathbf{Q}_{j'}) | \mathbf{s}_n \rangle = \left(\frac{1}{2} g_n \mu_N \right)^2 \mathbf{Q}_j \cdot \mathbf{Q}_{j'}, \end{aligned}$$

as may readily be shown by using the Pauli-matrix representation, in which $\text{Tr}\{\sigma_\alpha \sigma_\beta\} = 2\delta_{\alpha\beta}$. We have further that $\mathbf{Q}_j \cdot \mathbf{Q}_{j'}$ may be written

$$\begin{aligned} & (\hat{\boldsymbol{\kappa}} \times \mathbf{J}_j \times \hat{\boldsymbol{\kappa}}) \cdot (\hat{\boldsymbol{\kappa}} \times \mathbf{J}_{j'} \times \hat{\boldsymbol{\kappa}}) = (\mathbf{J}_j - \hat{\boldsymbol{\kappa}}(\mathbf{J}_j \cdot \hat{\boldsymbol{\kappa}})) \cdot (\mathbf{J}_{j'} - \hat{\boldsymbol{\kappa}}(\mathbf{J}_{j'} \cdot \hat{\boldsymbol{\kappa}})) \\ &= \mathbf{J}_j \cdot \mathbf{J}_{j'} - (\mathbf{J}_j \cdot \hat{\boldsymbol{\kappa}})(\mathbf{J}_{j'} \cdot \hat{\boldsymbol{\kappa}}) = \sum_{\alpha\beta} (\delta_{\alpha\beta} - \hat{\kappa}_\alpha \hat{\kappa}_\beta) J_{j\alpha} J_{j'\beta}, \end{aligned}$$

in terms of the Cartesian components. Defining $(\mathbf{J}_\perp)_j$ to be the projection of \mathbf{J}_j on the plane perpendicular to $\boldsymbol{\kappa}$, we have

$$\sum_{\alpha\beta} (\delta_{\alpha\beta} - \hat{\kappa}_\alpha \hat{\kappa}_\beta) J_{j\alpha} J_{j'\beta} = (\mathbf{J}_\perp)_j \cdot (\mathbf{J}_\perp)_{j'}.$$

The various factors in these expressions may be combined to give

$$\frac{k'}{k} \left(\frac{M}{2\pi\hbar^2} 8\pi\mu_B \frac{1}{2} g_n \mu_N \right)^2 = \frac{k'}{k} \left(\frac{\hbar\gamma e^2}{mc^2} \right)^2 \quad ; \quad \gamma = \frac{1}{2\hbar} g_n.$$

γ is the gyromagnetic ratio of the neutron, and $e^2/mc^2 = 2.82$ fm is the classical electron radius. The differential cross-section, in the dipole approximation, for the scattering of unpolarized neutrons is then finally

$$\begin{aligned} \frac{d^2\sigma}{dE d\Omega} &= \frac{k'}{k} \left(\frac{\hbar\gamma e^2}{mc^2} \right)^2 \sum_{\alpha\beta} (\delta_{\alpha\beta} - \hat{\kappa}_\alpha \hat{\kappa}_\beta) \sum_{jj'} \left\{ \frac{1}{2} g F(\kappa) \right\}_j \left\{ \frac{1}{2} g F(\kappa) \right\}_{j'} \\ &\times \sum_{if} P_i \langle i | J_{j\alpha} e^{-i\kappa \cdot \tilde{\mathbf{R}}_j} | f \rangle \langle f | J_{j'\beta} e^{i\kappa \cdot \tilde{\mathbf{R}}_{j'}} | i \rangle \delta(\hbar\omega + E_i - E_f), \end{aligned} \quad (4.1.16)$$

where the total magnetic cross-section is $4\pi(\hbar\gamma e^2/mc^2)^2 = 3.65$ barns.

4.2 Elastic and inelastic neutron scattering

If the scattering system is assumed to be in thermal equilibrium at temperature T , the average over initial states in (4.1.16) is the same as the thermal average $\langle \dots \rangle = \text{Tr}\{\rho_0 \dots\}$, where ρ_0 is the density operator defined in eqn (3.1.1). The atom at the position $\tilde{\mathbf{R}}_j = \mathbf{R}_j + \mathbf{u}_j$ vibrates around its equilibrium position, the lattice point \mathbf{R}_j , and we may write

$$\langle e^{-i\kappa \cdot (\tilde{\mathbf{R}}_j - \tilde{\mathbf{R}}_{j'})} \rangle = e^{-2W(\kappa)} e^{-i\kappa \cdot (\mathbf{R}_j - \mathbf{R}_{j'})},$$

where $W(\kappa)$ is the *Debye-Waller factor* $\approx \frac{1}{6}\kappa^2 \langle u^2 \rangle$, discussed in detail by, for example, Marshall and Lovesey (1971). We insert this term in (4.1.16), and thereby neglect contributions from inelastic phonon-scattering processes, the so-called magneto-vibrational part of the magnetic cross-section. The integral representation of the δ -function is

$$\delta(\hbar\omega + E_i - E_f) = \frac{1}{2\pi\hbar} \int_{-\infty}^{\infty} e^{i(\hbar\omega + E_i - E_f)t/\hbar} dt,$$

which allows us to write

$$\begin{aligned} &\sum_{if} P_i \langle i | J_{j\alpha} | f \rangle \langle f | J_{j'\beta} | i \rangle \delta(\hbar\omega + E_i - E_f) \\ &= \sum_{if} \frac{1}{2\pi\hbar} \int_{-\infty}^{\infty} dt e^{i\omega t} P_i \langle i | e^{i\hbar t/\hbar} J_{j\alpha} e^{-i\hbar t/\hbar} | f \rangle \langle f | J_{j'\beta} | i \rangle \\ &= \frac{1}{2\pi\hbar} \int_{-\infty}^{\infty} dt e^{i\omega t} \sum_i P_i \langle i | J_{j\alpha}(t) J_{j'\beta}(0) | i \rangle \\ &= \frac{1}{2\pi\hbar} \int_{-\infty}^{\infty} dt e^{i\omega t} \langle J_{j\alpha}(t) J_{j'\beta}(0) \rangle, \end{aligned}$$

where $J_{j\alpha}(t)$ is the angular-momentum operator in the Heisenberg picture, as in (3.2.1),

$$J_{j\alpha}(t) = e^{i\mathcal{H}t/\hbar} J_{j\alpha} e^{-i\mathcal{H}t/\hbar}.$$

At thermal equilibrium, the differential cross-section can then be written

$$\begin{aligned} \frac{d^2\sigma}{dEd\Omega} = & \frac{k'}{k} \left(\frac{\hbar\gamma e^2}{mc^2} \right)^2 e^{-2W(\kappa)} \sum_{\alpha\beta} (\delta_{\alpha\beta} - \hat{\kappa}_\alpha \hat{\kappa}_\beta) \sum_{jj'} \left\{ \frac{1}{2} g F(\boldsymbol{\kappa}) \right\}_j \left\{ \frac{1}{2} g F(-\boldsymbol{\kappa}) \right\}_{j'} \\ & \times \frac{1}{2\pi\hbar} \int_{-\infty}^{\infty} dt e^{i\omega t} e^{-i\boldsymbol{\kappa}\cdot(\mathbf{R}_j - \mathbf{R}_{j'})} \langle J_{j\alpha}(t) J_{j'\beta}(0) \rangle. \end{aligned} \quad (4.2.1)$$

If the magnetic atoms are all identical, the form factor may be taken outside the summation and the cross-section reduces to

$$\frac{d^2\sigma}{dEd\Omega} = N \frac{k'}{k} \left(\frac{\hbar\gamma e^2}{mc^2} \right)^2 e^{-2W(\kappa)} \left| \frac{1}{2} g F(\boldsymbol{\kappa}) \right|^2 \sum_{\alpha\beta} (\delta_{\alpha\beta} - \hat{\kappa}_\alpha \hat{\kappa}_\beta) \mathcal{S}^{\alpha\beta}(\boldsymbol{\kappa}, \omega), \quad (4.2.2a)$$

where we have introduced the *Van Hove scattering function* (Van Hove 1954)

$$\mathcal{S}^{\alpha\beta}(\boldsymbol{\kappa}, \omega) = \frac{1}{2\pi\hbar} \int_{-\infty}^{\infty} dt e^{i\omega t} \frac{1}{N} \sum_{jj'} e^{-i\boldsymbol{\kappa}\cdot(\mathbf{R}_j - \mathbf{R}_{j'})} \langle J_{j\alpha}(t) J_{j'\beta}(0) \rangle, \quad (4.2.2b)$$

which is $(2\pi\hbar)^{-1}$ times the Fourier transform, in space and time, of the pair-correlation function $\langle J_{j\alpha}(t) J_{j'\beta}(0) \rangle$. If $\langle J_{j\alpha} \rangle \langle J_{j'\beta} \rangle$ is added and subtracted, the scattering function may be written as the sum of a static and a dynamic contribution:

$$\mathcal{S}^{\alpha\beta}(\boldsymbol{\kappa}, \omega) = \mathcal{S}^{\alpha\beta}(\boldsymbol{\kappa}) + \mathcal{S}_d^{\alpha\beta}(\boldsymbol{\kappa}, \omega), \quad (4.2.3a)$$

where the static or *elastic* component is

$$\mathcal{S}^{\alpha\beta}(\boldsymbol{\kappa}) = \delta(\hbar\omega) \frac{1}{N} \sum_{jj'} \langle J_{j\alpha} \rangle \langle J_{j'\beta} \rangle e^{-i\boldsymbol{\kappa}\cdot(\mathbf{R}_j - \mathbf{R}_{j'})} \quad (4.2.3b)$$

and the *inelastic* contribution is

$$\mathcal{S}_d^{\alpha\beta}(\boldsymbol{\kappa}, \omega) = \frac{1}{2\pi\hbar} S_{\alpha\beta}(\boldsymbol{\kappa}, \omega) = \frac{1}{\pi} \frac{1}{1 - e^{-\beta\hbar\omega}} \chi''_{\alpha\beta}(\boldsymbol{\kappa}, \omega). \quad (4.2.3c)$$

We have introduced the dynamic correlation function $S_{\alpha\beta}(\boldsymbol{\kappa}, \omega)$, defined by eqn (3.2.13), with

$$\hat{\alpha} = N^{-\frac{1}{2}} \sum_j J_{j\alpha} e^{-i\boldsymbol{\kappa} \cdot \mathbf{R}_j} \quad \text{and} \quad \hat{\beta} = N^{-\frac{1}{2}} \sum_{j'} J_{j'\beta} e^{i\boldsymbol{\kappa} \cdot \mathbf{R}_{j'}},$$

and the corresponding susceptibility function $\chi_{\alpha\beta}(\boldsymbol{\kappa}, \omega)$, utilizing the relation between the two functions given by the fluctuation–dissipation theorem (3.2.18).

An important consequence of (4.2.2–3) is that the *inelastic scattering of neutrons* is proportional to the correlation function $S_{\alpha\beta}(\boldsymbol{\kappa}, \omega)$, which is essentially the Fourier transform of the probability that, if the moment at site j has some specified vector value at time zero, then the moment at site j' has some other specified value at time t . An inelastic neutron-scattering experiment is thus extremely informative about the dynamics of the magnetic system. Poles in the correlation function, or in $\chi_{\alpha\beta}(\boldsymbol{\kappa}, \omega)$, are reflected as peaks in the intensity of the scattered neutrons. According to (4.1.2) and (4.1.3), each neutron in such a scattering peak has imparted energy $\hbar\omega$ and momentum $\hbar\boldsymbol{\kappa}$ to the sample, so the peak is interpreted, depending on whether $\hbar\omega$ is positive or negative, as being due to the creation or annihilation of *quasi-particles* or *elementary excitations* in the system, with energy $|\hbar\omega|$ and crystal momentum $\hbar\mathbf{q} = \hbar(\boldsymbol{\kappa} - \boldsymbol{\tau})$, where $\boldsymbol{\tau}$ is a reciprocal lattice vector. A part of the momentum $\hbar\boldsymbol{\tau}$ may be transferred to the crystal as a whole. If the sample is a single crystal, with only one magnetic atom per unit cell, $S_{\alpha\beta}(\boldsymbol{\kappa}, \omega) = S_{\alpha\beta}(\mathbf{q} = \boldsymbol{\kappa} - \boldsymbol{\tau}, \omega)$, where $\boldsymbol{\tau}$ is normally chosen so that \mathbf{q} lies within the primitive Brillouin zone. The form factor in the scattering amplitude is not however invariant with respect to the addition of a reciprocal lattice vector. This interpretation of the poles in $S_{\alpha\beta}(\mathbf{q}, \omega)$ governs the choice of sign in the exponential arguments in both the temporal and the spatial Fourier transforms.

The relation (4.2.3c) between the scattering function and the generalized susceptibility implies that the neutron may be considered as a magnetic probe which effectively establishes a frequency- and wave-vector-dependent magnetic field in the scattering sample, and detects its response to this field. This is a particularly fruitful way of looking at a neutron scattering experiment because, as shown in Chapter 3, the susceptibility may be calculated from linear response theory, and thus provides a natural bridge between theory and experiment. Using the symmetry relation (3.2.15), which may here be written $\chi_{\alpha\beta}^*(\mathbf{q}, z) = \chi_{\alpha\beta}(-\mathbf{q}, -z^*)$, it is straightforward to show that $\chi_{\alpha\beta}''(\mathbf{q}, \omega) + \chi_{\beta\alpha}''(\mathbf{q}, \omega)$ is real and equal to $\text{Im}\{\chi_{\alpha\beta}(\mathbf{q}, \omega) + \chi_{\beta\alpha}(\mathbf{q}, \omega)\}$. In addition, the form of the inelastic cross-section, and also the result (3.3.2) for the dissipation rate, impose another analytic condition on the function $\chi_{\alpha\beta}''(\mathbf{q}, \omega) + \chi_{\beta\alpha}''(\mathbf{q}, \omega)$.

It must be either zero, or positive or negative with ω (such functions are called *herglotz functions*), because a negative value of the cross-section is clearly unphysical.

If the magnetic moments in a Bravais lattice are ordered in a static structure, described by the wave-vector \mathbf{Q} , we may write

$$\langle J_{j\alpha} \rangle = \frac{1}{2} (\langle J_\alpha \rangle e^{i\mathbf{Q}\cdot\mathbf{R}_j} + \langle J_\alpha \rangle^* e^{-i\mathbf{Q}\cdot\mathbf{R}_j}), \quad (4.2.4)$$

allowing $\langle J_\alpha \rangle$ to be complex in order to account for the phase. The static contribution to the cross-section is then proportional to

$$\begin{aligned} \sum_{\alpha\beta} (\delta_{\alpha\beta} - \hat{\kappa}_\alpha \hat{\kappa}_\beta) \mathcal{S}^{\alpha\beta}(\boldsymbol{\kappa}) &= \sum_{\alpha\beta} (\delta_{\alpha\beta} - \hat{\kappa}_\alpha \hat{\kappa}_\beta) \operatorname{Re} \{ \langle J_\alpha \rangle \langle J_\beta \rangle^* \} \\ &\times \delta(\hbar\omega) \frac{(2\pi)^3}{v} \sum_{\boldsymbol{\tau}} \frac{1}{4} (1 + \delta_{\mathbf{Q}0}) \{ \delta(\boldsymbol{\tau} + \mathbf{Q} - \boldsymbol{\kappa}) + \delta(\boldsymbol{\tau} - \mathbf{Q} - \boldsymbol{\kappa}) \}, \end{aligned} \quad (4.2.5)$$

where $\delta_{\mathbf{Q}0}$ is equal to 1 in the ferromagnetic case $\mathbf{Q} = \mathbf{0}$, and zero otherwise, and v is the volume of a unit cell. The magnetic ordering of the system leads to δ -function singularities in momentum space, corresponding to *magnetic Bragg scattering*, whenever the scattering vector is equal to $\pm\mathbf{Q}$ plus a reciprocal lattice vector $\boldsymbol{\tau}$. The static and dynamic contributions from $\mathcal{S}^{\alpha\beta}(\boldsymbol{\kappa})$ and $\mathcal{S}_d^{\alpha\beta}(\boldsymbol{\kappa}, \omega)$ to the total integrated scattering intensity may be comparable, but the dynamic contributions, including possibly a quasi-elastic diffusive term, are distributed more or less uniformly throughout reciprocal space. Consequently, the elastic component, determined by $\mathcal{S}^{\alpha\beta}(\boldsymbol{\kappa})$, in which the scattering is condensed into points in reciprocal space, is overwhelmingly the most intense contribution to the cross-section $d\sigma/d\Omega$, obtained from the differential cross-section (4.2.2a) by an energy integration:

$$\begin{aligned} \frac{d\sigma}{d\Omega} &\simeq N \left(\frac{\hbar\gamma e^2}{mc^2} \right)^2 e^{-2W(\boldsymbol{\kappa})} \left| \frac{1}{2} g F(\boldsymbol{\kappa}) \right|^2 \sum_{\alpha\beta} (\delta_{\alpha\beta} - \hat{\kappa}_\alpha \hat{\kappa}_\beta) \operatorname{Re} \{ \langle J_\alpha \rangle \langle J_\beta \rangle^* \} \\ &\times \frac{(2\pi)^3}{v} \sum_{\boldsymbol{\tau}} \frac{1}{4} (1 + \delta_{\mathbf{Q}0}) \{ \delta(\boldsymbol{\tau} + \mathbf{Q} - \boldsymbol{\kappa}) + \delta(\boldsymbol{\tau} - \mathbf{Q} - \boldsymbol{\kappa}) \}. \end{aligned} \quad (4.2.6)$$

$d\sigma/d\Omega$ is the cross-section measured in *neutron diffraction* experiments, in which all neutrons scattered in the direction of \mathbf{k}' are counted without energy discrimination, i.e. without the analyser crystal in Fig. 4.1. This kind of experiment is more straightforward to perform than one in which, for instance, only elastically scattered neutrons are counted. In the ordered phase, (4.2.6) is a good approximation, except close to a second-order phase transition, where $\langle J_\alpha \rangle$ is small and where *critical fluctuations*

may lead to strong inelastic or quasi-elastic scattering in the vicinity of the magnetic Bragg peaks.

Independently of whether the magnetic system is ordered or not, the total integrated scattering intensity in the Brillouin zone has a definite magnitude, determined by the size of the local moments and the following sum rule:

$$\begin{aligned}
 \frac{1}{N} \sum_{\mathbf{q}} \sum_{\alpha} \int_{-\infty}^{\infty} S^{\alpha\alpha}(\mathbf{q}, \omega) d(\hbar\omega) \\
 &= \frac{1}{N} \sum_j \sum_{\alpha} \langle J_{j\alpha} \rangle^2 + \frac{1}{N} \sum_{\mathbf{q}} \sum_{\alpha} S_{\alpha\alpha}(\mathbf{q}, t=0) \\
 &= \frac{1}{N} \sum_j \sum_{\alpha} \langle J_{j\alpha} J_{j\alpha} \rangle = J(J+1), \quad (4.2.7)
 \end{aligned}$$

and taking into account the relatively slow variation of the other parameters specifying the cross-section. This implies, for instance, that $d\sigma/d\Omega$ is non-zero in the paramagnetic phase, when $\langle J_{\alpha} \rangle = 0$, but the distribution of the available scattered intensity over all solid angles makes it hard to separate from the background. In this case, much more useful information may be obtained from the differential cross-section measured in an inelastic neutron-scattering experiment.

For a crystal with a basis of p magnetic atoms per unit cell, the ordering of the moments corresponding to (4.2.4) is

$$\langle J_{j_s\alpha} \rangle = \frac{1}{2} (\langle J_{s\alpha} \rangle e^{i\mathbf{Q}\cdot\mathbf{R}_{j_s}} + \langle J_{s\alpha} \rangle^* e^{-i\mathbf{Q}\cdot\mathbf{R}_{j_s}}), \quad (4.2.8a)$$

where

$$\mathbf{R}_{j_s} = \mathbf{R}_{j_0} + \mathbf{d}_s, \quad \text{with } s = 1, 2, \dots, p. \quad (4.2.8b)$$

Here \mathbf{R}_{j_0} specifies the position of the unit cell, and \mathbf{d}_s is the vector determining the equilibrium position of the s th atom in the unit cell. The summation over the atoms in (4.2.2) may be factorized as follows:

$$\begin{aligned}
 &\sum_{ij} e^{-i\boldsymbol{\kappa}\cdot(\mathbf{R}_i - \mathbf{R}_j)} \\
 &= \sum_{i_0 j_0} e^{-i\boldsymbol{\kappa}\cdot(\mathbf{R}_{i_0} - \mathbf{R}_{j_0})} \sum_{s=1}^p e^{-i\boldsymbol{\kappa}\cdot(\mathbf{R}_{i_s} - \mathbf{R}_{i_0})} \sum_{r=1}^p e^{i\boldsymbol{\kappa}\cdot(\mathbf{R}_{j_r} - \mathbf{R}_{j_0})} \\
 &= \sum_{i_0 j_0} e^{-i\boldsymbol{\kappa}\cdot(\mathbf{R}_{i_0} - \mathbf{R}_{j_0})} |F_G(\boldsymbol{\kappa})|^2 \quad ; \quad F_G(\boldsymbol{\kappa}) = \sum_{s=1}^p e^{-i\boldsymbol{\kappa}\cdot\mathbf{d}_s},
 \end{aligned}$$

where $F_G(\boldsymbol{\kappa})$ is the *geometric structure factor*. The elastic cross-section then becomes

$$\begin{aligned} \frac{d\sigma}{d\Omega} &= N_0 \left(\frac{\hbar\gamma e^2}{mc^2} \right)^2 e^{-2W(\boldsymbol{\kappa})} \left| \frac{1}{2} g F(\boldsymbol{\kappa}) \right|^2 \sum_{\alpha\beta} (\delta_{\alpha\beta} - \hat{\kappa}_\alpha \hat{\kappa}_\beta) |\langle J_\alpha \rangle \langle J_\beta \rangle| \times \\ &\frac{(2\pi)^3}{v} \sum_{\boldsymbol{\tau}} \frac{1}{4} (1 + \delta_{Q0}) \text{Re} \{ F_\alpha(\boldsymbol{\tau}) F_\beta^*(\boldsymbol{\tau}) \} \{ \delta(\boldsymbol{\tau} + \mathbf{Q} - \boldsymbol{\kappa}) + \delta(\boldsymbol{\tau} - \mathbf{Q} - \boldsymbol{\kappa}) \} \end{aligned} \quad (4.2.9a)$$

where N_0 is the number of unit cells, and the *structure factor* is

$$F_\alpha(\boldsymbol{\tau}) = |\langle J_\alpha \rangle|^{-1} \sum_{s=1}^r \langle J_{s\alpha} \rangle e^{-i\boldsymbol{\tau} \cdot \mathbf{d}_s}. \quad (4.2.9b)$$

As an example, we return to the Heisenberg ferromagnet discussed in Chapter 3. The magnitude of the ordered moments and their direction relative to the crystal lattice, defined to be the z -axis, may be determined by neutron diffraction, since

$$\frac{d\sigma}{d\Omega} = N \left(\frac{\hbar\gamma e^2}{mc^2} \right)^2 e^{-2W(\boldsymbol{\kappa})} \left| \frac{1}{2} g F(\boldsymbol{\kappa}) \right|^2 (1 - \hat{\kappa}_z^2) \langle S_z \rangle^2 \frac{(2\pi)^3}{v} \sum_{\boldsymbol{\tau}} \delta(\boldsymbol{\tau} - \boldsymbol{\kappa}). \quad (4.2.10)$$

The Bragg-peak intensity is thus proportional to the square of the ordered moment and to $\sin^2 \theta$, where θ is the angle between the magnetization and the scattering vector. The elastic scattering is therefore strongest when $\boldsymbol{\kappa} = \boldsymbol{\tau}$ is perpendicular to the magnetization. On the other hand, the inelastic scattering is strongest when the scattering vector $\boldsymbol{\kappa} = \mathbf{q} + \boldsymbol{\tau}$ is along the magnetization, in which case, from (3.4.11),

$$\begin{aligned} \sum_{\alpha\beta} (\delta_{\alpha\beta} - \hat{\kappa}_\alpha \hat{\kappa}_\beta) \mathcal{S}^{\alpha\beta}(\boldsymbol{\kappa}, \omega) &= \frac{1}{\pi} \frac{1}{1 - e^{-\beta\hbar\omega}} (\chi''_{xx}(\mathbf{q}, \omega) + \chi''_{yy}(\mathbf{q}, \omega)) \\ &= \langle S_z \rangle \frac{1}{1 - e^{-\beta\hbar\omega}} \{ \delta(\hbar\omega - E_{\mathbf{q}}) - \delta(\hbar\omega + E_{\mathbf{q}}) \} \\ &= \langle S_z \rangle \{ (n_{\mathbf{q}} + 1) \delta(\hbar\omega - E_{\mathbf{q}}) + n_{\mathbf{q}} \delta(\hbar\omega + E_{\mathbf{q}}) \}, \end{aligned} \quad (4.2.11)$$

where $n_{\mathbf{q}} = (e^{\beta E_{\mathbf{q}}} - 1)^{-1}$ is the Bose population factor. The magnon-scattering intensity is thus proportional to the ordered moment, and the *stimulated emission and absorption* of the boson excitations, i.e. the magnons, due to the neutron beam, are proportional respectively to $(n_{\mathbf{q}} + 1)$ and $n_{\mathbf{q}}$, which may be compared with the equivalent result for light scattering from a gas of atoms.

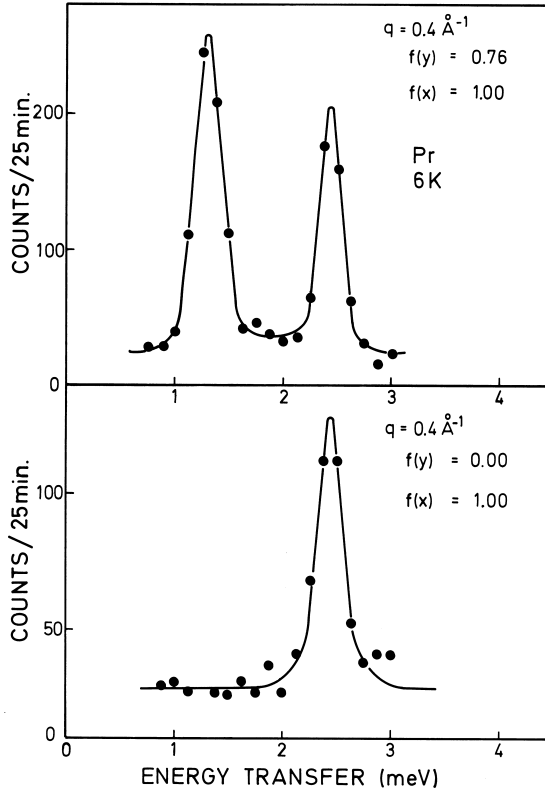


Fig. 4.2. A typical spectrum of inelastically-scattered neutrons in a constant- κ experiment, illustrating the determination of the dispersion relation and the polarization vector of the magnetic excitations. The peaks in the spectrum establish the energies of excitations which have a wave-vector \mathbf{q} , defined by the scattering vector through $\kappa = \mathbf{q} + \boldsymbol{\tau}$, and thus determine points on the dispersion relation for Pr, shown in Fig. 7.1. The cross-section is proportional to the factor $f(\alpha) = 1 - (\kappa_\alpha/\kappa)^2$. Since \mathbf{q} is along the ΓM (y)-axis, the absence of the peak of lower energy in the bottom figure shows unambiguously that it corresponds to a longitudinal mode.

The dependence of the intensity of inelastically scattered neutrons on the relative orientation of κ and the direction of the moment fluctuations is illustrated for the example of Pr in Fig. 4.2, which is discussed in more detail in Chapter 7. As in this figure, the scattering is normally measured as a function of $\hbar\omega$ at a fixed value of \mathbf{q} , a so-called *constant- \mathbf{q}* or *constant- κ scan*, but occasionally *constant-energy scans*

may also be employed. In an actual experiment the directions and the lengths of \mathbf{k} and \mathbf{k}' are only defined with a limited degree of accuracy, and the δ -functions occurring in (4.2.10–11) are broadened into peaks with the shape of the *instrumental resolution function*, which to a good approximation is a Gaussian in the four-dimensional $(\boldsymbol{\kappa}, \omega)$ -space. If the resolution function is known, it is possible to deconvolute the scattering peaks obtained in constant \mathbf{q} -scans from the broadening due to instrumental effects, and thereby determine the lifetimes of the excitations.

In this chapter, we have concentrated on the magnetic scattering of neutrons, but they may also be scattered through the interaction, via nuclear forces, with the nuclei in the sample. This interaction leads to a cross-section of the same order of magnitude as in the magnetic case, and it results in analogous phenomena to those discussed above, with the positions of the atoms replacing the magnetic moments as the fluctuating variables. The elastic Bragg scattering reveals the positions of the atoms in the crystal, and the elementary excitations appearing in the correlation functions are phonons. The fluctuations in the nuclear cross-section, due to the different spin states of the nuclei, give rise to an *incoherent* scattering, determined by the self-correlation of the individual atoms, in contrast to the *coherent* scattering, which is governed by the atomic pair-correlation function, in analogy with the magnetic scattering discussed above. Incoherence can also be produced by different isotopes of a particular element in a crystal, just as the variation of the magnetic moments in disordered alloys leads to incoherent magnetic scattering.

The magnetic scattering may be difficult to separate experimentally from the nuclear component. One possibility is to utilize the different temperature dependences of the two contributions, since the nuclear scattering normally changes relatively slowly with temperature. If this is not adequate, it may be necessary to perform *polarized* neutron scattering, in which the spin states of the incoming and scattered neutrons are determined, making it possible to isolate the scattering of purely magnetic origin (Moon, Riste and Koehler 1969). For further details of neutron scattering by nuclei in solids we refer to the texts mentioned at the beginning of this chapter.

SPIN WAVES IN THE FERROMAGNETIC HEAVY RARE EARTHS

As discussed in Section 1.5, the exchange interaction dominates the magnetic behaviour of the heavy rare earth metals, and the ordered moments at low temperatures are consequently close to the saturation values. The excitations of such a system are *spin waves*, which may be viewed semi-classically as coupled precessions of the moments about their equilibrium directions, with well-defined frequencies which are determined by the phase relations between the precessing moments on different sites. From the viewpoint of quantum mechanics, these modes are *magnons*, which are linear combinations of single-ion excitations from the ground state to the first excited molecular-field state, which is to a good approximation $|J_z = J - 1\rangle$, with phase factors between the coefficients for different ions which determine the dispersion relation $E_{\mathbf{q}}$ for the magnon energy. A useful review of the excitations of magnetic systems has been given by Stirling and McEwen (1987).

These spin waves have been very extensively studied in the heavy rare earths, both experimentally and theoretically. In this chapter, we consider the simplest case of the *ferromagnet*, in which all the sites are equivalent. Since the magnetic heavy rare earths are all hcp, we begin by extending the earlier treatment of the linear response of the isotropic Heisenberg ferromagnet to this structure. These results are immediately applicable to Gd, where the anisotropy is indeed negligible, with the consequence that the excitation spectrum is the simplest to be found among the magnetic rare earths. Crystal-field and magneto-elastic anisotropies modify the excitation spectrum significantly, inducing an *elliptical polarization* of the precessing moments, and a *spin-wave energy gap* at long wavelengths. To treat such systems, we employ *linear spin-wave theory*, determining the magnon energies via the *Holstein-Primakoff transformation*. We consider in particular the basal-plane ferromagnet, comparing the calculated excitation spectrum throughout with experimental measurements on Tb, which has been very comprehensively studied. The magnon energies and their temperature dependence are discussed, and the energy gap associated with the uniform spin-wave mode is treated in some detail and related to the macroscopic magnetic anisotropy. The contribution to this energy gap of the *magnetoelastic coupling*, via the *static* deformation of the crystal, is then

calculated and its *dynamic* manifestation in the *magnon-phonon* interaction is discussed. *Anisotropic two-ion coupling* between the moments alters the form of the dispersion relations, both quantitatively and, on occasions, qualitatively. The classical *dipole-dipole interaction*, though weak, is highly anisotropic and long-ranged, and may therefore have an important influence at long wavelengths. Since its form is known exactly, we can calculate its effects in detail, but we can say much less about the two-ion anisotropy in general. Its possible origins and symmetry are however discussed, and examples of observable effects to which it gives rise are presented. The mutual solubility of the rare earths allows the formation of an enormous variety of *binary alloys*, with magnetic properties which may be adjusted with the concentration. We show how the excitation spectrum of such systems can be calculated by the *virtual crystal approximation* and the *coherent potential approximation*, and illustrate the phenomena which may be observed by experiments on Tb alloys. Finally, we consider the interaction between the conduction electrons and the localized *4f* moments, and its influence on both the spin waves and the conduction electrons themselves. The *indirect-exchange interaction* is derived more rigorously than in Section 1.4, and the lifetime of the magnons due to electron scattering is deduced. The *mass enhancement* of the conduction electrons is determined, and the effects of magnetic ordering on the band structure, and of magnetic scattering on the conductivity, are discussed.

5.1 The ferromagnetic hcp-crystal

In Chapter 3, we considered the linear response of a system of magnetic moments placed on a Bravais lattice and coupled by the Heisenberg interaction. We shall now generalize this treatment to the hexagonal close-packed crystal structure of the heavy rare earth metals, in which there is a basis of two ions per unit cell, constituting two identical sublattices which, for convenience, we number 1 and 2. The surroundings of the atoms belonging to each of the two sublattices are identical, except for an inversion. Introducing the following Fourier transforms:

$$\mathcal{J}_{ss'}(\mathbf{q}) = \sum_{j \in s' - \text{subl.}} \mathcal{J}(ij) e^{-i\mathbf{q} \cdot (\mathbf{R}_i - \mathbf{R}_j)} \quad ; \quad i \in s\text{-sublattice}, \quad (5.1.1a)$$

we have, for an hcp crystal,

$$\begin{aligned} \mathcal{J}_1(\mathbf{q}) &\equiv \mathcal{J}_{11}(\mathbf{q}) = \mathcal{J}_{22}(\mathbf{q}) \\ \mathcal{J}_2(\mathbf{q}) &\equiv \mathcal{J}_{12}(\mathbf{q}) = \mathcal{J}_{21}(-\mathbf{q}) = \mathcal{J}_{21}^*(\mathbf{q}), \end{aligned} \quad (5.1.1b)$$

where $\mathcal{J}_1(\mathbf{q})$ is real. Defining the four Fourier transforms $\overline{\overline{\chi}}_{ss'}(\mathbf{q}, \omega)$ of the susceptibility tensor equivalently to (5.1.1a), we obtain from the

RPA equation (3.5.7):

$$\begin{aligned}\bar{\chi}_{11}(\mathbf{q}, \omega) &= \bar{\chi}^o(\omega) \{1 + \mathcal{J}_{11}(\mathbf{q}) \bar{\chi}_{11}(\mathbf{q}, \omega) + \mathcal{J}_{12}(\mathbf{q}) \bar{\chi}_{21}(\mathbf{q}, \omega)\} \\ \bar{\chi}_{21}(\mathbf{q}, \omega) &= \bar{\chi}^o(\omega) \{\mathcal{J}_{21}(\mathbf{q}) \bar{\chi}_{11}(\mathbf{q}, \omega) + \mathcal{J}_{22}(\mathbf{q}) \bar{\chi}_{21}(\mathbf{q}, \omega)\},\end{aligned}\quad (5.1.2)$$

assuming that the MF susceptibility $\bar{\chi}^o(\omega)$ is the same for all the sites, as in a paramagnet or a ferromagnet. These matrix equations may be solved straightforwardly, and using (5.1.1b) we find

$$\begin{aligned}\bar{\chi}_{11}(\mathbf{q}, \omega) &= \bar{D}(\mathbf{q}, \omega)^{-1} \{1 - \bar{\chi}^o(\omega) \mathcal{J}_1(\mathbf{q})\} \bar{\chi}^o(\omega) \\ \bar{\chi}_{21}(\mathbf{q}, \omega) &= \bar{D}(\mathbf{q}, \omega)^{-1} \{\bar{\chi}^o(\omega)\}^2 \mathcal{J}_2(-\mathbf{q}),\end{aligned}\quad (5.1.3a)$$

where

$$\begin{aligned}\bar{D}(\mathbf{q}, \omega) &= \{1 - \bar{\chi}^o(\omega) \mathcal{J}_1(\mathbf{q})\}^2 - \{\bar{\chi}^o(\omega) |\mathcal{J}_2(\mathbf{q})|\}^2 \\ &= (1 - \bar{\chi}^o(\omega) \{\mathcal{J}_1(\mathbf{q}) + |\mathcal{J}_2(\mathbf{q})|\}) (1 - \bar{\chi}^o(\omega) \{\mathcal{J}_1(\mathbf{q}) - |\mathcal{J}_2(\mathbf{q})|\}),\end{aligned}\quad (5.1.3b)$$

and, by symmetry,

$$\bar{\chi}_{22}(\mathbf{q}, \omega) = \bar{\chi}_{11}(\mathbf{q}, \omega) \quad \text{and} \quad \bar{\chi}_{12}(\mathbf{q}, \omega) = \bar{\chi}_{21}(-\mathbf{q}, \omega). \quad (5.1.3c)$$

If $\bar{\chi}^o(\omega)$ contains only one pole, as in the case of the Heisenberg ferromagnet, then $\bar{D}(\mathbf{q}, \omega)^{-1}$ in (5.1.3a) generates two poles, corresponding to the existence of both an *acoustic* and an *optical* mode at each \mathbf{q} -vector. $\mathcal{J}_2(\mathbf{0})$ must be real and, since it is also positive in a ferromagnet, the acoustic mode arises from the zero of the first factor in (5.1.3b), its energy therefore being determined by the effective coupling parameter $\mathcal{J}_1(\mathbf{q}) + |\mathcal{J}_2(\mathbf{q})|$. On the other hand, if $\mathcal{J}_2(\mathbf{0})$ is negative, as it is in paramagnetic Pr, it is the second factor which gives the acoustic mode. The nomenclature results from the circumstance that the deviations of the moments from their equilibrium values are in phase in the acoustic mode in the limit of $\mathbf{q} \rightarrow \mathbf{0}$, and it therefore dominates the neutron cross-section. The inelastic neutron scattering is determined by (4.2.2) and (4.2.3), i.e. by

$$\begin{aligned}\bar{\chi}(\boldsymbol{\kappa}, \omega) &= \frac{1}{N} \sum_{ij} \bar{\chi}(ij, \omega) e^{-i\boldsymbol{\kappa} \cdot (\mathbf{R}_i - \mathbf{R}_j)} = \frac{1}{2} \sum_{ss'} \bar{\chi}_{ss'}(\boldsymbol{\kappa}, \omega) \\ &= \bar{D}(\boldsymbol{\kappa}, \omega)^{-1} \left\{ 1 - \bar{\chi}^o(\omega) (\mathcal{J}_1(\boldsymbol{\kappa}) - \frac{1}{2} [\mathcal{J}_2(\boldsymbol{\kappa}) + \mathcal{J}_2(-\boldsymbol{\kappa})]) \right\} \bar{\chi}^o(\omega),\end{aligned}\quad (5.1.4)$$

where $N = 2N_0$ is the number of atoms. Introducing $\boldsymbol{\kappa} = \mathbf{q} + \boldsymbol{\tau}$, with \mathbf{q} lying in the primitive zone, we may write this result as a sum of the acoustic and optical response functions:

$$\begin{aligned}\bar{\chi}_{\text{Ac}}(\mathbf{q}, \omega) &= \{1 - \bar{\chi}^o(\omega) (\mathcal{J}_1(\mathbf{q}) + \nu |\mathcal{J}_2(\mathbf{q})|)\}^{-1} \bar{\chi}^o(\omega) \\ \bar{\chi}_{\text{Op}}(\mathbf{q}, \omega) &= \{1 - \bar{\chi}^o(\omega) (\mathcal{J}_1(\mathbf{q}) - \nu |\mathcal{J}_2(\mathbf{q})|)\}^{-1} \bar{\chi}^o(\omega),\end{aligned}\quad (5.1.5)$$

where $\nu = \pm 1$ denotes the sign of $\mathcal{J}_2(\mathbf{0})$. $\mathcal{J}_1(\boldsymbol{\kappa}) = \mathcal{J}_1(\mathbf{q})$ is real, whereas

$$\mathcal{J}_2(\boldsymbol{\kappa}) = \mathcal{J}_2(\mathbf{q}) e^{i\boldsymbol{\tau} \cdot \boldsymbol{\rho}} = \nu |\mathcal{J}_2(\mathbf{q})| e^{i\varphi}, \quad (5.1.6a)$$

defining the phase $\varphi = \varphi(\boldsymbol{\kappa})$, and $\boldsymbol{\rho} = \mathbf{d}_2 - \mathbf{d}_1$ is the vector joining the two sublattices. In terms of these quantities, the susceptibility (5.1.4) may be written

$$\overline{\chi}(\mathbf{q} + \boldsymbol{\tau}, \omega) = \frac{1}{2}(1 + \cos \varphi) \overline{\chi}_{\text{Ac}}(\mathbf{q}, \omega) + \frac{1}{2}(1 - \cos \varphi) \overline{\chi}_{\text{Op}}(\mathbf{q}, \omega). \quad (5.1.6b)$$

The phase φ vanishes in the limit $\mathbf{q} \rightarrow \mathbf{0}$ if $\boldsymbol{\tau} = \mathbf{0}$, and the scattering cross-section then only depends on the isolated pole in the acoustic response function, in accordance with our definition above. Introducing the following lattice vectors of the hexagonal lattice:

$$\mathbf{a}_1 = (a, 0, 0) \quad \mathbf{a}_2 = \left(-\frac{a}{2}, \frac{\sqrt{3}a}{2}, 0\right) \quad \mathbf{a}_3 = (0, 0, c), \quad (5.1.7a)$$

we find the corresponding reciprocal lattice vectors:

$$\mathbf{b}_1 = \left(\frac{2\pi}{a}, \frac{2\pi}{\sqrt{3}a}, 0\right) \quad \mathbf{b}_2 = \left(0, \frac{4\pi}{\sqrt{3}a}, 0\right) \quad \mathbf{b}_3 = \left(0, 0, \frac{2\pi}{c}\right). \quad (5.1.7b)$$

Since $\boldsymbol{\rho} = \left(\frac{a}{2}, \frac{a}{2\sqrt{3}}, \frac{c}{2}\right)$,

$$\boldsymbol{\tau} \cdot \boldsymbol{\rho} = \frac{4\pi}{3}h + \frac{2\pi}{3}k + \pi l \quad \text{with} \quad \boldsymbol{\tau} = (hkl) = h\mathbf{b}_1 + k\mathbf{b}_2 + l\mathbf{b}_3. \quad (5.1.8)$$

If \mathbf{q} is parallel to the c -axis, $\mathcal{J}_2(\mathbf{q})$ is real. The phase φ in (5.1.6) is then $\boldsymbol{\tau} \cdot \boldsymbol{\rho}$ and, if the Miller indices h and k are both zero, $\varphi = \boldsymbol{\tau} \cdot \boldsymbol{\rho} = l\pi$. In this case, with $\boldsymbol{\kappa}$ in the c -direction, the inelastic scattering detects only the acoustic or the optical excitations, depending on whether l is respectively even or odd, and no energy gap appears at the zone boundary, even though l changes, because $\mathcal{J}_2(\mathbf{b}_3/2) = 0$ by symmetry. We may therefore use a *double-zone representation*, in which the dispersion relation for the excitations is considered as comprising a single branch extending twice the distance to the Brillouin zone boundary, corresponding to an effective unit cell of height $c/2$. We shall generally use this representation when discussing excitations propagating in the c -direction.

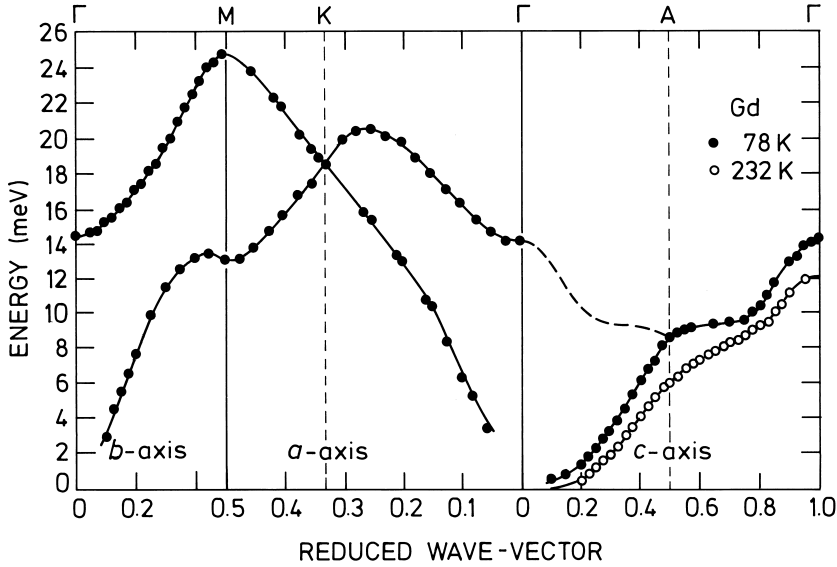


Fig. 5.1. Spin-wave dispersion relations for Gd, after Koehler *et al.* (1970). The two atoms of the hcp structure give rise to acoustic and optical branches. Since the single-ion anisotropy is negligible, the acoustic mode rises quadratically from the origin.

Because $L = 0$, so that $J = S$, anisotropy effects are small in Gd, and it is therefore a good approximation to a Heisenberg ferromagnet. Using the above procedure to generalize (3.5.26) to the hcp structure, we obtain the two branches of the excitation spectrum

$$\begin{aligned} E_{\mathbf{q}}^{\text{Ac}} &= \langle J_z \rangle \{ \mathcal{J}_1(\mathbf{0}) + \mathcal{J}_2(\mathbf{0}) - \mathcal{J}_1(\mathbf{q}) - |\mathcal{J}_2(\mathbf{q})| \} \\ E_{\mathbf{q}}^{\text{Op}} &= \langle J_z \rangle \{ \mathcal{J}_1(\mathbf{0}) + \mathcal{J}_2(\mathbf{0}) - \mathcal{J}_1(\mathbf{q}) + |\mathcal{J}_2(\mathbf{q})| \}, \end{aligned} \quad (5.1.9)$$

since $\mathcal{J}_2(\mathbf{0})$ is positive. The dispersion relations measured by inelastic neutron scattering by Koehler *et al.* (1970) are shown in Fig. 5.1. This figure illustrates the use of the double-zone representation when \mathbf{q} is along the c -axis, resulting in a single spin-wave branch. The renormalization predicted by the simple RPA theory, that $E_{\mathbf{q}}(T)$ is proportional to σ , is not followed very precisely. σ changes from about 0.97 at 78 K to 0.66 at 232 K. As may be seen from Fig. 5.1, and from more extensive studies by Cable *et al.* (1985), the energies in the c -direction vary approximately like $\sigma^{0.5}$ at the largest wave-vectors, like σ in the middle of the branch, and faster than σ at small wave-vectors. However, it is also evident from the figure that the form of $\mathcal{J}(\mathbf{q})$ changes with decreasing magnetization, so some of the discrepancy between the simple

prediction and the observed behaviour at low temperatures may be due to changes of $\mathcal{J}(\mathbf{q})$. At higher temperatures, the RPA renormalization breaks down completely. The spin-wave energy at the zone boundary has only fallen by about a factor two at 292 K, very close to T_C . Furthermore, strongly-broadened neutron peaks are observed even at 320 K, well above the transition, close to the zone boundary in the basal plane, with energies of about $k_B T_C$. On the other hand, the low-energy spin waves progressively broaden out into diffusive peaks as T_C is approached from below.

5.2 Spin waves in the anisotropic ferromagnet

In the heavy rare earth metals, the two-ion interactions are large and of long range. They induce magnetically-ordered states at relatively high temperatures, and the ionic moments approach closely their saturation values at low temperatures. These circumstances allow us to adopt a somewhat different method, *linear spin-wave theory*, from those discussed previously in connection with the derivation of the correlation functions. We shall consider the specific case of a hexagonal close-packed crystal ordered ferromagnetically, with the moments lying in the basal plane, corresponding to the low-temperature phases of both Tb and Dy. For simplicity, we shall initially treat only the anisotropic effects introduced by the single-ion crystal-field Hamiltonian so that, in the case of hexagonal symmetry, we have

$$\mathcal{H} = \sum_i \left[\sum_{l=2,4,6} B_l^0 Q_l^0(\mathbf{J}_i) + B_6^6 Q_6^6(\mathbf{J}_i) - g\mu_B \mathbf{J}_i \cdot \mathbf{H} \right] - \frac{1}{2} \sum_{i \neq j} \mathcal{J}(ij) \mathbf{J}_i \cdot \mathbf{J}_j. \quad (5.2.1)$$

The system is assumed to order ferromagnetically at low temperatures, a sufficient condition for which is that the maximum of $\mathcal{J}(\mathbf{q})$ occurs at $\mathbf{q} = \mathbf{0}$. $Q_l^m(\mathbf{J}_i)$ denotes the Stevens operator of the i th ion, but defined in terms of (J_ξ, J_η, J_ζ) instead of (J_x, J_y, J_z) , where the (ξ, η, ζ) -axes are fixed to be along the symmetry a -, b - and c -directions, respectively, of the hexagonal lattice. The (x, y, z) -coordinate system is chosen such that the z -axis is along the magnetization axis, specified by the polar angles (θ, ϕ) in the (ξ, η, ζ) -coordinate system. Choosing the y -axis to lie in the basal plane, we obtain the following relations:

$$\begin{aligned} J_\xi &= J_z \sin \theta \cos \phi - J_x \cos \theta \cos \phi + J_y \sin \phi \\ J_\eta &= J_z \sin \theta \sin \phi - J_x \cos \theta \sin \phi - J_y \cos \phi \\ J_\zeta &= J_z \cos \theta + J_x \sin \theta, \end{aligned} \quad (5.2.2)$$

from which

$$Q_2^0 = 3\{J_z^2 \cos^2 \theta + J_x^2 \sin^2 \theta + (J_z J_x + J_x J_z) \cos \theta \sin \theta\} - J(J+1). \quad (5.2.3)$$

Initially we assume that $\langle J_z \rangle = J$ at $T = 0$, which implies that the ground state is the product of $|J_z = J\rangle$ -states of the single ions. In this case, we find, consistently with eqn (2.2.14),

$$\langle Q_2^0 \rangle = \langle J | Q_2^0 | J \rangle = J^{(2)} (3 \cos^2 \theta - 1),$$

where, as before, $J^{(n)} = J(J - \frac{1}{2}) \cdots (J - \frac{n-1}{2})$, and we have used the expectation values $\langle J_z^2 \rangle = J^2$, $\langle J_x^2 \rangle = \frac{1}{2}J$ and $\langle J_z J_x \rangle = 0$. Analogously, though with considerably more labour, we can show that, for instance,

$$\langle Q_6^6 \rangle = \langle J | \frac{1}{2}(J_\xi + iJ_\eta)^6 + \frac{1}{2}(J_\xi - iJ_\eta)^6 | J \rangle = J^{(6)} \sin^6 \theta \cos 6\phi. \quad (5.2.4)$$

For simplicity, we neglect for the moment B_4^0 and B_6^0 , and specifying the direction of the magnetic field by the polar angles (θ_H, ϕ_H) , we find that the ground-state energy is, within this approximation,

$$\begin{aligned} U(T=0) \simeq & N [B_2^0 J^{(2)} (3 \cos^2 \theta - 1) + B_6^6 J^{(6)} \sin^6 \theta \cos 6\phi \\ & - g\mu_B JH \{ \cos \theta \cos \theta_H + \sin \theta \sin \theta_H \cos(\phi - \phi_H) \} - \frac{1}{2} \mathcal{J}(\mathbf{0}) J^2], \end{aligned} \quad (5.2.5)$$

where θ and ϕ are determined so that they minimize this expression. In zero magnetic field, $H = 0$, (5.2.5) only gives two possibilities for θ , viz. $\theta = 0$ for $B_2^0 J^{(2)} < -\frac{1}{3} |B_6^6| J^{(6)}$ or $\theta = \frac{\pi}{2}$ for $B_2^0 J^{(2)} > -\frac{1}{3} |B_6^6| J^{(6)}$. We shall here be concerned with the second case of $\theta = \frac{\pi}{2}$, i.e. the basal-plane ferromagnet. In this case, the angle ϕ is determined by the sign of B_6^6 . The magnetic moments will be along an a - or a b -axis ($\phi = 0$ or $\phi = \frac{\pi}{2}$) if B_6^6 is respectively negative or positive. Having specified the (approximate) ground state, we turn to the excitations, i.e. the spin waves.

Instead of utilizing the standard-basis operators, defined by (3.5.11), we shall introduce a Bose operator a_i for the i th ion, satisfying

$$[a_i, a_j^+] = \delta_{ij} \quad ; \quad [a_i, a_j] = [a_i^+, a_j^+] = 0, \quad (5.2.6)$$

which acts on the $|J_z\rangle$ -state vector of this ion (the site index is suppressed) in the following way:

$$a |J\rangle = 0 \quad ; \quad a |J - m\rangle = \sqrt{m} |J - m + 1\rangle \quad (5.2.7)$$

Holstein and Primakoff (1940) introduced the following representation of the angular momentum operators:

$$\begin{aligned} J_z &= J - a^+ a \\ J_+ &= (2J - a^+ a)^{\frac{1}{2}} a \\ J_- &= a^+ (2J - a^+ a)^{\frac{1}{2}}. \end{aligned} \quad (5.2.8)$$

If the usual basis vectors in the Hilbert space created by the Bose operators are denoted by $|n\rangle$, i.e. $a|n\rangle = \sqrt{n}|n-1\rangle$ where $n = 0, 1, 2, \dots, \infty$, then by the definition (5.2.7), $|n\rangle = |J_z = J - n\rangle$ for $n = 0, 1, 2, \dots, 2J$, but there is no physical $|J_z\rangle$ -state corresponding to $|n\rangle$ when $n > 2J$. It is straightforward to see that the Bose representation (5.2.8) produces the right matrix-elements of the angular momentum operators, as long as $|n\rangle$ is restricted to the physical part of the Hilbert space, $n \leq 2J$, but this representation presupposes the presence of an infinite number of states. In the ferromagnetic case, the unphysical states are at high energies, if J is large and T is low, and their influence on the thermal averages is negligible. In this regime of J and T , the *Holstein-Primakoff transformation* is useful and the results derived from it are trustworthy.

In order to be able to treat the Bose operators under the square roots in eqn (5.2.8), we shall utilize $1/J$ as an expansion parameter. This means that, instead of the J_{\pm} given by (5.2.8), we shall use

$$J_+ = (J_-)^\dagger \simeq \sqrt{2J} \left(a - \frac{1}{4J} a^+ a a \right). \quad (5.2.9)$$

It is important here to realize that the expansion parameter is $1/J$ and not, for instance, ‘the number of deviation operators’. If the latter were the case, a well-ordered expansion of J_+ (Lindgård and Danielsen 1974) would suggest instead $J_+ = \sqrt{2J} \{ a - (1 - \sqrt{1 - 1/2J}) a^+ a a + \dots \}$, corresponding to a replacement of $\frac{1}{4J}$ in (5.2.9) by $\frac{1}{4J} (1 + \frac{1}{8J} + \dots)$. We emphasize that we shall be expanding the *reduced* operators $(1/J^{(l)}) O_l^m$, leaving no ambiguities either in (5.2.9) or in the following. Using eqn (5.2.9) and $J_z = J - a^+ a$, it is straightforward to express the Stevens operators in terms of the Bose operators. For O_2^0 , we get

$$\begin{aligned} O_2^0 &= 3J_z^2 - J(J+1) = 3(J - a^+ a)^2 - J(J+1) \\ &= 2J(J - \frac{1}{2}) - 6(J - \frac{1}{2}) a^+ a + 3a^+ a^+ a a \\ &= 2J^{(2)} \left\{ 1 - \frac{3}{J} a^+ a + \frac{3}{2J^2} a^+ a^+ a a + \mathcal{O}(1/J^3) \right\}. \end{aligned} \quad (5.2.10)$$

Here we have used $[a, a^+] = 1$ to arrange the operators in ‘well-ordered’ products, with all the creation operators to the left, and in the last line $1/J^{(2)}$ has been replaced by $1/J^2$ in the term of second order in $1/J$. In the same way, we obtain

$$\begin{aligned} O_2^2 &= \frac{1}{2} (J_+^2 + J_-^2) = J^{(2)} \left\{ \frac{1}{J} (a^+ a^+ + a a) \right. \\ &\quad \left. + \frac{1}{4J^2} (a^+ a^+ + a a - 2a^+ a^+ a^+ a - 2a^+ a a a) + \mathcal{O}(1/J^3) \right\}. \end{aligned} \quad (5.2.11)$$

The expression for Q_2^0 is then determined using $Q_2^0(\theta = \frac{\pi}{2}) = -\frac{1}{2}O_2^0 + \frac{3}{2}O_2^2$. For the case of Q_6^6 , we refer to Lindgård and Danielsen (1974), who have established the Bose operator expansion of the tensor operators up to the eighth rank. Introducing these expansions into (5.2.1), and grouping the terms together according to their order in $1/J$, we may write the Hamiltonian

$$\mathcal{H} = \mathcal{H}_0 + \mathcal{H}_1 + \mathcal{H}_2 + \cdots + \mathcal{H}', \quad (5.2.12)$$

where $\mathcal{H}_0 = U_0$ is the zero-order term, and

$$U_0 = N \left[-B_2^0 J^{(2)} + B_6^6 J^{(6)} \cos 6\phi - g\mu_B JH \cos(\phi - \phi_H) - \frac{1}{2} J^2 \mathcal{J}(\mathbf{0}) \right], \quad (5.2.13)$$

corresponding to (5.2.5), when we restrict ourselves to the case $\theta = \theta_H = \pi/2$. \mathcal{H}_1 comprises the terms of first order in $1/J$, and is found to be

$$\mathcal{H}_1 = \sum_i \left[A a_i^+ a_i + B \frac{1}{2} (a_i^+ a_i^+ + a_i a_i) \right] - \sum_{ij} J \mathcal{J}(ij) (a_i^+ a_j - a_i^+ a_i), \quad (5.2.14)$$

where the parameters A and B are

$$\begin{aligned} A &= \frac{1}{J} \{ 3B_2^0 J^{(2)} - 21B_6^6 J^{(6)} \cos 6\phi + g\mu_B JH \cos(\phi - \phi_H) \} \\ B &= \frac{1}{J} \{ 3B_2^0 J^{(2)} + 15B_6^6 J^{(6)} \cos 6\phi \}. \end{aligned} \quad (5.2.15)$$

If we consider only the zero- and first-order part of the Hamiltonian, i.e. assume $\mathcal{H} \simeq \mathcal{H}_0 + \mathcal{H}_1$, it can be brought into diagonal form via two transformations. The first step is to introduce the spatial Fourier transforms of $\mathcal{J}(ij)$, eqn (3.4.2), and of a_i :

$$a_{\mathbf{q}} = \frac{1}{\sqrt{N}} \sum_i a_i e^{-i\mathbf{q}\cdot\mathbf{R}_i} \quad ; \quad a_{\mathbf{q}}^+ = \frac{1}{\sqrt{N}} \sum_i a_i^+ e^{i\mathbf{q}\cdot\mathbf{R}_i}, \quad (5.2.16)$$

for which the commutators are

$$[a_{\mathbf{q}}, a_{\mathbf{q}'}^+] = \frac{1}{N} \sum_i e^{-i(\mathbf{q}-\mathbf{q}')\cdot\mathbf{R}_i} = \delta_{\mathbf{q}\mathbf{q}'}.$$

In the case of an hcp lattice, with its two ions per unit cell, the situation is slightly more complex, as discussed in the previous section. However, this complication is inessential in the present context, and for simplicity we consider a Bravais lattice in the rest of this section, so that the results which we obtain are only strictly valid for excitations propagating in

the c -direction, for which the double-zone representation may be used. Introducing the Fourier transforms, we may write

$$\mathcal{H}_1 = \sum_{\mathbf{q}} \left[A_{\mathbf{q}} a_{\mathbf{q}}^+ a_{\mathbf{q}} + B \frac{1}{2} (a_{\mathbf{q}}^+ a_{-\mathbf{q}}^+ + a_{\mathbf{q}} a_{-\mathbf{q}}) \right], \quad (5.2.17)$$

with

$$A_{\mathbf{q}} = A + J\{\mathcal{J}(\mathbf{0}) - \mathcal{J}(\mathbf{q})\}. \quad (5.2.18)$$

\mathcal{H}_1 is quadratic in the Bose operators, and it can be diagonalized by performing a *Bogoliubov transformation*. A new Bose operator $\alpha_{\mathbf{q}}$ is introduced, such that

$$a_{\mathbf{q}} = u_{\mathbf{q}} \alpha_{\mathbf{q}} - v_{\mathbf{q}} \alpha_{-\mathbf{q}}^+ \quad ; \quad |u_{\mathbf{q}}|^2 - |v_{\mathbf{q}}|^2 = 1, \quad (5.2.19)$$

in terms of which $\mathcal{H}_0 + \mathcal{H}_1$ is transformed into

$$\mathcal{H}_0 + \mathcal{H}_1 = U_0 + U_1 + \sum_{\mathbf{q}} E_{\mathbf{q}} \alpha_{\mathbf{q}}^+ \alpha_{\mathbf{q}}, \quad (5.2.20)$$

when $u_{\mathbf{q}}$ and $v_{\mathbf{q}}$ are adjusted appropriately. Here they can both be chosen to be real quantities, and are determined by the equation

$$(u_{\mathbf{q}} \pm v_{\mathbf{q}})^2 = (A_{\mathbf{q}} \pm B)/E_{\mathbf{q}}. \quad (5.2.21)$$

The energy parameters are

$$U_1 = \frac{1}{2} \sum_{\mathbf{q}} (E_{\mathbf{q}} - A_{\mathbf{q}}) \quad ; \quad E_{\mathbf{q}} = \sqrt{A_{\mathbf{q}}^2 - B^2}. \quad (5.2.22)$$

When B is different from zero, as occurs if either B_2^0 or B_6^6 is non-zero, the product of the $|J_{iz} = J\rangle = |0\rangle_i$ -states is no longer the (MF) ground state. Q_2^0 and Q_6^6 give rise to couplings between the single-ion states $|J\rangle$, $|J-2\rangle$ etc. as reflected in the term proportional to B in (5.2.17). The new ground state established by the Bogoliubov transformation has the energy $U_0 + U_1$ ($= U_0 - \sum_{\mathbf{q}} B^2/4E_{\mathbf{q}}$ to leading order in B), which is always smaller than U_0 . The admixture of (predominantly) the $|J-2\rangle$ -state into the ground state implies that the system is no longer fully polarized at $T = 0$, as assumed in (5.2.5). Using (5.2.19) and the conditions $\langle \alpha_{\mathbf{q}} \alpha_{\mathbf{q}} \rangle = \langle \alpha_{\mathbf{q}}^+ \alpha_{\mathbf{q}}^+ \rangle = 0$, whereas

$$\langle \alpha_{\mathbf{q}}^+ \alpha_{\mathbf{q}} \rangle = n_{\mathbf{q}} = \frac{1}{e^{\beta E_{\mathbf{q}}} - 1} \quad (5.2.23)$$

is the usual Bose population-factor, we find to first order in $1/J$:

$$\langle J_z \rangle = \langle J - \frac{1}{N} \sum_{\mathbf{q}} a_{\mathbf{q}}^+ a_{\mathbf{q}} \rangle = J(1 - m), \quad (5.2.24)$$

with

$$m = \frac{1}{N} \sum_{\mathbf{q}} \frac{1}{J} \langle a_{\mathbf{q}}^+ a_{\mathbf{q}} \rangle = \frac{1}{N} \sum_{\mathbf{q}} m_{\mathbf{q}}$$

and

$$\begin{aligned} m_{\mathbf{q}} &= \frac{1}{J} \langle (u_{\mathbf{q}} \alpha_{\mathbf{q}}^+ - v_{\mathbf{q}} \alpha_{-\mathbf{q}})(u_{\mathbf{q}} \alpha_{\mathbf{q}} - v_{\mathbf{q}} \alpha_{-\mathbf{q}}^+) \rangle \\ &= \frac{1}{J} \{ u_{\mathbf{q}}^2 n_{\mathbf{q}} + v_{\mathbf{q}}^2 (n_{\mathbf{q}} + 1) \} \\ &= \frac{1}{J} \left\{ \frac{A_{\mathbf{q}}}{E_{\mathbf{q}}} \left(n_{\mathbf{q}} + \frac{1}{2} \right) - \frac{1}{2} \right\}, \end{aligned} \quad (5.2.25)$$

which is positive and non-zero, even when $n_{\mathbf{q}} = 0$ at $T = 0$.

The second-order contribution to the Hamiltonian is

$$\begin{aligned} \mathcal{H}_2 &= \sum_i \left[B \frac{1}{8J} (a_i^+ a_i^+ + a_i a_i) + C_1 a_i^+ a_i^+ a_i a_i \right. \\ &\quad \left. + C_2 (a_i^+ a_i^+ a_i^+ a_i + a_i^+ a_i a_i a_i) + C_3 (a_i^+ a_i^+ a_i^+ a_i^+ + a_i a_i a_i a_i) \right] \\ &\quad - \frac{1}{4} \sum_{ij} \mathcal{J}(ij) (2a_i^+ a_j^+ a_i a_j - a_i^+ a_j^+ a_j a_j - a_i^+ a_i^+ a_j a_j), \end{aligned} \quad (5.2.26)$$

with

$$\begin{aligned} C_1 &= -\frac{1}{J^2} \left(\frac{3}{2} B_2^0 J^{(2)} - 105 B_6^6 J^{(6)} \cos 6\phi \right) \\ C_2 &= -\frac{1}{J^2} \left(\frac{3}{4} B_2^0 J^{(2)} + \frac{195}{4} B_6^6 J^{(6)} \cos 6\phi \right) \\ C_3 &= \frac{1}{J^2} \frac{15}{4} B_6^6 J^{(6)} \cos 6\phi. \end{aligned} \quad (5.2.27)$$

Introducing the Fourier transforms of the Bose operators in \mathcal{H}_2 , we find straightforwardly that

$$\begin{aligned} i\hbar \partial a_{\mathbf{q}} / \partial t &= [a_{\mathbf{q}}, \mathcal{H}] \simeq [a_{\mathbf{q}}, \mathcal{H}_1 + \mathcal{H}_2] = A_{\mathbf{q}} a_{\mathbf{q}} + B \left(1 + \frac{1}{4J} \right) a_{-\mathbf{q}}^+ + \\ &\frac{1}{N} \sum_{\mathbf{k}, \mathbf{k}'} \left[\left\{ -\mathcal{J}(\mathbf{q} - \mathbf{k}') + \frac{1}{2} \mathcal{J}(\mathbf{k}') + \frac{1}{4} \mathcal{J}(\mathbf{k}) + \frac{1}{4} \mathcal{J}(\mathbf{q}) + 2C_1 \right\} a_{\mathbf{k}}^+ a_{\mathbf{k}'} a_{\mathbf{q}+\mathbf{k}-\mathbf{k}'} \right. \\ &\quad \left. + C_2 \{ 3a_{\mathbf{k}}^+ a_{-\mathbf{k}'}^+ a_{\mathbf{q}+\mathbf{k}-\mathbf{k}'} + a_{-\mathbf{k}} a_{\mathbf{k}'} a_{\mathbf{q}+\mathbf{k}-\mathbf{k}'} \} + 4C_3 a_{\mathbf{k}}^+ a_{-\mathbf{k}'}^+ a_{-\mathbf{q}-\mathbf{k}+\mathbf{k}'}^+ \right], \end{aligned} \quad (5.2.28)$$

for the operator $[a_{\mathbf{q}}, \mathcal{H}]$, which appears in the equation of motion of, for instance $\langle \langle a_{\mathbf{q}} ; a_{\mathbf{q}}^+ \rangle \rangle$. When the thermal averages of terms due to \mathcal{H}_2

are considered, the replacement of \mathcal{H} by $\mathcal{H}_0 + \mathcal{H}_1$ in the density matrix only gives rise to errors of higher-order in $1/J$. Because $\mathcal{H}_0 + \mathcal{H}_1$ is quadratic in the Bose operators, this replacement results in a decoupling of the \mathcal{H}_2 -terms (according to *Wick's theorem*) which is equivalent to the RPA decoupling utilized previously. Hence, when considering thermal averages, we have to leading order in $1/J$, for instance,

$$\begin{aligned} a_{\mathbf{k}}^+ a_{\mathbf{k}'} a_{\mathbf{q}+\mathbf{k}-\mathbf{k}'} &\simeq a_{\mathbf{k}'}^+ \langle a_{\mathbf{k}'} a_{\mathbf{q}+\mathbf{k}-\mathbf{k}'} \rangle + a_{\mathbf{k}'} \langle a_{\mathbf{k}}^+ a_{\mathbf{q}+\mathbf{k}-\mathbf{k}'} \rangle + a_{\mathbf{q}+\mathbf{k}-\mathbf{k}'} \langle a_{\mathbf{k}} a_{\mathbf{k}'} \rangle \\ &= \delta_{\mathbf{k},-\mathbf{q}} a_{-\mathbf{q}}^+ \langle a_{\mathbf{k}'} a_{-\mathbf{k}'} \rangle + \delta_{\mathbf{k}',\mathbf{q}} a_{\mathbf{q}} \langle a_{\mathbf{k}}^+ a_{\mathbf{k}} \rangle + \delta_{\mathbf{k},\mathbf{k}'} a_{\mathbf{q}} \langle a_{\mathbf{k}}^+ a_{\mathbf{k}} \rangle, \end{aligned} \quad (5.2.29)$$

where the last line follows from the diagonality of $\mathcal{H}_0 + \mathcal{H}_1$ in reciprocal space. We note that it is convenient here that the single-ion operators are expressed as products of Bose operators which are well-ordered. When this decoupling is introduced in (5.2.28), it reduces to

$$[a_{\mathbf{q}}, \mathcal{H}] = \tilde{A}_{\mathbf{q}}(T) a_{\mathbf{q}} + \tilde{B}_{\mathbf{q}}(T) a_{-\mathbf{q}}^+, \quad (5.2.30)$$

where the effective, renormalized parameters are

$$\begin{aligned} \tilde{A}_{\mathbf{q}}(T) &= A + 4JC_1 m + 6JC_2 b + J\{\mathcal{J}(\mathbf{0}) - \mathcal{J}(\mathbf{k})\}(1 - m) \\ &\quad + \frac{1}{N} \sum_{\mathbf{k}} J\{\mathcal{J}(\mathbf{k}) - \mathcal{J}(\mathbf{k} - \mathbf{q})\} m_{\mathbf{k}} \end{aligned} \quad (5.2.31a)$$

and

$$\begin{aligned} \tilde{B}_{\mathbf{q}}(T) &= B(1 + \frac{1}{4J}) + 2JC_1 b + 6JC_2 m + 12JC_3 b - \frac{1}{2} J\{\mathcal{J}(\mathbf{0}) - \mathcal{J}(\mathbf{q})\} b \\ &\quad + \frac{1}{2N} \sum_{\mathbf{k}} J\{\mathcal{J}(\mathbf{0}) - \mathcal{J}(\mathbf{k})\} b_{\mathbf{k}} + \frac{1}{N} \sum_{\mathbf{k}} J\{\mathcal{J}(\mathbf{k}) - \mathcal{J}(\mathbf{k} - \mathbf{q})\} b_{\mathbf{k}}. \end{aligned} \quad (5.2.31b)$$

$m_{\mathbf{k}}$ and $b_{\mathbf{k}}$ are respectively the correlation functions $(1/J)\langle a_{\mathbf{k}}^+ a_{\mathbf{k}} \rangle$ and $(1/J)\langle a_{\mathbf{k}}^+ a_{-\mathbf{k}}^+ \rangle = (1/J)\langle a_{\mathbf{k}} a_{-\mathbf{k}} \rangle$, and m and b are the corresponding averages over \mathbf{k} . Equation (5.2.30) implies that the operator $[a_{\mathbf{q}}, \mathcal{H}]$, in the equations of motion of any Green function involving $a_{\mathbf{q}}$, can be replaced by the expression on the right-hand side. The same result is obtained if, instead, \mathcal{H}_2 is neglected, and $A_{\mathbf{q}}$ and B in \mathcal{H}_1 are replaced by $\tilde{A}_{\mathbf{q}}(T)$ and $\tilde{B}_{\mathbf{q}}(T)$ in (5.2.17). Consequently, the system behaves as if the Hamiltonian $\mathcal{H}_0 + \mathcal{H}_1 + \mathcal{H}_2$ is replaced by $\tilde{\mathcal{H}}_0 + \tilde{\mathcal{H}}_1$, which is similar to $\mathcal{H}_0 + \mathcal{H}_1$ except for the introduction of the effective, temperature-dependent parameters. The RPA decoupling (5.2.29) introduces errors in the Green functions, but only in the third order of $1/J$, and as it leads to an effective Hamiltonian which is quadratic in the Bose operators, it is a valid procedure. This internal consistency of the theory to second order in

$1/J$ means that the RPA contributions to the correlation functions are reliably estimated, and that all second-order contributions are included when $\tilde{\mathcal{H}}_0 + \tilde{\mathcal{H}}_1$ is used, instead of $\mathcal{H}_0 + \mathcal{H}_1$, in the calculation of the thermal averages. We shall therefore use the following self-consistent expressions for the characteristic correlation functions, $m_{\mathbf{k}}$ and $b_{\mathbf{k}}$, determined straightforwardly by utilizing the correspondence between $\mathcal{H}_0 + \mathcal{H}_1$ and $\tilde{\mathcal{H}}_0 + \tilde{\mathcal{H}}_1$:

$$m_{\mathbf{k}} = \frac{1}{J} \left\{ \frac{\tilde{A}_{\mathbf{k}}(T)}{E_{\mathbf{k}}(T)} \left(n_{\mathbf{k}} + \frac{1}{2} \right) - \frac{1}{2} \right\}, \quad (5.2.32a)$$

corresponding to (5.2.25), and

$$b_{\mathbf{k}} = -\frac{1}{J} \frac{\tilde{B}_{\mathbf{k}}(T)}{E_{\mathbf{k}}(T)} \left(n_{\mathbf{k}} + \frac{1}{2} \right). \quad (5.2.32b)$$

In order to express the result in a convenient form, we rewrite one of the second-order terms in $\tilde{B}_{\mathbf{q}}(T)$ as

$$\frac{1}{2N} \sum_{\mathbf{k}} J \{ \mathcal{J}(\mathbf{0}) - \mathcal{J}(\mathbf{k}) \} b_{\mathbf{k}} = -\frac{1}{2} B \left(m + \frac{1}{2J} \right) - \frac{1}{2} A b + \mathcal{O}(1/J^3), \quad (5.2.33)$$

since, to leading order, $J \{ \mathcal{J}(\mathbf{0}) - \mathcal{J}(\mathbf{k}) \} = \tilde{A}_{\mathbf{k}}(T) - A$, and $\tilde{B}_{\mathbf{k}}(T)$ in $b_{\mathbf{k}}$ can be approximated by B . We note that $A_{\mathbf{q}}$ and B are parameters of the order $1/J$, as are m and b (at low temperatures). In addition to introducing (5.2.33) into (5.2.31b), it is adequate for calculating the spin-wave energies to define a transformed set of parameters:

$$\begin{aligned} A_{\mathbf{q}}(T) &= \tilde{A}_{\mathbf{q}}(T) + \frac{1}{2} \tilde{B}_{\mathbf{q}}(T) b \\ B_{\mathbf{q}}(T) &= \tilde{B}_{\mathbf{q}}(T) + \frac{1}{2} \tilde{A}_{\mathbf{q}}(T) b \end{aligned} \quad (5.2.34)$$

and these are then, to the order considered,

$$\begin{aligned} A_{\mathbf{q}}(T) &= A + 4JC_1 m + 6JC_2 b + \frac{1}{2} B b \\ &\quad + J \{ \mathcal{J}(\mathbf{0}) - \mathcal{J}(\mathbf{q}) \} (1 - m) + \frac{1}{N} \sum_{\mathbf{k}} J \{ \mathcal{J}(\mathbf{k}) - \mathcal{J}(\mathbf{k} - \mathbf{q}) \} m_{\mathbf{k}} \end{aligned} \quad (5.2.35a)$$

and

$$\begin{aligned} B_{\mathbf{q}}(T) &= B + 2JC_1 b + 6JC_2 m + 12JC_3 b - \frac{1}{2} B m \\ &\quad + \frac{1}{N} \sum_{\mathbf{k}} J \{ \mathcal{J}(\mathbf{k}) - \mathcal{J}(\mathbf{k} - \mathbf{q}) \} b_{\mathbf{k}}. \end{aligned} \quad (5.2.35b)$$

This transformation leaves the expression for the excitation energies unchanged, i.e.

$$E_{\mathbf{q}}(T) = \left\{ [A_{\mathbf{q}}(T) + B_{\mathbf{q}}(T)][A_{\mathbf{q}}(T) - B_{\mathbf{q}}(T)] \right\}^{\frac{1}{2}}, \quad (5.2.36)$$

when higher-order corrections are neglected. Inserting the eqns (5.2.15), (5.2.18), and (5.2.27) into (5.2.35), we finally obtain, at zero wave-vector,

$$A_{\mathbf{0}}(T) - B_{\mathbf{0}}(T) = \frac{1}{J} \left\{ -36B_6^6 J^{(6)} (1 - 20m + 15b) \cos 6\phi \right. \\ \left. + g\mu_B JH \cos(\phi - \phi_H) \right\} \quad (5.2.37a)$$

and

$$A_{\mathbf{0}}(T) + B_{\mathbf{0}}(T) = \frac{1}{J} \left\{ 6B_2^0 J^{(2)} (1 - 2m - b) \right. \\ \left. - 6B_6^6 J^{(6)} (1 - 20m + 5b) \cos 6\phi + g\mu_B JH \cos(\phi - \phi_H) \right\}, \quad (5.2.37b)$$

and, at non-zero wave-vector,

$$A_{\mathbf{q}}(T) = A_{\mathbf{0}}(T) + J \{ \mathcal{J}(\mathbf{0}) - \mathcal{J}(\mathbf{q}) \} (1 - m) + \frac{1}{N} \sum_{\mathbf{k}} J \{ \mathcal{J}(\mathbf{k}) - \mathcal{J}(\mathbf{k} - \mathbf{q}) \} m_{\mathbf{k}} \quad (5.2.38a)$$

and

$$B_{\mathbf{q}}(T) = B_{\mathbf{0}}(T) + \frac{1}{N} \sum_{\mathbf{k}} J \{ \mathcal{J}(\mathbf{k}) - \mathcal{J}(\mathbf{k} - \mathbf{q}) \} b_{\mathbf{k}}. \quad (5.2.38b)$$

The spin-wave energies deduced here, to second order in the expansion in $1/J$, depend on temperature and on the crystal-field mixing of the J_z -eigenstates, and both dependences are introduced via the two correlation functions $m_{\mathbf{k}}$ and $b_{\mathbf{k}}$, given self-consistently by (5.2.32) in terms of the energy parameters. $B_{\mathbf{q}}(T)$ vanishes if there is no anisotropy, i.e. if B_2^0 and B_6^6 are zero. In the case of single-ion anisotropy, $B_{\mathbf{q}}(T)$ is independent of \mathbf{q} if the small second-order term in (5.2.38b) is neglected, nor does it depend on the magnetic field, except for the slight field-dependence which may occur via the correlation functions m and b .

When the spin-wave excitation energies have been calculated, it is a straightforward matter to obtain the corresponding response functions. Within the present approximation, the xx -component of the susceptibility is

$$\chi_{xx}(\mathbf{q}, \omega) = -\frac{1}{4N} \sum_{ij} \langle \langle (J_+ + J_-)_i e^{-i\mathbf{q}\cdot\mathbf{R}_i}; (J_+ + J_-)_j e^{i\mathbf{q}\cdot\mathbf{R}_j} \rangle \rangle \\ = -\frac{J}{2} \left(1 - \frac{1}{2}m - \frac{1}{4}b \right)^2 \langle \langle a_{\mathbf{q}} + a_{-\mathbf{q}}^+; a_{\mathbf{q}}^+ + a_{-\mathbf{q}} \rangle \rangle. \quad (5.2.39)$$

The Bogoliubov transformation, eqns (5.2.19) and (5.2.21), with the parameters replaced by renormalized values, then leads to

$$\chi_{xx}(\mathbf{q}, \omega) = -\frac{J}{2} \left(1 - m - \frac{1}{2}b \right) \frac{\tilde{A}_{\mathbf{q}}(T) - \tilde{B}_{\mathbf{q}}(T)}{E_{\mathbf{q}}(T)} \langle \langle \alpha_{\mathbf{q}} + \alpha_{-\mathbf{q}}^+; \alpha_{\mathbf{q}}^+ + \alpha_{-\mathbf{q}} \rangle \rangle,$$

which is a simple combination of Bose Green-functions determined by (5.2.20), with $E_{\mathbf{q}}$ replaced by $E_{\mathbf{q}}(T)$. Introducing these functions and the parameters given by (5.2.34), we finally obtain

$$\chi_{xx}(\mathbf{q}, \omega) = J(1 - m) \frac{A_{\mathbf{q}}(T) - B_{\mathbf{q}}(T)}{E_{\mathbf{q}}^2(T) - (\hbar\omega)^2}, \quad (5.2.40a)$$

neglecting third-order terms. A rotation of the coordinate system by $\pi/2$ around the z -axis changes the sign of $B_{\mathbf{q}}(T)$, and hence we have

$$\chi_{yy}(\mathbf{q}, \omega) = J(1 - m) \frac{A_{\mathbf{q}}(T) + B_{\mathbf{q}}(T)}{E_{\mathbf{q}}^2(T) - (\hbar\omega)^2}. \quad (5.2.40b)$$

These results show that the ratio between the neutron-scattering intensities due to the spin-wave at \mathbf{q} , neglecting $S_{zz}(\mathbf{q}, \omega)$, in the two cases where the scattering vector is perpendicular to the basal y - z plane and to the x - z plane is

$$R_{\mathbf{q}}(T) = \left. \frac{S_{xx}(\mathbf{q}, \omega)}{S_{yy}(\mathbf{q}, \omega)} \right|_{\hbar\omega = \pm E_{\mathbf{q}}(T)} = \frac{\chi_{xx}(\mathbf{q}, 0)}{\chi_{yy}(\mathbf{q}, 0)} = \frac{A_{\mathbf{q}}(T) - B_{\mathbf{q}}(T)}{A_{\mathbf{q}}(T) + B_{\mathbf{q}}(T)}. \quad (5.2.41)$$

The measured intensities from Tb, which differ substantially from those calculated for the Heisenberg ferromagnet, agree well with this expression, especially if the correction for anisotropic two-ion coupling is taken into account (Jensen *et al.* 1975).

In the Heisenberg ferromagnet without rotational anisotropy, corresponding to $B_{\mathbf{q}}(T) = 0$, the elementary excitations at low temperatures are *circularly* polarized spin waves, in which the local moments precess in circles around the equilibrium direction. In the presence of anisotropy, $R_{\mathbf{q}}(T)$ differs from unity, and the excitations become *elliptically* polarized spin waves. The eccentricity of the ellipse depends on the wave-vector of the excited spin wave, and by definition $R_{\mathbf{q}}(T)$ is the square of the ratio of the lengths of the principal axes which, at least to the order in $1/J$ which we have considered, is equal to the ratio between the corresponding static susceptibility components. So the static anisotropy is reflected, in a direct way, in the normal modes of the system. The result (5.2.41) justifies the transformation (5.2.34) by attributing observable effects to the parameters $A_{\mathbf{q}}(T) \pm B_{\mathbf{q}}(T)$, whereas the parameters which are defined via the Hamiltonian alone, here $\tilde{A}_{\mathbf{q}}(T) \pm \tilde{B}_{\mathbf{q}}(T)$, depend on the particular Bose representation which is employed.

The longitudinal correlation function $S_{zz}(\mathbf{q}, \omega)$, which is neglected above, contains a diffusive mode at zero frequency, but no well-defined normal modes of non-zero frequency. There is inelastic scattering, but

the inelastic response, as well as the elastic mode, are purely of second order in $1/J$ and we shall not consider the longitudinal fluctuations further here.

The method developed in this section may be utilized, essentially unchanged, to calculate the MF susceptibility $\overline{\chi}^o(\omega)$ of the *single* sites. The result to first order in $1/J$ is:

$$\begin{aligned}\chi_{xx}^o(\omega) &= \langle J_z \rangle \frac{A - B + h_{\text{ex}}}{E_{\text{ex}}^2 - (\hbar\omega)^2} \\ \chi_{yy}^o(\omega) &= \langle J_z \rangle \frac{A + B + h_{\text{ex}}}{E_{\text{ex}}^2 - (\hbar\omega)^2} \\ \chi_{xy}^o(\omega) &= -\chi_{yx}^o(\omega) = \langle J_z \rangle \frac{i\hbar\omega}{E_{\text{ex}}^2 - (\hbar\omega)^2},\end{aligned}\tag{5.2.42a}$$

where $\langle J_z \rangle$ is the MF expectation value of J_z , h_{ex} is the exchange field, and E_{ex} is the energy of the first excited MF state:

$$h_{\text{ex}} = \langle J_z \rangle \mathcal{J}(\mathbf{0}) \quad ; \quad E_{\text{ex}}^2 = (A + h_{\text{ex}})^2 - B^2.\tag{5.2.42b}$$

Introducing this expression for $\overline{\chi}^o(\omega)$ into the RPA equation (3.5.8), we may derive $\overline{\chi}(\mathbf{q}, \omega)$ by the same method as was used for the Heisenberg ferromagnet in Section 3.5.2, in which case $A = B = 0$. The results for the xx - and yy -components are then found to agree with eqn (5.2.40) to leading order in $1/J$. To the next order in $1/J$, the parameters are replaced by renormalized values, but this procedure is not here easily generalized so as to become fully self-consistent. However, most of the corrections may be included by substituting $A_{\mathbf{0}}(T) \pm B_{\mathbf{0}}(T)$ for $A \pm B$ in the expression for $\overline{\chi}^o(\omega)$, and the self-consistent value of $\langle J_z \rangle$ for its MF value. The only terms which are not included in $\overline{\chi}(\mathbf{q}, \omega)$ by this procedure, as we may see by a comparison with eqn (5.2.40), are the \mathbf{q} -dependent contributions to $A_{\mathbf{q}}(T) \pm B_{\mathbf{q}}(T)$ determined by the \mathbf{k} -sums in (5.2.38). At low temperatures, these contributions are small and may safely be neglected in systems with long-range interactions. This formulation therefore represents a valid alternative, which is useful for generalizing the linear spin-wave theory to the hcp structure, discussed in Section 5.1, or to the helically or conically ordered systems which we will consider in Chapter 6.

As an example of the *magnon dispersion relations* for the anisotropic basal-plane ferromagnet, we show in Fig. 5.2 experimental measurements on Tb at 4K (Mackintosh and Bjerrum Møller 1972). The principal differences between these results and the corresponding excitations for Gd in Fig. 5.1 are the pronounced interactions which are observed between the magnons and phonons, which we shall discuss in some detail in

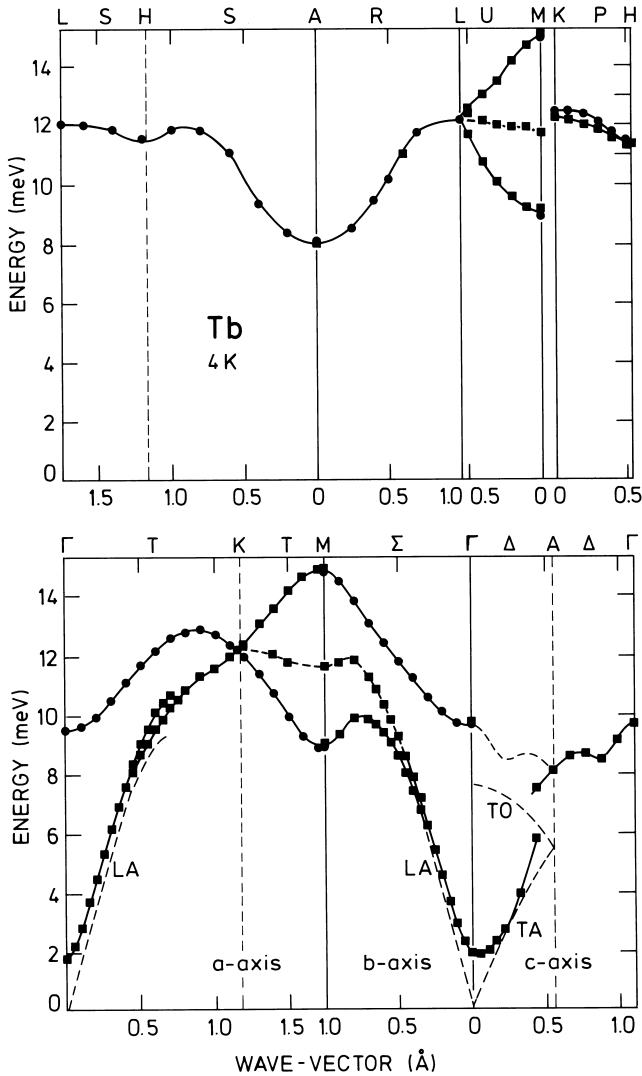


Fig. 5.2. The spin-wave dispersion relations along the symmetry lines in the Brillouin zone for Tb. In contrast to Gd, the anisotropy gives rise to an energy gap at the origin, and there are large effects due to interactions with the phonons. The third branch along, for example, Γ M may also be due to phonon interactions, or it may be a manifestation of the breaking of the hexagonal symmetry by the ordered moment in a particular domain, in the multi-domain sample. The lifting of the double degeneracy along the line KH provides evidence for anisotropic two-ion coupling.

Section 5.4.2, and the appearance of an energy gap at long wavelengths. This gap has its origin in the magnetic anisotropy. Even though the exchange energy required to excite a magnon vanishes in the long-wavelength limit, work is still required to turn the moments away from the easy direction against the anisotropy forces. If we neglect the small terms due to the sums over \mathbf{k} in (5.2.38), the dispersion relation along the c -axis in zero field becomes, from eqns (5.2.36–38),

$$E_{\mathbf{q}}(T) = \{[A_{\mathbf{0}}(T) + B_{\mathbf{0}}(T) + \langle J_z \rangle \{ \mathcal{J}(\mathbf{0}) - \mathcal{J}(\mathbf{q}) \}] \\ \times [A_{\mathbf{0}}(T) - B_{\mathbf{0}}(T) + \langle J_z \rangle \{ \mathcal{J}(\mathbf{0}) - \mathcal{J}(\mathbf{q}) \}]\}^{\frac{1}{2}}. \quad (5.2.43)$$

For an arbitrary direction in the zone, this relation is generalized analogously to eqn (5.1.9), giving rise again to acoustic and optical modes. From the dispersion relations, the *magnon density of states* and $\mathcal{J}(\mathbf{q})$ may readily be determined and hence, by a Fourier transform, the nominal Heisenberg exchange interaction $\mathcal{J}(ij)$ between moments on different atomic sites (Houmann 1968). The energy gap at zero wave-vector is given by

$$E_{\mathbf{0}}(T) = \{[A_{\mathbf{0}}(T) + B_{\mathbf{0}}(T)][A_{\mathbf{0}}(T) - B_{\mathbf{0}}(T)]\}^{\frac{1}{2}}, \quad (5.2.44)$$

and as we shall see in the next section, it is proportional to the geometrical mean of the axial- and hexagonal-anisotropy energies. We shall return to the dependence of this energy gap on the temperature and the magnetoelastic effects in the following two sections.

5.3 The uniform mode and spin-wave theory

The spin-wave mode at zero wave-vector is of particular interest. In comparison with the Heisenberg ferromagnet, the non-zero energy of this mode is the most distinct feature in the excitation spectrum of the anisotropic ferromagnet. In addition, the magnitude of the energy gap at $\mathbf{q} = \mathbf{0}$ is closely related to the bulk magnetic properties, which may be measured by conventional techniques. We shall first explore the connection between the static magnetic susceptibility and the energy of the uniform mode, leading to an expression for the temperature dependence of the energy gap. In the light of this discussion, we will then consider the general question of the validity of the spin-wave theory which we have presented in this chapter.

5.3.1 The magnetic susceptibility and the energy gap

The static-susceptibility components of the bulk crystal may be determined as the second derivatives of the free energy

$$F = U - TS = -\frac{1}{\beta} \ln Z. \quad (5.3.1)$$

The specific heat C may be derived in a simple way, within our current spin-wave approximation, by noting that the excitation spectrum is the same as that for a non-interacting Bose system, so that the entropy is fully determined by the statistics of independent bosons of energies $E_{\mathbf{q}}(T)$:

$$S = k_B \sum_{\mathbf{q}} [(1 + n_{\mathbf{q}}) \ln(1 + n_{\mathbf{q}}) - n_{\mathbf{q}} \ln n_{\mathbf{q}}], \quad (5.3.2)$$

and hence

$$C = T \partial S / \partial T = k_B T \sum_{\mathbf{q}} (dn_{\mathbf{q}} / dT) \ln \{(1 + n_{\mathbf{q}}) / n_{\mathbf{q}}\},$$

or, with $n_{\mathbf{q}} = [e^{\beta E_{\mathbf{q}}(T)} - 1]^{-1}$,

$$\begin{aligned} C &= \sum_{\mathbf{q}} E_{\mathbf{q}}(T) dn_{\mathbf{q}} / dT \\ &= \beta \sum_{\mathbf{q}} n_{\mathbf{q}} (1 + n_{\mathbf{q}}) E_{\mathbf{q}}(T) \{E_{\mathbf{q}}(T) / T - \partial E_{\mathbf{q}}(T) / \partial T\}, \end{aligned} \quad (5.3.3)$$

as in (3.4.17).

The first derivative of F with respect to the angles θ and ϕ can be obtained in two ways. The first is to introduce S , as given by (5.3.2) into (5.3.1), so that

$$\begin{aligned} \frac{\partial F}{\partial \theta} &= \frac{\partial U}{\partial \theta} - \sum_{\mathbf{q}} E_{\mathbf{q}}(T) \frac{\partial n_{\mathbf{q}}}{\partial \theta} \\ &= \frac{\partial U}{\partial \theta} \Big|_{m_{\mathbf{q}}, b_{\mathbf{q}}} + \sum_{\mathbf{q}} \left(\frac{\partial U}{\partial m_{\mathbf{q}}} \frac{\partial m_{\mathbf{q}}}{\partial \theta} + \frac{\partial U}{\partial b_{\mathbf{q}}} \frac{\partial b_{\mathbf{q}}}{\partial \theta} - E_{\mathbf{q}}(T) \frac{\partial n_{\mathbf{q}}}{\partial \theta} \right) \\ &= \frac{\partial U}{\partial \theta} \Big|_{m_{\mathbf{q}}, b_{\mathbf{q}}}, \end{aligned} \quad (5.3.4)$$

as it can be shown that $\partial U / \partial m_{\mathbf{q}} = J \tilde{A}_{\mathbf{q}}(T)$ and $\partial U / \partial b_{\mathbf{q}} = J \tilde{B}_{\mathbf{q}}(T)$, when $U = \langle \mathcal{H}_0 + \mathcal{H}_1 + \mathcal{H}_2 \rangle$, and hence that each term in the sum over \mathbf{q} in the second line of (5.3.4) vanishes, when (5.2.32) is used. This result is only valid to second order in $1/J$. However, a result of general validity is

$$\partial F / \partial \theta = \langle \partial \mathcal{H} / \partial \theta \rangle, \quad (5.3.5)$$

as discussed in Section 2.1, in connection with eqn (2.1.5). The two different expressions for $\partial F / \partial \theta$, and corresponding expressions for $\partial F / \partial \phi$, agree if \mathcal{H} in (5.3.5) is approximated by $\mathcal{H}_0 + \mathcal{H}_1 + \mathcal{H}_2$, i.e. to second order in $1/J$. However, the results obtained up to now are based on the

additional assumption, which we have not stated explicitly, that \mathcal{H}' in the starting Hamiltonian (5.2.12) is negligible. \mathcal{H}' is the sum of the terms proportional to Stevens operators O_l^m with m odd, and it includes for instance the term $3B_2^0(J_z J_x + J_x J_z) \cos \theta \sin \theta$ associated with $B_2^0 Q_2^0$ in eqn (5.2.3). \mathcal{H}' vanishes by symmetry if the magnetization is along a high-symmetry direction, i.e. $\theta = 0$ or $\pi/2$ and ϕ is a multiple of $\pi/6$. In these cases, the results obtained previously are valid. If the magnetization is not along a high-symmetry direction, \mathcal{H}' must be taken into account. The first-order contributions arise from terms proportional to $(1/J)^{1/2}$ in \mathcal{H}' , which can be expressed effectively as a linear combination of J_x and J_y . In this order, $\langle \partial \mathcal{H}' / \partial \theta \rangle = 0$ therefore, because $\langle J_x \rangle = \langle J_y \rangle = 0$ by definition. For a harmonic oscillator, corresponding in this system to the first order in $1/J$, the condition for the elimination of terms in the Hamiltonian linear in a and a^\dagger coincides with the equilibrium condition $\partial F / \partial \theta = \partial F / \partial \phi = 0$. Although the linear terms due to \mathcal{H}' can be removed from the Hamiltonian by a suitable transformation, terms cubic in the Bose operators remain. Second-order perturbation theory shows that, if \mathcal{H}' is non-zero, $\langle \partial \mathcal{H}' / \partial \theta \rangle$ and the excitation energies include contributions of the order $1/J^2$. Although it is straightforward to see that \mathcal{H}' makes contributions of the order $1/J^2$, it is not trivial to calculate them. The effects of \mathcal{H}' have not been discussed in this context in the literature, but we refer to the recent papers of Rastelli *et al.* (1985, 1986), in which they analyse the equivalent problem in the case of a helically ordered system.

In order to prevent \mathcal{H}' from influencing the $1/J^2$ -contributions derived above, we may restrict our discussion to cases where the magnetization is along high-symmetry directions. This does not, however, guarantee that \mathcal{H}' is unimportant in, for instance, the second derivatives of F . In fact $\partial \langle \partial \mathcal{H}' / \partial \theta \rangle / \partial \theta \propto \mathcal{O}(1/J^2)$ may also be non-zero when $\theta = 0$ or $\pi/2$, and using (5.3.4) we may write

$$\begin{aligned} F_{\theta\theta} &= \frac{\partial^2 F}{\partial \theta^2} = \frac{\partial^2 U}{\partial \theta^2} \Big|_{m_{\mathbf{q}}, b_{\mathbf{q}}} + \mathcal{O}(1/J^2) \\ &= \left\langle \frac{\partial^2}{\partial \theta^2} (\mathcal{H}_0 + \mathcal{H}_1 + \mathcal{H}_2) \right\rangle + \mathcal{O}(1/J^2) \quad ; \quad \theta = 0, \frac{\pi}{2}, \end{aligned} \quad (5.3.6a)$$

and similarly

$$F_{\phi\phi} = \left\langle \frac{\partial^2}{\partial \phi^2} (\mathcal{H}_0 + \mathcal{H}_1 + \mathcal{H}_2) \right\rangle + \mathcal{O}(1/J^2) \quad ; \quad \phi = p \frac{\pi}{6}, \quad (5.3.6b)$$

where the corrections of order $1/J^2$ are exclusively due to \mathcal{H}' . Here we have utilized the condition that the first derivatives of $m_{\mathbf{q}}$ and $b_{\mathbf{q}}$ vanish when the magnetization is along a symmetry direction.

The derivatives $F_{\theta\theta}$ and $F_{\phi\phi}$ are directly related to the static susceptibilities, as shown in Section 2.2.2. When $\theta_0 = \frac{\pi}{2}$, we obtain from eqn (2.2.18)

$$\chi_{xx}(\mathbf{0}, 0) = N\langle J_z \rangle^2 / F_{\theta\theta} \quad ; \quad \chi_{yy}(\mathbf{0}, 0) = N\langle J_z \rangle^2 / F_{\phi\phi}. \quad (5.3.7)$$

These results are of general validity, but we shall proceed one step further and use $F(\theta, \phi)$ for estimating the frequency dependence of the bulk susceptibilities. When considering the uniform behaviour of the system, we may to a good approximation assume that the equations of motion for all the different moments are the same:

$$\hbar\partial\langle\mathbf{J}\rangle/\partial t = \langle\mathbf{J}\rangle \times \mathbf{h}(\text{eff}). \quad (5.3.8)$$

By equating it to the average field, we may determine the effective field from

$$F = F(0) - N\langle\mathbf{J}\rangle \cdot \mathbf{h}(\text{eff}), \quad (5.3.9a)$$

corresponding to N isolated moments placed in the field $\mathbf{h}(\text{eff})$. The free energy is

$$F = F(\theta_0, \phi_0) + \frac{1}{2}F_{\theta\theta}(\delta\theta)^2 + \frac{1}{2}F_{\phi\phi}(\delta\phi)^2 - N\langle\mathbf{J}\rangle \cdot \mathbf{h}, \quad (5.3.9b)$$

and, to leading order, $\delta\theta = -\langle J_x \rangle / \langle J_z \rangle$ and $\delta\phi = -\langle J_y \rangle / \langle J_z \rangle$. Hence

$$h_x(\text{eff}) = -\frac{1}{N} \frac{\partial F}{\partial \langle J_x \rangle} = h_x - \frac{1}{N} F_{\theta\theta} \frac{\langle J_x \rangle}{\langle J_z \rangle^2}, \quad (5.3.10a)$$

and similarly

$$h_y(\text{eff}) = h_y - \frac{1}{N} F_{\phi\phi} \frac{\langle J_y \rangle}{\langle J_z \rangle^2}. \quad (5.3.10b)$$

Introducing a harmonic field applied perpendicular to the z -axis into eqn (5.3.8), we have

$$\begin{aligned} i\hbar\omega\langle J_x \rangle &= \frac{1}{N\langle J_z \rangle} F_{\phi\phi} \langle J_y \rangle - h_y \langle J_z \rangle \\ i\hbar\omega\langle J_y \rangle &= -\frac{1}{N\langle J_z \rangle} F_{\theta\theta} \langle J_x \rangle - h_x \langle J_z \rangle, \end{aligned} \quad (5.3.11)$$

and $\partial\langle J_z \rangle/\partial t = 0$, to leading order in \mathbf{h} . Solving the two equations for $h_x = 0$, we find

$$\chi_{yy}(\mathbf{0}, \omega) = \langle J_y \rangle / h_y = \frac{1}{N} \frac{F_{\theta\theta}}{E_0^2(T) - (\hbar\omega)^2}, \quad (5.3.12a)$$

and, when $h_y = 0$,

$$\chi_{xx}(\mathbf{0}, \omega) = \frac{1}{N} \frac{F_{\phi\phi}}{E_0^2(T) - (\hbar\omega)^2}, \quad (5.3.12b)$$

where the uniform-mode energy is

$$E_0(T) = \frac{1}{N\langle J_z \rangle} \{F_{\theta\theta}F_{\phi\phi}\}^{1/2}. \quad (5.3.13)$$

This result for the uniform mode in an anisotropic ferromagnet was derived by Smit and Beljers (1955). It may be generalized to an arbitrary magnetization direction by defining (θ, ϕ) to be in a coordinate system in which the polar axis is *perpendicular* to the z -axis (as is the case here), and by replacing $F_{\theta\theta}F_{\phi\phi}$ by $F_{\theta\theta}F_{\phi\phi} - F_{\theta\phi}^2$ if $F_{\theta\phi} \neq 0$.

The introduction of the averaged effective-field in (5.3.8) corresponds to the procedure adopted in the RPA, and a comparison of the results (5.3.12–13) with the RPA result (5.2.40), at $\mathbf{q} = \mathbf{0}$ and $\omega = 0$, shows that the relations

$$\begin{aligned} A_0(T) - B_0(T) &= \frac{1}{N\langle J_z \rangle} F_{\phi\phi} \\ A_0(T) + B_0(T) &= \frac{1}{N\langle J_z \rangle} F_{\theta\theta} \end{aligned} \quad (5.3.14)$$

must be valid to second order in $1/J$. In this approximation, $A_0(T) \pm B_0(T)$ are directly determined by that part of the time-averaged two-dimensional potential, experienced by the single moments, which is quadratic in the components of the moments perpendicular to the magnetization axis. The excitation energy of the uniform mode is thus proportional to the geometric mean of the two force constants characterizing the parabolic part of this potential. Since $A_0(T) \pm B_0(T)$ are parameters of order $1/J$, the second-order contributions of \mathcal{H}' in (5.3.6), which are not known, appear only in order $1/J^3$ in (5.3.14), when the magnetization is along a high-symmetry direction.

B_2^0 does not appear in $A_0(T) - B_0(T)$, and this is in accordance with eqn (5.3.14), as Q_2^0 is independent of ϕ . Considering instead the θ -dependence, we find that the contribution to $F_{\theta\theta}$ is determined by

$$\begin{aligned} \left\langle \frac{\partial^2 Q_2^0}{\partial \theta^2} \right\rangle &= \left\langle -6(J_z^2 - J_x^2) \cos 2\theta - 6(J_z J_x + J_x J_z) \sin 2\theta \right\rangle_{\theta=\pi/2} \\ &= 3\langle O_2^0 - O_2^2 \rangle. \end{aligned} \quad (5.3.15)$$

From (5.2.10) and (5.2.11), the thermal average is found to be

$$\begin{aligned} \langle O_2^0 - O_2^2 \rangle &= 2J^{(2)} \left\langle 1 - \frac{3}{J} a^+ a + \frac{3}{2J^2} a^+ a^+ a a \right. \\ &\quad \left. - \frac{1}{2J} \left(1 + \frac{1}{4J}\right) (a a + a^+ a^+) + \frac{1}{4J^2} (a^+ a a a + a^+ a^+ a^+ a) \right\rangle, \end{aligned}$$

or

$$\langle O_2^0 - O_2^2 \rangle = 2J^{(2)} \left\{ 1 - 3m + 3m^2 + \frac{3}{2}b^2 - \left(1 + \frac{1}{4J}\right)b + \frac{3}{2}mb + \mathcal{O}(1/J^3) \right\}. \quad (5.3.16)$$

Hence, according to (5.3.6a) and (5.3.14), the B_2^0 -term contributes to the spin-wave parameter $A_0(T) + B_0(T)$ by

$$\begin{aligned} 3B_2^0 \langle O_2^0 - O_2^2 \rangle / \langle J_z \rangle &\simeq 6B_2^0 J^{(2)} (1 - 3m - b) / J(1 - m) \\ &\simeq 6B_2^0 J^{(2)} (1 - 2m - b) / J, \end{aligned}$$

in agreement with (5.2.37b). When b is zero, this result is consistent with the classical Zener power-law (Zener 1954), $\langle O_l^m \rangle \propto \delta_{m0} \sigma^{l(l+1)/2}$, where $\sigma = 1 - m$ is the relative magnetization, since, to the order considered, $\langle O_2^0 - O_2^2 \rangle_{b=0} = \langle O_2^0 \rangle_{b=0} = 2J^{(2)}(1 - m)^3$. If we include the diagonal contribution of third order in m or $1/J$ to $\langle O_2^0 \rangle$ in (5.3.16), the result differs from the Zener power-law, but agrees, at low temperatures, with the more accurate theory of Callen and Callen (1960, 1965) discussed in Section 2.2. The results of the linear spin-wave theory obtained above can be utilized for generalizing the theory of Callen and Callen to the case of an anisotropic ferromagnet. The elliptical polarization of the spin waves introduces corrections to the thermal expectation values, which we express in the form

$$\langle O_2^0 - O_2^2 \rangle = 2J^{(2)} \hat{I}_{5/2}[\sigma] \eta_{\pm}^{-1}, \quad (5.3.17)$$

where the factor $\hat{I}_{l+1/2}[\sigma]$ represents the result (2.2.5) of Callen and Callen, and where η_{\pm} differs from 1 if b is non-zero. The two correlation functions m and b are determined through eqn (5.2.32), in terms of the intermediate parameters $\hat{A}_{\mathbf{k}}(T) \pm \hat{B}_{\mathbf{k}}(T)$, but it is more appropriate to consider instead

$$\begin{aligned} m_o &= \frac{1}{NJ} \sum_{\mathbf{k}} \left\{ \frac{A_{\mathbf{k}}(T)}{E_{\mathbf{k}}(T)} \left(n_{\mathbf{k}} + \frac{1}{2} \right) - \frac{1}{2} \right\} \\ b_o &= -\frac{1}{NJ} \sum_{\mathbf{k}} \frac{B_{\mathbf{k}}(T)}{E_{\mathbf{k}}(T)} \left(n_{\mathbf{k}} + \frac{1}{2} \right), \end{aligned} \quad (5.3.18)$$

defined in terms of the more fundamental parameters. The transformation (5.2.34) then leads to the following relations:

$$m_o + \frac{1}{2J} = m + \frac{1}{2J} - \frac{1}{2}b^2 \quad \text{and} \quad b_o = b - \frac{1}{2}b(m + \frac{1}{2J}).$$

Separating the two contributions in (5.3.16), we find

$$\tilde{b} \equiv \langle O_2^2 \rangle / \langle O_2^0 \rangle \simeq \left(1 + \frac{1}{4J}\right)b(1 - m)^{-3/2}, \quad (5.3.19a)$$

which, to the order calculated, may be written

$$\tilde{b} = \left(1 - \frac{1}{2J}\right)^{-1} \frac{b_o}{\sigma^2}, \quad (5.3.19b)$$

where

$$\sigma = \langle J_z \rangle / J = 1 - m = 1 - m_o - \frac{1}{2} b_o \tilde{b}. \quad (5.3.20)$$

The function η_{\pm} is then determined in terms of \tilde{b} as

$$\eta_{\pm} = (1 \pm \tilde{b})(1 - \frac{1}{2}\tilde{b}^2). \quad (5.3.21)$$

The spin-wave theory determines the correlation functions σ and η_{\pm} to second order in $1/J$, but for later convenience we have included some higher-order terms in (5.3.20) and (5.3.21). It may be straightforwardly verified that the thermal expectation values of $\langle O_2^0 - O_2^2 \rangle$ given by (5.3.16) and (5.3.17) agree with each other to order $1/J^2$. In the absence of anisotropy, the latter has a wider temperature range of validity than the former, extending beyond the regime where the excitations can be considered to be bosons. This should still be true in the presence of anisotropy, as long as \tilde{b} is small.

The combination of the spin-wave theory and the theory of Callen and Callen has thus led to an improved determination of the thermal averages of single-ion Stevens operators, as shown in Figs. 2.2 and 2.3. The quantity $O_2^0 - O_2^2$ was chosen as an example, but the procedure is the same for any other single-ion average. It is tempting also to utilize this improvement in the calculation of the excitation energies, and the relation (5.3.14) between the free energy and the spin-wave parameters $A_{\mathbf{0}}(T) \pm B_{\mathbf{0}}(T)$ is useful for this purpose. Neglecting the modifications due to \mathcal{H}' in (5.3.6), i.e. using $F_{\theta\theta} \simeq \langle \partial^2 \mathcal{H} / \partial \theta^2 \rangle$ and similarly for $F_{\phi\phi}$, we find from (5.3.14) the following results:

$$A_{\mathbf{0}}(T) - B_{\mathbf{0}}(T) = -\frac{1}{J\sigma} 36B_6^6 J^{(6)} \hat{I}_{13/2}[\sigma] \eta_-^{-15} \cos 6\phi + g\mu_B H \cos(\phi - \phi_H) \quad (5.3.22a)$$

and

$$\begin{aligned} A_{\mathbf{0}}(T) + B_{\mathbf{0}}(T) = & \frac{1}{J\sigma} \left[6B_2^0 J^{(2)} \hat{I}_{5/2}[\sigma] \eta_+^{-1} - 60B_4^0 J^{(4)} \hat{I}_{9/2}[\sigma] \eta_+^7 \eta_-^{-1} \right. \\ & \left. + 210B_6^0 J^{(6)} \hat{I}_{13/2}[\sigma] \eta_-^{18} \eta_+^{-1} - 6B_6^6 J^{(6)} \hat{I}_{13/2}[\sigma] \eta_-^{-30} \eta_+^{-25} \cos 6\phi \right] \\ & + g\mu_B H \cos(\phi - \phi_H), \quad (5.3.22b) \end{aligned}$$

which for completeness include all contributions from the starting Hamiltonian (5.2.1). The spin-wave spectrum at non-zero wave-vectors is adjusted accordingly by inserting $A_{\mathbf{0}}(T) \pm B_{\mathbf{0}}(T)$ given above, instead

of (5.2.37), in eqns (5.2.36), (5.2.38), and (5.2.40). If the out-of-plane anisotropy is stronger than the in-plane anisotropy, as in Tb and Dy, B is positive and \tilde{b} is negative. This means that η_+ and η_- are respectively smaller and greater than 1 (for small \tilde{b}), with the result that the axial contributions to $A_0(T) + B_0(T)$ are increased, whereas the planar contribution to $A_0(T) - B_0(T)$ is diminished, due to \tilde{b} . This is consistent with the fact that the out-of-plane fluctuations are suppressed in comparison with the in-plane fluctuations by the anisotropy. Hence we find, as a general result, that the elliptical polarization of the spin waves enhances, in a self-consistent fashion, the effects of the anisotropy. We note that Q_6^6 , which depends on both θ and ϕ , contributes to both anisotropy parameters, but that the anisotropy of the fluctuations affects the two contributions differently.

If \tilde{b} and the \mathbf{k} -sums in (5.2.38) are neglected, the above result for the spin-wave energies $E_{\mathbf{q}}(T)$ reduces to that derived by Cooper (1968b). The modifications due to the non-spherical precession of the moments, $\tilde{b} \neq 0$, were considered first by Brooks *et al.* (1968) and Brooks (1970), followed by the more systematic and comprehensive analysis of Brooks and Egami (1973). They utilized directly the equations of motion of the angular-momentum operators, without introducing a Bose representation. Their results are consistent with those above, except that they did not include all the second-order modifications considered here. We also refer to Tsuru (1986), who has more recently obtained a result corresponding to eqn (5.2.31), when B_6^6 is neglected, using a variational approach. The procedure outlined above essentially follows that of Lindgård and Danielsen (1974, 1975), which was further developed by Jensen (1975). This account only differs from that given by Jensen in the use of η_{\pm} instead of \tilde{b} as the basis for the ‘power-law’ generalization (and by the alternative choice of sign for B and \tilde{b}) and, more importantly, by the explicit use of $1/J$ as the expansion parameter.

As illustrated in Fig. 5.1 for Gd, and in Fig. 5.3 for Tb, the observed temperature dependence of the spin-wave spectrum is indeed substantial, both in the isotropic and the anisotropic ferromagnet. In the case of Tb, the variation of the exchange contribution is augmented by the temperature dependence of the anisotropy terms, which is reflected predominantly in the rapid variation of the energy gap at $\mathbf{q} = \mathbf{0}$. A comparison of Figs. 5.1 and 5.3 shows that the change in the form of $\mathcal{J}(\mathbf{q})$ appears to be more pronounced in Tb than in Gd. In Tb, the variation of $\mathcal{J}(\mathbf{q})$ with \mathbf{q} at a particular temperature is also modified if the magnetization vector is rotated from the b -axis to a hard a -axis (Jensen *et al.* 1975). Most of these changes with magnetization can be explained as the result of two-ion anisotropy, which we will consider in Section 5.5. Anisotropic two-ion terms may also affect the energy gap. In addition,

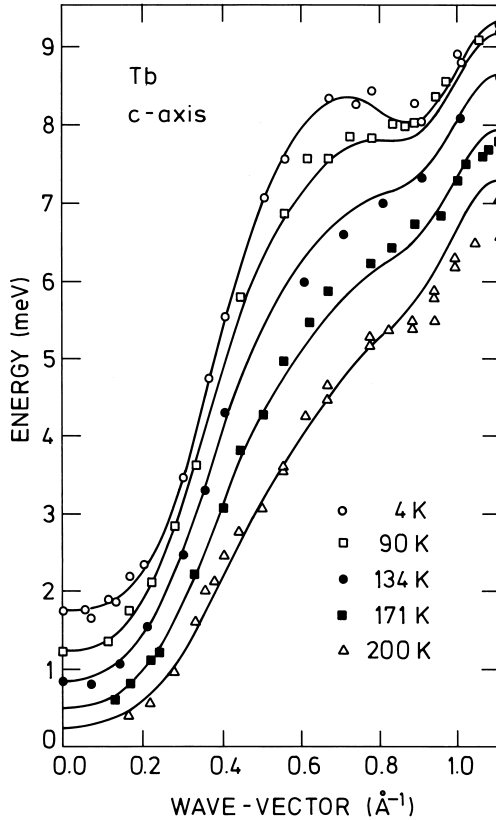


Fig. 5.3. The temperature dependence of the dispersion relations for the unperturbed spin waves in the c -direction in Tb. Both the energy gap and the \mathbf{q} -dependence renormalize with temperature. The results have been corrected for the magnon-phonon interaction, and the lines show the calculated energies.

the magnetoelastic coupling introduces qualitatively new effects, not describable by eqn (5.3.22), to which we will return after a short digression to summarize our understanding of the spin-wave theory.

5.3.2 The validity of the spin-wave theory

In presenting the spin-wave theory, we have neglected phenomena which first appear in the third order of $1/J$, most importantly the finite lifetimes of the excitations. In the presence of anisotropy, when B is different from zero, the total moment is not a conserved quantity, since $[\sum_i J_{iz}, \mathcal{H}] \neq 0$, unlike in the Heisenberg model. On the microscopic

plane, this means that the number of spin-wave excitations, i.e. magnons, is not necessarily conserved in a scattering process. In contrast to the behaviour of the isotropic ferromagnet, the linewidths do not therefore vanish at zero temperature, although energy conservation, combined with the presence of an energy gap in the magnon spectrum, strongly limit the importance of the allowed decay processes at low temperatures.

The two-ion interactions are assumed to involve only tensor operators of the lowest rank, so that these terms in the $1/J$ -expansion only have small numerical factors multiplying the Bose operator products. Therefore, if J is large, as in heavy rare earth-ions, the third-order terms due to the exchange coupling, which are neglected in the spin-wave theory, are expected to be small, as long as the number of excited magnons is not very large. The weak influence, at low temperatures, of the higher-order contributions of the exchange coupling is also indicated by a comparison with the low-temperature expansion of Dyson (1956) of the free energy in a Heisenberg ferromagnet with only nearest-neighbour interactions, also discussed by Rastelli and Lindgård (1979). If $A = B = 0$, the results derived earlier, to second order in $1/J$, are consistent with those of Dyson, except that we have only included the leading-order contribution, in the Born approximation or in powers of $1/J$, to the T^4 -term in the magnetization and in the specific heat. The higher-order corrections to the T^4 -term are significant if $J = \frac{1}{2}$, but if $J = 6$ as in Tb, for example, they only amount to a few per cent of this term and can be neglected.

If only the two-ion terms are considered, the RPA decoupling of the Bose operator products (5.2.29) is a good approximation at large J and at low temperatures. However, this decoupling also involves an approximation to the single-ion terms, and these introduce qualitatively new features into the spin-wave theory in the third order of $1/J$. For example, the C_3 -term in (5.2.26) directly couples the $|J_z = J\rangle$ state and $|J - 4\rangle$, leading to an extra modification of the ground state not describable in terms of B or η_{\pm} . Furthermore, the Bogoliubov transformation causes the (J_x, J_y) -matrix elements between the ground state and the third excited state to become non-zero. This coupling then leads to the appearance of a new pole in the transverse susceptibilities, in addition to the spin-wave pole, at an energy which, to leading order, is roughly independent of \mathbf{q} and close to that of the third excited MF level, i.e. $3E_{\mathbf{q}_o}(T)$, with \mathbf{q}_o defined as a wave-vector at which $\mathcal{J}(\mathbf{q}_o) = 0$. A qualitative analysis indicates that the third-order contribution to e.g. $\chi_{xx}(\mathbf{0}, 0)$, due to this pole, must cancel the second-order contribution of \mathcal{H}' to $F_{\theta\theta}$ in the relation (5.3.12b) between the two quantities. Hence the approximation $F_{\theta\theta} \simeq \langle \partial^2 \mathcal{H} / \partial \theta^2 \rangle$, used in (5.3.22), corresponds to the neglect of this additional pole.

The higher-order exchange contributions can thus be neglected at low temperatures, if J is large. This condition is not, however, sufficient to guarantee that the additional MF pole is unimportant, and the spin-wave result (5.3.22), combined with (5.2.36), (5.2.38), and (5.2.40), can only be trusted as long as the modification of the ground state, due to the single-ion anisotropy, is weak. This condition is equivalent to the requirement that $|\tilde{b}|$ be much less than 1. The regime within which the spin-wave theory is valid can be examined more closely by a comparison with the MF-RPA theory. In the latter, only the two-ion interactions are treated approximately, whereas the MF Hamiltonian is diagonalized exactly. The MF-RPA decoupling utilized in Section 3.5 leads here to a cancellation of the \mathbf{k} -sums in (5.3.38), and to a replacement of the correlation functions m_o and b_o by their MF values

$$m_o \simeq m_o^{\text{MF}} = \frac{1}{J} \left\{ \frac{A_{\mathbf{q}_o}(T)}{E_{\mathbf{q}_o}(T)} \left(n_{\mathbf{q}_o} + \frac{1}{2} \right) - \frac{1}{2} \right\}, \quad (5.3.23)$$

with a similar expression for b_o^{MF} . The wave-vector \mathbf{q}_o is defined as above, such that $\mathcal{J}(\mathbf{q}_o) = 0$. If the single-ion anisotropy is of second rank only, including possibly a Q_2^2 -term as well as the Q_2^0 -term of our specific model, all the predictions obtained with the MF-RPA version of the spin-wave theory agree extremely well with the numerical results obtained by diagonalizing the MF Hamiltonian exactly, even for relatively large values of $|b_o^{\text{MF}}|$ (≈ 0.1). Even though $1/J$ is the expansion parameter, the replacement of $(1 + \frac{1}{2J})$ by $(1 - \frac{1}{2J})^{-1}$ in (5.3.19b) extends the good agreement to the limit $J = 1$, in which case the MF Hamiltonian can be diagonalized analytically.

The applicability of the $1/J$ -expansion for the anisotropy is much more restricted if terms of high rank, such as Q_6^6 , dominate. This is a simple consequence of the relatively greater importance of the contributions of higher-order in $1/J$, like for instance the C_3 -term in (5.2.26), for higher-rank anisotropy terms. We have analysed numerically models corresponding to the low-temperature phases of Tb and Er, which include various combinations of anisotropy terms with ranks between 2 and 6. In the case of the basal-plane ferromagnet Tb, we find that the $1/J$ -expansion leads to an accurate description of the crystal-field effects on both the ground-state properties and the excitation energies. The MF-RPA excitation-energies calculated with the procedure of Section 3.5 differ relatively only by $\sim 10^{-3}$ at $T = 0$ from those of the spin-wave theory (Jensen 1976c). We furthermore find that this good agreement extends to non-zero temperatures, and that the $1/J$ -expansion is still acceptably accurate when $\sigma \simeq 0.8$. Consequently, the effective power-laws predicted by the spin-wave theory at low temperatures (Jensen 1975) are valid.

The renormalization of the anisotropy parameters appearing in the spin-wave energies, in the second order of $1/J$, is expected to be somewhat more important in the conical phase of Er than in Tb. In Er, the moments are not along a symmetry direction (they make an angle of about 28° with the c -axis) and the second-order modifications due to \mathcal{H}' in (5.2.12) might be expected to be important. The $1/J$ -results do not allow a precise estimate of the second-order contributions, but by introducing two scaling parameters, one multiplying the exchange terms by σ , and the other scaling the constant crystal-field contribution in the $1/J$ -expression for the spin-wave energies in the cone phase, it is possible (Jensen 1976c) to give an accurate account of the excitation energies derived by diagonalizing the MF Hamiltonian exactly, the relative differences being only of the order 10^{-2} . The two scaling parameters are found to have the expected magnitudes, although σ turns out to be slightly smaller ($\simeq 0.94$ in the model considered) than the relative magnetization predicted by the MF Hamiltonian ($\sigma^{\text{MF}} \simeq 0.98$). An analysis of the MF Hamiltonian shows that the excitations can be described in terms of an elliptical precession of the single moments, as expected, but surprisingly the ellipsoid lies in a plane with its normal making an angle ($\simeq 33^\circ$) with the c -axis which differs from the equilibrium cone-angle ($\simeq 28^\circ$), so the polarization of the spin waves is not purely transverse. In terms of the $1/J$ -expansion, this modification of the excited states can only be produced by \mathcal{H}' . This observation indicates that \mathcal{H}' has significant effects in Er, since it explains the difference between σ and σ^{MF} , as σ becomes equal to σ^{MF} if the angle appearing in the renormalized spin-wave energies is considered to be that defining the excited states, i.e. 33° , rather than the equilibrium value.

We may conclude that the $1/J$ -expansion is a valid procedure for describing the low-temperature magnetic properties of the heavy rare earth metals. This is an important conclusion for several reasons. To first order in $1/J$, the theory is simple and transparent. It is therefore feasible to include various kinds of complication in the model calculations and to isolate their consequences. This simplicity is retained in the second order of $1/J$, as long as \mathcal{H}' can be neglected, in which case the first-order parameters are just renormalized. Accurate calculations of the amount of renormalization of the different terms may be quite involved, but because of the long range of the two-ion interactions in the rare earth metals, the MF values of m_o and b_o utilized above normally provide good estimates. The spin-wave theory in the harmonic approximation, to first order in $1/J$, has been employed quite extensively in the literature, both for analysing experimental results and in various theoretical developments. It is therefore fortunate that these analyses are not invalidated, but only modified, or renormalized, by the

presence of moderate anisotropy. However, it is necessary to be aware that the renormalization itself may cause special effects not expected in the harmonic approximation, as the amount of renormalization may change when the system is perturbed by an external magnetic field or pressure, or when the temperature is altered.

There have been attempts (Lindgård 1978, and references therein) to construct an analytical spin-wave theory starting with a diagonalization of the MF Hamiltonian. In principle, this should be an appropriate starting-point, since the ground state is closer to the MF ground-state than to the fully polarized state, as soon as the planar anisotropy becomes significant. As in the model calculations discussed above, the MF Hamiltonian can be diagonalized numerically without difficulty, but in this form the method is non-analytical and the results are not easily interpretable. In order to diagonalize the MF Hamiltonian analytically, one is forced to make a perturbative expansion, unless J is small. If the MF Hamiltonian is expressed in the $|J_z\rangle$ -basis, the natural expansion parameter is $\sim |B_{\mathbf{q}_0}/A_{\mathbf{q}_0}| \simeq 2J|b_o|$ at $T = 0$. The use of this expansion parameter and the $1/J$ -expansion considered above lead to identical results in the limit $2J|b_o| \ll 1$ (Rastelli and Lindgård 1979). However, the expansion parameter is not small when the anisotropy is moderately large ($2J|b_o| \simeq 0.35$ in Tb at $T = 0$), which severely limits the usefulness of this procedure as applied by Lindgård (1978, 1988) to the analysis of the spin waves in the anisotropic heavy rare earths. It gives rise to a strong renormalization of all the leading-order spin-wave-energy parameters, which are thus quite sensitive, for example, to an external magnetic field, and it is extremely difficult to obtain a reasonable estimate of the degree of renormalization. In contrast, the $1/J$ -expansion leads, at low temperatures, to results in which only the high-rank terms (which are quite generally of smaller magnitude than the low-rank terms) are renormalized appreciably, and the amount of renormalization can be determined with fair accuracy. In the numerical example corresponding to Tb, the B_6^6 -term is renormalized by -38% at $T = 0$, according to the spin-wave theory, which agrees with the value obtained by diagonalizing the MF Hamiltonian exactly, as indicated in Fig. 2.3.

To recapitulate, we have developed a self-consistent RPA theory for the elementary excitations in a ferromagnet, i.e. the spin waves, valid when the magnetization is close to its saturation value. The major complication is the occurrence of anisotropic single-ion interactions, which were treated by performing a systematic expansion in $1/J$. To first order in $1/J$, the theory is transparent and simple, and it is straightforwardly generalized to different physical situations. Much of the simplicity is retained in second order, as long as the magnetization is along a

symmetry axis, but the first-order parameters are replaced by effective values. These effective parameters are determined self-consistently in terms of the spin-wave parameters $A_{\mathbf{q}}(T) \pm B_{\mathbf{q}}(T)$, which depend on T , and on an eventual applied magnetic field. One advantage of the use of $1/J$ as the expansion parameter is that the second-order modifications are smallest for the low-rank couplings, which are quite generally also the largest terms. If the magnetization is not along a symmetry axis, the elementary excitations may no longer be purely transverse. This additional second-order phenomenon may, however, be very difficult to detect experimentally within the regime of validity of the second-order spin-wave theory.

5.4 Magnetoelastic effects

The magnetoelastic coupling between the magnetic moments and the lattice modifies the spin waves in two different ways. The *static* deformations of the crystal, induced by the ordered moments, introduce new anisotropy terms in the spin-wave Hamiltonian. The *dynamic* time-dependent modulations of the magnetic moments furthermore interfere with the lattice vibrations. We shall start with a discussion of the static effects, and then consider the magnon–phonon interaction. The magnetoelastic crystal-field Hamiltonian was introduced in Section 1.4, where the different contributions were classified according to the symmetry of the strain parameters. The two-ion coupling may also change with the strain, as exemplified by eqn (2.2.32). We shall continue considering the basal-plane ferromagnet and, in order to simplify the discussion, we shall only treat the low-rank magnetoelastic couplings of single-ion origin. In the ferromagnetic case, the magnetoelastic two-ion couplings do not introduce any effects which differ qualitatively from those due to the crystal-field interactions. Consequently, those interactions which are not included in the following discussion only influence the detailed dependence of the effective coupling parameters on the magnetization and, in the case of the dynamics, on the wave-vector.

5.4.1 Magnetoelastic effects on the energy gap

The static effects of the α -strains on the spin-wave energies may be included in a straightforward manner, by replacing the crystal-field parameters in (5.2.1) with effective strain-dependent values, i.e. $B_2^0 \rightarrow B_2^0 + B_{\alpha 1}^{(2)} \bar{\epsilon}_{\alpha 1} + B_{\alpha 2}^{(2)} \bar{\epsilon}_{\alpha 2}$, with α -strains proportional to $\langle Q_2^0 \rangle$. Equivalent contributions appear in the magnetic anisotropy, discussed in Section 2.2.2. This simplification is not possible with the γ - or the ϵ -strain contributions, because these, in contrast to the α -strains, change the symmetry of the lattice. When $\theta = \pi/2$, the ϵ -strains vanish, and the

γ -strain part of the magnetoelastic Hamiltonian is given by eqn (2.2.23):

$$\begin{aligned} \mathcal{H}_\gamma = \sum_i & \left[\frac{1}{2} c_\gamma (\epsilon_{\gamma 1}^2 + \epsilon_{\gamma 2}^2) - B_{\gamma 2} \{ Q_2^2(\mathbf{J}_i) \epsilon_{\gamma 1} + Q_2^{-2}(\mathbf{J}_i) \epsilon_{\gamma 2} \} \right. \\ & \left. - B_{\gamma 4} \{ Q_4^4(\mathbf{J}_i) \epsilon_{\gamma 1} - Q_4^{-4}(\mathbf{J}_i) \epsilon_{\gamma 2} \} \right]. \end{aligned} \quad (5.4.1)$$

The equilibrium condition, $\partial F / \partial \epsilon_\gamma = 0$, leads to eqn (2.2.25) for the static strains $\bar{\epsilon}_\gamma$. The static-strain variables are distinguished by a bar from the dynamical contributions $\epsilon_\gamma - \bar{\epsilon}_\gamma$. The expectation values of the Stevens operators may be calculated by the use of the RPA theory developed in the preceding section, and with $\theta = \pi/2$ we obtain, for instance,

$$\begin{aligned} \langle Q_2^2 \rangle &= \langle \frac{1}{2} (O_2^0 + O_2^2) \cos 2\phi + 2O_2^{-1} \sin 2\phi \rangle = J^{(2)} \hat{I}_{5/2}[\sigma] \eta^{-1} \cos 2\phi \\ \langle Q_2^{-2} \rangle &= \langle \frac{1}{2} (O_2^0 + O_2^2) \sin 2\phi - 2O_2^{-1} \cos 2\phi \rangle = J^{(2)} \hat{I}_{5/2}[\sigma] \eta^{-1} \sin 2\phi. \end{aligned} \quad (5.4.2)$$

We note that $\langle O_2^{-1} \rangle$ vanishes only as long as \mathcal{H}' in (5.2.12) can be neglected. Introducing the magnetostriction parameters C and A via eqn (2.2.26a), when $\theta = \pi/2$,

$$\begin{aligned} \bar{\epsilon}_{\gamma 1} &= C \cos 2\phi - \frac{1}{2} A \cos 4\phi \\ \bar{\epsilon}_{\gamma 2} &= C \sin 2\phi + \frac{1}{2} A \sin 4\phi, \end{aligned} \quad (5.4.3)$$

and calculating $\langle Q_4^{\pm 4} \rangle$, we obtain

$$\begin{aligned} C &= \frac{1}{c_\gamma} B_{\gamma 2} J^{(2)} \hat{I}_{5/2}[\sigma] \eta^{-1} \\ A &= -\frac{2}{c_\gamma} B_{\gamma 4} J^{(4)} \hat{I}_{9/2}[\sigma] \eta^{-6}, \end{aligned} \quad (5.4.4)$$

instead of eqn (2.2.26b), including the effects of the elliptical precession of the moments. The equilibrium conditions allow us to split the magnetoelastic Hamiltonian into two parts:

$$\begin{aligned} \mathcal{H}_\gamma(\text{sta}) &= \sum_i \left[\frac{1}{2} c_\gamma (\bar{\epsilon}_{\gamma 1}^2 + \bar{\epsilon}_{\gamma 2}^2) - B_{\gamma 2} \{ Q_2^2(\mathbf{J}_i) \bar{\epsilon}_{\gamma 1} + Q_2^{-2}(\mathbf{J}_i) \bar{\epsilon}_{\gamma 2} \} \right. \\ & \left. - B_{\gamma 4} \{ Q_4^4(\mathbf{J}_i) \bar{\epsilon}_{\gamma 1} - Q_4^{-4}(\mathbf{J}_i) \bar{\epsilon}_{\gamma 2} \} \right], \end{aligned} \quad (5.4.5)$$

depending only on the static strains, and

$$\begin{aligned} \mathcal{H}_\gamma(\text{dyn}) &= \sum_i \left[\frac{1}{2} c_\gamma \{ (\epsilon_{\gamma 1} - \bar{\epsilon}_{\gamma 1})^2 + (\epsilon_{\gamma 2} - \bar{\epsilon}_{\gamma 2})^2 \} \right. \\ & - (B_{\gamma 2} \{ Q_2^2(\mathbf{J}_i) - \langle Q_2^2 \rangle \} + B_{\gamma 4} \{ Q_4^4(\mathbf{J}_i) - \langle Q_4^4 \rangle \}) (\epsilon_{\gamma 1} - \bar{\epsilon}_{\gamma 1}) \\ & \left. - (B_{\gamma 2} \{ Q_2^{-2}(\mathbf{J}_i) - \langle Q_2^{-2} \rangle \} - B_{\gamma 4} \{ Q_4^{-4}(\mathbf{J}_i) - \langle Q_4^{-4} \rangle \}) (\epsilon_{\gamma 2} - \bar{\epsilon}_{\gamma 2}) \right] \end{aligned} \quad (5.4.6)$$

depending only on the dynamical part of the strains.

To leading order, the magnetoelastic energy is determined by the static part (5.4.5), corresponding to eqn (2.2.27). \mathcal{H}_γ influences the equilibrium condition determining ϕ and, in the spin-wave approximation (\mathcal{H}' is neglected), we have

$$\begin{aligned} \frac{1}{N} \frac{\partial F}{\partial \phi} &= \frac{1}{N} \left\langle \frac{\partial}{\partial \phi} \{ \mathcal{H} + \mathcal{H}_\gamma \} \right\rangle \simeq \frac{1}{N} \left\langle \frac{\partial}{\partial \phi} \{ \mathcal{H} + \mathcal{H}_\gamma(\text{sta}) \} \right\rangle \\ &= -6B_6^6 J^{(6)} \hat{I}_{13/2} [\sigma] \eta_-^{-15} \sin 6\phi + g\mu_B H J \sigma \sin(\phi - \phi_H) \\ &\quad + 2c_\gamma C (\bar{\epsilon}_{\gamma 1} \sin 2\phi - \bar{\epsilon}_{\gamma 2} \cos 2\phi) - 2c_\gamma A (\bar{\epsilon}_{\gamma 1} \sin 4\phi + \bar{\epsilon}_{\gamma 2} \cos 4\phi), \end{aligned} \quad (5.4.7)$$

or, using the equilibrium values of $\bar{\epsilon}_{\gamma 1}$ and $\bar{\epsilon}_{\gamma 2}$,

$$\frac{1}{N} \frac{\partial F}{\partial \phi} = g\mu_B J \sigma \left\{ H \sin(\phi - \phi_H) - \frac{1}{6} \tilde{H}_c \sin 6\phi \right\}, \quad (5.4.8a)$$

with the definition

$$g\mu_B \tilde{H}_c = 36\kappa_6^6 / (J\sigma) = 36 \{ B_6^6 J^{(6)} \hat{I}_{13/2} [\sigma] \eta_-^{-15} + \frac{1}{2} c_\gamma C A \} / (J\sigma). \quad (5.4.8b)$$

If $H = 0$, the equilibrium condition $\partial F / \partial \phi = 0$ determines the stable direction of magnetization to be along either a b -axis or an a -axis, depending on whether \tilde{H}_c is positive or negative respectively.

The additional anisotropy terms introduced by \mathcal{H}_γ and proportional to the static strains, as for instance the term $-B_{\gamma 2} Q_2^2(\mathbf{J}_i) \bar{\epsilon}_{\gamma 1}$ in (5.4.5), contribute to the spin-wave energies. Proceeding as in Section 5.3, we find the additional contributions to $A_0(T) \pm B_0(T)$ in (5.3.22), proportional to the static γ -strains,

$$\begin{aligned} \Delta \{ A_0(T) + B_0(T) \} &= \frac{c_\gamma}{J\sigma} \{ 2C^2 + A^2 \eta_+^{-8} \eta_-^{-4} - CA(2 + \eta_+^{-8} \eta_-^{-4}) \cos 6\phi \} \eta_+^{-1} \eta_- \\ \Delta \{ A_0(T) - B_0(T) \} &= \frac{c_\gamma}{J\sigma} \{ 4C^2 + 4A^2 - 10CA \cos 6\phi \}. \end{aligned} \quad (5.4.9)$$

The contribution to $A_0(T) - B_0(T)$ is expressible directly in terms of the strain-parameters, C and A , without the further correction factors necessary for $A_0(T) + B_0(T)$. By using \tilde{H}_c and the non-negative quantity

$$\Lambda_\gamma = \frac{4c_\gamma}{J\sigma} (C^2 + A^2 + 2CA \cos 6\phi), \quad (5.4.10)$$

we can write the *total* spin-wave parameter

$$A_0(T) - B_0(T) = \Lambda_\gamma - g\mu_B \tilde{H}_c \cos 6\phi + g\mu_B H \cos(\phi - \phi_H). \quad (5.4.11)$$

This parameter does not obey the relation (5.3.14) with the second derivative $F_{\phi\phi}$ of the free energy. A differentiation $\partial F/\partial\phi$, as given by (5.4.8), with respect to ϕ shows that (5.3.14) accounts for the last two terms in (5.4.11), but not for Λ_γ . A calculation from (5.4.7) of the second derivative of F , when the strains are kept constant, instead of under the constant (zero) stress-condition assumed above, yields

$$A_0(T) - B_0(T) = \frac{1}{NJ\sigma} \frac{\partial^2 F}{\partial\phi^2} \Big|_{\epsilon=\bar{\epsilon}} = \Lambda_\gamma + \frac{1}{NJ\sigma} F_{\phi\phi}, \quad (5.4.12)$$

which replaces (5.3.14). The relation (5.3.14), determining $A_0(T) - B_0(T)$, was based on a calculation of the frequency dependence of the bulk susceptibility and, as we shall see later, it is the influence of the lattice which invalidates this argument. The Λ_γ term was originally suggested by Turov and Shavrov (1965), who called it the ‘frozen lattice’ contribution because the dynamic strain-contributions were not considered. However, as we shall show in the next section, the magnon-phonon coupling does not change this result.

The modifications caused by the magnetoelastic γ -strain couplings are strongly accentuated at a second-order phase transition, at which $F_{\phi\phi}$ vanishes. Let us consider the case where \tilde{H}_c is positive, $\tilde{H}_c = |\tilde{H}_c| \equiv H_c$, i.e. the b -axis is the easy axis. If a field is applied along an a -axis, $\phi_H = 0$, then the magnetization is pulled towards this direction, as described by eqn (5.4.8):

$$H = H_c \frac{\sin 6\phi}{6 \sin \phi} = H_c \left(1 - \frac{16}{3} \sin^2 \phi + \frac{16}{3} \sin^4 \phi\right) \cos \phi, \quad (5.4.13)$$

as long as the field is smaller than H_c . At the critical field $H = H_c$, the moments are pulled into the hard direction, so that $\phi = 0$ and the second derivative of the free energy,

$$F_{\phi\phi} = Ng\mu_B \{H \cos \phi - H_c \cos 6\phi\} J\sigma, \quad (5.4.14)$$

vanishes. So a second-order phase transition occurs at $H = H_c$, and the order parameter can be considered to be the component of the moments perpendicular to the a -axis, which is zero for $H \geq H_c$. An equally good choice for the order parameter is the strain $\bar{\epsilon}_{\gamma 2}$, and these two possibilities reflect the nature of the linearly coupled magnetic-structural phase transition. The free energy does not contain terms which are cubic in the order parameters, but the transition might be changed into one of first-order by terms proportional to $\cos 12\phi$, e.g. if σ or η_\pm , and thereby \tilde{H}_c , depend sufficiently strongly on ϕ (Jensen 1975). At the transition, eqn (5.4.11) leads to

$$A_0(T) - B_0(T) = \Lambda_\gamma \quad \text{at} \quad H = H_c, \quad (5.4.15)$$

which shows the importance of the constant-strain contribution Λ_γ . It ensures that the spin-wave energy gap $E_0(T)$, instead of going to zero as $|H - H_c|^{1/2}$, remains non-zero, as illustrated in Fig. 5.4, when the transition at $H = H_c$ is approached. Such a field just cancels the macroscopic hexagonal anisotropy, but energy is still required in the spin wave to precess the moments against the strain field of the lattice.

By symmetry, the γ -strains do not contain terms linear in $(\theta - \frac{\pi}{2})$, and the choice between constant-stress and constant-strain conditions therefore has no influence on their contribution to the second derivative of F with respect to θ , at $\theta = \pi/2$. Consequently, the γ -strains do not change the relation between $A_0(T) + B_0(T)$ and $F_{\theta\theta}$, given by eqn (5.3.14). The ε -strains vanish at $\theta = \pi/2$, but they enter linearly with $(\theta - \frac{\pi}{2})$. Therefore they have no effect on $A_0(T) + B_0(T)$, but they contribute to $F_{\theta\theta}$. To see this, we consider the ε -strain part of the Hamiltonian, eqn (2.2.29):

$$\mathcal{H}_\varepsilon = \sum_i \left[\frac{1}{2} c_\varepsilon (\epsilon_{\varepsilon 1}^2 + \epsilon_{\varepsilon 2}^2) - B_{\varepsilon 1} \{ Q_2^1(\mathbf{J}_i) \epsilon_{\varepsilon 1} + Q_2^{-1}(\mathbf{J}_i) \epsilon_{\varepsilon 2} \} \right]. \quad (5.4.16)$$

The equilibrium condition is

$$\bar{\epsilon}_{\varepsilon 1} = \frac{1}{c_\varepsilon} B_{\varepsilon 1} \langle Q_2^1 \rangle = \frac{1}{4} H_\varepsilon \sin 2\theta \cos \phi,$$

in terms of the magnetostriction parameter H_ε . In the basal-plane ferromagnet, $\bar{\epsilon}_{\varepsilon 1}$ and $\bar{\epsilon}_{\varepsilon 2}$ both vanish. The transformation (5.2.2) leads to

$$Q_2^1 = \frac{1}{4} (O_2^0 - O_2^2) \sin 2\theta \cos \phi - O_2^1 \cos 2\theta \cos \phi + O_2^{-1} \cos \theta \sin \phi + \frac{1}{2} O_2^{-2} \sin \theta \sin \phi, \quad (5.4.17)$$

and Q_2^{-1} is given by the same expression, if ϕ is replaced by $\phi - \frac{\pi}{2}$. This implies that

$$H_\varepsilon = \frac{4}{c_\varepsilon} B_{\varepsilon 1} \langle \frac{1}{4} (O_2^0 - O_2^2) \rangle = \frac{2}{c_\varepsilon} B_{\varepsilon 1} J^{(2)} \hat{I}_{5/2} [\sigma] \eta_+^{-1}. \quad (5.4.18)$$

The static ε -strains are zero and do not contribute to the spin-wave parameters $A_0(T) \pm B_0(T)$, but they affect the second derivative of F , with respect to θ , under zero-stress conditions and, corresponding to (5.4.12), we have

$$A_0(T) + B_0(T) = \left. \frac{1}{NJ\sigma} \frac{\partial^2 F}{\partial \theta^2} \right|_{\epsilon=\bar{\epsilon}} = \Lambda_\varepsilon + \frac{1}{NJ\sigma} F_{\theta\theta}, \quad (5.4.19)$$

with

$$\Lambda_\varepsilon = \frac{c_\varepsilon}{4J\sigma} H_\varepsilon^2, \quad (5.4.20)$$

where Λ_ε in (5.4.19) just cancels the ε -contribution to $F_{\theta\theta}/(NJ\sigma)$ determined from eqn (2.2.34).

The dependence of the magnon energy gap in Tb on magnetic field and temperature has been studied in great detail by Houmann *et al.* (1975a). They expressed the axial- and hexagonal-anisotropy energies of eqn (5.2.44) in the form

$$A_0(T) \pm B_0(T) = P_0(\pm) - P_6(\pm) \cos 6\phi + g\mu_B H \cos(\phi - \phi_H) \quad (5.4.21)$$

and, by a least-squares fitting of their results, some of which are shown in Fig. 5.4, they were able to deduce the values of the four parameters $P_{0,6}(\pm)$, shown as a function of magnetization in Fig. 5.5. According to eqns (5.3.22) and (5.4.9), these parameters are given at low temperatures by:

$$P_0(+) = \{6B_2^0 J^{(2)} - 60B_4^0 J^{(4)} + 210B_6^0 J^{(6)} + c_\gamma(2C^2 + A^2)\}/J \quad (a)$$

$$P_6(+) = \{6B_6^6 J^{(6)} + 3c_\gamma CA\}/J \quad (b)$$

$$P_0(-) = 4c_\gamma\{C^2 + A^2\}/J \quad (c)$$

$$P_6(-) = \{36B_6^6 J^{(6)} + 10c_\gamma CA\}/J, \quad (d)$$

(5.4.22)

where, for convenience, we have set the renormalization parameters σ and η_\pm to unity. These expressions for the parameters $P_{0,6}(\pm)$ are derived from a particular model. In general, additional contributions may appear due to other magnetoelastic interactions, and to anisotropic two-ion couplings. Nevertheless, within the RPA, the relations between the spin-wave energy parameters $A_0(T) \pm B_0(T)$ and the bulk anisotropy parameters, (5.4.12) and (5.4.19) combined with (5.3.7), should still be valid. The values of the anisotropy parameters, and their temperature dependences, determine the static magnetic and magnetoelastic properties, and can thus be obtained from bulk measurements on single crystals. A comparison between such static parameters and the dynamic values $P_{0,6}(\pm)$, derived from the field dependence of the spin-wave energy gap, can therefore elucidate the extent to which the spin-wave theory of the anisotropic ferromagnet is complete and correct.

Such a comparison has been made by Houmann *et al.* (1975a). The axial-anisotropy parameter $P_0(+) + P_6(+)$, when the moments are along the easy axis, agrees with the values deduced from torque and magnetization experiments, to within the rather large uncertainties of the

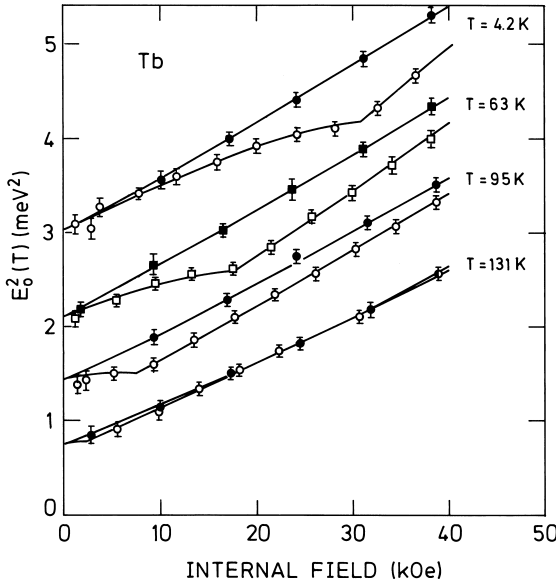


Fig. 5.4. The dependence of the square of the magnon energy gap in Tb on the internal magnetic field. Open symbols represent results for the field in the hard direction, and closed symbols are for the easy direction. The non-zero value of the gap at the critical field, which just turns the moments into the hard direction, is due to the constant-strain contribution Λ_γ . The full lines are least-squares fits of the theoretical expressions for the energy gap, given in the text, to the experimental results.

latter. The basal-plane anisotropies, as determined from the critical field H_c and the magnetoelastic γ -strain parameters, are well established by bulk measurements. Here $P_0(-)$ agrees, within the small combined uncertainties, with that derived from (5.4.22c) and (5.4.11), both in magnitude and temperature dependence. On the other hand, the small parameter $P_6(-)$ differs from the static value, so that

$$\delta_6(-) \equiv P_6(-) - g\mu_B\tilde{H}_c + 8c_\gamma CA/(J\sigma) \quad (5.4.23a)$$

is found to be non-zero. A part of this discrepancy may be explained by a twelve-fold anisotropy term, but this would also affect $P_0(-)$, and is expected to decrease more rapidly with increasing temperature than the experiments indicate. Within the accuracy of the experimental results, the non-zero value of $\delta_6(-)$ is the only indication of an additional renormalization of the spin-wave energy gap, compared with that derived from the second derivatives of the free energy.

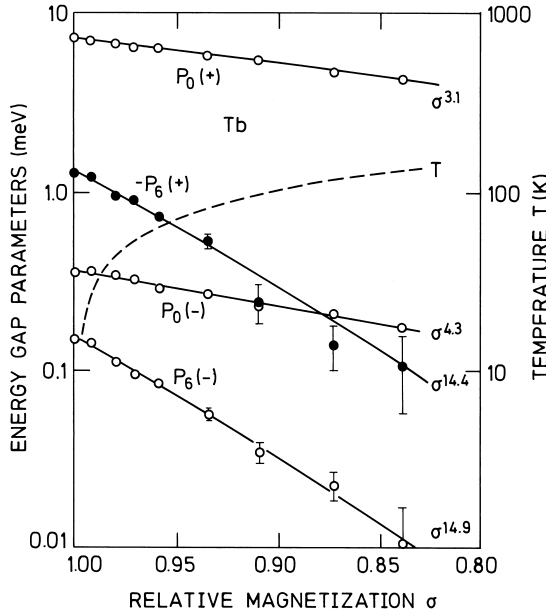


Fig. 5.5. Anisotropy parameters in Tb as a function of the relative magnetization, deduced from results of the type illustrated in Fig. 5.4.

The σ^3 -dependence of $P_0(+)$ on temperature is consistent with the σ^2 -renormalization of the dominant two-fold term in (5.4.22a) predicted by the Callen–Callen theory, but a comparison with the studies of dilute Tb-alloys by Høg and Touborg (1975) suggests that a large part of the axial anisotropy may have its origin in the two-ion coupling. The effect of the two-ion anisotropy is directly apparent in that part of the axial anisotropy $P_6(+)$ which depends on the orientation of the moments in the basal plane. If only single-ion anisotropy of the type which we have considered is important, $P_6(+)$ in (5.4.22b) is directly related to the critical field necessary to turn the moments into the hard direction. However, the experimental value of $P_6(+)$ bears little relation to $g\mu_B\tilde{H}_c/6$, even having the opposite sign. We can express this discrepancy by the parameter ΔM , defined by

$$\Delta M = P_6(+)-g\mu_B\tilde{H}_c/6. \quad (5.4.23b)$$

The influence of ΔM can be directly seen in the results of Fig. 5.4, since it is responsible for the difference between the slopes when the field is applied in the easy and hard directions. Although it could in principle be due to higher-rank γ -strain magnetoelastic terms, the large magnitude

of ΔM , compared to the contributions of C and A to the energy gap, effectively precludes this possibly. We must therefore ascribe it to two-ion anisotropy.

In the analysis of the field dependence of the magnon energy gap, the possible dependences of the renormalization parameters σ and η_{\pm} on magnetic field and the orientation of the moments were neglected at zero temperature, but included at non-zero temperatures, assuming the different parameters effectively to be functions of σ only. In the case of Dy, the zero-temperature change of the renormalization as a function of ϕ is of some importance (Egami 1972; Jensen 1975; Egami and Flanders 1976), whereas in Tb we have estimated by various means that both approximations are justified. There are some indications that there might be a systematic error involved in the determination of the ϕ -dependent energy-gap parameters $P_6(\pm)$, possibly arising from the influence of the classical dipole forces on the inelastic neutron-scattering at long wavelength, discussed in Section 5.5.1. An extrapolation of the results found at non-zero wave-vectors to $\mathbf{q} = \mathbf{0}$ suggests that both $P_6(+)$ and $P_6(-)$ may be about a factor of two smaller than shown in Fig. 5.5. If this were the case, ΔM would still be too large to be explained by the γ -strain couplings, but $\delta_6(-)$ would be reduced almost to the level of the experimental uncertainties. Otherwise a non-zero value of $\delta_6(-)$ can only be explained by theories beyond the RPA, e.g. by effects, proportional to the frequency, due to the interaction between the spin-waves and the electron-hole pair-excitations of the conduction electrons.

5.4.2 The magnon-phonon interaction

The displacement of the i th ion from its equilibrium position, $\delta\mathbf{R}_i = \mathbf{u}(\mathbf{R}_i)$, can be expanded in normal phonon coordinates in the usual way:

$$\mathbf{u}(\mathbf{R}_i) = \sum_{\nu\mathbf{k}} \mathbf{F}_{\mathbf{k}}^{\nu} (\beta_{\nu\mathbf{k}} + \beta_{\nu-\mathbf{k}}^+) e^{i\mathbf{k}\cdot\mathbf{R}_i}, \quad (5.4.24a)$$

with

$$F_{\mathbf{k},\alpha}^{\nu} = \left[\frac{\hbar}{2NM\omega_{\nu\mathbf{k}}} \right]^{\frac{1}{2}} f_{\mathbf{k},\alpha}^{\nu}. \quad (5.4.24b)$$

M is the mass of the ions and $f_{\mathbf{k},\alpha}^{\nu}$ is the α -component of the phonon-polarization vector. $\beta_{\nu\mathbf{k}}$ is the phonon-annihilation operator and $\omega_{\nu\mathbf{k}}$ the corresponding phonon frequency, where ν denotes one of the three (acoustic) branches. The polarization vectors are normalized and are mutually orthogonal:

$$\sum_{\alpha} (f_{\mathbf{k},\alpha}^{\nu})^* f_{\mathbf{k},\alpha}^{\nu'} = \delta_{\nu\nu'}. \quad (5.4.24c)$$

For simplicity, we assume that there is only one ion per unit cell, but the results we shall derive are also applicable to the hcp lattice, at least for the acoustic modes at long wavelengths. In this limit $\mathcal{H}_\gamma(\text{dyn})$, eqn (5.4.6), augmented by the kinetic energy of the ions, is adequate for discussing dynamical effects due to the γ -strains, if $\epsilon_{\alpha\beta}$ are replaced by their local values

$$\epsilon_{\alpha\beta}(i) = \bar{\epsilon}_{\alpha\beta} + \frac{i}{2} \sum_{\nu\mathbf{k}} (k_\alpha F_{\mathbf{k},\beta}^\nu + k_\beta F_{\mathbf{k},\alpha}^\nu) (\beta_{\nu\mathbf{k}} + \beta_{\nu-\mathbf{k}}^+) e^{i\mathbf{k}\cdot\mathbf{R}_i}. \quad (5.4.25)$$

We shall initially concentrate on the most important dynamical effects, and consider only the inhomogeneous-strain terms involving Stevens operators with odd m . Assuming for the moment that $\phi = p\frac{\pi}{2}$, we obtain the contribution $-B_{\gamma 2}\{-2O_2^{-1}(\mathbf{J}_i) \cos 2\phi\}(\epsilon_{\gamma 2}(i) - \bar{\epsilon}_{\gamma 2})$ from eqn (5.4.6), and a corresponding term in $B_{\gamma 4}$. Introducing the spin-deviation operators through (5.2.8) and (5.2.9), we obtain, to leading order in m and b ,

$$\begin{aligned} B_{\gamma 2}O_2^{-1}(\mathbf{J}_i) &= J^{(2)}B_{\gamma 2}\frac{i}{\sqrt{2J}}\{a_i^+ - a_i - \frac{5}{4J}(a_i^+a_i^+a_i - a_i^+a_ia_i)\} \\ &= J^{(2)}B_{\gamma 2}\frac{i}{\sqrt{2J}}(1 - \frac{5}{2}m + \frac{5}{4}b)(a_i^+ - a_i) \\ &= c_\gamma C \frac{i}{\sqrt{2J}}(1 + \frac{1}{2}m + \frac{1}{4}b)(a_i^+ - a_i) \\ &= ic_\gamma C \sum_{\mathbf{q}} \left[\frac{A_{\mathbf{q}}(T) + B_{\mathbf{q}}(T)}{2NJ\sigma E_{\mathbf{q}}(T)} \right]^{\frac{1}{2}} (\alpha_{\mathbf{q}}^+ - \alpha_{-\mathbf{q}}) e^{-i\mathbf{q}\cdot\mathbf{R}_i}, \end{aligned} \quad (5.4.26)$$

utilizing the RPA decoupling (5.2.29) and introducing the (renormalized) magnon operators $\alpha_{\mathbf{q}}^+$ and $\alpha_{-\mathbf{q}}$, analogously with (5.2.39) and (5.2.40). The $B_{\gamma 4}$ -term is treated in the same way, and introducing the phonon-operator expansion of the strains (5.4.25) into (5.4.6), we find that $\mathcal{H} + \mathcal{H}_\gamma$ leads to the following Hamiltonian for the system of magnons and phonons:

$$\mathcal{H}_{\text{mp}} = \sum_{\mathbf{k}} E_{\mathbf{k}}(T)\alpha_{\mathbf{k}}^+\alpha_{\mathbf{k}} + \sum_{\nu\mathbf{k}} \{ \hbar\omega_{\nu\mathbf{k}}\beta_{\nu\mathbf{k}}^+\beta_{\nu\mathbf{k}} + W_{\mathbf{k}}^\nu(\alpha_{\mathbf{k}}^+ - \alpha_{-\mathbf{k}})(\beta_{\nu\mathbf{k}} + \beta_{\nu-\mathbf{k}}^+) \} \quad (5.4.27)$$

with a *magnon-phonon interaction* given by

$$W_{\mathbf{k}}^\nu = -c_\gamma\sqrt{N}(k_1F_{\mathbf{k},2}^\nu + k_2F_{\mathbf{k},1}^\nu) \left[\frac{A_{\mathbf{k}}(T) + B_{\mathbf{k}}(T)}{2J\sigma E_{\mathbf{k}}(T)} \right]^{\frac{1}{2}} (C \cos 2\phi + A \cos 4\phi). \quad (5.4.28)$$

This Hamiltonian includes the part of \mathcal{H}_γ which is linear in the magnon operators when $\phi = p\frac{\pi}{2}$. The effects of the static deformations are

included in $E_{\mathbf{k}}(T)$ through (5.4.11). In general, $W_{\mathbf{k}}^{\nu}$ couples all three phonon modes with the magnons. A simplification occurs when \mathbf{k} is along the 1- or 2-axis, i.e. when \mathbf{k} is either parallel or perpendicular to the magnetization vector. In this case, $W_{\mathbf{k}}^{\nu}$ is only different from zero when ν specifies the mode as a transverse phonon with its polarization vector parallel to the basal plane. In order to analyse this situation, we introduce the four Green functions:

$$\begin{aligned} G_1(\mathbf{k}, \omega) &= \langle\langle \alpha_{\mathbf{k}}; \alpha_{\mathbf{k}}^+ - \alpha_{-\mathbf{k}} \rangle\rangle & G_2(\mathbf{k}, \omega) &= \langle\langle \alpha_{-\mathbf{k}}^+; \alpha_{\mathbf{k}}^+ - \alpha_{-\mathbf{k}} \rangle\rangle \\ G_3(\mathbf{k}, \omega) &= \langle\langle \beta_{\mathbf{k}}; \alpha_{\mathbf{k}}^+ - \alpha_{-\mathbf{k}} \rangle\rangle & G_4(\mathbf{k}, \omega) &= \langle\langle \beta_{-\mathbf{k}}^+; \alpha_{\mathbf{k}}^+ - \alpha_{-\mathbf{k}} \rangle\rangle, \end{aligned} \quad (5.4.29)$$

where the phonon mode is as specified above (the index ν is suppressed). \mathcal{H}_{mp} then leads to the following coupled equations of motion for these Green functions:

$$\begin{aligned} \{\hbar\omega - E_{\mathbf{k}}(T)\}G_1(\mathbf{k}, \omega) - W_{\mathbf{k}}\{G_3(\mathbf{k}, \omega) + G_4(\mathbf{k}, \omega)\} &= 1 \\ \{\hbar\omega + E_{\mathbf{k}}(T)\}G_2(\mathbf{k}, \omega) - W_{\mathbf{k}}\{G_3(\mathbf{k}, \omega) + G_4(\mathbf{k}, \omega)\} &= 1 \\ \{\hbar\omega - \hbar\omega_{\mathbf{k}}\}G_3(\mathbf{k}, \omega) + W_{-\mathbf{k}}\{G_1(\mathbf{k}, \omega) - G_2(\mathbf{k}, \omega)\} &= 0 \\ \{\hbar\omega + \hbar\omega_{\mathbf{k}}\}G_4(\mathbf{k}, \omega) - W_{-\mathbf{k}}\{G_1(\mathbf{k}, \omega) - G_2(\mathbf{k}, \omega)\} &= 0. \end{aligned} \quad (5.4.30)$$

These four equations may be solved straightforwardly and, using $W_{-\mathbf{k}} = -W_{\mathbf{k}}$, we obtain, for instance,

$$\begin{aligned} \langle\langle \alpha_{\mathbf{k}} - \alpha_{-\mathbf{k}}^+; \alpha_{\mathbf{k}}^+ - \alpha_{-\mathbf{k}} \rangle\rangle &= G_1(\mathbf{k}, \omega) - G_2(\mathbf{k}, \omega) \\ &= 2E_{\mathbf{k}}(T)\{(\hbar\omega)^2 - (\hbar\omega_{\mathbf{k}})^2\}/\mathcal{D}(\mathbf{k}, \omega), \end{aligned} \quad (5.4.31)$$

where the denominator is

$$\mathcal{D}(\mathbf{k}, \omega) = \{(\hbar\omega)^2 - E_{\mathbf{k}}^2(T)\}\{(\hbar\omega)^2 - (\hbar\omega_{\mathbf{k}})^2\} - 4W_{\mathbf{k}}^2\hbar\omega_{\mathbf{k}}E_{\mathbf{k}}(T). \quad (5.4.32)$$

In a similar way, introducing the appropriate Green functions, we find

$$\langle\langle \alpha_{\mathbf{k}} + \alpha_{-\mathbf{k}}^+; \alpha_{\mathbf{k}}^+ + \alpha_{-\mathbf{k}} \rangle\rangle = [2E_{\mathbf{k}}(T)\{(\hbar\omega)^2 - (\hbar\omega_{\mathbf{k}})^2\} + 8W_{\mathbf{k}}^2\hbar\omega_{\mathbf{k}}]/\mathcal{D}(\mathbf{k}, \omega). \quad (5.4.33)$$

In this situation, the polarization factor is $(k_1 f_{\mathbf{k},2} + k_2 f_{\mathbf{k},1}) = \pm k$, with $k = |\mathbf{k}|$. At long wavelengths, the velocity $v = \omega_{\mathbf{k}}/k$ of the transverse sound waves is related to the elastic constant $c_{66} = \rho v^2$, and hence

$$c_{\gamma} = 4c_{66}V/N = 4M\omega_{\mathbf{k}}^2/k^2, \quad (5.4.34)$$

and the coupling term in $\mathcal{D}(\mathbf{k}, \omega)$ can be written

$$4W_{\mathbf{k}}^2\hbar\omega_{\mathbf{k}}E_{\mathbf{k}}(T) = \{A_{\mathbf{k}}(T) + B_{\mathbf{k}}(T)\}(\hbar\omega_{\mathbf{k}})^2\Lambda_{\gamma}, \quad (5.4.35)$$

where the parameter Λ_γ is given by (5.4.10). The magnetic susceptibilities can be expressed in terms of the Green functions calculated above, using (5.2.39) and (5.2.40), and we finally arrive at

$$\chi_{xx}(\mathbf{q}, \omega) = J\sigma [A_{\mathbf{q}}(T) - B_{\mathbf{q}}(T)] \{(\hbar\omega_{\mathbf{q}})^2 - (\hbar\omega)^2\} - \Lambda_\gamma (\hbar\omega_{\mathbf{q}})^2 / \mathcal{D}(\mathbf{q}, \omega) \quad (5.4.36a)$$

and

$$\chi_{yy}(\mathbf{q}, \omega) = J\sigma [A_{\mathbf{q}}(T) + B_{\mathbf{q}}(T)] \{(\hbar\omega_{\mathbf{q}})^2 - (\hbar\omega)^2\} / \mathcal{D}(\mathbf{q}, \omega). \quad (5.4.36b)$$

Because $\omega_{\mathbf{q}} \propto q$ and $E_{\mathbf{0}}(T) > 0$, it is possible to satisfy the inequality $E_{\mathbf{q}}(T) \gg \hbar\omega_{\mathbf{q}}$ by choosing a sufficiently small q . As mentioned earlier, $E_{\mathbf{0}}(T)$ is always greater than zero, if the magnetoelastic coupling is non-zero, on account of the constant-strain term Λ_γ . Under these circumstances the elementary-excitation energies, determined by the poles of the susceptibilities or by $\mathcal{D}(\mathbf{q}, \omega) = 0$, are found to be

$$(\hbar\omega)^2 = \begin{cases} E_{\mathbf{q}}^2(T) + 4W_{\mathbf{q}}^2 \hbar\omega_{\mathbf{q}} / E_{\mathbf{q}}(T) \\ (\hbar\omega_{\mathbf{q}})^2 - 4W_{\mathbf{q}}^2 \hbar\omega_{\mathbf{q}} / E_{\mathbf{q}}(T), \end{cases} \quad (5.4.37)$$

to leading order in $\hbar\omega_{\mathbf{q}}/E_{\mathbf{q}}(T)$. The different excitations have become mixed magnetoelastic modes, which mutually repel due to the magnetoelastic coupling, and their squared energies are shifted up or down by an equal amount. When $E_{\mathbf{q}}(T) \gg \hbar\omega_{\mathbf{q}}$, the change in energy of the upper, predominantly magnon-like branch can be neglected, whereas the frequency of the lower phonon-like mode, as obtained from (5.4.37), using the relation (5.4.35),

$$\omega^2 = \omega_{\mathbf{q}}^2 \left(1 - \frac{\Lambda_\gamma}{A_{\mathbf{0}}(T) - B_{\mathbf{0}}(T)} \right) + \mathcal{O}(\{\hbar\omega_{\mathbf{q}}/E_{\mathbf{q}}(T)\}^4), \quad (5.4.38a)$$

may be modified appreciably relative to the unperturbed phonon frequency. This relation implies that the elastic constant, relative to the unperturbed value, as determined by the velocity of these magnetoacoustic sound waves, is

$$\frac{c_{66}^*}{c_{66}} = 1 - \frac{\Lambda_\gamma}{A_{\mathbf{0}}(T) - B_{\mathbf{0}}(T)} \quad ; \quad \mathbf{q} \parallel \text{ or } \perp \langle \mathbf{J} \rangle. \quad (5.4.38b)$$

At $\mathbf{q} = \mathbf{0}$, the dynamic coupling vanishes identically and the spin-wave energy gap is still found at $\hbar\omega = E_{\mathbf{0}}(T) = \{A_{\mathbf{0}}^2(T) - B_{\mathbf{0}}^2(T)\}^{1/2}$, with the static-strain contributions included in $A_{\mathbf{0}}(T) \pm B_{\mathbf{0}}(T)$. Due to the vanishing of the eigenfrequencies of the elastic waves at zero wave-vector, the lattice cannot respond to a uniform precession of the magnetic moments

at a non-zero frequency. Therefore the spin-wave mode at $\mathbf{q} = \mathbf{0}$ perceives the lattice as being completely static or ‘frozen’. This is clearly consistent with the result (5.4.12), that the spin-wave energy gap is proportional to the second derivative of the free energy under constant-strain, rather than constant-stress, conditions.

If the lattice is able to adapt itself to the applied constant-stress condition, in the static limit $\omega \ll \omega_{\mathbf{q}}$, then, according to (5.4.36b),

$$\chi_{yy}(\mathbf{q} \rightarrow \mathbf{0}, 0) = \chi_{yy}(\mathbf{q} \equiv \mathbf{0}, 0) = \frac{J\sigma}{A_{\mathbf{0}}(T) - B_{\mathbf{0}}(T) - \Lambda_{\gamma}} = N \frac{(J\sigma)^2}{F_{\phi\phi}}, \quad (5.4.39)$$

in agreement with (5.3.7). However, the first equality is not generally valid. The susceptibility depends on the direction from which \mathbf{q} approaches $\mathbf{0}$. If the direction of \mathbf{q} is specified by the spherical coordinates $(\theta_{\mathbf{q}}, \phi_{\mathbf{q}})$, then eqn (5.4.39) is valid only in the configuration considered, i.e. for $\theta_{\mathbf{q}} = \frac{\pi}{2}$ and $\phi_{\mathbf{q}} = 0$ or $\frac{\pi}{2}$. If we assume elastically isotropic conditions ($c_{11} = c_{33}$, $c_{44} = c_{66}$, and $c_{12} = c_{13}$), which is a reasonable approximation in Tb and Dy, we find that (5.4.39) is replaced by the more general result

$$\chi_{yy}(\mathbf{q} \rightarrow \mathbf{0}, 0) = \frac{J\sigma}{A_{\mathbf{0}}(T) - B_{\mathbf{0}}(T) - \Lambda_{\gamma} \sin^2 \theta_{\mathbf{q}} \{1 - (1 - \xi) \sin^2 \theta_{\mathbf{q}} \sin^2 2\phi_{\mathbf{q}}\}}, \quad (5.4.40)$$

when $\phi = 0$ or $\frac{\pi}{2}$, and $\xi = c_{66}/c_{11}$ ($\simeq 0.3$ in Tb or Dy). The reason for this modification is that discussed in Section 2.2.2; the ability of the lattice to adapt to various static-strain configurations is limited if these strains are spatially modulated. If \mathbf{q} is along the c -axis ($\theta_{\mathbf{q}} = 0$), the γ -strains are ‘clamped’, remaining constant throughout the crystal, so that the susceptibilities at both zero and finite frequencies are determined by the uniform γ -strain contributions alone. We note that, according to (5.4.28), $W_{\mathbf{k}}^{\nu}$ vanishes if \mathbf{k} is parallel to the c -axis ($k_1 = k_2 = 0$). The opposite extreme occurs when $\theta_{\mathbf{q}} = \frac{\pi}{2}$ and $\phi_{\mathbf{q}} = 0$ or $\frac{\pi}{2}$. The relevant strain-mode is determined by the equilibrium conditions (5.4.3) at zero constant stress, but generalized to the non-uniform case where the y -component of the moments has a small modulation, with the wave-vector \mathbf{q} along the x -direction. This strain mode $(\bar{\epsilon}_{\gamma_2}(i) + \bar{\omega}_{21}(i) \propto \cos(\mathbf{q} \cdot \mathbf{R}_i + \varphi))$ coincides with a phonon eigenstate, the transverse phonon at \mathbf{q} with its polarization vector in the basal plane. This coincidence makes the equilibrium strain-mode viable, which then explains the constant-stress result (5.4.39) obtained for χ_{yy} in this situation.

We shall now return to the discussion of the second-order transition occurring at $H = H_c$, when the field is applied along a hard direction

in the basal plane. From (5.4.36a), we see that $\chi_{xx}(\mathbf{q} \rightarrow \mathbf{0}, 0)$ does not show an anomaly at the transition. The critical behaviour is confined to the yy -component of the static susceptibility. At the transition, $A_0(T) - B_0(T) = \Lambda_\gamma$, according to eqn (5.4.15), and (5.4.40) then predicts a very rapid variation of $\chi_{yy}(\mathbf{q} \rightarrow \mathbf{0}, 0)$ with the direction of \mathbf{q} , with a divergent susceptibility in the long wavelength limit in the two cases where \mathbf{q} is along the z - or the y -axis, both lying in the basal plane, parallel or perpendicular to the magnetic moments. These divergences reflect a softening of two modes in the system, the transverse phonons propagating parallel to either of the two axes ($\theta_{\mathbf{q}} = \frac{\pi}{2}$ and $\phi_{\mathbf{q}} = p\frac{\pi}{2}$), with their polarization vectors in the basal plane. Equation (5.4.38) predicts that the velocity of these modes is zero, or $c_{66}^* = 0$, at $H = H_c$, at which field the dispersion is quadratic in q instead of being linear. The softening of these modes was clearly observed in the ultrasonic measurements of Jensen and Palmer (1979). Although the ultrasonic velocity could not be measured as a function of magnetic field all the way to H_c , because of the concomitant increase in the attenuation of the sound waves, the mode with \mathbf{q} parallel to the magnetization could be observed softening according to (5.4.38b), until the elastic constant was roughly halved. On the other hand, as discussed in the next section, the dipolar interaction prevents the velocity of the mode in which the ionic motion is along the magnetization from falling to zero, and (5.4.38b) is replaced by (5.5.13). When they took this effect into account, Jensen and Palmer (1979) could fit their results over a wide range of fields and temperatures with the RPA theory, without adjustable parameters or corrections for critical phenomena, using the bulk values of the three basal-plane anisotropy parameters C , A , and \tilde{H}_c ,

The absence of such corrections may be explained by the behaviour of the *critical fluctuations*, which is the same as that found in a pure structural phase-transition in an orthorhombic crystal, where c_{66} is again the soft elastic constant (Cowley 1976; Folk *et al.* 1979). The strong bounds set by the geometry on the soft modes in reciprocal space constrain the transition to exhibit mean-field behaviour. The *marginal dimensionality* d^* , as estimated for example by Als-Nielsen and Birgeneau (1977), using a real space version of the Ginzburg criterion, is $d^* = 2$ in this kind of system. Whenever the dimensionality d of the system is larger than d^* , as in this case, Wilson's *renormalization group* theory predicts no corrections to Landau's mean-field theory. The transition at $H = H_c$ is thus profoundly influenced by the magnetoelastic effects. Without them, i.e. with $C = A = 0$, the spin-wave energy gap would vanish at the transition, and the critical fluctuations, the long-wavelength magnons, would not be limited to certain directions in \mathbf{q} -space. Under such circumstances, the system would behave analogously to a three-

dimensional Ising model, $d^* = 4$, with pronounced modifications induced by the critical fluctuations. The original treatment by Turov and Shavrov (1965) of the γ -strain contributions, which prevent the uniform magnon mode from going soft at the critical field, included only the static-strain components. The more complete analyses, including the phonon dynamics, were later given by Jensen (1971a,b), Liu (1972b), and Chow and Keffer (1973).

When the wave-vector is in the c -direction, the γ -strain couplings vanish, but instead the ε -strains become important. The O_2^1 -term in Q_2^1 , given by eqn (5.4.17), leads to a linear coupling between the magnons and the phonons, and proceeding as in eqns (5.4.26–27), we find the additional contribution to \mathcal{H}_{mp}

$$\Delta\mathcal{H}_{\text{mp}} = \sum_{\mathbf{k}} iW_{\mathbf{k}}^\nu(\varepsilon)(\alpha_{\mathbf{k}}^+ + \alpha_{-\mathbf{k}})(\beta_{\nu\mathbf{k}} + \beta_{\nu-\mathbf{k}}^+), \quad (5.4.41a)$$

with

$$W_{\mathbf{k}}^\nu(\varepsilon) = -\frac{1}{4}c_\varepsilon\sqrt{N}\{(k_1F_{\mathbf{k},3}^\nu + k_3F_{\mathbf{k},1}^\nu)\cos\phi + (k_2F_{\mathbf{k},3}^\nu + k_3F_{\mathbf{k},2}^\nu)\sin\phi\} \\ \times \left[\frac{A_{\mathbf{k}}(T) - B_{\mathbf{k}}(T)}{2J\sigma E_{\mathbf{k}}(T)} \right]^{\frac{1}{2}} H_\varepsilon, \quad (5.4.41b)$$

in the long-wavelength limit. When \mathbf{k} is parallel to the c -axis, (5.4.28) and (5.4.41) predicts that only the transverse phonons with their polarization vectors parallel to the magnetization are coupled to the magnons. The calculation of the velocity of this coupled mode leads, by analogy to (5.4.38), to an elastic constant

$$\frac{c_{44}^*}{c_{44}} = 1 - \frac{\Lambda_\varepsilon}{A_{\mathbf{0}}(T) + B_{\mathbf{0}}(T)} \quad \text{when } \mathbf{f}_{\mathbf{k}}^\nu \parallel \langle \mathbf{J} \rangle. \quad (5.4.42)$$

The same result is obtained for the transverse-phonon mode propagating in the direction of the ordered moments, with the polarization vector parallel to the c -axis. These are the two modes which go soft in the case of a second-order transition to a phase with a non-zero c -axis moment.

We have so far only considered the dynamics in the long-wavelength limit. At shorter wavelengths, where the phonon and spin-wave energies may be comparable, the magnon–phonon interaction leads to a strong hybridization of the normal modes, with energy gaps at points in the Brillouin zone where the unperturbed magnon and phonon dispersion relations cross each other, as illustrated in Fig. 5.6. The interaction amplitudes (5.4.28) and (5.4.41b) are correct only for small wave-vectors. At shorter wavelengths, we must consider explicitly the relative positions

of neighbouring ions, instead of the local strains. Evenson and Liu (1969) have devised a simple procedure for replacing the local-strain variables in the magnetoelastic Hamiltonian with the relative displacements of the neighbouring ions. Using their procedure, and assuming the nearest-neighbour interactions to be dominant, we find that eqn (5.4.41*b*) is replaced by

$$W_{\mathbf{k}}^{\nu}(\varepsilon) = -\frac{1}{4}c_{\varepsilon}\sqrt{N}\left(\frac{2}{c}\sin(kc/2)\right)F_{\mathbf{k},\parallel}^{\nu}\left[\frac{A_{\mathbf{k}}(T)-B_{\mathbf{k}}(T)}{2J\sigma E_{\mathbf{k}}(T)}\right]^{\frac{1}{2}}H_{\varepsilon}, \quad (5.4.43)$$

when \mathbf{k} is along the c -axis. c is the lattice constant and $F_{\mathbf{k},\parallel}^{\nu}$ is the component of $\mathbf{F}_{\mathbf{k}}^{\nu}$ parallel to the magnetization vector, which is only non-zero for one of the transverse-phonon modes. This interaction does not distinguish between the two sublattices in the hcp crystal. This means that $W_{\mathbf{k}}^{\nu}(\varepsilon)$ only couples the magnons with the phonons at a certain \mathbf{k} if the modes are either both acoustic or both optical, consistent with the double-zone representation in the c -direction. Except for the replacement of (5.4.41*b*) by (5.4.43), the interaction Hamiltonian (5.4.41*a*) is unchanged. From the equations of motion of the Green functions, we may derive the susceptibilities, when \mathbf{k} is along the c -direction, in the same way as before, eqns (5.4.29–36), and the results are found to be:

$$\begin{aligned} \chi_{xx}(\mathbf{k}, \omega) &= J\sigma\{A_{\mathbf{k}}(T) - B_{\mathbf{k}}(T)\}\{(\hbar\omega_{t\mathbf{k}})^2 - (\hbar\omega)^2\}/\mathcal{D}_{\varepsilon}(\mathbf{k}, \omega) \\ \chi_{yy}(\mathbf{k}, \omega) &= J\sigma\{A_{\mathbf{k}}(T) + B_{\mathbf{k}}(T)\} \\ &\quad \times \{(\hbar\omega_{t\mathbf{k}})^2 - (\hbar\omega)^2 - 4W_{\mathbf{k}}^2(\varepsilon)\hbar\omega_{t\mathbf{k}}/E_{\mathbf{k}}(T)\}/\mathcal{D}_{\varepsilon}(\mathbf{k}, \omega), \end{aligned} \quad (5.4.44)$$

with

$$\mathcal{D}_{\varepsilon}(\mathbf{k}, \omega) = \{E_{\mathbf{k}}^2(T) - (\hbar\omega)^2\}\{(\hbar\omega_{t\mathbf{k}})^2 - (\hbar\omega)^2\} - 4W_{\mathbf{k}}^2(\varepsilon)\hbar\omega_{t\mathbf{k}}E_{\mathbf{k}}(T), \quad (5.4.45)$$

where $\omega_{t\mathbf{k}}$ is the angular frequency of the transverse phonon mode at \mathbf{k} . Introducing the parameter

$$\mathcal{Y}_{\mathbf{k}} = \left[1 + \frac{16\hbar\omega_{t\mathbf{k}}E_{\mathbf{k}}(T)W_{\mathbf{k}}^2(\varepsilon)}{\{E_{\mathbf{k}}^2(T) - (\hbar\omega_{t\mathbf{k}})^2\}^2}\right]^{\frac{1}{2}}, \quad (5.4.46)$$

we find the poles in the susceptibilities at

$$\hbar\omega = \pm E_{\mathbf{k}}^{\pm} = \pm \left[\frac{1}{2}\{E_{\mathbf{k}}^2(T) + (\hbar\omega_{t\mathbf{k}})^2\} \pm \frac{1}{2}\{E_{\mathbf{k}}^2(T) - (\hbar\omega_{t\mathbf{k}})^2\}\mathcal{Y}_{\mathbf{k}}\right]^{\frac{1}{2}}, \quad (5.4.47a)$$

corresponding to

$$\mathcal{D}_{\varepsilon}(\mathbf{k}, \omega) = \{(E_{\mathbf{k}}^+)^2 - (\hbar\omega)^2\}\{(E_{\mathbf{k}}^-)^2 - (\hbar\omega)^2\}. \quad (5.4.47b)$$

By a straightforward manipulation of these expressions, we obtain

$$\begin{aligned} \chi''_{yy}(\mathbf{k}, \omega) = \text{Im}[\chi_{yy}(\mathbf{k}, \omega)] &= \pi J\sigma \frac{A_{\mathbf{k}}(T) + B_{\mathbf{k}}(T)}{2E_{\mathbf{k}}(T)} \\ &\times \left[\frac{E_{\mathbf{k}}^+}{E_{\mathbf{k}}(T)} \frac{\Upsilon_{\mathbf{k}} + 1}{2\Upsilon_{\mathbf{k}}} \{ \delta(E_{\mathbf{k}}^+ - \hbar\omega) - \delta(E_{\mathbf{k}}^+ + \hbar\omega) \} \right. \\ &\quad \left. + \frac{E_{\mathbf{k}}^-}{E_{\mathbf{k}}(T)} \frac{\Upsilon_{\mathbf{k}} - 1}{2\Upsilon_{\mathbf{k}}} \{ \delta(E_{\mathbf{k}}^- - \hbar\omega) - \delta(E_{\mathbf{k}}^- + \hbar\omega) \} \right]. \end{aligned} \quad (5.4.48)$$

Almost the same expression is obtained for $\chi''_{xx}(\mathbf{k}, \omega)$; the sign before $B_{\mathbf{k}}(T)$ is reversed and the factors $E_{\mathbf{k}}^{\pm}/E_{\mathbf{k}}(T)$ are replaced by their reciprocals. If $W_{\mathbf{k}}(\varepsilon) = 0$, then $\Upsilon_{\mathbf{k}} = 1$ and $E_{\mathbf{k}}^{\pm} = E_{\mathbf{k}}(T)$, and (5.4.48) is equivalent to eqn (5.2.40b). When $W_{\mathbf{k}}(\varepsilon)$ is non-zero, $\Upsilon_{\mathbf{k}} > 1$ and there are two poles in the magnetic susceptibilities, one at $E_{\mathbf{k}}^+$ closest to $E_{\mathbf{k}}(T)$, and the other at $E_{\mathbf{k}}^-$ closest to the energy of the transverse-phonon mode. Both poles lie outside the energy interval between $E_{\mathbf{k}}(T)$ and $\hbar\omega_{t\mathbf{k}}$. The two normal modes at \mathbf{k} , the magnons and the transverse phonons polarized parallel to the magnetization, are transformed into two magnetoelastic modes, both of which give rise to a magnetic scattering of neutrons. The cross-section for neutrons scattered by a pure phonon-mode is proportional to $(\boldsymbol{\kappa} \cdot \mathbf{f}_{\mathbf{k}}^{\nu})^2$. If the scattering vector $\boldsymbol{\kappa}$ is along the c -axis, the transverse phonons in this direction do not therefore scatter neutrons, unless they are coupled to the magnons. With $\boldsymbol{\kappa}$ parallel to the c -axis, the (magnetic) scattering amplitude is proportional to $\chi''_{yy}(\mathbf{k}, \omega)$ and, in this situation, eqn (5.4.48), combined with (4.2.2) and (4.2.3), determines the total scattered intensity due to the coupled magnon and transverse-phonon modes. If the energy difference between the two uncoupled modes at some \mathbf{k} is large, $\Upsilon_{\mathbf{k}}$ is only slightly greater than 1, and the coupling induces only a small repulsion of the mode energies. The pole at energy $E_{\mathbf{k}}^+$, close to the unperturbed magnons, then dominates the magnetic scattering cross-section. The strongest modification occurs at the \mathbf{k} -vector where $E_{\mathbf{k}}(T) = \hbar\omega_{t\mathbf{k}}$, at which $\Upsilon_{\mathbf{k}} \rightarrow \infty$ and eqn (5.4.48) predicts nearly equal scattering intensities of the two modes at energies determined by

$$(\hbar\omega)^2 = E_{\mathbf{k}}^2(T) \pm 2E_{\mathbf{k}}(T)|W_{\mathbf{k}}(\varepsilon)| \quad ; \quad E_{\mathbf{k}}(T) = \hbar\omega_{t\mathbf{k}}, \quad (5.4.49a)$$

corresponding to an energy splitting, or energy gap, between the two modes of magnitude

$$\Delta \simeq 2|W_{\mathbf{k}}(\varepsilon)|, \quad (5.4.49b)$$

to leading order. These *resonance* or *hybridization* phenomena, the redistribution of the scattered intensity and the creation of an energy gap,

are observed whenever two normal modes are coupled linearly with each other, and the value of the energy gap at the \mathbf{k} -point where the two coupled modes are closest in energy, or where their scattering intensities are equal, gives a direct measure of the coupling amplitude at that particular \mathbf{k} -vector. The effect of the magnon-phonon interaction on the excitation spectrum in Tb is illustrated in Fig. 5.6.

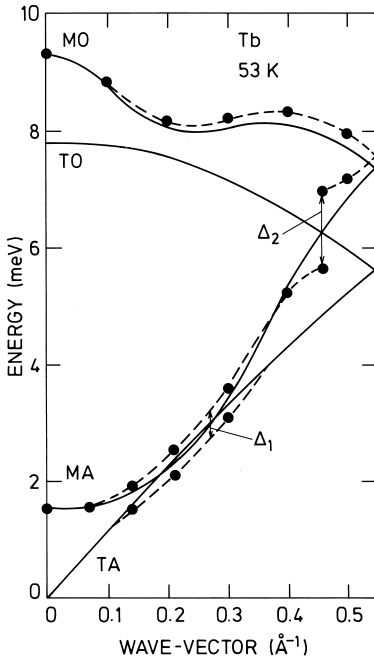


Fig. 5.6. The dispersion relations for the magnons and phonons propagating in the c -direction of Tb at 53 K, illustrating the magnon-phonon interaction. The calculated unperturbed modes are depicted by the full curves. The normal modes are mixed magnon-phonon states, and energy gaps appear at the crossing points of the unperturbed dispersion relations. The acoustic magnons interact both with the acoustic and the optical phonons.

The method described above, based on the magnetoelastic Hamiltonian, is not sufficiently general to enable a prediction of all possible couplings allowed by symmetry, i.e. the *selection rules*. To accomplish this, it is necessary either to use group-theoretical arguments, or to derive a general version of the magnon-phonon Hamiltonian based exclusively on symmetry considerations. These two methods have been applied to this system by respectively Cracknell (1974) and Jensen and Houmann (1975). Their analyses show that, when \mathbf{k} is along the c -direction, a further mixing is allowed in addition to that considered above. This requires the single-zone representation in the c -direction, since it couples an acoustic mode to an optical mode at the same \mathbf{k} -vector. The phonon modes in question are once more transverse, but their coupling to the magnons depends on the polarization relative to the direction of magnetization. In an a -axis magnet, the polarization vector should be parallel

to the magnetization, as is assumed in eqn (5.4.43), whereas in a b -axis magnet, the acoustic-optical coupling involves the transverse phonons polarized perpendicular to the magnetization (i.e. still along an a -axis). The symmetry arguments show that this coupling must be quadratic in k in the long wavelength limit, instead of linear as is $W_{\mathbf{k}}(\varepsilon)$. It therefore has no influence on the uniform strains or the elastic constants, and accordingly no counterpart in the magnetoelastic Hamiltonian. Liu (1972a) has discussed the possible origin of such an acoustic-optical interaction, and he concludes that it cannot be a crystalline-field effect, but must be mediated indirectly via the conduction electrons and be proportional to the spin-orbit coupling forces. As is illustrated in Fig. 5.6, the acoustic-optical magnon-phonon interaction is clearly observed in Tb, where it leads to the energy gap Δ_2 , the strongest hybridization effect seen in the metal. However, a closer examination (Jensen and Houmann 1975) shows that the transverse phonon modes involved are those polarized parallel to the magnetization, in spite of the fact that Tb has its magnetization vector in the b -direction. Hence this interaction violates the selection rules deduced from the general symmetry arguments, leading to the conclusion that the ground-state of Tb cannot be a simple b -axis ferromagnet as assumed. The $4f$ moments are undoubtedly along an easy b -axis, but the spins of the conduction electrons are not necessarily polarized collinearly with the angular momenta of the core electrons, because of their spin-orbit coupling. If the ground-state spin-density wave of the conduction electrons in Tb has a polarization which varies in space within a single unit cell, a coupling mediated by this spin-density wave may violate the selection rules based on the symmetry properties of the simple ferromagnet. The presence of the 'symmetry-breaking' acoustic-optical interaction in Tb demonstrates that the conduction electrons play a more active role than passively transmitting the indirect-exchange interaction. This magnon-phonon coupling is directly dependent on spin-orbit effects in the band electrons, in accordance with Liu's explanation, and its appearance demonstrates that the polarization of the conduction-electron spins must have a component perpendicular to the angular momenta.

To complete this section, we shall briefly discuss the additional magnon-phonon interaction terms which are linear in the phonon operators, but quadratic in the magnon operators:

$$\mathcal{H}_{\text{mp}}^{(2)} = \sum_{\mathbf{q}\mathbf{k}\nu} [U_{\nu}(\mathbf{k}, \mathbf{q})\alpha_{\mathbf{q}+\mathbf{k}}^+\alpha_{\mathbf{q}} + \frac{1}{2}V_{\nu}(\mathbf{k}, \mathbf{q})\alpha_{\mathbf{q}+\mathbf{k}}^+\alpha_{-\mathbf{q}} + \frac{1}{2}V_{\nu}^*(-\mathbf{k}, -\mathbf{q})\alpha_{\mathbf{q}}\alpha_{-\mathbf{q}-\mathbf{k}}](\beta_{\nu\mathbf{k}} + \beta_{\nu-\mathbf{k}}^+). \quad (5.4.50)$$

Referring back to the magnetoelastic Hamiltonian, we find that such an

interaction may originate from, for instance, the term

$$-B_{\gamma 2}\{(O_2^0 + O_2^2) - \langle O_2^0 + O_2^2 \rangle\} \frac{1}{2} \cos 2\phi(\epsilon_{\gamma 1} - \bar{\epsilon}_{\gamma 1})$$

in (5.4.6), or the corresponding terms in (5.4.16). In contrast to the linear couplings considered above, the symmetry-preserving α -strain part of the magnetoelastic Hamiltonian makes a contribution to the quadratic interaction terms. Using the procedure of Evenson and Liu (1969), it is straightforward, if somewhat tedious, to relate the interaction amplitudes in eqn (5.4.50) to the magnetoelastic coupling parameters. We shall not perform this analysis here, but refer instead to the detailed calculations of Jensen (1971a,b). The interactions in eqn (5.4.50) have the consequence that the equations of motion of the magnon Green function $\langle\langle \alpha_{\mathbf{q}}; \alpha_{\mathbf{q}}^+ \rangle\rangle$ involve new, higher-order mixed Green functions like $\langle\langle \alpha_{\mathbf{q}-\mathbf{k}}\beta_{\mathbf{k}}; \alpha_{\mathbf{q}}^+ \rangle\rangle$. Performing an RPA or Hartree–Fock decoupling, as in (5.2.29), of the three-operator products which occur in the equations of motion of the new Green functions, we obtain a closed expression for the magnon Green function, which may be written

$$\langle\langle \alpha_{\mathbf{q}}; \alpha_{\mathbf{q}}^+ \rangle\rangle = \frac{1}{\hbar\omega - E_{\mathbf{q}}(T) - \Sigma(\mathbf{q}, \omega)}, \quad (5.4.51)$$

where $\Sigma(\mathbf{q}, \omega)$ is the *self-energy*, due to the interactions in (5.4.50), of the magnons of wave-vector \mathbf{q} . Neglecting $V_{\nu}(\mathbf{q}, \mathbf{k})$, we find that the self-energy at $T = 0$ is

$$\Sigma(\mathbf{q}, \omega) = \lim_{\epsilon \rightarrow 0^+} \sum_{\mathbf{k}\nu} \frac{|U_{\nu}(\mathbf{k}, \mathbf{q})|^2}{\hbar\omega + i\hbar\epsilon - E_{\mathbf{q}+\mathbf{k}}(0) - \hbar\omega_{\nu\mathbf{k}}}. \quad (5.4.52)$$

These interactions are not diagonal in reciprocal space and the magnons are therefore affected by all the phonons. Whenever \mathbf{k} has a value such that $E_{\mathbf{q}}(0) \simeq E_{\mathbf{q}+\mathbf{k}}(0) + \hbar\omega_{\nu\mathbf{k}}$, the real part of the denominator in (5.4.52) vanishes close to the magnon pole at \mathbf{q} , as determined by (5.4.51). This implies a negative imaginary contribution to $\Sigma(\mathbf{q}, \omega)$, when $\hbar\omega \simeq E_{\mathbf{q}}(0)$, and hence a reduction in the lifetime of the magnons. The energy of the magnons at \mathbf{q} is approximately given by $E_{\mathbf{q}}(0) + \text{Re}[\Sigma(\mathbf{q}, \omega)]$, with $\hbar\omega \simeq E_{\mathbf{q}}(0)$. At non-zero temperatures, the self-energy terms increase in proportion to the Bose population-factors of the magnons and phonons involved. These interactions, quadratic in the magnon operators, do not lead to the kind of hybridization effects produced by the linear couplings, but rather give rise to a (small) renormalization of the normal-mode energies and to a finite lifetime of the excitations. These effects are entirely similar to those due to the magnon–magnon interactions appearing in the spin-wave theory in the third order

of $1/J$. Equation (5.4.52) shows that the ‘zero-point’ motion of the ions, at $T = 0$, has a slight effect on the magnons. A similar effect occurs due to the magnon–magnon interactions, but only in an anisotropic ferromagnet where B is non-zero, as we discussed in the previous section. In most cases, the contributions due to the magnon–magnon interactions are expected to predominate, because the magnon–phonon coupling parameters are usually quite small, in comparison with the spin-wave interactions. Although the interactions in (5.4.50) may not be important for the magnons, they may have observable effects on the phonons at finite temperatures. For instance, they affect the velocity of the transverse sound waves propagating in the c -direction and polarized perpendicular to the magnetization, but not those polarized parallel to the magnetization, which are modified by the linear couplings as discussed above. Deriving the perturbed phonon Green functions in the same way as the magnon Green function, and taking the long-wavelength limit, we find (Jensen 1971a,b)

$$\frac{c_{44}^*}{c_{44}} = 1 - \Lambda_\varepsilon \frac{1}{NJ} \sum_{\mathbf{q}} \frac{n_{\mathbf{q}}}{E_{\mathbf{q}}(T)} \quad \text{when } \mathbf{f}_{\mathbf{k}}^\nu \perp \langle \mathbf{J} \rangle. \quad (5.4.53)$$

We note that this result is of higher order in $1/J$ than the effect due to the linear coupling, given in (5.4.42). However, the extra factor $1/J$ may be compensated by the magnon population-factor $n_{\mathbf{q}}$ in the sum over \mathbf{q} , at elevated temperatures.

Modifications of the results obtained above may occur, due to anharmonic terms of third order in the strains, or magnetoelastic terms quadratic in the strains. These higher-order contributions may possibly be of some importance for the temperature dependence of the elastic constants and the spin-wave parameters. However, they should be of minor significance under the nearly constant-strain conditions which obtain, for instance, when the magnetic-field dependence of the elastic constants is considered.

5.5 Two-ion anisotropy

In this section, we discuss the components of the two-ion coupling which cannot be included in the *isotropic* Heisenberg Hamiltonian considered hitherto, i.e. the two-ion term in eqn (5.2.1). We first consider the classical magnetic *dipole–dipole interaction* in some detail, and show how it may affect the spin-wave energies and ultrasonic velocities. Thereafter we discuss some of the complexities resulting from the presence of *general two-ion couplings*, which are consistent with the symmetry properties of the magnetic phase. The experimental manifestations of such interactions, which either have been observed in the excitation spectrum of Tb, or could in principle be observed, are finally summarized.

5.5.1 The dipole–dipole interaction

A general two-ion Hamiltonian involving only the dipolar moments of the $4f$ electrons is

$$\mathcal{H}_{\text{dd}} = -\frac{1}{2} \sum_{ij} \sum_{\alpha\beta} \mathcal{J}_{\alpha\beta}(ij) J_{i\alpha} J_{j\beta}. \quad (5.5.1)$$

The Heisenberg interaction, when expressed in this way, is diagonal, with the form $\mathcal{J}(ij)\delta_{\alpha\beta}$. The most familiar example of an *anisotropic* two-ion coupling is the classical magnetic dipole–dipole interaction, which gives a contribution

$$\Delta \mathcal{J}_{\alpha\beta}(ij) = \frac{N}{V} (g\mu_B)^2 D_{\alpha\beta}(ij), \quad (5.5.2a)$$

where $D_{\alpha\beta}(ij)$ is the dimensionless coupling parameter

$$D_{\alpha\beta}(ij) = \frac{V}{N} \frac{3(R_{i\alpha} - R_{j\alpha})(R_{i\beta} - R_{j\beta}) - \delta_{\alpha\beta} |\mathbf{R}_i - \mathbf{R}_j|^2}{|\mathbf{R}_i - \mathbf{R}_j|^5}, \quad (5.5.2b)$$

recalling that the magnetic moment of the i th ion is $g\mu_B \mathbf{J}_i$. This coupling is weak, being typically one or two orders of magnitude smaller than the indirect exchange between near neighbours, but it is extremely long-range and anisotropic and may therefore have important consequences for the magnetic properties, as we shall discuss in the following.

We wish to calculate the spatial Fourier transform

$$D_{\alpha\beta}(\mathbf{q}) = \frac{1}{N} \sum_i \sum_j D_{\alpha\beta}(ij) e^{-i\mathbf{q}\cdot(\mathbf{R}_i - \mathbf{R}_j)}. \quad (5.5.3)$$

If \mathbf{q} is along the c -axis, which is a three-fold axis of the hcp lattice, the symmetry dictates that the only non-zero elements of $\mathcal{J}_{\alpha\beta}(\mathbf{q})$ are $\mathcal{J}_{\xi\xi}(\mathbf{q}) = \mathcal{J}_{\eta\eta}(\mathbf{q})$ and $\mathcal{J}_{\zeta\zeta}(\mathbf{q})$. In addition, the condition $\sum_{\alpha} D_{\alpha\alpha}(\mathbf{q}) = 0$ implies that

$$D_{\zeta\zeta}(\mathbf{q}) = -2D_{\xi\xi}(\mathbf{q}) = -2D_{\eta\eta}(\mathbf{q}) \quad ; \quad \mathbf{q} \parallel c\text{-axis}, \quad (5.5.4)$$

with the extra stipulation that $\mathbf{q} \neq \mathbf{0}$, in which case the surface of the sample does not contribute. In the limit of long wavelengths, the shape of the sample becomes important, and for convenience we assume it to be an ellipsoid, with the principal axes along the symmetry ξ -, η -, and ζ -axes. We consider first the limit $\mathbf{q} = \mathbf{0}$ where, because the sample is an ellipsoid, the summation over j in (5.5.3) leads to a result independent of i , since an ellipsoid placed in a constant magnetic field has a uniform magnetization throughout its interior. Furthermore, when $\mathbf{r} = \mathbf{R}_i - \mathbf{R}_j$ becomes large, it may be replaced by a continuous variable, and the sum

over j may be split into a sum over the lattice points lying within a large sphere plus an integral over the rest of the sample:

$$\sum_j \cdots = \sum_{j \in \text{sphere}} \cdots + \frac{N}{V} \int_{\text{sphere}}^{\text{sample}} \cdots d\mathbf{r}.$$

The value of the integral for the zz -component is

$$\begin{aligned} \int \frac{1}{r^3} \left(\frac{3z^2}{r^2} - 1 \right) d\mathbf{r} &= - \int \nabla \cdot \left(\frac{\mathbf{z}}{r^3} \right) d\mathbf{r} = \int_{\text{sphere}} \frac{\mathbf{z} \cdot d\mathbf{S}}{r^3} - \int_{\text{sample}} \frac{\mathbf{z} \cdot d\mathbf{S}}{r^3} \\ &= \frac{4\pi}{3} - N_z, \end{aligned}$$

where $d\mathbf{S}$ is a vectorial surface element of the sphere/sample, and N_ξ is the *demagnetization factor*

$$N_\xi = \int_{\text{sample}} \left(\frac{\hat{\boldsymbol{\xi}} \cdot \mathbf{r}}{r^3} \right) \hat{\boldsymbol{\xi}} \cdot d\mathbf{S}, \quad (5.5.5)$$

where $\hat{\boldsymbol{\xi}}$ is a unit vector along the ξ -axis. It is easily seen that $N_\xi + N_\eta + N_\zeta = 4\pi$. Hence we obtain

$$D_{\xi\xi}(\mathbf{0}) = \frac{4\pi}{3} + [D_{\xi\xi}(\mathbf{0})]_L - N_\xi, \quad (5.5.6)$$

plus equivalent results for the other diagonal components. The first term is the *Lorentz factor*, and $[D_{\xi\xi}(\mathbf{0})]_L$ is the value of the lattice sum over the sphere, satisfying the relations $[D_{\zeta\zeta}(\mathbf{0})]_L = -2[D_{\xi\xi}(\mathbf{0})]_L = -2[D_{\eta\eta}(\mathbf{0})]_L$. In the case of a cubic lattice, the lattice sums vanish by symmetry. This is nearly also true for an hcp lattice with an ideal c/a -ratio, because of the close relationship between the fcc lattice and the ideal hcp lattice. The hcp lattice of the heavy rare earths is slightly distorted, as may be seen from Table 1.2, in which case the lattice sums become non-zero, approximately proportionally to the deviation from the ideal c/a -ratio; $[D_{\xi\xi}(\mathbf{0})]_L = -0.0024 + 1.50(c/a - \sqrt{8/3})$. Brooks and Goodings (1968) overestimate the anisotropy in the free energy due to the dipole interaction by a factor of two.

When considering the lattice sum determining $D_{\alpha\beta}(\mathbf{q}) - D_{\alpha\beta}(\mathbf{0})$, we may immediately apply the continuum approximation in the long-wavelength limit $2\pi/q \gg a$, and replace the sum with the corresponding integral. In the calculation above at $\mathbf{q} = \mathbf{0}$, this approximation is not directly applicable, because the corresponding integral contains a divergence at the origin, which is however removed in the difference

$D_{\alpha\beta}(\mathbf{q}) - D_{\alpha\beta}(\mathbf{0})$. In addition to the condition $q \ll 2\pi/a$, we shall assume that $q \gg 2\pi/L$, or more specifically $q \geq 10/L$ (Keffer 1966), where L is a length dimension of the crystal, in which case the effects of the boundaries on $D_{\alpha\beta}(\mathbf{q})$ are averaged out because of the relatively rapid variation of the exponential factor on the surface. Using these two conditions, we find

$$\begin{aligned} D_{\alpha\beta}(\mathbf{q}) &= D_{\alpha\beta}(\mathbf{0}) + \int \frac{3(\hat{\boldsymbol{\alpha}} \cdot \mathbf{r})(\hat{\boldsymbol{\beta}} \cdot \mathbf{r}) - \delta_{\alpha\beta} r^2}{r^5} (e^{i\mathbf{q} \cdot \mathbf{r}} - 1) d\mathbf{r} \\ &= [D_{\alpha\beta}(\mathbf{0})]_L + \\ &\iint \frac{3(\hat{\boldsymbol{\alpha}} \cdot \mathbf{r})(\hat{\boldsymbol{\beta}} \cdot \mathbf{r}) - \delta_{\alpha\beta} r^2}{r^5} \left[\sum_{l=0}^{\infty} [4\pi(2l+1)]^{1/2} i^l j_l(qr) Y_{l0}(\theta, \phi) \right] r^2 dr d\Omega. \end{aligned}$$

The \mathbf{q} -independent term in the first integral leads to the same result as in (5.5.6), but without the lattice-sum contribution, and adding $D_{\alpha\beta}(\mathbf{0})$, we are left with the term $[D_{\alpha\beta}(\mathbf{0})]_L$. The \mathbf{q} -dependent exponential is expanded in terms of the spherical Bessel functions, as in (4.1.8), with the polar axis chosen to be parallel to \mathbf{q} . The dipole factor in the resulting integral may be written as a linear combination of the spherical harmonics of second rank $Y_{2m}(\theta, \phi)$, multiplied by r^{-3} , ensuring that only the term with $l = 2$ in the sum over l survives the integration over solid angles. Further, if $\hat{\boldsymbol{\alpha}}$ and $\hat{\boldsymbol{\beta}}$ are either parallel or perpendicular to \mathbf{q} , only the diagonal components may differ from zero. With $\hat{\boldsymbol{\alpha}}$ and $\hat{\boldsymbol{\beta}}$ both parallel to \mathbf{q} , the longitudinal component is

$$\begin{aligned} D_{\parallel}(\mathbf{q}) - [D_{\parallel}(\mathbf{0})]_L &= \iint [16\pi/5]^{1/2} Y_{20}(\theta, \phi) r^{-3} [4\pi \cdot 5]^{1/2} (-1) j_2(qr) Y_{20}(\theta, \phi) r^2 dr d\Omega \\ &= -8\pi \int_0^{\infty} \frac{1}{\rho} j_2(\rho) d\rho = -8\pi \left[-\frac{j_1(\rho)}{\rho} \right]_0^{\infty} = -\frac{8\pi}{3}, \end{aligned}$$

recalling that $j_1(\rho)/\rho \rightarrow \frac{1}{3}$ or 0, for respectively $\rho \rightarrow 0$ or ∞ . This result implies that the two transverse components are

$$\begin{aligned} D_{\perp}(\mathbf{q}) - [D_{\perp}(\mathbf{0})]_L &= -\frac{1}{2} \{ D_{\parallel}(\mathbf{q}) - [D_{\parallel}(\mathbf{0})]_L \} = \frac{4\pi}{3}; \quad (5.5.7) \\ &\text{when } 2\pi/L \ll q \ll 2\pi/a. \end{aligned}$$

The dipole-coupling components change from the values given by (5.5.6) to those above within a very narrow range of q , i.e. when q goes from zero to about $10/L$, as shown by the detailed analysis of Keffer (1966). At larger wave-vectors, the variation of $D_{\alpha\beta}(\mathbf{q})$ is smooth and gradual,

and it may be described by a few interplanar coupling parameters of the type used for other two-ion interactions. Cohen and Keffer (1955) have calculated the \mathbf{q} -dependence for the three cubic Bravais lattices, and their results also determine approximately $D_{\alpha\beta}(\mathbf{q})$, with \mathbf{q} along the c -axis, in the hcp lattice with the ideal c/a -ratio, since this is equivalent to \mathbf{q} along a (111)-direction in the fcc crystal. In the distorted case, with $c/a = 0.963\sqrt{8/3}$ (corresponding to Ho), a numerical calculation gives

$$D_{\xi\xi}(\mathbf{q}) + 0.0221 \frac{4\pi}{3} = \{0.9190 + 0.0816 \cos(qc/2) - 0.0006 \cos(qc)\} \frac{4\pi}{3}$$

when $\mathbf{q} \parallel c$ -axis and $q \geq 10/L$, so that the \mathbf{q} -dependence in the c -direction is very weak, except for the jump at small \mathbf{q} , which is illustrated for the example of Ho in Fig. 5.7.

In a uniform ferromagnet, the demagnetization factor leads to a positive contribution to the internal energy. Without any external applied

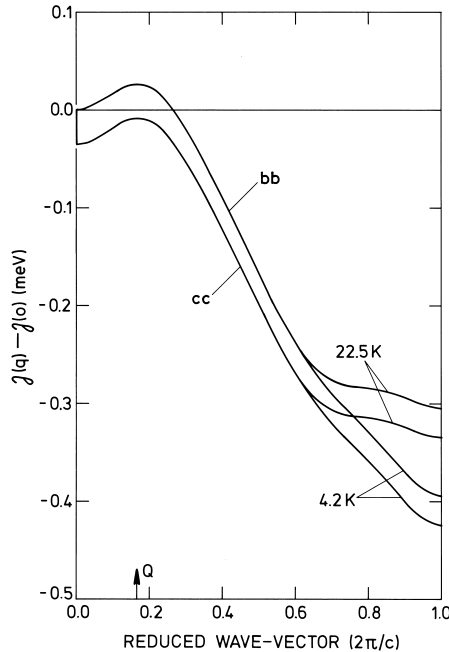


Fig. 5.7. Parallel and perpendicular components of the Fourier transform, for \mathbf{q} along the c -direction, of the two-ion coupling in Ho, deduced from the spin-wave energies. The coupling is assumed to comprise an isotropic indirect-exchange contribution and the classical dipole-dipole interaction, which gives rise to the discontinuity at $\mathbf{q} = \mathbf{0}$ in the parallel component, and stabilizes the cone structure at low temperatures.

field, it is therefore energetically favourable for the system to split up in *domains*, in which the magnetization vector points in different directions, so that the magnetization almost vanishes at the surface. The greater the number of domains, the more effectively the demagnetization contribution may be eliminated, but this tendency is opposed by the cost in energy of the *domain-walls*. It is only the contribution due to the demagnetization factor (as determined by the magnetization at the surface) which is affected by the creation of domains, and in a simple model in which the energy of the domain-walls is neglected, the internal energy per unit volume, due to the dipole coupling and including the Zeeman energy, is

$$U_D + U_Z \simeq -\frac{1}{2}D_{zz}^{\text{eff}}(\mathbf{0})M^2 + \frac{1}{2}N_z\langle M \rangle^2 - H_A\langle M \rangle.$$

The demagnetization factor is considered separately, so that $D_{zz}^{\text{eff}}(\mathbf{0}) = 4\pi/3 + [D_{zz}(\mathbf{0})]_L$, and H_A is the field applied in the z-direction. M is the magnetization,

$$M = \frac{N}{V}g\mu_B\langle J_z \rangle \quad (5.5.8)$$

in each domain, whereas $\langle M \rangle$ is the magnetization averaged over the whole crystal. If the *internal field* H_I and the *demagnetization field* H_D are defined by

$$H_I = H_A - H_D \quad ; \quad H_D = N_z\langle M \rangle, \quad (5.5.9)$$

the energy is minimized by the conditions; $H_I = 0$ when $\langle M \rangle < M$, and $\langle M \rangle = M$ when $H_I > 0$. As a function of H_I , the magnetization jumps from zero to its 'saturation' value at $H_I = 0$.

The strong \mathbf{q} -dependence of the dipole coupling at small \mathbf{q} is reflected in the energies of the magnetic excitations. In the case of the anisotropic ferromagnet, it is straightforward to deduce that the two-ion coupling of eqn (5.5.1) leads to spin-wave energies determined by

$$\begin{aligned} E_T^2(\mathbf{q}) = & [A_{\mathbf{0}}(T) + B_{\mathbf{0}}(T) + \langle J_z \rangle \{ \mathcal{J}_{\xi\xi}(\mathbf{0}) - \mathcal{J}_{\zeta\zeta}(\mathbf{q}) \}] \\ & \times [A_{\mathbf{0}}(T) - B_{\mathbf{0}}(T) + \langle J_z \rangle \{ \mathcal{J}_{\xi\xi}(\mathbf{0}) - \mathcal{J}_{\eta\eta}(\mathbf{q}) \}] - [\langle J_z \rangle \mathcal{J}_{\eta\zeta}(\mathbf{q})]^2, \end{aligned} \quad (5.5.10)$$

assuming that the magnetization vector in the basal plane is parallel to the ξ -axis, and that $\mathcal{J}_{\eta\zeta}(\mathbf{q}) = \mathcal{J}_{\zeta\eta}(\mathbf{q})$. This result may be obtained by an extension of the procedure used in Section 5.2, most easily from the MF susceptibility (5.2.42). Introducing the above results into this expression, we find, at $\mathbf{q} \equiv \mathbf{0}$,

$$E_T^2(\mathbf{0}) = [A'_{\mathbf{0}}(T) + B'_{\mathbf{0}}(T) + g\mu_B\langle M \rangle N_{\zeta}] [A_{\mathbf{0}}(T) - B_{\mathbf{0}}(T) + g\mu_B\langle M \rangle N_{\eta}], \quad (5.5.11a)$$

where the H appearing in $A_0(T)$ in (5.2.37) or (5.3.22) is the internal field H_I , and

$$A'_0(T) + B'_0(T) = A_0(T) + B_0(T) + g\mu_B M([D_{\xi\xi}(\mathbf{0})]_L - [D_{\zeta\zeta}(\mathbf{0})]_L). \quad (5.5.11b)$$

In comparison with the other anisotropy terms, the lattice-sum contribution to $A'_0(T) + B'_0(T)$ is very small (except in Gd) and may be neglected. Equation (5.5.11) demonstrates that the energy gap at $\mathbf{q} = \mathbf{0}$ depends on the shape of the sample, as was first pointed out by Kittel (1948). The same is the case with all other spin-wave modes in the *magneto-static region* $q \leq 10/L$, which are the observable states in ferromagnetic resonance experiments. In a neutron-scattering experiment, the volume in reciprocal space enclosed by the resolution function is normally several orders of magnitude larger than the volume of the magnetostatic region. The spin-waves in the long-wavelength limit, detected by inelastic neutron-scattering, therefore emanate from the much larger region where $q \geq 10/L$, but is still much smaller than $2\pi/a$, so that any two-ion coupling, except for the dipole coupling, is the same as that at $\mathbf{q} = \mathbf{0}$. The spin-wave energies in this regime are determined by eqn (5.5.10), when the dipole-coupling tensor in (5.5.7) is transformed to the $(\xi\eta\zeta)$ -coordinate system, and are

$$E_T^2(\mathbf{q} \approx \mathbf{0}) = E_T^2(\tilde{\mathbf{0}}) + 4\pi g\mu_B M[\{A_0(T) - B_0(T)\} \cos^2 \theta_{\mathbf{q}} + \{A'_0(T) + B'_0(T)\} \sin^2 \theta_{\mathbf{q}} \sin^2 \phi_{\mathbf{q}}], \quad (5.5.12a)$$

where $(\theta_{\mathbf{q}}, \phi_{\mathbf{q}})$ are the polar angles of \mathbf{q} with respect to the c -axis or ζ -axis, and

$$E_T^2(\tilde{\mathbf{0}}) = [A'_0(T) + B'_0(T)][A_0(T) - B_0(T)]. \quad (5.5.12b)$$

As long as the magnetization is in the basal-plane, this result is generally valid if $\phi_{\mathbf{q}}$ is redefined to be the angle between the magnetization vector and the projection of \mathbf{q} on the basal-plane. $E_T(\tilde{\mathbf{0}})$ is the minimum excitation energy, and the corresponding spin waves propagate parallel to the magnetization vector. If $A'_0(T) + B'_0(T)$ is significantly larger than $A_0(T) - B_0(T)$ (in Tb it is an order of magnitude greater at $T = 0$), the maximum value of $E_T(\mathbf{q} \approx \mathbf{0})$ occurs when \mathbf{q} lies in the basal plane perpendicular to the magnetic moments, whereas the spin waves propagating in the c -direction only have an energy slightly greater than $E_T(\tilde{\mathbf{0}})$. An inelastic neutron-scattering experiment, with the mean value of the scattering vector equal to a reciprocal lattice vector, will sample a whole spectrum of spin waves with energies between the two extremes. The shape of the scattering peak will be dependent on the

form of the resolution function. With a spherical resolution, the scattering will be quite sharply peaked at the intermediate energy of the spin waves propagating in the c -direction, as illustrated in the case of Tb in Fig. 5.8. The calculated sharp peak at about 1.8 meV and the high-energy shoulder are clearly apparent in the experimental measurements of Houmann *et al.* (1975a). In the measurements of Bjerrum Møller and Mackintosh (1979), on the other hand, the resolution function was such that the modes propagating in the basal plane perpendicular to the magnetization were most heavily weighted, so that the predominant peak occurs at about 2.0 meV. In Ho, the effect of the dipole interaction on the long-wavelength spin waves is even more pronounced. This is an example of the opposite extreme, where $A'_0(T) + B'_0(T)$ is much smaller than $A_0(T) - B_0(T)$, so that the maximum value of $E_T(\mathbf{q} \approx \mathbf{0})$ occurs when \mathbf{q} lies along the c -direction. As illustrated in Fig. 5.9, the dipolar splitting in this case is sufficiently great that the neutron scattering at $\mathbf{q} \approx \mathbf{0}$ can be resolved into two peaks.

Another consequence of the strong directional dependence of the dipolar contributions to the spin-wave energies is found in the behaviour of the coupled magneto-acoustic sound waves, discussed in the previous section. The region in \mathbf{q} -space sampled in ultrasonic measurements (with frequencies in the MHz regime) is just that in which eqn (5.5.12)

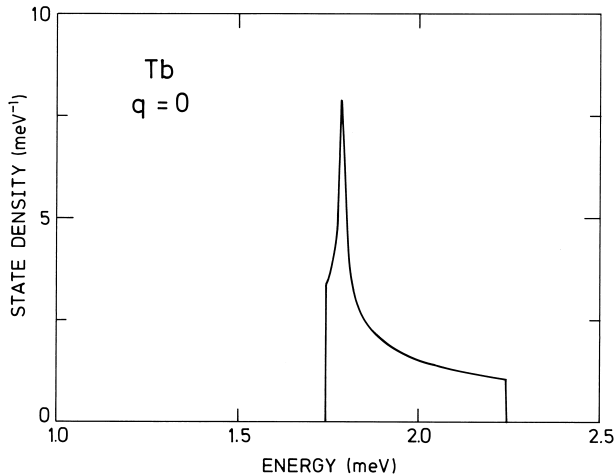


Fig. 5.8. The state density of the long-wavelength spin-wave mode $E_T(\mathbf{q} \approx \mathbf{0})$ in Tb at 4 K, calculated from eqn (5.5.12), taking into account the splitting of the dispersion relations by the dipole-dipole interaction. The sharp peak is due to the branch in the c -direction.

applies. If \mathbf{q} is parallel to the magnetization, the spin-wave energies are unchanged from the values deduced in Sections 5.2–4, provided that the lattice-sum contribution is included in the axial anisotropy term (5.5.11*b*), and eqn (5.4.38) is still valid. On the other hand, when \mathbf{q} is in the basal-plane and perpendicular to the magnetization, the ultrasonic

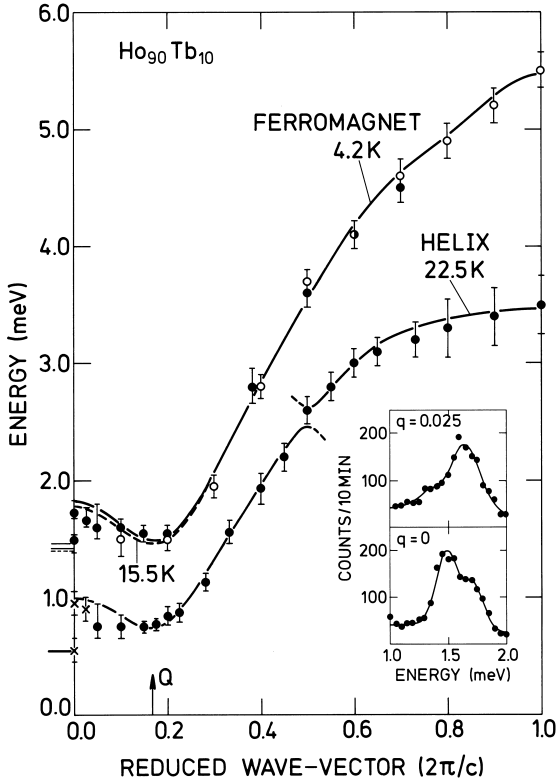


Fig. 5.9. Dispersion relations, in the double-zone representation, for magnetic excitations propagating in the c -direction of $\text{Ho}_{90}\text{Tb}_{10}$ in the ferromagnetic phase (upper branch), and the bunched helical structure (lower branch). The full and dashed lines for the ferromagnetic phase show the theoretical dispersion relations at 4 K and 16 K respectively, and the open and filled symbols are the corresponding experimental results. The calculated long-wavelength energies in the basal plane are shown to the left of the ordinate axis and the discontinuity, which is due to the dipole-dipole interaction, is clearly manifested in the neutron-scattering spectra in the inset. This discontinuity also appears in the helical phase, and the bunching causes an energy gap on the ALH face of the Brillouin zone, which is not resolved in these measurements.

velocities are determined by

$$\frac{c_{cc}^*}{c_{66}} = 1 - \frac{\Lambda_\gamma}{A_0(T) - B_0(T) + 4\pi g\mu_B M} \quad ; \quad \mathbf{q} \perp \langle \mathbf{J} \rangle. \quad (5.5.13)$$

This modification means that only the velocity of those magneto-acoustic modes which propagate parallel to the magnetization vanishes at the critical field $H_I = H_c$ where, according to (5.4.15), $A_0(T) - B_0(T) = \Lambda_\gamma$, whereas the velocity of the modes propagating in the basal-plane perpendicular to the field remains non-zero. This difference in the velocities of the ultrasonic modes was very clearly manifested in the ultrasonic experiment on Tb discussed in Section 5.4 (Jensen and Palmer 1979). This example shows that the dipolar coupling is able to lift the degeneracy in the velocities of two transverse sound-waves which are related to each other by an interchange of the directions of the wave-vector and the polarization vector. The same effect may be produced by the torque exerted on the moments when the local magnetic anisotropy axes are rotated by the transverse phonons relative to the direction of an external magnetic field. As discussed by Melcher (1972) and Dohm and Fulde (1975) the influence of this mechanism on the sound velocities may be derived from the principle that the total system has to be *rotationally invariant*. Their theory has been extended by Jensen (1988b), who finds that the dipolar-coupling contribution strongly dominates in a ferromagnet, but that the importance of the two mechanisms may be comparable in paramagnets.

5.5.2 General two-ion interactions

The two-ion couplings described by eqn (5.5.1) only involve the dipolar moments of the $4f$ electrons. A more general two-ion Hamiltonian is

$$\begin{aligned} \mathcal{H}_{JJ} = & -\frac{1}{2} \sum_{ij} \sum_{l+l':\text{even}} \sum_{mm'} [K_{ll'}^{mm'}(ij) \tilde{O}_{lm}(\mathbf{J}_i) \tilde{O}_{l'm'}(\mathbf{J}_j) \\ & + (-1)^{m+m'} \{K_{ll'}^{mm'}(ij)\}^* \tilde{O}_{l-m}(\mathbf{J}_i) \tilde{O}_{l'-m'}(\mathbf{J}_j)], \end{aligned} \quad (5.5.14)$$

expressed in terms of the *Racah operators* or *tensor operators* $\tilde{O}_{lm}(\mathbf{J}_i)$ introduced in Section 1.4, rather than the Stevens operators. Tables of these operators and a discussion of their properties may be found in Buckmaster *et al.* (1972) and in Lindgård and Danielsen (1974). Here we neglect the possible effects of the *polar* tensors, which vanish for the isolated ions. In principle, these polar tensors may be non-zero in the hcp metals, because the surroundings lack inversion symmetry, but they occur only because of odd-parity configuration-mixing of the $4f$ wave-functions, which should be insignificant for the ground-state multiplet.

This leaves only the *axial* tensors, i.e. magnetic multipoles of odd rank and electric multipoles of even rank. Time reversal of these tensors effects the transformation $c\tilde{O}_{lm} \rightarrow c^*(-1)^{l+m}\tilde{O}_{l-m}$, whereas Hermitian conjugation gives $(c\tilde{O}_{lm})^\dagger = c^*(-1)^m\tilde{O}_{l-m}$. The requirement that \mathcal{H}_{JJ} should be invariant under both transformations allows only those terms in eqn (5.5.14) for which $l+l'$ is even. The violation of time-reversal symmetry which occurs when the system is magnetically ordered implies that \mathcal{H}_{JJ} should be supplemented by interactions proportional to $\langle \tilde{O}_{\lambda\mu} \rangle \tilde{O}_{lm}(\mathbf{J}_i) \tilde{O}_{l'm'}(\mathbf{J}_j)$, satisfying the condition that $\lambda+l+l'$ is even. An obvious example is magnetoelastic contributions to the Hamiltonian such as eqn (5.4.5). The tensor operators in (5.5.14) emanate from localized $4f$ wavefunctions with the orbital quantum number $l_f = 3$, which puts the further restriction on the phenomenological expansion of \mathcal{H}_{JJ} that l and l' cannot be larger than $2l_f+1 = 7$, as the operator-equivalents of higher rank than this vanish identically.

In the rare earth metals, several different mechanisms may give rise to such anisotropic two-ion couplings, and these have been listed by, for instance, Wolf (1971) and Jensen *et al.* (1975). We have already considered the magnetostatic coupling of lowest rank in the magnetic multipole expansion, namely the classical magnetic dipole–dipole interaction. This is of importance only because of its long range. The higher order magnetostatic couplings are of shorter range ($\propto (1/r)^{l+l'+1}$) and have negligible effects. The electrostatic Coulomb interaction gives rise to terms in (5.5.14) in which both l and l' are even. The single-ion contributions ($l' = 0$) are of decisive importance, when $L \neq 0$, but even the lowest-order electrostatic two-ion term, which contributes to the quadrupole–quadrupole interactions, is so small that it may be neglected.

The overlap between the $4f$ wavefunctions of neighbouring ions is so weak that it cannot generate any two-ion coupling of significance. The dominant terms in the two-ion Hamiltonian \mathcal{H}_{JJ} therefore arise indirectly via the propagation of the conduction electrons. We have already mentioned in Section 1.4 the most important of these, due to the exchange interaction between the band electrons and the $4f$ electrons, and it will be discussed in more detail in Section 5.7. In the simplest approximation, the indirect exchange is invariant with respect to a uniform rotation of the angular momenta, i.e. this RKKY interaction is *isotropic*. However, the neglect of the contribution of the orbital moment in the scattering process is not generally justified. If L is non-zero, the orbital state of the $4f$ electrons may change in an exchange-scattering process, if the conduction electron is scattered into a state with a different orbital momentum relative to the ion. The leading-order corrections to the isotropic RKKY interaction due to such processes have been

considered by Kaplan and Lyons (1963) and Kasuya and Lyons (1966). In order to obtain an estimate of the importance of the corrections, they assumed plane-wave states for the conduction electrons, expanded in a series of spherical Bessel functions centred at the ion. These calculations indicated anisotropic two-ion couplings with a magnitude of the order of 10% of the isotropic coupling, or greater (Specht 1967). As discussed in Section 1.3, the free-electron model does not provide a very satisfactory description of the conduction electrons in the rare earths. It is particularly inadequate when orbital effects are involved, since the expansion of the plane-wave states clearly underestimates the ($l = 2$)-character of the d -like band-electrons, which dominates the exchange interaction in the ($L = 0$)-case of Gd (Lindgård *et al.* 1975). When L is non-zero, the *Kaplan-Lyons* terms may be of comparable importance to the RKKY interaction in the rare earth metals. The relativistic modification of the band states, due to the spin-orbit coupling, may enhance the orbital effects and also lead to anisotropic interactions in Gd. In addition to the exchange, the direct Coulomb interaction between the $4f$ and the band electrons may contribute to eqn (5.5.14), with terms in which l and l' are both even. This coupling mechanism, via the conduction electrons, is probably more important for this kind of term than the direct electrostatic contribution mentioned above.

The RKKY interaction is derived on the assumption that the $4f$ electrons are localized in the core, and that their mixing with the conduction electrons is exclusively due to the exchange. However, the Coulomb interaction may lead to a slight hybridization of the localized $4f$ states with the band states. In recent years, Cooper and his co-workers (Cooper *et al.* 1985; Wills and Cooper 1987) have analysed the consequences of a weak hybridization between an ion with one or two f electrons and the band electrons, with special reference to the magnetic behaviour of Ce compounds and the actinides. They find that the magnetic two-ion coupling becomes highly anisotropic in the Ce compounds. Although Ce is the rare earth element in which the strongest hybridization effects would be expected to occur, these results and the analysis of Kaplan and Lyons (1963) suggest that the presence of anisotropic two-ion couplings should be a common feature in rare earth metals with orbital angular momentum on the ion.

As is clear from the above discussion, an analysis from first principles cannot at present give a reliable estimate of the relative magnitude of the Heisenberg exchange interaction and the various possible anisotropic two-ion couplings in the rare earth metals. We cannot a priori exclude any terms of the form given by eqn (5.5.14). In order to arrive at such an estimate, it is necessary to calculate the consequences of the anisotropic two-ion terms and compare the predictions with exper-

imental observations. In the case of the nearly saturated ferromagnet, it is straightforward to take into account the effects of \mathcal{H}_{JJ} on the ground-state properties and the spin-waves. The Racah operators, defined with reference to the (ξ, η, ζ) -coordinate system, may be expanded in terms of the spin deviation operators. When the moments in the basal-plane ($\theta = \pi/2$) are close to their saturation value ($\langle J_z \rangle \simeq J$),

$$\langle \tilde{O}_{lm} \rangle \simeq \left(\frac{4\pi}{2l+1} \right)^{1/2} J^{(l)} Y_{lm}(\theta = \frac{\pi}{2}, \phi) = J^{(l)} \Gamma_{lm} e^{im\phi}, \quad (5.5.15a)$$

where

$$\Gamma_{lm} = \begin{cases} (-1)^{(l+m)/2} \frac{[(l+m)!(l-m)!]^{1/2}}{(l+m)!!(l-m)!!} & , l+m \text{ even} \\ 0 & , l+m \text{ odd.} \end{cases} \quad (5.5.15b)$$

Utilizing the equivalence between the Racah operators and the spherical harmonics, and the connection between the spin-wave energies and the angular derivatives of the expectation values (which leads to the relation (5.3.14)), we have to first order in $1/J$ (Jensen *et al.* 1975):

$$\begin{aligned} \tilde{O}_{lm}(\mathbf{J}_i) = & \\ & \left(1 - \frac{m}{\sqrt{2J}}(a_i^+ - a_i) - \frac{l(l+1)}{2J}a_i^+a_i - \frac{l(l+1) - 2m^2}{4J}(a_i^+a_i^+ + a_i a_i) \right) \\ & \times J^{(l)} \Gamma_{lm} e^{im\phi}, \end{aligned} \quad (5.5.16a)$$

if $l+m$ is even, and if $l+m$ is odd

$$\begin{aligned} \tilde{O}_{lm}(\mathbf{J}_i) = & \\ & [(l+1)^2 - m^2]^{1/2} \left(\frac{1}{\sqrt{2J}}(a_i^+ + a_i) - \frac{m}{2J}(a_i^+a_i^+ - a_i a_i) \right) J^{(l)} \Gamma_{l+1m} e^{im\phi}. \end{aligned} \quad (5.5.16b)$$

Introducing these expressions into the two-ion Hamiltonian, we may derive the spin-wave energies, to leading order in $1/J$. The number of terms in eqn (5.5.14) which contribute to the excitation energies, in this order, may be reduced by the symmetry elements of the lattice which leave the \mathbf{q} -vector unchanged. In the simplest case, where \mathbf{q} is along the c -axis, the three-fold symmetry about this axis plus the mirror-plane perpendicular to the ξ -axis (i.e. the a -axis) ensure that only terms with $m+m' = 3p$, where p is an integer, contribute, and that their contribution is proportional to $\cos(3p\phi)$. The terms in which p is an odd integer couple the acoustic and optical magnons, but they do not

lift the degeneracy of the modes at A on the Brillouin-zone boundary of Fig 1.4. When \mathbf{q} is parallel to the c -axis, a direct calculation of the spin-wave energies (Jensen *et al.* 1975) shows that the two-ion terms in \mathcal{H}_{JJ} lead to the following modifications of the earlier results (5.2.38) and (5.3.22):

- (i) The two-ion anisotropy may contribute to the parameters $A_{\mathbf{q}}(T) \pm B_{\mathbf{q}}(T)$ at zero wave-vector.
- (ii) $B_{\mathbf{q}}(T)$ becomes dependent on \mathbf{q} to leading order in $1/J$.
- (iii) The \mathbf{q} -dependent parts of $A_{\mathbf{q}}(T) \pm B_{\mathbf{q}}(T)$ may change when the direction of magnetization is changed.

There are no direct ways of separating the single- and two-ion contributions to the energy gap at zero wave-vector. However, a strong \mathbf{q} -dependence of $B_{\mathbf{q}}(T)$ is only possible if the two-ion Hamiltonian is anisotropic. One way to determine $B_{\mathbf{q}}(T)$ is to utilize the dependence of the neutron cross-section on this parameter, given by eqn (5.2.41). This method requires accurate intensity measurements and is not straightforward. The other possibility is to measure the field dependence of the spin-wave energies since, from (5.2.38) or (5.3.22),

$$\alpha_{\mathbf{q}}(T) \equiv \partial E_{\mathbf{q}}^2(T) / \partial (g\mu_B H) \simeq 2A_{\mathbf{q}}(T), \quad (5.5.17)$$

when the field is parallel to the magnetization. This relation is only true to first order in $1/J$, and corrections have to be made for the influence of any field-dependent changes of the correlation functions σ and η_{\pm} . Both $A_{\mathbf{q}}(T)$ and $B_{\mathbf{q}}(T)$ may be determined from the energies and initial slopes, since

$$A_{\mathbf{q}}(T) \pm B_{\mathbf{q}}(T) \simeq \frac{1}{2}\alpha_{\mathbf{q}}(T) \pm \frac{1}{2}[\alpha_{\mathbf{q}}^2(T) - 4E_{\mathbf{q}}^2(T)]^{\frac{1}{2}}. \quad (5.5.18)$$

This method was used by Jensen *et al.* (1975) for a comprehensive study of the two-ion anisotropy in Tb. The values of $A_{\mathbf{q}}(T)$ and $B_{\mathbf{q}}(T)$, deduced from eqn (5.5.18), were parametrized in various ways, and clearly the best least-squares fit was obtained with expressions of the form

$$\begin{aligned} (A_{\mathbf{q}} + B_{\mathbf{q}}) - (A_0 + B_0) &= \mathcal{I}(\mathbf{q}) + \mathcal{K}(\mathbf{q}) - \mathcal{C}(\mathbf{q}) \cos 6\phi \\ (A_{\mathbf{q}} - B_{\mathbf{q}}) - (A_0 - B_0) &= \mathcal{I}(\mathbf{q}) - \mathcal{K}(\mathbf{q}) - \mathcal{D}(\mathbf{q}) \cos 6\phi, \end{aligned} \quad (5.5.19)$$

where $A_0 \pm B_0$ were taken from the simultaneous measurements of the magnetic anisotropy at $\mathbf{q} = \mathbf{0}$, discussed in the previous section. The low-temperature isotropic coupling $\mathcal{I}(\mathbf{q})$, which in the absence of anisotropy would just be $J[\mathcal{J}(\mathbf{0}) - \mathcal{J}(\mathbf{q})]$, and the ϕ -independent two-ion anisotropy $\mathcal{K}(\mathbf{q})$ are shown in Fig. 5.10. The ϕ -dependent axial

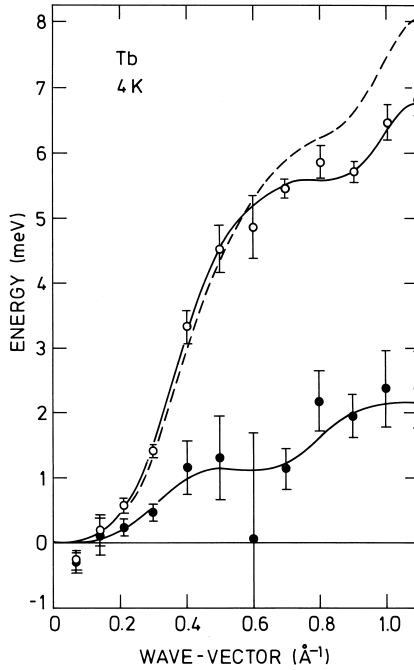


Fig. 5.10. Isotropic and anisotropic two-ion coupling parameters $\mathcal{I}(\mathbf{q})$ (upper curve) and $\mathcal{K}(\mathbf{q})$ (lower curve) for Tb at 4 K, deduced from the field dependence of the spin-wave energies. The former is closely related to $J[\mathcal{J}(\mathbf{0}) - \mathcal{J}(\mathbf{q})]$, an estimate of which is indicated by the dashed line. The magnon-phonon interaction causes relatively large uncertainties at intermediate wave-vectors.

anisotropy $\mathcal{C}(\mathbf{q})$ is about the same magnitude as $\mathcal{K}(\mathbf{q})$, while $\mathcal{D}(\mathbf{q})$ is very small. The ϕ -dependent anisotropy is detected very clearly in the experiments, since it gives rise to a change in the dispersion $E_{\mathbf{q}}(T)$, when the moments are rotated from the the easy to the hard planar direction. $\mathcal{C}(\mathbf{q})$ is the \mathbf{q} -dependent generalization of the ϕ -dependent anisotropy ΔM in $A_0 + B_0$, introduced in the previous section, and $\Delta M \approx -\langle \mathcal{C}(\mathbf{q}) \rangle_{\mathbf{q}}$.

As mentioned in Section 5.4.1, the corrections to the field dependence of the magnon energies in (5.5.17) were included in an effective fashion, neglecting changes due to the rotation of the moments and assuming $\eta_- \simeq 1/\eta_+ \simeq \{1 - b(T = 0)\}\sigma^{-k}$, where k may be estimated to be about 0.3. The renormalization effects are thus taken as proportional to σ raised to a power which depends on the term considered. We estimate that the effects neglected in this approach only introduce corrections of the order of the experimental uncertainties. The two-ion coupling

parameters decrease with increasing temperature or decreasing magnetization. The three anisotropy component all decrease very rapidly, roughly proportionally to σ^{15} (like ΔM), which means that they are only important at low temperatures and may be neglected above about 150 K. The strong temperature dependence of the anisotropic components indicates, according to the Callen–Callen theory, that higher-rank couplings make the dominant contribution. The lowest-order term in eqn (5.5.14) which contributes to $\mathcal{C}(\mathbf{q})$ involves K_{44}^{33} , and it should renormalize approximately as σ^{19} . The renormalization is observed to be \mathbf{q} -dependent for all the parameters, being slower at larger wave-vectors, and it lies in the range σ^2 – $\sigma^{0.1}$ for $\mathcal{I}(\mathbf{q})$. In Tb, $\mathcal{I}(\mathbf{q})$ may include higher-rank contributions besides the RKKY-exchange term, but the way in which it renormalizes resembles quite closely the behaviour observed in Gd and shown in Fig. 5.1. A \mathbf{q} -dependent renormalization may partially be accounted for, in the self-consistent RPA theory, by the \mathbf{k} -sum terms in (5.2.38).

When \mathbf{q} is not along the c -axis, there are other ways in which the presence of two-ion anisotropy may be detected in the ferromagnetic excitation spectrum:

- (iv) Spin-wave energy gaps may appear at the boundaries of the Brillouin zone.

The isotropic two-ion coupling alone does not lead to energy gaps at these boundaries, whereas anisotropic two-ion couplings may lift those degeneracies which are not dictated by symmetry. In fact, the first indication of the presence of two-ion anisotropy in the rare earth metals, other than the classical magnetic-dipolar interaction, was the splitting shown in Fig. 5.2 along the KH edge of the Brillouin zone in the ferromagnetic phase of Tb (Lindgård and Houmann 1971). Finally, we have the related effect:

- (v) The spin-wave energies, at a particular \mathbf{q} , in domains with different angles between the \mathbf{q} -vector and the magnetization vectors, need not be equal if two-ion anisotropy is important.

In a single domain, the two-ion anisotropy forces may lift the ‘accidental’ degeneracies between spin waves at \mathbf{q} -vectors which are equivalent in the paramagnetic phase, but which are no longer equivalent in the Brillouin zone of the ferromagnet. This manifestation of the two-ion anisotropy has not yet been subjected to experimental investigation, but it may provide a useful supplement to studies of the \mathbf{q} -dependence of $B_{\mathbf{q}}(T)$.

As we have seen, the expectation values $\langle \tilde{O}_{lm} \rangle$ are approximately proportional to $\sigma^{l(l+1)/2}$, if the extra modification due to the elliptical polarization of the spin-waves is neglected. This means that the importance of the higher-rank couplings declines relatively rapidly with tem-

perature. The effects of these interactions on the ground state and the spin waves are therefore most pronounced in the low-temperature limit, whereas the behaviour of the system at high temperatures which, in the heavy rare earths, includes the critical region around the phase transition between the ordered and paramagnetic phases, is dominated by the coupling between the dipolar moments, and the single-ion quadrupole interaction, i.e. by the terms in eqn (5.5.14) with $l + l' = 2$.

5.6 Binary rare earth alloys

The great similarity in the chemical properties of the different rare earth metals allows almost complete mutual solubility. It is therefore possible to fabricate rare earth alloys with nearly uniform electronic properties, but containing ions with disparate magnetic properties, distributed randomly on a single lattice. By a judicious choice of the constituents, the macroscopic magnetic properties, such as the ordering temperatures and the anisotropy parameters, may be continuously adjusted as desired. From a macroscopic viewpoint, such an alloy resembles a uniform and homogeneous crystal, with magnetic properties reflecting the characteristics and concentrations of the constituents. The spectrum of magnetic excitations also displays such average behaviour (Larsen *et al.* 1986), but in addition, there are effects which depend explicitly on the disparity between the different sites.

We restrict ourselves to binary alloys, which are described by the Hamiltonian,

$$\begin{aligned} \mathcal{H} = & \sum_i \{c_i \mathcal{H}_1(\mathbf{J}_{1i}) + (1 - c_i) \mathcal{H}_2(\mathbf{J}_{2i})\} \\ & - \frac{1}{2} \sum_{i \neq j} \mathcal{J}(ij) \{c_i \mathbf{J}_{1i} + \gamma(ij)(1 - c_i) \mathbf{J}_{2i}\} \cdot \{(c_j \mathbf{J}_{1j} + \gamma(ij)(1 - c_j) \mathbf{J}_{2j})\}, \end{aligned} \quad (5.6.1)$$

where c_i is a variable which is 1 if the ion on site i is of type 1, and 0 if the i th ion is of type 2. The configurational average of c_i is the atomic concentration of the type-1 ions, $\langle c_i \rangle_{\text{cf}} = c$. In addition to the simplifications made earlier in the Hamiltonian, we shall assume that $\gamma(ij)$ is a constant γ , independent of i and j . This approximation is consistent with a model in which the indirect exchange is assumed to dominate the two-ion coupling, in which case

$$\gamma(ij) = \gamma = (g_2 - 1)/(g_1 - 1), \quad (5.6.2)$$

where the indices 1 and 2 refer to the two types of ions with angular momenta J_1 and J_2 .

In order to derive the excitation spectrum of the alloy system, we first make the assumption that the surroundings of each ion are

so close to the average that individual variations can be neglected. Thus we replace the actual MF Hamiltonian of the i th ion with the configurationally-averaged MF Hamiltonian and, considering a type 1 ion ($c_i = 1$), obtain

$$\begin{aligned} \mathcal{H}_{\text{MF}}(i) &\simeq \langle \mathcal{H}_{\text{MF}}(i) \rangle_{\text{cf}} = \\ \mathcal{H}_1(\mathbf{J}_{1i}) - (\mathbf{J}_{1i} - \frac{1}{2}\langle \mathbf{J}_{1i} \rangle) \cdot \sum_j \mathcal{J}(ij) \{c\langle \mathbf{J}_{1j} \rangle + (1-c)\gamma\langle \mathbf{J}_{2j} \rangle\}. \end{aligned} \quad (5.6.3)$$

From this equation, and the similar one for $c_i = 0$, we may determine the MF values of the two moments $\langle \mathbf{J}_1 \rangle$ and $\langle \mathbf{J}_2 \rangle$, and the corresponding susceptibilities $\bar{\chi}_1^o(\omega)$ and $\bar{\chi}_2^o(\omega)$. For a paramagnetic or ferromagnetic system these quantities are all site-independent, in the present approximation. We note that (5.6.3) is correct in the case of a paramagnet, as possible environmental variations on the individual ions are already neglected in the starting Hamiltonian. The next step is the introduction of a 2×2 matrix of susceptibility tensors $\bar{\bar{\chi}}_{rs}(ij, \omega)$, where the elements with $r = 1$ or 2 are defined in terms of $c_i \mathbf{J}_{1i}$ or $(1 - c_i) \mathbf{J}_{2i}$ respectively, and $s = 1$ or 2 similarly specifies the other component. We may then write the RPA equation (3.5.7):

$$\bar{\bar{\chi}}_{rs}(ij, \omega) = \bar{\bar{\chi}}_r(i, \omega) \left(\delta_{rs} \delta_{ij} + \sum_{j'} \sum_{s'} \gamma_{rs'} \mathcal{J}(ij') \bar{\bar{\chi}}_{s's}(j'j, \omega) \right), \quad (5.6.4a)$$

where

$$\bar{\bar{\chi}}_1(i, \omega) = c_i \bar{\chi}_1^o(\omega) \quad ; \quad \bar{\bar{\chi}}_2(i, \omega) = (1 - c_i) \bar{\chi}_2^o(\omega), \quad (5.6.4b)$$

recalling that $c_i^2 = c_i$ ($= 0$ or 1), and defining $\mathcal{J}_{rs}(ij) = \gamma_{rs} \mathcal{J}(ij)$, with

$$\gamma_{11} = 1 \quad ; \quad \gamma_{12} = \gamma_{21} = \gamma \quad ; \quad \gamma_{22} = \gamma^2. \quad (5.6.4c)$$

In spite of the great simplification introduced through the random-phase approximation, the RPA equation for the alloy is still very complicated, because $\bar{\bar{\chi}}_r(i, \omega)$ depends on the randomness, and it cannot be solved without making quite drastic approximations. The simplest result is obtained by neglecting completely the site-dependence of $\bar{\bar{\chi}}_r(i, \omega)$, and consequently replacing c_i in (5.6.4b) by its average value c . This procedure corresponds to the replacement of each individual angular momentum \mathbf{J}_{ri} by the average $c\mathbf{J}_{1i} + (1 - c)\mathbf{J}_{2i}$, and it is known as the *virtual crystal approximation* (VCA). In this approximation, (5.6.4) may be solved straightforwardly after a Fourier transformation, and defining the T -matrices according to

$$\bar{\bar{\chi}}_{rs}(\mathbf{q}, \omega) = \bar{\bar{\chi}}_r(\omega) \delta_{rs} + \bar{\bar{\chi}}_r(\omega) \bar{\bar{T}}_{rs}(\mathbf{q}, \omega) \bar{\bar{\chi}}_s(\omega), \quad (5.6.5a)$$

where

$$\bar{\bar{\chi}}_1(\omega) = c\bar{\bar{\chi}}_1^o(\omega) \quad \text{and} \quad \bar{\bar{\chi}}_2(\omega) = (1-c)\bar{\bar{\chi}}_2^o(\omega), \quad (5.6.5b)$$

we find that these T-matrices are given by

$$\bar{\bar{T}}_{rs}(\mathbf{q}, \omega) = \gamma_{rs} \mathcal{J}(\mathbf{q}) \bar{\bar{D}}(\mathbf{q}, \omega)^{-1}, \quad (5.6.6a)$$

with

$$\bar{\bar{D}}(\mathbf{q}, \omega) = 1 - \{c\bar{\bar{\chi}}_1^o(\omega) + (1-c)\gamma^2\bar{\bar{\chi}}_2^o(\omega)\} \mathcal{J}(\mathbf{q}). \quad (5.6.6b)$$

This result is simplified by the assumption, (5.6.2) or (5.6.4c), that $\mathcal{J}_{12}(\mathbf{q})$ is the geometric mean of $\mathcal{J}_{11}(\mathbf{q})$ and $\mathcal{J}_{22}(\mathbf{q})$. In this and in more complex cases, the introduction of the T-matrices in (5.6.5) makes it somewhat easier to handle the RPA equations. The configurationally-averaged susceptibility is $\bar{\bar{\chi}}(\mathbf{q}, \omega) = \sum_{rs} \bar{\bar{\chi}}_{rs}(\mathbf{q}, \omega)$, but this does not directly determine the inelastic neutron-scattering cross-section. We must take into account the difference in the form factor $\{\frac{1}{2}gF(\boldsymbol{\kappa})\}$ for the two kinds of ions, in the differential cross-section (4.2.1). At small scattering vectors, $F(\boldsymbol{\kappa})$ is generally close to one and the most important variation is due to the g -factor. In this case, the inelastic scattering is proportional to the susceptibility:

$$\begin{aligned} g^2\bar{\bar{\chi}}(\mathbf{q}, \omega) &\equiv \sum_{rs} g_r g_s \bar{\bar{\chi}}_{rs}(\mathbf{q}, \omega) \\ &= g_1^2 c \bar{\bar{\chi}}_1^o(\omega) + g_2^2 (1-c) \bar{\bar{\chi}}_2^o(\omega) + \bar{\bar{\chi}}_3(\omega) \mathcal{J}(\mathbf{q}) \bar{\bar{D}}(\mathbf{q}, \omega)^{-1} \bar{\bar{\chi}}_3(\omega), \end{aligned} \quad (5.6.7a)$$

with

$$\bar{\bar{\chi}}_3(\omega) = g_1 c \bar{\bar{\chi}}_1^o(\omega) + g_2 (1-c) \gamma \bar{\bar{\chi}}_2^o(\omega). \quad (5.6.7b)$$

If $\bar{\bar{\chi}}_r(i, \omega)$ only depends on c_i , as assumed in (5.6.4b), the RPA equation (5.6.4a) is equivalent to that describing the phonons in a crystal with *diagonal disorder*, in the harmonic approximation. The possible variation of the molecular field (or other external fields) from site to site, which is neglected in (5.6.3), introduces *off-diagonal disorder*. If such off-diagonal disorder is neglected, the main effects of the randomness, in 3-dimensional systems, are very well described in the *coherent potential approximation* (CPA) (Taylor 1967; Soven 1967; Elliott *et al.* 1974; Lage and Stinchcombe 1977; Whitelaw 1981). In the CPA, the different types of ion are treated separately, but they are assumed to interact with a common surrounding medium. This configurationally-averaged medium, i.e. the *effective medium*, is established in a self-consistent fashion. The method may be described in a relatively simple manner, following the

approach of Jensen (1984). We first consider the case where $\bar{\chi}_2^o(\omega)$ vanishes identically, corresponding to the presence of non-magnetic impurities with a concentration $1 - c$. The RPA equation (5.6.4a) may then be solved formally by iteration:

$$\begin{aligned} \bar{\chi}(ij, \omega) &= c_i \bar{\chi}^o(\omega) \delta_{ij} + c_i \bar{\chi}^o(\omega) \mathcal{J}(ij) c_j \bar{\chi}^o(\omega) \\ &\quad + \sum_{j'} c_i \bar{\chi}^o(\omega) \mathcal{J}(ij') c_{j'} \bar{\chi}^o(\omega) \mathcal{J}(j'j) c_j \bar{\chi}^o(\omega) + \dots \end{aligned} \quad (5.6.8)$$

The VCA result is obtained by assuming $\langle c_{j'}^n \rangle_{\text{cf}} = c^n$, which is incorrect since $\langle c_{j'}^n \rangle_{\text{cf}} = \langle c_j^n \rangle_{\text{cf}} = c$. Consequently, the VCA leads to errors already in the fourth term in this expansion, or in the third term if $i = j$, even though $\mathcal{J}(ii)$ is zero. In order to ameliorate these deficiencies, we first consider the series for $\bar{\chi}(ii, \omega)$, where $i = j$. The different terms in this series may be collected in groups according to how many times the i th site appears, which allows us to write

$$\begin{aligned} \bar{\chi}(ii, \omega) &= c_i \left[\bar{\chi}^o(\omega) + \bar{\chi}^o(\omega) \bar{K}(i, \omega) \bar{\chi}^o(\omega) \right. \\ &\quad \left. + \bar{\chi}^o(\omega) \bar{K}(i, \omega) \bar{\chi}^o(\omega) \bar{K}(i, \omega) \bar{\chi}^o(\omega) + \dots \right] \\ &= c_i \{1 - \bar{\chi}^o(\omega) \bar{K}(i, \omega)\}^{-1} \bar{\chi}^o(\omega), \end{aligned} \quad (5.6.9)$$

where $\bar{K}(i, \omega)$ is the infinite sum of all the ‘interaction chains’ involving the i th site only at the ends, but nowhere in between. A similar rearrangement of the terms in the general RPA series leads to

$$\bar{\chi}(ij, \omega) = \bar{\chi}(ii, \omega) \delta_{ij} + \bar{\chi}(ii, \omega) \bar{T}(ij, \omega) \bar{\chi}(jj, \omega), \quad (5.6.10)$$

where $\bar{T}(ij, \omega)$ is only non-zero if $i \neq j$ and, by exclusion, is the sum of all the interaction chains in which the i th site appears only at the beginning, and the j th site only at the end of the chains. Introducing this expression in the RPA equation (5.6.4), we may write it

$$\begin{aligned} \bar{\chi}(ij, \omega) &= \\ c_i \bar{\chi}^o(\omega) & \left[\delta_{ij} + \mathcal{J}(ij) \bar{\chi}(jj, \omega) + \sum_{j'} \mathcal{J}(ij') \bar{\chi}(j'j', \omega) \bar{T}(j'j, \omega) \bar{\chi}(jj, \omega) \right]. \end{aligned}$$

From (5.6.9), we have $\bar{\chi}^o(\omega)^{-1} \bar{\chi}(ii, \omega) = c_i \{1 + \bar{K}(i, \omega) \bar{\chi}(ii, \omega)\}$, and a comparison of this equation for $\bar{\chi}(ij, \omega)$ with (5.6.10), leads to the result:

$$\begin{aligned} \delta_{ij} + \mathcal{J}(ij) \bar{\chi}(jj, \omega) + \sum_{j'} \mathcal{J}(ij') \bar{\chi}(j'j', \omega) \bar{T}(j'j, \omega) \bar{\chi}(jj, \omega) \\ = \{1 + \bar{K}(i, \omega) \bar{\chi}(ii, \omega)\} \{ \delta_{ij} + \bar{T}(ij, \omega) \bar{\chi}(jj, \omega) \}, \end{aligned} \quad (5.6.11)$$

leaving out the common factor c_i . Although this means that $\overline{\overline{K}}(i, \omega)$ and $\overline{\overline{T}}(ij, \omega)$ may be non-zero even when c_i is zero, this has no consequences in eqn (5.6.10). In order to derive the configurational average of this equation, we make the assumption that each site is surrounded by the same effective medium. Hence $\overline{\overline{K}}(i, \omega) \simeq \overline{\overline{K}}(\omega)$ is considered to be independent of the site considered, and therefore we have, from (5.6.9),

$$\overline{\overline{\chi}}(ii, \omega) = c_i \overline{\overline{\chi}}(\omega) \quad ; \quad \overline{\overline{\chi}}(\omega) = \{1 - \overline{\overline{\chi}}^o(\omega) \overline{\overline{K}}(\omega)\}^{-1} \overline{\overline{\chi}}^o(\omega). \quad (5.6.12)$$

With this replacement, the configurational average of eqn (5.6.11) may be derived straightforwardly, as we can take advantage of the condition that, for instance, $c_{j'}$ only occurs once in the sum over j' . It is important here that the common factor c_i was cancelled, because $\overline{\overline{T}}(j'j, \omega)$ involves the site i , making the averaging of $c_i \overline{\overline{T}}(j'j, \omega)$ more complicated. Introducing the notation $\overline{\overline{T}}_E(ij, \omega) = \langle \overline{\overline{T}}(ij, \omega) \rangle_{cf}$, we get from (5.6.11) the CPA equation

$$\begin{aligned} \delta_{ij} + c \mathcal{J}(ij) \overline{\overline{\chi}}(\omega) + \sum_{j'} c^2 \mathcal{J}(ij') \overline{\overline{\chi}}(\omega) \overline{\overline{T}}_E(j'j, \omega) \overline{\overline{\chi}}(\omega) \\ = \{1 + c \overline{\overline{K}}(\omega) \overline{\overline{\chi}}(\omega)\} \{\delta_{ij} + c \overline{\overline{T}}_E(ij, \omega) \overline{\overline{\chi}}(\omega)\} \end{aligned} \quad (5.6.13)$$

for the effective medium, which may be diagonalized by a Fourier transformation. Introducing the effective coupling parameter

$$\overline{\overline{\mathcal{J}}}_E(\mathbf{q}) = \mathcal{J}(\mathbf{q}) - \overline{\overline{K}}(\omega), \quad (5.6.14)$$

where the scalar appearing in a matrix equation is, as usual, multiplied by the unit matrix, we get

$$\overline{\overline{T}}_E(\mathbf{q}, \omega) = \overline{\overline{\mathcal{J}}}_E(\mathbf{q}) \overline{\overline{D}}_E(\mathbf{q}, \omega)^{-1} \quad ; \quad \overline{\overline{D}}_E(\mathbf{q}, \omega) = 1 - c \overline{\overline{\chi}}(\omega) \overline{\overline{\mathcal{J}}}_E(\mathbf{q}) \quad (5.6.15)$$

and, from (5.6.10),

$$\overline{\overline{\chi}}(\mathbf{q}, \omega) = c \overline{\overline{\chi}}(\omega) + c^2 \overline{\overline{\chi}}(\omega) \overline{\overline{T}}_E(\mathbf{q}, \omega) \overline{\overline{\chi}}(\omega) = \overline{\overline{D}}_E(\mathbf{q}, \omega)^{-1} c \overline{\overline{\chi}}(\omega). \quad (5.6.16)$$

Hence the result is similar to that obtained in the VCA, except that the parameters are replaced by the effective quantities introduced by eqns (5.6.12) and (5.6.14). These effective values are determined from the 'bare' parameters in terms of $\overline{\overline{K}}(\omega)$. It is easily seen that we retain the VCA result, i.e. $\overline{\overline{K}}(\omega)$ cancels out of (5.6.15), if (5.6.12) is replaced by the corresponding VCA equation $\overline{\overline{\chi}}(\omega) \simeq \{1 - c \overline{\overline{\chi}}^o(\omega) \overline{\overline{K}}(\omega)\}^{-1} \overline{\overline{\chi}}^o(\omega)$.

In the case $c = 1$, both the VCA and the CPA results coincide with the usual RPA result. $K(\omega)$ is itself determined by the effective parameters, and (5.6.13), with $i = j$, leads to the following self-consistent equation

$$\overline{\overline{K}}(\omega) = \frac{1}{N} \sum_{\mathbf{q}} c \mathcal{J}(\mathbf{q}) \overline{\overline{\chi}}(\omega) \overline{\overline{T}}_{\text{E}}(\mathbf{q}, \omega). \quad (5.6.17a)$$

This result may be written

$$\overline{\overline{K}}(\omega) = \frac{1}{N} \sum_{\mathbf{q}} \mathcal{J}(\mathbf{q}) \overline{\overline{D}}_{\text{E}}(\mathbf{q}, \omega)^{-1} = \sum_{\mathbf{q}} \mathcal{J}(\mathbf{q}) \overline{\overline{\chi}}(\mathbf{q}, \omega) / \sum_{\mathbf{q}} \overline{\overline{\chi}}(\mathbf{q}, \omega), \quad (5.6.17b)$$

corresponding to the condition that the *effective* T-matrix vanishes when summed over \mathbf{q} , $\sum_{\mathbf{q}} \overline{\overline{T}}_{\text{E}}(\mathbf{q}, \omega) = 0$, in accordance with our starting assumption, (5.6.10).

In order to derive the effective medium result (5.6.13), $\overline{\overline{\chi}}(j'j', \omega)$ in (5.6.11) was replaced by $c_{j'} \overline{\overline{\chi}}(\omega)$, which is an approximation, as this response depends on the actual surroundings, including the sites i and j . The CPA incorporates the same type of mistake as in the VCA, but it is clear that the frequency of such errors is substantially reduced. The dependence of $\overline{\overline{\chi}}(j'j', \omega)$ on c_i and c_j , corresponding to a site dependence of $\overline{\overline{K}}(j', \omega)$, becomes relatively unimportant if the configuration number Z is large, since i or j may only be one of the Z neighbours of the site j' .

The effective medium procedure is straightforwardly generalized to the case where $\overline{\overline{\chi}}_2(i, \omega)$ is non-zero (Jensen 1984). Again the CPA result may be expressed in the same way as the VCA result, (5.6.5–6), except that all the quantities are replaced by their effective CPA counterparts; $\mathcal{J}(\mathbf{q})$ becomes $\overline{\overline{\mathcal{J}}}_{\text{E}}(\mathbf{q})$, given by (5.6.14), and $\overline{\overline{\chi}}_r(\omega)$ in (5.6.6) is replaced by

$$\overline{\overline{\chi}}_r(\omega) = \left\{ 1 - \gamma_{rr} \overline{\overline{\chi}}_r^o(\omega) \overline{\overline{K}}(\omega) \right\}^{-1} \overline{\overline{\chi}}_r^o(\omega), \quad (5.6.18)$$

where the effective-medium parameter $\overline{\overline{K}}(\omega)$ is determined by the same self-consistent equation (5.6.17) as above. To a first approximation, $\overline{\overline{D}}_{\text{E}}(\mathbf{q}, \omega)^{-1}$ in this equation may be replaced by the simpler virtual-crystal result. Because of the poles in $\overline{\overline{D}}(\mathbf{q}, \omega)^{-1}$, both the real and imaginary parts of $\overline{\overline{K}}(\omega)$ are usually non-zero, and the imaginary contribution then predicts a finite lifetime for the excitations, due to the static disorder. This leading-order result may serve as the starting point in an iterative calculation of $\overline{\overline{K}}(\omega)$, and thus of a more accurate CPA result.

It is much more complicated to include the effects of off-diagonal disorder. They have been considered in the papers referred to above, but

only in relatively simple models like the dilute Heisenberg ferromagnet with nearest-neighbour interactions. This model may be considered as the extreme example of off-diagonal disorder, and the CPA concept of an effective medium loses its meaning completely below the *percolation* concentration, where all clusters of interacting spins are of finite size, precluding any long-range order. If the molecular field is independent of the site considered, i.e. $\mathcal{H}_{\text{MF}}(i) = \langle \mathcal{H}_{\text{MF}}(i) \rangle_{\text{cf}}$ in (5.6.3), as happens in the paramagnetic case or if $\langle \mathbf{J}_1 \rangle = \gamma \langle \mathbf{J}_2 \rangle$, then the CPA result above should apply. However, except in a pure boson or fermion system, the ‘dynamical’ disorder due to thermal fluctuations introduces corrections to the RPA equation (5.6.4), with consequences of the same order of magnitude as $\overline{\overline{K}}(\omega)$ in (5.6.16), at least at elevated temperatures. In most magnetic systems, the two kinds of disorder may lead to damping effects of the same magnitude, and furthermore the use of the CPA result (5.6.16), without taking into account the dynamic renormalization of the RPA, occasionally leads to misleading results, as discussed for instance by Jensen (1984).

The excitations of binary heavy-rare-earth alloys have been studied much less extensively than their magnetic structures. However, the effect of 10% of Y, Dy, Ho, and Tm on the spin-wave spectrum of Tb has been examined, and the characteristic influence of the different solutes observed. The results of Larsen *et al.* (1986) for the Y and Dy alloys could be interpreted in terms of a simple average-crystal model, in which all sites are considered as equivalent, and the effect of the solute atoms is to modify the average exchange and the effective single-ion anisotropy. Thus Dy reduces the effective hexagonal anisotropy, and the spin-wave energy gap therefore decreases. On the other hand, Y dilutes the two-ion coupling, and therefore decreases T_N and the spin-wave energies, although the relative magnitude of the peak in $\mathcal{J}(\mathbf{q})$ increases, extending the temperature range over which the helical structure is stable. The first excited state of the Ho ion in the Tb host lies in the spin-wave energy band, and the dispersion relation is consequently strongly perturbed (Mackintosh and Bjerrum Møller 1972).

However, the most pronounced effects were observed by Larsen *et al.* (1988) in Tb₉₀Tm₁₀, where the Tm ions, with a spin $S = 1$, are relatively weakly coupled to the surrounding Tb moments, with $S = 3$. Furthermore, the axial anisotropy of the Tm ions is large and of opposite sign to that of Tb. As a result, well-defined quasi-localized states may be excited on the Tm sites, as shown in Fig. 5.11. These rather complex results were interpreted by means of a VCA calculation, in which the crystal-field parameters for the Tm ions were deduced from the dilute-alloy experiments of Touborg (1977), while the single-ion anisotropy and the two-ion coupling between the Tb ions were taken from the analysis

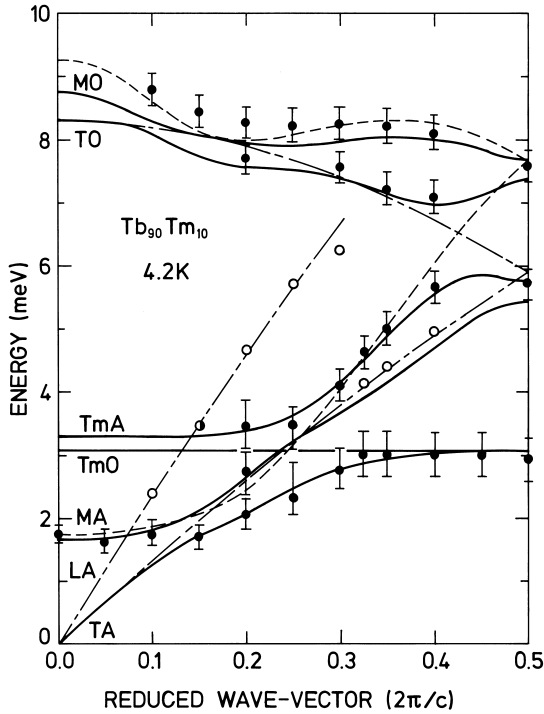


Fig. 5.11. Excitations in the c -direction of $\text{Tb}_{90}\text{Tm}_{10}$ at 4 K. The Tb magnon modes, the crystal-field excitations on the Tm ions, and the transverse phonons polarized parallel to the magnetization mutually interfere to produce the calculated dispersion relations shown by the thick lines. The dashed lines indicate the unperturbed Tb magnons, and the short and long dashes the phonons. A and O signify acoustic and optical respectively.

of Jensen *et al.* (1975) of the magnon dispersion relations. The magnon-phonon interaction, which plays an important role in determining the dispersion relations, was incorporated in the calculations by the method which will be presented in Section 7.3.1, which leads to results consistent with those derived in Section 5.4.2. The effective exchange between the moments on the different ions was scaled as in eqn (5.6.1-2), but γ was given the value 0.24, instead of the 0.33 which (5.6.2) yields, in order to fix correctly the energy of the first excited state on the Tm ions. Such a departure from the simple de Gennes scaling is not particularly surprising for ions with very different orbital angular momenta. In the system $\text{Pr}_{95}\text{Er}_5$, for example, Rainford *et al.* (1988b) found that

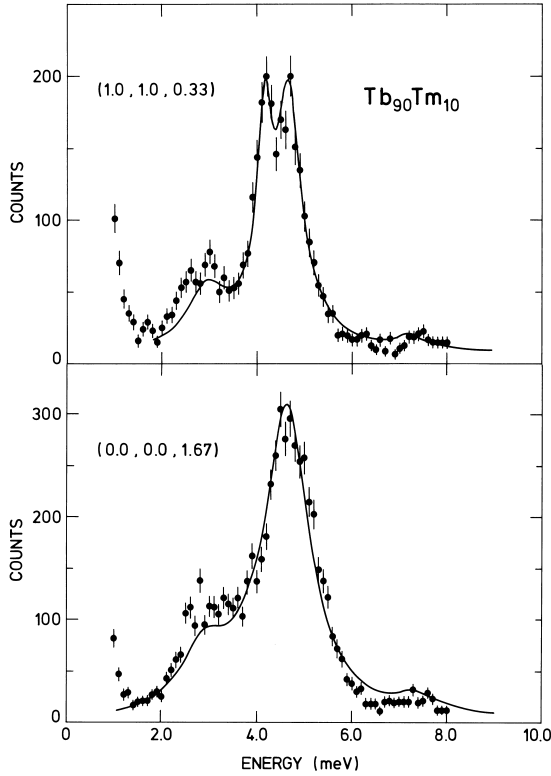


Fig. 5.12. Experimental and calculated neutron-scattering spectra in $\text{Tb}_{90}\text{Tm}_{10}$ for the indicated scattering vectors, which correspond to a reduced wave-vector of 0.33 in Fig. 5.11. In the lower curve, the scattering vector is in the c -direction, while it is close to the hexagonal plane in the upper, where an unperturbed transverse phonon is observed. The ratio of the impurity intensity to the magnon peak is roughly doubled when the scattering vector moves from the c -direction to the plane, showing that the magnetic fluctuations in the impurity mode are predominantly along the c -axis.

the Er ions modify the two-ion coupling of the host substantially.

The theoretical results give a good account both of the excitation energies and of the observed neutron-scattering spectra, as illustrated in Fig. 5.12. They reveal that the difference between the interactions of the Tb and Tm ions in this alloy has a profound influence on the magnetic behaviour at the two types of site. The exchange forces the Tm moment to lie in the plane at low concentrations but, according to the calculations, the crystal fields reduce it from the saturation value of

$7\mu_B$ to about $5.9\mu_B$, whereas the Tb moment is very close to saturation. Furthermore, the first excited-state on the Tm ions is at a relatively low energy, and the associated magnetic fluctuations are predominantly in the c -direction, reflecting an incipient realignment of the moments, which actually occurs at higher concentrations (Hansen and Lebech 1976). The Tb fluctuations, on the other hand, are largely confined to the plane, with the result that the neutron-scattering intensity stemming from the c -axis fluctuations is comparable for the two types of site, even though only 10% of the ions are Tm.

The CPA theory has not yet been applied to heavy rare earth-alloys. The extra linewidth-effects due to the randomness are not expected to be very pronounced in the 10% alloys. At low temperatures, they are of the order of the contribution of the scattering against the electron-hole pair excitations of the conduction electrons, and they become decreasingly important compared with intrinsic effects at higher temperatures. The CPA theory has been applied to the light rare earth-alloy $\text{Pr}_{95}\text{Nd}_5$ (Jensen 1979a) in the paramagnetic phase, where the linewidth effects predicted by the CPA at 9K are found to be of the same order as the intrinsic effects due to thermal disorder.

5.7 Conduction-electron interactions

As we have already discussed in Section 1.4, the conduction electrons in the rare earth metals act as the medium through which the coupling is established between the $4f$ electrons localized on the ions. In this section, we shall investigate this *RKKY* coupling in more detail, and consider its influence on both the *spin waves* in the ferromagnetic phase, and also on the *conduction electrons* themselves. The indirect-exchange interaction is first derived, and its effects in limiting the *lifetimes* of the spin waves and in *polarizing* the conduction electrons are deduced. The enhancement of the *effective mass* of the conduction electrons by the dynamical magnetic fluctuations is then calculated. Finally, the modification of the *electrical resistivity* by the exchange interaction is discussed, including the *scattering* of the conduction electrons by the spin-wave excitations, and the influence of the magnetic ordering on the conduction-electron band structure. For completeness, we include the effect of *magnetic superzones* in periodic structures in this section.

5.7.1 The indirect-exchange interaction

The starting point for our consideration of the indirect exchange, or RKKY coupling, of the localized moments is the Heisenberg-Dirac exchange between the $4f$ electrons and the conduction electrons. The $4f$ -core electrons of the ion at site i are assumed to be described to a good approximation by non-overlapping atomic wavefunctions $\phi_{4f}(\mathbf{r} - \mathbf{R}_i)$.

We shall neglect the spin-orbit coupling of the conduction electrons, and assume their wavefunctions to be the Bloch functions

$$\psi_{n\mathbf{k}}(\mathbf{r}) = u_{n\mathbf{k}}(\mathbf{r}) e^{i\mathbf{k}\cdot\mathbf{r}} = \psi_{n\mathbf{k}}(\mathbf{r} - \mathbf{R}_i) e^{i\mathbf{k}\cdot\mathbf{R}_i}, \quad (5.7.1)$$

independent of the spin state σ . $u_{n\mathbf{k}}(\mathbf{r}) = u_{n\mathbf{k}}(\mathbf{r} - \mathbf{R}_i)$ has the periodicity of the lattice, and n is the band index. The Hamiltonian of the conduction electrons in *second quantization* is

$$\mathcal{H}_s = \sum_{n\mathbf{k}\sigma} \varepsilon_{n\mathbf{k}} c_{n\mathbf{k}\sigma}^+ c_{n\mathbf{k}\sigma}, \quad (5.7.2)$$

where the index s is conventionally used for the conduction electrons even though, as we saw in Section 1.3, they have predominantly d character. $c_{n\mathbf{k}\uparrow}^+$ creates and $c_{n\mathbf{k}\uparrow}$ annihilates a spin-up electron in the band-state ($n\mathbf{k}$), and they are Fermi-operators which satisfy the *anticommutation relations*

$$\begin{aligned} \{c_{n\mathbf{k}\sigma}, c_{n'\mathbf{k}'\sigma'}^+\} &\equiv c_{n\mathbf{k}\sigma} c_{n'\mathbf{k}'\sigma'}^+ + c_{n'\mathbf{k}'\sigma'}^+ c_{n\mathbf{k}\sigma} = \delta_{nn'} \delta_{\mathbf{k}\mathbf{k}'} \delta_{\sigma\sigma'} \\ \{c_{n\mathbf{k}\sigma}^+, c_{n'\mathbf{k}'\sigma'}^+\} &= \{c_{n\mathbf{k}\sigma}, c_{n'\mathbf{k}'\sigma'}\} = 0. \end{aligned} \quad (5.7.3)$$

An exposition of second quantization may be found, for example, in White (1983). The exchange interaction between a pair of electrons is $-2I\mathbf{s}_1 \cdot \mathbf{s}_2$, where I is the exchange integral. If \mathbf{s}_1 is the spin of a $4f$ electron at site i , then the sum over all the $4f$ electrons at this site gives

$$\sum_{4f \text{ el.}} -2I\mathbf{s}_1 \cdot \mathbf{s}_2 = -2I\mathbf{S}_i \cdot \mathbf{s}_2 = -2I(g-1)\mathbf{J}_i \cdot \mathbf{s}_2,$$

where I is an average value of the exchange integral for the $4f$ electrons, and states other than those in the ground-state J -multiplet are neglected. The spin-density of the conduction electrons at \mathbf{r} may be expressed in second-quantized form so that, for instance,

$$s_{2z}(\mathbf{r}) = \sum_{nn'} \sum_{\mathbf{k}\mathbf{k}'} \psi_{n'\mathbf{k}'}^*(\mathbf{r}) \psi_{n\mathbf{k}}(\mathbf{r}) \frac{1}{2} (c_{n'\mathbf{k}'\uparrow}^+ c_{n\mathbf{k}\uparrow} - c_{n'\mathbf{k}'\downarrow}^+ c_{n\mathbf{k}\downarrow}). \quad (5.7.4)$$

The introduction of the Bloch functions implies that the *sf-exchange interaction* depends on:

$$\begin{aligned} \int d\mathbf{r}_1 d\mathbf{r}_2 \psi_{n'\mathbf{k}'}^*(\mathbf{r}_1) \phi_{4f}^*(\mathbf{r}_2 - \mathbf{R}_i) \frac{e^2}{|\mathbf{r}_1 - \mathbf{r}_2|} \psi_{n\mathbf{k}}(\mathbf{r}_2) \phi_{4f}(\mathbf{r}_1 - \mathbf{R}_i) \\ = \frac{1}{N} I(n'\mathbf{k}', n\mathbf{k}) e^{-i(\mathbf{k}' - \mathbf{k})\cdot\mathbf{R}_i}, \end{aligned}$$

with

$$I(n'\mathbf{k}', n\mathbf{k}) = N \int d\mathbf{r}_1 d\mathbf{r}_2 \psi_{n'\mathbf{k}'}^*(\mathbf{r}_1) \phi_{4f}^*(\mathbf{r}_2) \frac{e^2}{|\mathbf{r}_1 - \mathbf{r}_2|} \psi_{n\mathbf{k}}(\mathbf{r}_2) \phi_{4f}(\mathbf{r}_1), \quad (5.7.5)$$

If there are several $4f$ electrons per ion, $I(n'\mathbf{k}', n\mathbf{k})$ should be averaged over their wavefunctions. The Hamiltonian \mathcal{H}_{sf} , describing the exchange interaction between the conduction electrons and the $4f$ electrons, is found to be

$$\begin{aligned} \mathcal{H}_{sf} = & -\frac{1}{N} \sum_i \sum_{nn'} \sum_{\mathbf{k}\mathbf{k}'} (g-1) I(n'\mathbf{k}', n\mathbf{k}) e^{-i(\mathbf{k}'-\mathbf{k})\cdot\mathbf{R}_i} \\ & \times [(c_{n'\mathbf{k}'\uparrow}^+ c_{n\mathbf{k}\uparrow} - c_{n'\mathbf{k}'\downarrow}^+ c_{n\mathbf{k}\downarrow}) J_{iz} + c_{n'\mathbf{k}'\uparrow}^+ c_{n\mathbf{k}\downarrow} J_i^- + c_{n'\mathbf{k}'\downarrow}^+ c_{n\mathbf{k}\uparrow} J_i^+], \end{aligned} \quad (5.7.6)$$

in second quantization, where N is the number of rare earth ions.

In the ordered ferromagnetic phase, we may use the MF approximation, in which case

$$\mathcal{H}_{sf}(\text{MF}) = - \sum_{nn'} \sum_{\mathbf{k}} (g-1) I(n'\mathbf{k}, n\mathbf{k}) (c_{n'\mathbf{k}\uparrow}^+ c_{n\mathbf{k}\uparrow} - c_{n'\mathbf{k}\downarrow}^+ c_{n\mathbf{k}\downarrow}) \langle J_z \rangle. \quad (5.7.7)$$

This Hamiltonian gives rise to both diagonal and off-diagonal contributions to the energies of the conduction electrons. The diagonal energies are

$$\begin{aligned} \varepsilon_{n\mathbf{k}\uparrow} &= \varepsilon_{n\mathbf{k}} - \langle J_z \rangle (g-1) I(n\mathbf{k}, n\mathbf{k}) \\ \varepsilon_{n\mathbf{k}\downarrow} &= \varepsilon_{n\mathbf{k}} + \langle J_z \rangle (g-1) I(n\mathbf{k}, n\mathbf{k}). \end{aligned} \quad (5.7.8)$$

Second-order perturbation theory then gives the energies of the band electrons as

$$\tilde{\varepsilon}_{n\mathbf{k}\sigma} = \varepsilon_{n\mathbf{k}\sigma} + \langle J_z \rangle^2 (g-1)^2 \sum_{n' \neq n} \frac{|I(n'\mathbf{k}, n\mathbf{k})|^2}{\varepsilon_{n\mathbf{k}} - \varepsilon_{n'\mathbf{k}}}. \quad (5.7.9)$$

This dependence of the energies of the perturbed band-electrons on their state of polarization implies that the electron gas itself develops a non-zero magnetization. In order to calculate this moment, we first note that (5.7.9) corresponds to a replacement of $\mathcal{H}_s + \mathcal{H}_{sf}(\text{MF})$ by an effective Hamiltonian for the band electron,

$$\tilde{\mathcal{H}}_s = \sum_{n\mathbf{k}\sigma} \tilde{\varepsilon}_{n\mathbf{k}\sigma} \tilde{c}_{n\mathbf{k}\sigma}^+ \tilde{c}_{n\mathbf{k}\sigma}, \quad (5.7.10)$$

where the new Fermi operators are determined in terms of the old by

$$\begin{aligned} c_{n\mathbf{k}\uparrow} &= \tilde{c}_{n\mathbf{k}\uparrow} + \sum_{n'} U_{\mathbf{k}}(n, n') \tilde{c}_{n'\mathbf{k}\uparrow} \\ c_{n\mathbf{k}\downarrow} &= \tilde{c}_{n\mathbf{k}\downarrow} - \sum_{n'} U_{\mathbf{k}}(n, n') \tilde{c}_{n'\mathbf{k}\downarrow}, \end{aligned} \quad (5.7.11a)$$

to leading order. $U_{\mathbf{k}}(n, n) = 0$ and, for $n' \neq n$,

$$U_{\mathbf{k}}(n, n') = (g - 1) \langle J_z \rangle \frac{I(n\mathbf{k}, n'\mathbf{k})}{\varepsilon_{n\mathbf{k}} - \varepsilon_{n'\mathbf{k}}}. \quad (5.7.11b)$$

The (approximately) diagonal form of (5.7.9) implies that the thermal expectation values are

$$\langle \tilde{c}_{n\mathbf{k}\sigma}^+ \tilde{c}_{n'\mathbf{k}'\sigma'} \rangle = \delta_{nn'} \delta_{\mathbf{k}\mathbf{k}'} \delta_{\sigma\sigma'} f_{n\mathbf{k}\sigma}, \quad (5.7.12a)$$

where

$$f_{n\mathbf{k}\sigma} = \frac{1}{e^{\beta(\tilde{\varepsilon}_{n\mathbf{k}\sigma} - \mu_F)} + 1} \quad (5.7.12b)$$

is the *Fermi-Dirac distribution function* and μ_F is the chemical potential, equal to the Fermi energy $\tilde{\varepsilon}_F$ in the temperature regime in which we shall be interested. The moment density is determined by (5.7.4), and introducing the new Fermi operators and using (5.7.12), we obtain

$$\begin{aligned} \langle \mu_z(\mathbf{r}) \rangle_{\text{c.el.}} &= \mu_B \sum_{nn'} \sum_{\mathbf{k}\mathbf{k}'} \psi_{n'\mathbf{k}'}^*(\mathbf{r}) \psi_{n\mathbf{k}}(\mathbf{r}) (\langle c_{n'\mathbf{k}'\uparrow}^+ c_{n\mathbf{k}\uparrow} \rangle - \langle c_{n'\mathbf{k}'\downarrow}^+ c_{n\mathbf{k}\downarrow} \rangle) \\ &= \mu_B \sum_{nn'} \sum_{\mathbf{k}} \psi_{n'\mathbf{k}}^*(\mathbf{r}) \psi_{n\mathbf{k}}(\mathbf{r}) [\{\delta_{nn'} + U_{\mathbf{k}}^*(n', n)\} (f_{n\mathbf{k}\uparrow} - f_{n\mathbf{k}\downarrow}) \\ &\quad + U_{\mathbf{k}}(n, n') (f_{n'\mathbf{k}\uparrow} - f_{n'\mathbf{k}\downarrow})]. \end{aligned} \quad (5.7.13)$$

The uniform, averaged part of this moment density can be obtained by an integration of eqn (5.7.13) over space, and remembering that the wavefunctions are orthogonal and normalized, we find the magnetic moment of the conduction electrons per ion to be

$$\langle \mu_z \rangle_{\text{c.el.}} = \mu_B \frac{1}{N} \sum_{n\mathbf{k}} (f_{n\mathbf{k}\uparrow} - f_{n\mathbf{k}\downarrow}). \quad (5.7.14)$$

We note that, in addition to this uniform polarization of the conduction electrons, there is a spatially non-uniform component of the polarization density with the periodicity of the lattice. This non-uniform component reflects the variation in the electronic density, including the perturbative changes due to the *interband* contributions proportional to $U_{\mathbf{k}}(n, n')$. Furthermore, when the spin-orbit coupling of the conduction electrons is of importance, the interband coupling may induce a positional dependence in the direction of the spin polarization.

In order to obtain order-of-magnitude estimates of the exchange effects, we introduce a reasonable but somewhat crude approximation for the exchange integral, which is due to Overhauser (1963) and has

been discussed in detail by Freeman (1972). First we assume that the Coulomb interaction in eqn (5.7.5) is strongly shielded, so that it can be replaced by a δ -function. Next, using plane waves for the Bloch functions, we obtain

$$(g-1)I(n\mathbf{k}', n\mathbf{k}) \approx j(\mathbf{q} = \mathbf{k}' - \mathbf{k}) \propto \int d\mathbf{r} |\phi_{4f}(\mathbf{r})|^2 e^{-i\mathbf{q}\cdot\mathbf{r}}, \quad (5.7.15)$$

which is the form factor of the $4f$ -electron density, approximately the same as the local moment density (4.1.15). In this simplified model, where the conduction electrons are assumed to be free-electron-like, the interband exchange integrals, in which $n' \neq n$, are obtained by adding reciprocal-lattice vectors $\boldsymbol{\tau}$ to \mathbf{q} in eqn (5.7.15). In this model, we obtain a rigid band-splitting, independent of \mathbf{k} , between the spin-down and spin-up bands, of magnitude

$$\Delta = \tilde{\varepsilon}_{n\mathbf{k}\downarrow} - \tilde{\varepsilon}_{n\mathbf{k}\uparrow} = 2\langle J_z \rangle j(\mathbf{0}). \quad (5.7.16)$$

Since $j(\mathbf{0})$ has the same sign as $(g-1)$, it is positive in the heavy rare earth metals. If $\mathcal{N}(\varepsilon)$ is the density of electronic states per ion and per spin state in the paramagnetic phase, the shifts of the spin-up and spin-down bands lead to an excess number of spin-up electrons proportional to

$$\overline{\mathcal{N}}(\tilde{\varepsilon}_F) = \frac{1}{\Delta} \int_{\tilde{\varepsilon}_F - \frac{\Delta}{2}}^{\tilde{\varepsilon}_F + \frac{\Delta}{2}} \mathcal{N}(\varepsilon) d\varepsilon, \quad (5.7.17)$$

when the small modification of the density of states due to the interband coupling is neglected, so that $\tilde{\varepsilon}_F$ is close to the Fermi energy ε_F of the non-magnetic system. In combination with eqn (5.7.14), this result predicts a (positive) augmentation of the ferromagnetic moment of the $4f$ electrons, due to the conduction electrons, of magnitude

$$\langle \mu_z \rangle_{\text{c.el.}} = \mu_B \overline{\mathcal{N}}(\tilde{\varepsilon}_F) \Delta, \quad (5.7.18)$$

when $k_B T \ll \tilde{\varepsilon}_F$. The total moment per ion may then be expressed in terms of an effective g -factor:

$$\langle \mu_z \rangle = g\mu_B \langle J_z \rangle + \langle \mu_z \rangle_{\text{c.el.}} = (g + \Delta g)\mu_B \langle J_z \rangle, \quad (5.7.19a)$$

where

$$\Delta g = 2j(\mathbf{0}) \overline{\mathcal{N}}(\tilde{\varepsilon}_F). \quad (5.7.19b)$$

In the metals, the effective exchange integral $j(\mathbf{0})$ is $\sim (g-1) \times 0.1$ eV, leading to an exchange splitting Δ which, in Gd for example, is nearly 1 eV. This relatively large splitting has the consequence that $\overline{\mathcal{N}}(\tilde{\varepsilon}_F)$ may

differ somewhat from the value $\mathcal{N}(\varepsilon_F)$ in the paramagnetic phase. In the hcp metals, the band structure calculations discussed in Section 1.3 reveal that ε_F is near a peak in the density of states due to the d electrons, and that $\mathcal{N}(\varepsilon_F) \simeq 1 \text{ eV}^{-1}$ per spin state per ion, corresponding to an electronic moment of the order of one-tenth of the local moment. In the example of Gd, for which $g = 2$, $\Delta g = 0.18$. The same value of $\Delta g/(g-1)$ accounts fairly well for the conduction-electron contribution to the moments of the other heavy rare earths in Table 1.6, bearing in mind the uncertainties in the experimental results, and the possible effects of the crystal fields in quenching the local moments.

The spin waves in the ferromagnetic phase are decisively influenced by the sf -exchange interaction. In order to consider such effects, we introduce the Bose operators acting on the angular-momentum states, as in eqns (5.2.6-8), and find, to first order in $1/J$,

$$\begin{aligned} \mathcal{H}_{sf} \simeq \mathcal{H}_{sf}(\text{MF}) - \frac{1}{N} \sum_{\mathbf{k}\mathbf{q}\boldsymbol{\tau}} \sum_i j(\mathbf{q} + \boldsymbol{\tau}) e^{-i\mathbf{q}\cdot\mathbf{R}_i} & \left[-\delta_{\mathbf{q}\mathbf{0}} (\langle c_{\mathbf{k}+\boldsymbol{\tau}\uparrow}^+ c_{\mathbf{k}\uparrow} \rangle \right. \\ & \left. - \langle c_{\mathbf{k}+\boldsymbol{\tau}\downarrow}^+ c_{\mathbf{k}\downarrow} \rangle) a_i^+ a_i + \sqrt{2J} c_{\mathbf{k}+\mathbf{q}+\boldsymbol{\tau}\uparrow}^+ c_{\mathbf{k}\downarrow} a_i^+ + \sqrt{2J} c_{\mathbf{k}+\mathbf{q}+\boldsymbol{\tau}\downarrow}^+ c_{\mathbf{k}\uparrow} a_i \right], \end{aligned}$$

using the simplified exchange of eqn (5.7.15), and neglecting effects of third or higher order in $j(\mathbf{q})$ due to $(c_{\mathbf{k}'\sigma}^+ c_{\mathbf{k}\sigma} - \langle c_{\mathbf{k}'\sigma}^+ c_{\mathbf{k}\sigma} \rangle) a_i^+ a_i$. \mathbf{q} is assumed to lie in the primitive Brillouin zone, but no such restriction is placed on \mathbf{k} . We note that $c_{\mathbf{k}}^+$ and $c_{\mathbf{k}+\boldsymbol{\tau}}^+$, where $\boldsymbol{\tau}$ is a reciprocal lattice vector, create electrons in different bands in the free-electron model. Introducing the crystal-field Hamiltonian to first order in $1/J$ (eqn (5.2.14) with $\mathcal{J}(ij) = 0$), and the Fourier transforms of the Bose operators (5.2.16), we find that the total magnetic Hamiltonian becomes

$$\begin{aligned} \mathcal{H} = \tilde{\mathcal{H}}_s + \sum_{\mathbf{q}} [\{A + J\tilde{\mathcal{J}}(\mathbf{0}, 0)\} a_{\mathbf{q}}^+ a_{\mathbf{q}} + B \frac{1}{2} (a_{\mathbf{q}} a_{-\mathbf{q}} + a_{\mathbf{q}}^+ a_{-\mathbf{q}}^+)] \\ - \sqrt{2J/N} \sum_{\mathbf{k}\mathbf{q}\boldsymbol{\tau}} j(\mathbf{q} + \boldsymbol{\tau}) (c_{\mathbf{k}+\mathbf{q}+\boldsymbol{\tau}\uparrow}^+ c_{\mathbf{k}\downarrow} a_{-\mathbf{q}}^+ + c_{\mathbf{k}+\mathbf{q}+\boldsymbol{\tau}\downarrow}^+ c_{\mathbf{k}\uparrow} a_{\mathbf{q}}), \end{aligned} \quad (5.7.20)$$

where

$$\tilde{\mathcal{J}}(\mathbf{0}, 0) = 2j^2(\mathbf{0})\overline{\mathcal{N}}(\tilde{\varepsilon}_F) + \frac{2}{N} \sum_{\mathbf{k}, \boldsymbol{\tau} \neq \mathbf{0}} |j(\boldsymbol{\tau})|^2 \frac{f_{\mathbf{k}\downarrow} - f_{\mathbf{k}+\boldsymbol{\tau}\uparrow}}{\varepsilon_{\mathbf{k}+\boldsymbol{\tau}} - \varepsilon_{\mathbf{k}}}, \quad (5.7.21)$$

including the ‘interband’ contributions as in (5.7.9). The spin-wave energies may be obtained from the poles in the Green function $\langle\langle a_{\mathbf{q}}; a_{\mathbf{q}}^+ \rangle\rangle$. The equation of motion (3.3.14) for this Green function is determined

from \mathcal{H} to be

$$\begin{aligned} & \{\hbar\omega - A - J\tilde{\mathcal{J}}(\mathbf{0}, 0)\} \langle\langle a_{\mathbf{q}}; a_{\mathbf{q}}^+ \rangle\rangle - B \langle\langle a_{-\mathbf{q}}^+; a_{\mathbf{q}}^+ \rangle\rangle \\ & + \sqrt{2J/N} \sum_{\mathbf{k}\tau} j(-\mathbf{q} - \boldsymbol{\tau}) \langle\langle c_{\mathbf{k}-\mathbf{q}-\boldsymbol{\tau}\uparrow}^+ c_{\mathbf{k}\downarrow}; a_{\mathbf{q}}^+ \rangle\rangle = 1. \end{aligned} \quad (5.7.22)$$

The equation of motion of the new Green function $\langle\langle c_{\mathbf{k}-\mathbf{q}-\boldsymbol{\tau}\uparrow}^+ c_{\mathbf{k}\downarrow}; a_{\mathbf{q}}^+ \rangle\rangle$ involves the following commutator:

$$\begin{aligned} [c_{\mathbf{k}-\mathbf{q}-\boldsymbol{\tau}\uparrow}^+ c_{\mathbf{k}\downarrow}, \mathcal{H}] &= (\varepsilon_{\mathbf{k}\downarrow} - \varepsilon_{\mathbf{k}-\mathbf{q}-\boldsymbol{\tau}\uparrow}) c_{\mathbf{k}-\mathbf{q}-\boldsymbol{\tau}\uparrow}^+ c_{\mathbf{k}\downarrow} \\ &+ \sqrt{2J/N} \sum_{\mathbf{q}'} j(\mathbf{q}') (c_{\mathbf{k}-\mathbf{q}-\boldsymbol{\tau}+\mathbf{q}'\downarrow}^+ c_{\mathbf{k}\downarrow} - c_{\mathbf{k}-\mathbf{q}-\boldsymbol{\tau}\uparrow}^+ c_{\mathbf{k}-\mathbf{q}'\uparrow}) a_{\mathbf{q}'} \\ &\simeq (\varepsilon_{\mathbf{k}\downarrow} - \varepsilon_{\mathbf{k}-\mathbf{q}-\boldsymbol{\tau}\uparrow}) c_{\mathbf{k}-\mathbf{q}-\boldsymbol{\tau}\uparrow}^+ c_{\mathbf{k}\downarrow} + \sqrt{2J/N} j(\mathbf{q} + \boldsymbol{\tau}) (f_{\mathbf{k}\downarrow} - f_{\mathbf{k}-\mathbf{q}-\boldsymbol{\tau}\uparrow}) a_{\mathbf{q}} \end{aligned} \quad (5.7.23)$$

obtained by applying the anticommutator relations (5.7.3) and, in the second equation, an RPA decoupling of the operator products. It is not necessary here to differentiate between the new and the old Fermi operators, as the differences introduce corrections only in the third order of $|j(\mathbf{q})|$. Introducing this RPA result in the equation of motion for the Green function $\langle\langle c_{\mathbf{k}-\mathbf{q}-\boldsymbol{\tau}\uparrow}^+ c_{\mathbf{k}\downarrow}; a_{\mathbf{q}}^+ \rangle\rangle$, we obtain

$$\begin{aligned} & (\hbar\omega - \varepsilon_{\mathbf{k}\downarrow} + \varepsilon_{\mathbf{k}-\mathbf{q}-\boldsymbol{\tau}\uparrow}) \langle\langle c_{\mathbf{k}-\mathbf{q}-\boldsymbol{\tau}\uparrow}^+ c_{\mathbf{k}\downarrow}; a_{\mathbf{q}}^+ \rangle\rangle \\ & - \sqrt{2J/N} j(\mathbf{q} + \boldsymbol{\tau}) (f_{\mathbf{k}\downarrow} - f_{\mathbf{k}-\mathbf{q}-\boldsymbol{\tau}\uparrow}) \langle\langle a_{\mathbf{q}}; a_{\mathbf{q}}^+ \rangle\rangle = 0, \end{aligned} \quad (5.7.24)$$

which, in combination with (5.7.22), leads to

$$\{\hbar\omega - A - J\tilde{\mathcal{J}}(\mathbf{0}, 0) + J\tilde{\mathcal{J}}(\mathbf{q}, \omega)\} \langle\langle a_{\mathbf{q}}; a_{\mathbf{q}}^+ \rangle\rangle - B \langle\langle a_{-\mathbf{q}}^+; a_{\mathbf{q}}^+ \rangle\rangle = 1, \quad (5.7.25)$$

where

$$\tilde{\mathcal{J}}(\mathbf{q}, \omega) = \lim_{\varepsilon \rightarrow 0^+} \frac{2}{N} \sum_{\boldsymbol{\tau}} |j(\mathbf{q} + \boldsymbol{\tau})|^2 \sum_{\mathbf{k}} \frac{f_{\mathbf{k}\downarrow} - f_{\mathbf{k}-\mathbf{q}-\boldsymbol{\tau}\uparrow}}{\hbar\omega + i\hbar\varepsilon - \varepsilon_{\mathbf{k}\downarrow} + \varepsilon_{\mathbf{k}-\mathbf{q}-\boldsymbol{\tau}\uparrow}}. \quad (5.7.26a)$$

This result may be expressed in terms of the susceptibility of the conduction electrons. Introducing the spin susceptibility per ion, which is the usual magnetic susceptibility times $(2\mu_B)^{-2}V/N$, so that

$$\begin{aligned} \chi_{c.e.l.}^{+-}(\mathbf{q}, \omega) &= -\frac{1}{N} \int d\mathbf{r}_1 d\mathbf{r}_2 \langle\langle s^+(\mathbf{r}_1); s^-(\mathbf{r}_2) \rangle\rangle e^{-i\mathbf{q}\cdot(\mathbf{r}_1 - \mathbf{r}_2)} \\ &= -\frac{1}{N} \sum_{\mathbf{k}'\mathbf{k}''} \langle\langle c_{\mathbf{k}'-\mathbf{q}\uparrow}^+ c_{\mathbf{k}'\downarrow}; c_{\mathbf{k}''+\mathbf{q}\downarrow}^+ c_{\mathbf{k}''\uparrow} \rangle\rangle \\ &= \lim_{\varepsilon \rightarrow 0^+} \frac{1}{N} \sum_{\mathbf{k}} \frac{f_{\mathbf{k}\downarrow} - f_{\mathbf{k}-\mathbf{q}\uparrow}}{\hbar\omega + i\hbar\varepsilon - \varepsilon_{\mathbf{k}\downarrow} + \varepsilon_{\mathbf{k}-\mathbf{q}\uparrow}}, \end{aligned} \quad (5.7.26b)$$

and neglecting the higher-order corrections to the spin-susceptibility, due to the coupling to the local moments, we can write the above result

$$\tilde{\mathcal{J}}(\mathbf{q}, \omega) = 2 \sum_{\boldsymbol{\tau}} |j(\mathbf{q} + \boldsymbol{\tau})|^2 \chi_{\text{c.el.}}^{+-}(\mathbf{q} + \boldsymbol{\tau}, \omega), \quad (5.7.26c)$$

where by the relation (3.2.15), $\chi_{\text{c.el.}}^{+-}(\mathbf{q}, \omega) = [\chi_{\text{c.el.}}^{-+}(-\mathbf{q}, -\omega)]^*$. In general, when the Coulomb interaction cannot be approximated by a δ -function, this factorization is not valid, and the indirect exchange is instead given by

$$\begin{aligned} \tilde{\mathcal{J}}(\mathbf{q}, \omega) = \\ \lim_{\varepsilon \rightarrow 0^+} \frac{2}{N} \sum_{nn'} \sum_{\mathbf{k}} (g-1)^2 |I(n'\mathbf{k} - \mathbf{q}, n\mathbf{k})|^2 \frac{f_{n\mathbf{k}\downarrow} - f_{n'\mathbf{k}-\mathbf{q}\uparrow}}{\hbar\omega + i\hbar\varepsilon - \varepsilon_{n\mathbf{k}\downarrow} + \varepsilon_{n'\mathbf{k}-\mathbf{q}\uparrow}}, \end{aligned} \quad (5.7.27)$$

where \mathbf{k} is now confined to the primitive Brillouin zone.

In the frequency regime of the spin waves, where $|\hbar\omega|$ is much smaller than the Fermi energy or the exchange splitting Δ , the frequency dependence of $\tilde{\mathcal{J}}(\mathbf{q}, \omega)$ can, to a good approximation, be neglected. The spins of the conduction electrons respond essentially instantaneously to any changes in the state of the local angular momenta, compared with the time-scale of these changes. For a Bravais-lattice, $\tilde{\mathcal{J}}(\mathbf{q}, \omega) \simeq \tilde{\mathcal{J}}(\mathbf{q}, 0) = \tilde{\mathcal{J}}(-\mathbf{q}, 0)$. A comparison of eqn (5.7.25) with the $1/J$ spin-wave result (5.2.18) shows that $\tilde{\mathcal{J}}(\mathbf{0}, 0) - \tilde{\mathcal{J}}(\mathbf{q}, 0)$ replaces the contribution of the Heisenberg interaction considered in eqn (5.2.1). In this equation, $\mathcal{J}(ii) \equiv 0$ by definition and, since this is not the case for $\tilde{\mathcal{J}}(ii) = (1/N) \sum_{\mathbf{q}} \tilde{\mathcal{J}}(\mathbf{q}, 0)$, $\tilde{\mathcal{J}}(\mathbf{q}, 0)$ cannot be associated directly with $\mathcal{J}(\mathbf{q})$. The instantaneous or frequency-independent part of the coupling of \mathbf{J}_i with itself leads to a contribution $\frac{1}{2}N\tilde{\mathcal{J}}(ii)\langle \mathbf{J}_i \cdot \mathbf{J}_i \rangle$ to the total energy, where $\langle \mathbf{J}_i \cdot \mathbf{J}_i \rangle = J(J+1)$, independently of the magnetic ordering or the temperature. This assertion may be verified (to first order in $1/J$) by a direct calculation of $\langle \mathcal{H} \rangle$ from (5.7.20). For this purpose $\langle c_{\mathbf{k}-\mathbf{q}-\boldsymbol{\tau}\uparrow}^+ c_{\mathbf{k}\downarrow} a_{\mathbf{q}}^+ \rangle$, for instance, is determined from eqn (5.7.24), but a *self-energy* correction of a factor $1/2$ must be included in its contribution to $\langle \mathcal{H} \rangle$. Taking this condition into account, we may finally write

$$\mathcal{J}(\mathbf{q}) = \tilde{\mathcal{J}}(\mathbf{q}, 0) - \frac{1}{N} \sum_{\mathbf{q}'} \tilde{\mathcal{J}}(\mathbf{q}', 0). \quad (5.7.28)$$

The exchange interaction between the $4f$ electrons and the conduction electrons thus leads to an effective Heisenberg interaction between the local angular momenta, as given in (5.2.1). This is the RKKY interaction discussed earlier in Section 1.4.

The above calculation has been performed for a Bravais lattice, but the result (5.7.26) is readily generalized to a crystal with a basis of p ions, as the conduction electrons, in the approximation adopted, are not affected by the presence of the basis. If the couplings between the different sublattices are introduced in an equivalent manner to (5.1.1), then

$$\tilde{\mathcal{J}}_{ss'}(\mathbf{q}, \omega) = \frac{2}{p} \sum_{\boldsymbol{\tau}} |j(\mathbf{q} + \boldsymbol{\tau})|^2 \chi_{\text{c.el.}}^{+-}(\mathbf{q} + \boldsymbol{\tau}, \omega) \exp(i\boldsymbol{\rho}_{ss'} \cdot \boldsymbol{\tau}) \quad (5.7.29)$$

replaces (5.7.26c), where $\boldsymbol{\rho}_{ss'}$ is the vector connecting the two sublattices s and s' .

The interaction between the localized moments is effectuated via virtual electron-hole pair-excitations of the conduction electrons. The transmission of any time-dependent event may be disturbed in two ways; either by the finite propagation-time of the pairs, or by a decay of the pair states into unbound electron and hole excitations, the so-called *Stoner* excitations. The second effect produces by far the most important correction to the instantaneous interaction, but we shall begin with a discussion of the frequency-dependence of the real part of $\tilde{\mathcal{J}}(\mathbf{q}, \omega)$, due to the finite transmission time. Returning to the simple model leading to (5.7.26), we find that the exchange coupling is proportional to the susceptibility function $\chi_{\text{c.el.}}^{+-}(\mathbf{q}, \omega)$, which for unpolarized free electrons is the same as the *Lindhard function* (Lindhard 1954). If corrections of the order $k_B T / \varepsilon_F$ are neglected, the real part at zero wave-vector is

$$\begin{aligned} \text{Re}[\chi_{\text{c.el.}}^{+-}(\mathbf{0}, \omega)] &= \frac{1}{N} \sum_{\mathbf{k}} \frac{f_{\mathbf{k}\downarrow} - f_{\mathbf{k}\uparrow}}{\hbar\omega - \varepsilon_{\mathbf{k}\downarrow} + \varepsilon_{\mathbf{k}\uparrow}} \\ &= \frac{1}{N} \sum_{\mathbf{k}} \frac{f_{\mathbf{k}\uparrow} - f_{\mathbf{k}\downarrow}}{\Delta - \hbar\omega} = \bar{N}(\tilde{\varepsilon}_F) \left(1 + \frac{\hbar\omega}{\Delta}\right). \end{aligned} \quad (5.7.30)$$

From this result, we find immediately that the intra-band contribution at zero frequency to $\tilde{\mathcal{J}}(\mathbf{q} \rightarrow \mathbf{0}, 0)$ in eqn (5.7.26a) is $2j^2(\mathbf{0})\bar{N}(\tilde{\varepsilon}_F)$, which is the same as in (5.7.21). On the other hand, the interband contributions differ in the two expressions, as the denominator in (5.7.26a) involves the exchange splitting Δ , whereas that in (5.7.21) does not. However, this difference can be neglected, as it is of the order $(\Delta/\varepsilon_F)^2$ times the intra-band contribution, which is beyond the order considered in these calculations. In fact, since the starting Hamiltonian (5.7.6) is invariant with respect to the choice of z -axis for the electronic spins and the angular momenta, the spin-wave frequency must vanish when $\mathbf{q} \rightarrow \mathbf{0}$ and $A = B = 0$, according to the *Goldstone theorem*, which will be discussed in the next chapter. Therefore $\tilde{\mathcal{J}}(\mathbf{q} \rightarrow \mathbf{0}, 0) = \tilde{\mathcal{J}}(\mathbf{0}, 0)$,

and we simply assume that eqn (5.7.26a), with $(\mathbf{q}, \omega) = (\mathbf{0}, 0)$, replaces eqn (5.7.21). In the presence of an external field, Δ in eqn (5.7.16) is increased by an amount $2\mu_B H$, which leads to the extra contribution $\Delta g\mu_B H$ to $\tilde{\mathcal{J}}(\mathbf{0}, 0)$ in (5.7.21), as the change with field of the interband terms may be neglected. To leading order, $\tilde{\mathcal{J}}(\mathbf{q} \rightarrow \mathbf{0}, 0)$ is not affected by the applied field, so to this order the extra polarization of the conduction electrons, due to an external field, may simply be accounted for by replacing $g\mu_B H$ by $(g + \Delta g)\mu_B H$, both in the Zeeman energy (5.7.19a) and in the spin-wave energy parameters (in A). Writing the susceptibility in eqn (5.7.26b) as the sum of two terms, and replacing $\mathbf{k} - \mathbf{q}$ by \mathbf{k} in the term involving $f_{\mathbf{k}-\mathbf{q}\uparrow}$, we obtain

$$\begin{aligned} \text{Re}[\chi_{\text{c.el.}}^{+-}(\mathbf{q}, \omega)] = & \\ & \frac{V}{(2\pi)^3} \frac{2\pi}{N} \int_0^{k_{F\downarrow}} k^2 dk \int_{-1}^1 d\mu \left[\hbar\omega - \Delta + \frac{(\hbar q)^2}{2m} - \frac{\hbar^2 k q}{m} \mu \right]^{-1} \\ & - \frac{V}{(2\pi)^3} \frac{2\pi}{N} \int_0^{k_{F\uparrow}} k^2 dk \int_{-1}^1 d\mu \left[\hbar\omega - \Delta - \frac{(\hbar q)^2}{2m} - \frac{\hbar^2 k q}{m} \mu \right]^{-1}, \end{aligned}$$

or

$$\begin{aligned} \text{Re}[\chi_{\text{c.el.}}^{+-}(\mathbf{q}, \omega)] = & \\ \frac{V}{N} \frac{m}{(2\pi\hbar)^2} \{ & k_{F\downarrow}(1 - \eta) \mathcal{F}\left(\frac{q}{2k_{F\downarrow}}(1 - \eta)\right) + k_{F\uparrow}(1 + \eta) \mathcal{F}\left(\frac{q}{2k_{F\uparrow}}(1 + \eta)\right) \} \end{aligned} \quad (5.7.31a)$$

where we have introduced the function

$$\mathcal{F}(x) = \frac{1}{2} + \frac{1 - x^2}{4x} \ln \left| \frac{1 + x}{1 - x} \right| \quad (5.7.31b)$$

and the parameter

$$\eta = \frac{\Delta - \hbar\omega}{\varepsilon_F} \left(\frac{k_F}{q} \right)^2. \quad (5.7.31c)$$

The Fermi energy is $\varepsilon_F = (\hbar k_F)^2/2m$, and the wave-vectors of the spin-up and the spin-down electrons at the Fermi surface are

$$k_{F\uparrow} = k_F \left(1 + \frac{\Delta}{2\varepsilon_F} \right)^{\frac{1}{2}} \quad ; \quad k_{F\downarrow} = k_F \left(1 - \frac{\Delta}{2\varepsilon_F} \right)^{\frac{1}{2}}. \quad (5.7.31d)$$

$\eta \rightarrow \infty$ in the limit $q \rightarrow 0$ and, using $\mathcal{F}(x) = 1/3x^2$ when $|x| \rightarrow \infty$, we may re-derive the result (5.7.30). At non-zero q , a numerical analysis shows that, to a good approximation,

$$\text{Re}[\chi_{\text{c.el.}}^{+-}(\mathbf{q}, \omega)] = \bar{\mathcal{N}}(\bar{\varepsilon}_F) \left\{ \mathcal{F}\left(\frac{q}{2k_F}\right) + \xi_q \frac{\hbar\omega}{\Delta} \right\}, \quad (5.7.32)$$

even when Δ/ε_F is as large as 0.5. The parameter ξ_q is equal to 1 at $q = 0$, and peaks at $q = q_0 = k_{F\uparrow} - k_{F\downarrow}$, after which it rapidly decreases ($\xi_q \simeq 0.25$ at $q = 2q_0$). For $\Delta/\varepsilon_F = 0.1$, the maximum value is about 4 and it decreases for increasing values of Δ , falling to about 3 at $\Delta/\varepsilon_F = 0.4$. Usually q_0 is much smaller than the length of any reciprocal-lattice vector, which means that the frequency dependence of the ‘interband’ term in the real part of $\tilde{\mathcal{J}}(\mathbf{q}, \omega)$ can be neglected. The intra-band contribution is $2|j(\mathbf{q})|^2 \overline{\mathcal{N}}(\tilde{\varepsilon}_F) \xi_q \hbar\omega/\Delta$, and using

$$\{\hbar\omega + A + J\tilde{\mathcal{J}}(\mathbf{0}, 0) - J\tilde{\mathcal{J}}^*(-\mathbf{q}, -\omega)\} \langle\langle a_{-\mathbf{q}}^+; a_{\mathbf{q}}^+ \rangle\rangle + B \langle\langle a_{\mathbf{q}}; a_{\mathbf{q}}^+ \rangle\rangle = 0, \quad (5.7.33)$$

which follows by symmetry from eqn (5.7.25), we may determine the spin-wave energies from the real part of $\tilde{\mathcal{J}}(\mathbf{q}, \omega)$ to be

$$\hbar\omega = E'_{\mathbf{q}} = E_{\mathbf{q}} [1 + \xi_q \overline{\mathcal{N}}(\tilde{\varepsilon}_F) |j(\mathbf{q})|^2 / j(\mathbf{0})]^{-1}, \quad (5.7.34a)$$

to first order in $1/J$, with $E_{\mathbf{q}}$ given by (5.2.22). The extra factor, which originates from the frequency dependence of $\chi_{\text{c.el.}}^{+-}(\mathbf{q}, \omega)$, differs from 1 by only a few per cent, and its \mathbf{q} -dependent contribution could scarcely be distinguished from that of $\mathcal{J}(\mathbf{q})$. However, the presence of this factor at $\mathbf{q} = \mathbf{0}$ means that the energy of the uniform spin-wave mode is no longer determined exclusively by the magnetic anisotropy of the bulk, according to (5.4.12) and (5.4.19), when the magnetoelastic effects are included, but instead the energy gap is

$$E'_{\mathbf{0}} = \frac{1}{N} \left(\frac{\partial^2 F}{\partial \theta^2} \frac{\partial^2 F}{\partial \phi^2} \Big|_{\tilde{\varepsilon}} \right)^{\frac{1}{2}} \frac{1}{\langle J_z \rangle (1 + \frac{1}{2} \Delta g)}. \quad (5.7.34b)$$

Although this modification is small, it demonstrates that the frequency dependence of $\chi_{\text{c.el.}}^{+-}(\mathbf{q}, \omega)$ may cause small deviations between the static anisotropy parameters and those derived from the energy gap, as possibly detected in Tb in the form of a non-zero value of $\delta_6(-)$, defined by eqn (5.4.23a).

The dominant term in the real part of $\chi_{\text{c.el.}}^{+-}(\mathbf{q}, \omega)$ is the frequency-independent contribution proportional to $\mathcal{F}(q/2k_F)$. Including only this contribution, and making the rather drastic simplifying assumption that $|j(\mathbf{q} + \boldsymbol{\tau})|$ in eqn (5.7.26c) is a constant $|j_0|$ at all wave-vectors, we may derive the exchange coupling in real space, which then depends only on the distance R between the different ions:

$$\mathcal{J}(R) = 2|j_0|^2 \frac{V}{N(2\pi)^3} \int \overline{\mathcal{N}}(\tilde{\varepsilon}_F) \mathcal{F}\left(\frac{q}{2k_F}\right) e^{i\mathbf{q}\cdot\mathbf{R}} d\mathbf{q}.$$

The sum over τ in (5.7.26c) corresponds to letting q vary between 0 and ∞ , and the result is

$$\mathcal{J}(R) = 12\pi\nu|j_0|^2\bar{\mathcal{N}}(\bar{\epsilon}_F) \frac{\sin(2k_F R) - 2k_F R \cos(2k_F R)}{(2k_F R)^4}, \quad (5.7.35)$$

where ν is the number of conduction electrons per ion; $\nu = V k_F^3 / 3\pi^2 N$. Although this result is not directly applicable to realistic systems, it demonstrates explicitly that the indirect coupling mediated by the conduction electrons is long range, $\mathcal{J}(R) \propto R^{-3}$ for large R , and that it oscillates. The period of the oscillation is here $2\pi/2k_F$ whereas, in a real system, such oscillations may occur as a result of large parallel areas of Fermi surface, the separation of which determines an effective value of $2k_F$. It is interesting that $\mathcal{J}(R)$, derived from the excitation spectrum in Pr and shown in Fig. 1.18 on page 49, is reasonably well described by the above function, especially when \mathbf{R} is in the basal plane, provided that an effective value of $2k_F$ of about 1.1 \AA^{-1} is used.

The magnetic scattering of the electron-hole pairs leads to a damping of the spin waves, which is determined by the imaginary part of the susceptibility (5.7.26b). The complementary result to eqn (5.7.31a) is then

$$\begin{aligned} \text{Im}[\chi_{\text{c.el.}}^{+-}(\mathbf{q}, \omega)] = & \\ & - \frac{V}{(2\pi)^3} \frac{2\pi}{N} \int_0^\infty k^2 dk \int_{-1}^1 d\mu \pi \delta(\hbar\omega - \Delta + \frac{(\hbar q)^2}{2m} - \frac{\hbar^2 k q}{m} \mu) f_{\mathbf{k}\downarrow} \\ & + \frac{V}{(2\pi)^3} \frac{2\pi}{N} \int_0^\infty k^2 dk \int_{-1}^1 d\mu \pi \delta(\hbar\omega - \Delta - \frac{(\hbar q)^2}{2m} - \frac{\hbar^2 k q}{m} \mu) f_{\mathbf{k}\uparrow}. \end{aligned}$$

Because $-1 < \mu < 1$, the δ -function argument in the first term can only be zero if $\varepsilon_q \equiv (\hbar q)^2 / (2m)$ lies between the two roots $\varepsilon_\pm = 2\varepsilon_k + \Delta - \hbar\omega \pm 2[\varepsilon_k(\varepsilon_k + \Delta - \hbar\omega)]^{1/2}$. For the second term, the same condition applies, except that the signs of Δ and $\hbar\omega$ are reversed, leading to the extra requirement that $\varepsilon_k > \varepsilon_K = \Delta - \hbar\omega$. If these conditions are satisfied,

$$\begin{aligned} \text{Im}[\chi_{\text{c.el.}}^{+-}(\mathbf{q}, \omega)] = & \\ & - \frac{V}{N(2\pi)^2} \int_0^\infty \frac{\pi m}{\hbar^2 q} k f(\varepsilon_k + \frac{\Delta}{2}) dk + \frac{V}{N(2\pi)^2} \int_K^\infty \frac{\pi m}{\hbar^2 q} k f(\varepsilon_k - \frac{\Delta}{2}) dk, \end{aligned}$$

where $f(\varepsilon) = 1 / [\exp(\varepsilon - \varepsilon_F) + 1]$. By a suitable change of variables, the two integrals acquire the same limits and the same condition on ε_q , and they may therefore be combined in a single integral:

$$\text{Im}[\chi_{\text{c.el.}}^{+-}(\mathbf{q}, \omega)] = \frac{V}{N(2\pi)^2} \frac{\pi m^2}{\hbar^4 q} \int_{\frac{\Delta - \hbar\omega}{2}}^\infty \left\{ -f\left(\varepsilon + \frac{\hbar\omega}{2}\right) + f\left(\varepsilon - \frac{\hbar\omega}{2}\right) \right\} d\varepsilon.$$

The integrand is only non-zero in a narrow interval of width $|\hbar\omega| \ll \Delta < \varepsilon_F$ around the Fermi surface, in which case the condition on ε_q can be written $k_{F\uparrow} - k_{F\downarrow} < q < k_{F\uparrow} + k_{F\downarrow}$ (if $\Delta = 0$ the lower boundary is replaced by $(\hbar\omega)^2/(4\varepsilon_F) < \varepsilon_q$). With this condition fulfilled,

$$\text{Im}[\chi_{\text{c.el.}}^{+-}(\mathbf{q}, \omega)] = \frac{V}{N(2\pi)^2} \frac{\pi m^2}{\hbar^4 q} \hbar\omega,$$

independent of T (as long as $k_B T \ll \varepsilon_F$). Using

$$\mathcal{N}_\sigma(\varepsilon_F) = (V/N)(2\pi\hbar)^{-2} 2mk_{F\sigma} \quad ; \quad (V/N)(2\pi)^{-2} \frac{2}{3}(k_{F\uparrow}^3 + k_{F\downarrow}^3) = \nu,$$

where ν is the number of conduction electrons per ion ($\nu = 3$), we may write the result:

$$\text{Im}[\chi_{\text{c.el.}}^{+-}(\mathbf{q}, \omega)] = \frac{\pi}{3\nu} \mathcal{N}_\uparrow(\varepsilon_F) \mathcal{N}_\downarrow(\varepsilon_F) \frac{k_F}{q} \hbar\omega; \quad (5.7.36)$$

$$k_{F\uparrow} - k_{F\downarrow} < q < k_{F\uparrow} + k_{F\downarrow},$$

neglecting corrections of second order in Δ/ε_F . In the zero-frequency limit considered here, q has to exceed the threshold value $q_0 = k_{F\uparrow} - k_{F\downarrow}$ before the imaginary part of $\chi_{\text{c.el.}}^{+-}(\mathbf{q}, \omega)$ becomes non-zero. This threshold value corresponds to the smallest distance in q -space between an occupied spin-down state and an unoccupied spin-up state, or vice versa, of nearly the same energy ($\simeq \varepsilon_F$). At $q = q_0$, the function makes a discontinuous step from zero to a finite value. The above result, combined with eqn (5.7.26), leads to

$$\text{Im}[\tilde{\mathcal{J}}(\mathbf{q}, \omega)] = \zeta(\mathbf{q}) \hbar\omega, \quad (5.7.37a)$$

with

$$\zeta(\mathbf{q}) = \frac{2\pi}{3\nu} \mathcal{N}_\uparrow(\varepsilon_F) \mathcal{N}_\downarrow(\varepsilon_F) \sum_{\boldsymbol{\tau}} |j(\mathbf{q} + \boldsymbol{\tau})|^2 \frac{k_F}{|\mathbf{q} + \boldsymbol{\tau}|}, \quad (5.7.37b)$$

where the sum is restricted to $k_{F\uparrow} - k_{F\downarrow} < |\mathbf{q} + \boldsymbol{\tau}| < k_{F\uparrow} + k_{F\downarrow}$. The imaginary part of $\tilde{\mathcal{J}}(\mathbf{q}, \omega)$ gives rise to a non-zero width in the spin-wave excitations. If the above result is inserted in eqns (5.7.25) and (5.7.33), the denominator of the Green functions may approximately be written $(\hbar\omega)^2 - (E'_{\mathbf{q}})^2 + 2i\Gamma_{\mathbf{q}}\hbar\omega$, where $\Gamma_{\mathbf{q}}$ is half the linewidth of the spin waves at the wave-vector \mathbf{q} , and is found to take the form

$$\Gamma_{\mathbf{q}} = J[A + J\{\mathcal{J}(\mathbf{0}) - \mathcal{J}(\mathbf{q})\}] \zeta(\mathbf{q}) = JA_{\mathbf{q}} \zeta(\mathbf{q}). \quad (5.7.38)$$

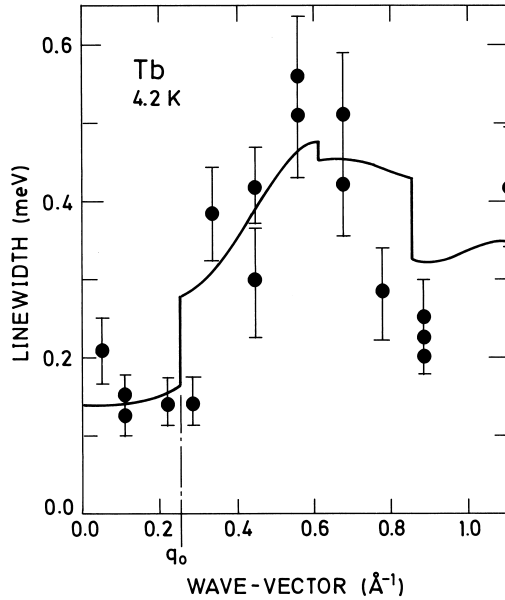


Fig. 5.13. The linewidths of magnons propagating in the c -direction of Tb at 4 K, compared with a theory based upon the nearly-free-electron model. The abrupt changes in the calculated lifetimes are due to the spin-splitting of the Fermi surface.

The lifetimes of the magnons propagating in the c -direction in Tb at 4 K, at which temperature the conduction electrons provide the dominant scattering process, were measured by Bjerrum Møller and Mackintosh (1979). As illustrated in Fig. 5.13, the linewidths are small, but non-zero, at small wave-vectors, rise abruptly at about a quarter of the way to the zone boundary, and fall again at large q . In order to interpret these results rigorously, it would be necessary to use eqn (5.7.27), with the correct band structure for Tb and realistic values for the exchange matrix elements $I(n'\mathbf{k}', n\mathbf{k})$. However, it is possible to obtain a semi-quantitative description by using the simple free-electron expression (5.7.37). As we shall see in the remainder of this section, this model, with an sf -interaction determined, for example, from the polarization of the conduction electrons (5.7.16–19), gives a surprisingly good account of the real scattering processes involving the interaction between the $4f$ and conduction electrons. Although the dominant d bands are far from parabolic in the rare earths, the nearly-free-electron Fermi surface for a trivalent hcp metal has a sheet with the form of a lens normal to the c -axis (Mackintosh *et al.* 1963), which mimics the Fermi-surface webbing

described in Section 1.3, and reproduces a number of observed features. In the calculations of Jensen (1982a), compared with the experimental results in Fig. 5.13, the spin-splitting of this surface gives rise to the critical value q_0 at which the linewidths abruptly increase. The finite lifetimes below this cut-off are due to interband transitions between states on sections of the Fermi surface with opposite spin, which intersect in the primitive Brillouin zone after translation through a reciprocal-lattice vector. These effects will also occur in calculations based on a realistic band structure, whereas the behaviour at higher q is much more dependent on the details of the energy bands.

5.7.2 The mass-enhancement of the conduction electrons

The processes in which the spin waves are scattered by the electron-hole pair excitations of the conduction electrons, and which therefore limit their lifetime, also have consequences for the conduction electrons. The energies of the conduction electrons are changed, and hence also their effective mass at the Fermi surface m^* , as measured directly by cyclotron resonance or the de Haas-van Alphen effect, or as determined from the low-temperature heat capacity. In the zero-temperature limit, the electronic part of the specific heat is

$$C = \gamma T = \frac{m^*}{m} \gamma_0 T \quad ; \quad \gamma_0 = \frac{1}{3} \pi^2 k_B^2 \{ \mathcal{N}_\uparrow(\tilde{\varepsilon}_F) + \mathcal{N}_\downarrow(\tilde{\varepsilon}_F) \} N, \quad (5.7.39)$$

where $m^* = (m_\uparrow^* + m_\downarrow^*)/2$ in the spin-polarized case. The use of $\tilde{\varepsilon}_F$ instead of ε_F is meant to indicate that all the effects of the MF Hamiltonian, including the interband couplings in (5.7.7), are assumed to be incorporated in γ_0 or m .

In order to calculate m^* , we shall utilize the Green functions of the conduction electrons. Because these particles are fermions, it is convenient to introduce an alternative type of Green function, in which an anticommutator bracket replaces the commutator bracket occurring in the definition (3.3.12), so that, for instance,

$$G_\uparrow(\mathbf{k}, t - t') \equiv \langle \langle c_{\mathbf{k}\uparrow}(t); c_{\mathbf{k}\uparrow}^\dagger(t') \rangle \rangle_+ = -\frac{i}{\hbar} \theta(t - t') \langle \{ c_{\mathbf{k}\uparrow}(t), c_{\mathbf{k}\uparrow}^\dagger(t') \} \rangle. \quad (5.7.40)$$

The Fourier transform obeys an equation of motion equivalent to eqn (3.3.14a), except that the commutator on the *right*-hand side of this equation is replaced by the anticommutator, or

$$\hbar\omega G_\uparrow(\mathbf{k}, \omega) - \langle \langle [c_{\mathbf{k}\uparrow}, \mathcal{H}]; c_{\mathbf{k}\uparrow}^\dagger \rangle \rangle_+ = \langle \{ c_{\mathbf{k}\uparrow}, c_{\mathbf{k}\uparrow}^\dagger \} \rangle = 1. \quad (5.7.41)$$

If \mathcal{H} is approximated by $\tilde{\mathcal{H}}_s$, given by eqn (5.7.10), we obtain the non-interacting value of the Green function

$$G_\uparrow(\mathbf{k}, \omega) \simeq G_\uparrow^o(\mathbf{k}, \omega) = \frac{1}{\hbar\omega - \varepsilon_{\mathbf{k}\uparrow}} \quad (5.7.42)$$

(neglecting the minor difference between ε and $\tilde{\varepsilon}$), showing that the poles of the Green function determine the energies of the conduction electrons. Considering the total Hamiltonian, in the approximation given by (5.7.20), we have instead

$$(\hbar\omega - \varepsilon_{\mathbf{k}\uparrow})G_{\uparrow}(\mathbf{k}, \omega) + \sqrt{2J/N} \sum_{\mathbf{q}\tau} j(\mathbf{q} + \boldsymbol{\tau}) \langle\langle c_{\mathbf{k}-\mathbf{q}-\tau\downarrow} a_{-\mathbf{q}}^+; c_{\mathbf{k}\uparrow}^+ \rangle\rangle_+ = 1. \quad (5.7.43)$$

The equation of motion of the new Green function is determined from

$$\begin{aligned} & [c_{\mathbf{k}-\mathbf{q}-\tau\downarrow} a_{-\mathbf{q}}^+, \mathcal{H}] \\ &= \{ \varepsilon_{\mathbf{k}-\mathbf{q}-\tau\downarrow} - A - J\tilde{\mathcal{J}}(\mathbf{0}, 0) \} c_{\mathbf{k}-\mathbf{q}-\tau\downarrow} a_{-\mathbf{q}}^+ - B c_{\mathbf{k}-\mathbf{q}-\tau\downarrow} a_{\mathbf{q}} \\ & \quad - \sqrt{2J/N} \sum_{\mathbf{k}'\tau'} j(-\mathbf{q} - \boldsymbol{\tau}') \left[c_{\mathbf{k}'-\mathbf{q}-\tau'\downarrow} c_{\mathbf{k}-\mathbf{q}-\tau\downarrow} c_{\mathbf{k}'\uparrow} \right. \\ & \quad \left. + \delta_{\mathbf{k}-\tau, \mathbf{k}'-\tau'} \langle a_{-\mathbf{q}}^+ a_{-\mathbf{q}} \rangle c_{\mathbf{k}+\tau'-\tau\uparrow} \right], \end{aligned}$$

using an RPA decoupling procedure to obtain the last term. To proceed further, we have to calculate $\langle\langle c_{\mathbf{k}'-\mathbf{q}-\tau'\downarrow} c_{\mathbf{k}-\mathbf{q}-\tau\downarrow} c_{\mathbf{k}'\uparrow}; c_{\mathbf{k}\uparrow}^+ \rangle\rangle_+$ and, within the RPA,

$$\begin{aligned} & \langle\langle c_{\mathbf{k}'-\mathbf{q}-\tau'\downarrow} c_{\mathbf{k}-\mathbf{q}-\tau\downarrow} c_{\mathbf{k}'\uparrow}; c_{\mathbf{k}\uparrow}^+ \rangle\rangle_+ \\ &= \delta_{\mathbf{k}'-\tau', \mathbf{k}-\tau} f_{\mathbf{k}-\mathbf{q}-\tau\downarrow} \langle\langle c_{\mathbf{k}+\tau'-\tau\uparrow}; c_{\mathbf{k}\uparrow} \rangle\rangle_+ \\ & \quad - \sqrt{2J/N} \frac{j(\mathbf{q} + \boldsymbol{\tau}') \{ f_{\mathbf{k}'\uparrow} - f_{\mathbf{k}'-\mathbf{q}-\tau'\downarrow} \}}{\hbar\omega - \varepsilon_{\mathbf{k}'\uparrow} - \varepsilon_{\mathbf{k}-\mathbf{q}-\tau\downarrow} + \varepsilon_{\mathbf{k}'-\mathbf{q}-\tau'\downarrow}} \langle\langle c_{\mathbf{k}-\mathbf{q}-\tau\downarrow} a_{-\mathbf{q}}^+; c_{\mathbf{k}\uparrow}^+ \rangle\rangle_+. \end{aligned}$$

Writing $\hbar\omega_1 = \hbar\omega - \varepsilon_{\mathbf{k}-\mathbf{q}-\tau\downarrow}$, we obtain from these equations

$$\begin{aligned} & \{ \hbar\omega_1 + A + J\tilde{\mathcal{J}}(\mathbf{0}, 0) - J\tilde{\mathcal{J}}^*(\mathbf{q}, -\omega_1) \} \langle\langle c_{\mathbf{k}-\mathbf{q}-\tau\downarrow} a_{-\mathbf{q}}^+; c_{\mathbf{k}\uparrow}^+ \rangle\rangle_+ \\ & \quad + B \langle\langle c_{\mathbf{k}-\mathbf{q}-\tau\downarrow} a_{\mathbf{q}}; c_{\mathbf{k}\uparrow}^+ \rangle\rangle_+ \\ &= -\sqrt{2J/N} \sum_{\tau'} j(-\mathbf{q} - \boldsymbol{\tau}') (f_{\mathbf{k}-\mathbf{q}-\tau\downarrow} + \langle a_{-\mathbf{q}}^+ a_{-\mathbf{q}} \rangle) \langle\langle c_{\mathbf{k}+\tau'-\tau\uparrow}; c_{\mathbf{k}\uparrow}^+ \rangle\rangle_+. \end{aligned} \quad (5.7.44)$$

In the sum, the terms with $\boldsymbol{\tau}' \neq \boldsymbol{\tau}$ only lead to higher-order corrections, of the same type as those arising from the difference between $c_{\mathbf{k}\uparrow}$ and $\tilde{c}_{\mathbf{k}\uparrow}$, and they can be neglected. Calculating $\langle\langle c_{\mathbf{k}-\mathbf{q}-\tau\downarrow} a_{\mathbf{q}}; c_{\mathbf{k}\uparrow}^+ \rangle\rangle_+$ in an equivalent way, and introducing the notation:

$$\begin{aligned} G_{m1}(\mathbf{q}, \omega) &= \langle\langle a_{\mathbf{q}}; a_{\mathbf{q}}^+ \rangle\rangle \quad ; \quad G_{m2}(\mathbf{q}, \omega) = \langle\langle a_{\mathbf{q}}^+; a_{\mathbf{q}} \rangle\rangle = G_{m1}^*(\mathbf{q}, -\omega) \\ G_{m3}(\mathbf{q}, \omega) &= \langle\langle a_{-\mathbf{q}}^+; a_{\mathbf{q}}^+ \rangle\rangle \end{aligned} \quad (5.7.45)$$

for the magnon Green functions determined by (5.7.25) and (5.7.33), we obtain

$$\begin{aligned} \langle\langle c_{\mathbf{k}-\mathbf{q}-\tau\downarrow}^+ a_{-\mathbf{q}}^+; c_{\mathbf{k}\uparrow}^+ \rangle\rangle_+ &= \sqrt{2J/N} j(-\mathbf{q}-\boldsymbol{\tau}) G_{\uparrow}(\mathbf{k}, \omega) \\ &\times [\{f_{\mathbf{k}-\mathbf{q}-\tau\downarrow} + \langle a_{\mathbf{q}}^+ a_{\mathbf{q}} \rangle\} G_{m2}(\mathbf{q}, \omega_1) - \langle a_{\mathbf{q}} a_{-\mathbf{q}} \rangle G_{m3}(\mathbf{q}, \omega_1)]. \end{aligned} \quad (5.7.46)$$

Defining the self-energy of the spin-up electrons by the relation

$$G_{\uparrow}(\mathbf{k}, \omega) = \frac{1}{\hbar\omega - \varepsilon_{\mathbf{k}\uparrow} - \Sigma_{\uparrow}(\mathbf{k}, \omega)}, \quad (5.7.47)$$

and using (3.1.10) to establish that

$$G_m(\mathbf{q}, \omega) = \frac{1}{i\pi} \int \frac{G_m(\mathbf{q}, \omega')}{\hbar\omega' - \hbar\omega} d(\hbar\omega'),$$

we obtain finally

$$\begin{aligned} \Sigma_{\uparrow}(\mathbf{k}, \omega) &= -\frac{2J}{N} \sum_{\mathbf{q}\boldsymbol{\tau}} |j(\mathbf{q}+\boldsymbol{\tau})|^2 \frac{1}{i\pi} \int_{-\infty}^{\infty} \frac{d(\hbar\omega')}{\hbar\omega' - \hbar\omega + \varepsilon_{\mathbf{k}-\mathbf{q}-\tau\downarrow}} \\ &\times [\{f_{\mathbf{k}-\mathbf{q}-\tau\downarrow} + \langle a_{\mathbf{q}}^+ a_{\mathbf{q}} \rangle\} G_{m2}(\mathbf{q}, \omega') - \langle a_{\mathbf{q}} a_{-\mathbf{q}} \rangle G_{m3}(\mathbf{q}, \omega')]. \end{aligned} \quad (5.7.48)$$

This result corresponds to that deduced by Nakajima (1967), as generalized by Fulde and Jensen (1983).

The average effective mass of the spin-up electrons at the Fermi surface is determined by

$$\frac{1}{m_{\uparrow}^*} = \frac{1}{\hbar^2 \mathbf{k}} \left. \frac{\partial \mathcal{E}_{\mathbf{k}\uparrow}}{\partial \mathbf{k}} \right|_{k=k_{F\uparrow}},$$

averaged over the direction of \mathbf{k} . Here $\mathcal{E}_{\mathbf{k}\uparrow} = \varepsilon_{\mathbf{k}\uparrow} + \text{Re}[\Sigma_{\uparrow}(\mathbf{k}, \mathcal{E}_{\mathbf{k}\uparrow})]$ is the corrected energy of the spin-up electrons. We can neglect the explicit \mathbf{k} -dependence of $\Sigma_{\uparrow}(\mathbf{k}, \omega)$ in comparison to its frequency dependence, disregarding terms of the order $E_{\mathbf{q}}/\varepsilon_F$ in the derivative of $\mathcal{E}_{\mathbf{k}\uparrow}$, so that

$$\frac{\partial \mathcal{E}_{\mathbf{k}\uparrow}}{\partial \mathbf{k}} = \frac{\partial \varepsilon_{\mathbf{k}\uparrow}}{\partial \mathbf{k}} + \frac{1}{\hbar} \frac{\partial}{\partial \omega} \text{Re}[\Sigma_{\uparrow}(\mathbf{k}, \omega)] \Big|_{\hbar\omega = \mathcal{E}_{\mathbf{k}\uparrow}} \frac{\partial \mathcal{E}_{\mathbf{k}\uparrow}}{\partial \mathbf{k}},$$

or

$$\frac{m_{\uparrow}^*}{m} = 1 - \frac{1}{\hbar} \frac{\partial}{\partial \omega} \text{Re}[\Sigma_{\uparrow}(\mathbf{k}_{F\uparrow}, \omega)] \Big|_{\hbar\omega = \mathcal{E}_F}, \quad (5.7.49)$$

averaged over the Fermi surface. Within the same approximation, the terms in eqn (5.7.48) proportional to the magnon correlation-functions

can be neglected and, to leading order, $\hbar\omega = \mathcal{E}_F$ in the ω -derivative may be replaced by $\varepsilon_{\mathbf{k}\uparrow}$, with $\mathbf{k} = \mathbf{k}_{F\uparrow}$. In the limit of zero temperature, the free-electron model then gives

$$\begin{aligned} \frac{m_{\uparrow}^*}{m} &= 1 + \frac{2J}{N} \sum_{\mathbf{q}\tau} |j(\mathbf{q} + \boldsymbol{\tau})|^2 \frac{1}{\pi} \int_{-\infty}^{\infty} d(\hbar\omega') \\ &\quad \times \frac{1}{2} \int_{-1}^1 d\mu \frac{\text{Im}[G_{m2}(\mathbf{q}, \omega')]}{(\hbar\omega' + \Delta + \frac{(\hbar|\mathbf{q} + \boldsymbol{\tau}|)^2}{2m} - \frac{\hbar^2 k|\mathbf{q} + \boldsymbol{\tau}|}{m} \mu)^2}, \end{aligned}$$

subject to the conditions that $k = k_{F\uparrow}$ and $|\mathbf{k} - \mathbf{q} - \boldsymbol{\tau}| < k_{F\downarrow}$. These conditions imply that $k_{F\uparrow} - k_{F\downarrow} < |\mathbf{q} + \boldsymbol{\tau}| < k_{F\uparrow} + k_{F\downarrow}$, and that the lower bound -1 of the μ -integral is replaced by $(\hbar^2 q^2 + 2m\Delta)/(2\hbar^2 k_{F\uparrow} |\mathbf{q} + \boldsymbol{\tau}|)$. Because $\text{Im}[G_{m2}(\mathbf{q}, \omega')]$ is odd in ω' , the contribution due to the upper bound in the μ -integral can be neglected (it is of the order $\hbar\omega'/\varepsilon_F$). Since

$$\frac{1}{\pi} \int_{-\infty}^{\infty} \frac{\text{Im}[G_{m2}(\mathbf{q}, \omega')]}{\hbar\omega'} d(\hbar\omega') = \text{Re}[G_{m2}(\mathbf{q}, 0)] = -\frac{A_{\mathbf{q}}}{E_{\mathbf{q}}^2},$$

the average mass-enhancement of the spin-up electrons at the Fermi surface is

$$\frac{m_{\uparrow}^*}{m} = 1 + \frac{\mathcal{N}_{\downarrow}(\varepsilon_F)}{2k_{F\uparrow}k_{F\downarrow}} \int_{k_{F\uparrow} - k_{F\downarrow}}^{k_{F\uparrow} + k_{F\downarrow}} dq \int \frac{d\Omega_{\mathbf{q}}}{4\pi} q |j(\mathbf{q})|^2 \frac{2JA_{\mathbf{q}}}{E_{\mathbf{q}}^2}, \quad (5.7.50)$$

and, by symmetry, m_{\downarrow}^*/m is given by the same expression, except that $\mathcal{N}_{\downarrow}(\varepsilon_F)$ is replaced by $\mathcal{N}_{\uparrow}(\varepsilon_F)$. We note that the mass-enhancement only depends on the static part of the susceptibility, i.e. $G_{m2}(\mathbf{q}, 0)$, and that the magnitude of the mass-renormalization is intimately related to the linewidth of the spin waves derived above in eqn (5.7.38). Utilizing this connection, we can write the specific heat, in the zero-temperature limit,

$$C = \frac{\pi^2}{3} k_B^2 T \left[\mathcal{N}_{\uparrow}(\varepsilon_F) + \mathcal{N}_{\downarrow}(\varepsilon_F) + \frac{1}{N} \sum_{\mathbf{q}} \frac{2\Gamma_{\mathbf{q}}}{\pi E_{\mathbf{q}}^2} \right] N, \quad (5.7.51)$$

where again the \mathbf{q} -sum only extends over the primitive Brillouin zone. With typical values of $E_{\mathbf{q}}\mathcal{N}(\varepsilon_F) \approx 0.01$ and $2\Gamma_{\mathbf{q}}/E_{\mathbf{q}} \approx 0.05$, this expression predicts a doubling of the linear term in the heat capacity due to the interaction between the conduction electrons and the spin waves, which therefore has an appreciable effect on the effective mass of the electrons near the Fermi surface. More detailed analyses (Nakajima 1967; Fulde and Jensen 1983) show that the deformation of the electronic bands is

pinned to the Fermi surface, and occurs within a narrow interval with a width corresponding to the spin-wave energies. This implies that, even if the electronic energies $\varepsilon_{\mathbf{k}\sigma}$ appearing in the magnon Green-functions were replaced with $\mathcal{E}_{\mathbf{k}\sigma}$, due to higher-order processes, this modification would not be of much importance. The total electronic heat capacity is $C_e = \sum_{\mathbf{k}\sigma} \mathcal{E}_{\mathbf{k}\sigma} df_{\mathbf{k}\sigma}/dT$, when the imaginary part of the self-energy is neglected. The extra contribution due to the coupling to the spin waves is linear only at the lowest temperatures ($k_B T < 0.05 E_{\mathbf{q}}$), after which it increases more rapidly than linearly to its maximum at $k_B T \simeq 0.15 E_{\mathbf{q}}$. Above $k_B T \simeq 0.3 E_{\mathbf{q}}$, this contribution becomes negative and finally dies out when $k_B T \approx E_{\mathbf{q}}$. This variation with temperature was described by Fulde and Jensen (1983), and has been discussed in the context of the phonon interaction by Grimvall (1981). The bosons (magnons and phonons) do not contribute directly to the linear term in the heat capacity, which is thus a characteristic phenomenon of the Fermi gas. However, the departure from the linear variation when $k_B T > 0.05 E_{\mathbf{q}}$ may be influenced by the spin-wave contribution

$$\begin{aligned}
 C_m &= \sum_{\mathbf{q}} \frac{1}{\pi} \int_{-\infty}^{\infty} d(\hbar\omega) \frac{2\Gamma_{\mathbf{q}}(\hbar\omega)^3}{\{(\hbar\omega)^2 - E_{\mathbf{q}}^2(T)\}^2 + \{2\Gamma_{\mathbf{q}}\hbar\omega\}^2} \frac{d}{dT} \left(\frac{1}{1 - e^{-\beta\hbar\omega}} \right) \\
 &\simeq \sum_{\mathbf{q}} E_{\mathbf{q}}(T) \frac{d}{dT} \left(n_{\mathbf{q}} + \frac{1}{2} \right) + \frac{\pi^2}{3} k_B^2 T \sum_{\mathbf{q}} \frac{2\Gamma_{\mathbf{q}}}{\pi E_{\mathbf{q}}^2} \left[\frac{2}{5y^2} + \frac{4}{7y^4} + \dots \right]_{y=\beta E_{\mathbf{q}}/2\pi},
 \end{aligned}
 \tag{5.7.52}$$

to first order in $\Gamma_{\mathbf{q}}/E_{\mathbf{q}}$. The first term is the RPA spin-wave contribution (5.3.3) derived before, which dominates strongly at elevated temperatures. However, in the low-temperature limit, the second term is of the same order of magnitude as the non-linear corrections to eqn (5.7.51). For comparison, the last term in this equation is multiplied by the factor $[1 + 3/(5y^2) + 5/(7y^4) + \dots]$ when the higher-order temperature effects are included. The additional contribution due to the non-zero linewidth of the bosons is normally not considered in the literature. It may be added to the pure electronic contribution derived by Fulde and Jensen (1983), by replacing $yL'(y)$ with $2yL'(y) + L(y)$ in their eqn (17a). The mass-enhancement effect increases proportionally to the inverse of $E_{\mathbf{q}}$ ($\Gamma_{\mathbf{q}} \propto A_{\mathbf{q}}$). On the other hand, the interval in which the linear variation occurs is diminished correspondingly, requiring a more careful consideration of the higher-order modifications.

In the metals, the itinerant electrons also interact with the phonons, and this leads to an entirely equivalent enhancement of their mass. This effect has been calculated for the whole rare earth series by Skriver and Mertig (1990), who find an increase of the band mass due to coupling to the phonons of typically about 35% for the heavy elements. Assuming

the different contributions to be additive, we may write the total mass-enhancement

$$\frac{m^*}{m} = 1 + \lambda_{\text{tot}} = 1 + \lambda_{\text{sw}} + \lambda_{\text{ph}} + \lambda_{\text{c}} \quad (5.7.53)$$

as a sum of contributions from the interactions with the spin waves and the phonons, and from the possible exchange and Coulomb interactions within the electron gas itself (λ_{c}). Although the different correlation effects may increase the effective mass derived from band structure calculations by a factor of two or more, it is difficult to isolate this enhancement in heat capacity measurements, because of the quite narrow temperature interval where a truly linear behaviour can be anticipated. This interval is bounded below because of the nuclear spins, which may give large contributions to the heat capacity in the mK-range. The upper bound is due partly to the higher-order temperature effects, but most importantly to the disturbance by the normal boson contributions, approximately proportional to $T^\alpha \exp(-E_0/k_B T)$ and T^3 for the magnons and the phonons respectively, which completely dominate the heat capacity at elevated temperatures. Because of this limitation, the most reliable method of determining the mass-enhancement is by measuring the temperature dependence of the dHvA effect, which also allows a separation of the contributions from the different sheets of the Fermi surface. Using this method, and comparing with the results of band structure calculations, Sondhelm and Young (1985) found values of λ_{tot} varying between 0.2 and 1.1 for Gd. The theoretical results of Fulde and Jensen (1983) lie within this range, but these measurements point to the necessity of discriminating between states of different symmetry in considering the mass-enhancement of the conduction electron gas.

5.7.3 Magnetic contributions to the electrical resistivity

The electrical resistivity of a metal can be calculated by solving the *Boltzmann equation*. We shall not discuss the theory of transport properties in detail here, but instead refer to the comprehensive treatments of Ziman (1960), and Smith and Højgaard Jensen (1989). The non-equilibrium distribution function $g_{\mathbf{k}\sigma}$, generated by the application of an external electric field \mathbf{E} , is written in terms of the equilibrium distribution function, and is determined by the Boltzmann equation:

$$g_{\mathbf{k}\sigma} = f_{\mathbf{k}\sigma} + f_{\mathbf{k}\sigma}(1 - f_{\mathbf{k}\sigma})\psi_{\mathbf{k}\sigma}, \quad \text{where} \quad \left. \frac{\partial g_{\mathbf{k}\sigma}}{\partial \mathbf{k}} \cdot \frac{d\mathbf{k}}{dt} = \frac{dg_{\mathbf{k}\sigma}}{dt} \right|_{\text{coll}}. \quad (5.7.54)$$

The electrical current-density is then determined as

$$\mathbf{j} = \bar{\sigma} \cdot \mathbf{E} = -\frac{e}{V} \sum_{\mathbf{k}\sigma} \mathbf{v}_{\mathbf{k}\sigma} f_{\mathbf{k}\sigma} (1 - f_{\mathbf{k}\sigma}) \psi_{\mathbf{k}\sigma},$$

with $\hbar \mathbf{v}_{\mathbf{k}\sigma} = \partial \varepsilon_{\mathbf{k}\sigma} / \partial \mathbf{k}$. In the linear regime, the left-hand side of the Boltzmann equation is

$$\frac{\partial g_{\mathbf{k}\sigma}}{\partial \mathbf{k}} \cdot \frac{d\mathbf{k}}{dt} \simeq -\frac{\partial f_{\mathbf{k}\sigma}}{\partial \varepsilon_{\mathbf{k}\sigma}} e \mathbf{v}_{\mathbf{k}\sigma} \cdot \mathbf{E} = e\beta f_{\mathbf{k}\sigma} (1 - f_{\mathbf{k}\sigma}) \mathbf{v}_{\mathbf{k}\sigma} \cdot \mathbf{E}.$$

The collision term on the right-hand side is

$$\left. \frac{dg_{\mathbf{k}\sigma}}{dt} \right|_{\text{coll}} = \sum_{\mathbf{k}'\sigma'} [g_{\mathbf{k}'\sigma'} (1 - g_{\mathbf{k}\sigma}) W(\mathbf{k}'\sigma', \mathbf{k}\sigma) - g_{\mathbf{k}\sigma} (1 - g_{\mathbf{k}'\sigma'}) W(\mathbf{k}\sigma, \mathbf{k}'\sigma')],$$

where $W(\mathbf{k}\sigma, \mathbf{k}'\sigma')$ is the probability per unit time for an electronic transition from an occupied state $|\mathbf{k}\sigma\rangle$ to an unoccupied state $|\mathbf{k}'\sigma'\rangle$. Linearizing the collision term, and using the principle of detailed balance, so that this term must vanish if $g_{\mathbf{k}\sigma} = f_{\mathbf{k}\sigma}$, we may reduce the Boltzmann equation to

$$e\beta f_{\mathbf{k}\sigma} (1 - f_{\mathbf{k}\sigma}) \mathbf{v}_{\mathbf{k}\sigma} \cdot \mathbf{E} = - \sum_{\mathbf{k}'\sigma'} (1 - f_{\mathbf{k}\sigma}) f_{\mathbf{k}'\sigma'} W(\mathbf{k}'\sigma', \mathbf{k}\sigma) (\psi_{\mathbf{k}\sigma} - \psi_{\mathbf{k}'\sigma'}).$$

It is possible to find an upper bound on the resistivity from this equation, with the use of a variational principle. Defining $\hat{\mathbf{u}}$ to be a unit vector along one of the principal axes of the resistivity tensor,

$$\rho_{uu} \leq \frac{V}{2\beta e^2} \frac{\sum_{\mathbf{k}\sigma} \sum_{\mathbf{k}'\sigma'} (1 - f_{\mathbf{k}'\sigma'}) f_{\mathbf{k}\sigma} W(\mathbf{k}\sigma, \mathbf{k}'\sigma') (\phi_{\mathbf{k}\sigma} - \phi_{\mathbf{k}'\sigma'})^2}{[\sum_{\mathbf{k}\sigma} \mathbf{v}_{\mathbf{k}\sigma} \cdot \hat{\mathbf{u}} (1 - f_{\mathbf{k}\sigma}) f_{\mathbf{k}\sigma} \phi_{\mathbf{k}\sigma}]^2}, \quad (5.7.55)$$

where $\phi_{\mathbf{k}\sigma}$ is an arbitrary trial function, and where the equality applies if $\phi_{\mathbf{k}\sigma} = \psi_{\mathbf{k}\sigma}$. In the case of the free-electron model, the Boltzmann equation possesses an exact solution, $\psi_{\mathbf{k}\sigma} \propto \mathbf{k} \cdot \hat{\mathbf{u}}$, if the scattering is purely elastic. As discussed, for instance, by Hessel Andersen *et al.* (1980), this trial function is still useful for treating possible inelastic scattering mechanisms, at least as long as the resistivity is dominated by elastic impurity scattering, so we shall use $\phi_{\mathbf{k}\sigma} = \mathbf{k} \cdot \hat{\mathbf{u}}$.

In the Born approximation, the transition probability per unit time is given by the Golden Rule (4.1.1), which we may here write

$$W(\mathbf{k}\sigma, \mathbf{k}'\sigma') = \frac{2\pi}{\hbar} \sum_{if} P_i |\langle \mathbf{k}\sigma; i | \mathcal{H}_{\text{int}} | \mathbf{k}'\sigma'; f \rangle|^2 \delta(\hbar\omega + E_i - E_f),$$

where $\hbar\omega = \varepsilon_{\mathbf{k}\sigma} - \varepsilon_{\mathbf{k}'\sigma'}$. Instead of basing the derivation of the magnetic resistivity on the linearized spin-wave expression (5.7.20) for \mathcal{H}_{int} , we shall be somewhat more general and use \mathcal{H}_{sf} from eqn (5.7.6) as the

interaction Hamiltonian. We assume that the system is uniform, paramagnetic or ferromagnetically ordered, continue to utilize the simple free-electron model, and replace $(g-1)I(n'\mathbf{k}', n\mathbf{k})$ by $j(\mathbf{k}' - \mathbf{k} + \boldsymbol{\tau})$. The MF part (5.7.7) of the Hamiltonian may lead to a modification $\varepsilon_{\mathbf{k}\sigma} \rightarrow \tilde{\varepsilon}_{\mathbf{k}\sigma}$ of the electronic band-states, but we can neglect this difference to leading order, and since the MF Hamiltonian does not lead to transitions between electronic states, we can replace J_{iz} by $\hat{J}_{iz} = J_{iz} - \langle J_z \rangle$ in \mathcal{H}_{int} , and obtain

$$\begin{aligned}
W(\mathbf{k}\sigma, \mathbf{k}'\sigma') &= \int_{-\infty}^{\infty} d(\hbar\omega) \delta(\hbar\omega - \varepsilon_{\mathbf{k}\sigma} + \varepsilon_{\mathbf{k}'\sigma'}) \\
&\times \frac{2\pi}{\hbar} \sum_{if} P_i \frac{1}{N^2} \sum_{jj'} |j(\mathbf{k}' - \mathbf{k})|^2 e^{-i(\mathbf{k}' - \mathbf{k}) \cdot (\mathbf{R}_j - \mathbf{R}_{j'})} \\
&\times \left\{ \langle i | J_{j'}^- | f \rangle \langle f | J_j^+ | i \rangle \delta_{\sigma\uparrow} \delta_{\sigma'\downarrow} + \langle i | J_{j'}^+ | f \rangle \langle f | J_j^- | i \rangle \delta_{\sigma\downarrow} \delta_{\sigma'\uparrow} \right. \\
&\quad \left. + \langle i | \hat{J}_{j'z} | f \rangle \langle f | \hat{J}_{jz} | i \rangle (\delta_{\sigma\uparrow} \delta_{\sigma'\uparrow} + \delta_{\sigma\downarrow} \delta_{\sigma'\downarrow}) \right\} \delta(\hbar\omega + E_i - E_f),
\end{aligned} \tag{5.7.56}$$

accounting explicitly for the condition on $\hbar\omega$ by the integral over the first δ -function. Using the same procedure as in the calculation of the neutron-scattering cross-section, when going from (4.1.16) to (4.2.1-3), we may write this:

$$\begin{aligned}
W(\mathbf{k}\sigma, \mathbf{k}'\sigma') &= \frac{2}{N\hbar} \int_{-\infty}^{\infty} d(\hbar\omega) \delta(\hbar\omega - \varepsilon_{\mathbf{k}\sigma} + \varepsilon_{\mathbf{k}'\sigma'}) \frac{1}{1 - e^{-\beta\hbar\omega}} |j(\mathbf{k} - \mathbf{k}')|^2 \\
&\times \left\{ \chi''_{+-}(\mathbf{k} - \mathbf{k}', \omega) \delta_{\sigma\uparrow} \delta_{\sigma'\downarrow} + \chi''_{-+}(\mathbf{k} - \mathbf{k}', \omega) \delta_{\sigma\downarrow} \delta_{\sigma'\uparrow} \right. \\
&\quad \left. + \chi''_{zz}(\mathbf{k} - \mathbf{k}', \omega) (\delta_{\sigma\uparrow} \delta_{\sigma'\uparrow} + \delta_{\sigma\downarrow} \delta_{\sigma'\downarrow}) \right\}.
\end{aligned}$$

Introducing this expression into (5.7.55), and using $\phi_{\mathbf{k}\sigma} = \mathbf{k} \cdot \hat{\mathbf{u}}$ and $\mathbf{k}' = \mathbf{k} - \mathbf{q} - \boldsymbol{\tau}$, we proceed as in the derivation of eqn (5.7.36) for $\text{Im}[\chi_{\text{c.el.}}^{+-}(\mathbf{q}, \omega)]$, obtaining

$$\begin{aligned}
&\frac{1}{N} \sum_{\mathbf{k}} f_{\mathbf{k}\downarrow} (1 - f_{\mathbf{k}-\mathbf{q}\uparrow}) \delta(\hbar\omega - \varepsilon_{\mathbf{k}\downarrow} + \varepsilon_{\mathbf{k}-\mathbf{q}\uparrow}) = \\
&\frac{V}{N(2\pi)^2} \int_0^{\infty} dk k^2 \int_{-1}^1 d\mu f(\varepsilon_{\mathbf{k}\downarrow}) \{1 - f(\varepsilon_{\mathbf{k}\downarrow} - \hbar\omega)\} \delta(\hbar\omega - \Delta + \varepsilon_q - \mu \frac{\hbar^2 q k}{m}) \\
&= \frac{V}{N(2\pi)^2} \int_{\frac{\Delta}{2}}^{\infty} d\varepsilon \frac{m^2}{\hbar^4 q} f(\varepsilon) \{1 - f(\varepsilon - \hbar\omega)\} = \frac{V}{N(2\pi)^2} \frac{m^2}{\hbar^4 q} \frac{\hbar\omega}{e^{\beta\hbar\omega} - 1},
\end{aligned}$$

where $k_{F\uparrow} - k_{F\downarrow} < q < k_{F\uparrow} + k_{F\downarrow}$ (when $k_B T \ll \varepsilon_F$). The denominator in (5.7.55) may be calculated in a straightforward fashion and

is $[N\nu/(\hbar\beta)]^2$, and we finally obtain the following expression for the resistivity, or rather its upper limit:

$$\begin{aligned} \rho_{uu}(T) \simeq \rho_0 \frac{3}{(4k_{F\uparrow}k_{F\downarrow})^2 \bar{j}_u^2} \int_{k_{F\uparrow}-k_{F\downarrow}}^{k_{F\uparrow}+k_{F\downarrow}} dq \int \frac{d\Omega_{\mathbf{q}}}{4\pi} \int_{-\infty}^{\infty} d(\hbar\omega) \\ \times |j(\mathbf{q})|^2 (\mathbf{q} \cdot \hat{\mathbf{u}})^2 q \frac{\beta\hbar\omega}{\sinh^2(\beta\hbar\omega/2)} \frac{1}{\pi} \sum_{\alpha} \chi''_{\alpha\alpha}(\mathbf{q}, \omega), \end{aligned} \quad (5.7.57a)$$

where

$$\rho_0 = \frac{3}{2} \frac{V}{N} \frac{\pi m}{\hbar e^2 \varepsilon_F} \bar{j}_u^2 = \frac{m}{ne^2} \frac{\pi}{\hbar} \{ \mathcal{N}_{\uparrow}(\varepsilon_F) + \mathcal{N}_{\downarrow}(\varepsilon_F) \} \bar{j}_u^2, \quad (5.7.57b)$$

$n = \nu N/V$ is the electron density, and

$$\bar{j}_u^2 = 4 \frac{3}{(2k_F)^4} \int_0^{2k_F} dq \int \frac{d\Omega_{\mathbf{q}}}{4\pi} |j(\mathbf{q})|^2 (\mathbf{q} \cdot \hat{\mathbf{u}})^2 q. \quad (5.7.57c)$$

For cubic symmetry, ρ_{uu} is independent of u and $(\mathbf{q} \cdot \hat{\mathbf{u}})^2$ can be replaced by $q^2/3$. In the high-temperature limit, we have

$$\begin{aligned} \frac{1}{\pi} \int_{-\infty}^{\infty} d(\hbar\omega) \frac{\beta\hbar\omega}{\sinh^2(\beta\hbar\omega/2)} \sum_{\alpha} \chi''_{\alpha\alpha}(\mathbf{q}, \omega) \simeq \\ \frac{1}{\pi} \int_{-\infty}^{\infty} d(\hbar\omega) \frac{4}{\beta\hbar\omega} \sum_{\alpha} \chi''_{\alpha\alpha}(\mathbf{q}, \omega) = \frac{4}{\beta} \sum_{\alpha} \chi'_{\alpha\alpha}(\mathbf{q}, 0) = 4J(J+1), \end{aligned}$$

recalling that $\chi'_{\alpha\alpha}(\mathbf{q}, 0) = \frac{1}{3}\beta J(J+1)$ in this limit. This result shows that the magnetic resistivity saturates at temperatures which are so high that the ions are uniformly distributed over the states in the ground-state J -multiplet, since the condition $k_B T \ll \varepsilon_F$ is always satisfied:

$$\rho_{uu}(T) \rightarrow J(J+1) \rho_0 \quad \text{for } T \rightarrow \infty, \quad (5.7.58)$$

and $J(J+1)\rho_0$ is called the saturation value of the *spin-disorder* resistivity. Since ρ_0 contains the factor $(g-1)^2$, the spin-disorder resistivity is proportional to the de Gennes factor, as observed (Legvold 1972). If the crystal-field splitting of the energy levels is neglected, this factor also determines the relative magnitudes of the contributions of magnetic rare earth-impurities to the resistivity of a non-magnetic host (Kasuya 1959). However, in analysing the measurements of Mackintosh and Smidt (1962) of the resistivity changes produced by small amounts of heavy rare earths in Lu, Hessel Andersen (1979) found that such crystal-field effects are indeed important at 4 K.

In a metal, the total collision rate $W(\mathbf{k}\sigma, \mathbf{k}'\sigma')$ in eqn (5.7.55) is actually the sum of contributions from several scattering mechanisms. If the trial function for elastic impurity-scattering still leads to a result reasonably close to that determined by the exact solution of the Boltzmann equation, then (5.7.55) implies that the different scattering mechanisms contribute additively to the total resistivity, in accordance with *Matthiessen's rule*:

$$\rho_{\text{total}}(T) = \rho_{\text{imp}} + \rho_{\text{m}}(T) + \rho_{\text{ph}}(T). \quad (5.7.59)$$

Here ρ_{imp} is the residual resistivity due to elastic scattering of the electrons from impurities and from lattice defects. $\rho_{\text{m}}(T)$ is the contribution, calculated above, due to the magnetic excitations, whereas $\rho_{\text{ph}}(T)$ is the equivalent term due to the phonons. The two last terms, associated with the excitations in the metal, vanish in the limit of zero temperature, so that $\rho_{\text{total}}(T = 0) = \rho_{\text{imp}}$. The problem of distinguishing between the magnetic and phonon scattering can be approximately solved by estimating the latter from the temperature dependence of the resistivity of Lu, which has an electronic structure and phonon spectrum very similar to those of the magnetic heavy rare earths, but no magnetic moment. Using this method, Mackintosh (1963) was able to show that the magnetic scattering in Tb increases as $\exp(-E_0/k_B T)$ at low temperatures, where the spin-wave energy gap E_0/k_B was estimated to be about 20 K, a value which was subsequently verified by neutron scattering. This analysis was refined by Hessel Andersen and Smith (1979), who used the free-electron model to show that the magnetic resistivity associated with the scattering by spin waves with an isotropic dispersion relation $E_{\mathbf{q}} = E_0 + \hbar^2 q^2 / 2m_{\text{sw}}$ is given by

$$\rho_{\text{m}}(T) = \frac{J m_{\text{sw}}^2 E_0 k_B T}{4 m^2 \varepsilon_F^2} e^{-E_0/k_B T} \left(1 + 2 \frac{k_B T}{E_0} + \frac{1}{2} e^{-E_0/k_B T} + \dots \right) \rho_0, \quad (5.7.60)$$

approximating the lower cut-off $k_{F\uparrow} - k_{F\downarrow}$ by 0 in (5.7.57a). A numerical calculation, utilizing the measured spin-wave energies and including one scaling parameter for the magnetic scattering and one for the phonon scattering, gave the excellent fit shown in Fig. 5.14. The disordered electric quadrupole moments of the $4f$ -charge distributions can also provide a mechanism for the scattering of the conduction electrons. This is normally very difficult to distinguish from the magnetic scattering, but in TmSb, where the exchange interaction is relatively small and the electric quadrupoles large, the latter appear to dominate the electrical resistivity at low temperatures (Hessel Andersen and Vogt 1979).

Even though $k_B T \ll \varepsilon_F$, the residual resistivity ρ_{imp} is only independent of temperature as long as the ground-state properties of the

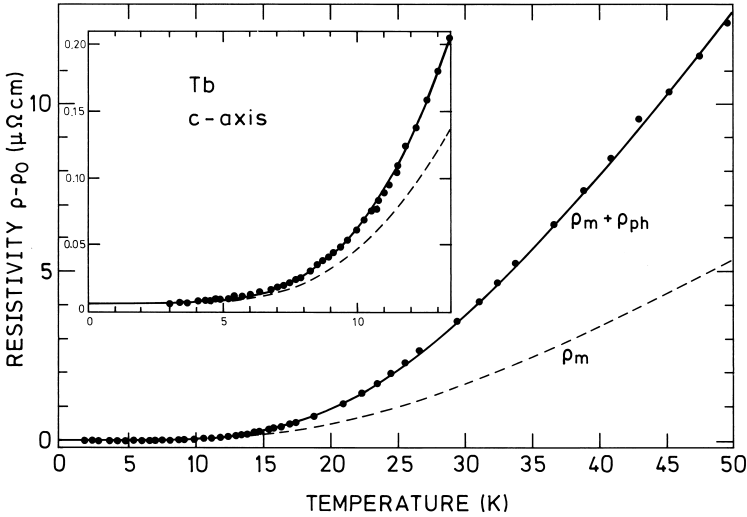


Fig. 5.14. A comparison of the measured and calculated resistivity of a Tb single crystal, as a function of temperature, after Hessel Andersen and Smith (1979). The residual resistivity has been subtracted from the experimental results. The full line includes the calculated contributions from both the magnon scattering and the phonons. The rapid increase around 20 K is predominantly due to the excitation of magnons across the energy gap.

electron gas remain unchanged. If the resistivity of the unpolarized electrons is $\rho_{\text{total}}^0(T)$ and their density of states at the Fermi surface is $\mathcal{N}(\varepsilon_F)$, the polarization (5.7.16) of the conduction electrons in the ferromagnetic state leads to a scaling of the *total* resistivity, which according to eqn (5.7.55) is

$$\rho_{\text{total}}(T) = \{1 + \zeta(T)\} \rho_{\text{total}}^0(T) \quad ; \quad \zeta(T) = \frac{\mathcal{N}_{\uparrow}(\tilde{\varepsilon}_F) + \mathcal{N}_{\downarrow}(\tilde{\varepsilon}_F)}{2\mathcal{N}(\varepsilon_F)} - 1. \quad (5.7.61)$$

In $\rho_{\text{total}}^0(T)$, the residual resistivity is temperature independent and the magnetic contribution is determined by the above result, if $\mathcal{N}_{\sigma}(\varepsilon_F)$ in (5.7.57b) is replaced by its paramagnetic value $\mathcal{N}(\varepsilon_F)$. The modification $\zeta(T)$, due to the polarization of the conduction electrons, depends on the temperature via the magnetization, and $\zeta(T) \propto \langle J_z \rangle^2$ at small magnetization.

The most important effect on the resistivity produced by the spin-polarization of the electronic states results from the change in the density of states at the Fermi surface, taken into account by $\zeta(T)$ in (5.7.61).

Since the other modification, the appearance of $k_{F\sigma}$ instead of the paramagnetic value k_F in (5.7.57b), generally only causes a minor correction to the value of the integral in this equation, the magnetic contribution to $\rho_{\text{total}}^0(T)$ is approximately independent of the spin-polarization, in this model. However, the spin-polarization in the real metals may be sufficiently great to alter the topology of the Fermi surface, as discussed in Section 1.4, so that the resistivity may change abruptly with temperature or magnetic field. Under these circumstances, the resistivity must be calculated from first principles, using a realistic model of the spin-polarized energy bands. The zz -contribution should be treated separately, as the q -integral for this case should go from 0 to $2k_F$, even when the electron spins are polarized, since no spin-flip is involved in the scattering process. This modification is, however, unimportant as the dominating contributions, in the ordered phase, arise from the perpendicular spin-wave components of the susceptibility.

The above results also apply, to a good approximation, when the moments are ordered antiferromagnetically, if the value of $\zeta(T)$ is calculated for a spatial modulation of the moments. The spin-polarization of the band electrons is determined by the MF Hamiltonian, and assuming $\langle J_{iz} \rangle = \langle J_z \rangle \cos(\mathbf{Q} \cdot \mathbf{R}_i)$, we may replace (5.7.7) by

$$\begin{aligned} \mathcal{H}_{sf}(\text{MF}) = & - \sum_{nn'} \sum_{\mathbf{k}\mathbf{k}'} (g-1) I(n'\mathbf{k}', n\mathbf{k}) (c_{n'\mathbf{k}'\uparrow}^+ c_{n\mathbf{k}\uparrow} - c_{n'\mathbf{k}'\downarrow}^+ c_{n\mathbf{k}\downarrow}) \\ & \times \frac{1}{2} (\delta_{\mathbf{k}', \mathbf{k} + \mathbf{Q} + \boldsymbol{\tau}} + \delta_{\mathbf{k}', \mathbf{k} - \mathbf{Q} + \boldsymbol{\tau}}) \langle J_z \rangle, \end{aligned} \quad (5.7.62)$$

showing that the modulated moments induce a coupling between the band electrons at the wave-vectors \mathbf{k} and $\mathbf{k} \pm \mathbf{Q} + \boldsymbol{\tau}$. In the same way as the periodic lattice potential lifts the degeneracy of the band states at the Brillouin-zone boundaries (passing through $\mathbf{k} = \boldsymbol{\tau}/2$), the above MF Hamiltonian gives rise to energy gaps at the *superzone boundaries*, the planes perpendicular to, and passing through, the vectors $\mathbf{k}_s = (\pm\mathbf{Q} + \boldsymbol{\tau})/2$. If \mathbf{k}_s is along the c -axis, the value of the energy gap δ is $(g-1)|I(n\mathbf{k}, n-\mathbf{k})|\langle J_z \rangle$ in the n th band. The importance of the superzone gaps for the resistivity was first pointed out by Mackintosh (1962), and detailed theories were developed by Elliott and Wedgwood (1963) and Miwa (1963). These theories utilized the free-electron model and the *relaxation time* approximation, $dg_{\mathbf{k}\sigma}/dt|_{\text{coll}} = -(g_{\mathbf{k}\sigma} - f_{\mathbf{k}\sigma})/\tau_{\mathbf{k}\sigma}$, giving a conductivity

$$\sigma_{uu} = \frac{e^2 \beta}{V} \sum_{\mathbf{k}\sigma} \tau_{\mathbf{k}\sigma} (\mathbf{v}_{\mathbf{k}\sigma} \cdot \hat{\mathbf{u}})^2 f_{\mathbf{k}\sigma} (1 - f_{\mathbf{k}\sigma})$$

or, if the relaxation time $\tau_{\mathbf{k}\sigma}$ is assumed to be constant over the Fermi

surface,

$$\sigma_{uu} \simeq \frac{e^2 \tau}{(2\pi)^3 \hbar^2} \sum_{\sigma} \int_{\varepsilon_{\mathbf{k}\sigma} = \varepsilon_F} \left(\frac{\partial \varepsilon_{\mathbf{k}\sigma}}{\partial k_u} \right)^2 \frac{1}{|\nabla_{\mathbf{k}} \varepsilon_{\mathbf{k}\sigma}|} dS, \quad (5.7.63)$$

where dS is a surface element of the Fermi surface. Even without detailed calculations, this expression shows that the conductivity may be reduced substantially if the superzone gaps are able to eliminate significant areas of the Fermi surface. Furthermore, the Fermi-velocity factor puts different weight on the various regions of the Fermi surface in the different components of the conductivity tensor. If \mathbf{k}_s is parallel to the c -axis, as in the heavy rare earths, and if its length is close to that of the Fermi wave-vector in the c -direction, only the cc -component of the conductivity is appreciably affected by the superzone boundary. For instance, an internal field of 2 kOe in the basal plane of Ho at 4 K, which eliminates the superzone energy gaps by inducing a transition from the cone to ferromagnetic ordering, increases the conductivity along the c -axis by about 30%, while decreasing the b -axis component by only about 1% (Mackintosh and Spanel 1964). As illustrated in Fig. 5.15, the anomalous increase in the resistivity in the helical phase of Tb is eliminated by a magnetic field which is large enough to suppress this structure, leaving only a weak maximum similar to that observed in Gd, which has been ascribed to critical scattering of the conduction electrons by magnetic fluctuations (de Gennes and Friedel 1958). This anomalous increase is not observed in the basal plane and the resistivity is little affected by a magnetic field (Hegland *et al.* 1963).

The theoretical calculations of the superzone effects within the free-electron model give a semi-quantitative account of the experimental observations, with a small number of adjustable parameters. For example, a superzone boundary normal to the c -axis, which intersects the Fermi surface, gives a positive contribution to $\zeta_{cc}(T)$ in (5.7.61) which is proportional to δ/ε_F , while $\zeta_{bb}(T)$ decreases like $(\delta/\varepsilon_F)^2$. Bearing in mind the analogy between the real and free-electron Fermi surfaces mentioned above, this corresponds well with the observations in, for example, Ho. In addition, the model calculations suggest that the superzone gaps are important for the value of the ordering wave-vector \mathbf{Q} , at which the exchange energy has its maximum (Elliott and Wedgwood 1964; Miwa 1965), by predicting a gradual reduction of the length of \mathbf{Q} with the increase of the size of the superzone gaps, which are proportional to $\langle J_z \rangle$ below the Néel temperature. Hence the exchange coupling $\mathcal{J}(\mathbf{q})$ is somewhat dependent on the magnetization, because the nearly elastic intra-band contributions to the exchange interaction depend on the density of states near the Fermi surface, as is also true in the ferromagnetic case, according to (5.7.21).

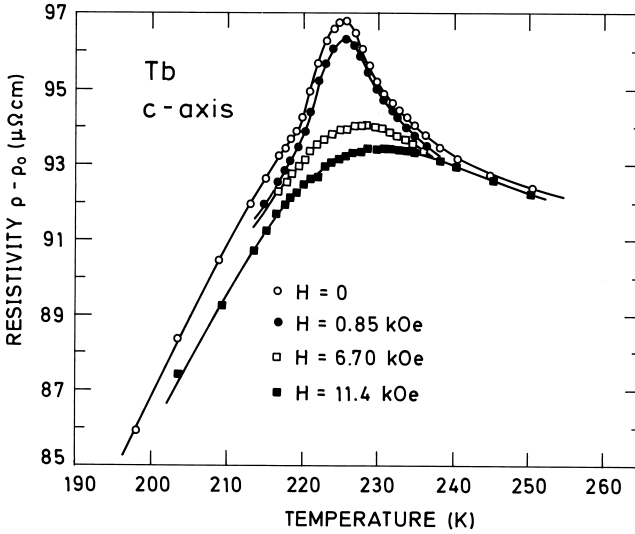


Fig. 5.15. The c -axis resistivity of Tb in the vicinity of $T_N = 230$ K, after Hegland *et al.* (1963). As the helical ordering develops, the magnetic superzones cause a sharp increase in the resistivity, which disappears at $T_C = 220$ K. The superzones may also be eliminated by a magnetic field in the b -direction, which suppresses the helical structure.

The agreement obtained between simple model calculations of the variation of \mathbf{Q} and that observed experimentally is surprisingly good, to some extent fortuitously so. The band electrons are far from free-electron-like in the rare earth metals, and the approximation in which $I(n'\mathbf{k}', n\mathbf{k})$ is replaced by $j(\mathbf{k}' - \mathbf{k} + \boldsymbol{\tau})$ is rather crude. The effective free-electron model, with $j(\mathbf{q})$ proportional to a form factor $[1 + (Aq)^2]^{-1}$ where $A \approx 0.2 \text{ \AA}^{-1}$ and $2k_F \approx 2.8 \text{ \AA}^{-1}$, leads to a maximum in $\mathcal{J}(\mathbf{q})$ at $\mathbf{q} \approx 0.3 \text{ \AA}^{-1}$ parallel to the c -axis, in the paramagnetic phase. In this model, $\frac{1}{N} \sum_{\mathbf{q}} \tilde{\mathcal{J}}(\mathbf{q})$ is found to be an order of magnitude larger than $\mathcal{J}(\mathbf{0})$, and the same is the case with the interband contributions ($\boldsymbol{\tau} \neq \mathbf{0}$) to the exchange interaction, compared to the intra-band contributions. However, various estimates indicate that all these terms are of the same order of magnitude. Lindgård *et al.* (1975) have made the only existing *ab initio* calculation of $\mathcal{J}(\mathbf{q})$ in a rare earth metal, considering the simplest case of Gd, and they obtained a reasonable account of the dependence on wave-vector, even though the magnitude differed by as much as a factor of four from that determined experimentally. Their calculations show that the exchange integral is dominated by the

contributions of the d -like band electrons, as is the density of states at the Fermi surface. Although the effective free-electron model is not adequate for determining the exchange interaction, other quantities derived above which depend on real scattering processes close to the Fermi surface (i.e. the contributions to the spin-wave linewidths, the mass enhancement, and the resistivity), may be more trustworthy, particularly if the actual density of states of the band electrons is substituted for the free-electron value. This should especially be true for the linewidth and mass-enhancement, but the strong polarization effect (5.7.60) on the resistivity in the ferromagnetic phase, for which the maximum effect occurs in Gd, with $\zeta(T)$ approaching -0.5 in the zero temperature limit (Fulde and Jensen 1983), may be somewhat exaggerated, because the conductivity is strongly influenced by the sp -band electrons.

SPIN WAVES IN PERIODIC STRUCTURES

Because of the modification of the translational symmetry, the spin waves in modulated magnetic structures display certain interesting aspects which are not shared by the simple ferromagnetic structure. However, this same feature makes their experimental study considerably more difficult, and the results which have been obtained on such systems are still relatively sparse. This chapter is correspondingly short, and in its two sections we distinguish between structures *incommensurable* with the lattice periodicity, when the translational symmetry in the direction of the wave-vector is, in principle, destroyed, and *commensurable* structures, in which this symmetry is only modified, though possibly quite drastically.

The stringent mathematical definition of an incommensurable structure is straightforward, but it presupposes that the coherence lengths of the lattice and of the magnetic system are both infinite. In this idealized case, an irrational ratio between the periodicities of the two subsystems breaks the translational invariance, the wave-vector \mathbf{q} is consequently no longer a good quantum number, and neutron-diffraction peaks acquire a non-zero width. Furthermore, the energy eigenvalues which determine the excitation spectrum also have a certain width when projected on to \mathbf{q} -space, which is the appropriate representation for interpreting constant- \mathbf{q} neutron-scattering experiments. The alternative method of distinguishing experimentally between the two types of structure is to follow the ratio between the two periodicities as a function of temperature or external field. If this ratio changes *discontinuously* between constant steps, the structure is commensurable. On the other hand, if the variation is observed to be *continuous*, the structure is usually classified as being incommensurable. As examples of transverse incommensurable structures, we shall accordingly take the *helix* in Tb, which exists only over a small range of temperature below T_N , and the low-temperature *cone* in Er. It is generally questionable whether any particular structure can strictly be classified as incommensurable but, as we shall see, the distinction in these cases is unimportant. The magnetic high-temperature phase of Er is treated as an example of an incommensurable *longitudinal-wave structure*, although it may only be truly incommensurable at the highest temperatures in the ordered phase. In

this case, the incommensurability has significant qualitative effects on the excitation spectrum.

In a commensurable structure, where $m|\mathbf{Q}| = mQ_c$ is p times the length $4\pi/c$ of the (effective) reciprocal lattice vector, the number m of layers between magnetically-identical lattice planes will have an important influence on the character of the excitations. If m is small, they will be well-defined, long-lived at low temperatures, and relatively easy to study experimentally. As examples of such ideal commensurable structures, we shall consider the low-temperature *bunched helix* in Ho, and the *longitudinal ferrimagnetic structure* in Tm, where the crystal fields make a decisive contribution. These relatively simple structures are stable at low temperatures but, in both cases, the configuration of the moments becomes more complicated as the temperature is increased. In Ho, for example, *spin-slip structures* of reduced symmetry and generally increasing m evolve, and the excitations, of which only preliminary studies have so far been made, become correspondingly complex. Although these excitations may be just as well-defined as when m is small, the extension of the magnetic Brillouin zone, in the c -direction, is reduced by the factor $1/m$, while the number of branches in the dispersion relation is multiplied by m . The different branches are separated from each other by energy gaps at the boundaries of the magnetic Brillouin zone, and the corresponding excitations scatter neutrons with different weight, depending on the scattering vector and described in terms of the *dynamical structure factor*. If m is large, however, it may be extremely difficult to resolve the different branches experimentally. As m increases towards the values of the order of 50 which characterize some of the commensurable structures presented in Section 2.3, imperfections in the lattice, or boundaries between different magnetic domains, become more important. We should also expect that disordering phase-slips would become relatively more frequent, leading to a less well-defined structure, and disturbing the very long-range periodicity. It is unlikely that a specific pattern involving 100 or more layers could be repeated many times in the crystal, without significant errors, and we might rather anticipate a somewhat chaotic arrangement, where the phase factor characterizing the moments changes systematically from layer to layer, but with an occasional minor phase slip, so that the structure never repeats itself exactly. This kind of structure may frequently in practice be described as incommensurable.

6.1 Incommensurable periodic structures

In this section, we shall first discuss the spin waves in the regular helix or cone, including the hexagonal anisotropy only as a minor perturbation. On account of the infinitely larger number of irrational than rational

numbers, these structures are most naturally classified as incommensurable, particularly as the distinction is immaterial in this case. If the hexagonal anisotropy and possible external fields are neglected, the translational symmetry is broken only formally, as a rigid rotation of the moments, or of the total system, around the spiral axis costs no energy. We then consider the longitudinally polarized phase, in which genuine effects due to incommensurability would be expected. On the other hand, the stronger coupling between the two periodicities increases the tendency of the magnetic-ordering wave-vector to lock into a value which is commensurable with the lattice. It may perhaps be questioned whether theoretical results derived for ideal incommensurable models are relevant to real, three-dimensional systems. However, it appears that the essential features of systems which are classified experimentally as incommensurable may be described theoretically as such, provided that the analysis includes an averaging or *coarse graining* of the results, of a magnitude somewhat smaller than the experimental resolution.

6.1.1 The helix and the cone

A helical ordering of the moments in an hcp lattice, with a wave-vector \mathbf{Q} along the c - or ζ -axis, is described by the following equations:

$$\begin{aligned}\langle J_{i\xi} \rangle &= \langle J_{\perp} \rangle \cos(\mathbf{Q} \cdot \mathbf{R}_i + \varphi) \\ \langle J_{i\eta} \rangle &= \langle J_{\perp} \rangle \sin(\mathbf{Q} \cdot \mathbf{R}_i + \varphi) \\ \langle J_{i\zeta} \rangle &= 0.\end{aligned}\tag{6.1.1}$$

As usual, we shall be most interested in excitations propagating in the c -direction, and hence may use the double-zone representation, corresponding to the case of a Bravais lattice. The moments of constant length $\langle J_{\perp} \rangle$ lie in the ξ - η plane perpendicular to \mathbf{Q} , and rotate uniformly in a right-handed screw along the \mathbf{Q} -vector. The elastic cross-section corresponding to this structure is, according to (4.2.6),

$$\begin{aligned}\frac{d\sigma}{d\Omega} &= N \left(\frac{\hbar\gamma e^2}{mc^2} \right)^2 e^{-2W(\kappa)} \left| \frac{1}{2} g F(\kappa) \right|^2 \langle J_{\perp} \rangle^2 (1 + \hat{\kappa}_{\zeta}^2) \\ &\times \frac{(2\pi)^3}{v} \sum_{\tau} \frac{1}{4} \{ \delta(\boldsymbol{\tau} + \mathbf{Q} - \boldsymbol{\kappa}) + \delta(\boldsymbol{\tau} - \mathbf{Q} - \boldsymbol{\kappa}) \}.\end{aligned}\tag{6.1.2}$$

In this system the molecular field in (3.5.3) changes from site to site, as does the MF susceptibility $\overline{\chi}_i^o(\omega)$ in (3.5.7). This complication may be alleviated by transforming into a rotating (xyz)-coordinate system with the z -axis parallel to the moments, i.e.

$$\begin{aligned}J_{i\xi} &= J_{iz} \cos \phi_i + J_{iy} \sin \phi_i \\ J_{i\eta} &= J_{iz} \sin \phi_i - J_{iy} \cos \phi_i \\ J_{i\zeta} &= J_{ix},\end{aligned}\tag{6.1.3}$$

where $\phi_i = \mathbf{Q} \cdot \mathbf{R}_i + \varphi$. Carrying out this transformation, we find that $\mathbf{J}_i \cdot \mathbf{J}_j$ becomes

$$(J_{iz}J_{jz} + J_{iy}J_{jy}) \cos(\phi_i - \phi_j) + (J_{iy}J_{jz} - J_{iz}J_{jy}) \sin(\phi_i - \phi_j) + J_{ix}J_{jx},$$

so that the Hamiltonian (3.5.1) may be written, in the (xyz) -coordinate system,

$$\mathcal{H} = \sum_i \mathcal{H}_J(J_{ix}^2) - \frac{1}{2} \sum_{i \neq j} \sum_{\alpha\beta} J_{i\alpha} \mathcal{J}_{\alpha\beta}(ij) J_{j\beta}, \quad (6.1.4)$$

where α and β signify the Cartesian coordinates x , y , and z . Here we have assumed that the dependence of the single-ion anisotropy on $J_{i\xi}$ and $J_{i\eta}$ can be neglected, and that only even powers of $J_{i\zeta} = J_{ix}$ occur, since otherwise the helical structure becomes distorted and (6.1.1) is no longer the equilibrium configuration. The ordering wave-vector \mathbf{Q} is determined by the minimum-energy condition that $\mathcal{J}(\mathbf{q})$ has its maximum value at $\mathbf{q} = \mathbf{Q}$. After this transformation, the MF Hamiltonian is the same for all sites:

$$\begin{aligned} \mathcal{H}_{\text{MF}}(i) &= \mathcal{H}_J(J_{ix}^2) - (J_{iz} - \frac{1}{2}\langle J_{\perp} \rangle) \sum_j \langle J_{\perp} \rangle \mathcal{J}(ij) \cos(\phi_i - \phi_j) \\ &= \mathcal{H}_J(J_{ix}^2) - (J_{iz} - \frac{1}{2}\langle J_{\perp} \rangle) \langle J_{\perp} \rangle \mathcal{J}(\mathbf{Q}) \quad ; \quad \langle J_{\perp} \rangle = \langle J_z \rangle, \end{aligned} \quad (6.1.5)$$

as is the corresponding MF susceptibility $\overline{\overline{\chi}}^o(\omega)$. The price we have paid is that the two-ion coupling $\overline{\overline{\mathcal{J}}}(ij)$ is now anisotropic, and its non-zero Fourier components are

$$\begin{aligned} \mathcal{J}_{xx}(\mathbf{q}) &= \mathcal{J}(\mathbf{q}) \quad ; \quad \mathcal{J}_{yy}(\mathbf{q}) = \mathcal{J}_{zz}(\mathbf{q}) = \frac{1}{2} \{ \mathcal{J}(\mathbf{q} + \mathbf{Q}) + \mathcal{J}(\mathbf{q} - \mathbf{Q}) \} \\ \mathcal{J}_{yz}(\mathbf{q}) &= -\mathcal{J}_{zy}(\mathbf{q}) = \frac{i}{2} \{ \mathcal{J}(\mathbf{q} + \mathbf{Q}) - \mathcal{J}(\mathbf{q} - \mathbf{Q}) \}. \end{aligned} \quad (6.1.6)$$

However, it is straightforward to take account of this complication in the RPA, and the result is the same as (3.5.8) or (3.5.21), with $\mathcal{J}(\mathbf{q})$ replaced by $\overline{\overline{\mathcal{J}}}(\mathbf{q})$,

$$\overline{\overline{\chi}}_t(\mathbf{q}, \omega) = \left\{ 1 - \overline{\overline{\chi}}^o(\omega) \overline{\overline{\mathcal{J}}}(\mathbf{q}) \right\}^{-1} \overline{\overline{\chi}}^o(\omega), \quad (6.1.7)$$

where the index t indicates that this is the (xyz) -susceptibility, and not the $(\xi\eta\zeta)$ -susceptibility $\overline{\overline{\chi}}(\mathbf{q}, \omega)$ which determines the scattering cross-section. From the transformation (6.1.3), it is straightforward, but somewhat cumbersome, to find the relation between the two susceptibility tensors.

In the general case, the MF susceptibility $\overline{\chi}^o(\omega)$ is determined by three distinct diagonal components, plus the two off-diagonal terms $\chi_{xy}^o(\omega) = -\chi_{yx}^o(\omega)$, with the same analytical properties, (3.5.24b) and (5.2.42), as in the Heisenberg ferromagnet. It may be seen that $\chi_{xy}^o(\omega)$, for instance, is imaginary by recalling that the MF Hamiltonian is independent of J_y , in which case the eigenvectors in the J_z -representation can all be chosen to be real, so that the products of the matrix elements of J_x and of J_y are imaginary. The vanishing of the other four off-diagonal terms follows from the two-fold symmetry about the z -axis of the MF Hamiltonian. In spite of this reduction, the analytical expression for $\overline{\chi}(\mathbf{q}, \omega)$ is still quite formidable. However, in most cases of interest, the single-ion anisotropy is relatively weak, and the inelastic modifications due to $\chi_{zz}^o(\omega)$ can be neglected, so that, for $\omega \neq 0$,

$$\begin{aligned}\chi_{xx}(\mathbf{q}, \omega) &= \{\chi_{xx}^o(\omega) - |\overline{\chi}^o(\omega)| \mathcal{J}_{yy}(\mathbf{q})\} / D(\mathbf{q}, \omega) \\ \chi_{xy}(\mathbf{q}, \omega) &= \{\chi_{xy}^o(\omega) + |\overline{\chi}^o(\omega)| \mathcal{J}_{xy}(\mathbf{q})\} / D(\mathbf{q}, \omega),\end{aligned}\quad (6.1.8a)$$

and the same relations hold with x and y interchanged. Here

$$D(\mathbf{q}, \omega) = 1 - \sum_{\alpha\beta} \chi_{\alpha\beta}^o(\omega) \mathcal{J}_{\beta\alpha}(\mathbf{q}) + |\overline{\chi}^o(\omega)| |\overline{\mathcal{J}}(\mathbf{q})|, \quad (6.1.8b)$$

where α or β are x or y , and $|\overline{\chi}^o(\omega)|$ or $|\overline{\mathcal{J}}(\mathbf{q})|$ are the determinants of the 2×2 matrices. In the weak-anisotropy limit, we may to a good approximation use the result (5.2.42) derived in Section 5.2, and to first order in $1/J$, we have

$$\begin{aligned}\chi_{xx}^o(\omega) &= \langle J_z \rangle \frac{A - B + h_{\text{ex}}}{E_{\text{ex}}^2 - (\hbar\omega)^2} \\ \chi_{yy}^o(\omega) &= \langle J_z \rangle \frac{A + B + h_{\text{ex}}}{E_{\text{ex}}^2 - (\hbar\omega)^2} \\ \chi_{xy}^o(\omega) &= -\chi_{yx}^o(\omega) = \langle J_z \rangle \frac{i\hbar\omega}{E_{\text{ex}}^2 - (\hbar\omega)^2}\end{aligned}\quad (6.1.9a)$$

and $\chi_{zz}^o(\omega) \simeq \beta(\delta J_z)^2 \delta_{\omega 0}$. The only modification is that the exchange field, given in eqn (6.1.5), is now

$$h_{\text{ex}} = \langle J_z \rangle \mathcal{J}(\mathbf{Q}) \quad \text{and} \quad E_{\text{ex}}^2 = (A + h_{\text{ex}})^2 - B^2. \quad (6.1.9b)$$

There are inelastic contributions to $\chi_{zz}^o(\omega)$, but they are of the order $A/2JE_{\text{ex}}$, relative to the other inelastic terms, and can be neglected.

The parameters A and B are the same as those derived in Section 5.2, when \mathcal{H}_J in (6.1.4) is replaced by the usual crystal-field Hamiltonian, except that we here neglect explicitly the hexagonal anisotropy

B_6^6 . The result above may be generalized to include most of the renormalization effects appearing in the second order of $1/J$, by replacing $A \pm B$ by $A_0(T) \pm B_0(T)$, in accordance with the discussion at the end of Section 5.2. After the transformation to the rotating coordinates, the system becomes equivalent to the basal-plane ferromagnet, except that the hexagonal anisotropy is neglected and the γ -strains vanish, due to the lattice-clamping effect discussed in Section 2.2.2. Hence we may take $A \pm B$ to be $A_0(T) \pm B_0(T)$, given by eqn (5.3.22), with $B_6^6 = 0$ and $H = 0$.

In the present situation, where \mathcal{H}_J in (6.1.4) only depends on J_x^2 , $A = B$ and (6.1.9) implies, for instance, that $\chi_{yy}^o(\omega = 0) = 1/\mathcal{J}(\mathbf{Q})$. This result is quite general and may be derived directly from (6.1.5); the addition of a small rotating field h_y in the y -direction, perpendicular to the exchange field, only has the consequence that the direction of the angular momentum is rotated through the angle ϕ , where $\tan \phi = h_y/h_{\text{ex}}$, and hence $\delta\langle J_y \rangle = \langle J_z \rangle \tan \phi = \{1/\mathcal{J}(\mathbf{Q})\} h_y$. Substituting (6.1.9) with $A = B$ into (6.1.8), we obtain

$$\chi_{xx}(\mathbf{q}, \omega) = \langle J_z \rangle \frac{A_{\mathbf{q}} - B_{\mathbf{q}}}{E_{\mathbf{q}}^2 - (\hbar\omega)^2} \quad ; \quad \chi_{yy}(\mathbf{q}, \omega) = \langle J_z \rangle \frac{A_{\mathbf{q}} + B_{\mathbf{q}}}{E_{\mathbf{q}}^2 - (\hbar\omega)^2}, \quad (6.1.10a)$$

with

$$E_{\mathbf{q}} = [A_{\mathbf{q}}^2 - B_{\mathbf{q}}^2]^{1/2} \quad (6.1.10b)$$

and

$$\begin{aligned} A_{\mathbf{q}} + B_{\mathbf{q}} &= 2A + \langle J_z \rangle \{ \mathcal{J}(\mathbf{Q}) - \mathcal{J}(\mathbf{q}) \} \\ A_{\mathbf{q}} - B_{\mathbf{q}} &= \langle J_z \rangle \left\{ \mathcal{J}(\mathbf{Q}) - \frac{1}{2} \mathcal{J}(\mathbf{q} + \mathbf{Q}) - \frac{1}{2} \mathcal{J}(\mathbf{q} - \mathbf{Q}) \right\}, \end{aligned} \quad (6.1.10c)$$

neglecting $\chi_{zz}^o(0)$. The absorptive components of $\overline{\overline{\chi}}_t(\mathbf{q}, \omega)$ are

$$\begin{aligned} \chi''_{xx}(\mathbf{q}, \omega) &= \frac{\pi}{2} \langle J_z \rangle \left(\frac{A_{\mathbf{q}} - B_{\mathbf{q}}}{A_{\mathbf{q}} + B_{\mathbf{q}}} \right)^{\frac{1}{2}} \{ \delta(E_{\mathbf{q}} - \hbar\omega) - \delta(E_{\mathbf{q}} + \hbar\omega) \} \\ \chi''_{yy}(\mathbf{q}, \omega) &= \frac{\pi}{2} \langle J_z \rangle \left(\frac{A_{\mathbf{q}} + B_{\mathbf{q}}}{A_{\mathbf{q}} - B_{\mathbf{q}}} \right)^{\frac{1}{2}} \{ \delta(E_{\mathbf{q}} - \hbar\omega) - \delta(E_{\mathbf{q}} + \hbar\omega) \}, \end{aligned} \quad (6.1.11)$$

demonstrating that the scattered intensities due to the two components are different, if $B_{\mathbf{q}}$ is non-zero. The neutron cross-section $d^2\sigma/dE d\Omega$, (4.2.2), is proportional to

$$\sum_{\alpha\beta} (\delta_{\alpha\beta} - \hat{\kappa}_{\alpha} \hat{\kappa}_{\beta}) \chi''_{\alpha\beta}(\boldsymbol{\kappa}, \omega) = (1 - \hat{\kappa}_{\zeta}^2) \chi''_{\zeta\zeta}(\boldsymbol{\kappa}, \omega) + (1 + \hat{\kappa}_{\zeta}^2) \chi''_{\eta\eta}(\boldsymbol{\kappa}, \omega), \quad (6.1.12a)$$

since the $\xi\xi$ - and $\eta\eta$ -components are equal. The components in this equation are derived from the equality $\overline{\chi}_t(\boldsymbol{\kappa}, \omega) = \overline{\chi}_t(\boldsymbol{\kappa} + \boldsymbol{\tau}, \omega)$, and

$$\begin{aligned}\chi_{\xi\xi}(\boldsymbol{\kappa}, \omega) &= \chi_{\eta\eta}(\boldsymbol{\kappa}, \omega) = \frac{1}{4} \{ \chi_{yy}(\boldsymbol{\kappa} - \mathbf{Q}, \omega) + \chi_{yy}(\boldsymbol{\kappa} + \mathbf{Q}, \omega) \} \\ \chi_{\zeta\zeta}(\boldsymbol{\kappa}, \omega) &= \chi_{xx}(\boldsymbol{\kappa}, \omega).\end{aligned}\quad (6.1.12b)$$

From this we deduce that, if the scattering vector is along the ζ -axis, we expect to observe both the spin waves propagating parallel to \mathbf{Q} , emerging from the magnetic Bragg peak at $\boldsymbol{\tau} + \mathbf{Q}$, and the spin waves propagating antiparallel to $-\mathbf{Q}$, but with their \mathbf{q} -vector determined relative to the Bragg peak at $\boldsymbol{\tau} - \mathbf{Q}$.

If $\langle J_z \rangle$ is zero, the system described by the Hamiltonian (6.1.4) is invariant with respect to a uniform rotation of all the angular momenta around the x - or ζ -axis, corresponding to the condition $[\sum_i J_{ix}, \mathcal{H}] = 0$. In the helical phase, this commutation relation is unchanged, but nevertheless the system is no longer invariant with respect to such a rotation, since it will alter the phase constant φ in (6.1.1). This system is thus an example of a situation where a *continuous symmetry* is spontaneously *broken*. In this case, a theorem of Goldstone (1961) predicts the existence of collective modes with energies approaching zero as their lifetimes go to infinity. A detailed discussion of this phenomenon is given by Forster (1975). The *Goldstone mode*, or the *broken-symmetry mode*, in the helix is the spin-wave excitation occurring in $\overline{\chi}_t(\mathbf{q}, \omega)$ in the limit of $\mathbf{q} \rightarrow \mathbf{0}$. Since this mode is related to a uniform change of the phase φ , it is also called the *phason*. In the long-wavelength limit, $A_{\mathbf{q}} - B_{\mathbf{q}} \simeq \frac{1}{2} \langle J_z \rangle (\mathbf{q} \cdot \nabla)^2 \mathcal{J}(\mathbf{0})$ goes to zero, and the spin wave energies $E_{\mathbf{q}} \simeq \{ \frac{1}{2} (A_{\mathbf{0}} + B_{\mathbf{0}}) \langle J_z \rangle (\mathbf{q} \cdot \nabla)^2 \mathcal{J}(\mathbf{0}) \}^{1/2}$ vanish linearly with q . The result (6.1.8) is valid in general at long wavelengths, independently of $\chi_{zz}^o(\omega)$, because the J_z -response is only mixed with the spin-wave response proportionally to $|\mathcal{J}_{yz}(\mathbf{q})|^2 \propto q^6$ in the limit of small q . In the static limit, $\chi_{xy}^o(\omega \rightarrow 0)$ vanishes by symmetry, and (6.1.8) then predicts that, in general,

$$\chi_{yy}(\mathbf{q}, 0) = 1 / \{ \mathcal{J}(\mathbf{Q}) - \frac{1}{2} \mathcal{J}(\mathbf{q} + \mathbf{Q}) - \frac{1}{2} \mathcal{J}(\mathbf{q} - \mathbf{Q}) \} \propto q^{-2}$$

when $\mathbf{q} \rightarrow \mathbf{0}$, which is also in accordance with (6.1.10). The divergence of $\chi_{yy}(\mathbf{q} \rightarrow \mathbf{0}, 0)$ is easily understood, as this susceptibility component determines the response $\langle J_y \rangle$ to the application of a constant rotating field h_y at every site, which causes the same rotation of all the moments, corresponding to a change of the phase constant φ in (6.1.1). A rigid rotation of the helix costs no energy, and the lack of restoring forces implies that the susceptibility diverges. A divergence in the static susceptibility is not sufficient to guarantee the presence of a *soft mode* in the system, as

there might be a diffusive mode in the excitation spectrum of the diverging susceptibility component, with an intensity ($\propto \chi''(\omega)/\omega$) which goes to infinity as the critical \mathbf{q} is approached. Outside the critical region, the inelastic excitation-energies must approach zero, in the absence of a diffusive mode, as a consequence of the Kramers–Kronig relation, but the excitations may be overdamped, i.e. still become diffusive, sufficiently close to the critical \mathbf{q} . In this case, the generator $1 - i\delta\varphi \sum_i J_{xi}$ of an infinitesimal rotation $\delta\varphi$ of the helix commutes with the Hamiltonian, and the Goldstone theorem applies, predicting that the spin waves are perfectly well-defined excitations in the limit of $\mathbf{q} \rightarrow \mathbf{0}$.

If \mathcal{H}_J can be neglected, the system contains one more Goldstone mode, since $\sum_i J_{i\xi}$ or $\sum_i J_{i\eta}$ now also commute with \mathcal{H} . The transformation $\exp(-i\theta \sum_i J_{i\xi})$ generates a tilting of the plane spanned by the moments, relative to the ξ – η plane perpendicular to \mathbf{Q} , giving rise to the tilted helix structure. In this configuration, the $J_{i\xi} = J_{ix}$ -component is non-zero and oscillates with the phase $\mathbf{Q} \cdot \mathbf{R}_i$. The magnitude of the modulation is determined by the susceptibility component $\chi_{xx}(\mathbf{q} = \mathbf{Q}, 0)$, which diverges in the limit where \mathcal{H}_J or $2A$ vanishes. The situation is very similar to the rotation of the helix considered above. The Goldstone mode is the spin-wave excitation at $\mathbf{q} = \mathbf{Q}$, and the spin-wave energy vanishes linearly with $|\mathbf{q} - \mathbf{Q}|$. The Heisenberg ferromagnet may be considered to be a helix with $\mathbf{Q} = \mathbf{0}$, and in this case the two Goldstone modes collapse into one at $\mathbf{q} = \mathbf{0}$, where the spin-wave dispersion now becomes quadratic in q .

The first study of the spin waves in a periodic magnetic structure was performed by Bjerrum Møller *et al.* (1967) on a Tb crystal, to which 10% Ho had been added to stabilize the helix over a wider temperature range. The results of these measurements are shown in Fig. 6.1. The hexagonal anisotropy in Tb is small, and $\langle O_6^6 \rangle$ has renormalized to negligible values in the helical phase, so the theory for the incommensurable structure would be expected to apply. The dispersion relations do indeed have the form of eqn (6.1.10), rising linearly from zero at small \mathbf{q} , and with a non-zero value of $E_{\mathbf{Q}}$, due to the axial anisotropy B_2^0 . An analysis of the experimental results in terms of this expression gives the exchange functions illustrated in Fig. 6.1. The decrease in the size of the peak in $\mathcal{J}(\mathbf{q})$ with decreasing temperature contributes towards the destabilization of the helix, as discussed in Section 2.3. The effects of the change in this function with temperature can be seen fairly directly in the dispersion relations since, from (6.1.10), the initial slope is proportional to the square root of the curvature $\mathcal{J}''(\mathbf{Q})$, and $E_{\mathbf{Q}}$ is proportional to $\{\mathcal{J}(\mathbf{Q}) - \frac{1}{2}\mathcal{J}(\mathbf{0}) - \frac{1}{2}\mathcal{J}(2\mathbf{Q})\}^{1/2}$. Similar results have been obtained for Dy by Nicklow *et al.* (1971b) and analysed in the same way, even though

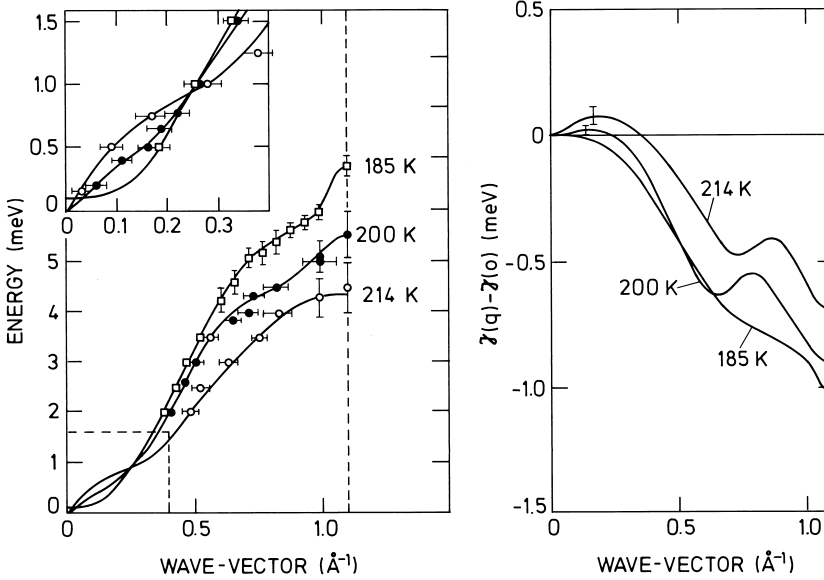


Fig. 6.1. Spin-wave dispersion relations and exchange in the c -direction, in the helical and ferromagnetic phases of $\text{Tb}_{90}\text{Ho}_{10}$. In the helical phase, the energy of the phason excitations goes linearly to zero at long wavelengths, owing to the broken rotational symmetry around the c -axis, but that of the mode at \mathbf{Q} remains non-zero, because of the axial anisotropy. The peak in the exchange function, which stabilizes the periodic structure, is reduced and shifted as the magnetic order increases. In the ferromagnetic phase at 185 K, the energy rises quadratically from a non-zero value, and the peak in the exchange is absent.

the relatively large hexagonal anisotropy makes the use of this theory somewhat marginal in this case. As we shall see in the next section, the very large value of B_6^0 has a decisive influence on the excitations in Ho.

The dispersion relation for the cone may be derived by the same procedure. In the conical structure the moments along the c -axis are non-zero, so that

$$\langle J_{i\zeta} \rangle = \langle J_{\parallel} \rangle = \langle J_z \rangle \cos \theta_0 \quad ; \quad \langle J_z \rangle^2 = \langle J_{\parallel} \rangle^2 + \langle J_{\perp} \rangle^2. \quad (6.1.13)$$

Introducing the transformation (2.2.8), which corresponds to (6.1.3) in the case where $\cos \theta_0 \neq 0$, we may derive the effective coupling parameters within the rotating coordinate system. For the (xy) -part of the

interaction matrix, the result is

$$\begin{aligned}\mathcal{J}_{xx}(\mathbf{q}) &= \frac{1}{2}\{\mathcal{J}(\mathbf{q} + \mathbf{Q}) + \mathcal{J}(\mathbf{q} - \mathbf{Q})\} \cos^2 \theta_0 + \mathcal{J}(\mathbf{q}) \sin^2 \theta_0 \\ \mathcal{J}_{yy}(\mathbf{q}) &= \frac{1}{2}\{\mathcal{J}(\mathbf{q} + \mathbf{Q}) + \mathcal{J}(\mathbf{q} - \mathbf{Q})\} \\ \mathcal{J}_{xy}(\mathbf{q}) &= -\mathcal{J}_{yx}(\mathbf{q}) = \frac{i}{2}\{\mathcal{J}(\mathbf{q} + \mathbf{Q}) - \mathcal{J}(\mathbf{q} - \mathbf{Q})\} \cos \theta_0,\end{aligned}\tag{6.1.14}$$

where $\mathcal{J}_{xy}(\mathbf{q})$ is now non-zero. Neglecting the longitudinal response, as we may in a weakly anisotropic system, we may calculate the response functions by introducing these coupling parameters in (6.1.8). In order to estimate the (xy) -components of the MF susceptibility, or $A \pm B + h_{\text{ex}}$ in eqn (6.1.9), we may utilize their relation to the derivatives of the free energy, as expressed in eqn (2.2.18). The free energy for the i th ion, including the Zeeman contribution from the exchange field of the surrounding ions, is

$$F(i) = f_0 + f(u = \cos \theta) - h_{\parallel} \langle J_z \rangle \cos \theta - h_{\perp} \langle J_z \rangle \sin \theta \cos(\phi - \phi_0),\tag{6.1.15a}$$

with $\phi_0 = \mathbf{Q} \cdot \mathbf{R}_i + \varphi$, and

$$h_{\parallel} = \langle J_z \rangle \mathcal{J}(\mathbf{0}) \cos \theta_0 \quad ; \quad h_{\perp} = \langle J_z \rangle \mathcal{J}(\mathbf{Q}) \sin \theta_0.\tag{6.1.15b}$$

\mathcal{H}_J is again, as in (6.1.4), the usual crystal-field Hamiltonian, except that B_6^6 is neglected. The function $f(u)$ is given by (2.2.17) in terms of $\kappa_l^m(T)$, with $\kappa_6^6 = 0$. From (6.1.15), the equilibrium angles are determined by

$$-f'(u_0) \sin \theta_0 + h_{\parallel} \langle J_z \rangle \sin \theta_0 - h_{\perp} \langle J_z \rangle \cos \theta_0 = 0,$$

and $\phi = \phi_0$. $f'(u)$ is the derivative of $f(u)$ with respect to u , and $u_0 = \cos \theta_0$. With $\sin \theta_0 \neq 0$, this equation leads to

$$f'(u_0) \cos \theta_0 = \langle J_z \rangle^2 \{\mathcal{J}(\mathbf{0}) - \mathcal{J}(\mathbf{Q})\} \cos^2 \theta_0.\tag{6.1.16}$$

The spin-wave parameters may then be derived as

$$\begin{aligned}\langle J_z \rangle (A + B + h_{\text{ex}}) &= F_{\theta\theta}(i) \\ &= f''(u_0) \sin^2 \theta_0 - f'(u_0) \cos \theta_0 + h_{\parallel} \langle J_z \rangle \cos \theta_0 + h_{\perp} \langle J_z \rangle \sin \theta_0 \\ \langle J_z \rangle (A - B + h_{\text{ex}}) &= F_{\phi\phi}(i) / \sin^2 \theta_0 = h_{\perp} \langle J_z \rangle / \sin \theta_0.\end{aligned}$$

Introducing the values of the exchange fields and applying the equilibrium condition (6.1.16), we then find that

$$\begin{aligned}A + B + h_{\text{ex}} &= \{f''(u_0) / \langle J_z \rangle\} \sin^2 \theta_0 + \langle J_z \rangle \mathcal{J}(\mathbf{Q}) \\ A - B + h_{\text{ex}} &= \langle J_z \rangle \mathcal{J}(\mathbf{Q}).\end{aligned}\tag{6.1.17}$$

These parameters determine the (xy) -components of $\bar{\chi}^o(\omega)$ in (6.1.9), and are valid, at least, to first order in $1/J$. From (6.1.8), we finally obtain

$$\begin{aligned}\chi_{xx}(\mathbf{q}, \omega) &= \langle J_z \rangle \frac{A_{\mathbf{q}} - B_{\mathbf{q}}}{A_{\mathbf{q}}^2 - B_{\mathbf{q}}^2 - (\hbar\omega - C_{\mathbf{q}})^2} \\ \chi_{yy}(\mathbf{q}, \omega) &= \langle J_z \rangle \frac{A_{\mathbf{q}} + B_{\mathbf{q}}}{A_{\mathbf{q}}^2 - B_{\mathbf{q}}^2 - (\hbar\omega - C_{\mathbf{q}})^2} \\ \chi_{xy}(\mathbf{q}, \omega) &= \langle J_z \rangle \frac{i(\hbar\omega - C_{\mathbf{q}})}{A_{\mathbf{q}}^2 - B_{\mathbf{q}}^2 - (\hbar\omega - C_{\mathbf{q}})^2},\end{aligned}\quad (6.1.18)$$

where the parameters are now

$$\begin{aligned}A_{\mathbf{q}} - B_{\mathbf{q}} &= \langle J_z \rangle \left\{ \mathcal{J}(\mathbf{Q}) - \frac{1}{2} \mathcal{J}(\mathbf{q} + \mathbf{Q}) - \frac{1}{2} \mathcal{J}(\mathbf{q} - \mathbf{Q}) \right\} \\ A_{\mathbf{q}} + B_{\mathbf{q}} &= (A_{\mathbf{q}} - B_{\mathbf{q}}) \cos^2 \theta_0 + [L + \langle J_z \rangle \{ \mathcal{J}(\mathbf{0}) - \mathcal{J}(\mathbf{q}) \}] \sin^2 \theta_0 \\ C_{\mathbf{q}} &= \frac{1}{2} \langle J_z \rangle \{ \mathcal{J}(\mathbf{q} - \mathbf{Q}) - \mathcal{J}(\mathbf{q} + \mathbf{Q}) \} \cos \theta_0,\end{aligned}\quad (6.1.19)$$

and the axial anisotropy constant is

$$\begin{aligned}L &= \langle J_z \rangle \{ \mathcal{J}(\mathbf{Q}) - \mathcal{J}(\mathbf{0}) \} + f''(u_0) / \langle J_z \rangle, \quad \text{with} \\ f''(u_0) &= 3\kappa_2^0(T) + \frac{15}{2}\kappa_4^0(T)(7\cos^2\theta_0 - 1) \\ &\quad + \frac{105}{8}\kappa_6^0(T)(33\cos^4\theta_0 - 18\cos^2\theta_0 + 1).\end{aligned}\quad (6.1.20)$$

This constant, to order $1/J$, is that determined by the c -axis bulk susceptibility: $\chi_{\zeta\zeta}(\mathbf{0}, 0) = \langle J_z \rangle / L$. The dispersion relation, derived from the pole at positive energies, is

$$E_{\mathbf{q}} = C_{\mathbf{q}} + [A_{\mathbf{q}}^2 - B_{\mathbf{q}}^2]^{1/2}, \quad (6.1.21)$$

which is no longer even with respect to \mathbf{q} , because the parameter $C_{\mathbf{q}}$ changes sign, whereas $A_{\mathbf{q}}$ and $B_{\mathbf{q}}$ are unaffected, if \mathbf{q} is replaced by $-\mathbf{q}$. The other pole, with a minus before the square root, lies at negative energies. If the two energies for \mathbf{q} were both positive, the two poles at $-\mathbf{q}$ would both lie at negative energies, indicating an instability of the magnetic system. Hence in a stable cone $C_{\mathbf{q}}^2 < A_{\mathbf{q}}^2 - B_{\mathbf{q}}^2$ (Cooper *et al.* 1962).

The scattering cross-section of the spin waves is still determined by (6.1.12a), but (6.1.12b) is replaced by

$$\begin{aligned}\chi_{\zeta\zeta}(\boldsymbol{\kappa}, \omega) &= \chi_{xx}(\boldsymbol{\kappa}, \omega) \sin^2 \theta_0 \\ \chi_{\xi\xi}(\boldsymbol{\kappa}, \omega) &= \chi_{\eta\eta}(\boldsymbol{\kappa}, \omega) = \frac{1}{4} \{ \chi_{xx}(\boldsymbol{\kappa} - \mathbf{Q}, \omega) + \chi_{xx}(\boldsymbol{\kappa} + \mathbf{Q}, \omega) \} \cos^2 \theta_0 \\ &\quad + \frac{1}{4} \{ \chi_{yy}(\boldsymbol{\kappa} - \mathbf{Q}, \omega) + \chi_{yy}(\boldsymbol{\kappa} + \mathbf{Q}, \omega) \} \\ &\quad - \frac{i}{2} \{ \chi_{xy}(\boldsymbol{\kappa} - \mathbf{Q}, \omega) - \chi_{xy}(\boldsymbol{\kappa} + \mathbf{Q}, \omega) \} \cos \theta_0.\end{aligned}\quad (6.1.22)$$

When $\boldsymbol{\kappa}$ is along the c -axis, the scattering is determined by the basal-plane component alone, and introducing (6.1.18) in this expression, we find for positive energies

$$\chi''_{\xi\xi}(\boldsymbol{\kappa}, \omega) = \sum_{\mathbf{q}} \frac{\pi \langle J_z \rangle}{8r_{\mathbf{q}}} \left\{ (r_{\mathbf{q}} \cos \theta_0 + 1)^2 \delta_{\mathbf{q}, \boldsymbol{\kappa} - \mathbf{Q} - \boldsymbol{\tau}} + (r_{\mathbf{q}} \cos \theta_0 - 1)^2 \delta_{\mathbf{q}, \boldsymbol{\kappa} + \mathbf{Q} - \boldsymbol{\tau}} \right\} \delta(E_{\mathbf{q}} - \hbar\omega), \quad (6.1.23)$$

where the ratio $r_{\mathbf{q}} = [(A_{\mathbf{q}} - B_{\mathbf{q}})/(A_{\mathbf{q}} + B_{\mathbf{q}})]^{1/2}$. This equation is consistent with the original result of Bar'yakhtar and Maleev (1963), who also considered the spin-polarized neutron cross-section. As in the helical case, there are two branches, emerging from either of the Bragg peaks at $\boldsymbol{\tau} \pm \mathbf{Q}$, but the intensities of the two branches are no longer equal. Furthermore, the crystal will normally split up into four distinct types of domain, as the energy of the cone structure depends on the sign of neither $\cos \theta_0$ nor $Q = \mathbf{Q} \cdot \hat{\zeta}$. The spin-wave parameter $C_{\mathbf{q}}$ changes sign with either of these two quantities, and this leads to two different values $E_{\mathbf{q}}^+$ and $E_{\mathbf{q}}^-$ of the spin-wave energies in the four domains, corresponding to regions where the signs of $\cos \theta_0$ and Q are respectively the same or different. All the vectors in (6.1.23) are along the ζ -axis, and we may therefore write the total response function at positive energies in terms of their magnitudes, in the presence of the four domains, as

$$\begin{aligned} \chi''_{\xi\xi}(\boldsymbol{\kappa}, \omega) = \sum_{\mathbf{q}} \frac{\pi \langle J_z \rangle}{8r_{\mathbf{q}}} & \left[\{ (r_{\mathbf{q}} |\cos \theta_0| + 1)^2 \delta_{q, \kappa - |Q| - \tau} \right. \\ & \left. + (r_{\mathbf{q}} |\cos \theta_0| - 1)^2 \delta_{q, \kappa + |Q| - \tau} \right] \delta(E_{\mathbf{q}}^+ - \hbar\omega) + \\ & \left[(r_{\mathbf{q}} |\cos \theta_0| - 1)^2 \delta_{q, \kappa - |Q| - \tau} + (r_{\mathbf{q}} |\cos \theta_0| + 1)^2 \delta_{q, \kappa + |Q| - \tau} \right] \delta(E_{\mathbf{q}}^- - \hbar\omega) \end{aligned} \quad (6.1.24)$$

showing that there will normally be four spin-wave resonances in a constant- $\boldsymbol{\kappa}$ scan, at positive energies. We shall denote the spin-waves with energies determined by $E_{\mathbf{q}}^{\pm}$, when q is positive or negative respectively, as the $+q$ branch or $-q$ branch. The energy difference $E_{\mathbf{q}}^+ - E_{\mathbf{q}}^- = E_{\mathbf{q}}^+ - E_{-\mathbf{q}}^+ = 2C_{\mathbf{q}}^+$ is normally positive, when $q = \mathbf{q} \cdot \hat{\zeta} > 0$, so that the $+q$ branch lies above the $-q$ branch. Equation (6.1.24) then predicts that neutron scans at a series of values of κ , starting from the Bragg peak at $\tau + |Q|$, will show both the $+q$ and the $-q$ branches, that the $+q$ branch will have the largest intensity when $\kappa > \tau + |Q|$, and that the response function is symmetrical around the lattice Bragg point $\kappa = \tau$. Although two of the four types of domain may be removed by the application of an external field along the c -axis, this does not remove the degeneracy with

respect to the helicity of the cone, and eqn (6.1.24) remains unchanged. Different sign conventions, stemming from whether θ_0 is determined by the ζ -component of the magnetic moments or of the angular momenta, may lead to a different labelling of the branches by $\pm q$, but this does not of course reflect any arbitrariness in, for instance, the relation between the spin-wave energies and their scattering intensities.

In Fig. 6.2 is shown the dispersion relations $E_{\mathbf{q}}^{\pm}$ obtained in the c -direction in the conical phase of Er at 4.5 K by Nicklow *et al.* (1971a). The length of the ordering wave-vector is about $\frac{5}{21}(2\pi/c)$ and the cone angle $\theta_0 \simeq 28^\circ$. The relatively small cone angle leads to a large splitting between the $+q$ and $-q$ branches. According to the dispersion relation (6.1.21), this splitting is given by $2C_{\mathbf{q}}$, from which $\mathcal{J}(\mathbf{q})$ may readily be derived. This leaves only the axial anisotropy L as a fitting parameter in the calculation of the mean values of the spin-wave energies. This parameter may be estimated from the magnetization measurements, $L = \langle J_z \rangle / \chi_{\zeta\zeta}(\mathbf{0}, 0)$, which indicate (Jensen 1976b) that it lies between 15–25 meV. Nicklow *et al.* (1971a) were not able to derive a satisfactory account of their experimental results from the dispersion relation given by (6.1.21) in terms of $\mathcal{J}(\mathbf{q})$ and L . In order to do so, they introduced a large anisotropic coupling between the dipoles $\mathcal{J}_{\zeta\zeta}(\mathbf{q}) - \mathcal{J}(\mathbf{q})$, corresponding to a \mathbf{q} -dependent contribution to $L = L(\mathbf{q})$ in (6.1.19). Although this model can account for the spin-wave energies, the value of $L(\mathbf{0})$ is much too large in comparison with that estimated above. This large value of $L(\mathbf{q})$ also has the consequence that $r_{\mathbf{q}}$ becomes small, so that the scattering intensities of the $+q$ and $-q$ branches are predicted to be nearly equal, since $(r_{\mathbf{q}} \cos \theta_0 - 1)^2 \simeq (r_{\mathbf{q}} \cos \theta_0 + 1)^2$, in disagreement with the experimental observations. A more satisfactory model was later suggested by Jensen (1974), in which an alternative anisotropic two-ion coupling was considered; $K_{ll'}^{mm'}(ij) \tilde{O}_{lm}(\mathbf{J}_i) \tilde{O}_{l'm'}(\mathbf{J}_j) + \text{h.c.}$, as in (5.5.14), with $m = -m' = 2$. This coupling modifies the close relationship between $C_{\mathbf{q}}$ and $A_{\mathbf{q}} - B_{\mathbf{q}}$ found above in the isotropic case, and it was thereby possible to account for the spin-wave energies, as shown in Fig. 6.2, and for the intensity ratio between the two branches at most wave-vectors, since $r_{\mathbf{q}}$ is much closer to 1, when $\pi/c < q < 2\pi/c$, than in the model of Nicklow *et al.* (1971a). Finally, the value of L used in the fit ($L = 20$ meV) agrees with that estimated from the magnetization curves. The anisotropic component of the two-ion coupling derived in this way was found to be of the same order of magnitude as the isotropic component, but the contributions of this anisotropic interaction (with $l = l' = 2$) to the spin-wave energies and to the free energy are effectively multiplied by respectively the factor $\sin^2 \theta_0$ and $\sin^4 \theta_0$, where $\sin^2 \theta_0 \simeq 0.2$ in the cone phase. It is in fact almost possible to reproduce the dispersion relations, within the experimental uncertainty, by including

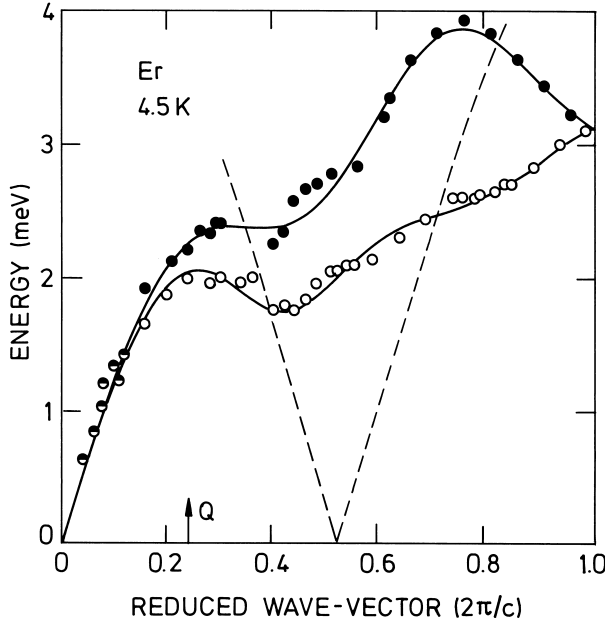


Fig. 6.2. Spin-wave dispersion relations in the c -direction, in the cone phase of Er at 4.5 K, after Nicklow *et al.* (1971a). The closed and open symbols represent the $+q$ and $-q$ branches respectively. The solid lines are the results of the spin-wave calculation described in the text, and the dashed lines are the dispersion relations for the transverse phonons originating from $2\pi/c \pm 2Q$.

only the isotropic part of the coupling, but this requires a value of $L \simeq 35$ meV, and the intensity ratio, in the interval $\pi/c < q < 2\pi/c$, is found to be wrong by a factor of three or more.

It has been suggested (Lindgård 1978) that the necessity of introducing anisotropic two-ion coupling in the description of the spin-waves in Er may be an artifact due to a breakdown of the linear spin-wave theory. As discussed in Section 5.3.2, the linear theory is not valid in strongly anisotropic systems, i.e. when the numerical value of the b -parameter is large and the length of the moments is significantly smaller than their saturation value, in the low-temperature limit. However, the model for Er presented in Section 2.3, which describes the magnetic structure as a function of temperature and magnetic field reasonably well, predicts that $\sigma(T = 0)$ is only reduced by 1–2%, and that $|b| \simeq 0.08$. The excitation spectrum in the cone phase may be derived,

in the presence of arbitrarily large anisotropy, by a numerical calculation of the MF susceptibility $\overline{\chi}^o(\omega)$, as determined by the crystal-field Hamiltonian and the exchange field, given by (6.1.15b). In the general case, it is necessary to include the total interaction-matrix $\overline{\mathcal{J}}(\mathbf{q})$, and not only the (xy) -part as in (6.1.14), when deriving the final susceptibility matrix (6.1.7). A numerical calculation of the excitation energies, for a model which also accounts fairly accurately for the anisotropy of Er, leads to energies which are very well described by the linear spin-wave theory (Jensen 1976c), the discrepancies being only of the order of a few per cent. The spin waves are not purely transverse, as the individual moments are calculated to precess in a plane whose normal makes an angle of about 33° with the c -axis. The relation between the difference and the sum of $E_{\mathbf{q}}^+$ and $E_{\mathbf{q}}^-$ is still found to be obeyed, when the two-ion anisotropy is neglected. The experimental results therefore attest to the importance of such anisotropy effects. Except for the tilting of the plane in which the moments precess, which is not easy to detect experimentally, the linear spin-wave theory is found to give an accurate account of the excitations at low temperatures in Er. In spite of this, it is not a good approximation to consider only the ground state and the first excited state of the MF Hamiltonian, when calculating the excitation spectrum, because 10–15% of the dispersive effects are due to the coupling between the spin waves and the higher-lying MF levels. These effects are included implicitly, to a first approximation, in the linear spin-wave theory, which gives an indication of the efficacy of the Holstein–Primakoff transformation (when J is large).

We have so far neglected the hexagonal anisotropy. In Section 2.1.3, we found that B_6^6 causes a bunching of the moments about the easy axes in the plane, leading to (equal) 5th and 7th harmonics in the static modulation of the moments. The cone is distorted in an analogous way, but the hexagonal anisotropy is effectively multiplied by the factor $\sin^6 \theta_0 \approx 0.01$ in Er. The effects of B_6^6 on the spin waves are therefore small, and may be treated by second-order perturbation theory, which predicts energy gaps in the spectrum whenever $E_{\mathbf{q}} = E_{\mathbf{q} \pm 6\mathbf{Q}}$ (for a further discussion, see Arai and Felcher, 1975). In the experimental spin-wave spectrum of Er, shown in Fig. 6.2, energy gaps are visible, but not at the positions expected from the coupling due to the hexagonal anisotropy. It seems very likely that the two gaps observed close to $q = 0.4(2\pi/c)$ are due to an interaction with the transverse phonons. Although the normal magnetoelastic ε -coupling, which leads to energy gaps when $E_{\mathbf{q}} = \hbar\omega_{\mathbf{q} \pm \mathbf{Q}}$, might be significant for the lower branch, the positions of both gaps agree very well with those expected from an acoustic–optical coupling, occurring when $E_{\mathbf{q}} = \hbar\omega_{\mathbf{q} \pm 2\mathbf{Q} + \mathbf{b}_3}$ (in the double-zone representation), as indicated in Fig. 6.2. Although the

two gaps are close to each other on the figure, they appear in practice on different sides of $\mathbf{q} = \mathbf{0}$, and do not interfere. This interaction is equivalent to the strong optical-magnon – acoustic-phonon coupling observed in Tb, shown in Fig. 5.6. However, in Er, it is not possible to say whether or not a non-collinear component of the spin-density wave of the polarized conduction electrons is involved, as this coupling is allowed independently of whether such a component is present or not.

6.1.2 The longitudinally polarized structure

In the helix or the cone, the magnitude of the moments is constant, and a transformation to the rotating coordinate system yields a Hamiltonian which is equivalent to that of a ferromagnet, independently of whether or not the ordering is commensurable. In the longitudinally polarized phase, the length of the moments is modulated and the magnitude of the exchange field changes from site to site. This results in a modulation of the *energies* of the MF levels, whereas in the helix or the cone, it is only the *matrix elements* of the dipole moments which change. In the commensurable case, which we shall discuss in more detail in the following section, the RPA always predicts well-defined excitations. If the magnetic ordering is incommensurable, the single-site energy levels change in a pattern which never repeats itself, introducing effectively random energy-barriers along the paths of the excitations. Hence it is not obvious whether well-defined excitations can exist in this phase (Cooper *et al.* 1962). We shall focus on the effects of incommensurable ordering by considering the simplest possible model. The single-ion anisotropy terms are neglected, but in order to confine the moments along the c -axis, the two-ion dipole coupling is assumed to be anisotropic, $\mathcal{J}_{\parallel}(\mathbf{q}) \neq \mathcal{J}_{\perp}(\mathbf{q})$. Furthermore, we assume that the temperature is so close to T_N that the tendency towards squaring-up, i.e. the higher harmonics discussed in Section 2.1.4, can be neglected, in which case

$$\langle J_{i\zeta} \rangle = \mathcal{A}_i = \mathcal{A} \cos(\mathbf{Q} \cdot \mathbf{R}_i + \varphi). \quad (6.1.25)$$

The exchange field acting on the i th site is then

$$h_{i\zeta}^{\text{eff}} = \sum_j \mathcal{J}_{\parallel}(ij) \mathcal{A} \cos(\mathbf{Q} \cdot \mathbf{R}_j + \varphi) = \mathcal{A}_i \mathcal{J}_{\parallel}(\mathbf{Q}),$$

and the transverse component of the MF Green function is

$$g_i^o(\omega) \equiv -\chi_{+-}^o(\omega) = \frac{2\mathcal{A}_i}{\hbar\omega - \mathcal{A}_i \mathcal{J}_{\parallel}(\mathbf{Q})}, \quad (6.1.26)$$

as in Section 3.5.2. Because $\chi_{++}^o(\omega)$ and $\chi_{--}^o(\omega)$ both vanish, the site-dependent equation determining the final RPA Green function $G(ij, \omega)$,

corresponding to $g_i^o(\omega)$, may be written

$$\{\hbar\omega - \mathcal{A}_i \mathcal{J}_{\parallel}(\mathbf{Q})\} G(ij, \omega) = 2\mathcal{A}_i \delta_{ij} - \sum_{j'} \mathcal{A}_i \mathcal{J}_{\perp}(ij') G(j'j, \omega), \quad (6.1.27)$$

obtained from the RPA equation (3.5.7) by multiplying with the energy denominator in $g_i^o(\omega)$. We introduce the Fourier transforms

$$G_n(\mathbf{q}, \omega) = \frac{1}{N} \sum_{ij} G(ij, \omega) e^{-i\mathbf{q}\cdot(\mathbf{R}_i - \mathbf{R}_j)} e^{-in\mathbf{Q}\cdot\mathbf{R}_i}, \quad (6.1.28)$$

where n is an integer, and the coupling parameter

$$\gamma_n(\mathbf{q}) = -\frac{1}{2} \mathcal{A} \{ \mathcal{J}_{\parallel}(\mathbf{Q}) - \mathcal{J}_{\perp}(\mathbf{q} + n\mathbf{Q}) \}, \quad (6.1.29)$$

which is always negative ($\mathcal{A} > 0$), as the stability of the structure requires $\mathcal{J}_{\parallel}(\mathbf{Q}) - \mathcal{J}_{\perp}(\mathbf{Q}) > 0$. From (6.1.27), we then obtain the infinite set of equations

$$\hbar\omega G_n(\mathbf{q}, \omega) + \gamma_{n+1}(\mathbf{q}) G_{n+1}(\mathbf{q}, \omega) + \gamma_{n-1}(\mathbf{q}) G_{n-1}(\mathbf{q}, \omega) = \mathcal{A}(\delta_{n,1} + \delta_{n,-1}) \quad (6.1.30)$$

whenever \mathbf{Q} is incommensurable. In a commensurable structure, for which $m\mathbf{Q} = p\boldsymbol{\tau}$, we determine $G_n(\mathbf{q}, \omega) = G_{n+m}(\mathbf{q}, \omega)$ by the corresponding finite set of m equations. Of the infinite number of Green functions, we wish to calculate the one with $n = 0$, as the transverse scattering function is proportional to $\text{Im}[G_0(\mathbf{q}, \omega)]$.

It is possible to rewrite eqn (6.1.30) so that $G_0(\mathbf{q}, \omega)$ is expressed in terms of *infinite continued fractions*. In order to derive such an expression, we shall introduce the semi-infinite determinant D_n , with n positive,

$$D_n = \begin{vmatrix} \hbar\omega & \gamma_{n+1} & 0 & 0 & 0 & 0 & \cdots \\ \gamma_n & \hbar\omega & \gamma_{n+2} & 0 & 0 & 0 & \cdots \\ 0 & \gamma_{n+1} & \hbar\omega & \gamma_{n+3} & 0 & 0 & \cdots \\ 0 & 0 & \gamma_{n+2} & \hbar\omega & \gamma_{n+4} & 0 & \cdots \\ \vdots & \vdots & & \ddots & \ddots & \ddots & \ddots \end{vmatrix} \quad (6.1.31)$$

leaving out the variables \mathbf{q} and ω . Expanding the determinant in terms of the first column, we have

$$D_n = \hbar\omega D_{n+1} - \gamma_n \gamma_{n+1} D_{n+2}. \quad (6.1.32)$$

When $n = 1$, eqn (6.1.30) may be written $\hbar\omega G_1 + \gamma_2 G_2 = \mathcal{A} - \gamma_0 G_0$, and the semi-infinite series of equations with $n \geq 1$ may be solved in terms of G_0 and D_n :

$$G_1 = (\mathcal{A} - \gamma_0 G_0) \frac{D_2}{D_1} = (\mathcal{A} - \gamma_0 G_0) \frac{1}{\hbar\omega - \gamma_1 \gamma_2 D_3 / D_2}, \quad (6.1.33)$$

utilizing (6.1.32) in the last step. In terms of the two infinite continued fractions ($n \geq 1$)

$$\begin{aligned} z_n(\mathbf{q}, \omega) &= \frac{\gamma_n(\mathbf{q})}{\hbar\omega - \gamma_n(\mathbf{q}) z_{n+1}(\mathbf{q}, \omega)} \\ z_{-n}(\mathbf{q}, \omega) &= \frac{\gamma_{-n}(\mathbf{q})}{\hbar\omega - \gamma_{-n}(\mathbf{q}) z_{-n-1}(\mathbf{q}, \omega)}, \end{aligned} \quad (6.1.34)$$

eqn (6.1.33) may be written $\gamma_1 G_1 = (\mathcal{A} - \gamma_0 G_0) z_1$, and in the same way, we have $\gamma_{-1} G_{-1} = (\mathcal{A} - \gamma_0 G_0) z_{-1}$. Introducing these expressions into (6.1.30), with $n = 0$, we finally obtain

$$G_0(\mathbf{q}, \omega) = \mathcal{A} \frac{z_1(\mathbf{q}, \omega) + z_{-1}(\mathbf{q}, \omega)}{\gamma_0 \{z_1(\mathbf{q}, \omega) + z_{-1}(\mathbf{q}, \omega)\} - \hbar\omega}. \quad (6.1.35)$$

A similar result was derived by Liu (1980). In this formal solution, there is no small parameter, except in the high-frequency limit, which allows a perturbative expansion of $G_0(\mathbf{q}, \omega)$. The infinite continued fraction determining z_n never repeats itself, but it is always possible to find an $n = s$ such that z_s is arbitrary close to, for instance, z_1 . This property may be used for determining the final response function when $\hbar\omega \rightarrow 0$. In this limit, we have from (6.1.34): $z_1 = -1/z_2 = z_3 = -1/z_4 = \dots$ and, using $z_1 \simeq z_s$ for s even, we get $z_1 = -1/z_1$ or $z_1 = \pm i$. At $\mathbf{q} = \mathbf{0}$, we have by symmetry $z_1 = z_{-1} = \pm i$, which also has to be valid at any other \mathbf{q} . The correct sign in front of the i is determined from a replacement of ω by $\omega + i\epsilon$, where ϵ is an infinitesimal positive quantity or, more easily, from the property that $\text{Im}[G_0(\mathbf{q}, \omega)]$ should have the opposite sign to ω , i.e.

$$G(\mathbf{q}, \omega \rightarrow 0) = \frac{\mathcal{A}}{\gamma_0} - i \frac{\mathcal{A}}{2\gamma_0^2} \hbar\omega. \quad (6.1.36a)$$

Since

$$\chi_{\xi\xi}(\mathbf{q}, \omega) = \chi_{\eta\eta}(\mathbf{q}, \omega) = -\frac{1}{4} \{G(\mathbf{q}, \omega) + G^*(\mathbf{q}, -\omega)\},$$

we get

$$\chi_{\xi\xi}(\mathbf{q}, \omega \rightarrow 0) = \frac{1}{\mathcal{J}_{\parallel}(\mathbf{Q}) - \mathcal{J}_{\perp}(\mathbf{q})} + i \frac{\hbar\omega}{\mathcal{A} \{\mathcal{J}_{\parallel}(\mathbf{Q}) - \mathcal{J}_{\perp}(\mathbf{q})\}^2}. \quad (6.1.36b)$$

The imaginary term linear in ω implies that the correlation function (4.2.3), which is proportional to $\chi''_{\alpha\beta}(\mathbf{q}, \omega)/\beta\hbar\omega$ for $\omega \rightarrow 0$, is non-zero in this limit. Hence the inelastic-scattering spectrum of the incommensurable system contains a tail down to zero frequency, with a magnitude at $\omega = 0$ proportional to T . At non-zero frequencies, eqn (6.1.35) can only be solved in special cases, such as if γ_n is independent of n , corresponding to $\mathcal{J}_\perp(\mathbf{q}) = 0$ (Liu 1980). In general, numerical methods must be applied. We may, for example, replace ω by $\omega + i\epsilon$ and, instead of considering the limit $\epsilon \rightarrow 0^+$, allow ϵ to stay small but non-zero (e.g. $\epsilon = 0.01|\omega|$). Then $G_0(\mathbf{q}, \omega)$ becomes insensitive to the value of $z_{\pm n}$, if n is sufficiently large ($n > 50$). ϵ acts as a coarse-graining parameter, of the type mentioned at the beginning of this section, and any energy gaps in the spectrum, smaller than $\hbar\epsilon$, are smeared out. A more careful treatment of this problem has been given by Lantwin (1990). Solutions of eqn (6.1.35) have been presented by Ziman and Lindgård (1986), Lovesey (1988), and Lantwin (1990), for various values of \mathbf{Q} and the axial anisotropy parameter $\mathcal{J}_\parallel(\mathbf{Q}) - \mathcal{J}_\perp(\mathbf{Q})$. The most important result is that the imaginary part of $G_0(\mathbf{q}, \omega)/\omega$ contains a number

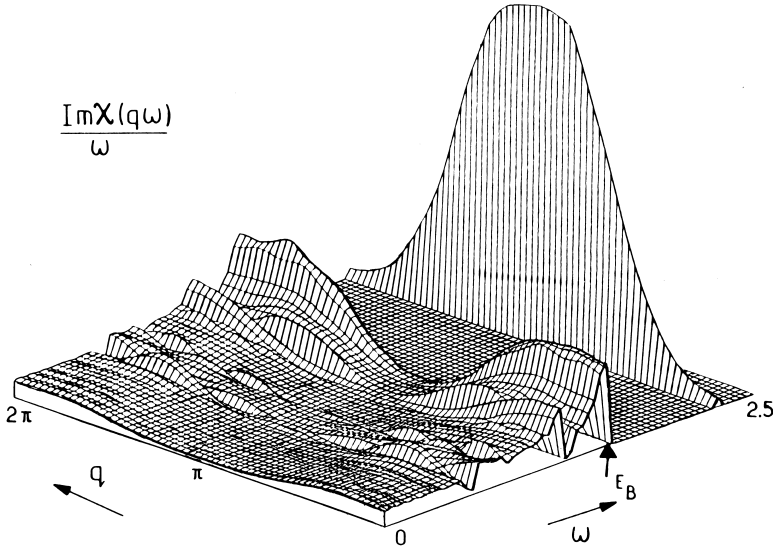


Fig. 6.3. The imaginary part of the response function $\chi_{\xi\xi}(\mathbf{q}, \omega)/\omega$ for an incommensurable longitudinal structure, as a function of ω and \mathbf{q} , from Ziman and Lindgård (1986). The sharp peaks indicate the presence of well-defined excitations in this structure.

of sharp peaks, as a function of ω at a constant value of \mathbf{q} ; one such example is shown in Fig. 6.3. These peaks indicate the presence of well-defined excitations. The variation of the energy with the component of \mathbf{q} parallel to \mathbf{Q} is very small, but the spectral weights of the different peaks change. This pattern indicates that the excitations propagating parallel to the ordering wave-vector are quasi-localized modes of composite angular momenta. This behaviour may be explained by a closer examination of the single-site response function (6.1.26). $g_i^o(\omega)$ becomes nearly zero, at non-zero frequencies, whenever $\mathcal{A}_i = \langle J_{i\zeta} \rangle$ is small, which generally occurs twice in every period. This explains the low-frequency diffusive response, and implies that the excitations become essentially trapped between the sites with small moments.

This theory may, with some modifications, be applicable to a description of Er in its high-temperature, longitudinally polarized phase ($T'_N < T < T_N$). The excitations in this temperature interval have been studied by Nicklow and Wakabayashi (1982). They found no sharp peaks in the transverse spectrum, but saw indications of relatively strong dispersive effects at small values of $\mathbf{q} \pm \mathbf{Q}$. The absence of sharp peaks in the spectrum may be explained by intrinsic linewidth effects, neglected in the RPA theory utilized above, which may be quite substantial at the relatively high temperatures of the experiments. However, the strong dispersive effects detected close to the magnetic Bragg peaks are not consistent with the results discussed above. One modification of the simple model which may be important is the squaring-up of the moments, which has been considered by Lantwin (1990). The higher harmonics lead to additional coupling terms in (6.1.30), and the analysis becomes correspondingly more complex. However, a simple argument shows that the higher harmonics result in less localized modes, and thus lead to a stronger dispersion, as also concluded by Lantwin. It is because the intervals along the c -axis in which the moments are small become narrower when the moments square up, so that the excitations may tunnel more easily through these regions. Another limitation of the theory, which may be important for Er, is that the single-site crystal-field anisotropy, neglected in the model, is probably more important than the two-ion axial anisotropy. The single-ion anisotropy splits the levels, even when the exchange field vanishes, and excited dipolar states may occur at energies suitable for allowing the excitations to propagate across sites with small moments, more freely than in the simple model. In the limit where the exchange field is small compared to the crystal-field splittings, which we shall discuss in the next chapter, the corresponding continued fractions in $G_0(\mathbf{q}, \omega)$ converge rapidly (Jensen *et al.* 1987), and the results become largely independent of whether the ordering is commensurable or not.

6.2 Commensurable periodic structures

In the preceding section, we discussed the spin-wave spectra in helical or conical systems, which are characterized by the important feature that the magnitude of the ordered moments, and hence of the exchange field, are constant. This simplification allowed an analytic derivation of the spin-wave energies, in weakly anisotropic systems. If B_6^6 only leads to a slight distortion of the structure, its effects on the spin waves may be included as a perturbation. If B_6^6 is large, however, as it is for instance in Ho, this procedure may not be sufficiently accurate. Instead it is necessary to diagonalize the MF Hamiltonian for the different sites, determine the corresponding MF susceptibilities, and thereafter solve the site-dependent RPA equation

$$\bar{\bar{\chi}}(ij, \omega) = \bar{\bar{\chi}}_i^o(\omega)\delta_{ij} + \sum_{j'} \bar{\bar{\chi}}_i^o(\omega)\bar{\bar{\mathcal{J}}}(ij')\bar{\bar{\chi}}(j'j, \omega). \quad (6.2.1)$$

In uniform para- or ferromagnetic systems, $\bar{\bar{\chi}}_i^o(\omega)$ is independent of the site considered, and the equation may be diagonalized, with respect to the site dependence, by a Fourier transformation. In an undistorted helix or cone, the transformation to the rotating coordinate system eliminates the variation of $\bar{\bar{\chi}}_i^o(\omega)$ with respect to the site index, and (6.2.1) may be solved as in the uniform case. If B_6^6 is large, the transformation to a (uniformly) rotating coordinate system leaves a residual variation in $\bar{\bar{\chi}}_i^o(\omega)$, and in the direction of the moments relative to the z -axis of the rotating coordinates. This complex situation can usually only be analysed by numerical methods. A strong hexagonal anisotropy will normally cause the magnetic structure to be commensurable with the lattice, as discussed in Section 2.3. We shall assume this condition, and denote the number of ferromagnetic hexagonal layers in one commensurable period by m , with \mathbf{Q} along the c -axis. The spatial Fourier transformation of (6.2.1) then leaves m coupled equations. In order to write down these equations explicitly, we define the Fourier transforms

$$\bar{\bar{\chi}}^o(n; \omega) = \frac{1}{N} \sum_i \bar{\bar{\chi}}_i^o(\omega) e^{-in\mathbf{Q}\cdot\mathbf{R}_i} \quad (6.2.2a)$$

and, corresponding to (6.1.28),

$$\bar{\bar{\chi}}(n; \mathbf{q}, \omega) = \frac{1}{N} \sum_{ij} \bar{\bar{\chi}}(ij, \omega) e^{-i\mathbf{q}\cdot(\mathbf{R}_i - \mathbf{R}_j)} e^{-in\mathbf{Q}\cdot\mathbf{R}_i}, \quad (6.2.2b)$$

where n is an integer. Equation (6.2.1) then leads to

$$\bar{\bar{\chi}}(n; \mathbf{q}, \omega) = \bar{\bar{\chi}}^o(n; \omega) + \sum_{s=0}^{m-1} \bar{\bar{\chi}}^o(n-s; \omega)\bar{\bar{\mathcal{J}}}(\mathbf{q} + s\mathbf{Q})\bar{\bar{\chi}}(s; \mathbf{q}, \omega), \quad (6.2.3)$$

where $\bar{\chi}^o(n+m; \omega) = \bar{\chi}^o(n; \omega)$. The m matrix equations may be solved by replacing ω by $\omega + i\epsilon$. Instead of taking the limit $\epsilon \rightarrow 0^+$, as required by the definition of the response function, ϵ is considered as non-zero but small, corresponding to a Lorentzian broadening of the excitations. Equation (6.2.3) may then be solved by a simple iterative procedure, after the diagonal term $\bar{\chi}(n; \mathbf{q}, \omega)$ has been isolated on the left-hand side of the equation. If m is not too large, and if ϵ is not chosen to be too small, this procedure is found to converge rapidly, requiring only 10–20 iterations at each (\mathbf{q}, ω) . The energies of the magnetic excitations at the wave-vector \mathbf{q} are then derived from the position of the peaks, of width $2\hbar\epsilon$, in the calculated response function $\text{Im}[\bar{\chi}(0; \mathbf{q}, \omega)]$.

The use of numerical methods, which is unavoidable in systems with complex moment-configurations, leads to less transparent results than those obtained analytically. However, compared with the linear spin-wave theory, they have the advantage that anisotropy effects may be included, even when they are large, without difficulty. The introduction of a non-zero value for ϵ means that the response function is only determined with a finite resolution, but this is not a serious drawback. The experimental results are themselves subject to a finite resolution, because of instrumental effects. Moreover, intrinsic linewidth phenomena, neglected within the RPA, provide a justification for adopting a non-zero ϵ .

The numerical method summarized above has been used for calculating the spin-wave energies in the various structures of Ho discussed in Section 2.3. In Fig. 5.9, we presented the dispersion relations in the c -direction of Ho containing 10% of Tb, in its ferromagnetic and helical phases (Larsen *et al.* 1987). The Tb content has the desirable effects of confining the moments to the basal plane, and inducing the simple bunched helix or zero-spin-slip structure (1.5.3) in the range 20–30 K, and ferromagnetism below 20 K. The commensurability of the 12-layer structure implies that the energy of the helix is no longer invariant under a uniform rotation, and an energy gap appears at long wavelengths, reflecting the force necessary to change the angle ϕ which the bunched moments make with the nearest easy axis. The excitations in this relatively straightforward structure can be treated by spin-wave theory, and the energies in the c -direction may be written in the form of eqn (6.1.10b):

$$E_{\mathbf{q}} = [A_{\mathbf{q}}^2 - B_{\mathbf{q}}^2]^{1/2},$$

where now

$$A_{\mathbf{q}} + B_{\mathbf{q}} = A + B + J\{\mathcal{J}_{\parallel}(\mathbf{0}) - \mathcal{J}_{\parallel}(\mathbf{q})\}, \quad (6.2.4a)$$

and

$$A_{\mathbf{q}} - B_{\mathbf{q}} = A - B + u^2 J \left\{ \mathcal{J}_{\perp}(\mathbf{Q}) - \frac{1}{2} \mathcal{J}_{\perp}(\mathbf{q} + \mathbf{Q}) - \frac{1}{2} \mathcal{J}_{\perp}(\mathbf{q} - \mathbf{Q}) \right\} \\ + v^2 J \left\{ \mathcal{J}_{\perp}(5\mathbf{Q}) - \frac{1}{2} \mathcal{J}_{\perp}(\mathbf{q} + 5\mathbf{Q}) - \frac{1}{2} \mathcal{J}_{\perp}(\mathbf{q} - 5\mathbf{Q}) \right\}. \quad (6.2.4b)$$

In this case, the axial- and hexagonal-anisotropy terms are

$$A + B = \frac{1}{J} \left\{ 6B_2^0 J^{(2)} - 60B_4^0 J^{(4)} + 210B_6^0 J^{(6)} + 6B_6^6 J^{(6)} \cos 6\phi \right\} \\ + J \left\{ u^2 \mathcal{J}_{\perp}(\mathbf{Q}) + v^2 \mathcal{J}_{\perp}(5\mathbf{Q}) - \mathcal{J}_{\parallel}(\mathbf{0}) \right\}, \quad (6.2.5a)$$

and

$$A - B = 36B_6^6 J^{(6)} \cos 6\phi, \quad (6.2.5b)$$

while u and v are determined from the bunching angle, by (1.5.3b), as respectively $\cos(\pi/12 - \phi)$ and $\sin(\pi/12 - \phi)$. As may be seen from the above expressions, the energy gap $E_{\mathbf{0}}$ in the periodic structure should be smaller than that in the ferromagnet by a factor of approximately $\cos 6\phi$, or about 0.8. The observed difference in Fig. 5.9 is considerably greater than this, and corresponds to an effective reduction of B_2^0 by about 50% in the helical phase. Such an effect can be accounted for by an anisotropic two-ion coupling of the type observed in Tb and considered in Section 5.5.2. Specifically, the term $\mathcal{C}(\mathbf{q})$ in eqn (5.5.19a) gives a contribution $\mathcal{C}(\mathbf{0})$ to $A + B$ in the ferromagnetic phase, and $\mathcal{C}(3\mathbf{Q}) \cos 6\phi$ in the bunched helical structure.

As in the ferromagnetic phase, treated in Section 5.5.1, the discontinuity in the dispersion relations at $\mathbf{q} = \mathbf{0}$ is due to the classical magnetic dipole–dipole interaction. As illustrated in Fig. 5.7, the basal-plane coupling $\mathcal{J}_{\perp}(\mathbf{q})$ has its maximum at $\mathbf{q} \simeq \mathbf{Q}$, but the jump in the long-wavelength limit in the dipolar contribution to $\mathcal{J}_{\parallel}(\mathbf{q}) - \mathcal{J}_{\parallel}(\mathbf{0})$, which has a magnitude $4\pi g\mu_B M$ or 0.28 meV, is sufficiently large that the absolute maximum in $\mathcal{J}_{\parallel}(\mathbf{q})$ is shifted from $\mathbf{q} = \mathbf{Q}$ to $\mathbf{q} = \mathbf{0}$. Consequently, the soft mode, whose energy goes to zero with the vanishing of the axial anisotropy at a temperature of 20 K in pure Ho, is the long-wavelength spin wave propagating perpendicular to the c -axis, rather than the mode of wave-vector \mathbf{Q} along the c -axis. As discussed in Section 2.3.1, the cone structure, rather than the tilted helix, is thereby stabilized. Near the second-order phase transition, the divergence of $\chi_{\zeta\zeta}(\mathbf{0}, 0)$ is accompanied by a vanishing of the energy gap as $(T - T_C)^{1/2}$.

The calculated small energy gap at the centre of the zone in the commensurate helix, shown in Fig. 5.9, is due to the bunching of the moments; $\varphi = \pi/2 + p\pi/3 \pm \phi$, where the sign before ϕ alternates from

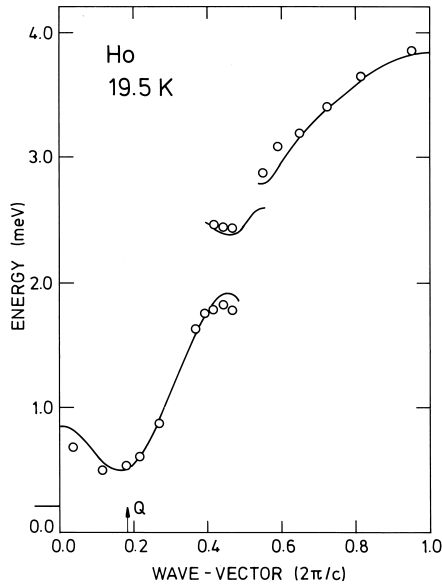


Fig. 6.4. Magnetic excitations propagating in the c -direction in the one-spin-slip structure of Ho at 20 K, after Patterson *et al.* (1990; and to be published). The full curve is the calculated dispersion relation and the points are the experimental results. The energy gap at $q = \frac{5}{11}(2\pi/c)$, due to the eleven-layer period, is resolved in these measurements. The linewidth of the scattering peaks behaves anomalously around $q = \frac{6}{11}(2\pi/c)$ suggesting a gap of the order of 0.3 meV at this wave-vector. The calculated energy of the long-wavelength modes in the basal plane is indicated by the line on the left. The discontinuity at $\mathbf{q} = \mathbf{0}$ is due to the dipolar coupling, and the transition to the cone structure is accompanied by a softening of this lowest-energy mode.

one layer to the next. This alternation doubles the periodicity in the rotating coordinate system, and thereby halves the Brillouin zone in the c -direction. The predicted gap is somewhat smaller than the experimental energy-resolution, and is therefore not observed in these measurements. The equivalent gap has however been measured in the one-spin-slip structure of Fig. 2.5 by Patterson *et al.* (1990), whose results are shown in Fig. 6.4. In this case, the 11-layer structure causes an eleven-fold reduction in the Brillouin zone, but only the first-order gap at $5/11$ times $2\pi/c$ is calculated to be readily observable. This gap, on the other hand, is amplified by about a factor two, as compared to that in the structure without spin slips. As the number of spin slips increases, the calculated excitation spectra (Jensen 1988a) become more complex,

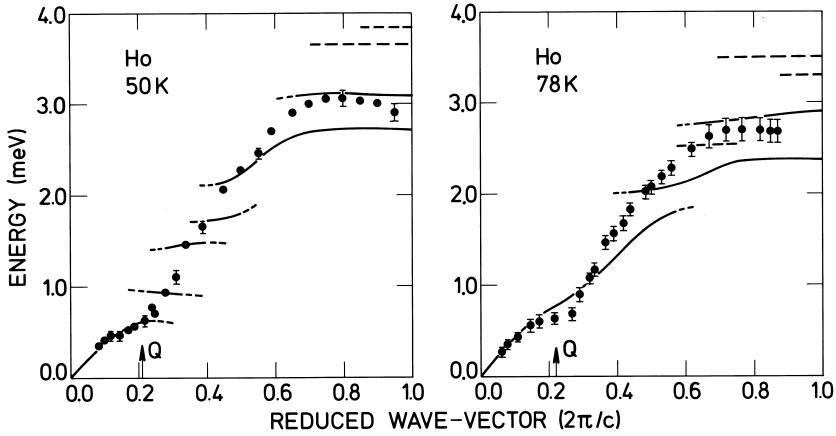


Fig. 6.5. The energies of the magnetic excitations propagating in the c -direction in the 19-layer and 9-layer spin-slip structures of Fig. 2.5. The solid lines indicate the positions of the main peaks in the calculated spectrum, whereas the dashed extensions designate peaks of relatively lower intensities. The energy gaps due to the reduced symmetry are not resolved in the experimental measurements of Nicklow (1971).

as illustrated in Fig. 6.5. The dispersion relations are broken into short segments by a succession of energy gaps, which may however be difficult to identify because of intrinsic broadening effects, neglecting in the RPA, which become more and more pronounced at increasing temperatures.

At temperatures above about 50 K, when $\langle O_6^6 \rangle$ in Ho is small and the distortion of the helix correspondingly weak, the large B_6^6 still plays an important role in mixing $|J_z\rangle$ molecular-field (MF) states. Indeed, as the temperature is increased and the exchange field decreases, this effect becomes relatively more important, so that, for example, the energy difference between the two lowest MF levels varies by an order of magnitude as the moment on the site moves from an easy to a hard direction at elevated temperatures, while this variation is much smaller in the low-temperature limit. The large changes in the MF states from site to site tend to disrupt the coherent propagation of the collective modes, providing a mechanism for the creation of energy gaps in the excitation spectrum. The spectrum thus becomes similar to that of the incommensurable longitudinal phase, illustrated in Fig. 6.3.

Whenever the moments are not along a direction of high symmetry, B_6^6 mixes the transverse and longitudinal components of the single-site susceptibility, so that the normal modes are no longer either pure transverse spin waves or longitudinal excitations. At low temperatures, where

$\langle J_z \rangle$ is close to its maximum value, this mixing is unimportant, but it has significant effects on the excitations at higher temperatures. In the RPA, the pure longitudinal response contains an elastic component, and the (mixed) excitation spectrum in the long-wavelength limit therefore comprises an elastic and an inelastic branch. The inelastic mode is calculated to lie around 1 meV in the temperature interval 50–80 K. In the RPA, this feature is independent of whether the magnetic periodicity is commensurable with the lattice. In the incommensurable structure, the free energy is invariant to a rotation of the helix around the c -axis, implying that $\bar{\chi}_t(\mathbf{q}, \omega)$ diverges in the limit $(\mathbf{q}, \omega) \rightarrow (\mathbf{0}, 0)$. However, the corresponding generator of rotations no longer commutes with the Hamiltonian, as in the regular helix, because B_0^6 is now non-zero. The divergence of $\bar{\chi}_t(\mathbf{q}, \omega)$ is therefore not reflected in a conventional Goldstone mode, but is rather manifested in the elastic, zero-energy phason mode, which coexists with the inelastic mode. Beyond the RPA, the elastic response is smeared out into a diffusive mode of non-zero width. This broadening may essentially eliminate the inelastic phason mode, leaving only a diffusive peak centred at zero energy in the long-wavelength limit. The intensity of this peak diverges, and its nominal width goes to zero, when the magnetic Bragg reflection is approached. However, a diffusive-like inelastic response is still present at $\mathbf{q} = \mathbf{0}$, and a true inelastic mode only appears some distance away. In the calculations, the elastic *single-site* response was assumed to be broadened by about 6 meV, corresponding to the spin-wave bandwidth. This assumption gives a reasonable account of the excitations in the long-wavelength limit, suggesting that they become overdamped if the wave-vector is less than about 0.1 times $2\pi/c$. Although the inelastic phason mode is largely eliminated, the calculations suggest that a residue may be observable. The most favourable conditions for detecting it would occur in a neutron-scattering scan with a large component of the scattering vector in the basal plane at about 50 K.

Another example to which the above theory has been applied is Tm (McEwen *et al.* 1991), where the c -axis moments order below 57.5 K in a longitudinally polarized structure, which becomes commensurable around 32 K. Below this temperature, as described in Section 2.3.1, the structure is ferrimagnetic, comprising four layers with the moments parallel to the c -axis, followed by three layers with the moments in the opposite direction. Although Tm belongs to the heavy end of the rare earth series, the scaling factor for the RKKY-exchange interaction, $(g-1)^2 = 1/36$, is small, and the Néel temperature is low compared to the crystal-field energy-splittings. The crystal-field effects are therefore more important in this element than in the other heavy rare earths. The energy difference between the MF ground state and the dipolar excited

state is calculated to vary between 8.0 and 10.2 meV, while the exchange field lies between 0 and 1.8 meV. Hence the exchange field acts as a minor perturbation, and incommensurable effects above 32 K in the excitation spectrum should be unimportant. In the low-temperature limit, the magnetic excitations are spin waves; the MF ground state and the first dipolar excited state are almost pure $|\pm 6\rangle$ and $|\pm 5\rangle$ levels (+ or – depending on the site considered). The excitations propagating in the c -direction are found to lie between 8.5 and 10 meV (Fernandez-Baca *et al.* 1990; McEwen *et al.* 1991). The magnetic period is seven times that of the lattice, and the exchange coupling splits the spin waves into seven closely lying bands, which cannot be separated experimentally. With a finite resolution, the exchange coupling leads to a single or, at some wave-vectors, a double peak, whose shape and width change with \mathbf{q} . At low temperatures, a relatively strong coupling between the spin waves and the transverse phonons is observed, and when this coupling is included in the determination of the RPA response functions, by the method presented in Section 7.3.1 in the next chapter, good agreement is obtained between the calculated neutron spectra and those observed experimentally. At elevated temperatures, both below and just above T_N , other excitations between the excited crystal-field (MF) levels are observed to be important, both in the transverse and the longitudinal components of the response function, and good agreement is again found between theory and experiment. With respect to its magnetic properties, Tm is thus an exceptional member of the heavy rare earths, as it is the only one in which well-defined crystal-field excitations have been detected. Hence it provides an appropriate termination of our discussion of spin-waves, as well as a natural transition to the crystal-field systems which are the topic of the next chapter.

CRYSTAL-FIELD EXCITATIONS IN THE LIGHT RARE EARTHS

A magnetic ion in a rare earth metal experiences a crystalline electric field from the surroundings, which gives rise to an overall splitting of the order 10–20 meV of the ionic ground-state J-multiplets. Crystal-field excitations are collective normal modes of the system, associated with transitions between the different levels of the ground-state multiplets. Even though there is an obvious qualitative difference between the crystal-field excitations in paramagnetic Pr and the spin waves in the isotropic ferromagnet Gd, it is not in general easy to give a precise prescription for differentiating between the two types of excitation. The spin-wave modes are derived from the precession which the moments execute when placed in a magnetic field. The two transverse components of a single moment change in time in a correlated fashion in such a precession, and this *phase-locking* is only possible when the time-reversal symmetry is broken. Hence the spin waves may be considered as the magnetic excitations related to the broken time-reversal symmetry of a magnetically ordered phase. However, spin waves may exist in the paramagnetic phase in the vicinity of the phase transition, if the time-reversal symmetry is broken locally. In the ordered phase, there may be additional magnetic excitations, associated either with the longitudinal fluctuations of the moments, or with further transitions between the MF levels, made possible by a strong mixing of the $|J_z\rangle$ -states in the crystal field, as discussed in Section 5.3.2. Depending on the circumstances, these additional excitations may be named crystal-field or molecular-field excitations. The effects of the crystal field, relative to that of the exchange field, are important in the four heavy rare earths Tb – Er, but not sufficiently to produce other well-defined magnetic excitations, in addition to the spin waves. In their paramagnetic phases, the temperature is sufficiently high, compared with the crystal-field splittings, that potential crystal-field excitations have such low intensity, and are so damped, as to be unobservable. Among the rare earth metals, crystal-field excitations are consequently only found in the light half of the series, and in Tm (McEwen *et al.* 1991) where, as discussed in the previous section, the crystal-field effects are relatively stronger because of the de Gennes scaling of the exchange.

We shall therefore concentrate our discussion on Pr, the paradigm

of crystal-field systems. We begin by using the RPA to analyse a number of model systems which, though oversimplified, contain much of the essential physics of the magnetic excitations, sometimes known as *magnetic excitons*, observed on both the hexagonal and the cubic sites in Pr. In the following section, it is shown how effects neglected in the RPA modify the *energies* and *lifetimes* of these excitations. The perturbations of the crystal-field system by the *lattice*, the *conduction electrons*, and the *nuclei* are then considered. This discussion is largely parallel to that of spin-wave systems in Chapter 5; the magnetoelastic interactions couple the phonons to the magnetic excitations and modify the elastic constants, and the conduction electrons limit the lifetimes of the excitations, especially at small q , while themselves experiencing a substantial increase in effective mass. The major effect of the *hyperfine interaction* has no counterpart in spin-wave systems, however, since it is able to induce *collective electronic–nuclear ordering* at low temperatures, and hence affect all magnetic properties drastically. Because the hexagonal sites in Pr constitute an *almost-critical system*, relatively small perturbations are able to drive it into a magnetically-ordered state. The effect of the *internal* interactions with the nuclei and magnetic impurities, and *external* perturbations by uniaxial stress or a magnetic field, are considered. Finally, we discuss a number of specific aspects of the magnetic excitations in Pr, in the paramagnetic and ordered phases.

7.1 MF-RPA theory of simple model systems

The general procedure for calculating the RPA susceptibility was outlined in Section 3.5. If we consider the Hamiltonian

$$\mathcal{H} = \sum_i \mathcal{H}_J(\mathbf{J}_i) - \frac{1}{2} \sum_{ij} \mathbf{J}_i \cdot \overline{\overline{\mathcal{J}}}(ij) \cdot \mathbf{J}_j, \quad (7.1.1)$$

which includes a general two-ion coupling between the dipolar moments, and assume the system to be in the paramagnetic state, we find the RPA susceptibility to be

$$\overline{\overline{\chi}}(\mathbf{q}, \omega) = \{1 - \overline{\overline{\chi}}^o(\omega) \overline{\overline{\mathcal{J}}}(\mathbf{q})\}^{-1} \overline{\overline{\chi}}^o(\omega), \quad (7.1.2)$$

which is a simple generalization of eqn (3.5.8), as in (6.1.7). The essence of the problem therefore lies in the calculation of the non-interacting susceptibility $\overline{\overline{\chi}}^o(\omega)$, as determined by the single-ion Hamiltonian $\mathcal{H}_J(\mathbf{J}_i)$. In the case of a many-level system, where J is large, this normally requires the assistance of a computer. Analytical expressions for $\overline{\overline{\chi}}(\mathbf{q}, \omega)$ may, however, be obtained for systems where the number of crystal-field levels is small, i.e. between 2–4 states corresponding to $J = \frac{1}{2}$, 1, or $\frac{3}{2}$. Such small values of J are rare, but the analysis of these models is also

useful for systems with larger J , if the higher-lying levels are not coupled to the ground state, and are so sparsely populated that their influence is negligible. According to *Kramers' theorem*, the states are at least doubly degenerate in the absence of an external magnetic field, if $2J$ is odd. In order to construct simple models with relevant level-schemes, we may consider a *singlet-singlet* or a *singlet-triplet* configuration, instead of systems with $J = \frac{1}{2}$ or $J = \frac{3}{2}$. These models may show some unphysical features, but these do not normally obscure the essential behaviour.

The simplest level scheme is that of the singlet-singlet model. This may be realized conceptually by lifting the degeneracy of the two states with $J = \frac{1}{2}$ with a magnetic field, and then allowing only one of the components of \mathbf{J} perpendicular to the field to interact with the neighbouring ions. This is the so-called *Ising model in a transverse field*. Assuming the coupled components to be along the α -axis, we need only calculate the $\alpha\alpha$ -component of $\overline{\chi}^o(\omega)$. The lower of the two levels, at the energy E_0 , is denoted by $|0\rangle$, and the other at E_1 by $|1\rangle$. The single-ion population factors are n_0 and n_1 respectively, and the use of eqn (3.5.20) then yields

$$\chi_{\alpha\alpha}^o(\omega) = \frac{2n_{01}M_\alpha^2\Delta}{\Delta^2 - (\hbar\omega)^2}, \quad (7.1.3)$$

where $M_\alpha = |\langle 0|J_\alpha|1\rangle|$ is the numerical value of the matrix element of J_α between the two states, while the two other (elastic) matrix elements are assumed to be zero. $\Delta = E_1 - E_0$ is the energy difference, and $n_{01} = n_0 - n_1$ is the difference in population between the two states. From eqn (7.1.2), we have immediately, since only $\mathcal{J}_{\alpha\alpha}(\mathbf{q})$ is non-zero,

$$\chi_{\alpha\alpha}(\mathbf{q}, \omega) = \frac{2n_{01}M_\alpha^2\Delta}{E_{\mathbf{q}}^2 - (\hbar\omega)^2}, \quad (7.1.4a)$$

where the *dispersion relation* is

$$E_{\mathbf{q}} = [\Delta\{\Delta - 2n_{01}M_\alpha^2\mathcal{J}_{\alpha\alpha}(\mathbf{q})\}]^{1/2}. \quad (7.1.4b)$$

These excitations are actually spin waves in this case of extreme axial anisotropy, but they have all the characteristics of crystal-field excitations. The energies are centred around Δ , the energy-splitting between the two levels, and the bandwidth of the excitation energies, due to the two-ion interaction, is proportional to the square of the matrix element, and to the population difference, between them. These factors also determine the neutron-scattering intensities which, from (3.2.18) and (4.2.3), are proportional to

$$\begin{aligned} S_d^{\alpha\alpha}(\mathbf{q}, \omega) &= \frac{1}{1 - e^{-\beta\hbar\omega}} \frac{n_{01}M_\alpha^2\Delta}{E_{\mathbf{q}}} \{\delta(\hbar\omega - E_{\mathbf{q}}) - \delta(\hbar\omega + E_{\mathbf{q}})\} \\ &\simeq M_\alpha^2 \frac{\Delta}{E_{\mathbf{q}}} \{n_0\delta(\hbar\omega - E_{\mathbf{q}}) + n_1\delta(\hbar\omega + E_{\mathbf{q}})\}. \end{aligned} \quad (7.1.5)$$

The approximate expression is obtained by using $\hbar\omega \simeq \pm\Delta$ in the temperature denominator.

The above results are only valid as long as the excitation energies remain positive for all \mathbf{q} . The mode of lowest energy is found at the wave-vector \mathbf{Q} at which $\mathcal{J}_{\alpha\alpha}(\mathbf{q})$ has its maximum. Introducing the critical parameter

$$R(T) = 1 - \frac{\chi_{\alpha\alpha}^{\circ}(0)}{\chi_{\alpha\alpha}(\mathbf{Q}, 0)}, \quad (7.1.6a)$$

which, in the present approximation, depends on T through n_{01} :

$$R(T) = 1 - (E_{\mathbf{Q}}/\Delta)^2 = n_{01}R_0 \quad ; \quad R_0 = \frac{2M_{\alpha}^2\mathcal{J}_{\alpha\alpha}(\mathbf{Q})}{\Delta}, \quad (7.1.6b)$$

we find that the excitation energies are all positive as long as $R(T) < 1$. This parameter increases monotonically when the temperature is lowered and, if the zero-temperature value R_0 is greater than one, the energy $E_{\mathbf{Q}}$ of the *soft mode* vanishes at a temperature $T = T_N$ (or T_C if $\mathbf{Q} = \mathbf{0}$) determined by $R(T_N) = 1$. Correspondingly, the susceptibility $\chi_{\alpha\alpha}(\mathbf{Q}, 0)$ becomes infinite at this temperature. This indicates that the system undergoes a second-order phase transition, from a paramagnetic phase to one which has the same symmetry as the soft mode. In this case, this means that $\langle J_{\alpha i} \rangle = \langle J_{\alpha} \rangle \cos(\mathbf{Q} \cdot \mathbf{R}_i + \varphi)$, where the MF equations have a non-zero solution for $\langle J_{\alpha} \rangle$ below, but not above, T_N .

We shall assume ferromagnetic ordering with $\mathbf{Q} = \mathbf{0}$. For the Ising model in a transverse field, the development of a ferromagnetic moment below T_C corresponds to a rotation of the moments away from the direction of the ‘transverse field’. The MF Hamiltonian in the ($|0\rangle$ $|1\rangle$)-basis is

$$\mathcal{H}_{\text{MF}}(i) = \begin{pmatrix} E_0 & -\delta \\ -\delta & E_1 \end{pmatrix} \quad ; \quad \delta = M_{\alpha}\mathcal{J}_{\alpha\alpha}(\mathbf{0})\langle J_{\alpha} \rangle. \quad (7.1.7)$$

Introducing the new eigenstates

$$\begin{aligned} |0'\rangle &= \cos\theta|0\rangle + \sin\theta|1\rangle \\ |1'\rangle &= \cos\theta|1\rangle - \sin\theta|0\rangle, \end{aligned} \quad (7.1.8a)$$

we find that the coupling parameter δ , due to the molecular field, gives rise to a non-zero moment $\langle 0'|J_{\alpha}|0'\rangle = M_{\alpha}\sin 2\theta$ in the ground state. Because it is a singlet, the ground state $|0\rangle$ in the paramagnetic phase is necessarily ‘non-magnetic’, in zero field. This condition does not apply in the ordered phase, so the nomenclature *induced-moment* system is frequently used. In the ordered phase, the splitting between the two singlets is $\Delta/\cos 2\theta$, and $\langle J_{\alpha} \rangle = n_{01}M_{\alpha}\sin 2\theta$ (where n_0 and n_1 are now

the population factors of the new eigenstates). The condition that \mathcal{H}_{MF} should be diagonal in the new basis requires that

$$\cos 2\theta = \frac{1}{n_{01}R_0}, \quad (7.1.8b)$$

which only has a solution if $n_{01}R_0 \geq 1$, in accordance with the critical condition $R(T_C) = 1$. The MF susceptibility is

$$\chi_{\alpha\alpha}^o(\omega) = \frac{2n_{01}M_\alpha^2\Delta \cos 2\theta}{(\Delta/\cos 2\theta)^2 - (\hbar\omega)^2} + \beta(n_0 + n_1 - n_{01}^2)M_\alpha^2 \sin^2 2\theta \delta_{\omega 0}, \quad (7.1.9)$$

revealing that there are now two kinds of excitation. The first is a continuation of the paramagnetic inelastic branch, with the dispersion relation

$$E_{\mathbf{q}}^2 = \frac{\Delta}{\cos 2\theta} \left(\frac{\Delta}{\cos 2\theta} - 2n_{01}M_\alpha^2\mathcal{J}(\mathbf{q}) \cos^2 2\theta \right), \quad (7.1.10)$$

which is again positive at all wave-vectors, consistent with the stability of the ordered phase. $E_{\mathbf{q}}$ therefore vanishes when T approaches T_C from above or below, and this kind of second-order phase transition is frequently known as a *soft-mode transition*. In addition to the inelastic mode, there appears a diffusive mode which, within the RPA, is purely elastic. The diffusive mode, but not the inelastic branch, has a parallel in the spectrum of the longitudinal fluctuations of a Heisenberg ferromagnet, described by eqn (3.5.27), since the spectrum analysed here is longitudinal relative to the polarization of the spontaneously ordered moment.

The behaviour discussed above is typical for a system where the crystal-field ground state is a singlet. The most characteristic feature of such a system is that the two-ion coupling must exceed a certain threshold value, relative to the crystal-field splitting, in order to force the system into a magnetically-ordered state at low temperatures. In this case, the condition is that the ratio R_0 must be greater than one. The general (MF) condition is that $\chi_{\alpha\alpha}^o(0)\mathcal{J}_{\alpha\alpha}(\mathbf{Q}) > 1$, for at least one of the α -components, where $\chi_{\alpha\alpha}^o(0)$ is the paramagnetic susceptibility at zero temperature. This condition is a consequence of the fact that the single-ion susceptibility remains finite in the zero-temperature limit, if the ground state is non-degenerate. If the ground state is degenerate, on the other hand, one or more components of the static single-ion susceptibility contains an elastic contribution proportional to $1/k_B T$, and its divergence in the $T = 0$ limit results in an ordering of the moments, within the MF approximation, no matter how weak the two-ion coupling. Fluctuations not included in the MF theory modify the critical

condition for $\mathcal{J}(\mathbf{Q})$, but the qualitative behaviour is unchanged. It is therefore possible to realize a system in which the moments are relatively strongly coupled to each other, but which remains paramagnetic at low temperatures, i.e. a crystal-field system in which cooperative effects are important. Perhaps the best example is elemental Pr, which is only slightly undercritical, with $R_0 \simeq 0.92$, and therefore exhibits a rich variety of unusual magnetic phenomena.

Pr crystallizes in the double hexagonal-close-packed (dhcp) structure, illustrated in Fig. 1.3, with the stacking sequence ABAC along the c -axis. This implies that there are two non-equivalent types of site of different symmetry in the crystal. The ions in A layers are in an approximately cubic environment, with nearest neighbours close to the fcc configuration, while those in the B and C layers experience a crystal field of hexagonal symmetry and form together an hcp structure. The tripositive Pr ion, with two $4f$ electrons, is a *non-Kramers* ion ($S = 1$, $L = 5$, and $J = 4$ for the ground-state multiplet) allowing the occurrence of singlet crystal-field states. Experimental observations, particularly of neutron scattering, have revealed that both kinds of site in fact have a singlet as the ground state. The lowest states of the *hexagonal* ions are the singlet $|J_\zeta = 0\rangle$ followed by the doublet $|J_\zeta = \pm 1\rangle$, with an energy difference of $\Delta_h \simeq 3.5$ meV, as illustrated in Fig. 1.16. If the distortion of the point symmetry of the *cubic* ions, due to the non-ideal c/a ratio, is neglected, their ground state is the Γ_1 -singlet, with the Γ_4 -triplet lying $\Delta_c \simeq 8.4$ meV above it. A complete survey of the classification and energies of crystal-field states in cubic surroundings has been given by Lea, Leask, and Wolf (1962). The possibility that the Γ_4 state is split into a singlet and a doublet, due to the deviation from cubic symmetry, has not yet been investigated experimentally. At temperatures well below 40 K (~ 3.5 meV), only the two ground states are populated significantly, and Pr may be considered to be a coupled singlet–doublet and singlet–triplet system. Furthermore, the difference between Δ_h and Δ_c is so large, compared to the two-ion interactions, that the excitation spectrum can be divided into two parts, related respectively to the crystal-field transitions on each kinds of ion. The weak coupling of the two components may be accounted for by second-order perturbation theory (Jensen 1976a), leading to an effective decoupling, with the two-ion parameters replaced by slightly different, effective values. Hence, at low temperature, Pr may be treated as a combination of a singlet–doublet system on an hcp lattice and a singlet–triplet system on a simple hexagonal lattice. Of these, the singlet–doublet system is much the more important because of the smaller value of the crystal-field splitting. The singlet–doublet scheme corresponds to an effective $J = 1$ and, if the two doublet states are defined to be $|1_s\rangle = (|+1\rangle + |-1\rangle)/\sqrt{2}$

and $|1_a\rangle = (|+1\rangle - |-1\rangle)/\sqrt{2}i$, the only non-zero matrix elements of \mathbf{J} are $\langle 1_a|J_\zeta|1_s\rangle = i$ and $\langle 0|J_\xi|1_s\rangle = \langle 0|J_\eta|1_a\rangle = \sqrt{J(J+1)}/2$, plus their Hermitian conjugates. In Pr, the matrix element of J_ζ is a factor of $\sqrt{10}$ smaller than the other matrix elements. This means that the transformation of the ($J = 4$) ion of Pr to an effective $J = 1$ system introduces a scaling of the two-ion couplings $\mathcal{J}_{\xi\xi}(\mathbf{q})$ and $\mathcal{J}_{\eta\eta}(\mathbf{q})$ by a factor of 10, compared to $\mathcal{J}_{\zeta\zeta}(\mathbf{q})$, and the latter may therefore be neglected to a first approximation. Hence the ($J = 1$) XY -model is an appropriate low-temperature description of the hexagonal ions in Pr.

The RPA theory of the XY -model, in the singlet-doublet case, is nearly identical to that developed above for the Ising model in a transverse field. One difference is that $n_0 + n_1 + n_2 = n_0 + 2n_1 = 1$, instead of $n_0 + n_1 = 1$, but since this condition has not been used explicitly (the population of any additional higher-lying levels is neglected), it may be considered as accounted for. The other modification of the above results is that there are now two components of $\bar{\chi}(\mathbf{q}, \omega)$ which are important: $\chi_{xx}^o(\omega) = \chi_{yy}^o(\omega)$ are given by the same expression as $\chi_{\alpha\alpha}^o(\omega)$ in eqn (7.1.3) (with $M_\alpha = 1$ when $J = 1$), whereas $\chi_{xy}^o(\omega) \equiv 0$ (the (xyz) -axes are assumed to coincide with the $(\xi\eta\zeta)$ -axes). This means that, for a Bravais lattice, there are two poles at positive energies in the RPA susceptibility (7.1.2) at each \mathbf{q} -vector. As long as $\mathcal{J}_{xy}(\mathbf{q}) = 0$, one of the modes describes a time variation of J_x alone, and the other J_y alone, and their dispersion relations are both given by eqn (7.1.4b), with α set equal to x or y . It is interesting to compare this result with the spin-wave case. Although the magnetic response is there also determined by a 2×2 matrix equation, it only leads to one (spin-wave) pole at positive energies, independently of whether the two-ion coupling is isotropic. The cancellation of one of the poles is due to the specific properties of $\chi_{xy}^o(\omega)$ in (5.1.3), produced by the molecular field (or the broken time-reversal symmetry) in the ordered phase. In the case considered above, the two modes may of course be degenerate, but only if $\mathcal{J}_{xx}(\mathbf{q})$ is equal to $\mathcal{J}_{yy}(\mathbf{q})$. In an hcp system, such a degeneracy is bound to occur, by symmetry, if \mathbf{q} is parallel to the c -axis. If the degeneracy is lifted by anisotropic two-ion couplings, which is possible in any other direction in \mathbf{q} -space, the x - and y -modes mix unless \mathbf{q} is parallel to a b -axis. The validity of the results derived above is not restricted to the situation where the doublet lies above the singlet. If the XY -model is taken literally, all the results apply equally well if Δ , and hence also n_{01} , is negative. However, if the z -components are coupled to some extent, as in Pr, the importance of this interaction is much reduced at low temperature if Δ is positive. In this case the zz -response, which is purely elastic,

$$\chi_{zz}(\mathbf{q}, \omega) \simeq \chi_{zz}^o(\omega) = 2\beta n_1 \delta_{\omega 0}$$

is frozen out exponentially in the low-temperature limit.

As shown in Fig. 7.1, the dispersion relations for the magnetic excitations on the hexagonal sites in Pr, measured by Houmann *et al.* (1979), illustrate many of the characteristic features of the ($J = 1$) XY -model. As mentioned above, when \mathbf{q} is along ΓM , the excitations are pure x - or y -modes. The hexagonal ions constitute an hcp structure, so there are an optical and an acoustic mode for each polarization. The excitation energies (7.1.4) are then generalized analogously to eqn (5.1.9), and since $\mathcal{J}_2(\mathbf{0})$ is negative in this case, the lower two branches are the optical modes. From intensity measurements of the type illustrated in Fig. 4.2, it may readily be deduced that the lowest branch is the longitudinal optical y -mode. The experimental dispersion relations show clearly that $\mathcal{J}_{xx}(\mathbf{q})$ and $\mathcal{J}_{yy}(\mathbf{q})$ have very different dependences on wave-vector, and that the anisotropic component is a substantial fraction of the two-ion coupling.

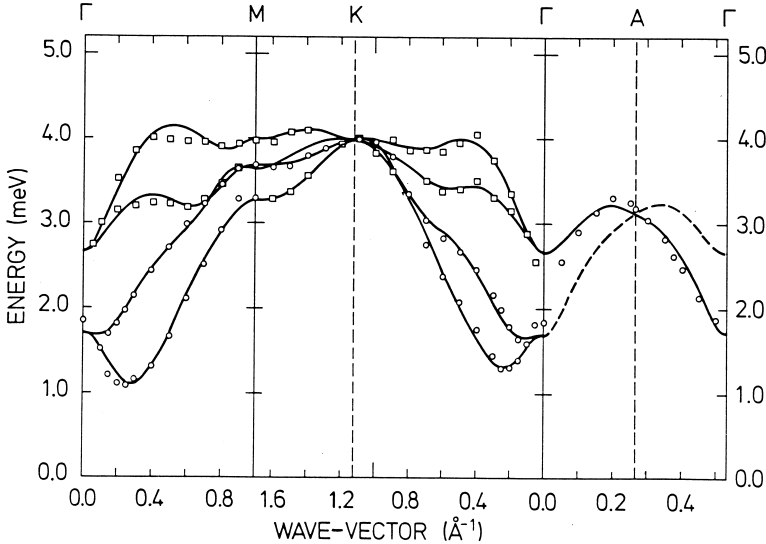


Fig. 7.1. Dispersion relations for the magnetic excitations propagating on the hexagonal sites of Pr at 6 K. In the basal plane, the squares and circles denote the experimental results for the acoustic and optical modes respectively. The double degeneracy of these excitations is lifted by anisotropic exchange, and the lower and upper branches correspond respectively to polarizations predominantly parallel and transverse to the wave-vector. The double-zone representation is used for the ΓA direction, along which the two transverse excitations are degenerate by symmetry, and therefore form a single branch.

The singlet–triplet model, relevant in the case of cubic symmetry and, with some modifications, also for the cubic ions in Pr, introduces one new feature; each component of the single-ion susceptibility includes a mixture of an elastic and an inelastic response. In surroundings with cubic symmetry, $\overline{\chi}^o(\omega)$ is proportional to the unit tensor, and the diagonal component is

$$\chi^o(\omega) = \frac{2n_{01}M_1^2\Delta}{\Delta^2 - (\hbar\omega)^2} + 2\beta n_1 M_2^2 \delta_{\omega 0}, \quad (7.1.11)$$

where now $n_0 + 3n_1 = 1$. This result follows from the circumstance that J_x , for instance, has a matrix element between the singlet state and one of the triplet states, and a matrix element between the two other triplet states, the numerical values of which are denoted by M_1 and M_2 respectively. In the $\Gamma_1 - \Gamma_4$ case with $J = 4$, corresponding to Pr, $M_1 = \sqrt{20/3}$ and $M_2 = 1/2$. The inelastic $\chi(\mathbf{q}, \omega \neq 0)$ is equivalent to (7.1.4) for the singlet–singlet system, but with M_α replaced by M_1 . Because of the elastic contribution, the critical condition $R(T_N) = 1$ is now determined from

$$R(T) = (2n_{01}M_1^2 + 2\beta\Delta n_1 M_2^2) \frac{\mathcal{J}_{\alpha\alpha}(\mathbf{Q})}{\Delta}. \quad (7.1.12)$$

The inelastic neutron-scattering spectrum is also determined by eqn (7.1.4) with $M_\alpha = M_1$ and $\alpha = x, y$, or z , when the off-diagonal coupling is neglected. The only difference is that there may now be three different branches, depending on the polarization. In addition to the inelastic excitations, the spectrum also includes a diffusive, elastic mode. In order to determine its contribution to the scattering function, $\delta_{\omega 0}$ in (7.1.11) may be replaced by $\delta^2 / \{\delta^2 - (\hbar\omega)^2\}$, and if the limit $\delta \rightarrow 0$ is taken at the end, the result is found to be:

$$\begin{aligned} S_d^{\alpha\alpha}(\mathbf{q}, \omega \approx 0) &= \frac{\chi^o(0) - \chi^o(\omega \rightarrow 0)}{\beta\{1 - \chi^o(\omega \rightarrow 0)\mathcal{J}_{\alpha\alpha}(\mathbf{q})\}\{1 - \chi^o(0)\mathcal{J}_{\alpha\alpha}(\mathbf{q})\}} \delta(\hbar\omega) \\ &= 2n_1 M_2^2 \left(\frac{\Delta}{E_{\mathbf{q}}}\right)^2 \frac{\chi_{\alpha\alpha}(\mathbf{q}, 0)}{\chi^o(0)} \delta(\hbar\omega). \end{aligned} \quad (7.1.13)$$

The two-ion coupling is assumed to be diagonal, and $\chi^o(\omega \rightarrow 0)$ is the static susceptibility without the elastic contribution. The scattering function at $\mathbf{q} = \mathbf{Q}$, integrated over small energies, diverges when T approaches T_N , as it also does in the singlet–singlet system. In the latter case, and in the singlet–doublet system, the divergence is related to the softening of the inelastic mode ($E_{\mathbf{Q}} \rightarrow 0$ when $T \rightarrow T_N$), as in eqn (7.1.5). In the singlet–triplet system, it is the intensity of the

elastic, diffusive mode which diverges, whereas the intensity of the inelastic mode stays finite and its energy is still non-zero at the transition. Within the simple MF-RPA theory, the critical behaviour has changed, because of the elastic term in the crystal-field susceptibility, so that the transition is no longer accompanied by a soft mode. The energy of the inelastic mode at $\mathbf{q} = \mathbf{Q}$, when T is close to T_N , depends on Δ and on how large the elastic term is at the transition. If this elastic contribution is small, the energy of the inelastic mode may be so small that it becomes overdamped because of the influence of the critical fluctuations, and therefore indistinguishable from the divergent diffusive peak. However, if the inelastic mode is sufficiently separated in frequency from the low-frequency critical fluctuations, it may persist as a reasonably well-defined excitation even near the phase transition.

The dhcp structure of Pr has four atoms per unit cell, so there are four branches of the dispersion relation for each polarization. If the hexagonal and cubic sites are decoupled, these decompose into two sets, each comprising two modes, which may be described as acoustic and optical, propagating on the sites of a particular symmetry. The complementary excitations to those of Fig. 7.1 propagate on the cubic sites, and their dispersion relations, also studied by Houmann *et al.* (1979), are illustrated in Fig. 7.2. If the hexagonal sites are ignored, the cubic sites lie on a simple hexagonal lattice, so that a double zone may be

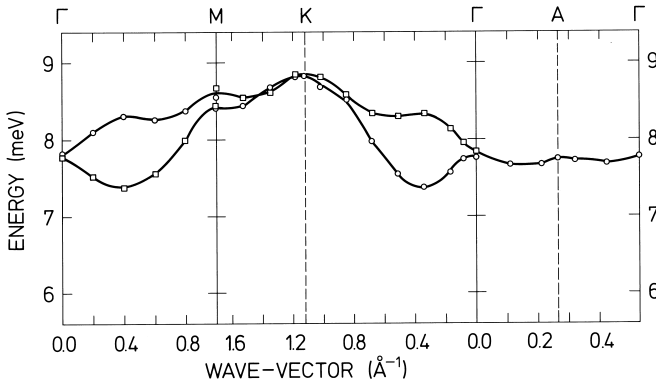


Fig. 7.2. Dispersion relations for the excitations propagating on the cubic sites of Pr at 6 K, plotted in the Brillouin zone of the dhcp structure. The upper and lower branches in the basal plane are respectively the acoustic and optical modes. The polarization vector of these excitations is perpendicular to the c -axis. In contrast to Fig. 7.1, no splitting of these branches by anisotropic two-ion coupling is observed, within the experimental resolution of about 0.5 meV.

used. However, it is both more convenient and, in general, more correct to use the true Brillouin zone for the dhcp structure, as in Fig. 7.2. The excitations in this figure are polarized in the plane, and may also be described by (7.1.4), with parameters appropriate to the cubic sites. The z -modes were not observed in these experiments, on account of the neutron scans employed. The dispersion is much smaller than that on the hexagonal sites and, in particular, it is negligible in the c -direction, indicating very weak coupling between planes of cubic ions normal to this axis. Again in contrast to the hexagonal ions, the splitting between modes of different polarization is not resolved, demonstrating that the anisotropy in the two-ion coupling is smaller.

7.2 Beyond the MF-RPA theory

When the temperature is raised, the available magnetic scattering intensity, from eqn (4.2.7) proportional to $J(J+1)$, is divided more and more equally among the $(2J)!$ different dipolar transitions, and in the high-temperature limit half the intensity is transferred to the emissive part of the spectrum. This means that the different crystal-field excitations become weaker and less dispersive, and correspondingly correlation effects become less important as the temperature is raised. An additional mechanism diminishing the correlation effects at elevated temperatures is the scattering of the excitations against random fluctuations, neglected in the MF-RPA theory. In this theory, all the ions are assumed to be in the same MF state, thus allowing an entirely coherent propagation of the excitations. However, at non-zero temperatures, the occupations of the different crystal-field levels differ from site to site, and these *single-site fluctuations* lead to a non-zero linewidth for the excitations. In fact, if two-ion interactions are important, such fluctuations already exist at zero temperature, as the MF ground state $\prod_i |0_i\rangle$ cannot be the true ground state, because $\sum_i |0_i\rangle\langle 0_i|$ does not commute with the two-ion part of the Hamiltonian. Hence, the occupation n_0 of the ‘ground-state’ is reduced somewhat below 1 even at $T = 0$. The response functions derived above already predict such a reduction of n_0 but, as discussed earlier in connection with eqn (3.5.23), the MF-RPA theory is not reliable in this order. A more satisfactory account of the influence of fluctuations, both at zero and non-zero temperatures, can only be obtained by calculations which go beyond the MF-RPA.

One way to proceed to higher order is to postpone the use of the RPA decoupling to a later stage in the Green-function hierarchy generated by the equations of motion. Returning to our derivation of the MF-RPA results in Section 3.5; instead of performing the RPA decoupling on the Green function $\langle\langle a_{\nu\xi}(i)a_{\nu'\mu'}(j); a_{rs}(i')\rangle\rangle$, as in eqn (3.5.16), we first apply this decoupling to the higher-order Green functions appearing in

the equation of motion of this function. This method requires rather extensive manipulation, but it is essentially straightforward, and we shall not discuss the details here. It has been applied to the ($J = 1$)-model, corresponding to Pr (Jensen 1982b), and the results may be interpreted by replacing the crystal-field splitting and the exchange coupling by renormalized quantities, while the excitations acquire a linewidth proportional to the fluctuations in the single-site population factors. As may be seen in Fig. 7.3, this *self-consistent RPA* gives a good account of the temperature dependence of the excitations on the hexagonal sites in Pr, and fits the results of Houmann *et al.* (1975b) somewhat better than their MF model. The mode of lowest energy varies very rapidly with

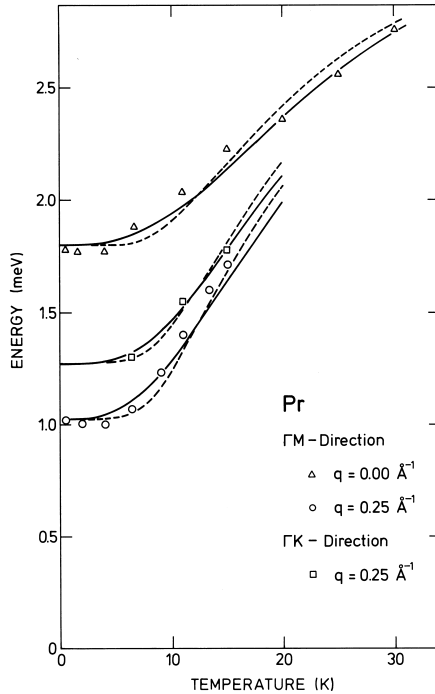


Fig. 7.3. The temperature dependence of the excitation energies at three different wave-vectors for the hexagonal sites in Pr. The dashed lines give the results of a MF calculation, and the full curves are based on the self-consistent RPA. The lowest-lying mode is the incipient soft mode, whose \mathbf{q} and longitudinal polarization correspond to the antiferromagnetic structure which may be induced in Pr by various perturbations.

temperature, but does not become soft, so Pr remains paramagnetic down to very low temperatures. However, these calculations indicate that $R_0 \simeq 0.92$, so that the exchange is very close to the critical value which would drive this *incipient soft mode* to zero energy. As we shall discuss in Section 7.4.1, under these circumstances a variety of perturbations may induce magnetic ordering.

A more elegant technique for obtaining such results is based on a diagrammatic-expansion technique. The introduction of this method requires a further development and refinement of the mathematical analysis of the Green functions, which falls outside the scope of this book. Nevertheless, we wish to discuss some essential problems connected with the use of the technique for rare earth systems, so we will present it very briefly and refer to the books by Abrikosov *et al.* (1965), Doniach and Sondheimer (1974), and Mahan (1990) for more detailed accounts.

Instead of the *retarded* Green function, introduced in eqn (3.3.12), we consider the Green function defined as the τ -ordered ensemble average: $G_{BA}^\tau(\tau_1 - \tau_2) \equiv -\langle T_\tau \hat{B}(\tau_1) \hat{A}(\tau_2) \rangle$. Here $\hat{B}(\tau)$ is the equivalent of the time-dependent operator in the Heisenberg picture, eqn (3.2.1), with t replaced by $-i\hbar\tau$. The τ -ordering operator T_τ orders subsequent operators in a sequence according to decreasing values of their τ -arguments, i.e. $T_\tau \hat{B}(\tau_1) \hat{A}(\tau_2) = \hat{B}(\tau_1) \hat{A}(\tau_2)$ if $\tau_1 \geq \tau_2$ or $\hat{A}(\tau_2) \hat{B}(\tau_1)$ otherwise. Restricting ourselves to considering the Green function $G_{BA}^\tau(\tau)$ only in the interval $0 \leq \tau \leq \beta$, where $\beta = 1/k_B T$, we may represent it by a Fourier series (corresponding to letting the function repeat itself with the period β):

$$G_{BA}^\tau(\tau) = -\langle T_\tau \hat{B}(\tau) \hat{A} \rangle = \frac{1}{\beta} \sum_n G_{BA}^\tau(i\omega_n) e^{-i\hbar\omega_n\tau} \quad ; \quad \hbar\omega_n = \frac{2\pi n}{\beta}. \quad (7.2.1a)$$

n is an integer and the ω_n are called the *Matsubara frequencies*. The Fourier coefficients are determined by

$$G_{BA}^\tau(i\omega_n) = \int_0^\beta G_{BA}^\tau(\tau) e^{i\hbar\omega_n\tau} d\tau. \quad (7.2.1b)$$

The most important property of the τ -ordered Green function is that it can be calculated by perturbation theory using the *Feynman-Dyson* expansion. By dividing the Hamiltonian into two parts, $\mathcal{H} = \mathcal{H}_0 + \mathcal{H}_1$, and denoting the ensemble average with respect to the ‘unperturbed’ Hamiltonian \mathcal{H}_0 by an index ‘0’, it can be shown that

$$G_{BA}^\tau(\tau) = -\frac{\langle T_\tau U(\beta, 0) \hat{B}(\tau) \hat{A}(0) \rangle_0}{\langle U(\beta, 0) \rangle_0}, \quad (7.2.2a)$$

where

$$U(\beta, 0) = 1 - \int_0^\beta \mathcal{H}_1(\tau_1) d\tau_1 + \cdots \\ \cdots + \frac{(-1)^n}{n!} \int_0^\beta \cdots \int_0^\beta T_\tau \mathcal{H}_1(\tau_1) \cdots \mathcal{H}_1(\tau_n) d\tau_1 \cdots d\tau_n + \cdots \quad (7.2.2b)$$

which is suitable for a diagrammatic representation in which the denominator in (7.2.2a) just eliminates all ‘un-linked’ diagrams. Furthermore, it can be shown that the retarded Green function is the analytic continuation of the τ -ordered function to the real axis in the complex ω -plane, or

$$\chi_{BA}(\omega) = - \lim_{\epsilon \rightarrow 0^+} G_{BA}^T(i\omega_n \rightarrow \omega + i\epsilon), \quad (7.2.3)$$

and we shall therefore use the frequency arguments $i\omega_n$ and ω to distinguish between respectively the τ -ordered and the retarded Green function.

Considering the simplest case of the Ising model, we wish to calculate the Fourier transform of $G(ij, \tau) = -\langle T_\tau J_{i\alpha}(\tau) J_{j\alpha} \rangle$. We take \mathcal{H}_0 to be the single-ion crystal-field Hamiltonian, and the perturbation \mathcal{H}_1 is then the two-ion part. With this partition, the ensemble average $\langle \rangle_0$ of a product of operators belonging to different sites is just the product of the averages of the operators, i.e. $\langle J_{i\alpha} J_{j\alpha} \rangle_0 = \langle J_{i\alpha} \rangle_0 \langle J_{j\alpha} \rangle_0$ if $i \neq j$. This concentrates attention on the Green function for a single site $G(ii, i\omega_n)$, for which the perturbation expansion leads to a series corresponding to that considered in the CPA calculation, eqn (5.6.9). The only differences are that $\overline{K}(i, \omega)$ is replaced by the $\alpha\alpha$ -component $K(i\omega_n)$ and, more significantly, that the products $(c_i \chi^o(\omega))^p = c_i (\chi^o(\omega))^p$ are replaced by the $2p$ th order *cumulant* averages or *semi-invariants*

$$\mathcal{S}^{(2p)} = \frac{1}{\beta^p} \int_0^\beta d\tau_1 \cdots \int_0^\beta d\tau_{2p} \langle T_\tau \prod_{l=1}^{2p} J_{i\alpha}(\tau_l) \rangle_0 \prod_{l=1}^{2p} \exp(i\hbar\omega_{nl}\tau_l), \quad (7.2.4)$$

with the conditions $\sum_l \omega_{nl} = 0$ and $\omega_{n1} = \omega_n$. The lowest-order semi-invariant is $\mathcal{S}^{(2)} = -g(i\omega_n) = 2n_{01} M_\alpha^2 \Delta / [\Delta^2 - (i\hbar\omega_n)^2]$, which is the Fourier transform of $\langle T_\tau J_{i\alpha}(\tau) J_{i\alpha} \rangle_0$, and $-g(i\omega_n \rightarrow \omega) = -g(\omega) = \chi^o(\omega)$. The calculation of the fourth- and higher-order cumulants is more involved. It is accomplished basically by utilizing the invariance of the trace (i.e. of the ensemble average) to a cyclic permutation of the operators, as is discussed, for instance, by Yang and Wang (1974) and Care and Tucker (1977). If the operators are proportional to Bose operators this results in *Wick's theorem*, which here implies that $\mathcal{S}_{\text{Bose}}^{(2p)} = [\mathcal{S}^{(2)}]^p$. The determination of the cumulant averages is facilitated by

expressing the angular-momentum components as linear combinations of the standard-basis operators introduced by eqn (3.5.11). These are not Bose operators, so the ‘contractions’ determined by the commutators of the different operators are not c -numbers, but operators which give rise to new contractions. In the singlet–singlet Ising model, the result is

$$\begin{aligned} G(ii, i\omega_n) &= G(i\omega_n) = g(i\omega_n) \\ &- \frac{1}{n_{01}^2} \left[(n_0 + n_1)g(i\omega_n)K(i\omega_n) + \frac{1}{\beta} \sum_{n'} g(i\omega_{n'})K(i\omega_{n'})u(n, n') \right] g(i\omega_n) \\ &+ \dots \end{aligned} \quad (7.2.5a)$$

with

$$u(n, n') = \frac{g(i\omega_n)}{M_\alpha^2} + \frac{g(i\omega_{n'})}{M_\alpha^2} \frac{(i\hbar\omega_{n'})^2 + \Delta^2}{2\Delta^2} + \frac{1}{2}(n_0 + n_1 - n_{01}^2)\beta. \quad (7.2.5b)$$

The sum over the Matsubara frequencies may be transformed into an integral over real frequencies, but it may be advantageous to keep the frequency sum in numerical calculations. Before proceeding further, we must clarify a few points. The first is that \mathcal{H}_1 cannot, in general, be considered as being ‘small’ compared to \mathcal{H}_0 . However, each time a term involving the two-ion coupling is summed over \mathbf{q} , we effectively gain a factor $1/Z$, where Z is the co-ordination number. Hence, if we use $1/Z$ as a small expansion parameter, the order of the different contributions may be classified according to how many \mathbf{q} -summations they involve. In the equation above, $K(i\omega_{n'})$ is derived from one summation over \mathbf{q} , as in (5.6.17), so the series can be identified as being equivalent to an expansion in $1/Z$. The second point to realize is that it is of importance to try to estimate how the expansion series behaves to infinite order. A truncation of the series after a finite number of terms will produce a response function with incorrect analytical properties. If we consider the corresponding series determining $G(\mathbf{q}, i\omega_n)$, it is clear that any changes in the position of the poles, i.e. energy changes and linewidth phenomena, are reflected throughout the whole series, whereas a (small) scaling of the amplitude of the response function, which might be determined by the first few terms, is not particularly interesting. In other words, what we wish to determine is the first- (or higher-) order correction in $1/Z$ to the denominator of the Green function, i.e. to determine the self-energy $\Sigma(\mathbf{q}, i\omega_n)$, defined by

$$G(\mathbf{q}, i\omega_n) = \frac{g(i\omega_n)}{1 + g(i\omega_n)\{\mathcal{J}_{\alpha\alpha}(\mathbf{q}) + \Sigma(\mathbf{q}, i\omega_n)\}}, \quad (7.2.6)$$

assuming the MF-RPA response function to be the starting point. A systematic prescription for calculating the Green function to any finite

order in $1/Z$ has been given by Stinchcombe (1973), see also Vaks *et al.* (1968). The zero-order result is obtained by the ‘boson’ approximation $\mathcal{S}^{(2p)} \simeq [\mathcal{S}^{(2)}]^p$. As is apparent from (7.2.5a), this corresponds to the replacement of the second and subsequent terms on the r.h.s. by the infinite series generated by $-g(i\omega_n)K(i\omega_n)G(i\omega_n)$, leading to an equation for the single-site Green function which is the equivalent to the *Dyson equation* for bosons (or fermions), or to the CPA equation with $c = 1$. The \mathbf{q} -dependent Green function may be obtained from the single-site function by the same procedure as in the CPA case, eqns (5.6.10–17). In this approximation, the final Green function is that given by the MF-RPA, corresponding to $\Sigma(\mathbf{q}, i\omega_n) = 0$ in (7.2.6). This does not involve any \mathbf{q} -summation and may therefore be classified as the $(1/Z)^0$ -order result. In the *cumulant-expansion*, developed by Stinchcombe (1973) and others, the difference $\mathcal{S}^{(4)} - (\mathcal{S}^{(2)})^2$ is included, to the next order in $1/Z$, as an additional *vertex* appearing in the interaction chain-diagrams of $G(\mathbf{q}, i\omega_n)$, independently of the appearance of the $\mathcal{S}^{(2)}$ -vertices. A different approach, which is made possible by the isolation of the single-site Green function in (7.2.5a), is to generalize this equation once more, so that it becomes a Dyson equation, by replacing $g(i\omega_n)$ with $G(i\omega_n)$ in the second term on the r.h.s. of (7.2.5a), retaining the correct coefficient in this term. The effective-medium equation (5.6.13), with $c = 1$, is valid to first order in $1/Z$, so that

$$G(\mathbf{q}, i\omega_n) = \frac{G(i\omega_n)}{1 + G(i\omega_n)\{\mathcal{J}_{\alpha\alpha}(\mathbf{q}) - K(i\omega_n)\}} \quad (7.2.7a)$$

and, in combination with the Dyson equation for the single-site Green function, this leads to a \mathbf{q} -dependent Green function derived from

$$\begin{aligned} \Sigma(\mathbf{q}, i\omega_n) &= \Sigma(i\omega_n) = \\ &= \frac{1}{n_{01}^2} \left[(n_0 + n_1 - n_{01}^2)K(i\omega_n) + \frac{1}{\beta g(i\omega_n)} \sum_{n'} g(i\omega_{n'})K(i\omega_{n'})u(n, n') \right], \end{aligned} \quad (7.2.7b)$$

where $K(i\omega_n)$ is determined self-consistently, as in (5.6.17),

$$K(i\omega_n) = \sum_{\mathbf{q}} \mathcal{J}_{\alpha\alpha}(\mathbf{q})G(\mathbf{q}, i\omega_n) / \sum_{\mathbf{q}} G(\mathbf{q}, i\omega_n). \quad (7.2.7c)$$

The result obtained in this way is close to that derived by Galili and Zevin (1987) using a more elaborate renormalization procedure, but in addition to the simplifications attained by utilizing the effective-medium approximation, the procedure which we have adopted has allowed us to achieve a fully self-consistent result. We note that, in the application

of the equations of motion, the population factors take the realistic values which may be calculated from eqn (3.5.23) using the more accurate Green functions, whereas the population factors here are by definition the unperturbed MF values. This means that the renormalization of the different RPA parameters predicted by the real part of $\Sigma(\omega)$ includes the possible effects on the population factors. $\Sigma(\omega)$ is the continuation of $\Sigma(i\omega_n)$ on to the real frequency-axis, and the imaginary part of $\Sigma(\omega)$, which is equal to $(n_0 + n_1 - n_{01}^2)/n_{01}^2$ times $\text{Im}[K(\omega)]$, since the sum in (7.2.7b) is real, predicts a non-zero linewidth for the crystal-field excitations. Introducing the spectral density of the excited states, at positive energies $E = \hbar\omega$,

$$\mathcal{N}(E) = \frac{2}{N} \sum_{\mathbf{q}} \frac{\text{Im}[G(\mathbf{q}, E/\hbar)]}{\pi E G(\mathbf{q}, 0)} \simeq \frac{1}{N} \sum_{\mathbf{q}} \delta(E_{\mathbf{q}} - E),$$

which may be compared with (3.3.17), we find that, at frequencies where $|g(\omega)K(\omega)|$ is small compared to one,

$$\text{Im}[K(\omega)] \simeq \pi n_{01} M_{\alpha}^2 \mathcal{N}(\hbar\omega) \Delta / \hbar\omega g^2(\omega),$$

corresponding to a linewidth $2\Gamma_{\mathbf{q}}$ of the excitation at \mathbf{q} , half of which is

$$\Gamma_{\mathbf{q}} \simeq \frac{n_0 + n_1 - n_{01}^2}{n_{01}^2} \left(\frac{\Delta^2 - E_{\mathbf{q}}^2}{2E_{\mathbf{q}}} \right)^2 \pi \mathcal{N}(E_{\mathbf{q}}). \quad (7.2.8a)$$

The linewidth is proportional to the density of states and to the squared energy-difference between the excitation and the crystal-field level (proportional to $\mathcal{J}_{\alpha\alpha}^2(\mathbf{q})$), where the \mathbf{q} -dependences of the two factors roughly balance each other. When $E_{\mathbf{q}}$ is close to Δ , this result is no longer valid. Instead, at $\hbar\omega = \tilde{\Delta}$, where $\tilde{\Delta}$ is the effective crystal-field splitting determined by $\text{Re}[\Sigma(\tilde{\Delta}/\hbar)] = -1/g(\tilde{\Delta}/\hbar)$, we find that $\text{Re}[K(\tilde{\Delta}/\hbar)] = 0$ and

$$\Gamma_{\mathbf{q}}(E_{\mathbf{q}} = \tilde{\Delta}) \simeq \frac{n_0 + n_1 - n_{01}^2}{n_{01}^2} \frac{1}{\pi \mathcal{N}(\tilde{\Delta})}. \quad (7.2.8b)$$

The first result (7.2.8a) for $\Gamma_{\mathbf{q}}$, but not (7.2.8b), agrees with that obtained by the cumulant-expansion method of Stinchcombe (1973) and others. One modification which appears when this method is used is that $K(\omega)$ in (7.2.7b) is replaced by $K(\omega)\{1 - G(\omega)K(\omega)\}$. This is a $(1/Z)^2$ -correction, which however becomes important when $\hbar\omega \approx \Delta$, and in this theory $\Gamma_{\mathbf{q}}(E_{\mathbf{q}} = \Delta) = 0$, in contrast to the result (7.2.8b). In order to decide which of the two procedures leads to the most trustworthy results, we have to some extent to rely on the effective-medium

approximation. It is known (Yonezawa 1968) that the cumulant expansion, in solving the dilute RPA equation (5.6.8), includes all terms proportional to $P_2(ij) = \langle c_i c_j \rangle - c^2$, but that this occurs at the expense of ‘self-containedness’, leading to unphysical features in the final results. Compared to this, the CPA neglects some of the products of $P_2(ii)P_2(jj)$ for neighbouring sites, which are of the order $(1/Z)^2$ (see the discussion following (5.6.17)), but it is self-contained and the results are well-behaved and accurate if Z is not small, as discussed by Elliott *et al.* (1974). Hence, referring to the analyses of the dilute systems, we expect the effective-medium approximation to be more adequate than the unrestricted cumulant expansion in the first order of $1/Z$. More importantly, the Hartree–Fock decoupling of the higher-order cumulants, i.e. $\mathcal{S}^{(6)} = (\mathcal{S}^{(2)})^3 + 3\mathcal{S}^{(2)}\{\mathcal{S}^{(4)} - (\mathcal{S}^{(2)})^2\}$ to first order in $1/Z$, which is one of the basic ideas behind the cumulant-expansion method considered here, does not appear to be a good approximation. The effective-medium model is not solved ‘exactly’, as this would require a determination of the whole series for $G(i\omega_n)$ in (7.2.5a), but a consideration of the second- and higher-order diagrams in this series indicates that the Dyson-equation generalization is much more reasonable. The sum rules, like (3.3.18) or the ‘monotopic restriction’ discussed by Haley and Erdős (1972), are satisfied to the considered order in $1/Z$. This is obviously true for the unrestricted cumulant expansion, but it also holds for the effective-medium approximation, as this is derived directly from the behaviour of the single sites. One may ask (Galili and Zevin 1987) whether there exists any other ‘conservation law’ which permits a more stringent distinction between the various possibilities. For this purpose, we propose to use the condition that the resultant Green function should be independent of adding the following constant to the Hamiltonian:

$$\Delta\mathcal{H} = -\lambda \sum_i \mathbf{J}_i \cdot \mathbf{J}_i = -N \lambda J(J+1), \quad (7.2.9)$$

corresponding to a replacement of $\mathcal{J}(\mathbf{q})$ by $\mathcal{J}(\mathbf{q}) + \lambda$. This change does not affect the effective-medium equation (5.6.9), other than by adding the constant to $\mathcal{J}(\mathbf{q})$, so $K(i\omega_n)$ is still determined by (7.2.7c), with λ added on the r.h.s. A replacement of $K(i\omega_n)$ by $K(i\omega_n) + \lambda$ in (7.2.5a) does not make any difference, as $(1/\beta) \sum_{n'} g(i\omega'_n) u(n, n') = -g(i\omega_n)$ when $n_0 + n_1 = 1$, so that $J_{i\alpha} J_{i\alpha}$ is a constant. The additions of λ to both $J(\mathbf{q})$ and $K(i\omega_n)$ cancel out in the \mathbf{q} -dependent Green function expressed in terms of the single-site Green function, as may be seen from (7.2.7a), so that the final result is independent of λ . This is not the case when the unrestricted cumulant expansion is used. Formally, the occurrence of λ is a $(1/Z)^2$ -effect, but this is an unphysical feature which is a serious defect, since λ may assume an arbitrary value. This

variational test is related to the sum rules (like that considered in eqn (4.2.7) or below), but it has the advantage that it applies directly to the \mathbf{q} -dependent Green function without involving any additional summations with respect to \mathbf{q} or ω_n . For a final comparison of the two methods, we may utilize the fact that the single-site series can be summed exactly in an Ising system with no crystal-field splitting. The result is $G(\omega) = -\beta\delta_{\omega 0}\langle J_\alpha^2 \exp\{\frac{1}{2}\beta K(0)J_\alpha^2\}\rangle_0 / \langle \exp\{\frac{1}{2}\beta K(0)J_\alpha^2\}\rangle_0$, which coincides with that deduced by Lines (1974b, 1975) from his *correlated effective-field* theory. When $J = 1/2$, the above method produces the correct result $G(0) = g(0) = -\beta/4$. For the ($J = 1$)-Ising model, $G(0) = -2\beta[2 + \exp\{-\frac{1}{2}\beta K(0)\}]^{-1}$, which may be compared with the prediction $G(0) = -2\beta[3 - \frac{1}{2}\beta K(0)]^{-1}$ of eqns (7.2.5-7). On the other hand, the unrestricted cumulant expansion, to first order in $1/Z$, leads to spurious contributions of second and higher powers in $K(0)$ and, for instance, suggests a second-order term in the denominator of $G(0)$ which is a factor of 14 larger than the correct value. We note that corrections to the effective-medium theory only appear in the order $(1/Z)^3$ in the *single-site* Green function. This comparison is discussed in more detail by Jensen (1984), in a paper where the $1/Z$ -expansion, in the effective-medium approximation, is combined with the CPA, thereby removing some of the difficulties encountered in the RPA and mentioned at the end of Section 5.6.

In a crystal-field system, the single-site fluctuations lead to a non-zero linewidth of the excitations, to first order in $1/Z$. This reflects the relative importance of corrections to the RPA, compared to spin-wave systems. In the latter, the excitation operators are, to a good approximation, Bose operators, neglecting the ‘kinematic’ effects, which means that a non-zero linewidth only appears in the second-order of $1/Z$. The linewidth $2\Gamma_{\mathbf{q}}$ derived above is exponentially small at low temperatures, but becomes important when $k_B T \approx \Delta$. The linewidth as a function of ω , $\Gamma_{\mathbf{q}}(\omega) \propto \text{Im}[K(\omega)]$, is only non-zero as long as $\hbar\omega$ lies within the excitation energy-band, which roughly corresponds to that determined by the RPA. This means that the linewidth, in this approximation, begins to decrease at higher temperatures when the RPA-excitation band becomes sufficiently narrow. The behaviour in both limits is modified by higher-order effects. Within the framework of the $1/Z$ -expansion, the effective-medium approximation ceases to be valid in second order. The leading-order scattering effects are due to the single-site fluctuations and, if the interactions are long-range, the correlation of the fluctuations on neighbouring sites only leads to minor modifications (provided that the system is not close to a second-order phase transition). In this kind of system, the effective-medium method should be satisfactory, and in order to avoid the complications encountered in more elaborate theo-

ries, we confine ourselves to the $(1/Z)^2$ -corrections which can be determined within this approximation. This provides a better estimate of the effects due to the single-site fluctuations, but neglects the possible \mathbf{q} -dependence of the self-energy. The correct $(1/Z)^2$ -terms in the effective-medium theory are obtained by introducing $\mathcal{S}^{(6)}$ in the third term of the single-site series in eqn (7.2.5). This calculation has been carried out by Jensen *et al.* (1987) for the ($J = 1$)-singlet-doublet case, and the most important effect of the second-order terms is to replace the MF population-factors in (7.2.7b) by approximately the actual population of the excitonic states. Furthermore, $\Gamma_{\mathbf{q}}(\omega)$ becomes non-zero outside the excitation band, and it stays non-zero (although small) in the $T = 0$ limit.

The ($J = 1$)-case has been analysed by Yang and Wang (1975), to first order in $1/Z$, and Bak (1975) independently derived the linewidth and applied the result to Pr. Psaltakis and Cottam (1982) have considered the ($J = 1$)-model in the ordered phase, in the presence of uniaxial anisotropy, where the ‘kinematic’ effects cannot be neglected. In the paramagnetic singlet-doublet XY -model, the $(1/Z)$ -results are close to those derived above for the Ising model. If the xx - and yy -couplings are assumed to be equal, it is found, to a good approximation, that $n_0 + n_1$ in eqn (7.2.7b) is replaced by $n_0 + 2n_1 = 1$, and that the frequency sum in this equation is multiplied by a factor $3/2$. If $\mathcal{J}_{zz}(\mathbf{q})$ is non-zero, it gives rise to additional contributions to the average \mathbf{q} -independent self-energy. Furthermore, it also leads to a \mathbf{q} -dependent contribution, even in the first order of $1/Z$. This occurs because the odd-rank cumulants (corresponding to half-integral p in (7.2.4)) involving all three components may be non-zero. The lowest-rank odd cumulant which is non-zero is $\langle T_{\tau} J_{ix}(\tau_1) J_{iy}(\tau_2) J_{iz}(\tau_3) \rangle_0$. Although this formally leads to a $(1/Z)$ -contribution to the \mathbf{q} -dependent part of $\Sigma(\mathbf{q}, \omega)$, which is not immediately compatible with the effective-medium results above, this should be a minor term in systems with long-range interactions and, if Δ is positive, its importance is much reduced at low temperatures under all circumstances.

The results of calculations of the lifetimes of the long-wavelength magnetic optical-modes in Pr, based on eqn (7.2.7), are compared with the experimental results of Houmann *et al.* (1979) in Fig. 7.4. This theory predicts very nearly the same temperature dependence of the energies as does the self-consistent RPA; the excitation depicted in Fig. 7.4 is the uppermost mode in Fig. 7.3. The theory to first order in $1/Z$ accounts very well for the temperature dependence of the energies, lifetimes, and intensities of these excitations, without adjustable parameters. The low temperature results are similar to those of Bak (1975), but the experiments at the highest temperatures in Fig. 7.4 are more

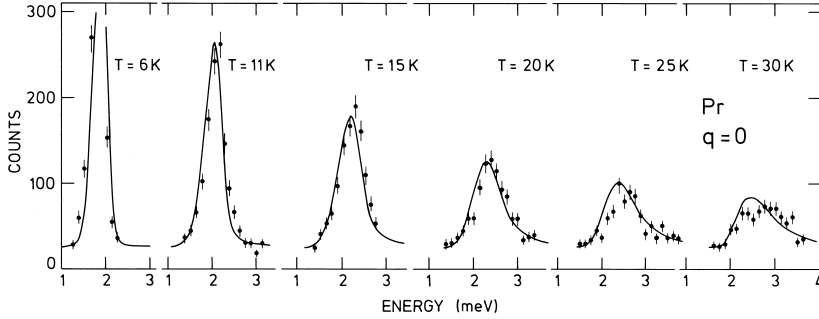


Fig. 7.4. The temperature dependence of the neutron-scattering intensities for the $\mathbf{q} = 0$ magnetic optical-mode on the hexagonal sites of Pr. The instrumental resolution and the overall scaling of the intensity are extracted from the experimental results at 6 K, and thereafter used unchanged in the calculations, which are based on a $1/Z$ -expansion, as described in the text.

accurately described by the effective-medium theory developed above, than by his unrestricted cumulant expansion.

An analysis of the $1/Z$ -corrections to the MF-RPA theory for the singlet-triplet model does not exist in the literature, to our knowledge. We shall not attempt such an analysis here, but we will discuss one aspect, that the elastic response due to the triplet states is predicted to be a diffusive peak of non-zero width, to first order in $1/Z$, within the effective-medium approximation. In order to consider this matter, we can omit the singlet and use instead the ($J = 1$) Heisenberg model, corresponding to the above model with $\Delta = 0$. In this case, the diagonal components of the single-site Green function are

$$G(i\omega_n) = -\frac{2}{3}\beta\left\{1 - \frac{1}{6}\beta K(0)\right\}\delta_{n0} + \frac{4}{3(i\hbar\omega_n)^2}\{K(0) - K(i\omega_n)\} + \dots \quad (7.2.10)$$

to first order in $1/Z$. In zero order, the response is purely elastic and $K(i\omega_n) \propto \delta_{n0}$. If this is introduced into (7.2.10), the second term predicts an inelastic contribution to $G(\omega)$, which further diverges proportionally to ω^{-2} in the zero-frequency limit. This divergence indicates that the elastic peak must broaden out to a Lorentzian, with a non-zero half-width Γ , as in (3.3.10–11), corresponding to the replacement of $(\hbar\omega)^2$ in the denominator by $(\hbar\omega)^2 + \Gamma^2$, when the higher-order terms in the series are included. The classification of $K(i\omega_n \neq 0)$ as a higher-order term in the series (7.2.9) is not consistent with a simple Lorentzian,

and a more appropriate form turns out to be

$$G(\omega) = G(0) \left(\frac{i\Gamma}{\hbar\omega + i\Gamma} \right)^2 = G(0) \frac{\Gamma^2 [\Gamma^2 - (\hbar\omega)^2 + 2i\hbar\omega\Gamma]}{[\Gamma^2 + (\hbar\omega)^2]^2}. \quad (7.2.11a)$$

The real and imaginary parts of this retarded Green function are connected by the Kramers–Kronig relation, and the expansion in powers of Γ agrees with (7.2.10), when

$$G(0) = -\frac{2}{3}\beta \left\{ 1 - \frac{1}{6}\beta K(0) \right\} \quad \text{and} \quad \Gamma = \sqrt{2K(0)/\beta}. \quad (7.2.11b)$$

In the high-temperature limit, $K(0) \simeq (2\beta/3N) \sum_{\mathbf{q}} \mathcal{J}^2(\mathbf{q})$, and hence Γ is independent of T in this limit. The most important reason for choosing the Green function given by (7.2.11a) is that it satisfies the sum rule:

$$\begin{aligned} -\frac{1}{\beta} \sum_n \sum_{\alpha=x,y,z} G(i\omega_n) &= -3 \frac{1}{\pi} \int_0^\infty d(\hbar\omega) \operatorname{Im}[G(\omega)] \coth(\beta\hbar\omega/2) \\ &= J(J+1) = 2, \end{aligned} \quad (7.2.12)$$

to the degree of accuracy with which $G(0)$ is determined (this is the same sum rule considered in (4.2.7)). The original expansion series satisfies this sum rule, to first order in $1/Z$, but this property is not easily conserved if a Lorentzian is chosen. The problem with the Lorentzian (with approximately the same Γ as above) is that it decreases only slowly with ω , and the tails lead to a divergence of the integral in (7.2.12), unless a high-frequency cut-off is introduced. In this system, there is no natural frequency-scale setting such a cut-off, and the only reasonable way of determining it is through the sum-rule itself, which is rather unsatisfactory.

In addition to the equations of motion and the Feynman–Dyson linked-cluster-expansion method discussed here, there are other many-body perturbation techniques which may be useful for analysing this kind of system. The most important supplementary theories are those based on the Mori technique (Mori 1965; Huber 1978; Ohnari 1980), or similar projection-operator methods (Becker *et al.* 1977; Micnas and Kishore 1981). However, no matter which theory is used, it cannot circumvent the essential complication of crystal-field systems; the more single-ion levels which are important, the greater is the complexity of the dynamical behaviour. This principle is illustrated by the fact that the methods discussed above have not yet been extended to systems with more than two levels, singlet or degenerate, per site.

7.3 Perturbations of the crystal-field system

In this section, we shall discuss various effects of the surrounding medium on a crystal-field system. The first subject to be considered is the magnetoelastic coupling to the lattice. Its contribution to the magnetic-excitation energies may be described in terms of frequency-dependent, anisotropic two-ion interactions, and we include a short account of the general effect of such terms. We next consider the coupling to the conduction electrons, which is treated in a manner which is very parallel to that used for spin-wave systems in Section 5.7. Finally, we discuss the hyperfine interaction between the angular momenta and the nuclear spins, which becomes important at the lowest temperatures, where it may induce an ordering of the moments in an otherwise undercritical singlet-ground-state system.

7.3.1 Magnetoelastic effects and two-ion anisotropy

The magnetoelastic interactions which, in the kind of system we are considering, primarily originate in the variation of the crystal-field parameters with lattice strain, produce a number of observable phenomena. The lattice parameters and the elastic constants depend on temperature and magnetic field, the crystal-field excitation energies are modified, and these excitations are coupled to the phonons. In addition, the magnetoelastic coupling allows an externally applied uniaxial strain to modify the crystal-field energies. All these magnetoelastic effects have their parallel in the ferromagnetic system discussed in Section 5.4 and, in the RPA, they may be derived by almost the same procedure as that presented there, provided that the spin-wave operators are replaced by the standard-basis operators, introduced in eqn (3.5.11).

In the paramagnetic phase in zero external field, only those strains which preserve the symmetry, i.e. the α -strains, may exhibit variations with temperature due to the magnetic coupling. The lowering of the symmetry by an applied external field may possibly introduce non-zero strains, proportional to the field, which change the symmetry of the lattice. In both circumstances, the equilibrium strains may be calculated straightforwardly within the MF approximation. As an example, we shall consider the lowest-order magnetoelastic γ -strain Hamiltonian

$$\mathcal{H}_\gamma = \sum_i \left[\frac{1}{2} c_\gamma (\epsilon_{\gamma 1}^2 + \epsilon_{\gamma 2}^2) - B_{\gamma 2} \{ O_2^2(\mathbf{J}_i) \epsilon_{\gamma 1} + O_2^{-2}(\mathbf{J}_i) \epsilon_{\gamma 2} \} \right], \quad (7.3.1)$$

corresponding to eqn (5.4.1) with $B_{\gamma 4} = 0$. The equilibrium strain $\bar{\epsilon}_{\gamma 1}$, for instance, is determined in the presence of an external magnetic field

and external stresses by

$$\frac{1}{N} \left\langle \frac{\partial \mathcal{H}_\gamma}{\partial \epsilon_{\gamma 1}} \right\rangle = c_\gamma \bar{\epsilon}_{\gamma 1} - B_{\gamma 2} \langle O_2^2 \rangle - (t_{11} - t_{22}) = 0,$$

with $\bar{t} = (V/N)\bar{T}$, where \bar{T} is the usual stress-tensor. Introducing the equilibrium condition into the Hamiltonian, we get

$$\mathcal{H}_\gamma(\text{sta}) = - \sum_i B_{\gamma 2} \{ O_2^2(\mathbf{J}_i) \bar{\epsilon}_{\gamma 1} + O_2^{-2}(\mathbf{J}_i) \bar{\epsilon}_{\gamma 2} \} + \mathcal{H}_\gamma^0, \quad (7.3.2a)$$

where

$$\mathcal{H}_\gamma^0 = N \left[\frac{1}{2} c_\gamma (\bar{\epsilon}_{\gamma 1}^2 + \bar{\epsilon}_{\gamma 2}^2) - (t_{11} - t_{22}) \bar{\epsilon}_{\gamma 1} - 2t_{12} \bar{\epsilon}_{\gamma 2} \right]. \quad (7.3.2b)$$

The thermal averages have to be calculated self-consistently, which implies that the static magnetoelastic Hamiltonian, (7.3.2), must itself be included in the total magnetic MF Hamiltonian, which determines the thermal averages such as $\langle O_2^2 \rangle$ in the equilibrium equation. The magnetoelastic coupling changes the magnetic-excitation energies if the crystal is strained, because the extra crystal-field term in (7.3.2a), introduced by $\mathcal{H}_\gamma(\text{sta})$, directly modifies $\bar{\chi}^o(\omega)$. In the ($J = 1$)-model corresponding to Pr, $O_2^{\pm 2}(\mathbf{J}_i)$ couples the two doublet states, and thus the degeneracy of this level is lifted in proportion to the γ -strains.

Having included the contributions of $\mathcal{H}_\gamma(\text{sta})$ to the single-ion susceptibility, we continue by discussing the influence of the coupling between the magnetic excitations and the phonons, as determined by the dynamic part of the magnetoelastic Hamiltonian $\mathcal{H}_\gamma(\text{dyn})$, given by eqn (5.4.6) with $B_{\gamma 4} = 0$. As an example, we consider the coupling to the transverse phonons propagating in the a - or the b -direction, with the polarization vector in the basal-plane, which is derived from

$$\begin{aligned} \Delta \mathcal{H}_\gamma(\text{dyn}) &= -B_{\gamma 2} \sum_i \{ O_2^{-2}(\mathbf{J}_i) - \langle O_2^{-2} \rangle \} \epsilon_i \\ &= -B_{\gamma 2} \sum_i \sum_{\nu\mu} N_{\nu\mu} a_{\nu\mu}(i) \epsilon_i, \end{aligned} \quad (7.3.3)$$

where ϵ_i is a shorthand notation for $\epsilon_{\gamma 2}(i) - \bar{\epsilon}_{\gamma 2}$, and $N_{\nu\mu}$ is the matrix element of the Stevens operator between $\langle \nu |$ and $|\mu \rangle$, cf. eqns (3.5.11–13). This Hamiltonian introduces an additional term on the l.h.s. of the equation of motion (3.5.15) for the Green function $\langle\langle a_{\nu\mu}(i); a_{rs}(i') \rangle\rangle$:

$$\begin{aligned} B_{\gamma 2} \sum_\xi \langle\langle \{ N_{\mu\xi} a_{\nu\xi}(i) - N_{\xi\nu} a_{\xi\mu}(i) \} \epsilon_i; a_{rs}(i') \rangle\rangle &\simeq \\ &B_{\gamma 2} (n_\nu - n_\mu) N_{\mu\nu} \langle\langle \epsilon_i; a_{rs}(i') \rangle\rangle, \end{aligned} \quad (7.3.4)$$

where the approximate result follows from the usual RPA decoupling introduced by eqn (3.5.16). According to eqn (5.4.25),

$$\epsilon_i = \sum_{\mathbf{k}} (ikF_{\mathbf{k}}/2)(\beta_{\mathbf{k}} + \beta_{-\mathbf{k}}^+) \exp(i\mathbf{k} \cdot \mathbf{R}_i),$$

where we assume, for simplicity, only one phonon mode. From the equations of motion determining the two Green functions $\langle\langle\beta_{\mathbf{q}}; a_{rs}(i')\rangle\rangle$ and $\langle\langle\beta_{-\mathbf{q}}^+; a_{rs}(i')\rangle\rangle$, we obtain

$$\begin{aligned} \langle\langle\beta_{\mathbf{q}} + \beta_{-\mathbf{q}}^+; a_{rs}(i')\rangle\rangle = \\ B_{\gamma 2} \sum_i \sum_{\nu\mu} (iqF_{\mathbf{q}}/2) D(\mathbf{q}, \omega) e^{-i\mathbf{q} \cdot \mathbf{R}_i} N_{\nu\mu} \langle\langle a_{\nu\mu}(i); a_{rs}(i')\rangle\rangle, \end{aligned} \quad (7.3.5)$$

where $D(\mathbf{q}, \omega)$ is the phonon Green function for the mode considered:

$$D_{\nu}(\mathbf{q}, \omega) = \frac{2\omega_{\nu\mathbf{q}}}{\hbar(\omega^2 - \omega_{\nu\mathbf{q}}^2)}. \quad (7.3.6)$$

If this is introduced into (7.3.4), and the resulting expression is added to the l.h.s. of (3.5.18), the procedure leading to eqn (3.5.21) yields the equivalent result

$$\overline{\overline{\chi}}(\mathbf{q}, \omega) - \overline{\overline{\chi}}^o(\omega) \overline{\overline{\mathcal{J}}}(\mathbf{q}, \omega) \overline{\overline{\chi}}(\mathbf{q}, \omega) = \overline{\overline{\chi}}^o(\omega). \quad (7.3.7)$$

However, these quantities are now four-dimensional matrices in the vector space defined by the operators J_{ix} , J_{iy} , J_{iz} , and $O_2^{-2}(\mathbf{J}_i)$, or more accurately by these operators minus their expectation values. The only extra element in $\overline{\overline{\mathcal{J}}}(\mathbf{q}, \omega)$, in addition to the normal Cartesian components $\mathcal{J}_{\alpha\beta}(\mathbf{q})$, is

$$\mathcal{J}_{44}(\mathbf{q}, \omega) = N \left(\frac{i}{2} q F_{\mathbf{q}} B_{\gamma 2} \right)^2 D(\mathbf{q}, \omega). \quad (7.3.8)$$

The excitation energies are determined by the condition

$$|1 - \overline{\overline{\chi}}^o(\omega) \overline{\overline{\mathcal{J}}}(\mathbf{q}, \omega)| = 0.$$

When \mathbf{q} is along an a - or b -direction, and the external fields are applied in the basal plane, parallel or perpendicular to \mathbf{q} , then $\overline{\overline{\mathcal{J}}}(\mathbf{q})$ and the 3×3 Cartesian components of $\overline{\overline{\chi}}^o(\omega)$, at low frequencies, are diagonal with respect to the $(\xi\eta\zeta)$ -axes. In this case, the most phonon-like pole is found at a frequency determined by

$$|1 - \overline{\overline{\chi}}^o(\omega) \overline{\overline{\mathcal{J}}}(\mathbf{q}, \omega)| / \prod_{\alpha} [1 - \chi_{\alpha\alpha}^o(\omega) \mathcal{J}_{\alpha\alpha}(\mathbf{q})] = 1 - \Xi(\mathbf{q}, \omega) \mathcal{J}_{44}(\mathbf{q}, \omega) = 0, \quad (7.3.9a)$$

where $\alpha = \xi, \eta,$ and $\zeta,$ and

$$\Xi(\mathbf{q}, \omega) = \chi_{44}^o(\omega) + \sum_{\alpha} \frac{\chi_{\alpha 4}^o(\omega)\chi_{4\alpha}^o(\omega)\mathcal{J}_{\alpha\alpha}(\mathbf{q})}{1 - \chi_{\alpha\alpha}^o(\omega)\mathcal{J}_{\alpha\alpha}(\mathbf{q})}. \quad (7.3.9b)$$

At long wavelengths, this pole determines the velocity of the magneto-acoustic sound waves, as measured in an ultrasonic experiment, and expressing this velocity in terms of the corresponding elastic constant, we find

$$\frac{c_{66}^*}{c_{66}} = 1 - \Xi(\mathbf{q}, 0)B_{\gamma 2}^2/c_{\gamma}, \quad (7.3.10)$$

by combining the above relation with eqns (5.4.24b) and (5.4.34). This result is valid when \mathbf{q} is along the ξ - or η -axes, provided that the external field is applied along one of the principal axes. In the general case, it is necessary to include the coupling to the other phonon branches in eqn (7.3.7), and also to take into account possible off-diagonal terms in the Cartesian part of the matrices, but these complications may be included in the above calculations in a straightforward fashion. One question raised by (7.3.10) is whether the magneto-acoustic sound velocities, measured at non-zero frequencies, depend on possible purely-elastic contributions to the RPA susceptibilities. That these should be included in (7.3.7), at $\omega = 0$, can be seen by the argument used in deriving (3.5.22). In the preceding section, we found that the coupling between the angular momenta broadens the elastic RPA response into a diffusive peak of width 2Γ , as in (7.2.11b), proportional to $T^{1/2}$ at low temperatures. Unless this coupling is very weak, Γ is likely to be much larger than the applied $\hbar\omega$ in an ultrasonic experiment, in which case the total elastic contribution to $\Xi(\mathbf{q}, 0)$ in (7.3.10) should be included. A more detailed investigation of this question is given by, for instance, Elliott *et al.* (1972), in a paper discussing systems with Jahn-Teller-induced phase transitions.

In the paramagnetic phase without any external *magnetic* field, the susceptibility components $\chi_{\alpha 4}^o(\omega)$ all vanish in the zero frequency limit, due to the time-reversal symmetry of the system. Replacing t by $-t$ generates the transformation $\chi_{\alpha 4}^o(\omega) \rightarrow \chi_{\alpha T_4 T}^o(-\omega)$, where the time-reversed operators are $J_{i\alpha}^T = -J_{i\alpha}$, and $O_2^{-2}(\mathbf{J}_i)^T = O_2^{-2}(\mathbf{J}_i)$. These results follows from the symmetry properties of the axial tensor operators, discussed after eqn (5.5.14), recalling that the operators are Hermitian, of rank $l = 1$ and $l = 2$ respectively. Hence, because of the time-reversal symmetry, $\chi_{\alpha 4}^o(\omega) = -\chi_{\alpha 4}^o(-\omega) = -(\chi_{\alpha 4}^o(\omega^*))^*$, where the last result follows from (3.2.15), and we assume implicitly that all poles lie on the real axis. This quantity must therefore vanish at zero frequency, and the reactive and absorptive components are either zero or purely imaginary at non-zero frequencies. If there is no ordered moment and no

external magnetic field, the coupling between the dipolar crystal-field excitations and the long-wavelength phonons must therefore vanish by symmetry, within the present approximation, and $\Xi(\mathbf{q}, 0) = \chi_{44}^o(0)$ in eqn (7.3.10). In the presence of an external magnetic field, the mixed dipolar–quadrupolar susceptibility-components may become non-zero, and hence produce a direct coupling of the elastic waves and the dipolar excitations. In this case, the magnetic dipole coupling, which gives rise to a directional dependence of $\mathcal{J}_{\alpha\alpha}(\mathbf{q})$, as discussed in Section 5.5, leads to different values of c_{66}^* (as determined from the transverse sound velocity in the $b(\eta)$ -direction), depending on whether the field is parallel to the ξ - or the η -axis or, if the field is fixed along one of these two axes, whether \mathbf{q} is along the ξ - or the η -direction. As mentioned earlier, this anisotropy is similar to that introduced by rotational invariance, and has a comparable magnitude in paramagnetic systems (Jensen 1988b).

The dynamic coupling between the magnetic and elastic excitations in Pr has been studied in the long-wavelength limit by Palmer and Jensen (1978), who measured the elastic constant c_{66} by ultrasonic means, as a function of temperature and magnetic field. At 4K, it was found to be very sensitive to a field applied in the basal plane, but insensitive to a field along the c -axis, reflecting the anisotropy of the susceptibility. At non-zero fields in the basal plane, there is furthermore a considerable anisotropy, due to B_6^6 . Using the crystal-field level scheme illustrated in Fig. 1.16, and a value of $B_{\gamma 2}$ consistent with that deduced from the field dependence of the magnetic excitations (Houmann *et al.* 1979), they were able to obtain a very good fit to the observed dependence of c_{66} on field, shown in Fig. 7.5, and on temperature.

The above theory is also valid at non-zero frequencies. However, if q is no longer small, we must take account of the discreteness of the lattice and replace q in (7.3.8) by a sinusoidal function of q and the lattice parameters, as in (5.4.43) in Section 5.4. Except for the change in the \mathbf{q} -dependence of $\mathcal{J}_{44}(\mathbf{q}, \omega)$, eqn (7.3.7) still applies, and it predicts hybridization effects between the phonons and the crystal-field excitations, equivalent to those derived from the linear magnon–phonon coupling in Section 5.4. The time-reversal symmetry of the paramagnetic system in zero magnetic field does not exclude the possibility that the phonons at non-zero frequencies are coupled to the crystal-field dipolar excitations and, in the case of Pr, the doublet excitations are allowed to interact with the transverse phonons, when \mathbf{q} is in the c -direction. Nevertheless, the application of a magnetic field will generally introduce new interactions via $\chi_{4\alpha}^o(\omega)$, leading to hybridization effects proportional to the field, as observed in Pr by Houmann *et al.* (1979) and interpreted by Jensen (1976a). Interactions between crystal-field excitations and

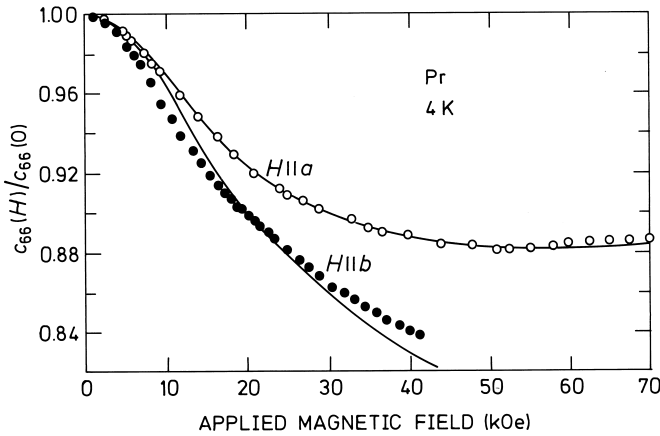


Fig. 7.5. The field dependence of the elastic constant c_{66} in Pr at 4 K, relative to the value at zero field. The elastic constant was determined from the velocity of the transverse sound waves propagating in an a -direction, and the open and closed symbols indicate the experimental results when the field was applied respectively in the a - or the perpendicular b -direction. The solid lines show the calculated field dependence.

the phonons are further discussed by Thalmeier and Fulde (1975), Fulde (1979), and Aksenov *et al.* (1981).

The coupling (5.4.50), quadratic in the magnon operators, also has its counterpart in crystal-field systems. Such interactions arise when, instead of applying the RPA decoupling in the first step, as in eqn (7.3.4), we proceed to the next step in the hierarchy of Green functions. The most important effect of these terms is to replace the crystal-field parameters by effective values, which might be somewhat temperature dependent, corresponding to an averaging of the effective crystalline field experienced by the $4f$ electrons over the finite volume spanned by the thermal vibration of the ions. As in the spin-wave case, these extra higher-order contributions do not lead to the kind of hybridization effects produced by the linear couplings. However, if the density of states of the phonons, weighted with the amplitude of the coupling to the crystal-field excitations, is particularly large at certain energies, resonance-like bound-states due to the higher-order terms may be observed in the magnetic spectrum. The *dynamic Jahn-Teller effect* observed in CeAl_2 (Loewenhaupt *et al.* 1979) seems to be due to these higher-order effects, according to the calculation of Thalmeier and Fulde (1982).

The expression (7.3.7) for the interaction of the crystal-field system with the phonons has essentially the same form as that derived from any

general two-ion coupling. Referring to (5.5.14), in which is introduced a general two-ion Hamiltonian in terms of the tensor operators $\tilde{O}_{lm}(\mathbf{J}_i)$, we may write

$$\mathcal{H}_{JJ} = -\frac{1}{2} \sum_{ij} \mathbf{J}_i^p \cdot \overline{\overline{\mathcal{J}}^p}(ij) \cdot \mathbf{J}_j^p, \quad (7.3.11)$$

where $\mathbf{J}^p \equiv (J_x, J_y, J_z, O_2^{-2}, \tilde{O}_{lm}, \dots)$ is a generalized p -dimensional moment operator, and the $\{lm\}$ -set of operators comprises the tensor couplings from the original Hamiltonian, except those between the first four components. It is then immediately clear that the final RPA susceptibility is given by an expression equivalent to (7.3.7), in terms of the $p \times p$ susceptibility-matrix with $\mathcal{J}_{\alpha\beta}(\mathbf{q}, \omega) = \mathcal{J}_{\alpha\beta}^p(\mathbf{q})$, except that (at long wavelengths) $\mathcal{J}_{44}(\mathbf{q}, \omega) = N(iqF_{\mathbf{q}}B_{\gamma 2}/2)^2 D(\mathbf{q}, \omega) + \mathcal{J}_{44}^p(\mathbf{q})$. If the frequency is not near a pole in $D(\mathbf{q}, \omega)$, the effect of the coupling to the phonons on the magnetic excitations is therefore similar to that stemming from the corresponding quadrupole-quadrupole interaction. If $\mathcal{J}_{44}^p(\mathbf{0})$ is non-zero, the ultrasonic velocities are influenced by this coupling, as we now have

$$\frac{c_{66}^*}{c_{66}} = \frac{1 - \Xi(\mathbf{q}, 0)\mathcal{J}_{44}(\mathbf{0}, 0)}{1 - \Xi(\mathbf{q}, 0)\mathcal{J}_{44}^p(\mathbf{0})} = 1 - \frac{\Xi(\mathbf{q}, 0)}{1 - \Xi(\mathbf{q}, 0)\mathcal{J}_{44}^p(\mathbf{0})} B_{\gamma 2}^2/c_{\gamma}, \quad (7.3.12)$$

where the sum over α in (7.3.9b) comprises all the $(p-1)$ components for which $\alpha \neq 4$, under the same condition that $\overline{\overline{\chi}}^o(\omega)$ and $\overline{\overline{\mathcal{J}}}(\mathbf{q}, \omega)$ are both diagonal for $\alpha \neq 4$. In general, $\chi_{4\alpha}^o(0)$ may be non-zero, in the paramagnetic phase in zero magnetic field, if the α -component is an even-rank tensor, and these interactions may contribute to $\Xi(\mathbf{q}, 0)$, whereas the odd-rank couplings are prevented from affecting the phonons in the zero-frequency limit by time-reversal symmetry.

In our discussion of crystal-field excitations, we have only been concerned with the excitation spectrum derived from the time variation of the *dipole* moments. There are two reasons for this. Most importantly, the coupling between the dipolar moments expressed in eqn (7.1.1) is normally dominant in rare earth systems, so that the collective phenomena are dominated by the dipolar excitations. The other reason is that the *magnetic* response, including the magnetic susceptibility and the (magnetic) neutron scattering cross-section, is determined exclusively by the upper-left 3×3 part of $\overline{\overline{\chi}}(\mathbf{q}, \omega)$, in the generalized p -dimensional vector space introduced through eqn (7.3.11). However, strong quadrupolar interactions may lead to collective effects and to an ordered phase of the quadrupole moments. The quadrupolar excitations are not directly visible in neutron-scattering experiments, but may be detected indirectly via their hybridization with the dipole excitations, in the same way as the phonons, or via their hybridization with the phonons, as measured

by the nuclear scattering of the neutrons. In a paramagnetic system in zero field, the $p \times p$ susceptibility-matrix partitions into two independent blocks, at zero frequency, the one depending only on the even-rank couplings and the other only on the odd-rank couplings. If one of the two parts of $\bar{\chi}(\mathbf{q}, 0)$ diverges at some temperature T^* , it signals the occurrence of a second-order phase transition at this temperature. If it is the block determined by the even-rank couplings which diverges, the order parameter below T^* is associated with the quadrupole moments, assuming the lowest-rank terms to be dominant. If there is any coupling between this order parameter and one of the phonon modes, the transition is accompanied by a softening of these phonons, provided that the pure quadrupolar excitations have higher energies than the phonons at the ordering wave-vector. If this vector \mathbf{Q} is zero, the corresponding elastic constant vanishes at the transition. In the case where $\mathbf{Q} \neq \mathbf{0}$, the situation corresponds to that considered in the magnetic case, and the phonon mode shows soft-mode behaviour according as there are pure elastic contributions to the (RPA) susceptibility or not. A quadrupolar phase-transition involving the phonons is usually referred to as being induced by the *Jahn-Teller* effect, and a more detailed discussion and relevant examples may be found in, for instance, Elliott *et al.* (1972). The presence of a non-zero quadrupole moment does not destroy the time-reversal symmetry, and an ordering of the dipole moments may follow only after an additional phase transition. In TmZn (Morin *et al.* 1980) an ordering of the quadrupole moments occurs below a first-order transition at $T_Q = 8.6$ K, and this phase is disrupted by the onset of ferromagnetic ordering at $T_C = 8.1$ K. In the opposite case of ordering of the dipole moments, the breaking of the time-reversal symmetry allows a direct coupling between the dipole and quadrupole moments, so that the latter are forced to order together with the dipoles, giving rise to, for example, crystal-field-induced magnetostriction effects, and the dipolar ordering will normally quench any tendency toward a purely quadrupolar-ordered phase.

In this chapter, we have formulated the various RPA results in terms of the generalized-susceptibility matrices. The results apply in paramagnetic as well as in ordered systems, so long as the order parameter is uniform throughout the crystal. They agree with the more explicit results derived previously in the case of a weakly-anisotropic ferromagnetic system. In a paramagnet or a strongly-anisotropic ferromagnet, the results above may also be given a more transparent and explicit form, but only if the number $(2J + 1)$ of different angular-momentum states can be taken as small; else the matrix-equations themselves are well-suited for solution by numerical methods. The reduction of the matrix-equations in, for instance, the $(J = 1)$ -case is straightforward

and the results, corresponding to Pr in the limit $T = 0$, are given by Jensen (1976a).

In the present approximation, the sound velocities are not affected by the interaction between the dipoles, in the paramagnetic phase at zero magnetic field. However, in the vicinity of a second-order transition to a ferromagnetic phase, strong softening of the long-wavelength phonons may be observed, depending on the symmetry properties, and this behaviour cannot be explained within the RPA. We have seen that, according to eqns (5.4.15) and (5.4.38), c_{66}^* vanishes in the basal-plane ferromagnet when a field equal to the critical field H_c is applied along the hard basal-plane direction. When T_C is approached from below, H_c vanishes rapidly, resulting in a strong softening of c_{66}^* even in zero field, and it seems likely that similar behaviour should be observed when T_C is approached from above, considering that just above T_C there will be large domains of nearly constant magnetization, allowing an ‘RPA’ coupling between the dipole moments and the sound waves similar to that occurring in the ferromagnetic phase. Clear indications of this kind of behaviour have been seen in for example Tb (Jensen 1971b), indicating that the RPA is not even qualitatively trustworthy when the fluctuations are a dominating feature of the system.

7.3.2 Conduction-electron interactions

The sf -exchange Hamiltonian (5.7.6) was derived without making any special assumptions about the rare earth metal involved, and it therefore applies equally well to a metallic crystal-field system. For the weakly-anisotropic ferromagnet considered in Section 5.7, this Hamiltonian leads to a Heisenberg two-ion coupling, $\tilde{\mathcal{J}}(\mathbf{q}, \omega)$, which to a first approximation is instantaneous, and is thus effectively $\mathcal{J}(\mathbf{q}) = \tilde{\mathcal{J}}(\mathbf{q}, 0) - (1/N) \sum_{\mathbf{q}'} \tilde{\mathcal{J}}(\mathbf{q}', 0)$, as given by eqn (5.7.28). This remains true in crystal-field systems, as may be demonstrated by expanding the angular-momentum operators in (5.7.6) in terms of the standard-basis operators, and then calculating the corresponding Green functions which determine $\bar{\chi}(\mathbf{q}, \omega)$, utilizing an RPA decoupling of the coupled Green functions.

In the ordered phase, $\mathcal{J}_{zz}(\mathbf{q}, \omega)$ may actually differ from the two other components of the exchange coupling, due to the polarization of the conduction electrons. However, in the paramagnetic phase in zero field, the coupling is isotropic, within the approximation made in Section 5.7. This may be seen by analysing the full expression (5.7.27) for $\tilde{\mathcal{J}}(\mathbf{q}, \omega)$, or the simpler result (5.7.26), in which the susceptibility of the conduction electrons becomes a scalar:

$$\chi_{\text{c.el.}}^{\alpha\beta}(\mathbf{q}, \omega) = \frac{1}{2} \chi_{\text{c.el.}}^{+-}(\mathbf{q}, \omega) \delta_{\alpha\beta}. \quad (7.3.13)$$

Here the reactive and absorptive parts of $\chi_{\text{c.el.}}^{+-}(\mathbf{q}, \omega)$, still given by (5.7.26b), are both real and even in \mathbf{q} , while the reactive part is even with respect to ω , whereas the absorptive part is odd. When considering the frequency dependence of the susceptibility, we must distinguish two separate regimes, defined by the parameter

$$\vartheta = -\eta q/2k_F = (\hbar\omega/2\varepsilon_F)(k_F/q) = (2/3\nu)\mathcal{N}(\varepsilon_F)\hbar\omega(k_F/q),$$

where η is the parameter introduced in (5.7.31c) (with $\Delta(\text{c.el.}) = 0$). If $|\vartheta|$ is small compared to one,

$$\chi_{\text{c.el.}}^{+-}(\mathbf{q}, \omega) = \mathcal{N}(\varepsilon_F) \left\{ \mathcal{F}\left(\frac{q}{2k_F}\right) + i\frac{\pi}{2}\vartheta \right\} \quad ; \quad |\vartheta| \ll 1, \quad (7.3.14)$$

where the correction to the real part, of the order ϑ^2 , may be neglected. This is the same result as obtained in the ordered phase, eqns (5.7.32) and (5.7.36), when the small frequency-dependent term in the former is neglected. When $|\vartheta|$ becomes larger than 1 (or $q > 2k_F$), the imaginary part vanishes, as shown in the calculations leading to (5.7.36), and the real part becomes strongly dependent on ω , vanishing for large values of ϑ as $\vartheta^{-2} \propto \omega^{-2}$. If $\hbar\omega = 1\text{--}10\text{ meV}$, then $\vartheta = (10^{-4} - 10^{-3})k_F/q$ in the rare earth metals, so that the corrections to (7.3.14) are only important in the immediate neighbourhood of $q = 0$. The physical origin of this particular effect is that the susceptibility of the free-electron gas is purely elastic in the limit $q = 0$, and it does not therefore respond to a uniform magnetic field varying with a non-zero frequency. In the polarized case, the contributions to the transverse susceptibility are all inelastic at long wavelengths, so this retardation effect does not occur when the polarization gap $\Delta(\text{c.el.})$ is large compared to $|\hbar\omega|$. The exchange coupling, in the limit $q = 0$, includes both the elastic and inelastic contributions, as in (5.7.26c), and the abnormal behaviour of the elastic term may be observable in paramagnetic microwave-resonance experiments, where the anomalies should be quenched by a magnetic field. On the other hand, it may not be possible to study such an isolated feature in \mathbf{q} -space by inelastic neutron-scattering experiments. Leaving aside the small- q regime, we have therefore that the effective exchange-coupling is

$$\mathcal{J}(\mathbf{q}, \omega) = \mathcal{J}(\mathbf{q}) + i\zeta(\mathbf{q})\hbar\omega, \quad (7.3.15)$$

where $\zeta(\mathbf{q})$ is given by (5.7.37b), and $\mathcal{J}(\mathbf{q})$ is the reduced zero-frequency coupling given above, or by (5.7.28).

In the case of the weakly-anisotropic ferromagnet, the frequency dependence of the exchange coupling affects the spin-wave excitations

in the same way as results when $\mathcal{J}(\mathbf{q})$ is replaced by $\mathcal{J}(\mathbf{q}, \omega)$ in the usual RPA expression for the susceptibility, i.e.

$$\bar{\chi}(\mathbf{q}, \omega) = \{1 - \bar{\chi}^o(\omega)\mathcal{J}(\mathbf{q}, \omega)\}^{-1}\bar{\chi}^o(\omega). \quad (7.3.16)$$

In order to establish that this procedure is valid in general, to leading order in $1/Z$, we must appeal to the $1/Z$ -expansion discussed in Section 7.2. It is clear that the usual RPA decoupling (3.5.16), $a_{\nu\xi}(i)a_{\nu'\mu'}(j) \simeq \langle a_{\nu\xi}(i)a_{\nu'\mu'}(j) + a_{\nu\xi}(i)\langle a_{\nu'\mu'}(j) \rangle$, is not a good approximation if $i = j$, and in (3.5.15) it is only applied in cases where $i \neq j$, as $\mathcal{J}(ii) = 0$ by definition. Here, however, $\mathcal{J}(\mathbf{q}, \omega)$ does contain a coupling of one ion with itself, since $\mathcal{J}(ii, \omega) = i\zeta_0\hbar\omega$, where

$$\zeta_0 = \frac{1}{N} \sum_{\mathbf{q}} \zeta(\mathbf{q}) = 2\pi \langle |j(\mathbf{q})|^2 \rangle \mathcal{N}^2(\varepsilon_F), \quad (7.3.17)$$

as is obtained by replacing $|j(\mathbf{q})|$ in (5.7.37b) by a constant averaged value in the integral determining ζ_0 . This indicates that it is also necessary to rely on the RPA decoupling when $i = j$, in order to obtain the result (7.3.16) when ζ_0 is not zero. On the other hand, the RPA decoupling may work just as well if only the time arguments of the two operators are different, which is the case as $\mathcal{J}(ii, t = 0) = 0$ independently of ζ_0 . Only when $t = 0$, is $a_{\nu\xi}(i, t)a_{\nu'\mu'}(i, 0)$ equal to $a_{\nu\mu'}(i, 0)\delta_{\xi\nu'}$, in direct conflict with the RPA decoupling. This indicates that it may not be necessary to consider separately the effects of $\zeta(\mathbf{q}) - \zeta_0$ and of ζ_0 . This point is treated more precisely by the $1/Z$ -expansion procedure developed in Section 7.2. Since $\mathcal{J}(\mathbf{q}, \omega)$ replaces $\mathcal{J}(\mathbf{q})$, it makes no difference whether $\mathcal{J}(\mathbf{q}, \omega)$ is frequency-dependent or not, nor whether $\mathcal{J}(ii, \omega) \neq 0$, and this procedure leads immediately to the result (7.3.16), in the zeroth order of $1/Z$. If $\mathcal{J}(\mathbf{q}, \omega)$ contains a constant term, resulting from $\mathcal{J}(ii, t) \propto \delta(t)$, it is removed automatically in the next order in $1/Z$, according to the discussion following eqn (7.2.9). The argument for subtracting explicitly any constant contribution to $\mathcal{J}(\mathbf{q}, \omega)$, in eqn (7.3.16), is then that this procedure minimizes the importance of the $1/Z$ and higher-order contributions. The modifications of the $1/Z$ contributions are readily obtained by substituting $\mathcal{J}(\mathbf{q}, \omega)$ for $\mathcal{J}(\mathbf{q})$ in the expression (7.2.7c), which determines $K(\omega)$, i.e.

$$\tilde{K}(\omega) = K(\omega) + \frac{1}{N} \sum_{\mathbf{q}} i\zeta(\mathbf{q})\hbar\omega G(\mathbf{q}, \omega)/G(\omega) = K(\omega) + i\langle \zeta(\omega) \rangle \hbar\omega, \quad (7.3.18a)$$

and the self-energy is then obtained as

$$\Sigma(\mathbf{q}, \omega) = i\zeta(\mathbf{q})\hbar\omega + \tilde{\Sigma}(\omega), \quad (7.3.18b)$$

where $\tilde{\Sigma}(\omega)$ is the previous function with $K(\omega)$ replaced by $\tilde{K}(\omega)$. The most interesting effects of the scattering of the magnetic excitations against the electron-hole pair excitations of the conduction electrons derive from the first term in the self-energy, which already appears in the ‘RPA’ in (7.3.16). The lifetime of the excitations becomes \mathbf{q} -dependent and remains finite in the zero-temperature limit, whereas the imaginary part of $\Sigma(\omega)$, and therefore also of $\tilde{\Sigma}(\omega)$, vanishes exponentially at low temperatures, in the order $1/Z$. The importance of the higher-order contributions associated with this scattering mechanism, as compared to those of the intrinsic processes, i.e. the relative magnitudes of $\langle \zeta(\omega) \rangle \hbar\omega$ and $K(\omega)$, may depend on the system considered, but in Pr, for example, $\text{Im}[K(\omega)]$ is much the dominant term at frequencies lying within the excitonic band. Hence, $\langle \zeta(\omega) \rangle$ may be neglected in $\tilde{K}(\omega)$ at temperatures where the linewidths are still somewhat smaller than the overall bandwidth.

In Pr, the effect of the conduction electrons on the linewidths at low temperatures only becomes visible due to the strong increase in the value of $\zeta(\mathbf{q})$ in the limit of small q , where it is approximately proportional to $1/q$. Houmann *et al.* (1979) were thus able to observe the remarkable broadening of the acoustic modes illustrated in Fig. 7.6, as q was reduced at 6 K. The width at $q = 0.2 \text{ \AA}^{-1}$ is only slightly greater than the experimental resolution, but the peak has become very broad by 0.05 \AA^{-1} , and it has almost vanished into the background at $q = 0$, even though the integrated intensity is expected to increase as the energy decreases. This behaviour is in sharp contrast to that observed in Tb where, as shown in Fig. 5.13 on page 269, the width at small q is greatly reduced by the spin-splitting of the Fermi surface, in accordance with eqn (5.7.37). Since the spin-splitting of the Pr Fermi surface becomes very substantial in a large field, as illustrated in Fig. 1.10, the scattering of the long-wavelength magnetic excitations by the conduction electrons should be quenched by the application of a field. A careful study of this phenomenon would allow a detailed investigation of the interaction between the conduction electrons and the $4f$ moments.

The modification of $\tilde{K}(\omega)$ also contributes to the broadening of the diffusive peak and, instead of (7.2.11), the result for $J = 1$ is now

$$G(\omega) = G(0) \frac{i\Gamma_1 \hbar\omega - \Gamma^2}{(\hbar\omega + i\Gamma)^2}, \quad (7.3.19a)$$

with

$$\Gamma_1 = 2\langle \zeta(0) \rangle / \beta \quad \text{and} \quad \Gamma = \Gamma_1 + \sqrt{2K(0)/\beta}. \quad (7.3.19b)$$

The term linear in $\langle \zeta(0) \rangle$, introduced in (7.2.10), predicts Lorentzian broadening, if $K(0)$ is neglected. The intrinsic contribution may also

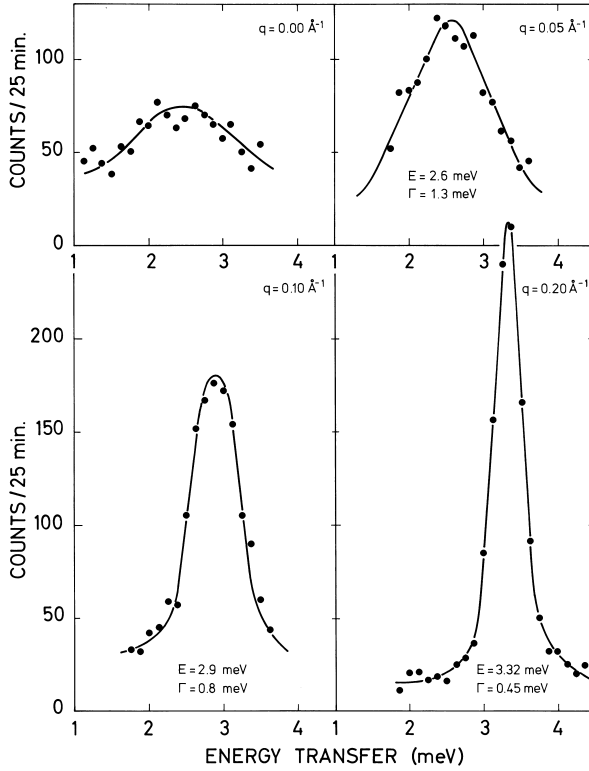


Fig. 7.6. Neutron-scattering spectra from the acoustic branch of the magnetic excitations propagating along the c -axis on the hexagonal sites of Pr at 6 K. The observed values of Γ , the full width at half maximum, increase rapidly as q decreases, due to scattering by the conduction electrons, and at $q = 0$ it is difficult to distinguish the peak from the background. The experimental energy resolution is about 0.35 meV.

here dominate at most temperatures, but it is clear that this cannot hold true in the high-temperature limit, where Γ_1 increases proportionally to T , whereas $K(0)/\beta$ approaches a constant value. So, in the high-temperature limit, (7.3.19) leads to the *Korringa law* (Korringa 1950) for the linewidth:

$$G(\mathbf{q}, \omega) \simeq G(\omega) \simeq G(0) \frac{i\Gamma_1}{\hbar\omega + i\Gamma_1}, \quad \text{with}$$

$$\Gamma_1 = 2\langle\zeta(0)\rangle k_B T = 4\pi\langle|j(\mathbf{q})|^2\rangle \mathcal{N}^2(\varepsilon_F) k_B T, \quad (7.3.20)$$

since $\langle\zeta(0)\rangle = \zeta_0$ in this limit. We argued above that $\langle\zeta(\omega)\rangle$ could be neglected, in comparison with the intrinsic effects, at relatively low

temperatures but, in the high-temperature limit, $\langle \zeta(\omega) \rangle$ is the dominant term. Becker *et al.* (1977) have deduced the influence of the electron-hole-pair scattering on the crystal-field excitations, with an accuracy which corresponds to the results obtained here to first order in $1/Z$, using an operator-projection technique. They performed their calculations for an arbitrary value of J , but without including the intrinsic damping effects which, as pointed out above, may be more important, except in the high-temperature limit.

The effects of the *sf*-exchange Hamiltonian on the effective mass and the heat capacity of the conduction electrons in a crystal-field system may be derived in an equivalent way to that used for the spin-wave system. The mass-enhancement, $m^*/m = 1 + \lambda_{\text{CF}}$, is deduced to be given by (White and Fulde 1981; Fulde and Jensen 1983):

$$\begin{aligned} \lambda_{\text{CF}} &= \mathcal{N}(\varepsilon_F) \frac{1}{2k_F^2} \int_0^{2k_F} dq \int \frac{d\Omega_{\mathbf{q}}}{4\pi} q |j(\mathbf{q})|^2 \sum_{\alpha} \chi_{\alpha\alpha}(\mathbf{q}, \omega \rightarrow 0) \\ &= \frac{1}{N} \sum_{\mathbf{q}} \frac{\zeta(\mathbf{q})}{2\pi\mathcal{N}(\varepsilon_F)} \sum_{\alpha} \chi_{\alpha\alpha}(\mathbf{q}, \omega \rightarrow 0), \end{aligned} \tag{7.3.21a}$$

and is a generalization of eqn (5.7.50), valid in the paramagnetic phase. The term $\chi_{\alpha\alpha}(\mathbf{q}, \omega \rightarrow 0)$ is the zero-frequency susceptibility, omitting possible elastic contributions, assuming the broadening effects to be small. At non-zero temperatures, it is found that excitations with energies small compared to $k_B T$ do not contribute to the mass-enhancement, and therefore, even in the low-temperature limit considered here, the purely elastic terms in $\chi_{\alpha\alpha}(\mathbf{q}, \omega)$ do not influence the effective mass. This is also one of the arguments which justifies the neglect to leading order of the effect on m^* of the longitudinal fluctuations in a ferromagnet, which appear in $\chi_{zz}(\mathbf{q}, \omega)$. In contrast, the elastic part of the susceptibility should be included in eqn (5.7.57), when the magnetic effects on the resistivity are derived in the general case, as in Section 5.7. In systems like Pr, with long-range interactions, the dispersive effects due to the \mathbf{q} -dependence of $\bar{\chi}(\mathbf{q}, \omega)$ are essentially averaged out, when summed over \mathbf{q} . In this case, we may, to a good approximation, replace $\bar{\chi}(\mathbf{q}, \omega)$ in sums over \mathbf{q} by its MF value $\bar{\chi}^o(\omega)$. The correction to the MF value of the low-temperature heat capacity in Pr, for example, is minute (Jensen 1982b). In the eqns (7.3.18–20) above, this means that, to a good approximation, $\langle \zeta(\omega) \rangle \simeq \frac{1}{N} \sum_{\mathbf{q}} \zeta(\mathbf{q}) = \zeta_0$ even at low temperatures, and that the mass-enhancement parameter is

$$\lambda_{\text{CF}} \simeq \frac{\zeta_0}{2\pi\mathcal{N}(\varepsilon_F)} \sum_{\alpha} \chi_{\alpha\alpha}^o(\omega \rightarrow 0). \tag{7.3.21b}$$

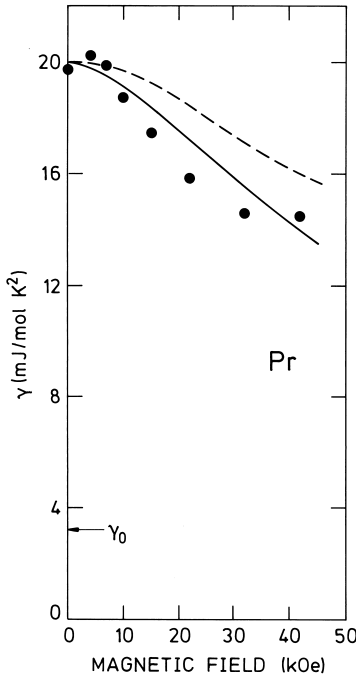


Fig. 7.7. The field dependence of the coefficient γ of the linear electronic heat capacity of Pr at low temperatures. The experimental results of Forgan (1981) are compared with a theory including the renormalization of the mass, due to the interaction of the conduction electrons with the magnetic excitations, and also taking into account the phonon enhancement and the dependence of the Fermi level on magnetic field. The dashed line shows the results of the theory when the change of the Fermi energy with field is neglected.

The mass-enhancement due to the crystal-field excitations is reflected directly in the effective mass measured in the de Haas-van Alphen effect, and in the linear term in the low-temperature electronic specific heat, analogously to the spin-wave system. The former effect has been studied by Wulff *et al.* (1988), who find that the theory of Fulde and Jensen (1983) accounts very well for the field dependence of the masses of several orbits, using the same values of the sf -exchange integral I , about 0.1 eV, as reproduce the variation of the orbit areas discussed in Section 1.3. The substantial field dependence of the electronic heat capacity, measured by Forgan (1981), is shown in Fig. 7.7, and compared with values calculated from eqn (7.3.21*b*), taking into account the field dependence of the electronic state density at the Fermi level, calculated by Skriver (private communication), and the phonon enhancement (Skriver and Mertig 1990). At higher temperatures, the imaginary part of $\mathcal{J}(\mathbf{q}, \omega)$ in (7.3.16) gives rise to the same contribution to the magnetic heat capacity as the extra term in (5.7.52) in the spin-wave case, with $\zeta(\mathbf{q}) \sum_{\alpha} \chi_{\alpha\alpha}(\mathbf{q}, \omega \rightarrow 0)$ replacing $2\Gamma_{\mathbf{q}}/E_{\mathbf{q}}^2$. This contribution should be added to the non-linear corrections to the total low-temperature heat capacity calculated by Fulde and Jensen (1983).

7.3.3 Coupling to the nuclear spins

The hyperfine coupling to the nuclear spins normally has a negligible influence on the properties of the electronic magnetic moments. However, in the special case of a crystal-field system with a singlet ground-state, where the two-ion coupling is smaller than the threshold value for magnetic ordering, this minute coupling may become of decisive importance. Under these circumstances, the hyperfine interaction may induce a cooperative ordering of the combined system of the electronic and nuclear magnetic moments at very low temperatures. The Hamiltonian describing the hyperfine interaction in a rare earth ion has been comprehensively discussed by Bleaney (1972) and McCausland and Mackenzie (1979), and the leading-order term is

$$\mathcal{H}_{\text{hf}} = A \mathbf{I} \cdot \mathbf{J}, \quad (7.3.22)$$

where \mathbf{I} is the nuclear spin. For the isotope of Pr with mass number 141, which has a natural abundance of 100%, $I = 5/2$ and $A = 52.5 \text{ mK} = 4.5 \mu\text{eV}$. This coupling modifies the MF susceptibility $\bar{\chi}^o(\omega)$ of the single ion, and since A is small, we may derive this modification by second-order perturbation theory. In order to simplify the calculations, we assume that the MF ground-state of the electronic system is a singlet, and that $k_B T$ is much smaller than the energy of the lowest excited J -state, so that any occupation of the higher-lying J -states can be neglected. Considering first a singlet-singlet system, with a splitting between the two states $|0\rangle$ and $|1\rangle$ of $\Delta \gg |A|$, where only $M_z = \langle 0 | J_z | 1 \rangle$ is non-zero, and denoting the combined electronic and nuclear states by $|0, m_I\rangle$ and $|1, m_I\rangle$, where $I_z |p, m_I\rangle = m_I |p, m_I\rangle$, we find that the only non-zero matrix elements of \mathcal{H}_{hf} are

$$\langle 0, m_I | \mathcal{H}_{\text{hf}} | 1, m_I \rangle = \langle 1, m_I | \mathcal{H}_{\text{hf}} | 0, m_I \rangle = m_I M_z A,$$

yielding the following modifications of the state vectors:

$$\begin{cases} |0', m_I\rangle = |0, m_I\rangle - (m_I M_z A / \Delta) |1, m_I\rangle \\ |1', m_I\rangle = |1, m_I\rangle + (m_I M_z A / \Delta) |0, m_I\rangle, \end{cases}$$

to leading order. If we neglect the shifts in energy of the different levels, due to the hyperfine coupling, and the change of the inelastic matrix element,

$$\langle 0', m_I | J_z | 1', m_I \rangle = M_z \{1 - (m_I M_z A / \Delta)^2\} \simeq M_z,$$

the susceptibility is only modified by the non-zero matrix-element,

$$\langle 0', m_I | J_z | 0', m_I \rangle = -2m_I M_z^2 A / \Delta,$$

within the $(2I + 1)$ -ground state manifold, i.e.

$$\delta\chi_{zz}^o(\omega) = \beta \frac{1}{2I+1} \sum_{m_I} (2m_I M_z^2 A/\Delta)^2 \delta_{\omega 0} = \beta \frac{1}{3} I(I+1) A^2 (2M_z^2/\Delta)^2 \delta_{\omega 0}. \quad (7.3.23)$$

This result may be straightforwardly generalized to an arbitrary level scheme, including non-zero matrix elements of the other \mathbf{J} -components, as the different contributions are additive. The susceptibility may then be written

$$\chi_{\alpha\beta}^o(\omega) = \chi_{\alpha\beta}^J(\omega) + A^2 \sum_{\gamma\gamma'} \chi_{\alpha\gamma}^J(\omega) \chi_{\gamma\gamma'}^I(\omega) \chi_{\gamma'\beta}^J(\omega), \quad (7.3.24)$$

to leading order in A , which is valid as long as the general assumptions made above are satisfied. $\chi_{\alpha\beta}^J(\omega)$ is the MF susceptibility for the electronic system alone, when the extra term $\delta\mathcal{H}_J(\text{MF}) = A\langle\mathbf{I}\rangle\cdot\mathbf{J}$ is included in its MF Hamiltonian. In order to derive the effective MF Hamiltonian $\mathcal{H}_I(\text{MF})$, determining the susceptibility of the nuclear spins $\chi_{\alpha\beta}^I(\omega)$, we must consider the possibility, neglected above, that \mathcal{H}_{hf} may lift the $(2I + 1)$ -fold degeneracy of the ground-state manifold. Calculating the energies of the ground-state levels, in the presence of an external field, by second-order perturbation theory, we find straightforwardly that the equivalent Hamiltonian, describing the splitting of these levels, is

$$\mathcal{H}_I(\text{MF}) = -g_N \mu_N \mathbf{H} \cdot \mathbf{I} + A \{ \langle\mathbf{J}\rangle + A\langle\mathbf{I}\rangle \cdot \bar{\bar{\chi}}^J(0) \} \cdot \mathbf{I} - \frac{1}{2} A^2 \mathbf{I} \cdot \bar{\bar{\chi}}^J(0) \cdot \mathbf{I}. \quad (7.3.25a)$$

This result can be interpreted as expressing the ability of \mathbf{J} to follow instantaneously any changes of \mathbf{I} . The molecular field due to $\langle\mathbf{J}\rangle$ is subtracted from the response to \mathbf{I} , which then instead gives rise to the last quadrupolar term. This quadrupolar contribution is the only effect which is missing in a simple RPA decoupling of the interactions introduced through \mathcal{H}_{hf} . If $\bar{\bar{\chi}}^J(0)$ is not a scalar, the last term gives rise to a quadrupole-splitting of the ground-state manifold, and the zero-frequency susceptibility is then, to leading order in this term,

$$\chi_{\alpha\alpha}^I(0) = \frac{1}{3} I(I+1) \beta \left[1 + \frac{1}{15} A^2 \beta (I + \frac{3}{2})(I - \frac{1}{2}) \{ 3\chi_{\alpha\alpha}^J(0) - \sum_{\gamma} \chi_{\gamma\gamma}^J(0) \} \right] \quad (7.3.25b)$$

if $\bar{\bar{\chi}}^J(0)$ is diagonal. The results above were first obtained and analysed by Murao (1971, 1975, 1979), except that he replaced $\chi_{\alpha\alpha}^J(0)$ in (7.3.25) by $(1/N) \sum_{\mathbf{q}} \chi_{\alpha\alpha}^J(\mathbf{q}, 0)$ which, according to the above interpretation, is to be expected in order $1/Z$. For the hexagonal ions in Pr-metal, $A\chi_{\alpha\alpha}^J(0) = 0.026$ for the two basal-plane components, but is

zero for the cc -component, which implies that the induced quadrupolar-interaction is a factor of about seven larger than the intrinsic value of the electric-quadrupole hyperfine-interaction for the ion ($\langle 0 | \mathcal{H}_Q | 0 \rangle = (5/7)P_{\parallel}(I_{\xi}^2 + I_{\eta}^2)$, with $P_{\parallel} = -0.128$ mK, using the notation of Bleaney (1972)). In any case, the quadrupole contribution to (7.3.25b) only makes a 1.5% correction at the transition temperature $T_N \approx 50$ mK in Pr. The induced quadrupole interaction, due to the highly anisotropic fluctuations of the electronic moments, may be important in nuclear-magnetic-resonance (NMR) experiments. The most important effect in NMR is, however, the strong enhancement of the Zeeman splitting between the nuclear levels by the hyperfine coupling. Introducing $\mathcal{H}_I(\text{MF}) = -g_N\mu_N\mathbf{H}_I^{\text{eff}} \cdot \mathbf{I}$ in (7.3.25a), we find an enhancement

$$|H_I^{\text{eff}}/H| \simeq |1 - (g\mu_B/g_N\mu_N)A\chi_{zz}(\mathbf{0}, 0)|, \quad (7.3.26)$$

which, for the hexagonal ions in Pr, gives a factor of about 40 in the low-temperature limit, when the field is applied in the basal-plane, but unity if H is along the c -axis. In addition to the hyperfine interactions considered above, the nuclear spins may also interact directly with the conduction electrons, leading to an extra *Knight shift* and Korringa broadening of the NMR-levels. The most important NMR-linewidth effect is, however, due to the fluctuations of the localized electronic moment. If $J = 1$, corresponding to Pr, these fluctuations lead to a Lorentzian broadening, so that $\chi_{\xi\xi}^I(0) \rightarrow \chi_{\xi\xi}^I(0)[i\Gamma_N/(\hbar\omega + i\Gamma_N)]$, with

$$\Gamma_N = 10(n_0n_1/n_{01})M_{\xi}^2\text{Im}[\tilde{K}(\omega = \Delta/\hbar)],$$

to first order in $1/Z$. In the case of Pr, this gives $\Gamma_N \simeq \exp(-\beta\Delta) \times 1.0$ meV (Jensen *et al.* 1987).

The magnetization and the neutron-scattering cross-section are determined in the RPA by the usual susceptibility expression (7.1.2), with $\bar{\chi}^o(\omega)$ now given by (7.3.24), provided that we neglect the contributions of the small nuclear moments. This means that, even though the electronic system has a singlet ground-state, the hyperfine interaction induces an elastic contribution, and assuming the electronic system to be undercritical, so that $R(0) < 1$ in (7.1.6), we obtain in the low temperature limit, where $k_B T \ll \Delta$,

$$\chi_{\xi\xi}(\mathbf{q}, 0) = \frac{\Delta^2\{1 + A^2\chi^J(0)\chi^I(0)\}}{E_{\mathbf{q}}^2 - (\Delta^2 - E_{\mathbf{q}}^2)A^2\chi^J(0)\chi^I(0)}\chi^J(0), \quad (7.3.27)$$

where $\chi^J(0) = 2M_{\xi}^2/\Delta$, and $E_{\mathbf{q}}$ is given by (7.1.4b), with $n_{01} = 1$. If we introduce the nuclear spin susceptibility, neglecting the quadrupolar contribution, into this expression, it predicts a second-order phase

transition, at a temperature determined by

$$k_B T_N = \frac{1}{3} I(I+1) A^2 \chi^J(0) \frac{\Delta^2 - E_{\mathbf{Q}}^2}{E_{\mathbf{Q}}^2} = \frac{1}{3} I(I+1) A^2 \chi^J(0) \frac{R_0}{1 - R_0}, \quad (7.3.28)$$

to a modulated phase described by the wave-vector \mathbf{Q} at which $\mathcal{J}(\mathbf{q})$ has its maximum value, where R_0 is the critical parameter defined by eqn (7.1.6). With $\Delta = 3.52$ meV and $E_{\mathbf{Q}} = 1.0$ meV for the hexagonal excitations in Pr, the electronic system is just undercritical, with a critical ratio $R_0 \simeq 0.92$. This means that the importance of the hyperfine interaction is much enhanced, and eqn (7.3.28) predicts $T_N = 45$ mK for the cooperative ordering of the nuclear and electronic moments in Pr. The transition is no longer accompanied by a soft mode, but there is rather an elastic peak, with a scattering intensity given by

$$S_d^{\xi\xi}(\mathbf{q}, \omega \approx 0) = \frac{1}{3} I(I+1) A^2 \frac{(2M_{\xi}^2/E_{\mathbf{q}})^2}{1 - \chi^J(0)\{1 + A^2\chi^J(0)\chi^I(0)\}\mathcal{J}(\mathbf{q})} \delta(\hbar\omega), \quad (7.3.29)$$

in the paramagnetic phase, which diverges at $\mathbf{q} = \mathbf{Q}$ when T approaches T_N , analogously to the behaviour of the singlet-triplet case described by (7.1.13).

7.4 Magnetic properties of Praseodymium

The magnetic behaviour of Pr has already been extensively discussed in this chapter, in order to illustrate a number of the phenomena which occur in crystal-field systems. In this section, we will collect together these threads into a coherent description of the magnetic ordering which may be induced by various perturbations, and of the excitations in the paramagnetic and ordered phases.

7.4.1 Induced magnetic ordering

As discussed at the end of the preceding section, the coupling of the nuclear spins to the electronic moments in Pr gives rise to a magnetic system whose ground state is degenerate. According to the third law of thermodynamics, this degeneracy must be lifted at sufficiently low temperatures and, within the MF approximation, this is accomplished by magnetic ordering at a temperature determined by eqn (7.3.28). The enhancement factor $R_0/(1 - R_0)$ is about 12 for the hexagonal sites, so that the calculated collective-ordering temperature for the nuclear spins and the electronic moments is raised into the more readily accessible range of about 45 mK. The strong neutron-diffraction peak illustrated in Fig. 7.8 was observed at 40 mK by Bjerrum Møller *et al.* (1982), at a value of \mathbf{Q} close to the minimum in the dispersion relations of the magnetic excitons. This mode of excitation comprises magnetic fluctuations

whose zero-frequency limit is a longitudinal-wave structure along the b -axis, and the electronic moment induced by the hyperfine coupling, in the zero-temperature limit, is

$$\langle J_\eta(\mathbf{Q}) \rangle_0 \simeq IA \frac{\chi^J(0)}{1 - \chi^J(0)\mathcal{J}(\mathbf{Q})} = IA \frac{2M_\eta^2}{\Delta(1 - R_0)}, \quad (7.4.1)$$

multiplied by $g\mu_B$, corresponding to about $0.6\mu_B$. Determining the electronic moment from the neutron-diffraction intensities is complicated by the coherent nuclear scattering of neutrons at the same \mathbf{Q} , due to the induced polarization of the nuclei. The two contributions can however be separated with the help of polarized neutrons, and Kawarazaki *et al.* (1988) thereby deduced that the electronic moment on the hexagonal sites is about $0.4\mu_B$ at 30 mK, while there is also an induced moment an order of magnitude smaller on the cubic sites. The nuclear polarization on both types of site is substantial at this temperature, which is consistent with the observation by Lindelof *et al.* (1975) and Eriksen *et al.* (1983) of a dramatic increase in the nuclear heat capacity, indicating a second-order transition of the nuclear spins to an ordered structure at about 50 mK.

As may be seen in Fig. 7.8, the magnetic ordering is preceded by a strong precursor scattering, which has been observed in single crystals by a number of investigators at temperatures as high as 10 K, and was first investigated in the millikelvin range by McEwen and Stirling (1981). The figure shows that the peak actually comprises two contributions, one centred at the critical wave-vector, and a broader component at a slightly smaller wave-vector. The narrower peak, which is usually known as the *satellite*, appears around 5 K and increases rapidly in intensity as T_N is approached, at which temperature it transforms into the magnetic Bragg peak. Since the width in κ of this peak is greater than the instrumental resolution, at temperatures above T_N , it does not reflect the presence of true long-range magnetic order, but rather very intense fluctuations, with a range of several hundred Å, which presumably also vary slowly in time. The RPA theory predicts such a peak only because of the elastic scattering from the nuclear spins, as given by eqn (7.3.29). However, the peak produced by this mechanism is estimated to be visible only very close to T_N , below 200 mK, and cannot therefore explain the observations. The satellite above T_N may be interpreted as a critical phenomenon, due to the strong increase in the fluctuations, neglected in the RPA, which develop as the second-order transition is approached. When the electronic susceptibility has saturated below about 7 K, the critical fluctuations in Pr would be expected

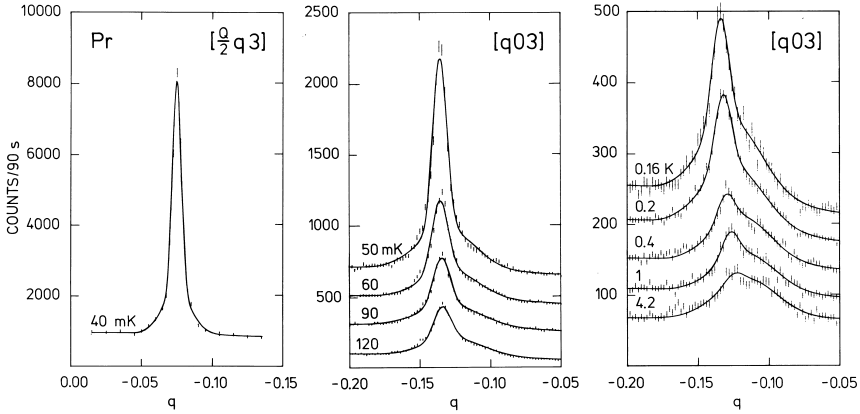


Fig. 7.8. Neutron-diffraction scans in Pr. The solid lines show the sum of two Gaussian functions fitted to the data. Only below 50 mK is the width of the narrower of these equal to the experimental resolution, indicating true long-range magnetic order.

to correspond to those of a normal degenerate system within 10% of its critical temperature. However, the satellite in Fig. 7.8 is much more intense than such fluctuations could normally give rise to. An alternative possibility, which has been analysed theoretically by Murao (1984), is that much of the intensity of the satellite above T_N is due to an ordering of the moments close to the surface of the crystal, which gives rise to a Bragg peak of non-zero width. The crystalline electric field acting on the surface ions is different from that determining the bulk properties, and the magnetic response of these ions will therefore also be different. For instance, the lowering of the symmetry near the surface splits the degeneracy of the $|\pm 1\rangle$ -states, thereby enhancing one of the basal-plane components of the susceptibility tensor.

The occurrence of the other peak in the scans shown in Fig. 7.8, known as the *central* or *quasielastic peak*, has been a long-standing mystery. It is much broader than the satellite and constitutes a ring of scattering around Γ in the basal- Γ MK-plane, with a radius which is slightly smaller than that of the contour of energy minima found in the excitation spectrum, illustrated in Fig. 7.1. The integrated quasielastic-scattering intensity from this ring is therefore rather large, and around 1 K it is found to correspond to a moment of the order of $0.1 \mu_B$ per hexagonal ion. In a polycrystalline sample, this ring of scattering cannot be distinguished from scattering from a single point in κ -space, which presumably explains why diffraction studies of polycrystalline Pr indicate that it is antiferromagnetic at 4 K (Cable *et al.* 1964).

The quasielastic peak cannot be classified as an additional critical phenomenon, because it is not centred at the critical ordering wave-vector. Furthermore, even though its intensity increases in the paramagnetic phase, as the system approaches criticality, it is still present, with a non-zero width in κ -space, below the transition and its intensity continues to increase as the temperature is further reduced (Burke *et al.* 1981; Bjerrum Møller *et al.* 1982; McEwen 1986). The dynamic effects associated with this quasielastic peak are very modest, as observed by Jensen *et al.* (1987); its width in energy is estimated to be less than 0.1 meV. Nevertheless, its integrated intensity is too large to be explained as a static phenomenon due to scattering from local *short-range* ordering of the crystal near the surface or around bulk defects, such as magnetic impurities or lattice defects. The only remaining possibility appears to be that the quasielastic peak is associated with the magnetic response of the itinerant electrons. This is consistent with one of the results of the neutron-scattering studies by Leuenberger *et al.* (1984) of the hexagonal *insulator* Cs₃Cr₂Br₉, in which the Cr dimers form a singlet-triplet system which has a number of analogies to Pr. Even though this system is very close to magnetic ordering, and the lowest excitation energies are only about 0.2 meV, there is no sign of either a satellite or a quasielastic peak. The spin fluctuations of band electrons are not normally expected to give rise to a quasielastic peak of the intensity observed in Pr, and its occurrence may therefore indicate the formation of resonant states near the Fermi surface in Pr, due to hybridization of the conduction electrons with the *4f* electrons. As discussed in Section 1.3, the *4f* electrons in Pr are very close to delocalization, and the incipient magnetic instability of the localized electrons would therefore be expected to be reflected in fluctuations in the conduction electron-gas. An indication of the sensitivity of the conduction electrons to the ordering process is provided by the resistivity measurements of Hauschultz *et al.* (1978), who found an increase of almost fifty per cent, over the temperature range in which the quasielastic peak develops, in the *c*-direction, where superzone effects in the ordered phase are expected to be of minor importance. Further studies of the quasielastic peak, and associated changes in the conduction electrons, particularly under high pressures with the corresponding progressive increase in *4f* hybridization, would clearly be of interest.

Antiferromagnetism can also be induced in Pr by an internal coupling to magnetic impurities. Assuming that the susceptibility of the single impurities of concentration *c* is proportional to $1/T$, we find that eqns (5.6.5-6) of the virtual crystal approximation lead to an ordering temperature determined by

$$T_N = T_N(c) = \frac{c}{1 - (1 - c)R(T_N)} T_N(c = 1), \quad (7.4.2)$$

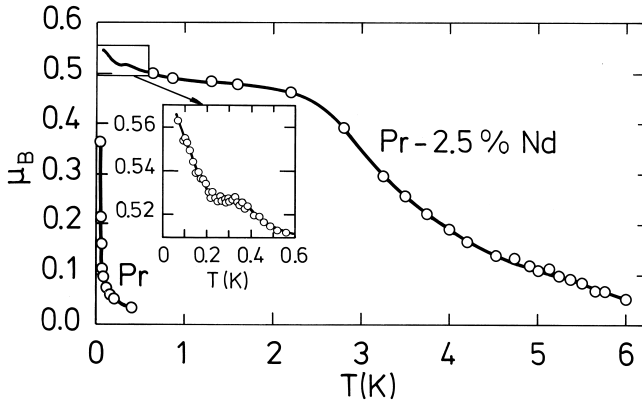


Fig. 7.9. The effective moments, deduced from the intensities of the narrower peaks in scans of the type illustrated in Fig. 7.8, in Pr and $\text{Pr}_{97.5}\text{Nd}_{2.5}$. Only below about 50 mK and 3.5 K respectively do these moments correspond to a long-range magnetically ordered state.

where $R(T)$ is the critical parameter of eqn. (7.1.6). This expression gives $T_N \simeq 12.5cT_N(c = 1)$, for $c \ll 1$. A rapid increase of T_N at small concentrations of Nd ions in Pr was indeed observed by Lebech *et al.* (1975). As illustrated in Fig. 7.9, the study of a single crystal of $\text{Pr}_{97.5}\text{Nd}_{2.5}$ by Bjerrum Møller *et al.* (1982) revealed a number of informative details. The temperature dependence of the scattered intensity follows qualitatively the behaviour observed in pure Pr. The quasielastic peak appears around 10 K, a strong satellite which is broader than the experimental resolution emerges from it around 6 K, and a diffraction peak, signifying true long-range order, develops below about 3.5 K. As in Pr, the quasielastic peak continues to grow below T_N . The rise in the magnetization below about 0.2 K is ascribed to the polarization of the nuclei and their hyperfine interaction with the $4f$ moments. Inelastic neutron-scattering experiments by Wulff *et al.* (1983) gave results consistent with a crystal-field model in which the Nd ions have a predominantly $|\pm \frac{3}{2}\rangle$ ground state, and excited $|\pm \frac{1}{2}\rangle$ and predominantly $|\pm \frac{5}{2}\rangle$ states at about 0.3 meV and 1.2 meV respectively.

The application of an external uniaxial pressure along the a -axis in the basal plane lifts the degeneracy of the $|\pm 1\rangle$ first excited-state and may therefore induce magnetic ordering, as predicted by Jensen (1976a) and observed by McEwen *et al.* (1978). The magnetoelastic phenomena described in Section 7.3.1, particularly the magnitude of the field-induced interaction between the magnetic excitations and the transverse phonons, may be used for estimating the coupling parameter $B_{\gamma 2}$

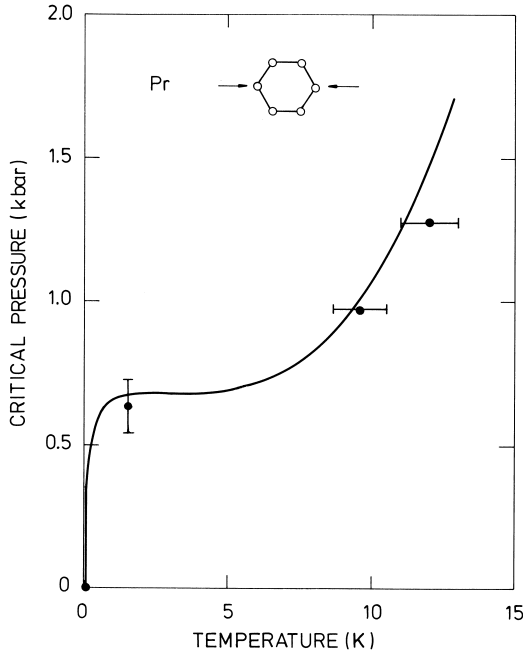


Fig. 7.10. MF calculation of the ordering temperature T_N in Pr, as a function of the uniaxial pressure in the a -direction, compared with the neutron-diffraction measurements of McEwen *et al.* (1983).

for the hexagonal ions. Neglecting the magnetoelastic coupling to the cubic ions, we obtain from eqn (7.3.2) the following γ -strain contribution to the magnetic Hamiltonian:

$$\mathcal{H}_\gamma(\text{sta}) = - \sum_{i \in \text{hex.ions}} B_{\gamma 2} O_2^2(\mathbf{J}_i) \left[\frac{1}{2} B_{\gamma 2} \langle O_2^2(\mathbf{J}_i) \rangle + t_{11} \right] / c_\gamma + \mathcal{H}_\gamma^0, \quad (7.4.3)$$

in the presence of a uniaxial stress along the ξ -axis. N in (7.3.2) is the total number of ions, or twice the number of hexagonal sites. At zero temperature and zero magnetic field, the only effect of $\mathcal{H}_\gamma(\text{sta})$, within the effective ($J = 1$)-model, is that the crystal-field splitting which determines the excitation spectrum becomes different for the two polarizations, and for instance Δ_η , giving the J_η -mode energies, is found to be

$$\Delta_\eta = \Delta_\eta(t_{11}) = \Delta - B_{\gamma 2} M_{22} t_{11} / c_\gamma,$$

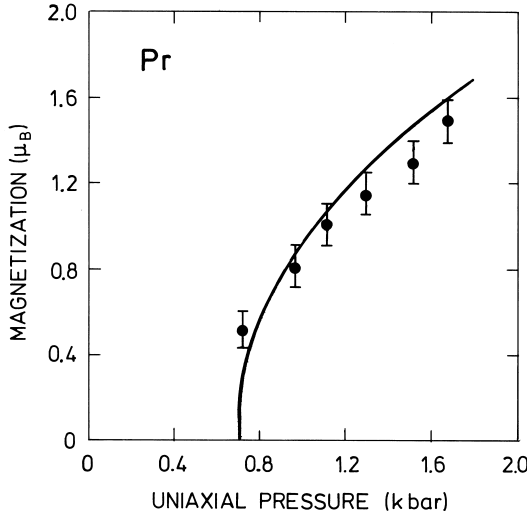


Fig. 7.11. Experimental measurements of the first harmonic of the magnetization on the hexagonal sites in Pr, deduced from the intensities of neutron-diffraction peaks at 1.5 K, compared with a MF calculation for the $J = 4$ ion.

where the matrix element

$$M_{22} \equiv \langle 1_a | O_2^2 | 1_a \rangle = - \langle 1_a | J_\eta^2 | 1_a \rangle = -10,$$

in Pr. Δ_ξ differs from Δ by the same amount, but with the opposite sign. At the incipient ordering wave-vector \mathbf{Q} along the η -axis, the excitations are purely transverse or longitudinal, J_ξ or J_η modes. The critical ratio R_0 , defined by eqn (7.1.6), for the optical longitudinal mode at \mathbf{Q} is then determined by

$$R_0(t_{11}) = R_0(0)\Delta/\Delta_\eta(t_{11}).$$

Hence the application of the stress alters the critical ratio, and it attains the threshold value 1 when

$$T_{11}^c = \frac{\{1 - R_0(0)\}\Delta}{M_{22}B_{\gamma_2}} c_\gamma N/V, \quad (7.4.4)$$

where $c_\gamma N/V = 4c_{66}$. With the following values of the parameters; $R_0(0) = 0.92$, $\Delta = 3.52$ meV, $B_{\gamma_2} \simeq 12$ meV, and $c_{66} = 1.6 \cdot 10^{10}$ N/m², the effective ($J = 1$)-model predicts that the critical stress necessary for inducing magnetic ordering in Pr at zero temperature is $T_{11}^c = -1.5$ kbar. However, the $|3_S\rangle$ -state lies just above the magnetic excitons

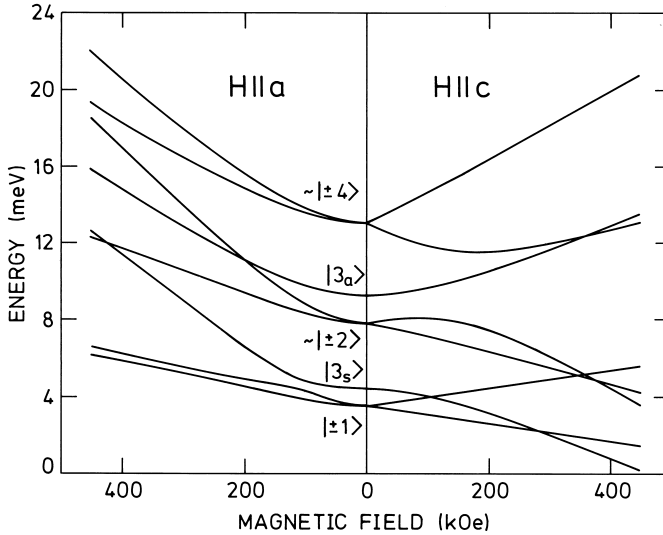


Fig. 7.12. The crystal-field levels of an isolated hexagonal ion in Pr, as a function of an applied magnetic field in the a - and c -directions. The zero-field wavefunctions are specified more precisely in Fig. 1.16.

and, as $\langle 1_a | O_2^2 | 3_s \rangle$ is non-zero, it has a significant effect on $\Delta_\eta(t_{11})$. A calculation which includes all the crystal-field levels of Pr predicts the critical uniaxial pressure $-T_{11}^c$ along the ξ -axis to be 0.7 kbar. As may be seen in Fig. 7.10, such a calculation is in good agreement with the experimental observations of McEwen *et al.* (1983), at temperatures sufficiently high that the hyperfine coupling is of no importance, and also accounts very well for the critical pressure at higher temperatures, where the thermal population of the magnetic excitons becomes significant. The dependence of the ordered moment at 1.5 K on the uniaxial pressure is also very well reproduced by this theory, as illustrated in Fig. 7.11. The stable configurations of the moments at zero pressure are expected to be analogous to those found in Nd and discussed in Sections 2.1.6 and 2.3.1, i.e. a single- \mathbf{Q} structure at small values of the magnetization and a double- \mathbf{Q} configuration when the first harmonic of the moments is larger than about $0.2\text{--}0.3\mu_B$. This behaviour has not been established experimentally, but a suggestive rotation of the ordering wave-vector away from the symmetry axis, as expected in the double- \mathbf{Q} structure, has been detected (McEwen *et al.* 1983). Uniaxial pressure stabilizes a longitudinal wave with \mathbf{Q} along the b -axis perpendicular to the strain, and a modest pressure of about 0.1 kbar is estimated to be sufficient to quench the double- \mathbf{Q} structure. Accordingly, the theoretical curve in

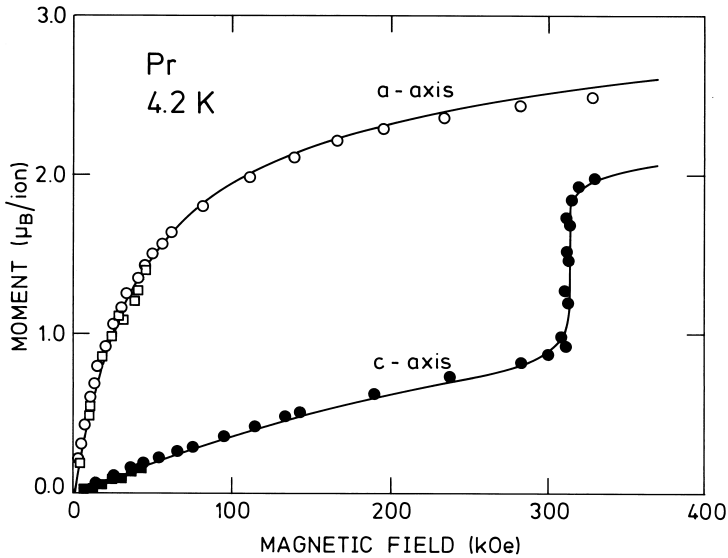


Fig. 7.13. MF calculation of the magnetization of Pr at 4.2 K as a function of a magnetic field applied in the a - and c -directions. The circles are the experimental measurements of McEwen *et al.* (1973), while the squares are deduced from the neutron-diffraction results of Lebech and Rainford (1971).

Fig. 7.11 is calculated with the assumption of a single- \mathbf{Q} ordering of the moments.

The final perturbation which may induce a magnetic state in Pr is an external magnetic field. The modification of the crystal-field levels of an isolated hexagonal ion by a magnetic field is illustrated in Fig. 7.12. If the field is in the basal plane, the excited states are increased in energy, relative to the ground state, but they mix strongly into it, giving rise to the large moment shown in Fig. 7.13. If the magnetic field is along the c -axis, on the other hand, the matrix elements between the ground and excited states on the hexagonal sites are zero, but the $|+1\rangle$ and $|3_S\rangle \rightarrow |+3\rangle$ states both decrease in energy, linearly and quadratically respectively. At about 320 kOe, the latter crosses the ground state and the moment increases abruptly, as observed by McEwen *et al.* (1973). As illustrated in Fig. 7.13, the model of Houmann *et al.* (1979), supplemented with a magnetoelastic coupling $B_{\alpha 2} = 7.0$ meV for the hexagonal ions, accounts well for these results. The jump in the magnetization rapidly becomes smeared out when the temperature is raised, due to the thermal population of the excited states, as observed experimentally at 14 K (McEwen 1978).

7.4.2 The magnetic excitations

The magnetic-excitation spectrum in Pr has been investigated experimentally in great detail as a function of various external constraints, such as the temperature, a magnetic field applied in the basal plane, and uniaxial pressure. Most of the knowledge about the (low-temperature) coupling parameters in the model Hamiltonian for Pr, which we have already utilized several times in the preceding sections, has been derived from these experiments. The first inelastic neutron-scattering experiments on Pr (Rainford and Houmann 1971; Houmann *et al.* 1975b) showed that the excitations behave as expected in a singlet ground-state system, and that the two-ion coupling is just below the threshold value for inducing magnetic ordering. A MF analysis of the temperature dependence of the excitations, shown by the dashed lines in Fig. 7.3, indicated that the crystal-field splitting Δ between the $|0\rangle$ ground-state and the first excited $|\pm 1\rangle$ -doublet state of the hexagonal ions is about 3.2 meV. An important discovery (Houmann *et al.* 1975b) was the observation, illustrated in Fig. 7.1, of a strong splitting of the doublet excitations, whenever such a splitting is allowed by symmetry, i.e. when \mathbf{q} is not along the c -axis. This effect demonstrates that the anisotropic contribution to the two-ion Hamiltonian of Pr,

$$\begin{aligned} \mathcal{H}_{JJ} = & -\frac{1}{2} \sum_{ij} \mathcal{J}(ij) \mathbf{J}_i \cdot \mathbf{J}_j \\ & + \frac{1}{2} \sum_{ij} \mathcal{K}(ij) [(J_{i\xi} J_{j\xi} - J_{i\eta} J_{j\eta}) \cos 2\phi_{ij} + (J_{i\xi} J_{j\eta} + J_{i\eta} J_{j\xi}) \sin 2\phi_{ij}], \end{aligned} \quad (7.4.5)$$

is important. Here ϕ_{ij} is the angle between the ξ -axis and the projection of $\mathbf{R}_i - \mathbf{R}_j$ on the basal plane. Real-space coupling parameters $\mathcal{J}(ij)$ and $\mathcal{K}(ij)$ derived from the excitation energies shown in Fig. 7.1, using the MF-RPA expression for the energies with $\Delta = 3.52$ meV, are shown in Fig. 1.18. This somewhat larger value of Δ was obtained from a study of the field dependence of the excitations (Houmann *et al.* 1979), but it is still consistent with their temperature dependence, as shown by the results of the self-consistent RPA, the solid lines in Fig. 7.3. Besides leading to the more accurate value of Δ , the field experiments revealed the presence of a rather strong magnetoelastic γ -strain coupling in Pr, which creates energy gaps proportional to the field at the crossing points of the magnetic-exciton and transverse-phonon branches in the basal-plane directions, as illustrated in Fig. 7.14.

The model Hamiltonian, with the two-ion and magnetoelastic terms given respectively by (7.4.5) and (7.4.3), together with the usual single-ion crystal-field Hamiltonian for a hexagonal system, describes very well the excitation-energy changes observed by Houmann *et al.* (1979) when

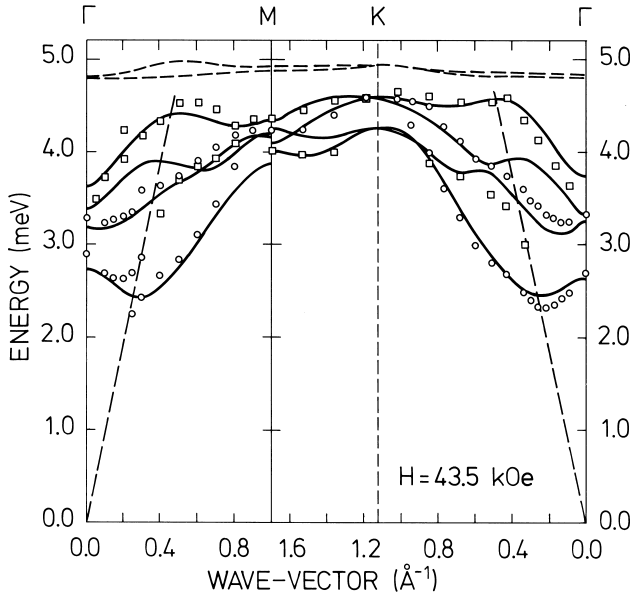


Fig. 7.14. Dispersion relations for the excitations propagating on the hexagonal sites of Pr at 6K, in an applied field of 43.5 kOe. The field is in the basal plane and perpendicular to the wave-vector, so that there is a discontinuity at M, corresponding to a rotation of the field through 90° . Compared with Fig. 7.1, the energy of the magnetic excitations has increased, and the field has induced couplings between the magnetic excitons and the transverse-acoustic phonons polarized in the basal plane, indicated by dashed lines. These phonons are coupled to the acoustic and optical longitudinal magnetic modes in the ΓM -direction, and to the (predominantly) acoustic longitudinal and optical transverse modes (the two branches of intermediate energy) in the ΓK -direction (Jensen 1976a). The full lines show the results of an RPA calculation of the magnetic excitations, neglecting the coupling to the phonons. The predicted low-intensity higher-lying modes, corresponding to transitions to the predominantly $|3_S\rangle$ crystal-field state, were not observed directly in the experiments, but their influence may be seen in the lowest branch along ΓK , since it is their mixing with this mode which holds the energies below those along ΓM .

a field is applied in the basal plane at low temperature. The dispersion relation was measured at three values of the field (14.5, 29.0, and 43.5 kOe), and the results obtained at the highest field are shown in Fig. 7.14.

The most important effect of the field is the admixture of $|1_{S,a}\rangle$ into the ground state. This causes Δ_ξ and Δ_η to increase, and the matrix elements M_ξ and M_η to decrease. The energies of the excita-

tions are thereby increased, while the dispersion becomes smaller. If the field is applied along the ξ -axis, the ξ -mode parameters are changed approximately twice as much, relative to their zero-field values, as the η -mode parameters. At $H = 43.5$ kOe, the total molecular field, which determines the energies in Fig. 7.12, is 100 kOe, and $\Delta_\xi = 4.29$ meV, whereas $\Delta_\eta = 3.86$ meV. This means that the field produces the largest effects on the excitations polarized (predominantly) parallel to it, which in Fig. 7.14 are the transverse modes, both when \mathbf{q} is along ΓM and along ΓK . The γ -strain coupling opposes the splitting of the transverse and longitudinal modes, but only quadratically in the field. The hexagonal anisotropy does not affect the effective ($J = 1$)-excitations in zero field, but B_6^6 causes a splitting between the $|3_s\rangle$ and $|3_a\rangle$ -states of nearly 5 meV. As B_6^6 is negative, the lower of the two states is $|3_s\rangle$ which, according to Fig. 1.16 or 7.12, should lie only 0.9 meV above the $|1_{s,a}\rangle$ -states. The magnetic field induces a coupling between this neighbouring level and the doublet excitations, so that it acquires a significant scattering cross-section at the energies indicated by the dashed lines in Fig. 7.14. Although the extra peak was not sufficiently distinct to be detected directly in the neutron-scattering experiments, the presence of this level is clearly manifested in the behaviour of the doublet excitations. The absolute minimum in the excitation spectrum at zero field is found along ΓM , whereas at $H = 43.5$ kOe the energy minimum in the ΓK -direction has become the lowest. The $|3_s\rangle$ -excitations are coupled to the doublet excitations polarized along the ξ -axis, both when the field is along the ξ - and the η -axis. This means that the energy increase of the longitudinal (optical) mode in the ΓK -direction is diminished, due to the repulsive effect of the field-induced coupling to the $|3_s\rangle$ -excitations. When the field is along the ξ -direction, the longitudinal modes in the ΓM -direction are coupled to the $|3_a\rangle$ -excitations, which lie at much higher energies and only perturb the lower modes very weakly. The basal-plane anisotropy is also clearly reflected in the field dependence of the elastic constant c_{66} , shown in Fig. 7.5.

The effects of the field on the hexagonal doublet-excitations are very strong. In comparison with the zero-field result of Fig. 7.1, the minimum-energy modes have more than doubled their energies, while the overall width of the excitation bands has been reduced by nearly a factor of two. Because of these large changes, the measurement of the field dependence of the excitation spectrum allowed a rather precise determination of Δ and the relative position of the $|3_s\rangle$ crystal-field level. With the assumption that $B_6^6 = -(77/8)B_6^0$, these results then led to the crystal-field level-scheme for the hexagonal ions shown in Figs. 1.16 and 7.12, leaving only the position of the highest-lying level somewhat arbitrary. The field experiment also determined the value of

the magnetoelastic parameter $(B_{\gamma_2})^2/c_\gamma$. This agrees with the value of B_{γ_2} for the hexagonal ions which accounts for the coupling between the magnetic excitations and the phonons, and for the field dependences of c_{66} (Fig. 7.5) and of the γ -strains (Hendy *et al.* 1979). It furthermore allowed the accurate prediction of the strain-induced antiferromagnetic transition in Pr, shown in Fig. 7.10.

The low-temperature magnetic properties of Pr are dominated by the hexagonal ions. One consequence of this is that it is more difficult to construct a reliable model for the cubic ions, based on experimentally derivable parameters. Although the model proposed by Houmann *et al.* (1979) accounts accurately for the bulk of the low-temperature experimental results, it is not uniquely specified and some deficiencies appear in comparison with experiments at elevated temperatures. The model is based on the following crystal-field Hamiltonian for the cubic ions:

$$\mathcal{H}_J = \sum_{i \in \text{cub. ions}} \left[B_4^0(c) \{ O_4^0(\mathbf{J}_i) - 20\sqrt{2} O_4^{-3}(\mathbf{J}_i) \} + B_6^0(c) \{ O_6^0(\mathbf{J}_i) + \frac{35}{4}\sqrt{2} O_6^{-3}(\mathbf{J}_i) - \frac{77}{8} O_6^6(\mathbf{J}_i) \} \right], \quad (7.4.6)$$

which neglects the departure of the local symmetry of these sites from cubic. We shall not present an extensive discussion of the model here (more details may be found in Houmann *et al.* (1979) and Jensen (1979b, 1982)), but it is clear that this MF model, which is the simplest description of Pr consistent with its magnetic behaviour in the low-temperature limit, must be extended in order to describe, for instance, the magnetostriction measurements of Hendy *et al.* (1979) and Ott (1975). In addition to introducing a non-zero value of B_{α_2} for the hexagonal ions, of the magnitude used to obtain agreement with experiment in Fig. 7.13, it is probably also necessary to include B_{α_1} . Moreover, the magnetoelastic parameters for the cubic ions are presumably of the same order of magnitude as those on the hexagonal ions. This probably also applies to $B_2^0(c)$, neglected in eqn (7.4.6). The separation of the contributions from the hexagonal and the cubic ions to the c -axis bulk susceptibility as a function of temperature, accomplished through neutron-diffraction experiments by Rainford *et al.* (1981), indicates that not only is $B_2^0(c)$ non-zero, but the exchange between the c -axis components of the moments is also different from the corresponding coupling between the basal-plane components. The development of a MF model for Pr which describes its properties more accurately at elevated temperatures would benefit greatly from a more detailed examination of the excitations on the cubic sites, i.e. a determination of the energies of the excitations polarized in the c -direction, and the field-induced changes of these excitations, and of those polarized in the basal-plane and shown in Fig. 7.2.

The missing ingredients in the model presented here to describe Pr have a negligible influence on the pressure-induced ordered structure, and most of the observations made in this phase were explained by Jensen *et al.* (1987) utilizing only the information obtained from the zero-pressure studies of Houmann *et al.* (1979). Because the ordered moments in the antiferromagnetic phase are parallel to \mathbf{Q} , the change of the ground state affects primarily the longitudinal excitations, and the low-energy optical branch close to the ordering wave-vector is particularly strongly modified. Fig. 7.15 shows the experimental excitation energies of the optical modes in the ΓM -direction at 5.5 K, in the presence of a uniaxial pressure of 1.28 kbar, compared with the predictions of the RPA theory.

Under the conditions of the measurements, the analysis shows that the induced moments

$$\langle J_{i\eta} \rangle = \langle J_{\eta}(\mathbf{Q}) \rangle \cos(\mathbf{Q} \cdot \mathbf{R}_i + \varphi) \quad (7.4.7a)$$

are so small that the effective ($J = 1$)-model is adequate to describe the excitations, and the value of the third harmonic of the longitudinally ordered moments is only a few per cent of $\langle J_{\eta}(\mathbf{Q}) \rangle$. A full account of the structure would require specifying two phase constants, one for

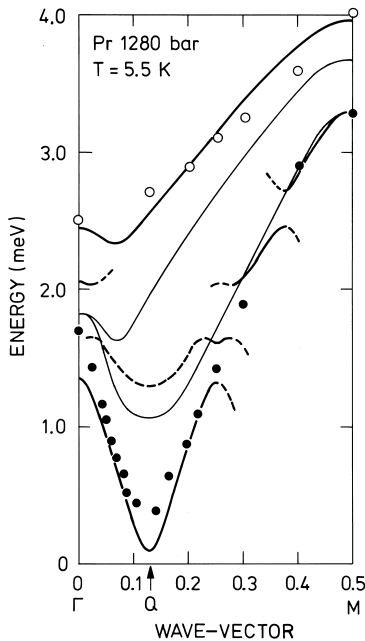


Fig. 7.15. The dispersion relations for the optical excitations in the antiferromagnetic phase of Pr at 5.5 K under an applied uniaxial pressure of 1.28 kbar. The ΓM direction shown is perpendicular to the pressure axis. The circles depict the experimental results obtained from inelastic neutron scattering, with solid and open symbols indicating the longitudinal and transverse branches respectively. The solid lines are the calculated RPA energies for the excitations, whereas the dashed lines indicate longitudinal modes of weaker intensity. The thin lines are the experimental dispersion relations in unstressed Pr, as in Fig. 7.1

each of the two sublattices. The difference between the two phases is approximately π , or approximately 0 if \mathbf{Q} , within the primitive zone, is replaced by $\mathbf{Q} + \mathbf{b}_3$. Introducing the relative magnetization σ by

$$\langle J_\eta(\mathbf{Q}) \rangle = M_\eta \sigma, \quad (7.4.7b)$$

where the matrix element is slightly dependent on the pressure ($M_\eta = 1.026\sqrt{10}$ at 1 kbar), we find that $\sigma \simeq 0.44$ under the conditions of Fig. 7.15. Because σ is still small, it may be utilized as an expansion parameter, both in the calculation of the ordered moments and also in the equations of motion determining the excitation spectrum. The ordering wave-vector is close to $\frac{1}{8}\mathbf{b}_2$, but whether the system is commensurate or not is not easy to decide from the experiments. In any case, this is not important for calculating the excitation spectrum, because distinctive effects of commensurability only appear in the order $\sigma^8 \approx 0.001$. The modulation of the length of the moments implies that the single-ion MF susceptibility is site-dependent, and the $\eta\eta$ -component is found to be

$$\chi_{\eta\eta}^o(j, \omega) = \frac{2n_{01}(j)M_\alpha^2\Delta \cos 2\theta_j}{(\Delta/\cos 2\theta_j)^2 - (\hbar\omega)^2} + \beta p_{01}(j)M_\alpha^2 \sin^2 2\theta_j \delta_{\omega 0}, \quad (7.4.8a)$$

equivalent to eqn (7.1.9) with $\langle J_{j\eta} \rangle = M_\eta n_{01}(j) \sin(2\theta_j)$, and $p_{01}(j)$ defined by

$$p_{01}(j) = n_0(j) + n_1(j) - n_{01}^2(j). \quad (7.4.8b)$$

$\Delta = \Delta_\eta(t_{11})$ is here the crystal-field splitting between the ground state $|0\rangle$ and the excited state $|1\rangle$ ($\equiv |1_a\rangle$ at zero stress) at the particular stress considered. In the incommensurate case, the coupling matrix determining the longitudinal component of the susceptibility tensor is of infinite extent. The situation is very similar to that considered in Section 6.1.2 and, as there, the coupling matrix may be solved formally in terms of infinite continued fractions. The only difference is that, in the present case, the single-site susceptibility is unchanged if the moments are reversed, which means that the coupling matrix only involves terms with n even (where n is the number of the Fourier component, as in (6.1.28)). Since the effective modulation wave-vector seen by the longitudinal excitations is $2\mathbf{Q}$ and not \mathbf{Q} , the acoustic and the optical modes propagating parallel to \mathbf{Q} may be treated separately, as the \mathbf{q} -dependent phase factor determining the effective coupling parameters $\mathcal{J}_{11}(\mathbf{q}) \pm |\mathcal{J}_{12}(\mathbf{q})|$, derived from the interactions in the two sublattices (see Section 5.1), is not affected.

To leading order, the modulation of the moments introduces a coupling between the excitations at wave-vectors \mathbf{q} and $\mathbf{q} \pm 2\mathbf{Q}$, and energy gaps appear on planes perpendicular to \mathbf{Q} passing through $n\mathbf{Q}$. When

$\mathbf{q} = \mathbf{Q}$, the coupling between the modes at \mathbf{Q} and $-\mathbf{Q}$ leads to an *amplitude mode* and a *phason mode*, corresponding respectively to an in-phase and a 90° out-of-phase modulation of the lengths of the moments. The energies of the two longitudinal modes at $\mathbf{q} = \mathbf{Q}$ are approximately given by

$$\begin{aligned} E_{\text{amplitude}} &\simeq \frac{\sqrt{3}}{2} \sigma \Delta \\ E_{\text{phason}} &\simeq \left(\frac{1}{8} \beta \Delta \bar{p}_{01}\right)^{1/2} \sigma \Delta, \end{aligned} \quad (7.4.9)$$

where \bar{p}_{01} is the average value of $p_{01}(j)$. The scattering intensity, proportional to $1/[\hbar\omega\{1 - \exp(-\beta\hbar\omega)\}]$, of the lowest-lying phason mode is much larger than that of the amplitude mode. The low-intensity amplitude mode is indicated by the dashed line at \mathbf{q} -vectors close to \mathbf{Q} in Fig. 7.15, and it was not clearly resolved in the experiments. The phason mode has a dispersion relation, indicated by the solid lines in the figure, which increases linearly from the magnetic Bragg peak at \mathbf{Q} , except for the presence of the small gap E_{phason} at $\mathbf{q} = \mathbf{Q}$. In the incommensurable case, the free energy is invariant to a change of the phase constant φ in (7.4.7), so that the longitudinal component of the zero-frequency susceptibility diverges at the wave-vector \mathbf{Q} . The corresponding generator of an infinitesimal phase shift is $1 - i\delta\varphi \sum_j (|1 \rangle \langle 1|)_j$. If this generator commuted with the Hamiltonian, a specific choice of φ would break a continuous symmetry of the system, implying the presence of a well-defined linearly-dispersive Goldstone mode, as discussed in Section 6.1. However, as may be verified straightforwardly, it does not in fact commute with the Hamiltonian. On the contrary, within the RPA the longitudinal response contains an elastic contribution, due to the final term in (7.4.8a), and hence the scattering function contains a diffusive peak at zero frequency. It is the intensity of this peak which is found to diverge in the limit $\mathbf{q} \rightarrow \mathbf{Q}$. As \mathbf{q} departs from \mathbf{Q} , the diffusive response at zero frequency rapidly weakens, and the phason mode begins to resemble a Goldstone mode. The presence of the inelastic phason mode at the wave-vector \mathbf{Q} can be explained as a consequence of the modulation of the population difference $n_{01}(j)$, which is proportional to \bar{p}_{01} . This mode corresponds to an oscillation of the phase-constant φ in (7.4.7), except that the adiabatic condition, which applies within the RPA as soon as the oscillation frequency is non-zero, constrains $n_{01}(j)$ to remain constant, without participating in the oscillations. This condition, in turn, gives rise to the restoring force which determines the frequency of the oscillations. However, if the oscillations are so slow (i.e. essentially zero in the present approximation) that $n_{01}(j)$ can maintain its thermal-equilibrium value, there are no restoring forces. In the zero-temperature limit, \bar{n}_1 vanishes exponentially, in which case $n_{01}(j) = 1$, and the diffusive elastic response disappears together with E_{phason} . The

gap also vanishes in the other limit when $\sigma \rightarrow 0$, as does the amplitude-mode energy gap, reflecting the soft-mode nature of the transition in this approximation. In the above discussion, we have assumed that the system is incommensurate. In a commensurate structure, the free energy is no longer invariant to an overall phase shift of the structure, and the longitudinal susceptibility does not diverge at \mathbf{Q} . Because of the small value of σ^8 , however, it is close to divergence. The phason-mode energy gap stays non-zero at $T = 0$ in the commensurate case, but it is estimated to be only about 0.03 meV at 1 kbar.

Even at the lowest temperatures reached in the inelastic neutron-scattering experiments, quite strong line-broadening of the low-lying longitudinal excitations was observed in the ordered phase. There are several mechanisms which may lead to non-zero linewidths. One possibility, if the ordering is incommensurate, is a broadening of the excitation peaks analogous to that illustrated in Fig. 6.3 in Section 6.1.2. However, the off-diagonal coupling terms, corresponding to γ_n in (6.1.30), are here multiplied by σ^2 , which means that the continued-fraction solution, although infinite, converges very rapidly without producing linewidth effects of any importance. The $1/Z$ -expansion, discussed in Section 7.2, accounts very well in first order in $1/Z$ for the lifetime effects observed in paramagnetic Pr, as shown in Fig. 7.4. In this order, the intrinsic-linewidth effects vanish exponentially at low temperature, and they should be negligible in the temperature range of the ordered phase, with the important exception that the elastic RPA response acquires a non-zero width. To first order in $1/Z$, δ_{ω_0} in eqn (7.4.8a) is replaced by a Lorentzian $i\Gamma/(\hbar\omega + i\Gamma)$, with $1/\Gamma \simeq \bar{n}_{01}^2 (\pi/2) \mathcal{N}_\eta(\Delta)$, where $\mathcal{N}_\eta(E)$ is the density of states of the η -polarized part of the excitation spectrum. Due to the large value of Γ , estimated to be about 1 meV, the RPA predictions for the behaviour of the phason modes near the ordering wave-vector are strongly modified. Instead of an elastic diffusive and an inelastic, adiabatic phason mode, the theory to this order predicts only one mode at zero energy, but with non-zero width, when \mathbf{q} is close to \mathbf{Q} . An inelastic low-energy peak develops only at a distance of about $0.03|\mathbf{b}_1|$ from \mathbf{Q} . The exchange-enhancement factor in the scattering function causes the width of the Lorentzian near \mathbf{Q} to be much less than 2Γ . Formally the width tends to zero when $\mathbf{q} \rightarrow \mathbf{Q}$, but it is more precisely the intensity which diverges, while strong inelastic tails remain at $\mathbf{q} = \mathbf{Q}$, in accordance with the experimental results.

As was mentioned in Section 7.2, the $1/Z$ -expansion of the effective medium theory was extended to second order in $1/Z$ by Jensen *et al.* (1987). The second-order modifications are important here, but not in the zero-stress case considered in Fig. 7.4, because the low-temperature energy gap of about 1 meV in the excitation spectrum is suppressed by

the uniaxial pressure. The gapless excitation-spectrum in the ordered phase implies that the linewidth effects are predicted to vary smoothly with temperature, and to stay non-zero at $T = 0$, when the second-order contributions are included. We note that the imaginary part of the self-energy is now non-zero below the RPA-excitonic band in the paramagnetic phase, and that it generates an appreciable low-energy scattering at the ordering wave-vector, just above T_N , changing the inelastic critical excitation into a diffusive mode of diverging intensity. Hence a true 'soft-mode transition', as found in the zeroth or first order of $1/Z$, is no longer predicted, but the low-energy effect is far too weak to account for the observed behaviour of the neutron-diffraction satellite. The inclusion of the second-order effects in the theory clearly improves the agreement with the experimental results. However, even though the $1/Z^2$ -theory predicts a non-zero linewidth in the limit $T \rightarrow 0$, the effect is so small, at energies below 1 meV, that it can be neglected in comparison with the contribution due to the scattering against electron-hole pair excitations of the conduction electrons, discussed in Section 7.3.2. The importance of this mechanism has been estimated reasonably accurately, and it leads to a linewidth of the order of 0.15 meV for the optical modes close to \mathbf{Q} . When all contributions are included, the theory indicates that the amplitude mode should have been observable at $\mathbf{q} = \mathbf{Q}$ at the lowest temperatures, in contrast to the experimental results, but otherwise its predictions are found to agree well with the main features of the observations.

PERSPECTIVES FOR RARE EARTH RESEARCH

During the last three decades, a remarkable transformation has occurred in our understanding of rare earth magnetism. This development has been described in the preceding chapters, and we conclude with a short epilogue, in which we attempt briefly to summarize the status of the field and the perspectives for future research in it. The close interplay between experiment and theory is particularly pronounced in rare earth research. It was measurements on pure materials and single crystals which stimulated the early development of the subject, but the construction of the standard model pointed the way to more refined and varied experiments, which in turn required more sophisticated explanations. At the moment, we appear to be in a period where the theory is in the ascendancy; it is able to account for the great majority of the observations, and also to suggest a wide variety of new investigations. Much of the following will therefore be concerned with the indication of promising directions for experimental study.

However, it is clear that the standard model is indeed a model, and transforming it into a fundamental theory will require a deeper quantitative understanding of the magnetic interactions. The key to such an understanding lies in the electronic structure. Band structure calculations are able to predict the ground-state properties of solids with impressive accuracy, and to the extent that comparisons with experimental results exist for the rare earth metals, they are highly successful. Nevertheless, this comparison between theory and experiment is incomplete for even the two most carefully studied examples, Gd and Pr. In both cases, the Fermi surface has been measured in considerable detail with the dHvA effect, but even though the general agreement with the calculations is satisfactory for the larger sheets, the small areas are still not fully accounted for. These discrepancies point to the necessity both of more accurate measurements and of first-principles self-consistent calculations, in which the spin-orbit coupling, the exchange splitting, and the external field are rigorously incorporated. A more complete description of the conduction electrons in Gd would allow further progress in the computation of the sf exchange, although it would not immediately solve the most intractable part of the problem, the screening of the exchange field of the $4f$ electrons, which reduces its effect by a large factor.

The contribution of the spin-orbit coupling in the conduction-electron gas to the single-ion anisotropy could also be estimated and compared with the low-temperature experimental results, taking into account the readily computed dipolar contribution. A knowledge of both the experimental and theoretical masses on a variety of orbits would allow a stringent test of the theory of mass-enhancement by the spin waves. The rich structure in the low-frequency dHvA spectrum of Pr may reflect the hybridization with the $4f$ electrons, which presumably gives rise to the quasielastic neutron-diffraction central peak, and also apparently makes a contribution to the binding in the light rare earths. An immediate goal of a first-principles calculation of the indirect exchange in Pr would be an explanation of the large anisotropy which is revealed by the dispersion relations for the magnetic excitations. This would require an extension of the theory of the influence of the orbital angular momentum on the two-ion coupling to more realistic electronic structures than the free-electron model which is normally considered. If this could be accomplished, a first-principles account of the observed scaling of the exchange with the de Gennes factor in the elements could be envisaged.

An accurate knowledge of the electronic structure would also open the way to a calculation of the source of the other primary interaction, the crystal field, which is determined by the charge distribution. The non-spherical terms, which give rise to the higher- l components of the crystal field, are neglected in the averaging procedure adopted in the construction of the muffin-tin potential, but both they and the non-uniformity of the charge distribution in the interstitial regions can in principle be calculated self-consistently. Such a calculation for Y, for example, would cast some light on the origin of the crystal-field splittings observed in dilute alloys with magnetic rare earths. However, the main barrier to calculating the full crystal-field Hamiltonian again resides in the other part of the problem, the screening of the fields by the atomic core and the $4f$ electrons themselves. This is indeed a formidable difficulty, but presumably not one which is insurmountable.

A constant theme, running in parallel with the steady improvement of the standard model, has been the question of the nature of the $4f$ states in Ce and its compounds. As has been apparent for some time, the standard model is not applicable to, for example, α -Ce, as the $4f$ electrons are itinerant, make a substantial contribution to the binding, and must be described by the band model. We have said relatively little about mixed-valent Ce compounds, primarily because they lie outside the main scope of this book, but also because the subject is in a very rapid state of development, making any kind of meaningful summary both difficult and ephemeral. Nevertheless, there is no question that the study of the magnetic properties of these materials, and of the

related actinide compounds, and of the possible connection between magnetism and superconductivity in heavy-fermion systems, is one of the most fruitful areas of research in solid state physics, and one in which great progress can be anticipated in the next few years.

We have emphasized the efficacy of neutron scattering for the experimental study of rare earth magnetism, but macroscopic measurements provide an invaluable complement. The macroscopic magnetic properties are frequently very sensitive to impurities, and many of the parameters on which we rely for comparison with theory were measured on crystals substantially less pure than can be prepared today. The measured value of the conduction-electron polarization in Gd, for instance, increased significantly with crystal purity. The magnetic moment of the conduction-electron gas is an important quantity, which gives valuable information on the exchange interaction with the $4f$ electrons, but since it is typically an order of magnitude smaller than the ionic moment, its accurate determination is not straightforward, either in the paramagnetic or the ordered phases, and the values of Table 1.6 could in many cases be improved upon. The anisotropy parameters, describing the angular dependence of the free energy in a field, are also difficult to determine precisely, paradoxically because they are frequently so large in the rare earths. It may consequently be very difficult to pull the moments out of the easy direction, and the torque on a crystal in a field can be huge. Apart from the question of sample purity, many of the values in the literature therefore suffer from substantial uncertainties for technical reasons. The same may be said for the multifarious magnetoelastic parameters, which characterize the dependence of the free energy of the magnetic systems on the lattice strain. The temperature dependence of this free energy is reflected in the heat capacity, which therefore in principle contains useful information on the energetics of magnetic materials. However, the unscrambling of the nuclear, lattice, magnetic and electronic components may be a formidable task, and small amounts of impurity may make the results essentially useless. Nevertheless, it would be worthwhile to attempt to improve upon the accuracy of the available measurements, and the effect of an external magnetic field on the heat capacity could be pursued further, since the few studies which have so far been made have been very informative.

It was the revelation by neutron diffraction of the exotic magnetic structures of the rare earths which initiated the revolutionary progress of the 1960s, and since that time countless studies have been performed of the patterns of the ordered moments. It is therefore remarkable that so much remains to be done. The temperature dependences of the structures of the heavy rare earths have been determined in great detail, although there is still scope for further study of some phases, for in-

stance in the intermediate temperature-range of Er. However, the effect of other external constraints, especially magnetic fields and pressure, have only been cursorily investigated. It is apparent, for instance, that a variety of helifan and analogous structures may be produced by applying a field to periodic structures, especially if the interactions are adjusted by taking advantage of the almost perfect mutual solubility of the elements. Apart from their intrinsic interest, measurements of the resistivity may provide a very sensitive method for determining the complex phase diagrams which frequently arise in a magnetic field. The same may be said of the lattice strain, and of the elastic constants (Bates *et al.* 1988). Since the magnetoelastic effects in the rare earths are so pronounced, external pressure or uniaxial stress can have a profound effect on the stability of different magnetic states, as the few examples which have been examined have demonstrated. The light rare earths remain a largely unexplored terrain. The more that is learned about the magnetic structures of Nd, the wider loom the areas which remain to be investigated. Our understanding of γ -Ce is still at a rudimentary stage, nor is the magnetic structure of Sm by any means completely resolved. Although its crystal structure is complicated, and neutron experiments require isotopically enriched samples to circumvent the large absorption in the natural state, there is no fundamental obstacle to attaining a more detailed description of the configurations of the moments under different conditions than we have at present. The form factor is particularly interesting and unusual, and the theoretical understanding of its variation with κ is still incomplete. A dhcp phase can also be stabilized in Sm; a comparison of its magnetic properties with those of the more common allotrope would further elucidate the relation between the crystal structure and the magnetic interactions. The magnetic structures of films and superlattices constitute a field which has only existed for a few years, and is in the process of rapid expansion. There appear to be unlimited possibilities for fabricating new systems, and for discovering new forms of ordering.

The mean-field theory, in conjunction with the standard model, has proved to be ideally suited for explaining the general features of the magnetic structures in terms of the interactions. Furthermore, detailed self-consistent calculations provide an accurate description of the arrangement of the moments determined by neutron diffraction and macroscopic measurements, under specified conditions of temperature and field, and also give a good account of the variation of the macroscopic anisotropy and magnetostriction parameters with the magnetization. Although the crystal-field parameters are adjusted to fit, for example, the low-temperature magnetic properties, they are not normally thereafter varied in the calculation. The indirect-exchange interaction

must be taken as explicitly temperature dependent, but its variation is constrained to be consistent with the excitation spectrum. Only in the vicinity of the critical temperature does the mean-field theory fail seriously in the rare earths. Apart from this, the most severe challenge which has so far been presented to the theory is the explanation of the manifold structures of Nd in terms of a set of fundamental interactions. This challenge has not yet been fully met, but this is probably more due to an incomplete knowledge of the interactions than to any fundamental limitation of the method.

The random-phase approximation, which is a time-dependent extension of the mean-field method, provides a similarly powerful theoretical technique for treating the excitations. It is also quite general, but the results usually have to be obtained by numerical means. The linear spin-wave theory is an attractive alternative when the low-temperature moment is close to its saturation value, since it may be treated analytically, may readily be made self-consistent, and allows the identification of the combinations of parameters which determine the essential features of the excitation spectrum. The corrections to the theory may be computed systematically as an expansion in $1/J$, and considerable progress has been made in the calculation of such higher-order terms. Experimental investigations of the finite lifetime effects which appear in the third order of $1/J$, due to the magnon-magnon interactions, have so far been limited. The theory of this effect is well established for the Heisenberg ferromagnet, but it remains to be combined with the $1/J$ -expansion in the anisotropic case.

The RPA theory has the merit of providing the leading-order results for the excitation spectrum in the systematic $1/Z$ -expansion. This expansion is particularly well-suited for the rare earth metals, as it takes advantage of the large value of the effective coordination number Z , due to the close packing and the long range of the indirect exchange. Except in the immediate vicinity of a second-order phase transition, where any perturbation theory will fail, it seems capable of giving a rather satisfactory account of the many-body correlations even in the first order of $1/Z$, if there is a gap in the excitation spectrum, as demonstrated by the example of Pr. The usefulness of the theory in this order is much improved by the fully self-consistent formulation presented in Section 7.2. However, a substantial effort is still required to calculate the $1/Z$ -terms in systems with more complicated single-ion level schemes than those considered there. Furthermore, in spin-wave systems, or system with gapless excitations, $(1/Z)^2$ -corrections are important for the linewidths. We can however conclude that the $1/Z$ -expansion indicates quite generally that the $(1/Z)^0$ -theory, i.e. the RPA, should be a good first-approximation in the low-temperature limit.

The study of the excitations by inelastic neutron scattering has provided diverse and detailed information on the magnetic interactions. A glance at the dispersion relations of, for instance, Gd, Tb, and Pr immediately reveals the relative importance of the exchange and crystal fields in these elements. Careful measurements as a function of temperature and external fields, combined with a systematic analysis, yield an abundance of knowledge about these and other interactions. Further information is contained in the neutron-scattering intensities, though these have so far been relatively little utilized. However, in some cases, relative intensities have allowed a discrimination between different models, and if the difficult experimental problems can be overcome, absolute intensity measurements could provide a valuable supplement to the energies and lifetimes. The philosophy adopted in analysing measurements of excitation spectra has generally been to use the simplest theory and set of interaction-parameters which can provide a satisfactory fit to the experimental results available at any particular time. The anisotropic exchange may, for example, be subsumed in effective isotropic exchange and crystal-field parameters, so that it is necessary to treat such quantities with caution when comparing with values deduced from different kinds of measurements, or from a fundamental theory.

The excitations to which the greatest efforts have been devoted are the spin waves in the heavy rare earths. Gd, with negligible anisotropy, is the simplest example and the dispersion relations have been carefully measured over a range of temperatures, in an isotopically pure sample. The lifetimes have also been studied, but not as a function of wave-vector at low temperatures, which would allow an examination of the scattering by the conduction electrons, without the interference by the magnon-phonon interaction which partially disturbed the experiments on Tb. Gd would also be the prime candidate for a detailed comparison with a realistic theory, using the calculated band structure and measured Fermi surface rather than the free electron model. The isotropy of the exchange could be examined, to within the limitations of the experimental resolution, by applying a magnetic field, and a study of dipolar effects at long wavelengths might also be possible. Despite the attention which has been devoted to elucidating the excitation spectrum of Tb, a number of questions remain. The relative importance of single- and two-ion contributions to the macroscopic anisotropy and spin-wave energies could be further clarified by more precise measurements in a field, taking full account of the influence of the dipolar coupling at long wavelengths. The origin of the hard-axis axial anisotropy, and the discrepancy between the macroscopic and microscopic hexagonal anisotropy, could thereby be further investigated. The study of the magnon-phonon interaction, which has earlier provided some fruitful surprises, could profitably be

extended to other branches, and the magnon energies should be measured in a single-domain crystal, in order to establish whether the modification of the hexagonal symmetry by the magnetic ordering is reflected in the dispersion relations. It would be interesting to extend the measurements of Nicklow *et al.* (1971b) on ferromagnetic Dy, and subject it to an equally rigorous investigation, since the anisotropy parameters are rather different from those in Tb, but its large hexagonal anisotropy restricts the range of measurements in a field. Studies of ferromagnetic Ho are even more constrained.

When the moments vary with position in a periodic structure, the excitations become less amenable to study and the available information on them is relatively sparse. Eu corresponds to Gd in the role of an isotropic model system, but with a simple helical rather than a ferromagnetic structure. It is unfortunate that its intractable neutron properties (even the more favourable isotope absorbs inconveniently strongly) have so far precluded any measurements of the spin waves. It would be particularly interesting to investigate the mode of wave-vector \mathbf{Q} , whose energy is determined by the small anisotropy, and its dependence on magnetic field. It is energetically favourable for the plane of the helix to rotate so that it is normal to the field direction, and this would be expected to occur via a soft-mode transition analogous to that observed in Ho at low temperature, with a similarly decisive influence of the dipolar interactions. Apart from Pr, to which we return shortly, the only observations of inelastic neutron scattering in the light rare earths are preliminary studies of crystal-field excitations in the longitudinal-wave structure of Nd by McEwen and Stirling (1982). It may be an advantage to apply to these complex systems a magnetic field large enough to induce ferromagnetic ordering, in order to decouple the complications of periodic ordering from the problems of the interplay of crystal-field and exchange interactions in the excitation spectrum.

A number of reasonably complete studies of the spin waves in the c -direction have been made in incommensurable periodic phases of the heavy rare earths, notably in the helical structure of $\text{Tb}_{90}\text{Ho}_{10}$ and the conical phase of Er. The former is a good example of how the mutual solubility of the rare earths can be utilized in modifying the magnetic properties in a convenient manner, in this case by extending the temperature range over which the helix is stable. The effect of varying the temperature has only been cursorily explored, however, and lifetimes and field effects have not yet been investigated. Experimental spectra for the longitudinal-wave structure of Er bear little resemblance to the predictions of the theory, and both will presumably have to be improved before they can be expected to converge. A fairly good understanding has been attained of the excitations in the commensurable spin struc-

tures of Tm and Ho, and the first effects of spin slips in introducing new energy gaps within the zone have been observed in the latter. However, no experiments have yet been carried out on the spin waves in the helifan and fan structures which may be induced by a magnetic field, nor has the soft mode which should accompany a second-order transition from the latter to the ferromagnet been observed.

Such is the richness of the excitation spectrum of Pr that a number of experiments of fundamental importance remain to be performed, despite the considerable efforts which have already been devoted to this unique element. The magnetic excitons on the hexagonal sites and their relationship to the process of magnetic ordering are well understood, and the anisotropic exchange, magnetoelastic, and crystal-field interactions have been measured with unprecedented accuracy. The $|3_s >$ level has not yet been detected directly, however, and a further study of the lifetimes of the long-wavelength acoustic modes as a function of magnetic field would give detailed information about their interaction with the conduction electrons. The excitations on the cubic sites are much less precisely described, and even though they are of lesser significance, a full characterization of their energies and the underlying interactions is essential for the explanation of the temperature dependence of the magnetic properties. In particular, a measurement of the missing branch of excitations polarized in the c -direction, its possible splitting from the branches polarized in the plane, and of the field dependence of the energies, would help to determine the remaining magnetoelastic and crystal-field parameters, especially $B_2^0(c)$ which is usually assumed to be zero, but is likely to be as large as the corresponding parameter on the hexagonal sites.

The magnetically ordered state in Pr provides a new set of challenges. The mechanism of ordering by different perturbations requires further investigation. The neutron-diffraction studies of the hyperfine-coupling-induced collective state should be taken to lower temperatures, and the electronic and nuclear components on the different sites disentangled. The excitations of this state would also naturally be of interest. The influence of magnetic impurities, such as Nd and Er, could be clarified by further inelastic-scattering experiments in a field. The energy of the $|+1 >$ state on the hexagonal sites of Pr can be reduced by a magnetic field in the c -direction, which should affect the quasielastic central peak and precursor satellite. The precise nature of these unusual scattering phenomena is still a mystery, which further measurements under different constraints, especially of external pressure, could help to unravel. The application of a uniaxial pressure in the a -direction creates in effect a new magnetically ordered element, and one with very interesting properties. Many informative results have already been obtained from

this phase, but the full characterization of the excitations as a function of the strain, temperature, and field is clearly a major enterprise. Of immediate interest would be a renewed effort to observe the amplitude mode, which should be visible at low temperatures.

Despite the impressive range of information which has been attained by accurate measurements of the magnetic structures and excitations under various external conditions, the investigation of the two-ion interactions which supplement the dominant isotropic RKKY exchange is by no means complete. Low-symmetry two-ion couplings are clearly important in Pr and Nd. In addition to the anisotropic contribution $\mathcal{K}(ij)$ in (2.1.41), which accounts for the stability of the longitudinal ordering of the moments and the splitting of the doublet-excitations in Pr, a further term must be included to explain the c -axis moments on the cubic sites in Nd, which are induced by the ordered basal-plane moments on the hexagonal sites. In the heavy rare earths Tb and Er, there is indirect but weighty evidence that anisotropic interactions are essential for explaining the excitation spectra. The strong optical-phonon – acoustic-magnon interaction in the c -direction of Tb is of fundamental significance, since it reveals that the spin-orbit coupling of the conduction electrons results in a spatially varying deviation between the direction in which their spins are polarized and that of the ferromagnetic ionic moments. The spin-orbit coupling may also be important for explaining the possible occurrence of interactions, such as the example given in (2.1.39), which reflect the reduced three-fold symmetry of the c -axis in the hcp lattice. Indications that this kind of coupling is present in Ho have appeared in the possible detection by Cowley and Bates (1988) of a modulated c -axis moment in the commensurable helical structures, and the unusual stability of the $Q = \pi/2c$ -structure around 96 K (Noakes *et al.* 1990). The c -axis moments should alternate in sign between each *pair* of planes in the spin-slip structures of Fig. 2.5, being zero on the spin-slip planes, so that $Q_c = 2\pi/c - 3Q = \pi/c$ in the twelve-layered zero-spin-slip structure.

The aforementioned mutual solubility of the rare earth elements gives unlimited possibilities for fabricating systems with adjustable magnetic properties. Dilute alloys of magnetic ions in non-magnetic hosts such as Y have proved particularly interesting, largely because the crystal fields may be studied in the absence of the exchange interaction and its possible anisotropy. The crystal-field levels have primarily been determined by measurements of the magnetic moments, but further neutron-scattering studies, which are possible with modern experimental techniques even in very dilute systems, would be even more enlightening, especially in a magnetic field. These systems can also be effectively investigated by the straightforward means of measuring the electrical resistivity as a function of temperature and field, and comparing with

the pure solvent element. As the concentration is increased, magnetic ordering is observed at correspondingly higher temperatures. Because of the long range of the indirect exchange interaction, all systems of rare earth Kramers-ions in Y which have so far been studied order in the c -direction at sufficiently low temperatures, although there may be some disorder in the plane (Caudron *et al.* 1990). It would be interesting to examine by neutron diffraction even more dilute systems, to clarify the mechanism by which the moments are aligned. As the concentration of heavy rare earths in Y is further increased, the alloys change rather rapidly from crystal-field to exchange-dominated systems. This process, and especially the transition from crystal-field to spin-wave excitations (Wakabayashi and Nicklow 1974), deserves detailed examination.

The potentiality for adjusting the interactions to fabricate concentrated alloys with novel magnetic properties is restricted only by the imagination. The Ho-Er system is a good example, in which the richness of the phase diagrams of the two constituents, and the competing crystal-field anisotropies, give rise to a great variety of structures, especially in a magnetic field. The excitations of such binary alloys have only been investigated to a limited extent. The most systematic studies have so far been those on Tb alloys, which are well described by the average crystal or virtual crystal approximations. It would be interesting to examine a system in which lifetime effects are sufficiently pronounced to allow a comparison with the predictions of the coherent potential approximation; Pr alloys may be good candidates in this context. It would also be informative to investigate the behaviour of light rare earths dissolved in the heavy elements, and vice-versa. Preliminary studies have been made of Er in Pr, and Pr in Tb would be a natural choice for a complementary system. We have only peripherally discussed compounds of rare earths with other elements, but they may possess novel and interesting properties. Of particular significance are compounds with magnetic transition metals, such as ErFe_2 (Clausen *et al.* 1982) and HoCo_2 (Castets *et al.* 1982), which display a striking interplay between itinerant and localized magnetism. As mentioned earlier, Ce compounds constitute a field of magnetism in themselves. Their properties vary from highly localized magnetism, often with very anisotropic interactions, through mixed-valent systems with heavily quenched moments, to non-magnetic heavy-fermion superconductors. They are thus ideally suited for investigations of the limits and breakdown of the standard model.

It is a vain ambition for any authors to aspire to write the last word on any subject; there is always more to say. We have rather attempted to summarize the present state of knowledge and understanding of rare earth magnetism, and indicate some directions for future research. It is

sometimes argued that, since the standard model with suitably chosen interaction parameters accounts so well for the overwhelming majority of the magnetic properties, the field is essentially closed and no problems of fundamental interest remain, apart from the question of determining the parameters from first principles, and of possible failures of the model. This statement is however no more or less true or relevant than the assertion that the Schrödinger equation, or perhaps the Dirac equation, solves all of the basic problems of chemistry. The interesting and fundamental physics is to be found in the manner in which the interactions express themselves under different circumstances. The same model applied to Pr and Tb gives very different, if equally striking, behaviour. A sufficiently careful examination of any rare earth system will inevitably produce surprises, puzzles, and ultimately deeper understanding. In the last few years, this process has been clearly exemplified by the structures and excitations of Ho, which were formerly believed to be essentially understood, and not particularly interesting. We are therefore confident that, when the time comes to present another review of this subject, it will contain physical principles and phenomena which are scarcely hinted at in this book.

REFERENCES

- Abrikosov, A.A., Gor'kov, L.P., and Dzyaloshinskii, I.Ye. (1965). *Quantum Field Theoretical Methods in Statistical Physics* (2nd edn). Pergamon Press, Oxford.
- Akhavan, M. and Blackstead, H.A. (1976). *Phys. Rev. B* **13**, 1209.
- Aksenov, V.L., Frauenheim, Th., Plakida, N.M., and Schreiber, J. (1981). *J. Phys. F* **11**, 905.
- Als-Nielsen, J. and Birgeneau, R.J. (1977). *Am. J. Phys.* **45**, 554.
- Andersen, O.K. (1975). *Phys. Rev. B* **12**, 3060.
- Arai, T. and Felcher, G.P. (1975). *J. Phys. C* **8**, 2095.
- Atoji, M. (1974). *Solid State Commun.* **14**, 1047.
- Axe, J.D., Bohr, J., and Gibbs, D. (1991). To be published.
- Bak, P. (1974). *Risø Report No. 312*. Risø, Denmark.
- Bak, P. (1975). *Phys. Rev. B* **12**, 5203.
- Bak, P. (1982). *Rep. Prog. Phys.* **45**, 587.
- Bak, P. and Lebech, B. (1978). *Phys. Rev. Lett.* **40**, 800.
- Bak, P. and Mukamel, D. (1976). *Phys. Rev. B* **13**, 5086.
- Barak, Z. and Walker, M.B. (1982). *Phys. Rev. B* **25**, 1969.
- Bartholin, H., Beille, J., Bloch, D., Boutron, P., and Féron, J.L. (1971). *J. Appl. Phys.* **42**, 1679.
- Bar'yakhtar, V.G. and Maleev, S.V. (1963). *Fiz. Tverd. Tela* **5**, 1175 [*Sov. Phys. - Solid State* **5**, 858].
- Bates, S., Patterson, C., McIntyre, G.J., Palmer, S.B., Mayer, A., Cowley, R.A., and Melville, R. (1988). *J. Phys. C* **21**, 4125.
- Becker, K.W., Fulde, P., and Keller, J. (1977). *Z. Physik B* **28**, 9.
- Behrendt, D.R., Legvold, S., and Spedding, F.H. (1957). *Phys. Rev.* **106**, 723.
- Bjerrum Møller, H. and Houmann, J.G. (1966). *Phys. Rev. Lett.* **16**, 737.
- Bjerrum Møller, H. and Mackintosh, A.R. (1979). *J. Phys. (Paris)* **40**, C5-28.

- Bjerrum Møller, H., Houmann, J.G., and Mackintosh, A.R. (1967). *Phys. Rev. Lett.* **19**, 312.
- Bjerrum Møller, H., Jensen, J.Z., Wulff, M., Mackintosh, A.R., McMasters, O.D., and Gschneidner, K.A. (1982). *Phys. Rev. Lett.* **49**, 482.
- Bleaney, B. (1963). *Proc. Roy. Soc. A* **276**, 39.
- Bleaney, B. (1972). In *Magnetic Properties of Rare Earth Metals* (ed. R.J. Elliott) p.383. Plenum Press. London.
- Bohr, J., Gibbs, D., Axe, J.D., Moncton, D.E., D'Amico, K.L., Majkrzak, C.F., Kwo, J., Hong, M., Chien, C.L., and Jensen, J. (1989). *Physica B* **159**, 93.
- Borchers, J.A., Nieuwenhuys, G., Salamon, M.B., Flynn, C.P., Du, R., Erwin, R.W., and Rhyne, J.J. (1988). *J. Phys. (Paris)* **49**, C8-1685.
- Bowden, G.J. (1977). *J. Phys. F* **7**, 1731.
- Brits, G.H.F. and du Plessis, P. de V. (1988). *J. Phys. F* **18**, 2659.
- Brooks, M.S.S. (1970). *Phys. Rev. B* **1**, 2257.
- Brooks, M.S.S. and Egami, T. (1973). *J. Phys. C* **6**, 513; *ibid.* 3719.
- Brooks, M.S.S. and Goodings, D.A. (1968). *J. Phys. C* **1**, 1279.
- Brooks, M.S.S., Goodings, D.A., and Ralph, H.I. (1968). *J. Phys. C* **1**, 132.
- Brun, T.O., Sinha, S.K., Wakabayashi, N., Lander, G.H., Edwards, L.R., and Spedding, F.H. (1970). *Phys. Rev. B* **1**, 1251.
- Buckmaster, H.A., Chatterjee, R., and Shing, Y.H. (1972). *Phys. Stat. Sol. (a)* **13**, 9.
- Burke, S.K., Stirling, W.G., and McEwen, K.A. (1981). *J. Phys. C* **14**, L967.
- Cable, J.W., Moon, R.M., Koehler, W.C., and Wollan, E.O. (1964). *Phys. Rev. Lett.* **12**, 553.
- Cable, J.W., Nicklow, R.M., and Wakabayashi, N. (1985). *Phys. Rev. B* **32**, 1710.
- Callen, E.R. and Callen, H.B. (1960). *J. Phys. Chem. Solids* **16**, 310.
- Callen, E.R. and Callen, H.B. (1963). *Phys. Rev.* **129**, 578.
- Callen, E.R. and Callen, H.B. (1965). *Phys. Rev.* **139**, A455.
- Callen, H.B. and Shtrikman, S. (1965). *Solid State Commun.* **3**, 5.

- Care, C.M. and Tucker, J.W. (1977). *J. Phys. C* **10**, 2773.
- Caudron, R., Bouchiat, H., Monod, P., Brown, P.J., Chung, R., and Tholence, J.L. (1990). *Phys. Rev. B* **42**, 2325.
- Castets, A., Gignoux, D., and Hennion, B. (1982). *Phys. Rev. B* **25**, 337.
- Chow, H. and Keffer, F. (1973). *Phys. Rev. B* **7**, 2028.
- Clausen, K., Rhyne, J.J., Lebeck, B., and Koon, N.C. (1982). *J. Phys. C* **15**, 3587.
- Cohen, M.H. and Keffer, F. (1955). *Phys. Rev.* **99**, 1128.
- Collins, M.F. (1989). *Magnetic Critical Scattering*. Oxford University Press, Oxford.
- Cooper, B.R. (1967). *Phys. Rev. Lett.* **19**, 900.
- Cooper, B.R. (1968a). *Phys. Rev.* **169**, 281.
- Cooper, B.R. (1968b). In *Solid State Physics* (ed. F. Seitz, D. Turnbull, and H. Ehrenreich) Vol. 21, p.393. Academic Press, New York.
- Cooper, B.R., Elliott, R.J., Nettel, S.J., and Suhl, H. (1962). *Phys. Rev.* **127**, 57.
- Cooper, B.R., Siemann, R., Yang, D., Thayamballi, P., and Banerjee, A. (1985). In *Handbook on the Physics and Chemistry of the Actinides* (ed. A.J. Freeman and G.H. Lander) Vol. 2, p.435. North-Holland, Amsterdam.
- Coqblin, B. (1977). *The Electronic Structure of Rare-Earth Metals and Alloys: the Magnetic Heavy Rare-Earths*. Academic Press, New York.
- Corner, W.D. and Tanner, B.K. (1976). *J. Phys. C* **9**, 627.
- Cowley, R.A. (1976). *Phys. Rev. B* **13**, 4877.
- Cowley, R.A. (1991). To be published.
- Cowley, R.A. and Bates, S.B (1988). *J. Phys. C* **21**, 4113.
- Cracknell, A.P. (1974). *J. Phys. F* **4**, 466.
- de Gennes, P.G. (1958). *Comptes Rendus* **247**, 1836.
- de Gennes, P.G. and Friedel, J. (1958). *J. Phys. Chem. Solids* **4**, 71.
- del Moral, A. and Lee, E.W. (1975). *J. Phys. C* **8**, 3881.
- des Cloizeaux, D. (1968). In *Theory of Condensed Matter*, p.325. IAEA, Vienna.

- Dieke, G.H. (1968). *Spectra and Energy Levels of Rare Earth Ions in Crystals*. Wiley, New York.
- Dimmock, J.O. and Freeman, A.J. (1964). *Phys. Rev. Lett.* **13**, 750.
- Dohm, V. and Fulde, P. (1975). *Z. Physik B* **21**, 369.
- Doniach, S. and Sondheimer, E.H. (1974). *Green's Functions for Solid State Physicists*. Benjamin/Cummings Publishing Company, Reading, Massachusetts.
- Duthie, J.C. and Pettifor, D.G. (1977). *Phys. Rev. Lett.* **38**, 564.
- Dyson, F.J. (1956). *Phys. Rev.* **102**, 1217; *ibid.* 1230.
- Egami, T. (1972). *J. Phys. C* **5**, L85.
- Egami, T. and Flanders, P.J. (1976). *J. Phys. Soc. Japan* **40**, 78.
- Elliott, R.J. (1961). *Phys. Rev.* **124**, 346.
- Elliott, R.J. (1971). *Atomic Energy of Canada Limited Report No.* 3805.
- Elliott, R.J. and Wedgwood, F.A. (1963). *Proc. Phys. Soc.* **81**, 846.
- Elliott, R.J. and Wedgwood, F.A. (1964). *Proc. Phys. Soc.* **84**, 63.
- Elliott, R.J., Harley, R.T., Hayes, W., and Smith, S.R.P. (1972). *Proc. Roy. Soc. A* **328**, 217.
- Elliott, R.J., Krumhansl, J.A., and Leath, P.L. (1974). *Rev. Mod. Phys.* **46**, 465.
- Enz, U. (1960). *Physica* **26**, 698.
- Eriksen, M., Forgan, E.M., Muirhead, C.M., and Young, R.C. (1983). *J. Phys. F* **13**, 929.
- Eriksson, O., Brooks, M.S.S., and Johansson, B. (1990). *Phys. Rev. B* **41**, 7311.
- Evenson, W.E. and Liu, S.H. (1969). *Phys. Rev.* **178**, 783.
- Fernandez-Baca, J.A., Nicklow, R.M., and Rhyne, J.J. (1990). *J. Appl. Phys.* **67**, 5283.
- Féron, J.L. (1969). Thesis. University of Grenoble.
- Folk, R., Iro, H., and Schwabl, F. (1979). *Phys. Rev. B* **20**, 1229.
- Forgan, E.M. (1981). *Physica B* **107**, 65.
- Forgan, E.M. (1982). *J. Phys. F* **12**, 779.
- Forgan, E.M., Gibbons, E.P., McEwen, K.A., and Fort, D. (1989). *Phys. Rev. Lett.* **62**, 470.

- Forster, D. (1975). *Hydrodynamic Fluctuations, Broken Symmetry, and Correlation Functions*. Benjamin/Cummings Publishing Company, Reading, Massachusetts.
- Freeman, A.J. (1972). In *Magnetic Properties of Rare Earth Metals* (ed. R.J. Elliott) p.245. Plenum Press, London.
- Fulde, P. (1979). In *Handbook on the Physics and Chemistry of Rare Earths* (ed. K.A. Gschneidner, Jr. and L.R. Eyring) Vol. 2, p.295. North-Holland, Amsterdam.
- Fulde, P. and Jensen, J. (1983). *Phys. Rev. B* **27**, 4085.
- Fulde, P. and Peschel, I. (1971). *Z. Physik* **241**, 82.
- Fulde, P. and Peschel, I. (1972). *Adv. in Phys.* **21**, 1.
- Galili, Y. and Zevin, V. (1987). *J. Phys. C* **20**, 2543.
- Gibbons, E.P., Forgan, E.M., and McEwen, K.A. (1987). *J. Phys. F* **17**, L101.
- Gibbs, D., Moncton, D.E., D'Amico, K.L., Bohr, J., and Grier, B.H. (1985). *Phys. Rev. Lett.* **55**, 234.
- Gibbs, D., Bohr, J., Axe, J.D., Moncton, D.E., and D Amico, K.L. (1986). *Phys. Rev. B* **34**, 8182.
- Glötzel, D. (1978). *J. Phys. F* **8**, L163.
- Goldstone, J. (1961). *Nuovo Cimento* **19**, 154.
- Green, R. W., Legvold, S., and Spedding, F.H. (1961). *Phys. Rev.* **122**, 827.
- Grimvall, G. (1981). *The Electron-Phonon Interaction in Metals*, Vol. XVI of *Selected Topics in Solid State Physics* (ed. E.P. Wohlfarth). North-Holland, Amsterdam.
- Gunnarsson, O. and Lundqvist, B.I. (1976). *Phys. Rev. B* **13**, 4274.
- Gustafson, D.R. and Mackintosh, A.R. (1964). *J. Phys. Chem. Solids* **25**, 389; *Bull. Am. Phys. Soc.* **10**, 376.
- Gustafson, D.R., McNutt, J.D., and Roellig, L.O. (1969). *Phys. Rev.* **183**, 435.
- Habenschuss, H., Stassis, C., Sinha, S.K., Deckman, H.W., and Spedding, F.H. (1974). *Phys. Rev. B* **10**, 1020.
- Haley, S.B. and Erdös, P. (1972). *Phys. Rev. B* **5**, 1106.
- Hansen, P. and Lebech, B. (1976). *J. Phys. F* **6**, 2179.

- Hauschultz, M., Andersen, N.H., Rasmussen, F.B., and Pickett, G.R. (1978). *Phys. Lett. A* **68**, 479.
- Hedin, L. and Lundqvist, B.I. (1971). *J. Phys. C* **4**, 2064.
- Hegland, D.E., Legvold, S., and Spedding, F.H. (1963). *Phys. Rev.* **131**, 158.
- Hendy, P., Al-Rawi, K.M., Lee, E.W., and Melville, D. (1979). *J. Phys. F* **9**, 2121.
- Hessel Andersen, N. (1979). *Phys. Lett. A* **72**, 236.
- Hessel Andersen, N. and Smith, H. (1979). *Phys. Rev. B* **19**, 384.
- Hessel Andersen, N. and Vogt, O. (1979). *J. Phys. (Paris)* **40**, C5-118.
- Hessel Andersen, N., Jensen, J., Smith, H., Splittorff, O., and Vogt, O. (1980). *Phys. Rev. B* **21**, 189.
- Hohenberg, P. and Kohn, W. (1964). *Phys. Rev.* **136**, B864.
- Holden, T.M. and Buyers, W.J.L. (1974). *Phys. Rev. B* **9**, 3797.
- Holstein, T. and Primakoff, H. (1940). *Phys. Rev.* **58**, 1098.
- Houmann, J.G. (1968). *Solid State Commun.* **6**, 479.
- Houmann, J.G., Jensen, J., and Touborg, P. (1975a). *Phys. Rev. B* **12**, 332.
- Houmann, J.G., Chapellier, M., Mackintosh, A.R., Bak, P., McMasters, O.D., and Gschneidner, K.A. (1975b). *Phys. Rev. Lett.* **34**, 587.
- Houmann, J.G., Rainford, B.D., Jensen, J., and Mackintosh A.R. (1979). *Phys. Rev. B* **20**, 1105.
- Huber, D.L. (1978). *Phys. Rev. B* **18**, 429.
- Hund, F. (1925). *Z. Physik* **33**, 855.
- Hutchings, M.T. (1964). In *Solid State Physics* (ed. F. Seitz, D. Turnbull, and H. Ehrenreich) Vol. 16, p. 227. Academic Press, New York.
- Høg, J. and Touborg, P. (1975). *Phys. Rev. B* **11**, 520.
- Jensen, J. (1971a). *Intern. J. Magn.* **1**, 271.
- Jensen, J. (1971b). *Risø Report No. 252*. Risø, Denmark.
- Jensen, J. (1974). *J. Phys. F* **4**, 1065.
- Jensen, J. (1975). *J. Phys. C* **8**, 2769.
- Jensen, J. (1976a). *J. Phys. C* **9**, 111.
- Jensen, J. (1976b). *J. Phys. F* **6**, 1145.

- Jensen, J. (1976c). *Phys. Rev. Lett.* **37**, 951.
- Jensen, J. (1979a). *J. Magn. Magn. Mater.* **14**, 224.
- Jensen, J. (1979b). *J. Phys. (Paris)* **40**, C5-1.
- Jensen, J. (1982a). *J. Magn. Magn. Mater.* **29**, 47.
- Jensen, J. (1982b). *J. Phys. C* **15**, 2403.
- Jensen, J. (1984). *J. Phys. C* **17**, 5367.
- Jensen, J. (1988a). *J. Phys. (Paris)* **49**, C8-351.
- Jensen, J. (1988b). *Phys. Rev. B* **37**, 9495.
- Jensen, J. and Houmann, J.G. (1975). *Phys. Rev. B* **12**, 320.
- Jensen, J. and Mackintosh, A.R. (1990). *Phys. Rev. Lett.* **64**, 2699.
- Jensen, J. and Palmer, S.B. (1979). *J. Phys. C* **12**, 4573.
- Jensen, J., Houmann, J.G., and Bjerrum Møller, H. (1975). *Phys. Rev. B* **12**, 303.
- Jensen, J., McEwen, K.A., and Stirling, W.G. (1987). *Phys. Rev. B* **35**, 3327.
- Johanson, W.R., Crabtree, G.W., Edelstein, A.S., and McMasters, O.D. (1981). *Phys. Rev. Lett.* **46**, 504.
- Johanson, W.R., Crabtree, G.W., and Schmidt, F.A. (1982). *J. Appl. Phys.* **53**, 2041.
- Johansson, B. (1974). *Phil. Mag.* **30**, 469.
- Johansson, T., Lebeck, B., Nielsen, M., Bjerrum Møller, H., and Mackintosh, A.R. (1970). *Phys. Rev. Lett.* **25**, 524.
- Kaplan, T.A. and Lyons, D.H. (1963). *Phys. Rev.* **129**, 2072.
- Kasuya, T. (1956). *Prog. Theor. Phys.* **16**, 45.
- Kasuya, T. (1959). *Prog. Theor. Phys.* **22**, 227.
- Kasuya, T. and Lyons, D.H. (1966). *J. Phys. Soc. Japan* **21**, 287.
- Kawarazaki, S., Kunitomi, N., Arthur, J.R., Moon, R.M., Stirling, W.G., and McEwen, K.A. (1988). *Phys. Rev. B* **37**, 5336.
- Keeton, S.C. and Loucks, T.L. (1968). *Phys. Rev.* **168**, 672.
- Keffer, F. (1966). In *Handbuch der Physik* (ed. H.P.J. Wijn) Vol. XVIII/2, p. 1. Springer-Verlag, Berlin.
- Kittel, C. (1948). *Phys. Rev.* **73**, 155.

- Klemm, W. and Bommer, H. (1937). *Z. Anorg. u. Allgem. Chem.* **231**, 138.
- Koehler, W.C. (1972). In *Magnetic Properties of Rare Earth Metals* (ed. R.J. Elliott) p.81. Plenum Press. London.
- Koehler, W.C. and Moon, R.M. (1972). *Phys. Rev. Lett.* **29**, 1468.
- Koehler, W.C. and Wollan, E.O. (1955). *Phys. Rev.* **97**, 1177.
- Koehler, W.C., Wollan, E.O., Wilkinson, M.K., and Cable, J.W. (1961). In *Rare Earth Research* (ed. E.V. Kleber) p.149. Macmillan, New York.
- Koehler, W.C., Cable, J.W., Wilkinson, M.K., and Wollan, E.O. (1966). *Phys. Rev.* **151**, 414.
- Koehler, W.C., Cable, J.W., Child, H.R., Wilkinson, M.K., and Wollan, E.O. (1967). *Phys. Rev.* **158**, 450.
- Koehler, W.C., Child, H.R., Nicklow, R.M., Smith, H.G., Moon, R.M., and Cable, J.W. (1970). *Phys. Rev. Lett.* **24**, 16.
- Kohn, W. and Sham, L.J. (1965). *Phys. Rev.* **140**, A1133.
- Kornstädt, U., Lässer, R., and Lengeler, B (1980). *Phys. Rev. B* **21**, 1898.
- Korringa, J. (1950). *Physica* **16**, 601.
- Kubo, R. (1957). *J. Phys. Soc. Japan* **12**, 570.
- Kubo, R. (1966). *Rep. Prog. Phys.* **29**, 255.
- Lage, E.J.S. and Stinchcombe, R.B. (1977). *J. Phys. C* **10**, 295.
- Lang, J.K., Baer, Y., and Cox, P.A. (1981). *J. Phys. F* **11**, 121.
- Lantwin, C.J. (1990). Thesis. Department of Theoretical Physics, University of Oxford; and *Z. Physik B* **79**, 47.
- Larsen, C.C., Mackintosh, A.R., Bjerrum Møller, H., Legvold, S., and Beaudry, B.J. (1986). *J. Magn. Magn. Mater.* **54-57**, 1165.
- Larsen, C.C., Jensen, J., and Mackintosh, A.R. (1987). *Phys. Rev. Lett.* **59**, 712.
- Larsen, C.C., Jensen, J., Mackintosh, A.R., and Beaudry, B.J. (1988). *J. Phys. (Paris)* **49**, C8-331.
- Lawson, A.W. and Tang, T.-Y. (1949). *Phys. Rev.* **76**, 301.
- Lea, K.R., Leask, M.J.M., and Wolf, W.P. (1962). *J. Phys. Chem. Solids* **23**, 1381.

- Lebech, B. and Rainford, B.D. (1971). *J. Phys. (Paris)* **32**, C1-370.
- Lebech, B., McEwen, K.A., and Lindgård, P.-A. (1975). *J. Phys. C* **8**, 1684.
- Lebech, B., Rainford, B.D., Brown, P.J., and Wedgwood, F.A. (1979). *J. Magn. Magn. Mater.* **14**, 298.
- Legvold, S. (1961). In *Rare Earth Research* (ed. E.V. Kleber) p.142. Macmillan, New York.
- Legvold, S. (1972). In *Magnetic Properties of Rare Earth Metals* (ed. R.J. Elliott) p.335. Plenum Press. London.
- Leuenberger, B., Güdel, H.U., Feile, R., and Kjems, J.K. (1985). *Phys. Rev. B* **31**, 597.
- Levy, P. (1969). *Phys. Rev.* **177**, 509.
- Lindelof, P.E., Miller, I.E., and Pickett, G.R. (1975). *Phys. Rev. Lett.* **35**, 1297.
- Lindgård, P.-A. (1978). *Phys. Rev. B* **17**, 2348.
- Lindgård, P.-A. (1988). In *Spin Waves and Magnetic Excitations* (ed. A.S. Borovik-Romanov and S.K. Sinha) p.287. North-Holland, Amsterdam.
- Lindgård, P.-A. and Danielsen, O. (1974). *J. Phys. C* **7**, 1523.
- Lindgård, P.-A. and Danielsen, O. (1975). *Phys. Rev. B* **11**, 351.
- Lindgård, P.-A. and Houmann, J.G. (1971). In *Proceedings of the Durham Conference on Rare Earths and Actinides* (ed. E.W. Lee) p.192. Institute of Physics, London.
- Lindgård, P.-A., Harmon, B.N., and Freeman, A.J. (1975). *Phys. Rev. Lett.* **35**, 383.
- Lindhard, J. (1954). *Kgl. Danske Videnskab. Selskab Mat. Fys. Medd.* **28**, 8.
- Lines, M.E. (1974a). *J. Phys. C* **7**, L287.
- Lines, M.E. (1974b). *Phys. Rev. B* **9**, 3927.
- Lines, M.E. (1975). *Phys. Rev. B* **12**, 3766.
- Liu, S.H. (1972a). *Phys. Rev. Lett.* **29**, 793.
- Liu, S.H. (1972b). *Intern. J. Magn.* **3**, 327.
- Liu, S.H. (1978). In *Handbook on the Physics and Chemistry of Rare Earths* (ed. K.A. Gschneidner, Jr. and L.R. Eyring) Vol. 1, p.233. North-Holland, Amsterdam.

- Liu, S.H. (1980). *J. Magn. Magn. Mater.* **22**, 93.
- Loewenhaupt, M., Rainford, B.D., and Steglich, F. (1979). *Phys. Rev. Lett.* **42**, 1709.
- Lonzarich, G.G. (1988). *J. Magn. Magn. Mater.* **76-77**, 1.
- Lovesey, S.W. (1984). *Theory of Neutron Scattering from Condensed Matter* Vols. 1 and 2. Oxford University Press, Oxford.
- Lovesey, S.W. (1986). *Condensed Matter Physics: Dynamic Correlations* (2nd edn). Benjamin/Cummings Publishing Company, Reading, Massachusetts.
- Lovesey, S.W. (1988). *J. Phys. C* **21**, 2805; *ibid.* 4967.
- Mackintosh, A.R. (1962). *Phys. Rev. Lett.* **9**, 90.
- Mackintosh, A.R. (1963). *Phys. Lett.* **4**, 140.
- Mackintosh, A.R. (1983). *Inst. Phys. Conf. Ser.* **64**, 199.
- Mackintosh, A.R. (1985). *Physica B* **130**, 112.
- Mackintosh, A.R. and Andersen, O.K. (1980). In *Electrons at the Fermi Surface* (ed. M.Springford) p.149. Cambridge University Press, Cambridge.
- Mackintosh, A.R. and Bjerrum Møller, H. (1972). In *Magnetic Properties of Rare Earth Metals* (ed. R.J. Elliott) p.187. Plenum Press, London.
- Mackintosh, A.R. and Jensen, J. (1990). In *Disorder in Condensed Matter Physics* (ed. J.A. Blackman and J. Taguena). Oxford University Press, Oxford.
- Mackintosh, A.R. and Smidt, F.A. (1962). *Phys. Lett.* **2**, 107.
- Mackintosh, A.R. and Spanel, L.E. (1964). *Solid State Commun.* **2**, 383.
- Mackintosh, A.R., Spanel, L.E., and Young, R.C. (1963). *Phys. Rev. Lett.* **10**, 434.
- Mahan, G.D. (1990). *Many-Particle Physics* (2nd edn). Plenum Press, New York.
- Majkrzak, C.F., Cable, J.W., Kwo, J., Hong, M., McWhan, D.B., Yafet, Y., Waszczak, V. and Vettier C. (1986). *Phys. Rev. Lett.* **56**, 2700.
- Marshall, W. and Lovesey, S.W. (1971). *Theory of Thermal Neutron Scattering*. Oxford University Press, Oxford.
- Martin, D.J. and Rhyne, J.J. (1977). *J. Phys. C* **10**, 4123.

- Mason, W.P. (1954). *Phys. Rev.* **96**, 302.
- Mattocks, P.G. and Young, R.C. (1977). *J. Phys. F* **7**, 1219.
- McCausland, M.A.H. and Mackenzie, I.S. (1979). *Adv. in Phys.* **28**, 305.
- McEwen, K.A. (1978). In *Handbook on the Physics and Chemistry of Rare Earths* (ed. K.A. Gschneidner and L. Eyring) Vol. 1, p.411. North-Holland, Amsterdam.
- McEwen, K.A. (1986). *Physica B* **136**, 385.
- McEwen, K.A. and Stirling, W.G. (1981). *J. Phys. C* **14**, 157.
- McEwen, K.A. and Stirling, W.G. (1982). *J. Magn. Magn. Mater.* **30**, 99.
- McEwen, K.A. and Walker, M.B. (1986). *Phys. Rev. B* **34**, 1781.
- McEwen, K.A., Cock, G.J., Roeland, L.W., and Mackintosh, A.R. (1973). *Phys. Rev. Lett.* **30**, 287.
- McEwen, K.A., Stirling, W.G., and Vettier, C. (1978). *Phys. Rev. Lett.* **41**, 343.
- McEwen, K.A., Stirling, W.G., and Vettier, C. (1983). *Physica B* **120**, 152.
- McEwen, K.A., Forgan, E.M., Stanley, H.B., Bouillot, J., and Fort, D. (1985). *Physica B* **130**, 360.
- McEwen, K.A., Steigenberger, U., and Jensen, J. (1991), *Phys. Rev. B* **43**, 3298.
- Melcher, R.L. (1972). *Phys. Rev. Lett.* **28**, 165.
- Micnas, R. and Kishore, R. (1981). *Physica A* **108**, 180.
- Millhouse, A.H. and McEwen, K.A. (1973). *Solid State Commun.* **13**, 339.
- Min, B.I., Jansen, H.J.F., Oguchi, T., and Freeman, A.J. (1986a). *J. Magn. Magn. Mater.* **61**, 139.
- Min, B.I., Oguchi, T., Jansen, H.J.F., and Freeman, A.J. (1986b). *Phys. Rev. B* **34**, 654.
- Mishima, A., Fujii, H., and Okamoto, T. (1976). *J. Phys. Soc. Japan* **40**, 962.
- Miwa, H. (1963). *Prog. Theor. Phys.* **29**, 477.
- Miwa, H. (1965). *Proc. Phys. Soc.* **85**, 1197.
- Miwa, H. and Yosida, K. (1961). *Prog. Theor. Phys.* **26**, 693.

- Moon, R.M. and Koehler, W.C. (1971). *Phys. Rev. Lett.* **27**, 407.
- Moon, R.M., Cable, J.W., and Koehler, W.C. (1964). *J. Appl. Phys.* **35**, 1041.
- Moon, R.M., Riste, T., and Koehler, W.C. (1969). *Phys. Rev.* **181**, 920.
- Mori, H. (1965). *Prog. Theor. Phys.* **33**, 423.
- Morin, P., Schmitt, D., Vettier, V., and Rossat-Mignod, J. (1980). *J. Phys. F* **10**, 1575.
- Mukamel, D. and Krinsky, S. (1976). *Phys. Rev. B* **13**, 5065, 5078.
- Murao, T. (1971). *J. Phys. Soc. Japan* **31**, 683.
- Murao, T. (1975). *J. Phys. Soc. Japan* **39**, 50.
- Murao, T. (1979). *J. Phys. Soc. Japan* **46**, 40.
- Murao, T. (1984). *J. Phys. Soc. Japan Suppl.* **80**, 139.
- Mårtensson, N., Reihl, B., and Parks, R.D. (1982). *Solid State Commun.* **41**, 573.
- Nagamiya, T. (1967). In *Solid State Physics* (ed. F. Seitz, D. Turnbull, and H. Ehrenreich) Vol. 20, p.305. Academic Press, New York.
- Nagamiya, T., Nagata, K., and Kitano, Y. (1962). *Prog. Theor. Phys.* **27**, 1253.
- Nakajima, S. (1967). *Prog. Theor. Phys.* **38**, 23.
- Nicklów, R.M. (1971). *J. Appl. Phys.* **42**, 1672.
- Nicklów, R.M. and Wakabayashi, N. (1982). *Phys. Rev. B* **26**, 3994.
- Nicklów, R.M., Wakabayashi, N., Wilkinson, M.K., and Reed, R.E. (1971a). *Phys. Rev. Lett.* **27**, 334.
- Nicklów, R.M., Wakabayashi, N., Wilkinson, M.K., and Reed, R.E. (1971b). *Phys. Rev. Lett.* **26**, 140.
- Nielsen, M., Bjerrum Møller, H., Lindgård, P.-A., and Mackintosh, A.R. (1970). *Phys. Rev. Lett.* **25**, 1451.
- Niira, K. (1960). *Phys. Rev.* **117**, 129.
- Noakes, D.R., Tindall, D.A., Steinitz, M.O., and Ali, N. (1990). *J. Appl. Phys.* **67**, 5274.
- Norman, M.R., Koelling, D.D., Freeman, A.J., Jansen, H.J.F., Min, B.I., Oguchi, T., and Ye, Ling (1984). *Phys. Rev. Lett.* **53**, 1673.
- Néel, L. (1938). *Comptes Rendus* **242**, 1824.
- Ohnari, I. (1980). *J. Phys. C* **13**, 5911.

- Orlov, V.G. and Jensen, J. (1988). *J. Magn. Magn. Mater.* **71**, 279.
- Ott, H.R. (1975). *Solid State Commun.* **16**, 1355.
- Overhauser, A.W. (1963). *J. Appl. Phys.* **34**, 1019.
- Palmer, S.B. and Jensen, J. (1978). *J. Phys. C* **11**, 2465.
- Palmer, S.B., Bates, S., McIntyre, G.J., Sousa, J.B., Fort, D., and Beaudry, B.J. (1986). *J. Magn. Magn. Mater.* **54-57**, 519.
- Parkinson, D.H., Simon, F.E., and Spedding, F.H. (1951). *Proc. Roy. Soc. A* **207**, 137.
- Patterson, C., McMorro, D.F., Godfrin, H., Clausen, K.N., and Lebech, B. (1990). *J. Phys. Condens. Matter* **2**, 3421; and to be published.
- Podloucky, R. and Glötzel, D. (1983). *Phys. Rev. B* **27**, 3390.
- Probst, C. and Wittig, J. (1975). In *Low Temperature Physics-LT14* (ed. M. Krusius and M. Vuorio) Vol. 5, p.453. North-Holland, Amsterdam.
- Psaltakis, G.C. and Cottam, M.G. (1982). *J. Phys. C* **15**, 4847.
- Purwins, H.-G., Houmann, J.G., Bak, P., and Walker, E. (1973). *Phys. Rev. Lett.* **31**, 1585.
- Rainford, B.D. (1972). In *AIP Conf. Proc. No. 5* (ed. C.D. Graham and J.J. Rhyne) p.591. AIP, New York.
- Rainford, B.D. and Houmann, J.G. (1971). *Phys. Rev. Lett.* **26**, 1254.
- Rainford, B.D., McEwen, K.A., Lebech, B., and Burke, S.K. (1981). ILL Report (unpublished).
- Rainford, B.D., Kilcoyne, S.H., Mohammed, K.A., Lanchester, P.C., Stanley, H.B., and Caudron, R. (1988a). *J. Phys. (Paris)* **49**, C8-355.
- Rainford, B.D., Cussen, L., Jensen, J., and Fort, D. (1988b). *J. Magn. Magn. Mater.* **76-77**, 399.
- Rastelli, E. and Lindgård, P.-A. (1979). *J. Phys. C* **12**, 1899.
- Rastelli, E. and Tassi, A. (1986). *J. Phys. C* **19**, 1993.
- Rastelli, E., Reatto, L., and Tassi, A. (1985). *J. Phys. C* **18**, 353.
- Rathmann, O. and Touborg, P. (1977). *Phys. Rev. B* **16**, 1212.
- Reinders, P.H.P., Springford, M., Coleridge, P.T., Boulet, R., and Ravot, D. (1986). *Phys. Rev. Lett.* **57**, 1631.

- Rhyne, J.J. (1972). In *Magnetic Properties of Rare Earth Metals* (ed. R.J. Elliott) p.129. Plenum Press, London.
- Rhyne, J.J. and Legvold, S. (1965a). *Phys. Rev.* **138**, A507.
- Rhyne, J.J. and Legvold, S. (1965b). *Phys. Rev.* **140**, A2143.
- Rhyne, J.J., Erwin, R.W., Borchers J., Salamon, M.B., Du, R., and Flynn, C.P. (1989). *Physica B* **159**, 111.
- Rosen, M., Kalir, D., and Klimker, H. (1973). *Phys. Rev. B* **8**, 4399.
- Ruderman, M.A. and Kittel, C. (1954). *Phys. Rev.* **96**, 99.
- Salamon, M.B., Sinha, S., Rhyne, J.J., Cunningham, J.E., Erwin, R.W., Borchers, J., and Flynn, C.P. (1986). *Phys. Rev. Lett.* **56**, 259.
- Sherrington, D. (1972). *Phys. Rev. Lett.* **28**, 364.
- Shoenberg, D. (1983). *Magnetic Oscillations in Metals*. Cambridge University Press, Cambridge.
- Sinha, S.K. (1978). In *Handbook on the Physics and Chemistry of Rare Earths* (ed. K.A. Gschneidner and L. Eyring) Vol. 1, p.489. North-Holland, Amsterdam.
- Skriver, H.L. (1981). In *Physics of Solids under High Pressure* (ed. J.S. Schilling and R.N. Shelton) p.279. North-Holland, Amsterdam.
- Skriver, H.L. (1983). In *Systematics and Properties of the Lanthanides* (ed. S.P. Sinha) p.213. Reidel, Dordrecht.
- Skriver, H.L. (1984). *The LMTO Method*. Springer-Verlag, Berlin.
- Skriver, H.L. (1985). *Phys. Rev.* **31**, 1909.
- Skriver, H.L. and Mertig, I. (1990). *Phys. Rev. B* **41**, 6553.
- Smit, J. and Beljers, H.G. (1955). *Philips Res. Rep.* **10**, 113.
- Smith, H. and Højgaard Jensen, H. (1989). *Transport Phenomena*. Oxford University Press, Oxford.
- Sondhelm, S.A. and Young, R.C. (1985). *J. Phys. F* **15**, L261.
- Soven, P. (1967). *Phys. Rev.* **156**, 809.
- Spano, M.L., Clark, A.E., Teter, J.P., and Cullen, J.R. (1988). *J. Phys. (Paris)* **49**, C8-347.
- Specht, F. (1967). *Phys. Rev.* **162**, 389.
- Spedding, F.H., Legvold, S., Daane, A.H., and Jennings, L.D. (1957). In *Progress in Low Temperature Physics* (ed. C.J. Gorter) Vol. II, p.368. North-Holland, Amsterdam.

- Stassis, C. and Deckman, H.W. (1975). *Phys. Rev. B* **12**, 1885.
- Stassis, C. and Deckman, H.W. (1976). *J. Phys. C* **9**, 2241.
- Staun Olsen, J., Gerward, L., Benedict, U., and Itié, J.-P. (1985). *Physica B* **133**, 129.
- Steglich, F., Aarts, J., Bredl, C.D., Lieke, W., Meschede, D., Franz, W., and Schäfer, H. (1979). *Phys. Rev. Lett.* **43**, 1892.
- Stevens, K.W.H. (1952). *Proc. Phys. Soc. A* **65**, 209.
- Stinchcombe, R.B. (1973). *J. Phys. C* **6**, 2459; *ibid.* 2484; *ibid.* 2507.
- Stirling, W.G. and McEwen, K.A. (1987). In *Neutron Scattering* (ed. D.L. Price and K. Sköld), Vol. 23 of *Methods of Experimental Physics* p.159. Academic Press, New York.
- Strandburg, D.L., Legvold, S., and Spedding, F.H. (1962). *Phys. Rev.* **127**, 2046.
- Suzuki, M. (1971). *Physica* **51**, 277.
- Tahir-Kheli, R.A. (1976). In *Phase Transitions and Critical Phenomena* (ed. C. Domb and M.S. Green) Vol. 5b, p.259. Academic Press, New York.
- Taylor, A.D., Osborn, R., McEwen, K., Stirling, W.G., Bowden, Z.A., Williams, W.G., Balcar, E., and Lovesey, S.W. (1988). *Phys. Rev. Lett.* **61**, 1309.
- Taylor, D.W. (1967). *Phys. Rev.* **156**, 1017.
- Temmerman, W.M. and Sterne, P.A. (1990). *J. Phys. Condens. Matter* **2**, 5529.
- Thalmeier, P. and Fulde, P. (1975). *Z. Physik B* **22**, 359.
- Thalmeier, P. and Fulde, P. (1982). *Phys. Rev. Lett.* **49**, 1588.
- Tibbetts, T.A. and Harmon, B.N. (1982). *Solid State Commun.* **44**, 1409.
- Touborg, P. (1977). *Phys. Rev. B* **16**, 1201.
- Touborg, P. and Høg, J. (1974). *Phys. Rev. Lett.* **33**, 775.
- Touborg, P., Nevald, R., and Johansson, T. (1978). *Phys. Rev. B* **17**, 4454.
- Trammell, G.T. (1953). *Phys. Rev.* **92**, 1387.
- Tsuru, K. (1986). *J. Phys. C* **19**, 2031.

- Turov, E.A. and Shavrov, V.G. (1965). *Fiz. Tverd. Tela* **7**, 217 [*Sov. Phys. - Solid State* **7**, 166].
- Urbain, G., Weiss, P., and Trompe, F. (1935). *Comptes Rendus* **200**, 2132.
- Vaks, V.G., Larkin, A.I., and Pikin, S.A. (1968). *Zh. Eksp. Teor. Fiz.* **53**, 1089 [*Sov. Phys. - JETP* **26**, 647].
- Van Hove, L. (1954). *Phys. Rev.* **95**, 1374.
- Van Vleck, J.H. (1932). *The Theory of Electric and Magnetic Susceptibilities*. Oxford University Press, London.
- von Barth, U. and Hedin, L. (1972). *J. Phys. C* **5**, 1629.
- Wakabayashi, N. and Nicklow, R.M. (1974). *Phys. Rev. B* **10**, 2049.
- Walker, M.B. and McEwen, K.A. (1983). *J. Phys. F* **13**, 139.
- Watson, R.E., Freeman, A.J., and Dimmock, J.P. (1968). *Phys. Rev.* **167**, 497.
- White, R.M. (1983). *Quantum Theory of Magnetism* (2nd edn). Springer-Verlag, Berlin.
- White, R.M. and Fulde P. (1981). *Phys. Rev. Lett.* **47**, 1540.
- Whitelaw, D.J. (1981). *J. Phys. C* **14**, 2871.
- Wieliczka, D.M., Weaver, J.H., Lynch, D.W., and Olson, C.G. (1982). *Phys. Rev. B* **26**, 7056.
- Wieliczka, D.M., Olson, C.G., and Lynch, D.W. (1984). *Phys. Rev. Lett.* **52**, 2180.
- Williams, R.W. and Mackintosh, A.R. (1968). *Phys. Rev.* **168**, 679.
- Williams, R.W., Loucks, T.L., and Mackintosh, A.R. (1966). *Phys. Rev. Lett.* **16**, 168.
- Wills, J.M. and Cooper, B.R. (1987). *Phys. Rev. B* **36**, 3809.
- Wittig, J. (1980). *Z. Physik B* **38**, 11.
- Wolf, W.P. (1971). *J. Phys. (Paris)* **32**, C1-26.
- Wulff, M. (1985). Thesis. University of Cambridge.
- Wulff, M., Jensen, J., Mackintosh, A.R., Bjerrum Møller, H., McMasters, O.D., and Gschneidner, K.A. (1983). *J. Magn. Magn. Mater.* **31-34**, 601.
- Wulff, M., Lonzarich, G.G., Fort, D., and Skriver, H.L. (1988). *Europhys. Lett.* **7**, 629.

- Yang, D.H.-Y. and Wang, Y.-L. (1974). *Phys. Rev. B* **10**, 4714.
- Yang, D.H.-Y. and Wang, Y.-L. (1975). *Phys. Rev. B* **12**, 1057.
- Yonezawa, F. (1968). *Prog. Theor. Phys.* **40**, 734.
- Yosida, K. (1957). *Phys. Rev.* **106**, 893.
- Young, R.C., Jordan, R.G., and Jones, D.W. (1973). *Phys. Rev. Lett.* **31**, 1473.
- Zener, C. (1951). *Phys. Rev.* **81**, 440.
- Zener, C. (1954). *Phys. Rev.* **96**, 1335.
- Ziman, J.M. (1960). *Electrons and Phonons*. Oxford University Press, Oxford.
- Ziman, T. and Lindgård, P.-A. (1986). *Phys. Rev. B* **33**, 1976.
- Zochowski, S.W. and McEwen, K.A. (1986). *J. Magn. Magn. Mater.* **54-57**, 515.
- Zochowski, S.W., Tindall, D.A., Kahrizi, M., Genossar, J., and Steinitz, M.O. (1986). *J. Magn. Magn. Mater.* **54-57**, 707.
- Zochowski, S.W., McEwen, K.A., and Fawcett, E. (1991). *J. Phys. Condens. Matter*. To be published.
- Zubarev, D.N. (1960). *Usp. Fiz. Nauk* **71**, 71 [*Sov. Phys. - Usp.* **3**, 320].

INDEX

- anisotropic ferromagnet, 64–7, 186–98
- anisotropic two-ion coupling, 48, 240–4
- atomic magnetism, 14
- atomic sphere approximation, 19

- binary alloys, 247–56
- Bloch’s theorem, 18
- Bogoliubov transformation, 190
- Brillouin function, 15
- broken symmetry, 291
- bunched helix, 52, 82, 239

- c*-axis modulated structure, 51
- Callen–Callen theory, 94–101, 203
- canonical bands, 22
- Cartesian strains, 44
- Cerium
 - atomic radius, 37
 - atomic wavefunctions, 11
 - band energies, 34
 - band structure, 27
 - d*-electron occupancy, 38
 - electronic parameters, 26
 - electronic pressure, 36
 - equation of state, 28
 - ionic properties, 13
 - magnetic properties, 57
 - magnetic structure, 61
 - magnetic-ordering temperatures, 57
 - paramagnetic and saturation moments, 57
 - photoemission, 29
 - positron annihilation, 28
 - promotional model, 3, 27
 - Stevens factors, 40
 - structural properties, 17
- CeSn₃ electronic structure, 29
- CeAl₂ Jahn–Teller effect, 339
- Clebsch–Gordan coefficients, 12
- coherent potential approximation, 249–52
- commensurable structures, 52, 82, 84, 115–23, 305–11
- competing interactions, 85–9
- conduction-electron polarization, 50, 258–61
- conduction-electron susceptibility, 47, 262–8
- cone structure, 52, 109, 121, 126, 293–9
- critical phenomena, 93
- crystal field, 39
- crystal-field excitations
 - conduction-electron interactions, 342–5
 - MF-RPA theory, 313–22
 - 1/*Z*-expansion, 324–33
- crystal-field parameters, 41
- Curie constant, 16
- Curie temperature, 56
- Curie’s law, 15
- Curie–Weiss law, 56
- cycloidal structure, 52, 81, 86, 120

- de Gennes factor, 2, 58
- Debye–Waller factor, 173
- density-functional theory, 8
- detailed balance, 141
- dhcp structure, 17
- diffusive mode, 146
- dilute alloys, 63
- dipole approximation, 171
- dipole–dipole interaction, 49, 116, 121, 232–6
- domains, 236, 246
- double-zone representation, 184
- Dysprosium
 - atomic radius, 37
 - band energies, 34
 - d*-electron occupancy, 38
 - electronic pressure, 36
 - ionic properties, 13
 - $\mathcal{J}(\mathbf{q})$, 47
 - magnetic properties, 57

- magnetic structure, 52, 66, 94, 113
- magnetic-ordering temperatures, 57
- magnetoelastic effects, 64
- paramagnetic Curie temperatures, 57
- paramagnetic and saturation moments, 57
- spin waves, 292, 376
- Stevens factors, 40
- structural properties, 17
- two-ion magnetoelastic coupling, 108
- Dy–Y superlattices, 131–3
- elastic constants, 44
- electrical resistivity
 - magnetic-superzone contribution, 281
 - quadrupolar scattering, 279
 - spin-disorder contribution, 278
 - spin-wave scattering, 279
- electronic pressure, 35
- elementary excitation, 146
- Erbium
 - atomic radius, 37
 - band energies, 34
 - crystal-field parameters, 114
 - d*-electron occupancy, 38
 - electronic pressure, 36
 - film, 132
 - ionic properties, 13
 - $\mathcal{J}(\mathbf{q})$, 47
 - magnetic properties, 57
 - magnetic structure, 52, 94, 119–22
 - magnetic-ordering temperatures, 57
 - magnon–phonon interaction, 299
 - paramagnetic Curie temperatures, 57
 - paramagnetic and saturation moments, 57
 - spin waves
 - 1/*J*-expansion, 209
 - cone structure, 297–300
 - longitudinal structure, 304
 - Stevens factors, 40
 - structural properties, 17
- Er–Y superlattices, 132
- ErFe₂ excitations, 379
- Europium
 - atomic radius, 37
 - ionic properties, 13
 - magnetic properties, 57
 - magnetic structure, 54
 - magnetic-ordering temperature, 57
 - paramagnetic and saturation moments, 57
 - structural properties, 17
- exchange-correlation energy, 9
- fan structure 62, 126–8
- Fermi-surface nesting, 48
- fluctuation–dissipation theorem, 142
- form factor, 171
- Friedel oscillations, 48
- Gadolinium
 - atomic radius, 37
 - band energies, 34
 - d*-electron occupancy, 38
 - electrical resistivity, 284
 - electronic pressure, 36
 - Fermi surface, 32
 - ionic properties, 13
 - $\mathcal{J}(\mathbf{q})$, 47, 283
 - magnetic properties, 57
 - magnetic structure, 52, 112
 - magnetic-ordering temperature, 57
 - mass-enhancement, 275
 - paramagnetic Curie temperature, 57
 - paramagnetic and saturation moments, 57
 - spin waves, 185
 - Stevens factors, 40
 - structural properties, 17
- Gd–Y alloys, 113
- generalized susceptibility, 136, 144–6, 154–60
- Goldstone mode, 291, 310
- Green function, 147–9
- hcp structure, 17
 - generalized susceptibility, 183

- heat capacity
 - conduction electrons, 273, 347
 - spin waves, 274
- Heisenberg ferromagnet
 - linear response, 149–54
 - MF-RPA theory, 160–2
 - neutron-scattering cross-section, 178
 - spin waves in hcp structure, 185
- helical structure, 51, 79, 286–93
- helifan structure, 126–30
- high-temperature susceptibility, 71–4
- Holmium
 - anisotropic two-ion coupling, 307
 - atomic radius, 37
 - band energies, 34
 - crystal-field parameters, 114
 - d*-electron occupancy, 38
 - dipole–dipole interaction, 307
 - electrical resistivity, 282
 - electronic pressure, 36
 - film, 131
 - ionic properties, 13
 - $\mathcal{J}(\mathbf{q})$, 47, 115, 235
 - magnetic properties, 57
 - magnetic structure, 52, 114–9, 126–30
 - magnetic-ordering temperatures, 57
 - magnetization, 53, 125–30
 - paramagnetic Curie temperatures, 57
 - paramagnetic and saturation moments, 57
 - spin waves
 - bunched helix, 306
 - spin-slip structures, 308
 - Stevens factors, 40
 - structural properties, 17
 - two-ion coupling, 235
- Ho₉₀Tb₁₀ spin waves, 239
- HoCo₂ excitations, 379
- Holstein–Primakoff transformation, 187
- Hund’s rules, 13
- hybridization, 25
- hyperfine interaction, 50, 349–52
- indirect exchange, 45, 256–64
- Kohn anomalies, 48
- Korringa law, 346
- Kramers’ theorem, 60, 314
- Kramers–Kronig relation, 137
- Kubo formula, 139
- Lanthanum
 - atomic radius, 37
 - band energies, 34
 - d*-electron occupancy, 38
 - electronic pressure, 36
 - ionic properties, 13
 - structural properties, 17
- Landau expansion, 78
- Landé *g*-factor, 15
- lattice clamping, 66, 109
- Lindhard function, 264
- LMTO method, 19
- longitudinal ordering, 83–5
- longitudinal-wave structure, 51, 123, 124, 300–4
- Lutetium
 - atomic radius, 37
 - band energies, 34
 - d*-electron occupancy, 38
 - electronic pressure, 36
 - Fermi surface, 33
 - ionic properties, 13
 - structural properties, 17
- magnetic anisotropy
 - axial, 53, 86, 102
 - energy, 58
 - hexagonal, 52, 81, 86, 102, 107
 - macroscopic, 62
 - magnetoelastic contribution, 106–11
 - microscopic and macroscopic, 101–6
 - and susceptibility, 103
- magnetic Bragg scattering, 176
- magnetic exciton–phonon coupling, 335–40
- magnetic structures
 - anisotropic ferromagnet, 64–7
 - bunched helix, 52, 82
 - commensurable, 52, 82, 84, 115–23
 - cone, 52, 109, 121, 126

- cycloid, 52, 81, 86, 120
- fan, 62, 126–8
- helix, 51, 79
- helifan, 126–30
- longitudinal wave, 51, 123, 124
- multiply periodic, 89–94, 124
- spin slips, 53, 117
- square wave, 52, 84, 123
- superlattices, 130–3
- tilted helix, 52, 81, 87
- magnetic superzones, 59, 281
- magneto-acoustic waves, 222, 338
- magnetoelastic coupling, 43
 - two-ion, 108, 122
- magnetostriction, 43
 - ferromagnet, 106
 - periodic structures, 109–11
- magnon–phonon interaction, 219–31
 - selection rules, 228
- magnon–phonon scattering, 229
- mass-enhancement of conduction electrons
 - crystal-field excitations, 347
 - spin waves, 270–5
- mean-field theory 55, 74–9, 116
- multilayers, 130–3
- multiply periodic structures, 89–94, 124

- Neodymium
 - atomic radius, 37
 - band energies, 34
 - crystal-field excitations, 376
 - d*-electron occupancy, 38
 - electronic pressure, 36
 - form factor, 172
 - ionic properties, 13
 - magnetic properties, 57
 - magnetic structure, 61, 89–94, 124, 130
 - magnetic-ordering temperatures, 57
 - paramagnetic and saturation moments, 57
 - Stevens factors, 40
 - structural properties, 17
- Néel temperature, 57
- neutron-scattering cross-section
 - anisotropic ferromagnet, 194
 - binary alloys, 249, 251
 - cone structure, 295
 - helical structure, 290
 - longitudinal structure, 303
 - magnon–phonon modes, 227
 - singlet–singlet system, 315
 - non-local susceptibility, 70
- paramagnetic Curie temperature, 56–7, 63, 73
- phason, 291, 310, 367
- Promethium
 - atomic radius, 37
 - band energies, 34
 - d*-electron occupancy, 38
 - electronic pressure, 36
 - ionic properties, 13
 - magnetic properties, 57
 - paramagnetic and saturation moments, 57
 - Stevens factors, 40
 - structural properties, 17
- positron annihilation, 32
- potential function, 22
- Praseodymium
 - anisotropic two-ion coupling, 361
 - atomic radius, 37
 - band energies, 34
 - band structure, 29
 - crystal-field excitations
 - conduction-electron scattering, 345
 - cubic sites, 321, 364
 - hexagonal sites 319, 361–4
 - lifetimes, 332
 - magnetic-field dependence, 361–4
 - neutron-scattering spectrum, 179
 - ordered structure, 365–9
 - temperature dependence, 323
 - crystal-field levels, 43, 317, 359
 - d*-electron occupancy, 38
 - de Haas–van Alphen effect, 30
 - diffusive response, 354, 367
 - elastic constants, 338
 - electrical resistivity, 355
 - electronic pressure, 36
 - electronic-nuclear ordering, 351–4

- Praseodymium (*cont.*)
 Fermi surface, 29
 form factor, 172
 induced magnetic ordering, 352–60
 ionic properties, 13
 magnetic exciton–phonon interaction, 362
 magnetic-field dependence
 crystal-field excitations, 362
 magnetic moment, 360
 magnetic impurities, 356
 magnetic properties, 57
 magnetic structure, 60, 89–93, 359
 magnetic susceptibility, 60
 magnetic-ordering temperature, 57, 352, 357
 magneto-acoustic waves, 338
 magnetoelastic effects, 334–9
 mass-enhancement, 348
 nuclear heat capacity, 353
 nuclear-magnetic resonance, 351
 paramagnetic and saturation moments, 57
 quasielastic peak, 354
 Stevens factors, 40
 structural properties, 17
 two-ion coupling, 49, 361
 uniaxial pressure, 357–9
 $\text{Pr}_{95}\text{Er}_5$ excitations, 254, 256
 $\text{Pr}_{97.5}\text{Nd}_{2.5}$ structure and excitations, 356
- Racah operators, 40
 random-phase approximation, 151–62
 relativistic effects, 11
 response functions, 135, 137–42
 Russell–Saunders coupling, 12
- scattering function, 140
 scattering vector, 165
 singlet–doublet system, 318
 singlet–singlet system, 314–17
 singlet–triplet system, 320
- Samarium
 atomic radius, 37
 band energies, 34
d-electron occupancy, 38
 electronic pressure, 36
 form factor, 172
 ionic properties, 13
 magnetic properties, 57
 magnetic structure, 61
 magnetic-ordering temperatures, 57
 paramagnetic and saturation moments, 57
 Stevens factors, 40
 structural properties, 17
 structure, 17
 Van Vleck paramagnetism, 16
 soft-mode transition, 307, 316
 spectral weight function, 148
- spin waves
 anisotropic ferromagnet, 186–98
 commensurable structures, 305–11
 conduction-electron scattering, 268
 cone structure, 293–99
 dipole–dipole coupling, 236
 elliptical polarization, 203
 energy gap, 186–205
 frozen-lattice effect, 214
 magnetoelastic contribution, 211–9
 relation to susceptibility, 198–205
 helical structure, 286–293
 incommensurable structures, 286–305
 longitudinally polarized structure, 300–4
 spin-slip structures, 308
 square-wave structure, 310
 two-ion anisotropy, 243–7
- spin-wave theory and corrections, 206–11
- spin–orbit coupling, 13
 spin-slip structure, 53, 117, 308
 square-wave structure, 52, 84, 123, 310
- standard model, 3
 standard-basis operators, 156
 Stevens factors, 40
 Stevens operators, 41
 temperature dependence, 94–101, 202–4, 212

- structure factor, 178
- superlattices, 130–3

- Terbium
 - anisotropy parameters, 216–8
 - atomic radius, 37
 - band energies, 34
 - critical behaviour, 224, 342
 - critical field, 65
 - d*-electron occupancy, 38
 - electrical resistivity, 279, 282
 - electronic pressure, 36
 - Fermi surface, 33
 - ionic properties, 13
 - $\mathcal{J}(\mathbf{q})$, 47, 293
 - magnetic anisotropy, 98–100
 - magnetic properties, 57
 - magnetic structure, 52, 66, 113
 - magnetic-ordering temperatures, 57
 - magneto-acoustic waves, 223, 238
 - magnetoelastic effects, 64
 - magnetostriction, 66
 - magnon–phonon interaction, 228
 - paramagnetic Curie temperatures, 57
 - paramagnetic and saturation moments, 57
 - spin waves
 - binary alloys, 253–5
 - dipolar effects, 238
 - dispersion relations, 197
 - energy gap, 216
 - helical structure, 292
 - lifetimes, 269
 - temperature dependence, 206
 - $1/J$ -expansion, 208
 - Stevens factors, 40
 - structural properties, 17
 - two-ion anisotropy, 218, 244–6
 - two-ion magnetoelastic coupling, 108
- Tb_{0.5}Dy_{0.5} structures, 114
- tilted helix, 52, 81, 87, 292
- Thulium
 - atomic radius, 37
 - atomic wavefunctions, 11
 - band energies, 34
 - crystal-field excitations, 311
 - crystal-field parameters, 114
 - d*-electron occupancy, 38
 - electronic pressure, 36
 - ionic properties, 13
 - $\mathcal{J}(\mathbf{q})$, 47
 - magnetic properties, 57
 - magnetic structure, 52, 123
 - magnetic-ordering temperatures, 57
 - paramagnetic Curie temperatures, 57
 - paramagnetic and saturation moments, 57
 - spin waves, 310
 - Stevens factors, 40
 - structural properties, 17
 - TmZn quadrupolar ordering, 341
 - transverse ordering, 79–3
 - triple-axis spectrometer, 165
- Van Hove scattering function, 174
- Van Vleck paramagnetism, 16, 76
- virtual crystal approximation, 248

- Wortis expansion, 152

- Y alloys, 113, 379
- Y positron annihilation, 32
- Y–Dy superlattices, 131–3
- Y–Er superlattices, 132
- Ytterbium
 - atomic radius, 37
 - ionic properties, 13
 - Stevens factors, 40
 - structural properties, 17

- Zener power-law, 58, 96, 203

APPENDIX

The appendix added here to the electronic version of the book is a (slightly adjusted) copy of the review paper:

J. Jensen, *Magnetic structures and excitations in rare earth metals*. In: Magnetic and Superconducting Materials, eds. M. Akhavan, J. Jensen, and K. Kitazawa (World Scientific, Singapore, 2000) Vol. B, 711-26.

The review is self-contained supplying the book with an overview of the magnetic properties of the rare earth metals. The emphasis is on the progress made in the studies of the structures and excitations in the rare earth metals during the 1990s, after the book was published.

Magnetic structures and excitations in rare earth metals

Jens Jensen

Niels Bohr Institute, Universitetsparken 5, 2100 Copenhagen, Denmark

Abstract

The recent development within the studies of magnetic structures and excitations in the rare earth metals is reviewed. The fine resolution obtainable in x-ray synchrotron experiments led to the discovery of a number of commensurable magnetic structures in Ho and Er which helped renew interest in these long-period, helically or cycloidally, modulated structures. Shortly after, the helifan phases in Ho were established and effects due to trigonal couplings were detected in Er and Ho. The development of the technique of molecular-beam epitaxy has allowed the fabrication of superlattices and alloys of rare earth metals. One of the important discoveries made possible by the use of this technique is the isolation of a pentacritical point in the magnetic phase diagram of the Ho-Er and Ho-Tm alloys. The investigation of the magnetic structures in the two light rare earth metals Nd and Pr gives rise to a number of challenging problems, because of the complexity of the different structures and, in Pr, because of the low value of the Néel temperature (50 mK). The extra excitation branch observed a couple of years ago, in the paramagnetic phase of the singlet-ground-state system Pr at small wave vectors, still awaits a full explanation.

A.1 Introduction

The two dominant magnetic couplings in the rare earth metals are the single-ion anisotropy term due to the crystalline electric field acting on the magnetic $4f$ -electrons, and the Ruderman-Kittel-Kasuya-Yoshida RKKY-exchange interaction by which the localized $4f$ -moments on different ions are coupled indirectly through the polarization of the conduction electrons. To a first approximation, the indirect exchange leads effectively to a Heisenberg Hamiltonian for the coupling between the $4f$ -moments, when assuming the conduction electrons to behave as free electrons. The conduction electrons at the Fermi surfaces of the rare earth metals are predominantly d -electron-like, and orbital impacts on the exchange coupling introduce anisotropic two-ion interactions in the magnetic Hamiltonian. It is difficult to separate two-ion anisotropy effects from those due to the single-ion crystal-field terms. However, the indications are that the coupling between the different moments in the rare earth metals involves a great variety of anisotropic two-ion interactions in addition to the isotropic Heisenberg interaction [1,2].

The heavy rare earth metals are all hexagonal close-packed, and the magnetically ordered phases of the $4f$ -moments found in these metals are either ferromagnetic or the moments are antiferromagnetically modulated along the c axis. In the latter structures, the individual hexagonal layers are uniformly magnetized in a direction which changes from one layer to the next. The basic arrangements of the moments in these systems were determined by neutron-diffraction experiments by Koehler and his colleagues during the 1960s [3].

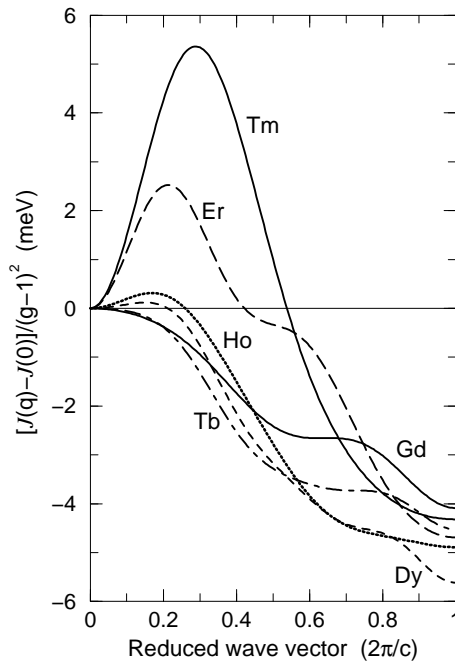


Fig. A.1. The exchange coupling $[\mathcal{J}(\mathbf{q}) - \mathcal{J}(0)] / (g - 1)^2$, with \mathbf{q} parallel to the c axis, determined experimentally in the magnetic heavy rare earth metals (after Ref. [6])

The first inelastic neutron-scattering experiment was carried out on ferromagnetic terbium in 1966 [4]. During the next two decades, similar measurements of the spin-wave energies in the other heavy rare earth metals were performed [5,1], and one main result is shown in Fig. A.1. The exchange interaction, $\mathcal{J}(\mathbf{q})$, is proportional to the magnetic susceptibility of the conduction electrons, and should according to the simple RKKY theory scale as $(g - 1)^2$. The metallic properties of the heavy rare earth metals are very similar; nevertheless, the results shown in Fig. A.1 indicate a pronounced variation of the exchange coupling in the c

direction with atomic number. The magnitude of the peak, which stabilizes the observed periodic magnetic structures, increases monotonically through the series. Here we shall be concerned mostly with the three heavy rare earths, Ho, Er, and Tm, in which a rich variety of different antiferromagnetically ordered phases have been detected.

The two “normal” light rare earths, Pr and Nd, are double hexagonal close-packed (dhcp) with an *ABAC* stacking sequence of the hexagonal layers, which has two non-equivalent sites. The nearest surroundings of the *A* sites is close to be fcc like, whereas the local surroundings of the *B* and *C* sites has hcp symmetry. The difference in lattice structure implies that the RKKY coupling in Pr and Nd does not have its maximum in the *c* direction, but at a wave vector lying in the basal plane at about $0.13 \mathbf{a}^*$. The $(g-1)^2$ -scaling of the RKKY coupling means that it is weak in Pr and Nd in comparison to the crystal-field splittings. Due to the Kramers degeneracy of the ground state the moments in Nd order at about 20 K, whereas Pr is a singlet-ground-state system in which the RKKY coupling is smaller than the threshold value required for inducing a magnetic ordering. This system eventually orders at about 50 mK because of the hyperfine interaction to the nuclear spins.

A.2 Long-period magnetic structures in the heavy rare earth elements

Tb, Dy, Ho are easy-planar magnets in which the moments order in a helical structure at T_N . At lower temperatures, Tb and Dy become basal-plane ferromagnets, whereas the ordered moments in Ho change into a cone structure at low temperatures, with a small ferromagnetic component along the *c* axis superimposed on the helical arrangement in the basal plane. In Er and Tm the *c* axis is the easy axis, which implies that they order in a longitudinally polarized structure where, just below T_N , the *c* component of the moments is sinusoidally modulated. In Tm there is a lock-in transition to a seven-layered structure and, in the low temperature limit, the *c* component saturates, being positive for four layers followed by three layers in which it is negative. The tendency towards a minimization of the variation of the magnitudes of the moments, which becomes more pronounced the lower the temperature, results in the case of Er in a phase in which one of the basal-plane components is non-zero, leading to an elliptic cycloidal structure. At the lowest temperatures, the cycloid is replaced by a *c*-axis cone structure.

The observation of long-period structures commensurate with the lattice, which was made in the high-resolution synchrotron x-ray experiments on Ho [7] and Er [8] by Gibbs and co-workers, has renewed interest in the magnetic ordering in these systems. In the low-temperature limit of Ho, the ordering wave vector locks in to $\frac{1}{6}\mathbf{c}^*$ [9], corresponding to

a period of twelve hexagonal layers. The hexagonal anisotropy in Ho causes the helical component of the moments to bunch around the easy b axes. In the twelve-layered structure, the moments of the different layers bunch pair wise about successive easy directions making angles of about $\pm 5.8^\circ$ with the nearest b axis. As the temperature is increased, the ordering wave vector becomes longer and commensurate structures with different periods are derived from the twelve-layered structure by replacing one or more of the pairs in a period with a single layer where the basal-plane moment is along the easy axis, forming the so-called “spin-slip” structures [7]. The formation of the spin-slip structures was confirmed by high-resolution neutron diffraction experiments performed on large crystals on a triple-axis spectrometer, allowing the observation of peaks of up to 4 orders of magnitude smaller than the main ones [10].

In the presence of an external field new magnetic structures appear in Ho as detected in resistivity measurements [11-13], in x-ray experiments [14], and in neutron diffraction experiments [9,15,16]. As the field applied perpendicular to the c axis of the helical structures is increased, the helix first distorts, giving rise to a moment along the field, and then undergoes a first order transition to a fan structure, in which the moments oscillate around the field direction. A further increase in the field reduces the opening angle of the fan which, in the absence of hexagonal anisotropy, goes continuously to zero. The hexagonal anisotropy causes the transition to the ferromagnet to be of first order or, if large enough, eliminates the fan phase. A detail mean-field analysis of the transition between the (distorted) helix and the fan [17] has shown that long period combinations of the two structures, “the helifans”, may appear as intermediate phases, in accordance with experimental findings in the case of Ho. Experiments on Dy do not show any indications of a helifan phase [18] consistent with mean-field analyzes which in this case predicts the helifan phases to be unstable. The magnetic structures in Er with a field applied in the basal plane have been studied by Jehan *et al.* [19], who followed the transformation of the cycloidal structure into different fan-like structures.

The symmetry of the hexagonal close-packed lattice of the heavy rare earth metals allows the presence of magnetic two-ion interactions with only three-fold symmetry around the c axis [1]. These so-called trigonal terms manifest themselves only under certain conditions, for instance they cancel out in the ferromagnetic case. To first order their contribution to the free energy is

$$\Delta F \propto \sum_p (-1)^p J_{\parallel} J_{\perp}^3 \cos(3\phi_p). \quad (A.1)$$

where J_{\parallel} and J_{\perp} are the components of the magnetic moments parallel and perpendicular to the c axis, respectively, and ϕ_p is the angle which

the basal-plane moments in the p th layer make with the a axis. Its change of sign from one layer to the next implies that the double-zone representation in the c direction ceases to be valid if this term is important. The first example of a trigonal coupling found in the heavy rare earths was the strong coupling between acoustic magnons and optical phonons propagating along the c direction in the ferromagnetic phase of Tb [2,20].

The high-resolution synchrotron x-ray studies of the intermediate cycloidal phase of Er by Gibbs *et al.* [8] indicated the presence of a number of long-period commensurate structures, which they explained to be regular arrangements of 3 or 4 layers of moments with an alternating positive or negative component along the c axis. The 7 layered or (43)-structure observed close to 50 K, thus comprises 4 hexagonal planes of moments with a positive c -component followed by 3 planes of moments with a negative c -component. As the temperature is lowered more and more triplets are replaced by quartets, until the system just above T_C only consists of quartets, which is the (44)-structure with $\mathbf{q} = \frac{1}{4}\mathbf{c}^*$. Cowley and Jensen [21] were able to determine the intensities of most of the harmonics in the commensurate structures of Er. The neutron-diffraction results were compared with the intensities of the corresponding structures predicted by a mean-field model. This comparison confirmed that the basic feature of the commensurate structures is the one proposed by Gibbs *et al.* Unexpectedly, the neutron experiments also showed the presence of scattering peaks along the c axis at $\pm(2n+1)q + mc^*$ for odd integer values of m . These indicate that the magnetic structures depend on the two orientations of the hexagonal layers in the hcp lattice, implying that the structures are distorted by trigonal couplings. The resulting structures are “wobbling cycloids”, in which there is a b -axis moment perpendicular to the cycloidal a - c plane, oscillating with a period different from that of the basic structure. This means that, for instance, the (43)-structure should rather be denoted as the 2(43)-structure as it only repeats itself after each 14 layers. In the case of Ho, the trigonal couplings have a weak, second order, effect on the helical structure. The application of a field in the c direction enhances the structural distortions due to the possible trigonal interactions and by analyzing various experiments, Simpsons *et al.* [22] were able to establish that these couplings are also of significance in Ho.

The tendency for the period of the magnetic ordered structures in the rare earths to lock into values which are commensurate with the lattice, is determined by a complex interplay between the exchange coupling and the magnetic anisotropy terms. The commensurate spin-slip structures detected in Ho at low temperatures by Gibbs *et al.* [7] are explained by the large basal-plane six-fold anisotropy. This hexagonal-

anisotropy energy and thus the bunching effect rapidly declines with the magnetization M , approximately like M^{21} , and the commensurate effects deriving from this anisotropy term should decrease when applying a field along the c axis. Nevertheless, neutron diffraction measurements indicate a strong increase with field of the lock-in of the 8 layered spin-slip structure at about 100 K [23] and of the 10 layered structure at about 40 K [24]. At 100 K the hexagonal anisotropy energy is so small that it only gives rise to a bunching of the order of a tenth of a degree and the spin-slip model of Gibbs *et al.* no longer applies. In comparison, the trigonal anisotropy energy decreases with a much lower rate with the magnetization (like M^7) and increases linearly with a c -axis field, as long as the c -axis moment is small, see Eq. (A.1). A mean-field analysis of the stability of the different commensurate structures in Ho has been carried out [25]. The model calculations show that the trigonal coupling is capable of explaining both observations. It was predicted that the width in temperature of the lock-in of the 8 layered structure should increase strongly, if the magnetic field is applied in a direction making a non-zero angle θ with the c axis, being proportional to $\sqrt{\theta}$ at small angles. As shown in Fig. A.2 this prediction has been confirmed by Tindall *et al.* [26]. The experimental lock-in is not as strong as predicted in the middle of the interval (it is weaker by a factor of 0.6 in the helix). However,

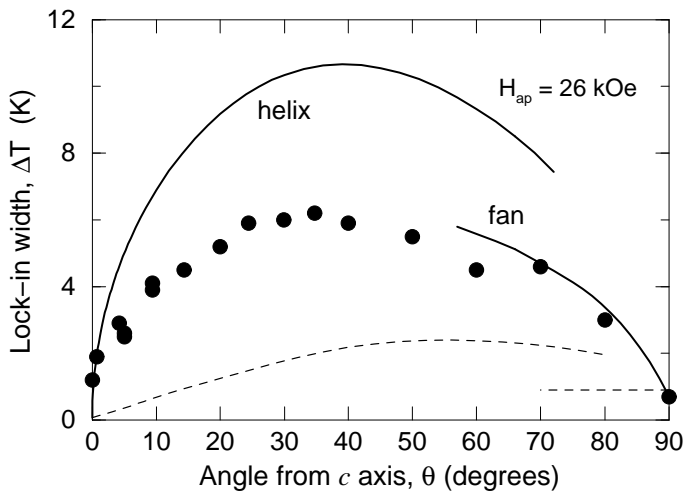


Fig. A.2. The experimental results (solid circles) of Tindall *et al.* [26] show the lock-in temperature width of the 8 layered structure versus the angle θ of the applied field of 26 kOe in the c - b plane of Ho. The lines show the theoretical results obtained from the mean-field model calculations [25] with (solid lines) and without (dotted lines) the trigonal coupling.

the over-all behaviour is very similar to that predicted when including the trigonal coupling determined from the low-temperature experiments [22], and contrast strongly with the behaviour expected when this coupling is neglected. Incidentally, the lock-in effect calculated in the case where the trigonal coupling is neglected, is due to the Zeeman energy.

The period of some of the commensurate structures observed in Ho and Er are remarkably long, as for instance the 2(444443) structure in Er with a repeat length of 46 hexagonal layers, and it is clear from the experiments that some disordering and hysteresis effects may occur noticeably at low temperatures. The neutron-diffraction experiment of Cowley *et al.* [27] shows that Ho may contain several domains with different spin-slip structures below 40 K. The regularity in the spacing of the spin-slip layers in the low-temperature spin-slip structures in Ho may be distorted. The x-ray diffraction measurements by Helgesen *et al.* [28] indicate that this is the case. They have observed a reduction of the longitudinal correlation length between 40 and 20 K by a factor of three, a reduction which is partly removed, when the spin-slip layers disappear at the lock-in transition to $\mathbf{q} = \frac{1}{6}\mathbf{c}^*$ at about 20 K. In the alloy $\text{Ho}_{0.9}\text{Er}_{0.1}$ the $\frac{7}{36}\mathbf{c}^*$ structure is stable at the lowest temperatures, and Rønnow [29] has observed that the widths of the neutron diffraction peaks in this phase are much larger for the higher harmonics than for the first one. The $\frac{7}{36}\mathbf{c}^*$ spin-slip structure consists of alternating two and three pairs of layers between the spin-slip planes, (2212221), and Rønnow has found that a structure in which the succession of the two sequences 221 and 2221 is completely random, predicts a diffraction spectrum close to the observed one.

A.3 Magnetic excitations in the heavy rare earth metals

The magnetic excitations in the heavy rare earths are in most cases well-defined spin waves at low temperatures [1]. Although Tm belongs to the heavy elements of the rare earth series the RKKY-exchange interaction, being proportional to $(g - 1)^2$, is weak compared to the crystal-field anisotropy energies. This implies that crystal-field excitations are important in Tm at elevated temperatures, both below and above T_N . In the low-temperature spin-wave regime the weakness of the exchange coupling implies that the bandwidth of the spin-wave spectrum, of the order of 2 meV, is small compared to the energy gap of approx. 8.5 meV [6,30]. One consequence of this is that the possible incommensurate broadening of the excitations occurring in the quasi-periodic regime (above 32 K), discussed for example by Lovesey [31], is of no importance in Tm. Using the infinite-continued-fraction formulation for the response function [1] the expansion rapidly converges in the case of Tm, because

$\mathcal{J}(\mathbf{q})$ is weak, and the response function becomes largely independent of whether the ordering is commensurate or not.

In Ref. [6] a complete RPA-theory for the magnetic excitations in Tm is developed. This theory accounts for the periodic magnetic ordering of the moments and for the interaction of the magnetic excitations with the phonons. Since the magnetic periodicity is seven times that of the lattice along the c axis, the spin waves are split into seven closely spaced energy bands. Because of the weak dispersion it was not possible to resolve experimentally the seven branches, instead, the calculated scattering function as a function of wave vector was compared directly with the experimental inelastic neutron-cross-section. A similar investigation of Er in its linearly polarized phase has been conducted by Nicklow and Wakabayashi [32]. The exchange coupling is relatively larger in Er than in Tm in comparison with the crystal-field splittings. However, the modifications of the spin waves in Er, due to the population of the different crystal-field levels, are important and dominate the possible effects caused by the quasi-periodic modulation of the magnitude of the moments.

The modulated (43)-structure in Tm is changed into a ferromagnetic structure when applying a c -axis field of more than 28 kOe. The model developed in Ref. [6] predicts this field to be about 42 kOe. Measurements [33] have later shown that there is a large change of the c -axis lattice parameter of about 0.7% at the transition, and the extra magnetoelastic energy gained in the ferromagnetic phase is able to explain the discrepancy. The spin-wave energies in the ferromagnetic phase of Tm have been measured [34]. The comparison with the excitations seen in the zero-field phase shows that both the crystal-field energy gap and the exchange coupling in the c direction is rather strongly modified at the transition. These changes must be the consequences of the disappearance of the superzone energy gaps and of the large shift in the c -axis lattice parameter.

The transport properties and among them the electrical resistivity of the rare earth metals were studied in many details during the 1960s, see for instance the review by Legvold [35]. The RKKY-coupling leads to a scattering of the electrons against the magnetic excitations. In addition, the effective number of conducting electrons is affected by the magnetic ordering. Particularly in the antiferromagnets, where the periodicity of the magnetic system introduces new zone boundaries with energy gaps in the conduction bands at the intersections. This so-called “superzone” effect was proposed by Mackintosh [36] and the theory worked out in detail by Elliott and Wedgwood [37]. The results shown in Fig. A.3 are from a recent study of the electrical resistivity in Tm [38]. They give a clear illustration of the superzone effect by comparing the c -axis

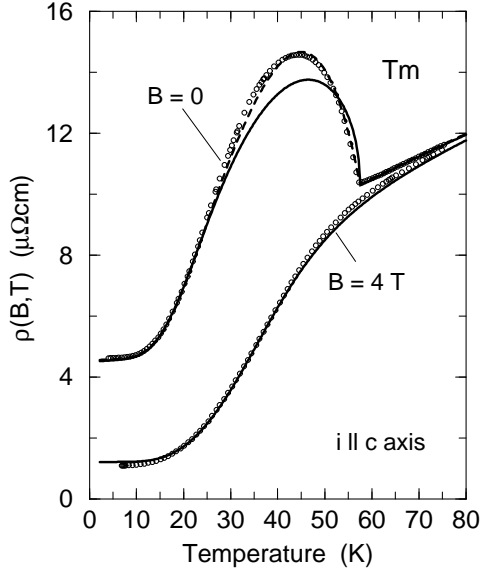


Fig. A.3. The c -axis resistivity in Tm at zero field and in a field of 4 T applied along the c axis. The solid lines show the calculated results, and the dashed line indicates the quadratic rather than linear dependence on magnetization of $\rho(B, T)$ just below T_N (after Ref. [38]).

resistivity obtained in the modulated, zero-field, phase with the one obtained in the ferromagnet. The superzone effect vanishes in the latter case and the c -axis resistivity in the low temperature limit is increased by a factor of 3.7 by the superzones in the zero-field phase corresponding to a reduction of the projection of the Fermi-surface on the plane perpendicular to the c -axis by 73%. The theoretical curves in Fig. 3 show that the resistance in Tm behaves in a way which is consistent with the RPA model developed by McEwen *et al.* [6]. A similar work on Er is in progress. According to model calculations [1] the cone phase in Er below 20 K is suppressed, when applying a hydrostatic pressure of about 2.5 kbar. Neutron-diffraction measurements at 11.5 and 14 kbar [39] show that the cycloid is indeed stable at 4 K at these values of the pressure. The resistivity of Er has been measured as a function of hydrostatic pressure [40]. The change of the magnetic phase from the cone to the cycloidal structure is observed to occur between 1 and 3 kbar. It is found that the superzone effects are a factor of 2–3 stronger in the cycloidal phase than in the cone. The combination of the calculated scattering rate with the Elliott-Wedgwood theory for the superzone effects accounts for most of the observations made in Er; except that the c -axis

resistivity in the intermediate phase at ambient pressure is somewhat smaller than predicted.

A.4 Films and superlattices of rare earth metals

The technique of molecular beam epitaxy (MBE) was utilized for producing the first superlattices of rare earth materials, Dy/Y [41] and Gd/Y [42], in the middle of the 1980s. Since then, a large number of different rare earth superlattices has been studied using x-ray and neutron-scattering techniques. Recent reviews are given by Majkzak [43] and by Cowley [44]. One of the central concerns in these systems is whether the magnetic ordering of one of the constituents is coherent over many bilayers or not. Some rare earth superlattices have coherent magnetic structures even when the magnetic layers are separated by non-magnetic layers of more than 40 atomic planes, as for instance Dy/Y, Ho/Y, and Ho/Lu. In the Pr/Ho or Nd/Y superlattices, or in the Ho/Sc case the magnetic coherence length is of the same size as the thickness of the magnetic layers. In the latter systems the lattice mismatch is important, and the same may be the case in films of a rare earth metals, where the mismatch may occur between the rare earth and the substrate on which the film is grown, see for instance the discussion of the Er thin films in Ref. [45,1]. The magnetoelastic effects are important for the transition to the cone phase in Er, or for the transition to the ferromagnet in Dy, but, in general, the magnetoelastic interactions are weak in comparison with the other magnetic couplings, and the films behave in most respect like the corresponding bulk materials.

The MBE-technique may be used for producing well-defined films of alloys, which has been utilized in an investigation of the $\text{Ho}_x\text{Er}_{1-x}$ [46] and $\text{Ho}_x\text{Tm}_{1-x}$ [47] alloy systems. Ho is an easy planar system whereas Tm and Er are both easy c -axis systems. This implies a *penta-critical* point in the both phase diagrams where the different anisotropy energies compensate each other. At this point, the plane in which the ordered moments are lying may rotate freely and five distinctly different phases are coexisting. The five phases are the paramagnetic, the longitudinally polarized, the cycloidal, the tilted cycloidal/helical, and the helical phase.

The experimental results obtained from neutron diffraction measurements are shown in Fig. A.4. In the case of the Ho-Er alloy system the results are supplemented with results obtained from bulk measurements at $x = 0.5, 0.9$ and 1.0 [29]. The topology of the phase diagrams was established from a Landau expansion by Cowley *et al.* [46]. Here, the theoretical lines are determined using the general mean-field models of the pure systems, Ho, Er, and Tm, known from previous investigations. The results for the different alloys are obtained using the virtual crystal

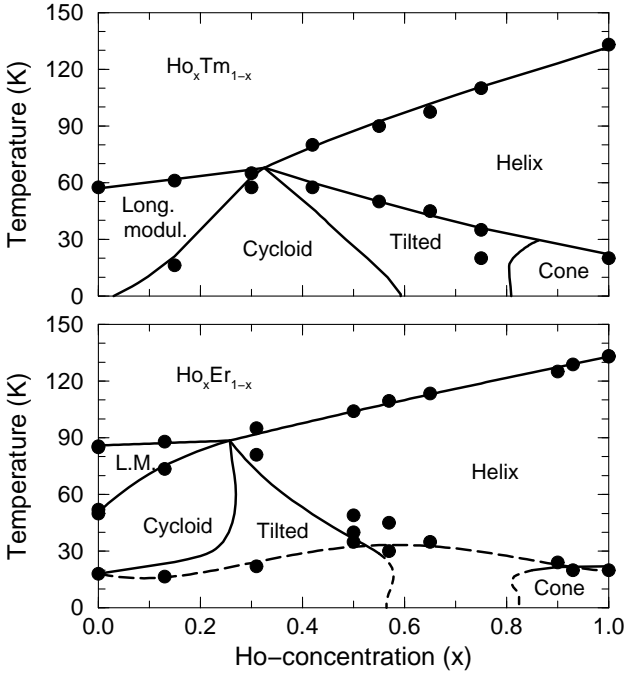


Fig. A.4. The magnetic phase diagrams of $\text{Ho}_x\text{Tm}_{1-x}$ and $\text{Ho}_x\text{Er}_{1-x}$ thin-film alloys. The circles show the transitions determined using neutron diffraction and the solid lines are mean-field calculations. The dotted lines in the $\text{Ho}_x\text{Er}_{1-x}$ case indicate that these transitions are predicted to be of first order.

approximation, and the RKKY coupling, scaled with the appropriated $(g-1)$ factors, is considered to be determined by an averaged conduction-electron gas. This procedure leaves no free parameters for determining the phase lines for x different from 0 or 1. In the case of Er, the model is not developed so to predict accurately the first-order transition to the cone [1], and the dashed line indicating this transition in the $\text{Ho}_x\text{Er}_{1-x}$ phase diagram is not the result of the calculations but a line through the points. The measurements shown in Fig. A.4 demonstrate for the first time the occurrence of the tilted helix, most clearly in the case of $\text{Ho}_x\text{Tm}_{1-x}$, which was advanced in 1972 by Sherrington [48] in relation to the phase diagram of pure Ho. The transition between the cycloid and the tilted cycloid, at which the plane of the cycloidal structures starts to tilt away from the c axis, is not isolated in the present experiments. A detection of this transition by neutron diffraction would require a preparation of the sample so to create a preferred orientation of the a - c cycloidal planes.

A.5 Structures and excitations in the light rare earths Pr and Nd

The magnetic structures in Nd have been studied extensively for more than 30 years [49-58]. The hexagonal B and C sites and the cubic A sites in the dhcp structure have different magnetic properties. The Néel temperature is 19.9 K, and below this temperature the moments on the hexagonal sites are ordered in a longitudinally polarized single- \mathbf{q} structure with $\mathbf{q} \simeq 0.14 \mathbf{a}^*$ [50]. The moments on the B and the C sublattice are antiparallel, and a small moment in predominantly the c direction is induced on the cubic sites. The transition is weakly discontinuous [51], and only about 0.8 K below T_N there is a new first-order transition to a structure, in which two of the three different single- \mathbf{q} domains combines into a double- \mathbf{q} structure [52]. At 8.3 K there is a transition to a triple- \mathbf{q} phase, in which a single- \mathbf{q} ordering of the moments on the cubic sites at a different $\mathbf{q} \simeq 0.18 \mathbf{a}^*$, is superimposed on the double- \mathbf{q} structure of the hexagonal moments. Finally, the low temperature phase, below 6.3 K, is a complex quadruple- \mathbf{q} structure [53] with two ordering wave vectors associated with each of the two sublattices. Thermal expansion measurements [54] indicate one more transition at 5.8 K, and it is suggested that the \mathbf{q} -vectors of the cubic moments may start to tilt out of the basal plane below this temperature, but the anomaly may also be the result of a lock-in transition to a commensurate structure.

The behaviour of the transition between the single- and double- \mathbf{q} structure is consistent with a mean-field analysis [55]. In the double- \mathbf{q} phase, the moments corresponding to each of the two \mathbf{q} -vectors rotate progressively towards each other as the magnetization increases. A numerical estimate [1], which predicts the transition to occur at about 0.9 K below T_N , indicates that the angle between the moments and their nearest b axis should be about 12° at maximum (8 K), corresponding to an angle of 96° between the two directions of the moments. The rotation of the moments is estimated to be accompanied by a rotation of the \mathbf{q} -vectors by an angle that is smaller by a factor of about three, in accordance with the observations. It is worth noting that the reason for the rotation of the moments, and for the stability of the double- \mathbf{q} structure in comparison with the single- \mathbf{q} structure, is the change in entropy [1,55]. The small value of the magnetization implies that the sixth-order hexagonal anisotropy is of no importance close to the transition, which is in contradiction with the proposal made in Ref. [56].

Lebech *et al.* [57] have examined whether the different multiple- \mathbf{q} structures in Nd may be commensurate with the lattice. Their neutron-diffraction experiments show clear lock-in effects in the low-temperature phases below 8.3 K. In the high temperature phases they suggest the presence of a series of two-dimensional higher-order com-

measurable structures, where the magnetic unit cell is rotated a certain angle around the c axis relatively to the crystallographic unit cell, so that commensurable structures are formed although each of the two basal-plane components of \mathbf{q} appears to be incommensurable. The high-resolution measurements of the ordering wave vector made by magnetic x-ray diffraction [58] indicate a smooth variation of \mathbf{q} between 11.5 K and T_N . The absence of lock-in effects in this experiment may be the result of the close spacing of the large number of higher-order commensurable structures. It does not necessarily indicate that the lock-in energies of the epitaxial structures proposed by Lebech *et al.* are negligible.

Pr have the same dhcp lattice structure as Nd, and the magnetic two-ion interactions seem to be very similar in the two metals. The ground state of both the cubic and the hexagonal ions in Pr is a singlet, and the maximum value of the exchange coupling is about 92% of that required for inducing a magnetic ordered state on the hexagonal sites. The coupling is close to the threshold value and small modifications, like a uniaxial pressure of about 0.7 kbar or the introduction of a small percentage of Nd ions, may change the situation [1]. Without external disturbances, magnetic ordering is produced via the hyperfine interaction between the $4f$ -electrons and the nuclear spins, and heat capacity measurements [59] indicate the Néel temperature to be 42 mK. As in Nd, the moments on the hexagonal ions in Pr order in a longitudinally polarized structure with $\mathbf{q} = 0.13 \mathbf{a}^*$, possibly accompanied by an induced moment along the c axis on the cubic ions. It is not yet known, whether the structure just below T_N is a single- or triple- \mathbf{q} structure, or whether, like in Nd, there is a transition between a single- and double- \mathbf{q} structure at a lower temperature. The ordered phase has recently been studied by neutron diffraction [60,61] well below T_N . The value of the first harmonic of the moments is determined to be $0.54 \mu_B$ at 10 mK, when assuming an equal population of domains, and as shown in Fig. A.5 it was found that the antiferromagnetic phase is quenched, when applying a field of about 4.2 kOe along an a direction. These numbers may be compared with the results derived from the MF/RPA-model presented in Ref. [1], which are shown by the solid line in Fig. A.5. The calculated moment is $0.63 \mu_B$ and the critical field is 5.4 kOe at 10 mK. Both values are larger than the experimental ones, although the exchange coupling is adjusted so that the energy gap in the excitation spectrum at the ordering wave vector has the right value, in which case the model correctly predicts $T_N = 43$ mK (using $A = 4.394$ meV). The discrepancies indicate that the single-site fluctuations [1] may be important in the determination of the field dependence of the ordered moment.

Most of the magnetic properties of Pr are well understood in terms of the MF/RPA-model, if including the leading-order corrections due

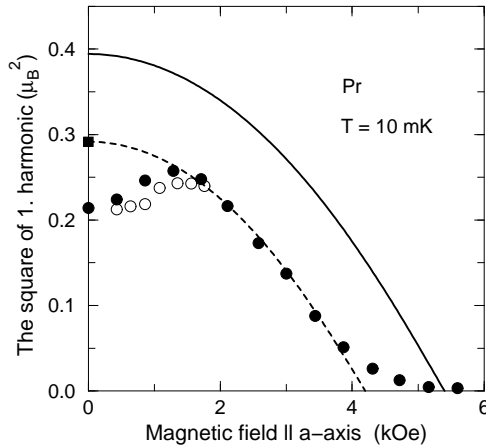


Fig. A.5. The square of the first harmonic of the modulated magnetic moments on the hexagonal sites in Pr as a function of a field applied along an a axis. The circles are the experimental results from Ref. [60,61]. The filled (open) circles are the results obtained for decreasing (increasing) values of the field. The square is the result obtained under zero-field conditions. The experimental results indicate that domains are formed in the field experiment below 2 kOe. The solid line is the variation predicted by the MF/RPA model for Pr [1], and the dashed line indicates the experimental variation.

to the single-site fluctuations in the description of, for instance, the linewidth of the magnetic excitations [1,62]. However, there are two phenomena in Pr which the “standard model” cannot easily explain. One is the broad quasielastic or central peak which appears at about 13 K as a ring in reciprocal space around Γ , which is perpendicular to the c axis and has a radius $|\mathbf{q}| \simeq 0.1 a^*$, see the discussion in Ref. [1]. The other phenomenon is the two extra excitations observed a couple of years ago, hybridizing at small wave vectors with the normal magnetic excitations which propagate on the hexagonal and on the cubic sites in the paramagnetic phase [63]. At 4.2 K the linewidth of the extra excitations shows a sharp drop when applying a field of about 15 kOe along the a axis. The quasielastic peak disappears [61] at this field (at 1.8 K) suggesting a connection between the two phenomena. The coincidence might be accidental, though it is proposed that both phenomena may involve a weak hybridization of the $4f$ electrons with the conduction electrons. Another proposal made recently [64] is that the quasielastic peak is due to transverse fluctuations locked to the critical longitudinal fluctuations in a kind of a spin-slip configuration. However, this theory

involves a number of postulates in the analysis of the dynamics, and it is inconsistent with the dominance of the quasielastic peak above 4 K. In addition, the excitation spectrum indicates that the transverse fluctuations are centered around $|\mathbf{q}| \simeq 0.07 a^*$, not $0.1 a^*$, and should be much weaker than the longitudinal ones in the critical regime. The energy difference between, for instance, the dhcp and the Sm-structure is small, and stacking faults in the *ABAC*-sequence of hexagonal layers along the *c* axis may occur relatively frequently. In case two layers, *B* and *C*, with local hcp symmetry happen to be neighbours, the effective $\mathcal{J}(\mathbf{q})$ within the two layers is probably increased. An increase by 23% would create a double-layered magnetic system with an estimated MF transition temperature of 14 K, a zero-temperature moment of $1.9 \mu_B/\text{ion}$, and a critical *a*-axis field of 14 kOe at 1.8 K. These numbers indicate that a distribution of hcp double-layers with a density of about one per 1000 layers, is a promising candidate for explaining the quasielastic peak in Pr. Although new normal modes would be associated with such a partial ordering, their intensities are probably all too weak to be able to explain the extra modes observed in Pr.

A.6 Conclusions

The rare earth metals display a large number of fascinating and exotic magnetic ordered structures, helifans, spin-slip and other commensurable structures, multiple- \mathbf{q} structures, and distorted structures induced by trigonal couplings. The RKKY-interaction is of long range and excluding the critical properties, the MF- and RPA-theories reasonably account for many of the properties of these systems. The parameters in the magnetic Hamiltonian are adjustable. It would be desirable to calculate these parameters from first principle, and some progress has been made recently [65]. Many aspects of the band properties of the conduction electrons, in the regime where the *4f*-electrons may be treated as localized core electrons, are well understood, see e.g. Ref. [1]. This may be utilized for calculating the change of the projected Fermi-surface areas due to the magnetic modulated moments in Tm and Er, as to be compared with the large reductions indicated by the resistivity measurements. A first-principle calculation of the RKKY interaction is a demanding task, however, a large amount of experimental data is available, and it would be valuable to get more theoretical insight into the behaviour of the RKKY interaction both in the homogeneous bulk systems and in the inhomogeneous superlattices.

References

- [1] J. Jensen and A. R. Mackintosh, *Rare Earth Magnetism: Structures and Excitations* (Oxford University Press, Oxford, 1991).
- [2] J. Jensen, J.G. Houmann and H. Bjerrum Møller, Phys. Rev. B **12**, 303 (1975); J. Jensen and J.G. Houmann, Phys. Rev. B **12**, 320 (1975); J.G. Houmann, J. Jensen and P. Touborg, Phys. Rev. B **12**, 332 (1975).
- [3] W. C. Koehler, in *Magnetic Properties of Rare Earth Metals*, ed. R. J. Elliott (Plenum Press, London, 1972), p. 81.
- [4] H. Bjerrum Møller and J. G. Houmann, Phys. Rev. Lett. **16**, 737 (1966).
- [5] A. R. Mackintosh and H. Bjerrum Møller, in *Magnetic Properties of Rare Earth Metals*, ed. R. J. Elliott (Plenum Press, London, 1972), p. 187.
- [6] K. A. McEwen, U. Steigenberger and J. Jensen, Phys. Rev. B **43**, 3298 (1991).
- [7] D. Gibbs, D. E. Moncton, K. L. D'Amico, J. Bohr and B. H. Grier, Phys. Rev. Lett. **55**, 234 (1985); J. Bohr, D. Gibbs, D. E. Moncton and K. L. D'Amico, Physica A **140**, 349 (1986).
- [8] D. Gibbs, J. Bohr, J. D. Axe, D. E. Moncton and K. L. D'Amico, Phys. Rev. B **34**, 8182 (1986).
- [9] W. C. Koehler, J. W. Cable, M. K. Wilkinson, and E. O. Wollan, Phys. Rev. **151**, 414 (1966); W. C. Koehler, J. W. Cable, H. R. Child, M. K. Wilkinson, and E. O. Wollan, Phys. Rev. **158**, 450 (1967).
- [10] R. A. Cowley and S. Bates, J. Phys. C **21**, 4113 (1988); S. Bates, C. Patterson, G. J. McIntyre, S. B. Palmer, A. Mayer, R. A. Cowley, and R. Melville, J. Phys. C **21**, 4125 (1988).
- [11] A. R. Mackintosh and L. E. Spanel, Solid State Commun. **2**, 383 (1964).
- [12] M. Akhavan and H. A. Blackstead, Phys. Rev. B **13**, 1209 (1976).
- [13] J. F. Gebhardt and N. Ali, J. Appl. Phys. **84**, 6299 (1998).
- [14] H. Ohsumi, K. Tajima, N. Wakabayashi, Y. Shinoda, K. Kamishima and T. Goto, J. Phys. Soc. Japan **66**, 1896 (1997); H. Ohsumi and K. Tajima, J. Phys. Soc. Japan **67**, 1883 (1998).
- [15] D. A. Jehan, D. F. McMorro, R. A. Cowley, and G. J. McIntyre, J. Magn. Magn. Mat. **104-107**, 1523 (1992) and Europhys. Lett. **17**, 553 (1992).

- [16] R. A. Cowley, R. C. C. Ward, M. R. Wells, M. Matsuda, and B. Sternlieb, *J. Phys. Condens. Matter* **6**, 2985 (1994).
- [17] J. Jensen and A. R. Mackintosh, *Phys. Rev. Lett.* **64**, 2699 (1990).
- [18] N. Wakabayashi, J. W. Cable, and J. L. Robertson, *Physica B* **241-243**, 517 (1998).
- [19] D. A. Jehan, D. F. McMorrow, J. A. Simpson, R. A. Cowley, P. P. Swaddling, and K. N. Clausen, *Phys. Rev. B* **50**, 3085 (1994).
- [20] J. Jensen, *Acta Phys. Pol. A* **91**, 89 (1997).
- [21] R. A. Cowley and J. Jensen, *J. Phys. Condens. Matter* **4**, 9673 (1992); J. Jensen and R. A. Cowley, *Europhys. Lett.* **21**, 705 (1993).
- [22] J. A. Simpson, D. F. McMorrow, R. A. Cowley and D. A. Jehan, *Phys. Rev. B* **51**, 16073 (1995).
- [23] D. R. Noakes, D. A. Tindall, M. O. Steinitz and N. Ali, *J. Appl. Phys.* **67**, 5274 (1990); D. A. Tindall, M. O. Steinitz, M. Kahrizi, D. R. Noakes and N. Ali, *J. Appl. Phys.* **69**, 5691 (1991).
- [24] D. A. Tindall, M. O. Steinitz and T. M. Holden, *Phys. Rev. B* **47**, 5463 (1993).
- [25] J. Jensen, *Phys. Rev. B* **54**, 4021 (1996).
- [26] D. A. Tindall, M. J. Small, M. O. Steinitz, and Z. Tun, *Physica B* **241-243**, 699 (1998).
- [27] R. A. Cowley, D. A. Jehan, D. F. McMorrow and G. J. McIntyre, *Phys. Rev. Lett.* **66**, 1521 (1991).
- [28] G. Helgesen, J. P. Hill, T. R. Thurston, D. Gibbs, J. Kwo and M. Hong, *Phys. Rev. B* **50**, 2990 (1994); G. Helgesen, J. P. Hill, T. R. Thurston and D. Gibbs, *Phys. Rev. B* **52**, 9446 (1995).
- [29] H. M. Rønnow, Thesis (Ørsted Laboratory, 1996).
- [30] J. A. Fernandez-Baca, R. M. Nicklow and J. J. Rhyne, *J. Appl. Phys.* **67**, 5283 (1990); J. A. Fernandez-Baca, R. M. Nicklow, Z. Tun and J. J. Rhyne, *Phys. Rev. B* **43**, 3188 (1991).
- [31] S. W. Lovesey, *J. Phys. Condens. Matter* **4**, 6275 (1992).
- [32] R. M. Nicklow and N. Wakabayashi, *Phys. Rev. B* **51**, 12425 (1995).
- [33] S. W. Zochowski and K. A. McEwen, *J. Magn. Magn. Mater.* **104-107**, 1515 (1992).
- [34] U. Steigenberger, K. A. McEwen, J. L. Martinez and J. Jensen, *Physica B* **180-181**, 158 (1992); K. A. McEwen, U. Steigenberger, L. Weiss, T. Zeiske and J. Jensen, *J. Magn. Magn. Mater.* **140-144**, 767 (1995).
- [35] S. Legvold, in *Magnetic Properties of Rare Earth Metals*, ed. R. J. Elliott (Plenum Press, London, 1972), p. 335.
- [36] A. R. Mackintosh, *Phys. Rev. Lett.* **9**, 90 (1962).
- [37] R. J. Elliott and F. A. Wedgwood, *Proc. Phys. Soc.* **81**, 846 (1963); *ibid.* **84**, 63 (1964).

- [38] M. Ellerby, K. A. McEwen, and J. Jensen, *Phys. Rev. B* **57**, 8416 (1998).
- [39] S. Kawano, B. Lebech, and N. Achiwa, *J. Phys. Condens. Matter* **5**, 1535 (1993); S. Kawano, S. Aa. Sørensen, B. Lebech, and N. Achiwa, *J. Magn. Magn. Mater.* **140-144**, 763 (1995).
- [40] M. Ellerby, K. A. McEwen, E. Bauer, R. Hauser, and J. Jensen, *Phys. Rev. B* **61**, 6790 (2000).
- [41] M. B. Salamon, S. Sinha, J. J. Rhyne, J. E. Cunningham, Ross W. Erwin, J. Borchers, and C. P. Flynn, *Phys. Rev. Lett.* **56**, 259 (1986).
- [42] C. Vettier, D. B. McWhan, E. M. Gyorgy, J. Kwo, B. M. Buntschuh, and B. W. Batterman, *Phys. Rev. Lett.* **56**, 757 (1986).
- [43] C. F. Majkrzak, *Physica B* **221**, 342 (1996).
- [44] R. A. Cowley, *J. Magn. Magn. Mater.* **177-181**, 1156 (1998).
- [45] J. A. Borchers, M. B. Salamon, R. W. Erwin, J. J. Rhyne, R. R. Du, and C. P. Flynn, *Phys. Rev. B* **43**, 3123 (1991).
- [46] R. A. Cowley, J. A. Simpson, C. Bryn-Jacobsen, R. C. C. Ward, M. R. Wells, and D. F. McMorrow, *Phys. Rev. B* **57**, 8394 (1998).
- [47] R. S. Sarthour, R. A. Cowley, R. C. C. Ward, M. R. Wells, D. F. McMorrow, and J. Jensen, *Phys. Rev. B* **62**, 14943 (2000).
- [48] D. Sherrington, *Phys. Rev. Lett.* **28**, 364 (1972).
- [49] R. M. Moon, J. W. Cable, and W. C. Koehler, *J. Appl. Phys.* **35**, 1041 (1964).
- [50] B. Lebech, *J. Appl. Phys.* **52**, 2019 (1981).
- [51] S. Zochowski and K. A. McEwen, *J. Magn. Magn. Mater.* **54-57**, 515 (1986).
- [52] K. A. McEwen, E. M. Forgan, H. B. Stanley, J. Bouillot, and D. Fort, *Physica B* **130**, 360 (1985).
- [53] E. M. Forgan, E. P. Gibbons, K. A. McEwen, and D. Fort, *Phys. Rev. Lett.* **62**, 470 (1989).
- [54] S. W. Zochowski, K. A. McEwen, and E. Fawcett, *J. Phys. Condens. Matter* **3**, 8079 (1991).
- [55] E. M. Forgan, *J. Phys. F* **12**, 779 (1982).
- [56] P.-A. Lindgård, *J. Magn. Magn. Mater.* **177-181**, 1016 (1998).
- [57] B. Lebech, J. Wolny, and R. M. Moon, *J. Phys. Condens. Matter* **6**, 5201 (1994).
- [58] D. Watson, E. M. Forgan, W. J. Nuttall, W. G. Stirling, and D. Fort, *Phys. Rev. B* **53**, 726 (1996).
- [59] M. Eriksen, E. M. Forgan, C. M. Muirhead, and R. C. Young, *J. Phys. F* **13**, 929 (1983).
- [60] A. Metz, B. Schröder-Smeibidl, A. A. Moolenaar, M. Ellerby, K. A. McEwen, M. Manns, and M. Steiner, *Physica B* **234-236**, 770 (1997).

- [61] K. A. McEwen, in *Magnetism in Metals*, ed. by D. F. McMorrow, J. Jensen, and H. M. Rønnow, Mat. Fys. Medd. Dan. Vid. Selsk. **45**, 79 (1997); and private communication.
- [62] J. Jensen, K. A. McEwen, and W. G. Stirling, Phys. Rev. B **35**, 3327 (1987).
- [63] K. N. Clausen, K. A. McEwen, J. Jensen, and A. R. Mackintosh, Phys. Rev. Lett. **72**, 3104 (1994); K. N. Clausen, S. Aa. Sørensen, K. A. McEwen, J. Jensen, and A. R. Mackintosh, J. Magn. Magn. Mater. **140-144**, 735 (1995).
- [64] P.-A. Lindgård, Phys. Rev. Lett. **78**, 4641 (1997).
- [65] M. S. S. Brooks, O. Eriksson, J. M. Wills, and B. Johansson, Phys. Rev. Lett. **79**, 2546 (1997).